ARTICLE IN PRESS Available online http://jopr.mpob.gov.my/category/article-in-press/

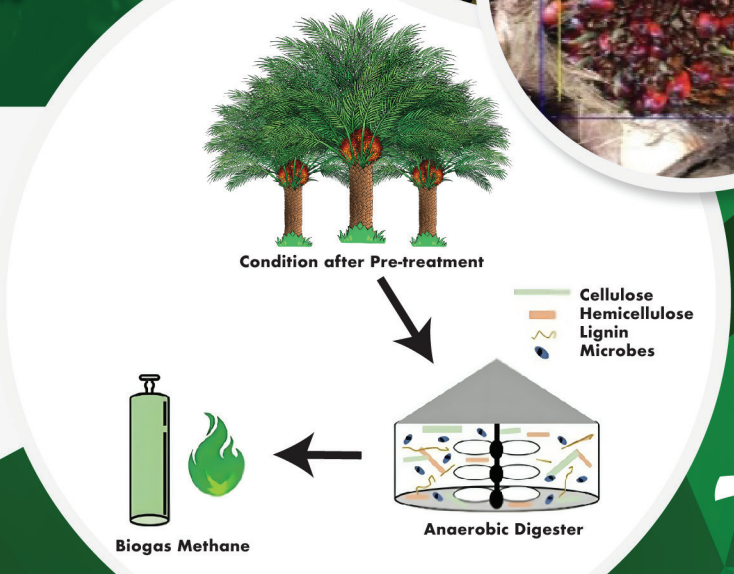
Journal of Oil Palm Research

Vol. 37 (1) • March 2025



REVIEW ARTICLES

- A Picture of Ripeness: Investigating Image-based Techniques for Oil Palm Fruit Grading
- Lignocellulosic Biomass-derived Biogas: A Review on Sustainable Energy in Malaysia



eISSN 2811-4701

JOURNAL OF OIL PALM RESEARCH (formerly known as ELAEIS)

JOURNAL OF OIL PALM RESEARCH (JOPR), an international refereed journal, carries full-length original research papers, short communications and scientific review papers on various aspects of oil palm and palm oil and other palms. JOPR is published four times per year, *i.e.* March, June, September and December.

© Malaysian Palm Oil Board (MPOB), 2025

All rights reserved. No part of this publication may be reproduced in any form or by any means without the written permission of MPOB.

Impact Factor:
1.2
data from *2023 Journal Citation Report*® Science Edition
– A Clarivate Analytics product.

For more information on advertisement for the JOPR, please write to:

Editor-in-Chief
Journal of Oil Palm Research
Malaysian Palm Oil Board
6, Persiaran Institusi, Bandar Baru Bangi
43000 Kajang, Selangor, Malaysia

Tel: *+603-8769 4400*
E-mail: *jopr.admin@mpob.gov.my*
Website: *jopr.mpob.gov.my*

DISCLAIMER
Views of writers expressed in this publication are not necessarily endorsed by or represent the views of MPOB.

MPOB Press
Malaysian Palm Oil Board
6, Persiaran Institusi, Bandar Baru Bangi
43000 Kajang, Selangor, Malaysia
Tel: +603-8769 4400 | Fax: +603-8925 9446
E-mail: *jopr.admin@mpob.gov.my*

JOURNAL OF OIL PALM RESEARCH

Vol. 37 (1) March 2025

CONTENTS

REVIEW ARTICLES

1 A Picture of Ripeness: Investigating Image-based Techniques for Oil Palm Fruit Grading
Munirah Rosbi; Zaid Omar and Marsyita Hanafi

16 Lignocellulosic Biomass-Derived Biogas: A Review on Sustainable Energy in Malaysia
Izzah Farhana Ab Aziz; Hasfalina Che Man; Ali Demirci; Muhammad Hazwan Hamzah; Rozita Omar; Nur Syakina Jamali; Kamil Kayode Katibi and Abdulsalam Mohammed

RESEARCH ARTICLES

44 Species Composition of Birds in Oil Palm Areas, Northern Sarawak, Borneo, Malaysia
Bettycopa Amit; Angie Sapis and Nik Sasha Khatrina Khairuddin

53 Application of Seaweed Extracts in Oil Palm (*Elaeis guineensis*) Seedlings Subjected to Water Deficit: Physiological, Biochemical and Enzymatic Responses
Muhammad Danial Mokhtaruddin; Nur Aifaa Abd Razak; Aisamuddin Ardi Zainal Abidin; Nor Izzati Husna Noorhisham; Nur Asna Faiqah Johari and Zetty Norhana Balia Yusof

64 *In Vitro* Cultural Studies for Callogenesis and Embryogenesis of Oil Palm (*Elaeis guineensis* Jacq.) Using Seedling and Spear Leaf Explants
B Kalyana Babu; R K Mathur; K Suresh; G Ravichandran; B Susanthi and S Tiwari

72 Analysis of Putative *EgBBM* Promoter Binding Proteins During Oil Palm Somatic Embryogenesis
Kamolwan Khianchaikhan; Suvichark Aroonluk; Supachai Vuttipongchaikij and Chatchawan Jantasuriyarat

85 Antifungal Volatile Organic Compounds (VOCs) from a Strain of *Fusarium foetens* Against *Ganoderma boninense*
Anisa Lutfia and Bedah Rupaedah

96 Insect Community Associated with *Ganoderma* Basidiocarps in Oil Palm Plantations of Sabah
Muhammad Nurul Yaqin Syarif; Shamala Sundram; Siti Nurulhidayah Ahmad; Mohamed Mazmira Mohd Masri and Idris Abu Seman

110 Analysis of the Energy Consumption of Motorised Circular Saw When Cutting Oil Palm Frond
Sun Qun and Zaidi Mohd Ripin

122 Corrosion Simulation of Automotive Materials Under Exposure in Biodiesel
S Y Cetin; M A Maleque; H H Masjuki; A Hamdani and M M Rahman

131 Experimental Investigations on Tribological Assessment and NO_x Emissions of Palm Biodiesel Blended with Oleic Acid and Ethanol
Karthic Raja M; Kamalesh A Sorate and Purnanand V Bhale

148 Sediment Formation in a Palm Oil Biodiesel Blend in a Ship Fuel Tank
Jajang Amir Hidayat; Bambang Sugiarto; Yulianto Sulistyo Nugroho; Ahmad Syihan Auzani; Hari Setiapraja and Siti Yubaidah

160 Physicochemical and Rheological Properties of Red Palm Olein Oleogels Made with Beeswax as the Oleogelator
Annisa Noor Rachmawati; Nur Wulandari and Eko Hari Purnomo

172 Inverse Vulcanised Polysulphide Adsorbent from Waste Cooking Palm Oil for Cu^{2+} Removal
Mohd Faizal Ali; Nancy Nubur Libat; Hannah Nisa Adawiyah; Abdullah Nayeem and Jun Haslinda Shariffuddin

SHORT COMMUNICATION

181 Development of qPCR Primer for *Ganoderma boninense* Detection in Soil
Hun Jiat, Tung; Yit Kheng, Goh and Wei Chee, Wong

Cover picture:

1 - Bounding box result of FFB localisation using YOLOv4 algorithm (in yellow), compared to ground truth (in blue) during data collection at estate in Yong Peng, Johor, Malaysia.
2 - Lignocellulosic biomass-derived biogas: A review on sustainable energy in Malaysia.

EDITORIAL BOARD

(1 January 2024 – 31 December 2025)

Datuk Dr. Ahmad Parveez Ghulam Kadir
Malaysia (Editor-in-Chief)

Dr. Carl Traeholt
Malaysia

Prof. Dr. Matthias Finkbenier
Germany

Prof. Dr. Dirk Prufer
Germany

Prof. Dr. Douglas G Hayes
USA

Prof. Dr. Tan Chin Ping
Malaysia

Prof. Dr. Takashi Hirano
Japan

Dr. Ahmad Aldrie Amir
Malaysia

Prof. Jonathan Wong Woon Chung
Hong Kong

Dr. Tristan Durand Gasselin
France

Prof. Fikret Isik
USA

Prof. Dr. Jan Stenlid
Sweden

PUBLICATION COMMITTEE

CHAIRPERSON
Datuk Dr. Ahmad Parveez Ghulam Kadir

SECRETARY
Dr. Anita Taib

MANAGING EDITOR
Dr. Laziana Ahmad

PRODUCTION EDITOR
Zaidiana Mohd Zaid
Mohamad Syaiful Mohd Yusof

COMMITTEE MEMBERS
Dr. Ramle Moslim
Ruba'ah Masri
Dr. Sivaruby Kanagaratnam
Dr. Rajinder Singh
Dr. Meilina Ong Abdullah
Dr. Aki @ Zaki Aman
Dr. Zafarizal Aldrin Azizul Hasan
Nasrin Abu Bakar
Johari Minal
Mohd Saufi Awang
Iptisam Abdul Wahab

REVIEW ARTICLES

Journal of Oil Palm Research Vol. 37 (1) March 2025 p. 1-15
DOI: https://doi.org/10.21894/jopr.2024.0015

A PICTURE OF RIPENESS: INVESTIGATING IMAGE-BASED TECHNIQUES FOR OIL PALM FRUIT GRADING

MUNIRAH ROSBI[1]*; ZAID OMAR[1] and MARSYITA HANAFI[2]

ABSTRACT

Oil palm is a highly efficient crop that can produce more oil per unit of land than any other type of oil seed. Palm oil is in high demand, and its production can significantly contribute to a country's economic growth. However, the traditional method of grading palm fruit is still prevalent in Malaysia, which requires skilled workers to classify the harvested fruit according to its ripeness. This approach can be costly and labour-intensive. Therefore, several studies have investigated automated palm fruit classification techniques that could reduce costs and labour in the industry. This article provides a review of these studies, with a specific focus on vision-based classification techniques. The article discusses approaches based on image processing encompassing pre-processing, feature extraction and classification steps. The survey's results indicate that there is a lack of technique to effectively address outdoor images, such as colour correction methods. Therefore, further research is necessary to develop a better segmentation and colour correction procedures. Overall, the findings of this study could help improve the efficiency and sustainability of palm oil production, thereby contributing to economic growth and environmental conservation.

Keywords: image processing, machine-vision technology, maturity detection, ripeness classification.

Received: 5 July 2023; **Accepted:** 27 November 2023; **Published online:** 14 February 2024.

INTRODUCTION

The palm oil industry is a major contributor to Malaysia's economy, with production expected to increase by 3.0% in 2023 (Chew, 2023). Despite covering around 18.0% of the country's land area (Parveez, 2021), the industry accounts for 66.1% of its total export earnings (Azuar, 2022). However, a sustainable production of palm oil is crucial to maximise yield and minimise loss. Approximately 30.0% of palm oil yield is lost (Woittiez *et al.*, 2017) due to the harvesting of unripe fruits, unharvested ripe bunches and uncollected loose fruits. Harvesting ripe fruits has been proven to increase oil yield (Platts & Leong, 2019), highlighting the need for an efficient harvesting process to reduce losses and promote sustainable production.

The oil palm fruit, scientifically known as *Elaeis guineensis*, originated in West Africa and was later cultivated in many Southeast Asian countries like Malaysia, Indonesia and Thailand (Forster *et al.*, 2017). In Malaysia, the *Tenera* species, a hybrid between the *Dura* and *Pisifera* species, is widely cultivated and can survive for over a century [Malaysian Palm Oil Council (MPOC), n.d]. A fresh fruit bunches (FFB) of palm fruits weighs up to 25 kg and consists of 1,000 to 3,000 fruitlets. The FFB are cut from the tree during conventional harvesting and transported to the mill within 24 hr (Jalil, 1995). Careful handling is essential to prevent damage and bruising, which can affect oil quality. At the mill, authorised workers grade and sort the FFBs before oil extraction, ensuring that only ripe and high-quality fruits are processed. The grader determines the payment based on the fruit's quality.

Human labour is required for the harvesting and sorting of FFBs, and additional workers must

[1] Faculty of Electrical Engineering,
Universiti Teknologi Malaysia,
81310 Skudai, Johor, Malaysia.

[2] Faculty of Engineering,
Universiti Putra Malaysia,
43400 Serdang, Selangor, Malaysia.

* *Corresponding author e-mail: munirah96@graduate.utm.my*

be trained to meet the demands of larger plantations or expanding industries. Due to the slow entry process of migrant workers caused by COVID-19 pandemic, Malaysia has faced a labour shortage in the plantation sector (Reuters, 2022). This led to a potential loss in palm oil production and a significant impact on the industry (Vethasalam, 2022). To ensure sustainable profitability in the palm oil industry, the harvesting process must ideally be mechanised to increase productivity (Shuib, 2011). By implementing artificial intelligence-based crop recognition technology, the harvesting process can be structured and the counting and sorting of crops can be performed faster by machines and computers, reducing the need for the already limited human labour (Ortenzi *et al*., 2021). Therefore, it is essential to incorporate an automated classification system with machinery harvesting technology, to minimise human effort and harvesting costs.

FFB Grading

The Malaysian Palm Oil Board (MPOB) has categorised palm fruit ripeness into four groups: Unripe, underripe, ripe, and overripe (MPOB, 2003). Ripeness can be determined by observing the external fruit colours (*Figure 1*), with purplish-black indicating unripe bunches and darkish-red indicating overripe fruits. Reddish-orange and reddish-purple colours represent ripe and underripe fruit bunches, respectively (Makky *et al*., 2013). The traditional manual grading process relied on human vision, which was slow and subjective, requiring experienced staff for grading and sorting (MPOB, 2003). This approach also involved multiple stages of ripeness identification, leading to increased sorting time. Implementing an automated grading system using machine-vision technology would greatly enhance the sorting process, improve efficiency, and provide standardised results (Makky *et al*., 2013). Automated ripeness detection technology could help farmers maximise crop production and reduce losses during harvesting.

This article aims to investigate and critically review the methods employed in machine vision-based classification of oil palm fruit ripeness. The survey explores the researches that have contributed to the maturity classification in palm fruit. The relevant studies in the image-based classification of FFBs, the techniques utilised in processing images, including pre-processing, feature extraction, and classification, will be deliberated, to determine the most effective practices for classifying the palm fruit, based on their maturity.

RELATED STUDIES

Several surveys have analysed the trend of studies related to palm fruit classification. One such study reviewed by Patkar *et al.* (2018) presented the challenges associated with automatic oil palm fruit grading and briefly explained the image processing and fuzzy techniques employed by researchers from 2006 to 2013. You *et al.* (2020) discussed the techniques used to monitor palm fruit maturity, limited to the configurations of microwave sensors for detecting water and oil percentage. In a recent study, Lai *et al.* (2023) reviewed the techniques used in

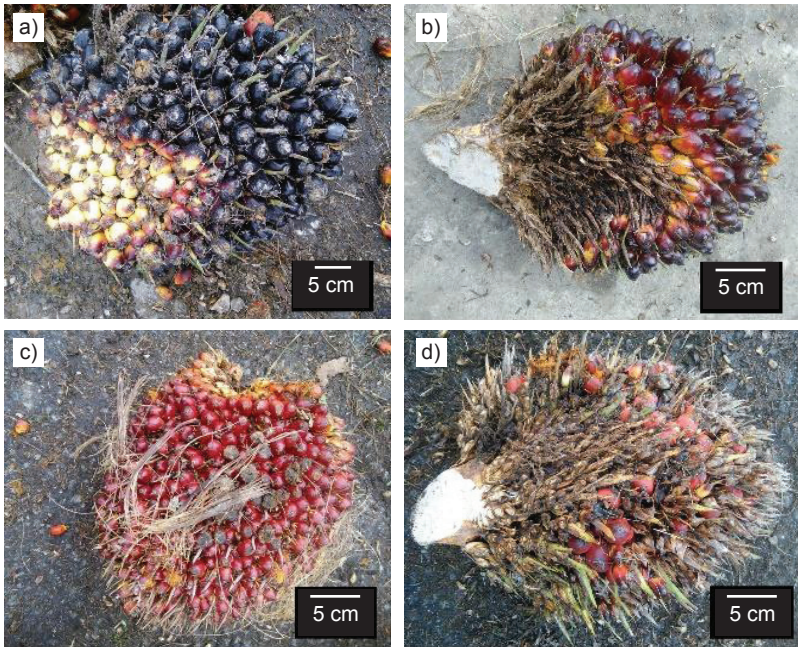


Figure 1. Different ripeness levels of FFB, (a) unripe, (b) underripe, (c) ripe, and (d) overripe.

detecting FFBs, such as using sensors and computer vision. They concluded that the in-field application of image detection is a feasible method for efficient fruit classification, although the authors did not delve into the techniques used in image processing for vision-based classification. Furthermore, machine learning could have significant potential for improving the palm oil industry, as discussed by Khan *et al.* (2021). Despite the notable increase in literature on palm oil ripeness, a comprehensive review of image processing techniques for FFB ripeness classification is necessary for further development. This article represents an early effort to analyse these techniques and address issues related to FFB maturity classification.

This survey aims to identify image-processing techniques used for classifying FFB. Research in this area has grown since the early 2000s, peaking in 2021, emphasising the importance of efficient image-processing techniques for sustainability. However, despite some advancements, the commercialisation of automated palm fruit classification remains limited, with only a few systems implemented in practice. While various harvesting machines have been introduced (Sowat *et al.*, 2018), ripeness detection applications are mostly at the research stage (Lai *et al.*, 2023). This highlights the need for further research and development to bridge the gap between academic studies and practical implementation in the industry.

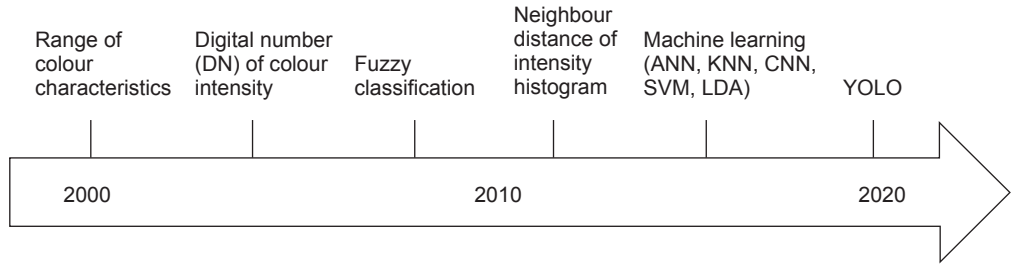
The evolution of the studies can be observed in *Figure 2*, beginning with the classification of colour range and advancing to the implementation of machine learning. The previous techniques involved manual observation of the image characteristics, such as the red, green and blue (RGB) colour channels and required the researcher to note any differences in the colour behaviour of each level of ripeness. However, with recent advances in deep learning, it is now possible to automate the process of palm fruit classification. Deep learning models can be trained on large datasets of palm fruit images, and they can learn to identify the subtle differences in colour and texture that distinguish ripe from unripe fruit. One of the key advantages of using deep learning for palm fruit classification is that it can handle variations in fruit position, lighting conditions and background noise. This makes the technique more robust and reliable than the past methods.

IMAGE-BASED CLASSIFICATION

The classification of FFB using machine learning involves several stages, as presented in *Figure 3*. Following subsections discuss the components of the classification process.

Pre-processing

Pre-processing of images is an essential step that significantly impacts the effectiveness of classifier algorithms. Its objective is to eliminate any noise present in the image. The input images usually undergo labelling and resizing processes. During the pre-processing of the images, the training images were labelled based on their maturity level and some images were resized to reduce their computational size (Septiarini *et al.*, 2020a; Suharjito *et al.*, 2021).



Note: YOLO - You-Only-Look-Once; ANN - Artificial neural network; KNN - K-nearest neighbour; CNN - Convolutional neural network; SVM - Support vector machine; LDA - Linear discriminant analysis.

Figure 2. Timeline of the FFB classification algorithm.

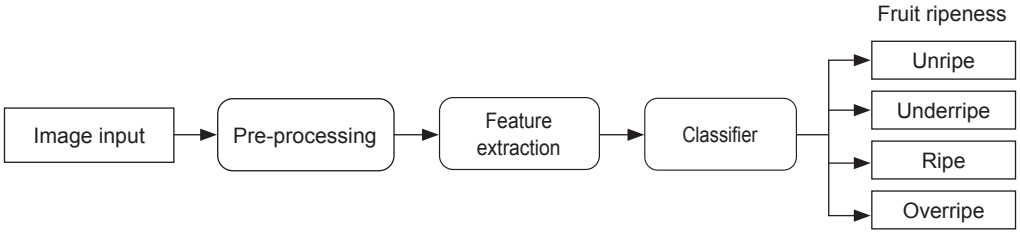


Figure 3. FFB image classification process.

Moreover, filters such as median filtering (Septiarini *et al.*, 2019) and Gaussian blur (Suharjito *et al.*, 2021) were employed to enhance the image and reduce degradation caused by the data acquisition process. Applying these filters to palm fruit images would ensure that the fruits at the edges are easier to distinguish and any noise is removed for better results.

Segmentation. Segmentation refers to the process of dividing an image into multiple parts or segments to facilitate the analysis process. This involves the removal of unwanted parts, such as the background, to eliminate any extraneous information (*Figure 4*). The resulting segmented image can greatly affect the colour detection process. Specifically, the segmented image shows noticeable differences in the RGB values for each maturity class. In contrast, the unsegmented image does not exhibit such variations in RGB values as mentioned by Jaffar *et al.* (2009).

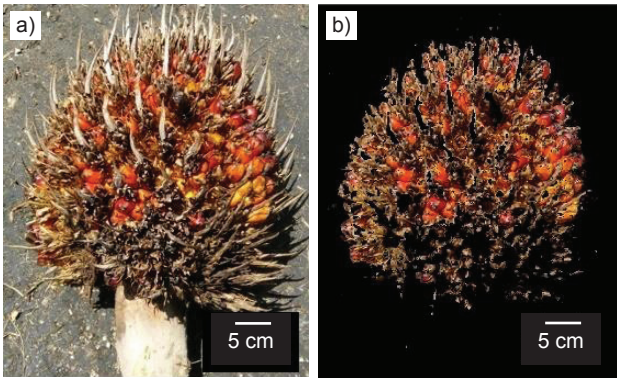


Figure 4. Example of FFB segmentation, (a) original image, and (b) segmented image.

The researchers employed a straightforward threshold method for image segmentation, comparing pixel values to a threshold and removing those below it. For instance, Fahmi *et al.* (2018) used saturation channel thresholding in the Hue Saturation Value (HSV) colour space and Pamornnak *et al.* (2015) set a threshold for grayscale palm fruitlet images to detect edges. Arulnathan *et al.* (2022) used the Otsu method for segmenting fruitlets from a white background, while Septiarini *et al.* (2019) applied the same method for complex background. Amosh *et al.* (2013) proposed the n-SRG method, which employs region-growing with a threshold derived from n-seed points. Thresholding is a simple and effective technique for palm fruit classification, with the choice of threshold value and additional processing techniques like morphological operations improving segmentation accuracy (Septiarini *et al.*, 2020a). Although adaptive thresholding (Makky *et al.*, 2013) has shown success with a constant background, its efficacy in a noisy background is still uncertain.

Other studies have used clustering methods for image segmentation, which involve partitioning images into clusters. However, the choice of clustering method and parameters significantly influences the segmentation quality. Siddesha *et al.* (2017) compared different clustering methods for palm fruit segmentation and found that the k-means method resulted in under-segmentation, while the fuzzy c-means (FCM) method led to over-segmentation. This emphasises the importance of selecting an appropriate clustering algorithm for the specific application. In another study by Ghazali *et al.* (2019), k-means clustering with 300 iterations was applied, but the segmentation still contained spikes attached to the fruit, requiring an additional process to remove them. Jaffar *et al.* (2009) used the k-means technique to segment spikes, preceded by a masking process to eliminate the image background. Similarly, Fadilah *et al.* (2012) adopted Jaffar's technique to separate spikes from fruits in cropped FFB images, without background interference. This approach improves segmentation accuracy by eliminating background noise, which is a challenge in palm fruit classification, due to the complex and cluttered plantation backgrounds.

In addition, Makky *et al.* (2013) performed texture analysis of FFB to distinguish spikes, leaves, and other components, but only for indoor images. They utilised a 3D surface contour graph to select pixel coordinates related to fruit RGB intensity. Septiarini *et al.* (2020a) employed edge and region information for loose fruit image segmentation, using the Canny edge algorithm after identifying regions of interest (ROI). Tan *et al.* (2021) applied the GrabCut algorithm for background removal, but had limited success, so they defined ROI for GrabCut processing. These edge-based segmentation methods effectively determined FFB boundaries, with a preference for working on ROI selection to reduce image noise. The ROI method selects specific areas in the image while discarding large backgrounds to reduce computational processing time (Septiarini *et al.*, 2020a; Suharjito *et al.*, 2021). However, manual cropping is time-consuming (Ibrahim *et al.*, 2018; Sabri *et al.*, 2018) while automatic cropping may yield inaccurate results (Alfatni *et al.*, 2014a). Nowadays, object detection-based ROI segmentation has emerged, enabling FFB detection in complex backgrounds and different environments. Junos *et al.* (2021) proposed the YOLO-P algorithm to detect objects in plantations, including grabbers, palm fruits and palm trees, achieving reliable results with 5,000 training images.

In outdoor settings, inconsistent lighting poses challenges for accurately segmenting FFB images (Razali *et al.*, 2008). Some studies have addressed this by capturing images in controlled conditions, such as closed chambers, to ensure fixed illumination (Jaffar *et al.*, 2009; Makky *et al.*, 2014; Roseleena *et al.*,

2011). While various studies have captured outdoor FFB images, different methodologies have been employed to ensure uniformity in the image frame. Some research employed a tripod stand to maintain a consistent distance between the camera and the fruit, as highlighted by references (Ismail *et al.*, 2010; Razali *et al.*, 2009). Haron *et al.*, 2012 utilised a pole setup with a camera and white LED, incorporating a distance marker to fixate the focus point within the image. Similarly, Fadilah *et al.* (2014) captured tree fruit images using a pole, while Wong *et al.* (2020) utilised the digital camera's zoom function to focus on the palm fruit on the tree. Additionally, research contributions in a study (Tan *et al.*, 2021) demonstrate that achieving an accuracy exceeding 78% is feasible even with a low-cost mobile phone equipped with a digital camera, provided that a reliable classifier algorithm is employed.

Nevertheless, occlusion and shadows in outdoor situations can affect the images, potentially leading to shadow detection as objects (Septiarini *et al.*, 2020a). The occlusion does significantly impact algorithm performance, prompting Junos *et al.* (2021) to exclude FFB images with 90% occlusion when using YOLO-P. Additionally, images of palm fruit on tall trees can suffer from backlighting, reducing contrast and making FFB colours appear darker. Addressing inconsistent outdoor lighting in FFB image classification requires careful selection and implementation of segmentation techniques, potentially incorporating new methods. *Table 1* provides a summary of the strengths and weaknesses of evaluated techniques and relevant research studies.

Image augmentation. Image augmentation is a technique used to increase the amount of training data by transforming the images in various ways, such as changing brightness, adding blur, rotating, and cropping. This technique is commonly used in deep learning for FFB detection to enhance the accuracy of the model. Several studies have applied image augmentation techniques, including adjusting intensity and brightness (Junos *et al.*, 2021; Lai *et al.*, 2022), performing Gamma correction and noise rejection (Robi *et al.*, 2022). The "Image Data Generator" function in TensorFlow library was also utilised by Arulnathan *et al.* (2022) to produce more images from a small number of training images. Another augmentation techniques have been proposed, including the "9-angle crop" (Suharjito *et al.*, 2021) and "TenCrop" methods (Harsawardana *et al.*, 2020), which produce a total of 10 augmented images from one original image. By increasing the amount of training data through image augmentation, the deep learning model can learn from a more diverse set of images, improving its performance in detecting FFB.

Feature Extraction

After preprocessing, image features are extracted for further analysis. This step is crucial in image processing and computer vision as it extracts meaningful information from the image. These features are organised into a matrix or vector and can be used for classification or other tasks using machine learning algorithms. Colour, texture, and shape features are commonly used to describe and determine the maturity level of FFB. Colour properties are often relied upon to assess ripeness, while shape and texture may not show significant differences across ripeness stages (Septiarini *et al.*, 2019). However, combining colour, texture, and shape features can lead to improved classification performance

TABLE 1. STRENGTHS AND LIMITATIONS OF SEGMENTATION METHODS IN FFB SEGMENTATION

Segmentation method	Strength	Limitation	Studies
Threshold	Simple	Brightness variations can affect results	Arulnathan *et al.* (2022); Fahmi *et al.* (2018); Makky *et al.* (2013); Pamornnak *et al.* (2015); Septiarini *et al.* (2019)
Clustering	Effective in separating parts	Accuracy depends on the method	Fadilah *et al.* (2012); Ghazali *et al.* (2019); Jaffar *et al.* (2009); Siddesha *et al.* (2017)
Texture-based segmentation	Spikes filtered by texture pattern	Limited research on outdoor images	Makky *et al.* (2013)
Edge-based segmentation	Fruit boundary detection	Background and noise removal required	Septiarini *et al.* (2020a); Tan *et al.* (2021)
ROI	Background elimination and fruit emphasis	Selection of optimal ROI can be challenging	Alfatni *et al.* (2014a; 2014b; 2018; 2020; 2022); Sabri *et al.* (2017); Septiarini *et al.* (2019; 2020a; 2020b; 2021)
Object detection	A fast and reliable fruit localisation	Requires extensive training data	Junos *et al.* (2021b); Khamis *et al.* (2022); Lai *et al.* (2022); Robi *et al.* (2022)

(Septiarini *et al.*, 2021). *Figure 5* summarises the image features used in the literature, and *Table 2* provides the advantages and disadvantages of these techniques.

Colour features. In the early 2000s, research explored the relationship between colour perception and fruit maturity. Choong *et al.* (2006) and Tan *et al.* (2010) found a correlation between colour characteristics and FFB oil content, making it suitable for maturity detection systems. RGB intensity values, representing average pixel values for each RGB channel, were commonly used for this purpose (Fahmi *et al.*, 2018; May *et al.*, 2011). Alfatni *et al.* (2008), Ghazali *et al.* (2009), Roseleena *et al.* (2011), Jaffar *et al.* (2009), and Jamil *et al.* (2009) referred to the mean of RGB intensity as a digital number (DN) in other studies. Derivatives of the RGB features, such as the ratio of R/G and R/B, could also reveal image characteristics (Melidawati *et al.*, 2021). Also, statistical colour features like the RGB histogram provide pixel characteristics through analysis of intensity colour vectors for each channel (Ismail *et al.*, 2010). Colour moments, another feature extraction method, utilise descriptive statistics such as mean, standard deviation, skewness, and kurtosis. It was stated that colour moments can yield better results than colour histograms, especially for outdoor images with small colour variations (Sabri *et al.*, 2017). However, Ibrahim *et al.* (2018) argued that texture feature analysis is superior to colour moments due to its sensitivity to sunlight illumination.

BBVBVBVBN have explored various colour spaces, including HSV, Hue Saturation and Intensity (HSI), YIQ, and YCbCr (*Figure 6*) to handle colour variations in outdoor images. These colour spaces consider human colour perception and incorporate luminance and brightness values. The HSV colour space, in particular, has been found suitable for outdoor applications (Wong *et al.*, 2020). Similar to the RGB colour space, it can be analysed using intensity, histograms, and statistical features. Several studies have highlighted the usefulness of the hue channel in identifying the dominant colour of outdoor FFB images (Fadilah *et al.*, 2012; Ismail *et al.*, 2010; Razali *et al.*, 2009). Yet, recent research has employed multiple colour spaces other than HSV and selected the most effective colour channels. For instance, the image has shown good performance under different lighting conditions (Sae-Tang, 2020), and the colour space has been found to yield the highest accuracy (Septiarini *et al.*, 2020b). Additionally, the YCbCr and YUV colour spaces have been recommended for FFB ripeness classification and segmentation due to their reduced sensitivity to glossy and silhouette surfaces, resulting in improved accuracy (Sabri *et al.*, 2018). Additionally, colour correction methods have been proposed to address inconsistent outdoor lighting. Haron *et al.* (2012) introduced an external white LED lighting during data acquisition, to minimise the effect of changing hue range in images over time. In another study, Taparugssanagorn *et al.* (2015) used histogram equalisation for image enhancement to adjust the brightness. These techniques can pre-process FFB images and reduce the effects of outdoor colour variation, potentially improving the accuracy of the FFB image classification algorithm. Despite their potential benefits, colour correction techniques are still underutilised by scholars in FFB classification.

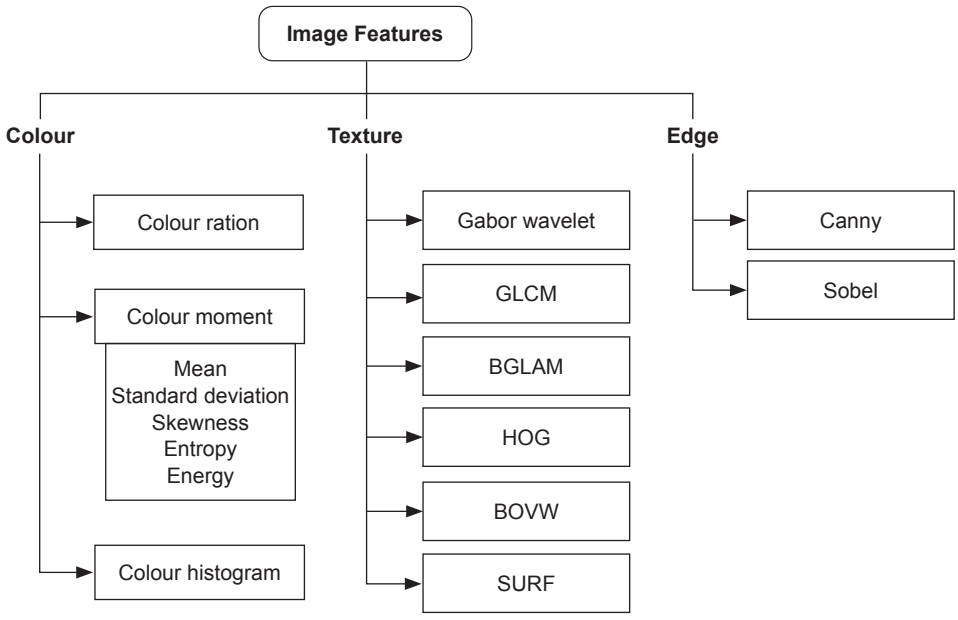


Figure 5. Feature extraction techniques.

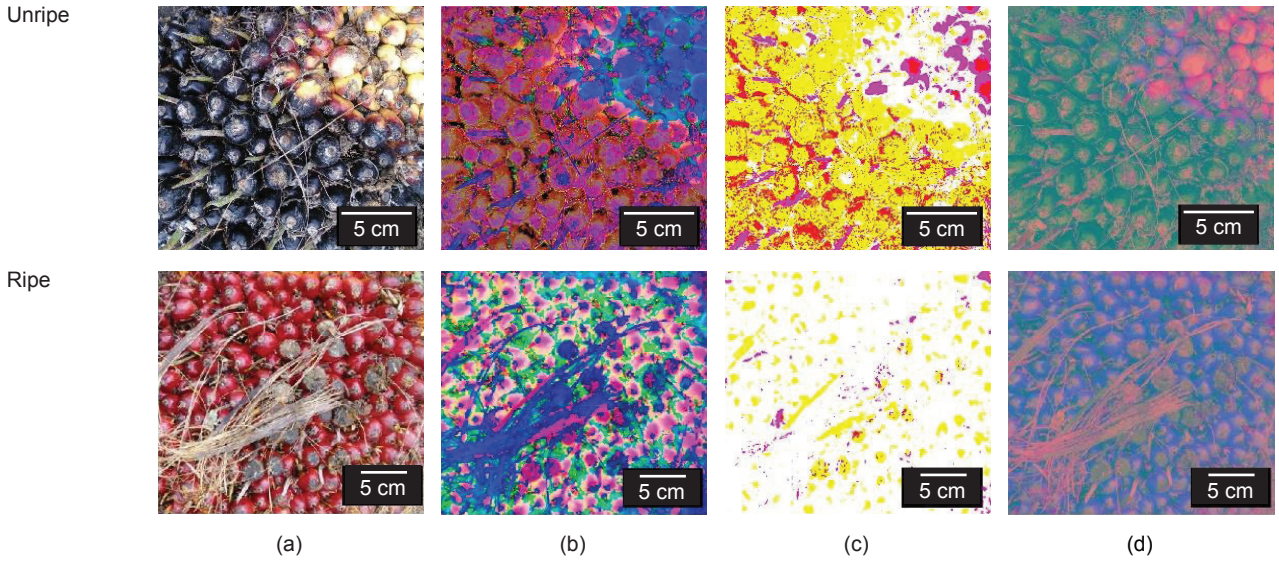


Figure 6. Example of FFB in different colour spaces representations, (a) RGB, (b) HSV, (c) CIELAB, and (d) YCbCr.

Texture features. Other studies have examined FFB texture characteristics for ripeness classification. Alfatni *et al.* (2018) used techniques like Gabor wavelet, grey-level co-occurrence matrix (GLCM), and basic grey-level aura matrix (BGLAM) to classify ripeness, with BGLAM achieving the highest accuracy of 93%. Histogram of oriented gradient (HOG), a gradient-based descriptor, was found effective by Ibrahim *et al.* (2018), outperforming other features but requiring more processing time. Moreover, Ghazali *et al.* (2019) utilised Bag of Visual Words (BOVW) and Speeded Up Robust Features (SURF) for texture descriptor extraction. In a different investigation, Alfatni *et al.* (2014b) directed their attention towards the attributes of thorns, specifically the variations in count and size, employing texture data. Meanwhile, Kassim *et al.* (2014) delved into the growth model of FFB by analysing alterations in spikes. Nonetheless, these two studies stand alone in their exploration of spikes changes, with no subsequent research continuing in this direction. Based on the author's observation, the utility of spikes features might be limited to specific subsets of the *Tenera* dataset, and their relevance could diminish in more recent datasets due to advancements in planting techniques. Texture feature extraction is a useful technique to analyse images that are affected by changes in illumination. However, many experiments involving FFB images were conducted in closed chambers, thereby minimising the impact of external lighting (Alfatni *et al.*, 2014b; 2018; 2022; Makky *et al.*, 2013). Furthermore, outdoor images have proven to be more challenging, with texture feature extraction producing only 70% accuracy according to Ghazalli *et al.* (2019) and 75% accuracy according to Ibrahim *et al.* (2018).

Edge features. Edge detection can provide more insight into the spikiness of the palm fruit, as a fruit that is overripe or rotten tends to show more spikes due to the detachment of fruitlets. Tan *et al.* (2021) used the canny edge algorithm to identify the long edges that were identified as spikes and then measured the ratio of the spikes to the total pixels of the image. Images with a higher number of spikes were classified as having empty and rotten fruits. However, the classification accuracy achieved by them was only 79% when combining colour and edge features. Astuti *et al.* (2019) utilised Sobel edge detection to determine the features of individual palm fruitlets within the boundary of the edge. Nevertheless, this approach only analysed the image of a single fruitlet, not an entire bunch of palm fruit. While the application of edge detection algorithms has the benefit of detecting spikes and fruitlets in FFB, it has not been fully explored by other researchers.

Classification

The final step in the FFB ripeness classification process involves using machine learning. The features that were extracted in the earlier stage are fed into a classifier. In some cases, machine-learning techniques are also used to select the most relevant features for classification, rather than using all the features that were extracted from the images.

Features selection. Classifier accuracy relies on feature quality, but excessive features can lead to overfitting. Therefore, feature selection techniques like Principal Component Analysis (PCA) are used to retain informative features while reducing their number (Fadilah *et al.*, 2012). Other

TABLE 2. STRENGTHS AND LIMITATIONS OF FEATURE EXTRACTION METHODS IN FFB RIPENESS CLASSIFICATION

Types of features	Strength	Limitation	Studies
Colour	Simple and adaptable to outdoor images based on colour space selection	Sensitive to outdoor lighting	Alfatni *et al.* (2008); Choong *et al.* (2006); Fadilah *et al.* (2012); Fahmi *et al.* (2018); Ghazali *et al.* (2009); Haron *et al.* (2012); Ismail *et al.* (2010); Jaffar *et al.* (2009); Jamil *et al.* (2009); May *et al.* (2011); Razali *et al.* (2009); Roseleena *et al.* (2011); Sabri *et al.* (2018; 2017); Sae-Tang, (2020); Septiarini *et al.* (2020b); Tan *et al.* (2010); Wong *et al.* (2020)
Texture	Less influenced by varying sunlight illuminations	Limited studies on outdoor texture recognition	Alfatni *et al.* (2014b; 2018; 2022); Ghazali *et al.* (2019); Ibrahim *et al.* (2018); Makky *et al.* (2013)
Edge	Capable of detecting spikes and empty socket	Recent studies show lower classification accuracy	Astuti *et al.* (2019); Tan *et al.* (2021)

techniques include correlation feature selection (CFS) (Septiarini *et al.*, 2021), backward regression (Syaifuddin *et al.*, 2020) and retrogressive method based on the fuzzy model (Patkar *et al.*, 2021). These methods eliminate redundant or irrelevant features while enhancing classification accuracy. Notably, scholars have achieved high accuracy with minimal features as Patkar *et al.* (2021) achieved over 90% accuracy with two features, and Septiarini *et al.* (2021) reached 98.2% accuracy with five features. Hence, feature selection and dimensionality reduction techniques greatly improve FFB classification accuracy.

Classifier. Researchers evaluated machine learning techniques for FFB classification. For example, Sepitiarini *et al.* (2020b) achieved 98.88% accuracy using linear discriminant analysis (LDA) for classifying three palm fruit maturity levels while Sameen *et al.* (2015) used the genetic algorithm to optimise separation of FFB classes. Other scholars commonly employ artificial neural network (ANN), convolutional neural network (CNN), K-nearest neighbour (KNN) and support vector machine (SVM) algorithms. ANN consists of interconnected neurons arranged in layers and effective for complex pattern recognition by learning from data. CNN is a specific type of deep neural network primarily used for image recognition and classification, where a network architecture with convolutional layers was applied for classification. CNN uses image input and the feature extraction was performed in the network. Next, KNN predicts the class or value of an instance based on majority voting among its k-nearest neighbours and SVM finds a hyperplane that best separates data points into different classes. Shabdin *et al.* (2016) found ANN to outperform linear regression in classifying oil palm fruit images and Alfatni *et al.* (2018) concluded that ANN had the highest accuracy and fastest algorithm compared to SVM and KNN. Multilayer perceptron (MLP), a type of ANN with multiple layers, was utilised by Fadilah *et al.* (2012) and Melidawati *et al.* (2021) to produce an appropriate FFB classification model.

In subsequent research, scholars have investigated the use of CNN-based algorithms for training labelled images and detecting FFB ripeness via sliding windows (Saleh *et al.*, 2020). To enhance the system's efficiency, networks such as AlexNet (Wong *et al.*, 2020), DenseNet (Herman *et al.*, 2021), and ResNet (Harsawardana *et al.*, 2020; Khamis *et al.*, 2022) have been implemented. Additionally, scholars have utilised the You-Only-Look-Once (YOLO) algorithm for single-stage FFB detection, which can accelerate the processing time of the classification process. Junos *et al.* (2021) successfully distinguished between FFB and trees while classifying fruits into three classes by adopting DenseNet in the YOLO-P algorithm. Robi *et al.* (2022) demonstrated that YOLOv4 outperforms previous YOLO versions, while Lai *et al.* (2022) found that 2000 iterations of trained YOLOv4 are appropriate for training images that are less than 500. *Figure 7* represents the trend of machine learning that was implemented in studies from 2012 to 2022.

DISCUSSION

The previous sections discussed the image processing techniques employed to classify FFB based on available research studies. It can be inferred that these techniques are not yet widely adopted, as a similar group of scholars is publishing most research. Out of the 36 works presented in *Table 3*, only 26 studies have introduced novel approaches, while the rest have focused on refining their techniques or continuing their previous research rather than exploring new methods. This suggests that there is still a lot of potential for exploring and developing new image processing techniques that can improve the accuracy of FFB image classification.

The pre-processing stage is an essential step in FFB image classification, as it can significantly affect the accuracy of the classification results. Clustering and ROI-based segmentation are two commonly used techniques for removing complex

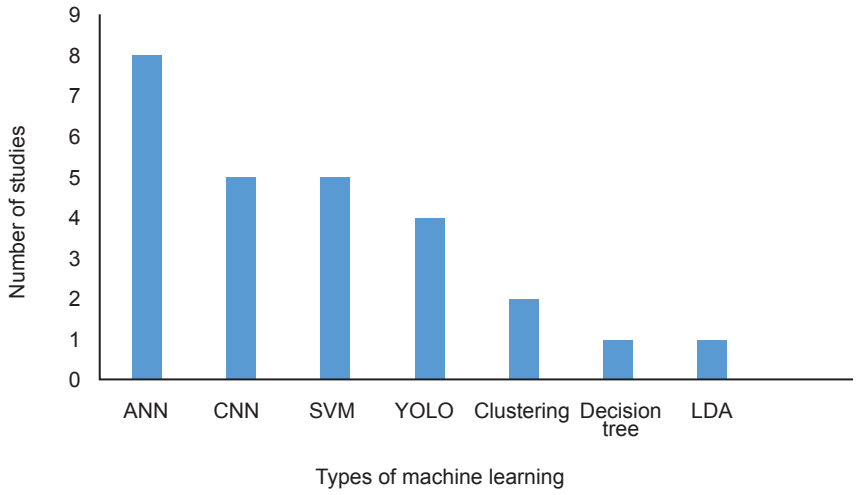


Figure 7. Types of machine learning used in related studies from 2012 to 2022.

backgrounds. Clustering can be a powerful tool for segmenting different parts of the FFB, such as spikes and fruit, but it requires a suitable selection of the algorithm and parameters, as well as pre-processing techniques such as masking, to achieve accurate results. ROI-based segmentation is another technique that can effectively discard most of the background noise, but it requires a precise region selection to avoid discarding important fruit colours outside of the cropped area. Object detection methods based on deep learning, such as YOLO and Faster R-CNN have shown promising results in improving ROI selection. The integration of object detection methods with clustering segmentation can potentially lead to precise segmentation of FFB images and emphasise the significant fruit features in the image. However, the requirement for a large amount of training data to develop a dependable system remains challenging in implementing such techniques. In addition, this survey revealed that salient image segmentation and deep-learning-based segmentation techniques, such as semantic segmentation, have not been widely used in FFB segmentation. This might be due to the inconsistent shape of the FFB, which makes it harder to determine the edges of the fruit and labelling the image is a cumbersome process. It also explains why there is a lack of texture-based and edge-based segmentation techniques implemented in FFB segmentation.

Moreover, researchers face the challenge of segmenting FFB images taken under inconsistent outdoor lighting conditions, which remains a critical task. As previously mentioned, selecting an appropriate segmentation technique, combined with a colour correction method, can help mitigate the effects of uneven outdoor lighting. However, it is important to note that colour correction methods have not been extensively used in FFB classification studies. Therefore, it is necessary to conduct further research to investigate the potential benefits of utilising colour correction methods to improve the accuracy of the FFB classification system. Researchers could explore colour correction methods applied to other types of images taken under natural sunlight and evaluate their impact on the colour features of FFB images. In addition to colour features, spikes texture can be useful for describing the maturity of FFBs, as the size and number of spikes change as the fruit ripens. Furthermore, texture features could be used to investigate the percentage of detached fruit, where Patkar *et al.* (2021) stated that the empty socket feature can improve the accuracy of classifying ripe and overripe fruits.

As an additional suggestion, the image-based FFB classification could be explored with other types of input images such as from multispectral (Groß *et al.*, 2017; Setiawan *et al.*, 2020) and thermal camera (Fauziah *et al.*, 2021; Makky *et al.*, 2021) to obtain the additional features of the FFB images. The depth of the images could also be extracted from a Kinect camera (Pamornnak *et al.*, 2017) which could increase the performance accuracy. The integration of colour, edge, texture and 3-D features analysis presents an opportunity to improve the accuracy of the FFB classification system. Conversely, it is crucial to strike a balance between having enough features to capture important information and avoiding overfitting due to having too many features. Careful consideration of feature selection and dimensionality reduction techniques can help to achieve this balance and improve the accuracy of classification models.

Table 3 compares various FFB classification techniques, revealing a recent trend towards

utilising reliable classifiers like CNN and YOLO that do not require extensive pre-processing or feature extraction. However, their performance is heavily reliant on the availability of a large number of training samples, with over 5,000 samples needed to achieve a mean average precision (mAP) of 98%. Conversely, handcrafted feature extraction techniques with appropriate segmentation methods have demonstrated good performance under outdoor lighting conditions, even with limited training data, as demonstrated in recent studies by Sabri *et al.* (2018) and Septiarini *et al.* (2021). Therefore, researchers should carefully consider the trade-off between using more sophisticated deep learning techniques and the amount of data required, versus using traditional techniques with fewer data requirements. Additionally, image augmentation methods could be applied to increase the training data.

CONCLUSION

This survey provides an overview of various techniques for processing palm fruit images, including pre-processing, feature extraction, and classification. Comparisons have been made, and best practices have been identified to form the basis of our future research. Based on the review, clustering and object detection using YOLO, combined with colour correction, can improve segmentation accuracy. Additionally, incorporating texture and edge features, plus colour features, can improve system accuracy, provided that feature selection is employed to avoid overfitting. Moreover, a neural network such as the MLP model can offer high classification accuracy and faster processing times. In conclusion, more research is needed to develop an effective and efficient palm fruit ripeness classification system.

TABLE 3. COMPARISONS OF RELATED STUDIES

Author, year	Image sample	Environment	Background removal technique	Image feature	Classifier	Highest accuracy (%)
Choong *et al.* (2006)	3	Indoor	-	Colour	DN ratio	-
Alfatni *et al.* (2008)	30	Indoor	Manual mask	Colour	RGB range	-
Jaffar *et al.* (2009)	16	Indoor	K-means clustering	Colour	Threshold	-
Jamil *et al.* (2009)	90	Unknown	Morphological process	Colour	Neuro-fuzzy	73.30
Ghazali *et al.* (2009)	90	Unknown	Threshold	Colour	RGB range	100.00
Roseleena *et al.* (2011)	30	Indoor	K-means clustering	Colour	DN ratio	93.10
May *et al.* (2011)	75	Indoor	-	Colour	Fuzzy logic	86.67
Fadilah *et al.* (2012)	208	Outdoor	K-means clustering	Colour	ANN	93.33
Amosh *et al.* (2013)	80	Outdoor	Region growing	Colour	DN ratio	86.00
Makky *et al.* (2013)	-	Indoor	Adaptive thresholding	Colour, texture	K-means clustering	88.70
Alfatni *et al.* (2014a)	-	Indoor	-	Colour	KNN, SVM	93.00
Alfatni *et al.* (2014b)	180	Indoor	ROI	Colour, texture	ANN	91.30
Makky *et al.* (2014)	-	Indoor	Adaptive thresholding	Colour, texture	ANN	93.50
Sameen *et al.* (2015)	-	Indoor	Threshold	Colour	Genetic algorithm	67.10
Taparugssanagorn *et al.* (2015)	-	Outdoor	K-means clustering	Colour	Relative entropy	-
Shabdin *et al.* (2016)	60	Indoor	Masking using ENVI classic	Colour	WEKA software, ANN	70.00
Sabri *et al.* (2017)	264	Outdoor	K-means clustering	Colour	SVM, naïve Bayes	96.59
Alfatni *et al.* (2018)	180	Indoor	-	Colour, texture	ANN, KNN, SVM	93.00
Fahmi *et al.* (2018)	40	Unknown	Threshold	Colour	ANN	100.00
Ibrahim *et al.* (2018)	120	Outdoor	ROI	Colour, texture	CNN	92.00
Sabri *et al.* (2018)	500	Outdoor	ROI	Colour	SVM	98.90
Astuti *et al.* (2019)	80	Indoor	-	Colour, texture	KNN	65.00
Septiarini *et al.* (2019)	160	Indoor	ROI, threshold	Colour	SVM	92.50

TABLE 3. COMPARISONS OF RELATED STUDIES (continued)

Author, year	Image sample	Environment	Background removal technique	Image feature	Classifier	Highest accuracy (%)
Ghazali *et al.* (2019)	400	Outdoor	K-means clustering	Colour, texture	SVM	70.00
Alfatni *et al.* (2020)	450	Indoor	-	Colour	ANN	94.00
Harsawardana *et al.* (2020)	400	Outdoor	-	-	CNN	71.34
Syaifuddin *et al.* (2020)	-	Outdoor	ROI	Texture	Clustering, fuzzy logic	73.07
Wong *et al.* (2020)	200	Outdoor	-	-	CNN	85.00
Septiarini *et al.* (2021)	240	Outdoor	ROI	Colour	Naïve Bayes, SVM, and ANN	98.30
Tan *et al.* (2021)	514	Outdoor	GrabCut	Colour, texture	Decision tree	71.11
Herman *et al.* (2021)	400	Outdoor	-	-	CNN	86.00
Suharjito *et al.* (2021)	653	Outdoor	ROI	-	CNN	89.30
Junos *et al.* (2021)	5,350	Outdoor	-	-	YOLO-P	98.96 mAP
Lai *et al.* (2022)	490	Outdoor	-	-	YOLOv4	87.90 mAP
Robi *et al.* (2022)	175	Outdoor	-	-	YOLOv4	77.20
Khamis *et al.* (2022)	299	Outdoor	-	-	YOLOv3	76.00

REFERENCES

Alfatni, M. S. M., Khairunniza-Bejo, S., Marhaban, M. H. B., Saaed, O. M. B., Mustapha, A., & Shariff, A. R. M. (2022). Towards a real-time oil palm fruit maturity system using supervised classifiers based on feature analysis. *Agriculture*, *12*(9), 1461. https://doi.org/10.3390/agriculture12091461

Alfatni, M. S. M., Shariff, A. R. M., Abdullah, M. Z., Marhaban, M. H., Shafie, S. B., Bamiruddin, M. D., & Saaed, O. M. B. (2014a). Oil palm fresh fruit bunch ripeness classification based on rule-based expert system of ROI image processing technique results. *IOP Conference Series Earth and Environmental Science*, *20*, 012018. https://doi.org/10.1088/1755-1315/20/1/012018

Alfatni, M. S. M., Shariff, A. R. M., Bejo, S. K., Saaed, O. M. B., & Mustapha, A. (2018). Real-time oil palm FFB ripeness grading system based on ANN, KNN and SVM classifiers. *IOP Conference Series Earth and Environmental Science*, *169*, 012067. https://doi.org/10.1088/1755-1315/169/1/012067

Alfatni, M. S. M., Shariff, A. R. M., Marhaban, M. H., Shafie, S. B., Saaed, O. M., Abdullah, M. Z., & Amiruddin, M. D. (2014b). Oil palm fruit maturity classification based on texture feature extraction of fruit thorns and supervised machine learning classifiers using image processing technique. *Acta Horticulturae, 1054*, 351–357. https://doi.org/10.17660/actahortic.2014.1054.42

Alfatni, M. S. M., Shariff, A. R. M., Saaed, O. M. B., Albhbah, A. M., & Mustapha, A. (2020). Colour feature extraction techniques for real time system of oil palm fresh fruit bunch maturity grading. *IOP Conference Series Earth and Environmental Science*, *540*(1), 012092. https://doi.org/10.1088/1755-1315/540/1/012092

Amosh, L. S., Abdullah, S. N. H. S., Mohd, C. R. C., & Jameson, J. (2013). Adaptive region growing for automated oil palm fruit quality recognition. In *Lecture notes in computer science* (pp. 184–192). Springer. https://doi.org/10.1007/978-3-319-02958-0_18

Arulnathan, D. N., Koay, B. C. W., Lai, W. K., Ong, T. K., & Lim, L. L. (2022, June 25). Background subtraction for accurate palm oil fruitlet ripeness detection. *Paper presented at the 2022 IEEE International Conference on Automatic Control and Intelligent Systems (I2CACIS)*, Kuala Lumpur.

Astuti, I. F., Nuryanto, F. D., Widagdo, P. P., & Cahyadi, D. (2019). Oil palm fruit ripeness detection using K-Nearest neighbour. *Journal of Physics Conference Series*, *1277*(1), 012028. https://doi.org/10.1088/1742-6596/1277/1/012028

Azri, N. A. (2021). Info about Malaysian palm oil. *Ministry of Foreign Affairs, Malaysia*. https://www.kln.gov.my/web/chl_santiago/events/-/asset_publisher/aaxAVFSn6K5B/blog/info-about-malaysian-palm-oil?inheritRedirect=false

Azuar, A. (2022, January 5). Malaysia's palm oil, products exports up 55.2% for 6M22. *The Malaysian Reserve*. https://themalaysianreserve.com/2022/08/09/malaysias-palm-oil-products-exports-up-55-2-for-6m22/

Chew, A. (2023, June 2). Malaysia palm oil production, exports expected to rise this year. *Nikkei Asia*. https://asia.nikkei.com/Business/Markets/Commodities/Malaysia-palm-oil-production-exports-expected-to-rise-this-year

Choong, T. S. Y., Abbas, S., Shariff, A. R., Halim, R., Ismail, M. H. S., Yunus, R., Ali, S., & Ahmadun, F. (2006). Digital image processing of palm oil fruits. *International Journal of Food Engineering, 2*(2). https://doi.org/10.2202/1556-3758.1090

Fadilah, N., & Mohamad-Saleh, J. (2014). Color feature extraction of oil palm fresh fruit bunch image for ripeness classification. *13th International Conference on Applied Computer and Applied Computational Science (ACACOS'14)*, Kuala Lumpur.

Fadilah, N., Mohamad-Saleh, J., Halim, Z. A., Ibrahim, H., & Ali, S. S. S. (2012). Intelligent color vision system for ripeness classification of oil palm fresh fruit bunch. *Sensors, 12*(10), 14179–14195. https://doi.org/10.3390/s121014179

Fahmi, F., Palti, H. M., Emerson, S. P., & Suherman, S. (2018, April 18). Oil palm fresh fruit bunch ripeness classification using back propagation and learning vector quantization. *IOP Conference Series: Materials Science and Engineering, 434*, 012066. https://doi.org/10.1088/1757-899x/434/1/012066

Fauziah, W. K., Makky, M., Santosa, & Cherie, D. (2021). Thermal vision of oil palm fruits under different ripeness quality. *IOP Conference Series: Earth and Environmental Science, 644*, 012044. https://doi.org/10.1088/1755-1315/644/1/012044

Forster, B. P., Sitepu, B., Setiawati, U., Kelanaputra, E. S., Nur, F., Rusfiandi, H., Rahmah, S., Ciomas, J., Anwar, Y., Bahri, S., & Caligari, P. D. S. (2017). Oil Palm (*Elaeis guineensis*). In *Genetic Improvement of Tropical Crops* (pp. 241–290). Springer.

Ghazali, K. H., Samad, R., Arshad, N. W., & Karim, R. A. (2009, October 20-22). Image processing analysis of oil palm fruits for automatic grading. *International Conference on Instrumentation, Control & Automation*, Bandung, Indonesia.

Ghazali, S. A., Selamat, H., Omar, Z., & Yusof, R. (2019). Image analysis techniques for ripeness detection of palm oil fresh fruit bunches. *ELEKTRIKA: J. Electrical Engineering, 18*, 57–62. https://doi.org/10.11113/elektrika.v18n3.192

Groß, T., Hashim, N., Khairunniza-Bejo, S., Aziz, S. A., & Zude-Sasse, M. (2017). Of maturity stages of oil palm fresh fruit bunches using multispectral imaging method. *Acta Horticulturae, 1152*, 71–76. https://doi.org/10.17660/ActaHortic.2017.1152.10

Haron, N. M. A. N., Halim, Z. A., Saleh, J. M., Ibrahim, H., Musa, K., & Fadzilah, N. (2012). White LED illumination for improving outdoor image analysis for palm oil fruit ripeness detection. *International Conference on Advanced Computer Science and Information Systems*. http://ieeexplore.ieee.org/iel7/6459621/6468717/06468775.pdf

Harsawardana, N., Rahutomo, R., Mahesworo, B., Cenggoro, T. W., Budiarto, A., Suparyanto, T., Atmaja, D. B. S., Samoedro, B., & Pardamean, B. (2020). AI-Based ripeness grading for oil palm fresh fruit bunch in smart crane Grabber. *IOP Conference Series Earth and Environmental Science*, *426*(1), 012147. https://doi.org/10.1088/1755-1315/426/1/012147

Herman, H., Cenggoro, T. W., Susanto, A., & Pardamean, B. (2021). Deep learning for oil palm fruit ripeness classification with DenseNet. *2022 International Conference on Information Management and Technology (ICIMTech)*, 116–119. https://doi.org/10.1109/icimtech53080.2021.9534988

Ibrahim, Z., Sabri, N., & Isa, D. (2018). Palm oil fresh fruit bunch ripeness grading recognition using convolutional neural network. *Journal of Telecommunication Electronic and Computer Engineering (JTEC)*, *10*, 109–113. http://journal.utem.edu.my/index.php/jtec/article/view/4720

Ismail, W. I. W., & Razali, M. H. (2010, January). *Hue optical properties to model oil palm fresh fruit bunches maturity index* [Paper presentation]. WMSCI 2010 - The 14th World Multi-Conference on Systemics, Cybernetics, and Informatics, Orlando, Florida, USA.

Jaffar, A., Jaafar, R., Jamil, N., Low, C. Y., & Abdullah, B. (2009). Photogrammetric grading of oil palm fresh fruit bunches. *International Journal of Mechanical and Mechatronic Engineering*, *9*(10), 18–24.

Jalil, A. M. (1995). Grading of FFB for palm oil mills in Malaysia. *Palm Oil Engineering Bulletin, 39*, 3–5.

Jamil, N., Mohamed, A., & Abdullah, S. (2009, December 4-7). *Automated grading of palm oil fresh fruit bunches (FFB) using neuro-fuzzy technique* [Paper Presentation]. International Conference of Soft Computing and Pattern Recognition, Malacca, Malaysia. https://doi.org/10.1109/socpar.2009.57

Junos, M. H., Khairuddin, A. S. M., Thannirmalai, S., & Dahari, M. (2021). An optimized YOLO-based object detection model for crop harvesting system. *IET Image Processing*, *15*(9), 2112–2125. https://doi.org/10.1049/ipr2.12181

Kassim, M. S. M., Ismail, W. I. W., Ramli, A. R., & Bejo, S. K. (2014). Image clustering technique in Oil Palm Fresh Fruit bunch (FFB) growth modeling. *Agriculture and Agricultural Science Procedia*, *2*, 337–344. https://doi.org/10.1016/j.aaspro.2014.11.047

Khamis, N., Selamat, H., Ghazalli, S., Saleh, N. I. M., & Yusoff, N. (2022, May 4-7). Comparison of palm oil fresh fruit bunches (FFB) ripeness classification technique using deep learning method [Paper presentation]. *13th Asian Control Conference (ASCC)*, Jeju, Republic of Korea. https://doi.org/10.23919/ascc56756.2022.9828345

Khan, N., Kamaruddin, M. A., Sheikh, U. U., Yusup, Y., & Bakht, M. P. (2021). Oil palm and machine learning: Reviewing one decade of ideas, innovations, applications, and gaps. *Agriculture*, *11*(9), 832. https://doi.org/10.3390/agriculture11090832

Lai, J. W., Ramli, H. R., Ismail, L. I., & Hasan, W. Z. W. (2022). Real-time detection of ripe oil palm fresh fruit bunch based on YOLOv4. *IEEE Access, 10*, 95763–95770. https://doi.org/10.1109/access.2022.3204762

Lai, J. W., Ramli, H. R., Ismail, L. I., & Wan Hasan, W. Z. (2023). Oil palm fresh fruit bunch ripeness detection methods: A systematic review. *Agriculture, 13*(1), 156. https://doi.org/10.3390/agriculture13010156

Makky, M., & Cherie, D. (2021). Thermal and optical properties of oil palm FFB for optimum harvest window prediction. *IOP Conference Series: Earth and Environmental Science, 757*(1), 012004. https://doi.org/10.1088/1755-1315/757/1/012004

Makky, M., & Soni, P. (2013). Development of an automatic grading machine for oil palm fresh fruits bunches (FFBs) based on machine vision. *Computers and Electronics in Agriculture, 93*, 129–139. https://doi.org/10.1016/j.compag.2013.02.008

Makky, M., Soni, P., & Salokhe, V. M. (2014). Automatic non-destructive quality inspection system for oil palm fruits. *International Agrophysics, 28*(3), 319–329. https://doi.org/10.2478/intag-2014-0022

Malaysian Palm Oil Board (MPOB). (2003). *Oil palm fruit grading manual*. MPOB.

Malaysian Palm Oil Council (MPOC) (n.d.). *The oil palm tree*. Retrieved October 22, 2022 from https://mpoc.org.my/the-oil-palm-tree/

May, Z., & Amaran, M. (2011). Automated oil palm fruit grading system using artificial intelligence. *International Journal of Video Image Processing and Network Security, 11*, 30. https://api.semanticscholar.org/CorpusID:10106358

Melidawati, N., Cherie, D., Fahmy, K., & Makky, M. (2021). Non destructive evaluation quality of oil palm fresh fruit bunch (FFB) (*Elaeis guineensis* Jacq.) based on optical properties using artificial neural network (ANN). *IOP Conference Series Earth and Environmental Science*, *644*(1), 012032. https://doi.org/10.1088/1755-1315/644/1/012032

Ortenzi, L., Figorilli, S., Costa, C., Pallottino, F., Violino, S., Pagano, M., Imperi, G., Manganiello, R., Lanza, B., & Antonucci, F. (2021). A machine vision rapid method to determine the ripeness degree of olive lots. *Sensors, 21*(9), 2940. https://doi.org/10.3390/s21092940

Pamornnak, B., Limsiroratana, S., & Chongcheawchamnan, M. (2015). Oil content determination scheme of postharvest oil palm for mobile devices. *Biosystems Engineering, 134*, 8–19. https://doi.org/10.1016/j.biosystemseng.2015.03.010

Pamornnak, B., Limsiroratana, S., Khaorapapong, T., Chongcheawchamnan, M., & Ruckelshausen, A. (2017). An automatic and rapid system for grading palm bunch using a Kinect camera. *Computers and Electronics in Agriculture, 143*, 227–237. https://doi.org/10.1016/j.compag.2017.10.020

Parveez, G. K. A., Tarmizi, A. H. A., Sundram, S., Loh, S. K., Ong-Abdullah, M., Palam, K. D. P., Salleh, K. M., Ishak, S. M., & Idris, Z. (2021). Oil palm economic performance in Malaysia and R&D progress in 2020. *Journal of Oil Palm Research, 33*(2), 181–214. https://doi.org/10.21894/jopr.2021.0026

Patkar, G., & Morajkar, S. (2021, August 27-28). *Feature selection approach for oil palm fruit grading expert system* [Paper presentation]. 6th International Conference on Recent Trends on Electronics, Information, Communication and Technology (RTEICT 2021). Bangalore, India. https://doi.org/10.1109/rteict52294.2021.9573633

Patkar, G. S., Anjaneyulu, G. S. G. N., & Chandra-Mouli, P. V. S. S. R. (2018). Challenging issues in automated oil palm fruit grading. *IAES International Journal of Artificial Intelligence*, *7*(3), 111. https://doi.org/10.11591/ijai.v7.i3.pp111-118

Platts, M., & Leong, Y. (2019). Achieving high soil fertility, efficient fruit harvesting, and low carbon footprint palm oil production in Malaysia. *Agricultural Sciences, 10*, 1396–1403. https://doi.org/10.4236/as.2019.1010102

Razali, M. H., Ismail, W. I. W., Ramli, A. R., & Sulaiman, M. N. (2008). Modeling of oil palm fruit maturity for the development of an outdoor vision system. *International Journal of Food Engineering*, *4*(3). https://doi.org/10.2202/1556-3758.1396

Razali, M. H., Ismail, W. I. W., Ramli, A. R., Sulaiman, M. N., & Harun, M. H. (2009). Development of image based modeling for determination of oil content and days estimation for harvesting of fresh fruit bunches. *International Journal of Food Engineering*, *5*(2). https://doi.org/10.2202/1556-3758.1633

Reuters. (2022, September 8). Labour shortages set up Malaysia for third year of palm oil losses. *New Straits Times*. https://www.nst.com.my/business/2022/09/829500/labour-shortages-set-malaysia-third-year-palm-oil-losses

Robi, S. N. A. B. M., Izhar, M. A. B. M., Sahrim, M. B., & Ahmad, N. B. (2022, July 26-28). *Image detection and classification of oil palm fruit bunches* [Paper presentation]. 4th International Conference on Smart Sensors and Application (ICSSA), Kuala Lumpur, Malaysia. https://doi.org/10.1109/icssa54161.2022.9870945

Roseleena, J., Nursuriati, J., Ahmed, J., & Low, C. (2011). Assessment of palm oil fresh fruit bunches using photogrammetric grading system. *International Food Research Journal*, *18*(3), 999–1005. http://www.ifrj.upm.edu.my/18%20(03)%202011/20)IFRJ-2010-151.pdf

Sabri, N., Ibrahim, Z., & Isa, D. (2018). Evaluation of color models for palm oil fresh fruit bunch ripeness classification. *Indonesian Journal of Electrical Engineering and Computer Science, 11*, 549–557. https://doi.org/10.11591/ijeecs.v11.i2.pp549-557

Sabri, N., Ibrahim, Z., Syahlan, S., Jamil, N., & Mangshor, N. N. A. (2018). Palm oil fresh fruit bunch ripeness grading identification using color features. *Journal of Fundamental and Applied Sciences*, *9*(4S), 563. https://doi.org/10.4314/jfas.v9i4s.32

Sae-Tang, S. (2020, November 18-20). *Estimation of oil content in oil palm fresh fruit bunch by its surface color* [Paper presentation]. 15th International Joint Symposium on Artificial Intelligence and Natural Language Processing (iSAI-NLP), Bangkok, Thailand. https://doi.org/10.1109/isai-nlp51646.2020.9376834

Saleh, A. Y., & Liansitim, E. (2020). Palm oil classification using deep learning. *Science Information Technology Letters, 1*(1), 1–8. https://doi.org/10.31763/sitech.v1i1.1

Sameen, M. I., & Shariff, A. R. B. M. (2015, October 24-28). *The use of genetic algorithm for palm oil fruit maturity detection* [Paper presentation]. 36th Asian Conference on Remote Sensing: Fostering Resilient Growth in Asia (ACRS), Manila, Philippines.

Septiarini, A., Hamdani, H., Hatta, H. R., & Kasim, A. A. (2019, October 23-24). *Image-based processing for ripeness classification of oil palm fruit* [Paper presentation]. 5th International Conference on Science in Information Technology: Embracing Industry 4.0: Towards Innovation in Cyber Physical System (ICSITech), Yogyakarta, Indonesia. https://doi.org/10.1109/icsitech46713.2019.8987575

Septiarini, A., Hamdani, H., Hatta, H. R., & Anwar, K. (2020a). Automatic image segmentation of oil palm fruits by applying the contour-based approach. *Scientia Horticulturae, 261*, 108939. https://doi.org/10.1016/j.scienta.2019.108939

Septiarini, A., Hatta, H. R., Hamdani, H., Oktavia, A., Kasim, A. A., & Suyanto, S. (2020b, November 3-4). *Maturity grading of oil palm fresh fruit bunches based on a machine learning approach* [Paper presentation]. 5th International Conference on Informatics and Computing (ICIC), Gorontalo, Indonesia. https://doi.org/10.1109/icic50835.2020.9288603

Septiarini, A., Sunyoto, A., Hamdani, H., Kasim, A. A., Utaminingrum, F., & Hatta, H. R. (2021).

Machine vision for the maturity classification of oil palm fresh fruit bunches based on color and texture features. *Scientia Horticulturae, 286*, 110245. https://doi.org/10.1016/j.scienta.2021.110245

Setiawan, A. W., & Prasetya, O. E. (2020). *Palm oil fresh fruit bunch grading system using multispectral image analysis in HSV* [Paper presentation]. IEEE International Conference on Informatics, IoT, and Enabling Technologies (ICIoT), Doha, Qatar. https://doi.org/10.1109/iciot48696.2020.9089431

Shabdin, M. K., Shariff, A. R. M., Johari, M. N. A., Saat, N. K., & Abbas, Z. (2016). A study on the oil palm fresh fruit bunch (FFB) ripeness detection by using hue, saturation and intensity (HSI) approach. *IOP Conference Series Earth and Environmental Science*, *37*, 012039. https://doi.org/10.1088/1755-1315/37/1/012039

Shuib, A. R., Khalid, M. R., & Deraman, M. S. (2011). Innovation and technologies for oil palm mechanisation. (2011). In *Further Advances in Oil Palm Research, 2000-2010* (pp. 569–597). MPOB.

Siddesha, S., Niranjant, S. K., & Aradhya, V. N. M. (2017). Segmentation of oil palm crop bunch from tree images. *2017 International Conference on Smart Technologies for Smart Nation (SmartTechCon)*, 1621–1626. https://doi.org/10.1109/smarttechcon.2017.8358639

Sowat, S. N., Wan Ismail, W. I., Mahadi, M.-R., Bejo, S., & Kassim, M. (2018). Trend in the development of oil palm fruit harvesting technologies in Malaysia. *Jurnal Teknologi, 80*. https://doi.org/10.11113/jt.v80.11298

Suharjito, N., Elwirehardja, G. N., & Prayoga, J. S. (2021). Oil palm fresh fruit bunch ripeness classification on mobile devices using deep learning approaches. *Computers and Electronics in Agriculture*, *188*, 106359. https://doi.org/10.1016/j.compag.2021.106359

Syaifuddin, A., Mualifah, L. N. A., Hidayat, L., & Abadi, A. M. (2020). Detection of palm fruit maturity level in the grading process through image recognition and fuzzy inference system to improve quality and productivity of crude palm oil (CPO). *Journal of Physics Conference Series*, *1581*(1), 012003. https://doi.org/10.1088/1742-6596/1581/1/012003

Tan, I. K. T., Lim, Y., & Hon, N. (2021). Towards palm bunch ripeness classification using colour and canny edge detection. In *Lecture notes in electrical engineering* (pp. 41–50). Springer. https://doi.org/10.1007/978-981-33-4069-5_4

Tan, Y. A., Low, K. W., Lee, C. K., & Low, K. S. (2010). Imaging technique for quantification of oil palm fruit ripeness and oil content. *European Journal of Lipid Science and Technology, 112*, 838-843. https://doi.org/10.1002/ejlt.201000020

Taparugssanagorn, A., Siwamogsatham, S., & Pomalaza-Ráez, C. (2015). A non-destructive oil palm ripeness recognition system using relative entropy. *Computers and Electronics in Agriculture, 118*, 340-349. https://doi.org/10.1016/j.compag.2015.09.018

Vethasalam, R. (2022, September 2). Palm oil output expected to drop due to acute labour shortages. *The Star*. https://www.thestar.com.my/news/nation/2022/09/02/palm-oil-output-expected-to-drop-due-to-acute-labour-shortages

Woittiez, L. S., Van Wijk, M. T., Slingerland, M., Van Noordwijk, M., & Giller, K. E. (2017). Yield gaps in oil palm: A quantitative review of contributing factors. *European Journal of Agronomy, 83*, 57-77. https://doi.org/10.1016/j.eja.2016.11.002

Wong, Z. Y., Chew, W. J., & Phang, S. K. (2020). Computer vision algorithm development for classification of palm fruit ripeness. *AIP Conference Proceedings*, *2233*, 030012. https://doi.org/10.1063/5.0002188

You, K. Y., Wee, F. H., Lee, Y. S., Abbas, Z., Lee, K. Y., Cheng, E. M., Khe, C. S., & Jamlos, M. F. (2020). A review of oil palm fruit ripeness monitoring using microwave techniques in Malaysia. *IOP Conference Series Materials Science and Engineering*, *767*(1), 012007. https://doi.org/10.1088/1757-899x/767/1/012007

Journal of Oil Palm Research Vol. 37 (1) March 2025 p. 16-43
DOI: https://doi.org/10.21894/jopr.2024.0021

LIGNOCELLULOSIC BIOMASS-DERIVED BIOGAS: A REVIEW ON SUSTAINABLE ENERGY IN MALAYSIA

IZZAH FARHANA AB AZIZ[1]*; HASFALINA CHE MAN[1,2,3]*; ALI DEMIRCI[4]; MUHAMMAD HAZWAN HAMZAH[1,2]; ROZITA OMAR[5]; NUR SYAKINA JAMALI[5]; KAMIL KAYODE KATIBI[6,7] and ABDULSALAM MOHAMMED[3,8]

ABSTRACT

Lignocellulosic Biomass (LCB) is regarded as a potentially sustainable alternative resource to fossil fuels. To address concerns related to environmental degradation and geopolitical tensions arising from resource scarcity, the global focus shifted towards developing and utilising sustainable and Renewable Energy (RE) technologies. Biogas technology has attracted attention due to its promising potential to generate energy from agro-waste and the preservation of natural resources. Therefore, this review explores the potential of utilising RE, specifically focusing on its practical implementation in Malaysia. It critically evaluates pre-treatment methods suitable for the country's prevalent biomass sources, offering insights into their applicability. Additionally, the article provides updated data on Malaysia's strategy to advance RE production, particularly in biogas. Despite considerable efforts, there is a notable gap in comprehensively assessing the impact of pre-treatment methods on LCB in Malaysia's biogas production. Hence, this article critically assesses recent advancements to address this gap, focusing on potential challenges and the comparative effectiveness of treatment techniques in Malaysian biogas production. It is with the aim to shed light on associated drawbacks and suggest means to enhance performance. Finally, this article ends by reviewing economic analyses for pre-treatment in LCB, focusing on efficient biogas production.

Keywords: agricultural waste, anaerobic digestion, biogas production, lignocellulosic materials, sustainable energy.

Received: 21 May 2023**; Accepted:** 22 December 2023**; Published online:** 18 March 2024.

INTRODUCTION

The global population's continued growth remains a significant driver of increasing energy demand in conjunction with societal and economic progress. Traditional fossil fuels, including natural gas, oil and coal, are the primary energy sources globally. However, their sustainability over the long term is questionable, especially for nations lacking fossil fuel reserves (Holechek *et al.*, 2022; Hossen *et al.*,

[1] Department of Biological and Agricultural Engineering, Faculty of Engineering, Universiti Putra Malaysia, 43400 Serdang, Selangor, Malaysia.

[2] SMART Farming Technology Research Centre (SFTRC), Faculty of Engineering, Universiti Putra Malaysia, 43400 Serdang, Selangor, Malaysia.

[3] International Institute of Aquaculture and Aquatic Sciences (I-AQUAS), Universiti Putra Malaysia, Batu 7, Jalan Kemang 5, 70150 Port Dickson, Negeri Sembilan, Malaysia.

[4] Department of Agricultural and Biological Engineering, Pennsylvania State University, 221 Agricultural Engineering Building, Shortlidge Road, University Park, Pennsylvania 16802, USA.

[5] Department of Chemical and Environmental Engineering, Faculty of Engineering, Universiti Putra Malaysia, 43400 Serdang, Selangor, Malaysia.

[6] Department of Process and Food Engineering, Faculty of Engineering, Universiti Putra Malaysia, 43400 Serdang, Selangor, Malaysia.

[7] Department of Agricultural and Biological Engineering, Faculty of Engineering and Technology, Kwara State University, Malete 23431, Nigeria.

[8] Department of Agricultural and Bio-Resources Engineering, Ahmadu Bello University, Zaria, Nigeria.

* *Corresponding author e-mail: hasfalina@upm.edu.my; izzahfarhana95@gmail.com*

2016). Renewable Energy (RE) sources have gained prominence in recent years, thus, amplifying the need for sustainable energy sources and the imperative to reduce Greenhouse Gas (GHG) emissions. This aligns with the objectives of the 2015 United Nations Conference on Climate Change, the Paris Climate Agreement and the 2030 Framework for Energy and Climate (European Commission, 2016). Furthermore, one of the latest policy developments in this domain is the European Union's (EU) revised Renewable Energy Directive (RED II) implemented in 2021, which aims to increase the target for resource consumption to 32% by 2030. Moreover, EU member states must also ensure that at least 14% of energy used in their road and rail transport is derived from renewable sources by 2030 (European Commission, 2023).

Bioenergy has risen to become the fourth most common energy source in the EU since 2015, trailing only nuclear energy, hydropower, geothermal, wind, solar, and fossil fuels. The European Biomass Association (2017) reported that bioenergy accounted for an impressive 130,200 kilotons of oil equivalent (ktoe). This has significantly surpassed energy generated from water sources (29,327 ktoe, *i.e.*, 14.30%). The recovery from the COVID-19 pandemic and the global responses to the energy crisis have resulted in a significant upsurge in global investments in clean energy. Additionally, the International Energy Agency (IEA, 2023c) has reported that the projections indicate that approximately USD2.8 trillion will be allocated to energy investments in 2023. Of this total, over USD1.7 trillion is earmarked for clean energy, encompassing sectors such as renewable power, nuclear energy, grid enhancements, energy storage, low-emission fuels, efficiency enhancements, and the expansion of end-use renewables and electrification. In contrast, over USD1.0 trillion is dedicated to unabated fossil fuel supply and power. Within this allocation, about 15% of the funding is directed towards coal, with the remaining portion allocated to oil and gas. This marks a significant shift, as for every USD1.0 invested in fossil fuels, a substantial USD1.7 is now being directed towards clean energy initiatives. It is noteworthy that this ratio was at parity just five years ago, with fossil fuels and clean energy receiving equal investment (IEA, 2023c).

In 2023, modern bioenergy which encompasses biogases, liquid biofuels, and solid bioenergy, already constitutes more than 50% of the global RE demand. Forecasts indicate that, by 2030, the combined installed capacity of all renewable power sources will be more than double in both the Stated Policies Scenarios (STEPS) and the Announced Pledges Scenario (APS) (IEA, 2023d). Remarkably, in the Net-Zero Emissions (NZE) scenario, the installed capacity of RE sources is set to triple by 2030. This represents a significant milestone in the collective effort to achieve the ambitious 1.5°C global temperature goal, emphasising the crucial role of RE expansion in this endeavour (IEA, 2023b). Moreover, we have witnessed consistent growth in the use of biomass as a sustainable energy source in the energy sector. This is attributed to various factors, including increased government initiatives for sustainable energy technologies, the demand for alternative energy sources, reduced emissions, and the vast untapped potential of biomass. However, the solar Photovoltaic (PV) and wind energy sectors are poised for remarkable future growth, particularly within the power industry (IEA, 2022; Jones & Olsson, 2017).

Malaysia, endowed with favourable climate conditions for agricultural production and dense tropical rainforests, are conducive to timber activities, which generates abundant biomass waste annually. The conversion of biomass into environmentally friendly energy and value-added products has been a focus of attention in Malaysia for several decades (Chan & Chong, 2019). Notably, the biomass waste generation in Malaysia is approximately 168 million tonnes (Zafar, 2022), with most of it comprising agricultural waste (90%), followed by municipal waste and forest residues. As a prominent agricultural commodity producer within the Association of Southeast Asian Nations (ASEAN) region, Malaysia is strategically positioned to advocate for and leverage biomass as a RE source. Accordingly, industrialisation which created the biomass industry in the 1900s, has led to the discovery of the vast potential economic benefits of biomass (Yatim *et al*., 2017).

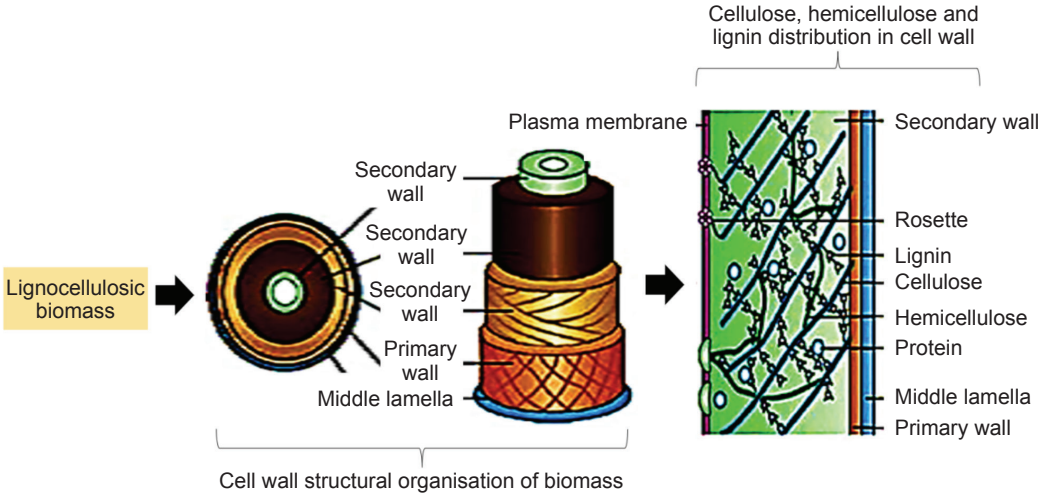
Lignocellulosic Biomass (LCB), recognised for its potential in addressing challenges posed by fossil fuels, especially coal, is a significant contributor to environmental degradation and is acknowledged for its sustainability and minimal carbon dioxide (CO_2) emissions. Furthermore, it boasts a heating value equivalent to energy crops, while producing no pollutants (Benti *et al.*, 2021). Biomass currently holds a significant position within Malaysia's energy composition. However, it still has yet to fully realise its potential, primarily due to uncertainties in biomass supply and various technical, financial, and policy-related obstacles (Rashidi *et al.*, 2022). The utilisation of biogas, primarily sourced from municipal solid waste, food waste, cattle manure, sewage, and palm oil mill effluent (POME), presents substantial prospects. With a potential capacity of approximately 2.3 gigawatt (GW), biomass stands as the most abundant resource in Malaysia, distributed across Peninsular Malaysia (1.3 GW), Sabah [561 megawatt (MW)], and Sarawak (448 MW). Furthermore, biogas and municipal solid waste exhibit promising potential, with a combined

capacity of 736 MW and 516 MW, respectively [International Renewable Energy Agency (IRENA), 2023].

Figure 1 presents the three main interwoven constituents of polymers that make up the LCB. Reports have revealed that cellulose constitutes the major part, of about 40%-45%, hemicelluloses from 25%-35%, while lignin made the remaining 20%-30% (Bhatia *et al.*, 2019; Yogalakshmi *et al.*, 2022). In addition, these biomasses contain a minor amount of extractives such as starch, lipids, resins, proteins, fats, simple sugars, fatty acids, phenolics and essential oils (Pattiya, 2018; Pecha & Garcia-Perez, 2020). These ingredients are indiscriminately dispersed along the cell wall as a skeletal arrangement, merging rigid solids and elements, respectively. Typically, cellulose clumps into pertinacious fibres and builds a skeletal structure along the cell wall. At the same time, the inner voids are loaded with lignin and hemicelluloses, functioning as connectors. Lignin and hemicellulose components link with cellulose via a hydrogen bond, while hemicellulose and lignin constituents are covalently and hydrogen-bonded, influencing biomass's pyrolysis properties. Several reports have suggested the potential of LCB to produce biogas (biomethane and biohydrogen) alongside the various treatment techniques for optimal performance (Kainthola *et al.*, 2019; Kim *et al.*, 2015; Koupaie, 2018; Ma *et al.*, 2019; Matheri *et al.*, 2018; Phuttaro *et al.*, 2019).

This article extensively explores the potential for generating RE from LCB, particularly highlighting its effective utilisation within Malaysia. Focussing on tropical countries like Malaysia, where agriculture significantly contributes to the national economy [Abu Dardak, 2022; International Trade Administration (ITA), 2022], this article underscores the importance of optimising biomass resources. Furthermore, biogas production using biomass has been extensively discussed and reviewed in Malaysia due to its widespread availability and efficient conversion potential. RE, particularly biogas, has garnered significant attention globally, with concerted efforts by governments to maximise the utilisation of biomass resources. Rashidi *et al.* (2022) conducted a comprehensive review focusing on biomass utilisation as an energy source. Their work examined the future growth of the biomass energy market in the country and emphasised effective implementation to address poor disposal issues while creating employment opportunities. Simultaneously, Aziz *et al.* (2019) conducted a comprehensive analysis employing the Life Cycle Assessment (LCA) methodology to evaluate the environmental performance of biogas generation, reflecting a collective effort towards understanding its ecological impact.

While various reviews have encompassed biomass utilisation in general, this article specifically centres its scope on LCB prevalent in Malaysia. This includes palm oil mill waste, sugarcane bagasse, corn stover and rice processing waste. It critically evaluates pre-treatment methods tailored for these specific lignocellulosic substrates, reflecting their suitability for implementation in Malaysia. This article also offers the most recent updates and current data concerning Malaysia's strategy and plan for enhancing RE production, specifically focusing on biogas. Despite considerable efforts, there remains a significant gap in comprehensive evaluations concerning the impact of pre-treatment methods on LCB in Malaysia's biogas production. Thus, to address this gap, this paper aims to critically assess recent advancements, focusing on the potential, challenges, and comparative effectiveness of various treatment techniques used in Malaysia's biogas production. The review aims to shed light on associated drawbacks and provides suggestions



Source: Tiwari *et al.* (2023).

Figure 1. Major polymeric constituents are present in lignocellulosic biomass.

for enhancing performance. Additionally, it delves into an economic analysis of pre-treatment methods specifically tailored for LCB in biogas production, hence offering insights into economic feasibility.

SUSTAINABLE ENERGY AND LIGNOCELLULOSIC BIOMASS UTILISATION IN MALAYSIA

Sustainable and Renewable Energy in Malaysia

Several studies have reported the assessments and analyses of Malaysia's evolving energy policy and strategies. These include Malaysia's sustainable energy (Basri *et al.*, 2015), Malaysia's sustainable power generation plan up to 2030, Malaysia's green RE policies and programmes, RE policies and initiatives for a sustainable energy future and the selection of energy sources for long-term electricity generation. These programmes and initiatives include an elaborate review of pre-treatment methods for LCB (Ahmad & Tahar, 2014). However, the recent issues regarding the high production of agricultural wastes rich in lignocellulose in Malaysia have generated some concerns. It is acknowledged that Malaysia generates a significant amount of agricultural waste, with an estimated 1.2 million tonnes produced and disposed of each year. Unfortunately, some of these wastes are improperly disposed of, through open burning or decomposition, hence increasing environmental problems (Sarangi *et al.*, 2023).

Malaysia is currently experiencing rapid urbanisation, and the population expansion is expected to rise to 37.4 million by 2030. This country is rich in natural energy resources and has been relying on fossil fuels, including oil, natural gas and coal, as its primary energy sources for a long time (Oh *et al.*, 2018). Its energy reserves had 4.553 billion barrels (bbl) of crude oil, 79.531 trillion cubic feet (Tcf) of natural gas, and 1,938.37 t of coal as of January 2018 (Zulkifli, 2021). Since fossil fuel resources are hard to be replenished quickly to meet the demands of such persistent consumption, the Malaysian government has been promoting RE since 2001, as a greener alternative using hydropower, biomass, and solar. However, the excessive utilisation of fossil fuel resources and the underutilisation of RE has since resulted in environmental pollution, climate change, and global warming (Oh *et al.*, 2018). Therefore, the Malaysian government has now shifted its paradigm towards sustainable, reliable and environmental-friendly energy sources. The government and critical stakeholders have embraced the need to diversify the fuel mix, which will serve as a stepping stone for enacting a policy on national energy security (Dharfizi *et al.*, 2020). In 1979, Malaysia's National Energy Policy was established for a much affordable and efficient energy usage (US Energy Information Administration, 2020). Subsequently, the government has consistently implemented several energy policies, targeting energy security (Lim & Goh, 2019), specifically gas, coal and oil. Accordingly, these efforts sought to lessen the overdependence on fossil fuel-based energy sources by increasing renewable energy as an alternative energy source.

It was later followed by the gazettement of the Renewable Energy Act (REA) in 2011, together with the Feed-in Tariff (FiT) strategy and the launching of Incentive-Based Regulation (IBR) in 2014. Moreover, the National Energy Efficiency Action Plan (NEEAP) was introduced into the Malaysian Action Plan from 2016 until 2025 to focus on sustainable energy usage under the 11th Malaysia Plan (2016-2020). A new Energy Efficiency and Conservation Act (EECA) have also been established to initiate early steps in reducing GHG emissions. The government's current goal for fuel diversification is to keep the Herfindahl-Hirschman Index (HHI) below 0.5 by 2025 to enhance energy security (Abdullah *et al.*, 2019). Recently, in 2021, Malaysia aimed to be a carbon-neutral nation (Bernama, 2021), with critical stakeholders such as Commerce International Merchant Bankers Berhad (CIMB) Group Holdings Berhad initiated its commitment to exempting coal from its portfolio by 2040 (Lo, 2020). Furthermore, Petroliam Nasional Berhad (PETRONAS), Malaysia's national oil company (Harun, 2021) and Malayan Banking Berhad (MAYBANK) aspired to achieve net-zero carbon emissions by 2050 (Greenpeace Southeast Asia, 2021).

By 2050, Malaysia anticipates that nearly one-fifth of its fuel demand will be sourced from renewables in the 1.5°C Scenario (1.5-S), encompassing bioenergy, renewable direct-use (*e.g.,* solar thermal), and hydrogen, which is a considerable shift from the current 1%, aiming to reach 70% of renewables in the power mix (EnerData, 2023; IRENA, 2023). A projected 40% of final energy consumption will be from electricity, meeting the increased demand for powering transportation and green hydrogen production. As of the end of 2021, Malaysia's grid was connected to a total installed electricity generation capacity of 33 GW. Coal and natural gas-fired power plants have constituted approximately a third of this capacity, while the remainder is comprised of a mix of large and small hydropower resources, biomass, and solar PV (IRENA, 2023). Over the last decade, the IRENA and the IEA reported that fossil fuels constituted around 95% of Malaysia's energy mix (IEA, 2023a; IRENA, 2023). As of 2020, Malaysia's national Total Primary Energy Supply (TPES) was primarily driven by four key energy sources. The largest share was natural gas, at 42.4%, followed by crude oil and petroleum products at

27.3%, with coal contributing 26.4% to the energy mix. Renewables, which include hydropower, solar and bioenergy, accounted for a minor portion, representing only 3.9% of the overall energy supply [Ministry of Economy (MoE), 2023].

Transitioning to 2023, IRENA's findings highlighted that renewables now constitute a modest 5% of Malaysia's energy composition, mainly attributed to hydropower and solar sources (IRENA, 2023). Malaysia's commitment to low-carbon development is reflected in the National Energy Transition Roadmap (NETR), aiming to reshape the economic landscape towards sustainability. NETR focuses on accelerating the energy transition by shifting from fossil fuel-based to greener and low-carbon energy systems. Furthermore, projections exhibit a marginal annual energy demand increase, with notable initiatives to reduce reliance on fossil fuels, phasing out coal and enhancing dependence on renewable sources such as solar, hydro and bioenergy. The plan includes 50 initiatives under six energy transition levers, five enablers and flagship projects announced in 2023. It also intends to support the nation through a combination of financing methods (MoE, 2023). The successful implementation of the NETR is anticipated to boost Gross Domestic Product (GDP) and job creation significantly. This has highlighted a vision that extends beyond achieving net-zero GHG emissions, aiming to fundamentally transform Malaysia's economy for a more resilient and robust future.

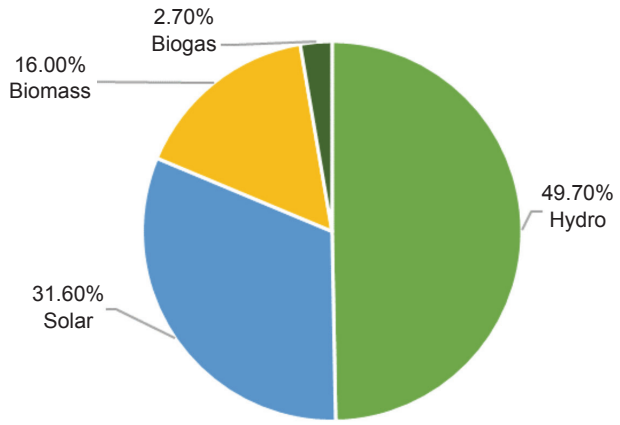
The 12th Malaysia Plan (RMK-12) recently introduced sets of an ambitious objective for the nation to achieve NZE by as early as 2050. This goal necessitates the incentivisation of clean energy adoption, the encouragement of enhanced energy efficiency, and the overall reduction of GHG emissions. The Hydrogen Economy has been expressly recognised as a key component in advancing green growth to attain Low-Carbon Nation status, particularly in the transportation sector. The facilitation of the RE industry's growth is accomplished through the implementation of the National RE Policy and Action Plan. This includes the execution of the Fuel Cells Roadmap and Hydrogen Roadmap for Malaysia (2005-2030), focusing on hydrogen generation from RE resources and the establishment of hydrogen networks for hydrogen fuel cell vehicles. The government has initiated a hydrogen energy roadmap to harness energy from hydropower resources in the state of Sarawak, which is naturally rich in hydropower resources [Minister of Science, Technology and Innovation (MOSTI), 2023].

The availability of biomass could eventually generate approximately USD4.4 billion in economic value annually, by presuming 30% accessibility with RM500/t value creation (Chan & Chong, 2019). Therefore, biomass retains the more significant proportion of 35%, outrunning the highest solar PV portions, with 11% recorded in 2014 by the Sustainable Energy Development Authority (SEDA) Malaysia (2021). This enormous abundance is usually left to decay as mulches or directly combusted as boiler fuel. Moreover, this tradition undermines the potential of lignocellulosic wastes to be recycled in a biorefinery to produce several value-added products, particularly RE and biochemicals (Yatim *et al.*, 2017). Notably, in 2021, the Ministry of Energy and Natural Resources of Malaysia (KeTSA) has established a target, aiming for a 31% share or 12.9 GW of RE in the national installed capacity mix by 2025, followed by 40% and 70% by 2035 and 2050, respectively [Malaysian Investment Development Authority (MIDA), 2023; SEDA, 2021a]. This ongoing evolution in Malaysia's energy strategy has underscored the country's commitment to diversifying its energy sources and expanding the role of renewables within its energy matrix. In 2022, Malaysia's GDP has surged to RM1,510.9 billion, marking an 8.7% increase from RM1,390.6 billion in 2021. The agriculture sector demonstrated a slight 0.1% growth in 2022, compared to a 0.1% decline the previous year, contributing 8.9% of the percentage share to the GDP of ASEAN countries [Department of Statistics Malaysia (DOSM), 2023].

Potentials of Agricultural Wastes for Biogas Production in Malaysia

Malaysia has a wide variety of agricultural wastes, including poultry waste, animal manure, sugarcane bagasse, rice husk, palm oil waste, and kitchen waste. It can be utilised for biogas production via Waste-to-Energy (WTE) to unravel the waste disposal challenges and energy exigencies of the country (SEDA, 2021b). SEDA Malaysia is responsible for implementing FiT and Net Energy Metering (NEM), together with the Energy Commission and Tenaga Nasional Berhad (TNB), for the Large Scale Solar and Large Hydro program, respectively (SEDA, 2021a). In November 2021, the initiation of a Green Electricity Tariff allowed individuals to choose electricity sourced from renewable resources by paying an extra fee per kWh. Subscribers participating in this program can also obtain a RE certificate (Aziz, 2023). Due to the efforts of these agencies, total RE capacity has grown tremendously, up to 8.2 GW in 2019 from 3.7 GW in 2012 (Hussin & Energy Watch, 2021). As of November 2021, the total installed capacity has vastly grown from 101.73 MW in 2012 to 661.22 MW under the FiT program. Resource types from these programs are solar PV, biogas, small hydro and biomass. The current share of biogas sources is 18% (119.74 MW), the second largest contributor after

solar energy (387.03 MW) in electricity production from RE in Malaysia, followed by small hydro (83.8 MW) and biomass (70.65 MW) resources (SEDA, 2014). POME is the primary feedstock, with over 93% of the biogas production, followed by the organic landfill waste, which accounts only for 5%. *Figure 2* presents shares of the installed capacity (Energy Commission, 2023) from all mentioned RE sources in Malaysia, out of the total installed capacity of 9.04 GW, up to the end of 2022 (Bhambhani, 2023).

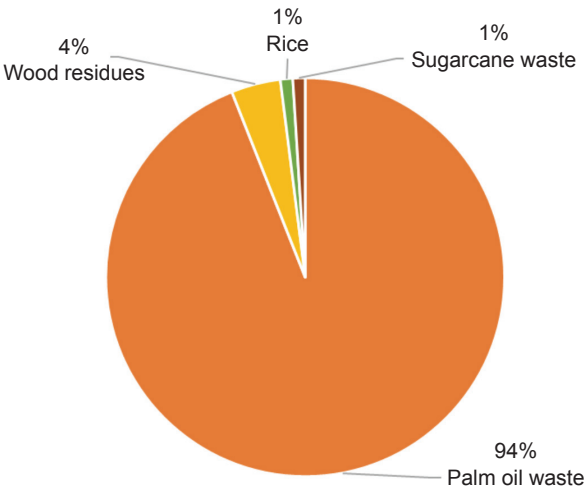


Source: Energy Commission (2023).

Figure 2. Shares of RE installed capacity for electricity generation in 2022.

Biogas production from agro-wastes has tremendous potential as an alternative source that can mitigate the utilisation of conventional fuels and significant global warming (Ardolino & Arena, 2019). Also, electricity production from biogas around the world is anticipated to rise from 331 terawatt-hours (TWh) in 2010 to 1,487 TWh by 2035, demonstrating growth from 8.0% of the total electrical energy produced from RE sources, which will rise to 13.0% by the year 2035. The EU drives the world to generate electricity from biogas by producing 61 TWh (Scarlat *et al.*, 2018). China forged 15.8 billion cubic meters (BCM) of biogas, substituting 5% of total natural gas and 11 t of coal in 2015 (Xue *et al.*, 2019). In Malaysia, researchers have analysed the impact of WTE policies on energy, economic and environmental factors. Based on their findings, Anaerobic Digestion (AD) is deemed as the most viable option for electricity production, compared to alternatives like gasification, landfill gas and municipal solid waste incineration (Tan *et al.*, 2015). The oil palm industry has been highlighted as one of the reliable biogas resources due to its expanding plantation area, around 5.67 million hectares in 2022 [Malaysian Palm Oil Board (MPOB), 2023b]. It covers approximately 17.2% of Malaysia's total land area of 33.02 million hectares (Sahabat Alam Malaysia, 2020). Hence, utilising resources from the oil palm industry for biogas production can aid in achieving the country's RE targets and promote sustainable waste management practices.

Malaysia has become one of the world's most crucial biofuel technology producers (Rezania *et al.*, 2020). On the other hand, agricultural wastes such as rice husks, wood, coconut stem fibres and biodegraded oil palm waste [such as empty fruit bunch (EFB)] can also become suitable substrates for biogas production. These wastes account for 168 t of biomass produced yearly in Malaysia and can be a viable alternative to fossil fuels (Wu *et al.*, 2017). Other agricultural produce, such as rubber, rice and other palm oil products (such as palm fronds, palm tree trunks and palm kernel shells), also have the potential to be utilised as biofuel sources (Su *et al.*, 2022). In 2019, various agricultural waste feedstocks for biogas production in Malaysia were observed, with POME identified as the most extensively used feedstock, accounting for 93%. The other sources included minimal quantities of manure (<1%), bagasse (<1%), landfills (5%), and sewage (<1%) (Lim *et al.*, 2021). In contrast, by 2023, as reported by the MOSTI, Malaysia's annual biomass waste production amounts to a minimum of 168 t. Palm oil waste is a primary constituent, representing 94% of the biomass feedstock. In comparison, *Figure 3* shows the remaining percentage which originates from agricultural and forestry by-products such as wood residues (4%), rice (1%), and sugarcane industry wastes (1%) (MOSTI, 2023).



Source: MOSTI (2023).

Figure 3. Biomass feedstock in Malaysia.

Similarly, animal manure has a high potential to be utilised as feedstock for biogas production in Malaysia. More manure waste is being produced since livestock farming keeps expanding due to the growing demand for dairy, beef, and chicken products (Abdeshahian *et al.*, 2016). However, it poses harmful environmental threats to the ecosystem and surroundings (Kumaran *et al.*, 2015). For instance, Gopinathan *et al.* (2018)

reported that most local farmers either dispose of their livestock wastes directly into the river or pile it up for natural decomposition, prior to being used as bio-fertilisers. Hence, using this waste for biogas production by deploying AD can also result in waste management to address the issue of odour and pathogens. In addition, sugarcane bagasse, composed of 50% cellulose, 25% hemicellulose and 25% lignin, is obtained from the fibrous residue of sugarcane after the juice extraction, can also be used as biogas substrates (Faizal *et al.*, 2019). In 2020, sugar cane production was reported to be almost 23,383 t in Malaysia (Knoema, 2021) and is processed into sugars and beverages, leaving a substantial amount of bagasse in the environment, with potential for biogas utilisation.

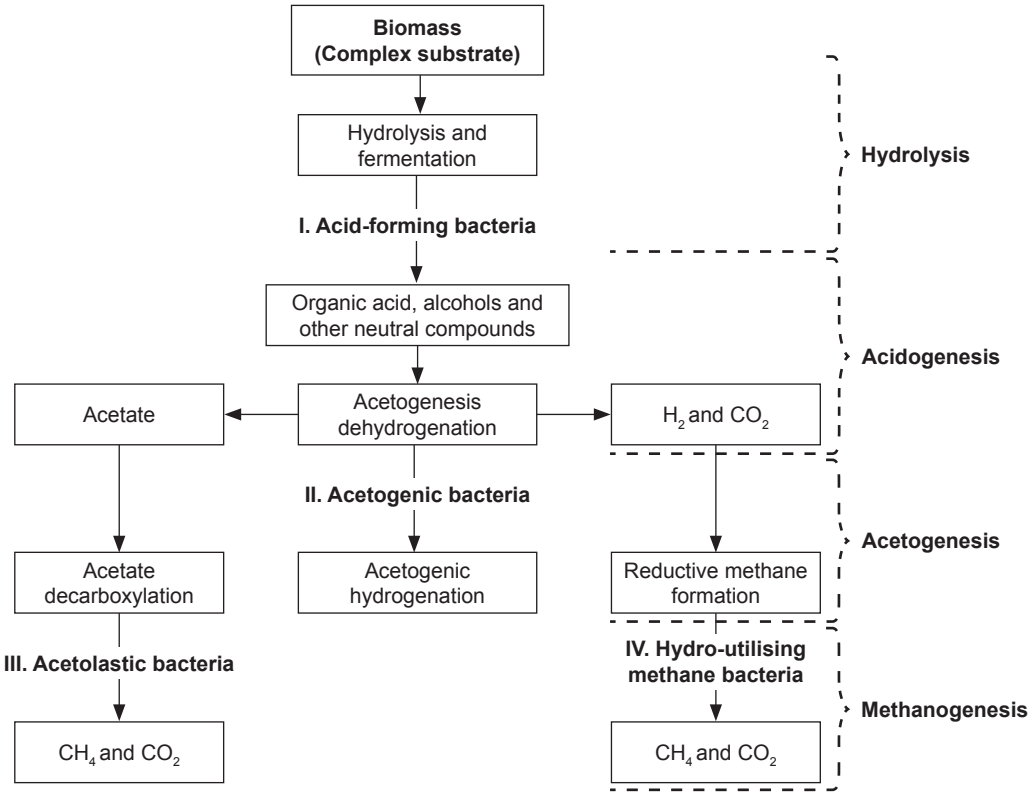
Biochemical Processes of Lignocellulosic Biomass Utilisation

As mentioned in the previous section, biogas has immense potential to be a cost-effective, growth-oriented, and environmental-friendly alternative energy source to generate electricity (Chien Bong *et al.*, 2017). It could be obtained from the biological breakdown of organic substances that contain 40%-75% methane (CH_4), 15%-60% CO_2, and trace amounts of hydrogen sulfide (H_2S), ammonia (NH_3), nitrogen (N_2), and carbon monoxide (CO). Biogas production is commonly produced using an AD method (Galván-Arzola *et al.*, 2021) by utilising food and garden wastes, landfill, sewage sludge, animal manure (Mong *et al.*, 2020; Zhang *et al.*, 2018), agricultural wastes (Pan *et al.*, 2021a; Riya *et al.*, 2020; Weide *et al.*, 2020), and municipal solid wastes (MSW) (Lopes *et al.*, 2021; Pera *et al.*, 2021; Riya *et al.*, 2020; Zulkifli *et al.*, 2019) as a viable feedstock. LCB may be converted into biogas, which can then be utilised as a RE source for various purposes, including heat and power production. Additionally, digestate, a by-product of biogas generation, may be utilised as a fertiliser since it is nutrient-rich (Fatma *et al.*, 2018).

Utilising organic plant materials from plant sources, such as agricultural leftovers, wood waste, and energy crops, is necessary for manufacturing biogas from LCB (Fatma *et al.*, 2018). Moreover, complex carbohydrates within the biomass, such as cellulose and hemicellulose, can be biochemically processed into biogas. Pre-treatment of the biomass materials is the initial stage in generating biogas from LCB to increase its accessibility to microbial breakdown and decrease recalcitrance. One may utilise physical, chemical, or biological techniques to disassemble the intricate structures and liberate the carbohydrates. Following pre-treatment, the biomass is put through an enzymatic hydrolysis process, in which enzymes convert the cellulose and hemicellulose into simple sugars. According to Baruah *et al.* (2018), these sugars act as substrates for microbial fermentation. Microorganisms, especially methanogenic bacteria, ferment the carbohydrates in an anaerobic digester to produce biogas. Most of the biogas produced from LCB comprised CH_4 and CO_2. Those gas ratios are influenced by a number of variables, such as feedstock and anaerobic digester operating parameters. The substrates undergo complex biochemical processes comprising four stages: Hydrolysis, acidogenesis, acetogenesis, and methanogenesis (Zulkifli *et al.*, 2019) (*Figure 4*).

Generally, the hydrolysis stage is much faster than the rest of the digestion phase in most AD processes (Vivekanand *et al.*, 2014). This is attributed to the fact that amorphous cellulose is easily digested during the step, depending on the pore size of the substrate. At the same time, crystalline cellulose is much harder for microbes to degrade during hydrolysis (Kucharska *et al.*, 2018). This phenomenon is due to the surface area and the compact structure of cellulose that affects the efficiency of hydrolysis. Cellulose is regarded as an essential component of plant cell walls, where its polymerisation degree and crystallinity can pose a detrimental effect on enzymatic hydrolysis (McNamara *et al.*, 2015). The crystallinity of cellulose is described in the percentage of the crystal-like structures which ranged from 30%-80%. The crystallisation zone consists of better chain orientation, compact organisation, high density, solid intermolecular bonding and *vice versa* for the amorphous (non-crystalline) area. The order of hydrolysed cellulose started with amorphous domains, followed by the crystalline domains, as reported by Ling *et al.* (2016), where the yield of monosaccharides dropped as the crystallinity of the substrate increased. Moreover, each cellulase component has its specific capabilities and activity for the adsorption of different types of cellulose through carbohydrate-binding modules (CBMs) during the breakdown of cellulose (Chaudhari *et al.*, 2023).

Furthermore, some digestion process-based factors could also contribute to the decline in biodegradation of lignocellulose biomass. For instance, the bioconversion process can generate additional inhibitors in the substrate during AD, such as NH_3, sulphide or sulphur, light metals, heavy metals, oxygen and organic compounds (Czatzkowska *et al.*, 2020), in addition to the harmful variation of the cell wall structure. The presence of inhibitors in the fermentation medium could undermine the microbial processes (Liu *et al.*, 2021). In addition, severe reduction of the substrates' pore size can trigger excessive generation of Volatile Fatty Acids (VFAs) as inhibitors and can delicately transform their chemical constituents (Magdalena *et al.*, 2019). Moreover, substrate delignification



Source: Zulkifli *et al.* (2019).

Figure 4. Mechanisms involved in biochemical degradation of substrates.

above 50% can cause the cellulose matrix to collapse, resulting in a compact and disordered structure and a subsequent reduction in cellulose availability (Ding *et al.*, 2018). Finally, bacterial decomposition processes of the organic matter/substrate without the presence of oxygen, yield the CH_4-rich biogas (Lim *et al.*, 2017).

DEVELOPMENT AND IMPLEMENTATION OF BIOGAS PLANTS IN MALAYSIA

In 2018, the World Biogas Association reported that Malaysia had installed 68 MW of biogas capacity, with an additional approved 73 MW, yielding 226 GWh of RE, which could avert the generation of almost 464 ktons of CO_2 emissions (US Energy Information Administration, 2020). Meanwhile, in the following year, biogas retained a total installed capacity of 148 MW 2019 (Energy Commission, 2021), which came from landfill and agricultural waste, with an estimation to reach up to 360-400 MW by 2020 and a projected energy reserve of 410 MW by 2030. A review of the resource potential for Malaysia RE was conducted by SEDA Malaysia (SEDA, 2021a), with the biogas potential identified to reach 736 MW, among other sources of bioenergy: Biomass (2.3 GW) and municipal solid waste (516 MW).

Lagoon systems and continuously stirred tank reactors are the two most frequently used technologies for producing biogas in Malaysia (Chan & Chong, 2019). However, in recent years, Malaysia's industry has started shifting attention towards high-level anaerobic bioreactors, comprising of advanced Anaerobic Expanded Granular Sludge Bed (AnaEG) and Integrated Anaerobic-Aerobic Bioreactor (IAAB) (Chan *et al.*, 2020; Lim *et al.*, 2021). The shifting is due to the bioreactors equipped with a biogas capture system, exhibiting better treatment efficiency, and producing lower carbon footprint (Chan & Chong, 2019). Usually, biogas production has lower purity of targeted gas, and the typical composition of biogas produced for CH_4, CO_2, N_2, O_2, CO, H_2S and NH_3 are 55.00%-77.00%, 19.00%-45.00%, <8.10%, 0.00%-2.10%, 0.00%-0.01%, 1-8,000 ppm and 0-7 ppm respectively (Korbag *et al.*, 2020). In order to obtain biogas with superior properties, the biogas produced must be cleaned and upgraded to improve the quality of biogas, to make it more suitable for power generation, gaseous car fuel and as a feedstock for the manufacturing of value-added chemicals (Zain & Mohamed, 2018).

Felda Sg. Tengi Palm Oil Mill in Selangor, Malaysia, a 400 m^3/hr biogas upgrading plant, was built in 2015 by Felda Palm Industries Sdn. Bhd. (FPISB), Sime Darby Offshore Engineering

Sdn. Bhd. (SDOE), and MPOB. The upgrading of the generated biogas using membrane technology produced CH_4 content of over 92%, CO_2 levels of 7%, and H_2S levels of 5 ppm (Lim *et al.*, 2021). The biogas upgrading also includes the following technologies- Pressure Swing Adsorption (PSA), water scrubbing, amine scrubbing, organic physical scrubbing, and membrane separation (Lim & Goh, 2019). Despite the adoption of industrial-scale AD in Malaysia, the application is still in its incipient stage compared to other developed countries. Against this background, several industries have begun to explore biogas production from agro wastes. *Table 1* summarises the significant activities of using AD to produce CH_4 from various agro wastes in Malaysia. It can be observed that POME has the highest energy potential compared to animal waste, with 40.19 GWh/yr, confirming its potential to convert waste into wealth (Kumaran *et al.*, 2015). *Table 1* also showcases different biogas plants utilising POME with an in-ground bioreactor system, generating electricity primarily for on-site use or to feed into the national power grid managed by Tenaga Nasional Berhad (TNB). *Table 1* also displays information about three different biogas plants - Cenergi Sri Ganda, FGV's Triang Palm Oil Mill, and GLT BP Power Sdn. Bhd., - highlighting their capacities and respective years of operation.

The biogas produced from POME is mainly used to generate energy for gas-powered appliances and on-site consumption. It was indicated that the collection of CH_4 via AD is expected to produce 16.91 TWh, resulting in a reduction of 11.35 million tonnes of CO_2 equivalent (Kumaran *et al.*, 2015). This also suggests that AD systems can provide 12.03% of the estimated power consumption in 2020, around 140.61 TWh, thereby lessening reliance on depletable fossil fuels. Given its significance, using POME as a biomass source has the potential to reduce environmental impact significantly (Jamali *et al.*, 2021). Apart from POME, the industries have also utilised animal wastes from cattle and chicken to produce biomethane. According to Abdeshahian *et al.* (2016), cows are the primary source of manure in Malaysia, generating approximately 5.45 t of waste annually. Due to the potential for odour issues and the emission of GHG, it is crucial to manage this manure production appropriately (Aili Hamzah *et al.*, 2020).

Almost 308.3 million chickens in the livestock subsector have been recorded by the DOSM, generating huge waste annually (Mahidin, 2019). This excessive quantity of animal waste can negatively affect the environment due to its high content of nutrients, which are N_2 and phosphorous (Gopinathan *et al.*, 2019), as well as harmful substances such as growth hormones, antibiotics, and heavy metals (Abdeshahian *et al.*, 2016). Excessive accumulation of these nutrients can lead to eutrophication phenomena that may affect water resources, including the aquatic environment. Besides that, dairy manure generation has also increased tremendously due to the increased number of cattle on the farms. In 2020, around 700,000 cattle were recorded across Peninsular Malaysia (FAOSTAT, 2023). Hence, it was estimated that in 2020, about 28,150 m^3 of CH_4 could be generated from cattle manure, resulting in the CH_4 production of 1,670,268 kWh/day (Gopinathan *et al.*, 2018).

There are 457 operated palm oil mills in Malaysia (MPOB, 2020; SEDA, 2021a), producing approximately 50-75 million m^3 of POME every

TABLE 1. LARGE-SCALE AGROWASTE METHANE PRODUCTION IN MALAYSIA

Agro-waste	Industries	Technology	Usage	Installed methane capacity	References
Cattle manure	Malaysian Veterinary Services	Fixed dome digester	On-site electricity and gas power	0.19 GWh/yr	Kumaran *et al.* (2015)
Chicken manure	QL Poultry Farm Sdn. Bhd.	Multi-stage anaerobic digester tank	On-site electricity	4.21 GWh/yr	Lim *et al.* (2021)
POME	FELDA Besout, Perak	Closed anaerobic pond	On-site electricity	40.19 GWh/yr	
POME	Cenergi Sri Ganda	In-ground bioreactor system	On-site electricity TNB's power grid	2.4 MW	Cenergi SEA Berhad (2023)
POME	FGV's Triang Palm Oil Mill	In-ground bioreactor system	On-site electricity (0.4 MW) TNB's power grid (2 MW)	2.4 MW	FGV Holding Berhad (2020)
POME	GLT BP Power Sdn. Bhd.	In-ground bioreactor system	TNB's power grid	3.6 MW	Green Lagoon Technology Sdn. Bhd. (2023)

year (Foong *et al*., 2021) with 95.5 million tonnes of fresh fruit bunches (FFB) annually (SEDA, 2021a). POME is generated from processing palm oil, which requires abundant water usage, and almost half of the waste produced ends up as liquid waste (Aziz & Hanafiah, 2017). The total annual production of POME has become a serious problem towards the ecosystem and public safety. In addition, POME can be linked to the high amount of biological oxygen demand (BOD) and chemical oxygen demand (COD) due to the elevated amount of organic content. Under the National RE policy, along with the glut production of POME and other agricultural wastes. With the rising interest in the biogas sector, the urgency to utilise these wastes as substrates for biogas production has received significant attention from the Malaysian government. From 2012-2017, more than 20 POME biogas plants and three landfill-based biogas plants were successfully constructed and commissioned (Gopinathan *et al*., 2018). The biogas plant's power output has gradually increased from 7,465-136,004 megawatt-hour (MWh). In 2020, within the FiT program, approvals were granted for 224 MW of biogas and 165 MW of biomass power plants (SEDA, 2021a). Notably, the predominant rise in capacity was observed in biogas plants. The statistics for biogas plants and power generation are expected to keep rising in the subsequent years since Malaysia is the second-largest producer of palm oil in Southeast Asia after Indonesia. The country recorded approximately 34.3% of global palm oil exports in 2020 [Malaysian Palm Oil Council (MPOC), 2021].

BIOGAS PRODUCTION FROM LIGNOCELLULOSIC BIOMASS

The primary feedstock for biogas production comes from lignocellulosic substrates derived from agricultural leftovers. This method is one of the key sources of sustainable bioenergy and aids in effective waste management. Despite their promise as a feedstock for biogas production, these materials exhibit biomass recalcitrance, defined as high resistance to biological breakdown due to their complex composition and structural organisation. The lignin-carbohydrate complex, also known as the lignin-hemicellulose complex, is a matrix of interlaced hemicellulose and lignin that contains cellulose microfibrils. It also provides a barrier to effective biological degradation (Mirmohamadsadeghi *et al*., 2020; Zoghlami & Paës, 2019). Therefore, methods to lessen biomass resistance are required to increase the availability of lignocellulosic materials for anaerobic microbial breakdown.

Pre-treatment is an essential component of the cellulose transformation process, and it is critical to alter the structure of the cellulosic biomass so that the enzymes which convert carbohydrate polymers into fermentable sugars may better utilise the cellulose (Ma *et al*., 2022). The various feedstock structures are altered at all fibre levels during pre-treatment. The pre-treatment of using biological, physical, chemical, and thermal agents, modifies the amount, proportion, and morphological properties of the lignocellulosic materials. However, none of these technologies has yet been proven to be efficient or cost-effective. Additionally, the ideal pre-treatment factors are not often specified. These findings are crucial for the efficient and useful utilisation of the diverse leftovers produced by agricultural activities.

Biohydrogen and Biomethane Production from Lignocellulosic Biomass

The recalcitrant character of LCB exhibits a technological problem for producing fermentable sugars from biomass and reduces the potential of its utilisation in biorefinery (Bhatia *et al*., 2020). The physicochemical properties of the biomass cells are significant factors contributing to the recalcitrant nature of LCB (Zoghlami & Paës, 2019). Furthermore, LCB has high stability and is highly recalcitrant, with standing enzymatic and bacterial attacks. Its intricate structure limits microbial degradation, thus slowing the substrate degradation during the hydrolysis stage. As indicated in *Figure 5*, biopolymers cellulose (11%-46%), hemicellulose (6%-42%) and lignin (1%-40%) are the three primary biopolymers discovered in lignocellulosic materials (Soares *et al*., 2019). Hemicellulose acts as a matrix surrounding the cellulose skeleton. In contrast, lignin acts as an encrusting substance that protects the cellulose skeleton (Amin *et al*., 2017), creating resistance towards effective biological breakdown. Based on studies from Thomsen *et al.* (2013), a 1% increase in lignin concentration results in an average decrease of 7.49 L CH_4/kg TS. This was further corroborated by Triolo *et al.* (2012), who stated that an excess of lignin of more than 100 g/kg VScan significantly reduces CH_4 output.

The relationship between lignin content and biomass degradation is further elucidated by two mechanisms. Firstly, lignin strengthens the cell wall structure by forming covalent bonds with other cell wall components, thereby increasing space resistance. This prevents carbohydrate breakdown by enzymes, and the second mechanism is the binding ability to enzymes (Lu *et al*., 2016). Lignin can alter enzymatic hydrolysis by adsorbing cellulase in a non-specific or non-productive manner. The accessible surface area also plays a vital role in the digestion and biodegradability of lignocellulosic materials, requiring the substrate to have sufficient pore sites available for optimal hydrolysis (Karimi & Taherzadeh, 2015).

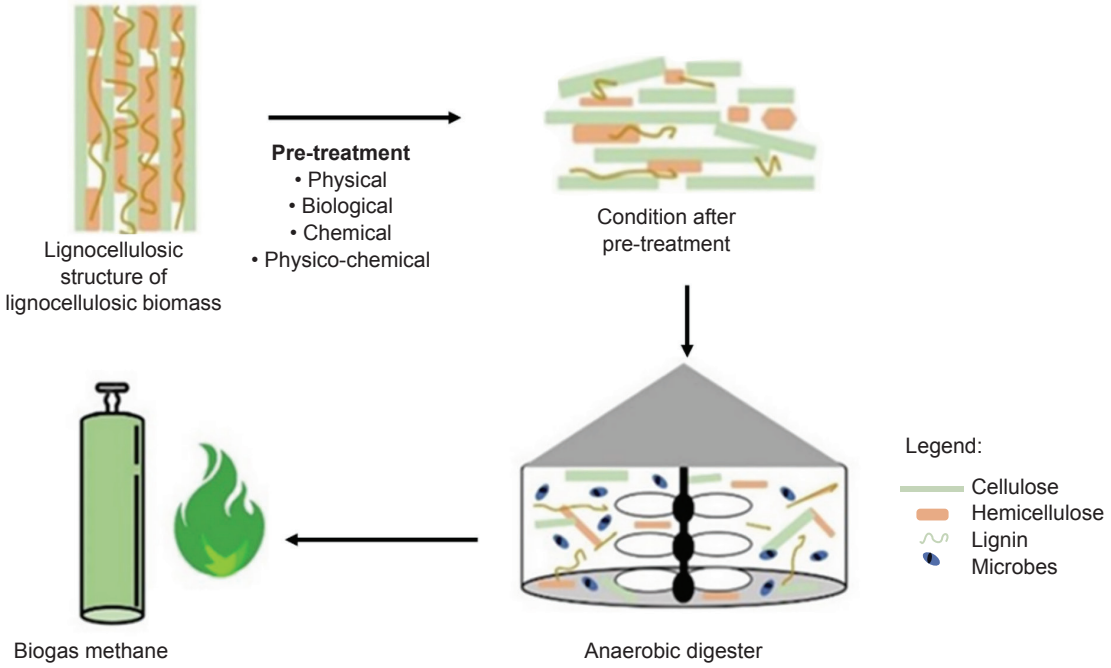


Figure 5. Schematic representation of pre-treatment of lignocellulose biomass during the AD process.

Several LCBs have been explored to produce biogas and bio-hydrogen, as reported in previous studies (Bhatia *et al.*, 2019; Yatim *et al.*, 2017). These LCBs include rice husk, oat straw, corn stover, sugarcane bagasse, EFB, poplar leaves, rice husk, wheat straw, empty palm fruit bunch, pine tree wood and others. These LCBs have generated substantial biogas and bio-hydrogen due to their inherent unique properties, nature or type of inoculum used and operating conditions. *Table 2* summarises the research findings on LCB utilisation for bio-hydrogen and biogas production. Based on these findings, LCB has demonstrated an outstanding performance in producing bio-hydrogen and biogas. Since LCB has abundant sources and feedstock, the utilisation and exploitation of LCB could play a significant role in advancing sustainable energy in Malaysia.

Pre-treatment Techniques of Lignocellulosic Biomass

The degradability of lignocellulose feedstock is affected by many variables, including lignin content, crystallinity, polymerisation grade, surface area, and solubility. Different researchers have applied different pre-treatment procedures to improve lignocellulosic feedstock bio-digestion and CH_4 release. Pre-treatment techniques are selected based on the physicochemical properties and structural makeup of the feedstock. It is anticipated that they will enhance the creation of organic feedstock while keeping the matter in the process. Thus, pre-treatment is essentially required to accelerate the hydrolysis process and break up the lignocellulose structure (Aftab *et al.*, 2019). Techniques for biological, chemical and physical pre-treatment include extrusion, steam explosion, liquid hot water, enzyme, fungi, acid, alkali, ionic liquids, organo-solvents, ozonolysis and size reduction (Olatunji *et al.*, 2021; Zhu & Pan, 2022). Pre-treatment of the substrate prior to both AD and ethanol production is performed for the same reasons. However, the only difference is that since microorganisms are involved in AD, crystalline compounds (cellulose and hemicelluloses) can be broken down with less cost for the pre-treatment process (Olatunji *et al.*, 2021).

The two primary aims of pre-treatment before AD are the dissolution of the bio-polymeric linkages and the opening of the materials. In general, pre-treatments aim to ensure easier interaction between the enzymes with the cellulose and hemicelluloses. This causes the feedstock to economically degrade, avoids degradation loss, thus preventing the release of potential inhibitors, as well as reduces the possible impact on the environment (Den *et al.*, 2018). Therefore, it is critical to have a detailed review of the biological, chemical, and physical pre-treatment techniques. Against this background, numerous preliminary treatment strategies have been identified and explored to advance the efficiency of the hydrolysis process during AD to enhance biogas production. *Table 3* compiles a thorough summary of research outcomes regarding biogas production from widely accessible LCB in Malaysia. It encompasses diverse pre-treatment methods feasible for implementation within the country. Additionally,

TABLE 2. SUMMARY OF FINDINGS ON LIGNOCELLULOSIC BIOMASS UTILISATION FOR BIOGAS PRODUCTION

Type of lignocellulosic biomass	Method	Inoculum used	Operating conditions	Biogas production	Challenges	References
Corn stover	Photo fermentation (PF), Dark fermentation (DF) and Dark-photo co-fermentation (DPCF)	DF: *Enterobacter aerogenes* PF: Photosynthetic bacteria *HAU-M1*	Working volume: 200 mL PF: pH: 6.5, light intensity of 3,500 Lux, Temp: 30°C DF: pH: 6.5, Temp: 35°C and without light DPCF: pH: 6.5, light intensity of 3,500 Lux, Temp: 30°C	Maximum cumulative H_2 HHH yield: 141.42 mL/g TS achieved by PF	High accumulation of volatile fatty acids during DF hampered the production of H_2	Riya *et al.* (2020)
Oat straw	Anaerobic digestion	Anaerobic granular sludge	Working volume: 80 mL, pH: 7.0, speed: 150 rpm and Temp: 35°C	H_2 yield: 94.4 mL H_2/g oat straw	Inhibitors (furfural, HMF, vanillin and syringaldehyde) causes low H_2 yield	Arreola-Vargas *et al.* (2015)
Empty palm fruit bunch (EFB), rice husk (RH), and pine tree wood (PTW)	Anaerobic dark fermentation	Heat-treated anaerobic digester sludge	Working volume: 40 mL pH: 7.0-7.5, speed: 150 rpm and Temp: 35°C	H_2 production yield: EFB = 2,640 mL/L/day RH = 2,960 mL/L/day PTW = 2,565 mL/L/day	Generation of inhibitors such as 5-HMF and furfural hinder the H_2 production rate	Gonzales *et al.* (2016)
Rice straw	Anaerobic digestion	Pond sediments sludge	Working volume: 2.2 L Incubation Temp: 35°C pH: 7.3	Biogas: 393.2 ± 13.6 mL/g VS CH_4: 224.4 ± 6.8 mL/g VS	Inconsistent performance of substrate digestion for co-substrate or fed-batch system	Pan *et al.* (2021b)
Rice straw and cow dung	Anaerobic co-digestion with cow dung	No inoculum used	Working volume: 30 L Dung-to-straw ratio: 3:1 (based on TS) 8 C/N ratio: 20:30	Biogas: 434.2 L/kg VSr CH_4: 217.6 L/kg CH_4 yield: 217.6 L/kgVSr	Rice straw has a high C/N ratio or low hydrolysis performance and digestibility	Haryanto *et al.* (2018)
Rice straw	Anaerobic digestion	Anaerobic wastewater sludge	Working volume: 500 mL Incubation Temp: 35°C, pH: 7	Biogas: 322.1 mL/g rice straw	No acknowledgement of this substrate for biogas production in Thailand	Amnuaycheewa *et al.* (2016)
Corn stover	Anaerobic digestion	Mesophilic biogas plant of pig manure sludge	Working volume: 8 L Organic loading rate: 90 g TS·L^{-1}, retention period: 60 days, pH: 7.2, Temp: 35°C, 38°C, 41°C and 44°C	Biogas: 598 mL/g VS/d CH_4: 308 mL/g VS/d	High incubation temperature for optimum biogas production leads to high energy usage	Liu *et al.* (2017)
Empty fruit bunch (EFB)	Anaerobic co-digestion with POME	Anaerobic sludge from palm oil mill	Different EFB to POME ratios EFB sizes: 0.5-6.0 cm Total solid of substrate: 2-10 g VS at 37°C	CH_4: 323 mL/g VS	Size reduction of EFB up to 0.5 cm requires high energy and is expensive	Saelor *et al.* (2017)
Poplar leaves	Anaerobic fermentation	No inoculum used	pH: (6.0-8.0), TS: (8%-12%) and Temp: (25°C-35°C)	Biogas: 39,625 mL	The substrate needs to be pre-treated with alkali to achieve optimum biogas production	Zhang *et al.* (2020)
Wheat straw, rice straw and sugarcane bagasse	Anaerobic co-digestion	Effluent of the operational biodigester of cow manure	Substrate to inoculum (S/I) ratio: 1.5:2.5 Working volume: 210 mL pH: 7.0-7.5, Temp: 35°C	Best S/I ratio: 1.5 CH_4: 393.08 NmlCH_4/g VS	Low hydrolysis rate, high lignin content and low pH value (accumulation of volatile fatty acids)	Meraj *et al.* (2021)

TABLE 3. INFLUENCE OF PRE-TREATMENT TECHNIQUES ON THE PRODUCTION OF BIOGAS

Type of lignocellulosic biomass	Method of biogas production	Pre-treatment methods		Treatment condition	Treatment mechanism	Major findings	References
		Type	Pre-treatment				
Rice straw	Anaerobic digestion	Chemical	Sodium carbonate, Na_2CO_3	0.25 and 0.5 M Na_2CO_3 at 90, 110, and 130°C for 1, 2, and 3 hr	Significantly reduce the crystallinity of cellulose and lignin content	0.5 M Na_2CO_3 at 110°C for 2 hr = 292 mL CH_4/g VS	Dehghani *et al.* (2015)
	Solid-state anaerobic digestion	Physical	Milling	Milled to the particle diameter of ≤2 mm	Can increase lignin and hemicellulose, and cellulose removal	Milling posterior to fungal pre-treatment results in the highest effect	Mustafa *et al.* (2016)
		Biological	*Pleurotus ostreatus* fungus	70% moisture content at 28°C for 10, 20 and 30 days	Degrade dry matter, cellulose, hemicellulose and lignin in rice straw		
	Anaerobic digestion	Chemical	Organic acid - acetic acid, $C_2H_4O_2$ - citric acid, $C_6H_8O_7$ - oxalic acid, $C_2H_2O_4$ Inorganic acid -Hydrochloric acid, HCl	Org. acid concentration (5%-15% wt), inorg. acid concentration (0.5-2.0 wt), treatment time (30-60 min), and reaction temperature (100°C-140°C)	Can reduce the large amount of rice straw mass into reducing sugar and lignin content to remove inhibitors of a hydrolysis reaction	$C_6H_8O_7$ pre-treated substrate is the best method Biogas yield: 197.86 mL/g VS_{total} COD removal: 73.2%	Amnuaycheewa *et al.* (2016)
Paddy straw	Anaerobic digestion	Physico-chemical	Sodium hydroxide microwave	Substrate soaked in sodium hydroxide (NaOH) solution at 2%-10% concentrations for 24 hr at 28°C. Then, irradiated with microwaves at 720 W, 180°C for 30 min	Co-pre-treatment reduced lignin and silica content while breaking lignocellulose structure by tearing different layers of the cell wall of paddy straw	Best pre-treatment at 4% NaOH-30 min microwave Biogas yield: 297 L biogas/kg substrate	Kaur & Phutela (2016)
Corn stover	Anaerobic digestion	Physico-chemical	Steam explosion	Steam explosion unit: 25 KW electric-heated steam boiler with pressure of 34 bar (maximum) Pre-treatment temperature ranges from 140°C to 220°C for 2 to 15 min	Acetyl groups in the hemicellulose fraction will be hydrolysed, producing a lot of acetic and uronic acids that reduce the pH value in the substrate sample	The best pre-treatment was conducted at 160°C for 2 min Biogas yield: 585 L/kg VS CH_4: 348 L/kg VS	Lizasoain *et al.* (2017)
Corn stalk	Anaerobic digestion	Physical	Dual-frequency ultrasound	Mass of corn stalk (40-64 g), ultrasonic duration time (10-50 mins), alkali pre-treatment (2% NaOH) time (0-72 hr), and single/dual-frequency ultrasound	Mechanisms of ultrasonic is the cavitation effect, where its intensity is related to the ultrasonic frequency and the ultrasonic intensity	Cum. Biogas yield: 0.501 L/g VS with higher 56.6% than other pre-treatment methods	Dong *et al.* (2018)

TABLE 3. INFLUENCE OF PRE-TREATMENT TECHNIQUES ON THE PRODUCTION OF BIOGAS (continued)

Type of lignocellulosic biomass	Method of biogas production	Pre-treatment methods		Treatment condition	Treatment mechanism	Major findings	References
		Type	Pre-treatment				
Sugarcane bagasse	Anaerobic digestion	Chemical	Ethanolic ammonia	10% v/v aqueous ammonia solution at 50 and 70°C for 12 and 24 hr Concentrations of ethanol added to the pre-treatment mixture: 5%-50% v/v	Pre-treatment increases lignin removal and reduces cellulose crystallinity to improve CH_4 yields	At 70°C, Highest CH_4 yield: Liquid fraction, 298.0 mL/g VS whole slurry, 299.3 mL/g VS solid fraction, 248.6 mL/g VS	Hashemi *et al.* (2019)
Empty fruit bunch (EFB)	Solid-state anaerobic digestion	Chemical	NaOH solutions	3%-7% w/v of NaOH	Those pre-treatments increase the surface area, cellulose content, and the concentration of reduced sugar	Size reduction gave the highest yield of CH_4: 429.9 mL/g VS, more than a 90% increase compared to raw substrate	Wadchasit *et al.* (2020)
		Physical	Size reduction	3.0 and 0.5 cm			
		Biological	Activated sludge (AS) and bio-scrubber effluent	10 g of substrate pre-treated with AS and effluent separately			

the overview focuses on several kinds of LCB often discovered and conveniently available in Malaysia, especially those produced by agricultural pursuits such as paddy cultivation, maize farming, sugarcane production, and palm oil plantations. Generally, most pre-treatment techniques can expand the surface area and produce readily available active binding sites for enzymes to thrive (Karthikeyan *et al.*, 2018). The benefits of various pre-treatments include increased surface area, lignin removal, and decreased cellulose crystallinity (Paudel *et al.*, 2017).

Physical Pre-treatment Method

In the physical pre-treatment technique, milling or grinding the LCB is conducted to break down the particle sizes (Arenas-Cárdenas *et al.*, 2017). The outputs of physical treatments could be influenced by the operating temperature, pressure, feedstock, and residence time. Mechanical pre-treatments are inadequate for the pre-treatment of LCB and are usually merged with chemical pre-treatments to enhance downstream carbohydrate products (Kumar & Sharma, 2017). The physical processes are undertaken at temperatures ranging between 180°C and 240°C, together with mechanical shearing. However, physical or mechanical pre-treatment methods such as mechanical comminution, microwave radiation, freezing method with a volumetric water change, extrusion, and sonication or ultrasound-assisted pre-treatment, do not use chemicals or microbes (Xu *et al.*, 2019).

Agricultural waste and forestry residues are commonly subjected to mechanical processing to improve the lignocellulosic material's accessibility to hydrolysable polymers (Amin *et al.*, 2017). These methods can improve the efficiency of hydrolysis and anaerobic breakdown of plant biomass into liquid and gaseous fuels and other essential organic compounds. Numerous physical pre-treatment approaches are employed to enhance biogas production. These physical techniques include grinding, ultrasound, milling, microwave, irradiation, external forces assisted and size reduction (Dong *et al.*, 2018; Mustafa *et al.*, 2016; Wadchasit *et al.*, 2020; Xu *et al.*, 2019). However, the utilisation of this pre-treatment approach requires prolonged retention times and high energy requirements (Baruah *et al.*, 2018).

Chemical Pre-treatment Method

For the chemical pre-treatment method, chemical reactions in aqueous solutions enable lignocellulose degradation to simple molecules (Kucharska *et al.*, 2018). These methods can be classified into acid hydrolysis, alkaline pre-treatment, ozonolysis, solvents (organic and others) and ionic liquid pre-treatment. However, this pre-treatment is more common than physical and biological pre-treatment procedures due to its efficacy and ability to increase the digestion of complicated feedstocks. Despite this efficacy, the formation of inhibitory compounds such as phenolic acids, furfurals, aldehydes and 5-hydroxymethylfurfural has restricted the more comprehensive application of this technique (Olatunji *et al.*, 2021). This technique also improves bioconversion performance due to its enhanced effectiveness in reducing resistive characteristics (Xu *et al.*, 2019). Chemicals often

utilised in chemical pre-treatment procedures for enhancing agricultural residue AD performance include hydrochloric acid (HCl) and sulfuric acid (H_2SO_4), sodium hydroxide (NaOH), acetic acid (CH_3COOH), lime [$Ca(OH)_2$], and potassium hydroxide (KOH) (González *et al.*, 2005; Olatunji *et al.*, 2021).

Acid pre-treatment can hydrolyse hemicellulose to monosaccharides, increasing the cell wall's pore size or volume and making cellulose more vulnerable to enzymatic breakdown. The addition of bases to biomass causes swelling, which increases internal surface, decreases polymerisation degree and crystallinity, disrupts connections between lignin and other polymers, and lignin breakdown (Badiei *et al.*, 2014), making it more effective for biomass with low lignin concentration. Chemical pre-treatment for biomethane production from LCB and acidic pre-treatment produces the highest biomethane production. This indicates that it could be considered as a good pre-treatment media, despite the substantial production of biomethane from LCB using chemical pre-treatment. Yet the application of this approach could generate high corrosivity and toxicity, environmental pollution, prolonged residence time, formation of inhibitors and toxic and high energy requirements (Amnuaycheewa *et al.*, 2016; Dehghani *et al.*, 2015; Hashemi *et al.*, 2019).

Physicochemical Pre-treatment Method

The physicochemical method combines oxidation and heat treatment to decompose lignocellulose structure. This method comprises steam explosion (autohydrolysis), Ammonia Fiber Explosion (AFEX) (Cai *et al.*, 2022), and CO_2 explosion (Mussatto *et al.*, 2021). Steam explosion is run by subjecting lignocellulosic material to high-pressure saturated steam at a temperature of 160°C-260°C and a pressure of 5-50 atm for several minutes (Amin *et al.*, 2017). The AFEX pre-treatment, also called NH_3, to recycle percolation or called Ammonia Recycle Percolation (ARP) or Soaking Aqueous Ammonia (SAA), utilises liquid NH_3 to pre-treat lignocellulose. This pre-treatment is conducted at room temperature, whereas the ARP approach is at high temperatures. For CO_2 explosion, feedstock is contained in a high-pressure vessel where supercritical CO_2 is released and acts as a solvent. It combines both chemical and physical techniques as a single pre-treatment method. However, the more comprehensive application of this technique is restricted by the formation of pseudo-lignin, which may hinder CH_4 yield (Sun *et al.*, 2021). However, some drawbacks of this technique include environmental pollution, high temperature, and high energy requirements (Sharma *et al.*, 2023).

Biological Pre-treatment Method

Biological pre-treatments are predominantly environmental-friendly and non-hazardous, with lesser energy consumption, without generating inhibitors for downstream conditions, and relying on microbes, enzymes, or consortia to promote lignocellulose biodegradation and biogas production (Tu & Hallett, 2019). The biologically discovered broad systematic array of microbes is utilised in biological pre-treatment. They degrade or change lignocellulose extracellularly by producing hydrolytic enzymes such as hydrolases and ligninolytic enzymes, which depolymerise lignin. Furthermore, fungal or bacterial pre-treatments can be employed to depolymerise, hydrolyse cellulose and eliminate lignin (Chen *et al.*, 2017). The working conditions for biological pre-treatments are affected by chemical (such as pH), biological (a strain of fungi or bacteria), and physical (for instance, the size of the particles and temperature) circumstances (Sharma *et al.*, 2017). Moreover, the generation of bioethanol from biogas carbohydrate fermentation can also be generated based on the nature of the bacteria/fungi and retreatment applied.

However, applying the biological pre-treatment approach requires prolonged retention times. It is not commercially feasible since it generally requires other pre-treatment techniques, such as chemical or biological, to function efficiently. Some emerging pre-treatment techniques, namely supercritical fluid-based, ionic liquids, Low Temperature Steep Delignification (LTSD) and Co-solvent Enhanced Lignocellulosic Fractionation (CELF), are regarded to be the most advanced approaches that produce superior sugar yield with a minimal quantity of by-products (Meng *et al.*, 2018; Sorn *et al.*, 2019). Accordingly, the released hexose and pentose sugars can be applied to produce polyols, organic acids, fatty acids, bioplastics and alcohols by various microbes (Jagtap *et al.*, 2019).

CURRENT CHALLENGES AND DRAWBACKS OF BIOGAS PRODUCTION FROM LIGNOCELLULOSIC BIOMASS IN MALAYSIA

Recently, the Malaysian government launched the Malaysia Energy Supply Industry 2.0 (MESI 2.0) plan in 2019, with a new target of 35% RE in installed power capacity by 2025. Malaysia has reiterated its commitment to increasing the percentage of carbon-neutral energy sources as part of its efforts to tackle global climate change. Notably, the country has revised its target for RE in the national energy mix, raising it from 20%-31% by the year 2025 (Rahman *et al.*, 2022). Despite the vast growth of biogas plant utilisation to generate energy in Malaysia, there

are several shortcomings which have hindered its development. These limitations include financial obstacles, market barriers, lack of indigenous technology, and poor access to grid connections for biogas power plants (Kumaran *et al.*, 2015). The principal financial hurdle is the investment cost of building biogas plant infrastructure with power production facilities. At the same time, the market barriers relating to the electricity market structure can be visibly observed to be very expensive compared to the current waste treatment practice.

Key challenges encountered by bioenergy developers, as listed by SEDA Malaysia, encompass various aspects: Firstly, issues of suboptimal plant size and capacity factors stem from challenges in acquiring feedstock. This is followed by concerns over fluctuating feedstock price and quality, complexities in accessing grid connections, and the utilisation of less efficient technologies for power generation. Furthermore, WTE players face their distinct issues, such as varying tipping fees across Malaysia, complicating investment decisions and logistical challenges in managing waste feedstocks due to scattered landfill sites across the country (SEDA, 2021a). The government also acknowledges the critical need to address both supply and demand challenges for agriculture-related bioenergy to meet its intended objectives. However, there are also supply-related hurdles, which involve potential concentration risks with bioenergy feedstock, global perceptions affecting the acceptance of palm oil biomass, biomass supply security and high aggregation costs of bio-based feedstock. On the other hand, demand challenges revolve around limited local demand for bioenergy (MoE, 2023).

Therefore, to curb the glut of agricultural waste generated in Malaysia, various agro-industries are currently considering strategies to reduce biomass waste generated by upgrading waste conversion or processing techniques. However, local funding institutions are still concerned about the sustainability of the biomass feedstock supply for an extended period. Malaysia's biogas sector is still in its early phases of growth (Amin *et al.*, 2022), and the main method of waste treatment is the use of anaerobic digesters, which employ microorganisms to break down waste. However, there is a dearth of biogas capture technology implementation, which could be secured by successful collaborations with government agencies (Hanafiah *et al.*, 2017). As of October 2023, Malaysia possessed a total of 447 palm oil mills with some of them equipped with biogas capture facilities as reported by the Malaysian Palm Oil Board (MPOB, 2023a). The majority of these biogas plants actively contributed to the national grid, showcasing a substantial commitment to sustainable energy practices within the country.

The utilisation of agricultural wastes as biogas substrates enhances waste management and serves as a critical renewable bioenergy source (Olatunji *et al.*, 2021). The application of agricultural wastes, especially lignocellulosic materials, has inherent limitations. Although LCB is rich in fermentable sugars, rendering them an ideal food source for microbes to produce biogas, their pre-treatment procedure still requires a huge sum of capital. In addition, their inherent drawbacks lie in their complicated compositional and structural arrangement that makes them recalcitrant to biological decomposition. Other challenges in utilising the lignocellulosic materials include their natural structure. Biomass recalcitrance and production of inhibitors are among the critical challenges limiting biogas and bioethanol production, leading to higher production costs and longer processing time (Xu *et al.*, 2019).

In addition, the biodegradability of LCB could be affected by the percentage or proportion of lignin, accessible surface area, cellulose polymerisation grade, crystallinity, cross-linkages of hemicellulose, solubility and other related factors (Xu *et al.*, 2019). Biomass degradation and modification to increase enzymatic digestibility are usually performed under severe conditions, requiring large amounts of chemicals, making the pre-treatment process more expensive (Capolupo & Faraco, 2016). In addition, the main challenge in biogas production from LCB, especially for small local industries, is the high cost of pre-treatment of the substrate to obtain higher biogas yield. The operating factors could also undermine the performance of various lignocellulose biomass (substrates) in biomethane production (Xu *et al.*, 2019).

ECONOMIC ANALYSIS OF PRE-TREATMENT METHODS FOR LIGNOCELLULOSIC BIOMASS IN BIOGAS PRODUCTION

In the quest for sustainable energy sources, LCB has emerged as a promising solution for biogas production. However, efficiently converting this abundant renewable resource into biogas poses significant challenges (Patel & Shah, 2021; Saini *et al.*, 2016). A critical aspect of this conversion process is the pre-treatment of LCB, which involves a series of physical, chemical, or biological processes, aimed at breaking down its complex structure and enhancing its accessibility for subsequent biogas production (Hernández *et al.*, 2019). The economic analysis of pre-treatment methods becomes crucial in evaluating their viability, optimising resource allocation and determining the overall financial feasibility of LCB-based biogas production systems.

Factors such as investment costs, operational expenses, biomass feedstock availability and costs and product revenues, significantly influence the potential economic profit of AD plants

(Bruno *et al.*, 2023). Moreover, the nascent nature of pre-treated LCBAD techniques introduces investment risks. This comprehensive analysis explores the economic factors and considerations associated with pre-treatment methods, providing valuable insights for policymakers, researchers and stakeholders invested in sustainable energy solutions. According to research, pre-treatment costs account for approximately 19%-22% of the total expenses in the bioenergy recovery process (Baral & Shah, 2017). Scientists have conducted techno-economic evaluations of the different pre-treatment methods to ensure energy efficiency and cost-effectiveness. The aim is to identify the optimal conditions that offer the best balance between cost and energy recovery in bioenergy production.

In the study by Dahunsi *et al.* (2019), acid pre-treatment of *Sorghum bicolor* stalk produces 312.3 LN biogas per kg of Volatile Solids (VS) added. However, there was a deficit in net thermal energy, which was -951 kWh/t of Total Solids (TS) and in net electrical energy, which was -753 kWh/t of TS. The capital investment for this project amounted to USD140 million. Note that the sulphuric acid pre-treatment used in the study on *S. bicolor* stalk demonstrated a high gas production. However, the negative net thermal and electrical energy values indicate a deficit in energy recovery. A thermo-alkaline method was employed for the pre-treatment of *Arachis hypogaea* (Peanut) hull. The pre-treatment resulted in gas production of 3,339.20 mL/kg of TS fed. The net thermal energy was -412 kWh/t of TS, while the net electrical energy was 303 kWh/t of TS. The capital investment for this project was USD450 million, with a Net Present Value (NPV) of USD381 million (Dahunsi *et al.*, 2017). The thermo-alkaline pre-treatment method applied to *A. hypogaea* hull demonstrated a favourable gas production, with a relatively balanced net thermal and electrical energy recovery. Accordingly, this pre-treatment indicates its potential for efficient bioenergy production.

Another study by Kabir *et al.* (2015) utilised organosolv pre-treatment on forest residue by comparing the performance of ethanol, CH_3COOH, and methanol on biogas production. The economic analysis indicates that using methanol for pre-treatment offers the highest NPV compared to alternatives utilising ethanol or CH_3COOH. This finding makes the methanol-based pre-treatment process the most economically attractive option. The primary factor contributing to its advantage is the low cost of methanol, priced at USD0.300/kg. Compared to the other alternatives, this cost advantage enhances the profitability and economic feasibility of the methanol-based pre-treatment method. Brand *et al.* (2013) investigated the economic analysis of mechanical pre-treatment for converting softwood biomass into fermentable sugars using three-phase milling. The cost of sugar production through this mechanical pre-treatment method was calculated to be USD0.496/kg. However, this study did not address the environmental and profitability aspects of the disintegration process. Furthermore, Safarian and Unnthorsson (2018) suggested that steam explosion pre-treatment is a highly efficient and profitable technique from an energetic, economic and ecological standpoint. Conversely, dilute acid pre-treatment is another effective method for LCB; however, it is less desirable due to higher production costs and increased GHG emissions. Soam *et al.* (2018) proposed treating LCB with alkali at lower doses prior to biological pre-treatment. This approach reduced the required enzyme dosage by 23%-39%. However, the authors also observed adverse ecological effects of this pre-treatment method.

Thus, further research is required to identify the optimal combination of disintegration methods and operational conditions that can effectively minimise ecological effects, reduce environmental impacts and decrease costs associated with pre-treatments. Notably, the expenses incurred for pre-treatment methods can be offset by producing excess bioenergy, resulting in a net gain. Nevertheless, when evaluating the profitability of the production process, it is crucial to consider both fixed capital investment and variable costs (Jamaldheen *et al.*, 2022). Additionally, it is recommended to assess the bioenergy productivity of all pre-treatment methods, when dealing with a fixed quantity of lignocellulosic feedstock. This comprehensive evaluation will provide a more accurate assessment of the process's profitability.

In evaluating pre-treatment methods, it is crucial to consider their environmental and economic impacts to ensure the sustainable production of bioenergy (Pérez-Almada *et al.*, 2023). Moreover, balancing economic gains with environmental sustainability through a comprehensive assessment of pre-treatment methods is vital for the long-term viability of biogas production from LCB (Preethi *et al.*, 2023). This balanced approach ensures economic profitability while mitigating adverse environmental effects.

FUTURE PROSPECTS

Though preliminary treatment is necessary to enhance bio-energy production, the constraining impact resulting from the lignin and hemicellulose degradation is unignorable. Therefore, it is a considerable concern to adequately balance functional bacteria actions and the lignocellulose derivative inhibitors production to optimise bioenergy generation from lignocellulose substrate. The commercial adoption of either pre-treatment

technique is relatively rare due to the significant drawbacks of each operation. Thus, the industrial-friendly and economical approach to pre-treat LCB should be explored and developed. Hence, lowering the treatment period together with reduced wastage may be favourable to reducing the overall pre-treatment cost. In this regard, the thermal-related pre-treatment (such as microwave) process could offer a reduction in residence time compared with other existing pre-treatment technologies.

This review suggests a robust comparative study of various pre-treatment technologies with a single variety of LCB. The main challenge has been the disparity in the makeup of lignocellulosic feedstock biomass with the differences in location. Thus, choosing a good pre-treatment technique could avert unnecessary difficulties during biogas production. A low-cost, practical, environmentally friendly and facile operation pre-treatment system should be exploited to enhance the existing AD reactors. Also, an integrated, optimised AD system with pre-treatment compartments is another grey area that can assist in minimising the residence time and the overall duration of biogas production. This echoes the need for further in-depth study on the inline pre-treatment-AD integrated system. Further study on the development of inline pre-treatment-AD integrated system may involve investigating the biomass feeding rate, retention time and operating conditions such as temperature and pH. This includes the design that ensures optimal biogas production conditions in terms of yield volume, feedstock retention time and reactor compatibility.

In addition, identifying the pre-treatment methods capable of breaking up the complex feedstock into simpler molecules is crucial in achieving a novel and efficient biogas production system. This demonstrates that the success of this inline integrated pre-treatment-AD system will significantly change the paradigm of biogas production in Malaysia and beyond. However, the meagre implementation and inadequate adoption of this technology among the stakeholders could undermine the impact on the biogas industries. To avoid this, the relevant government agencies in Malaysia, such as NEEAP in conjunction with the EECA, may be charged with demonstrating and promoting the technology to get it across to the stakeholders (such as the farmers and biogas industries).

CONCLUSION

This article presents a review of biogas production from LCB in Malaysia. Initially, it deliberates on the energy sources, the potentials of the abundant biomass generated, the chemistry compositions of the biomass and its applications. This should assist the Malaysian government in initiating several policies to develop biogas plants with the aim of reducing dependence on fossil fuels. This improved the contribution of the biogas energy value to the national energy requirement compared to other energy sources. Furthermore, the various sources of LCB in Malaysia and the respective potential utilisations are deliberated. The yearly generation of lignocellulosic biomass (LCB) is substantial; however, its potential for biogas production remains largely untapped. Despite this underutilisation, the energy value derived from biogas is comparable to other sources like hydro and solar energy. The hydrolysis process during LCB degradation is notably prolonged due to the intricate nature of cellulose compounds, thereby impeding the initial biochemical reactions. To expedite biogas production, physical, chemical and biological pre-treatments are predominantly employed. The delay in biochemical degradation triggers hydrogen partial pressure, resulting in the formation of volatile fatty acids (VFAs) that inhibit the methanogenesis process. This underscores the imperative for further investigation into the development of an inline integrated pre-treatment-anaerobic digestion (AD) system, coupled with an exploration of optimal operating conditions. The prospect of efficient biogas development and production from LCB in Malaysia hinges on various factors, including governmental policies, inherent physicochemical attributes of the feedstocks and operational conditions. These economic analyses provide valuable insights for policymakers, researchers, and stakeholders engaged in sustainable energy solutions utilising LCB. Therefore, enabling policies and availability of an efficient inline integrated pre-treatment-AD system capable of utilising the ever-generating biomass will not only consolidate its national energy contribution but also improve environmental conditions.

ACKNOWLEDGEMENT

This work is funded and supported by the Malaysia Ministry of Higher Education through the grant of Fundamental Research Grant Scheme [FRGS/1/2020/TK0/UPM/02/7]. All authors contributed to the interpretation of the article. All authors have read and agreed to the published version of the manuscript.

REFERENCES

Abdeshahian, P., Lim, J. S., Ho, W. S., Hashim, H., & Lee, C. T. (2016). The potential of biogas production from farm animal waste in

Malaysia. *Renewable and Sustainable Energy Reviews, 60*, 714–723. https://doi.org/10.1016/j.rser.2016.01.117

Abdullah, W. S. W., Osman, M., Kadir, M. Z. A. A., & Verayiah, R. (2019). The potential and status of renewable energy development in Malaysia. *Energies, 12*(12), 2347. https://doi.org/10.3390/en12122437

Abu Dardak, R. (2022, March 21). *Overview of the agriculture sector during the 11th Malaysian Development Plan (2016–2020)*. FFTC Agricultural Policy Platform, 1–10. https://ap.fftc.org.tw/article/3010

Aftab, M. N., Iqbal, I., Riaz, F., Karadag, A., & Tabatabaei, M. (2019). Different pretreatment methods of lignocellulosic biomass for use in biofuel production. In *IntechOpen eBooks*. https://doi.org/10.5772/intechopen.84995

Ahmad, S., & Tahar, R. M. (2014). Selection of renewable energy sources for sustainable development of electricity generation system using analytic hierarchy process: A case of Malaysia. *Renewable Energy, 63*, 458–466. https://doi.org/10.1016/j.renene.2013.10.001

Amin, F. R., Khalid, H., Zhang, H., Rahman, S., Zhang, R., Liu, G., & Chen, C. (2017). Pretreatment methods of lignocellulosic biomass for anaerobic digestion. *AMB Express, 7*(72), 1–12. https://doi.org/10.1186/s13568-017-0375-4

Amin, M. A., Shukor, H., Yin, L. S., Kasim, F. H., Shoparwe, N. F., Makhtar, M. M. Z., & Yaser, A. Z. (2022). Methane biogas production in Malaysia: Challenge and future plan. *International Journal of Chemical Engineering, 2022*, 1–16. https://doi.org/10.1155/2022/2278211

Amnuaycheewa, P., Hengaroonprasan, R., Rattanaporn, K., Kirdponpattara, S., Cheenkachorn, K., & Sriariyanun, M. (2016). Enhancing enzymatic hydrolysis and biogas production from rice straw by pretreatment with organic acids. *Industrial Crops and Products, 87*, 247–254. https://doi.org/10.1016/j.indcrop.2016.04.069

Ardolino, F., & Arena, U. (2019). Biowaste-to-biomethane: An LCA study on biogas and syngas roads. *Waste Management, 87*, 441–453. https://doi.org/10.1016/j.wasman.2019.02.030

Arenas-Cárdenas, P., López-López, A., Moeller-Chávez, G. E., & León-Becerril, E. (2017). Current pretreatments of lignocellulosic residues in the production of bioethanol. *Waste Biomass Valorization, 8*(1), 161–181. https://doi.org/10.1007/s12649-016-9559-4

Arreola-Vargas, J., Razo-Flores, E., Celis, L. B., & Alatriste-Mondragón, F. (2015). Sequential hydrolysis of oat straw and hydrogen production from hydrolysates: Role of hydrolysates constituents. *International Journal of Hydrogen Energy, 40*(34), 10756–10765. https://doi.org/10.1016/j.ijhydene.2015.05.200

Aziz, A. (2023, November 1). *Govt launches Green Electricity Tariff for renewable energy subscription, replaces myGreen+*. The *Edge Malaysia*. https://theedgemalaysia.com/article/domestic-industrial-consumers-can-opt-green-electricity-get-says-takiyuddin

Aziz, N. I. H. A., & Hanafiah, M. M. (2017). The potential of palm oil mill effluent (POME) as a renewable energy source. *Acta Scientiae Malaysia, 1*(2), 9–11. https://doi.org/10.26480/asm.02.2017.09.11

Aziz, N. I. H. A., Hanafiah, M. M., & Gheewala, S. H. (2019). A review on life cycle assessment of biogas production: Challenges and future perspectives in Malaysia. *Biomass and Bioenergy, 122*, 361–374. https://doi.org/10.1016/j.biombioe.2019.01.047

Badiei, M., Asim, N., Jahim, J. M., & Sopian, K. (2014). Comparison of chemical pretreatment methods for cellulosic biomass. *APCBEE Procedia, 9*, 170–174. https://doi.org/10.1016/j.apcbee.2014.01.030

Jamaldheen, S. B., Kurade, M. B., Basak, B., Yoo, C. G., Oh, K. K., Jeon, B., & Kim, T. H. (2021). A review on physico-chemical delignification as a pretreatment of lignocellulosic biomass for enhanced bioconversion. *Bioresource Technology, 346*, 126591. https://doi.org/10.1016/j.biortech.2021.126591

Baral, N. R., & Shah, A. (2017). Comparative techno-economic analysis of steam explosion, dilute sulfuric acid, ammonia fiber explosion and biological pretreatments of corn stover. *Bioresource Technology, 232*, 331–343. https://doi.org/10.1016/j.biortech.2017.02.068

Baruah, J., Nath, B. K., Sharma, R., Kumar, S., Deka, R. C., Baruah, D. C., & Kalita, E. (2018). Recent trends in the pretreatment of lignocellulosic biomass for value-added products. *Frontiers in Energy Research, 6*, 1–19. https://doi.org/10.3389/fenrg.2018.00141

Basri, N. A., Ramli, A. T., & Aliyu, A. S. (2015). Malaysia energy strategy towards sustainability: A panoramic overview of the benefits and challenges. *Renewable and Sustainable Energy Reviews, 42*, 1094–1105. https://doi.org/10.1016/j.rser.2014.10.056

Benti, N. E., Gurmesa, G. S., Argaw, T., Aneseyee, A. B., Gunta, S., Kassahun, G. B., Aga, G. S., & Asfaw, A. A. (2021). The current status, challenges and prospects of using biomass energy in Ethiopia. *Biotechnology for Biofuels, 14*(1), 1–14. https://doi.org/10.1186/s13068-021-02060-3

Bernama. (2021, May 6). *Malaysia aspires to be carbon neutral nation*. The Malaysian Reserve. https://themalaysianreserve.com/2021/05/06/malaysia-aspires-to-be-carbon-neutral-nation/

Bhambhani, A. (2023, May 10). *Malaysia announces new renewables target.* TaiyangNews. https://taiyangnews.info/malaysia-announces-new-renewables-target/

Bhatia, S. K., Gurav, R., Choi, T. R., Han, Y. H., Park, Y. L., Park, J. Y., Jung, H. R., Yang, S. Y., Song, H. S., Kim, S. H., Choi, K. Y., & Yang, Y. H. (2019). Bioconversion of barley straw lignin into biodiesel using *Rhodococcus* sp. YHY01. *Bioresource Technology, 289*, 121704. https://doi.org/10.1016/j.biortech.2019.121704

Bhatia, S. K., Jagtap, S. S., Bedekar, A. A., Bhatia, R. K., Patel, A. K., Pant, D., Rajesh Banu, J., Rao, C. V., Kim, Y. G., & Yang, Y. H. (2020). Recent developments in pretreatment technologies on lignocellulosic biomass: Effect of key parameters, technological improvements, and challenges. *Bioresource Technology, 300*, 122724. https://doi.org/10.1016/j.biortech.2019.122724

Brand, S., Susanti, R. F., Kim, S. K., Lee, H. S., Kim, J., & Sang, B. I. (2013). Supercritical ethanol as an enhanced medium for lignocellulosic biomass liquefaction: Influence of physical process parameters. *Energy, 59*, 173–182. https://doi.org/10.1016/j.energy.2013.06.049

Bruno, M., Marchi, M., Ermini, N., Niccolucci, V., & Pulselli, F. M. (2023). Life cycle assessment and cost-benefit analysis as combined economic-environmental assessment tools: Application to an anaerobic digestion plant. *Energies, 16*(9), 3686. https://doi.org/10.3390/en16093686

Cai, Z., Zhang, W., Zhang, J., Zhang, J., Ji, D., & Gao, W. (2022). Effect of ammoniated fiber explosion combined with H_2O_2 pretreatment on the hydrogen production capacity of herbaceous and woody waste. *ACS Omega, 7*(25), 21433–21443. https://doi.org/10.1021/acsomega.2c00598

Capolupo, L., & Faraco, V. (2016). Green methods of lignocellulose pretreatment for biorefinery development. *Applied Microbiology and Biotechnology, 100*(22), 9451–9467. https://doi.org/10.1007/s00253-016-7884-y

Cenergi SEA Berhad. (2023, October 23). *Cenergi Sri Ganda 2.4MW Biogas Power Plant*. https://www.cenergi-sea.com/our-projects/2-0mw-biogas-power-plant-2/

Chan, Y. J., & Chong, M. F. (2019). Palm oil mill effluent (POME) treatment - Current technologies, biogas capture and challenges. In D. Foo, M. Tun Abdul Aziz, (eds.), *Green Energy and Technology* (pp. 71–92). Springer. https://doi.org/10.1007/978-981-13-2236-5_4

Chan, Y. J., Hue, F. S., Chong, M. F., Ng, D. K. S., & Lim, D. L. K. (2020). Pre-commercialized integrated anaerobic-aerobic bioreactor (IAAB) for palm oil mill effluent (POME) treatment & biogas generation. *Journal of Oil Palm Environment and Health, 11*(40), 57–66.

Chaudhari, Y. B., Várnai, A., Sørlie, M., Horn, S. J., & Eijsink, V. G. H. (2023). Engineering cellulases for conversion of lignocellulosic biomass. *Protein Engineering, Design & Selection, 36*, 1–12. https://doi.org/10.1093/protein/gzad002

Chen, H., Liu, J., Chang, X., Chen, D., Xue, Y., Liu, P., Lin, H., & Han, S. (2017). A review on the pretreatment of lignocellulose for high-value chemicals. *Fuel Processing Technology, 160*, 196–206. https://doi.org/10.1016/j.fuproc.2016.12.007

Chien Bong, C. P., Ho, W. S., Hashim, H., Lim, J. S., Ho, C. S., Peng Tan, W. S., & Lee, C. T. (2017). Review on the renewable energy and solid waste management policies towards biogas development in Malaysia. *Renewable and Sustainable Energy Reviews, 70*, 988–998. https://doi.org/10.1016/j.rser.2016.12.004

Czatzkowska, M., Harnisz, M., Korzeniewska, E., & Koniuszewska, I. (2020). Inhibitors of the methane fermentation process with particular emphasis on the microbiological aspect: A review. *Energy Science & Engineering, 8*(5), 1880–1897. https://doi.org/10.1002/ese3.609

Dahunsi, S. O., Oranusi, S., & Efeovbokhan, V. E. (2017). Pretreatment optimization, process control, mass and energy balances, and economics of anaerobic co-digestion of *Arachis*

hypogaea (peanut) hull and poultry manure. *Bioresource Technology, 241*, 454–464. https://doi.org/10.1016/j.biortech.2017.05.152

Dahunsi, S. O., Adesulu-Dahunsi, A. T., Osueke, C. O., Lawal, A. I., Olayanju, T. M. A., Ojediran, J. O., & Izebere, J. O. (2019). Biogas generation from *Sorghum bicolor* stalk: Effect of pretreatment methods and economic feasibility. *Energy Reports, 5*, 584–593. https://doi.org/10.1016/j.egyr.2019.04.002

Dehghani, M., Karimi, K., & Sadeghi, M. (2015). Pretreatment of rice straw for the improvement of biogas production. *Energy & Fuels, 29*(6), 3770–3775. https://doi.org/10.1021/acs.energyfuels.5b00718

Den, W., Sharma, V. K., Lee, M., Nadadur, G., & Varma, R. S. (2018). Lignocellulosic biomass transformations via greener oxidative pretreatment processes: Access to energy and value-added chemicals. *Frontiers in Chemistry, 6*, 141. https://doi.org/10.3389/fchem.2018.00141

Dharfizi, A. D. H., Ghani, A. B. A., & Islam, R. (2020). Evaluating Malaysia's fuel diversification strategies 1981–2016. *Energy Policy, 137*, 111083. https://doi.org/10.1016/j.enpol.2019.111083

Ding, D., Zhou, X., You, T., Zhang, X., Zhang, X., & Xu, F. (2018). Exploring the mechanism of high degree of delignification inhibits cellulose conversion efficiency. *Carbohydrate Polymers, 181*, 931–938. https://doi.org/10.1016/j.carbpol.2017.11.057

Dong, C., Chen, J., Guan, R., Li, X., & Xin, Y. (2018). Dual-frequency ultrasound combined with alkali pretreatment of corn stalk for enhanced biogas production. *Renewable Energy, 127*, 444–451. https://doi.org/10.1016/j.renene.2018.03.088

Department of Statistics Malaysia. (DOSM) (2023). *Selected Agricultural Indicators 2023*. https://www.dosm.gov.my/portal-main/publication?search_keyword=selected+Agricultural+indicator&search_month=&search_year=2023

EnerData. (2023, May 12). *Malaysia sets new target to reach 70% of renewables in the power mix by 2050*. https://www.enerdata.net/publications/daily-energy-news/malaysia-sets-new-target-reach-70-renewables-power-mix-2050.html

Energy Commission. (2021). *Malaysia Energy Statistics Handbook 2020*. https://www.st.gov.my/en/contents/files/download/116/Malaysia_Energy_Statistics_Handbook_20201.pdf

Energy Commission. (2023). *Energy Malaysia, Volume 23/2023*. https://www.st.gov.my/contents/files/download/112/Energy_Malaysia_Vol_23.pdf

European Commission. (2016). *Communication from the Commission to the European Parliament and the Council - Clean Energy for All Europeans*.

European Commission. (2023). *Renewable Energy - Recast to 2030 (RED II)*. Joint Research Centre. https://joint-research-centre.ec.europa.eu/welcome-jec-website/reference-regulatory-framework/renewable-energy-recast-2030-red-ii_en

Faizal, M., Ang, W. Y., Amirah, A., & Tan, Y. H. (2019). Energy, economic and environmental impact of sugarcane bagasse in Malaysia. *International Journal of Advanced Science and Research Management, 4*(2), 104–110.

FAOSTAT. (2023,). *Crops and livestock products*. Food and Agriculture Organization of the United Nations. https://www.fao.org/faostat/en/#data/QCL

Fatma, S., Hameed, A., Noman, M., Ahmed, T., Sohail, I., Shahid, M., Tariq, M., & Tabassum, R. (2018). Lignocellulosic biomass: A sustainable bioenergy source for the future. *Protein and Peptide Letters, 25*(2), 148–163. https://doi.org/10.2174/0929866525666180122144504

FGV Holdings Berhad. (2020, October 28). *FGV's biggest renewable energy biogas power plant powers up 15,000 homes in Pahang*. https://www.fgvholdings.com/press_release/fgvs-biggest-renewable-energy-biogas-power-plant-powers-up-15000-homes-in-pahang/

Galván-Arzola, U., Moreno-Medina, C. U., Lucho-Chigo, R., Rodríguez-Rosales, M. D. J., & Valencia-Vázquez, R. (2021). Biochemical methane potential of residual biomass for energy generation. *Environmental Technology, 42*(8), 1165–1178. https://doi.org/10.1080/09593330.2019.1660412

Gonzales, R. R., Sivagurunathan, P., & Kim, S. H. (2016). Effect of severity on dilute acid pretreatment of lignocellulosic biomass and the following hydrogen fermentation. *International Journal of Hydrogen Energy, 41*(46), 21678–21684. https://doi.org/10.1016/j.ijhydene.2016.06.198

González, G., Urrutia, H., Roeckel, M., & Aspé, E. (2005). Protein hydrolysis under anaerobic, saline conditions in presence of acetic acid. *Journal of Chemical Technology & Biotechnology, 80*(2), 151–157. https://doi.org/10.1002/jctb.1165

Gopinathan, M., Kumaran, P., Rahaman, A. A., & Ismail, Z. (2018, October 24-26). *Progress of biogas industry in Malaysia: Cattle manure as potential substrate for biogas production and issues and challenges* [Paper Presentation]. International Conference and Utility Exhibition on Green Energy for Sustainable Development, Phuket, Thailand. https://doi.org/10.23919/ICUE-GESD.2018.8635771

Greenpeace Southeast Asia. (2021, May 7). Maybank committed to achieving net-zero emissions by 2050, a decade later than the world needs. https://www.greenpeace.org/malaysia/press/4275/maybanks-2050-net-zero-emissions-a-decade-too-late/

Green Lagoon Technology Sdn. Bhd., (2023). *Powering waste into profit*. https://glt.my/wp-content/uploads/2023/09/Green-Lagoon-Brochure-2023.pdf

Hamzah, A. F. A., Hamzah, M. H., Mazlan, F. N. A., Man, H. C., Jamali, N. S., & Siajam, S. I. (2020). Anaerobic co-digestion of pineapple wastes with cow dung: Effect of different total solid content on biomethane yield. *Advances in Agricultural and Food Research Journal, 1*(1), 1–12. https://doi.org/10.36877/aafrj.a0000109

Hanafiah, M. M., Ali, M. Y. M., Aziz, N. I. H. A., & John, A. (2017). Biogas production from agrowaste and effluents. *Acta Chemica Malaysia, 1*(1), 13–15. https://doi.org/10.26480/acmy.01.2017.13.15

Harun, H. N. (2021, March 19). PETRONAS leads charge towards net zero carbon emissions. *New Straits Times*. https://www.nst.com.my/news/nation/2021/03/675130/petronas-leads-charge-towards-net-zero-carbon-emissions

Hashemi, S. S., Karimi, K., & Karimi, A. M. (2019). Ethanolic ammonia pretreatment for efficient biogas production from sugarcane bagasse. *Fuel*, *248*, 196–204. https://doi.org/10.1016/j.fuel.2019.03.080

Hernández, C., Alamilla-Ortiz, Z. L., Escalante, A. E., Navarro-Díaz, M., Carrillo-Reyes, J., Moreno-Andrade, I., & Valdez-Vázquez, I. (2019). Heat-shock treatment applied to inocula for H2 production decreases microbial diversities, interspecific interactions, and performance using cellulose as substrate. *International Journal of Hydrogen Energy, 44*(26), 13126–13134. https://doi.org/10.1016/j.ijhydene.2019.03.124

Holechek, J. L., Geli, H. M. E., Sawalhah, M. N., & Valdez, R. (2022). A global assessment: Can renewable energy replace fossil fuels by 2050? *Sustainability, 14*(8), 4792. https://doi.org/10.3390/su14084792

Hossen, M. M., Rahman, A. S., Kabir, A. S., Hasan, M. F., & Ahmed, S. (2016). Systematic assessment of the availability and utilization potential of biomass in Bangladesh. *Renewable and Sustainable Energy Reviews, 67*, 94–105. https://doi.org/10.1016/j.rser.2016.09.008

Hussin, H. & Energy Watch (2021, August 20). *A decade of renewables growth in Malaysia, where do we go from here?* https://www.energywatch.com.my/blog/2021/08/20/a-decade-of-renewables-growth-in-malaysia-where-do-we-go-from-here/

International Energy Agency (IEA). (2022). *Renewables 2022: Analysis and forecast to 2027*. https://iea.blob.core.windows.net/assets/ada7af90-e280-46c4-a577-df2e4fb44254/Renewables2022.pdf

International Energy Agency (IEA). (2023a). *Malaysia - Key energy statistics, 2020*. https://www.iea.org/countries/malaysia

International Energy Agency (IEA). (2023b). *Net zero roadmap: A global pathway to keep the 1.5°C goal in reach.* https://iea.blob.core.windows.net/assets/8ad619b9-17aa-473d-8a2f-4b90846f5c19/NetZeroRoadmap_AGlobalPathwaytoKeepthe1.5CGoalinReach-2023Update.pdf

International Energy Agency (IEA). (2023c). *World energy investment 2023*. https://iea.blob.core.windows.net/assets/8834d3af-af60-4df0-9643-72e2684f7221/WorldEnergyInvestment2023.pdf

International Energy Agency (IEA). (2023d). *World energy outlook 2023*. https://iea.blob.core.windows.net/assets/86ede39e-4436-42d7-ba2a-edf61467e070/WorldEnergyOutlook2023.pdf

International Renewable Energy Agency (IRENA). (2023). *Malaysia energy transition outlook*. https://www.irena.org/-/media/Files/IRENA/Agency/Publication/2023/Mar/IRENA_Malaysia_energy_transition_outlook_2023.pdf

International Trade Administration (ITA). (2022, October 31). *Malaysia - Agricultural sector*. https://www.trade.gov/country-commercial-guides/malaysia-agricultural-sector

Jagtap, S. S., Bedekar, A. A., Liu, J. J., Jin, Y. S., & Rao, C. V. (2019). Production of galactitol from galactose by the oleaginous yeast *Rhodosporidium*

toruloides IFO0880. *Biotechnology for Biofuels, 12*(250), 1–13. https://doi.org/10.1186/s13068-019-1586-5

Jamali, N. S., Jahim, J. M., Mumtaz, T., & Abdul, P. M. (2021). Dark fermentation of palm oil mill effluent by *Caldicellulosiruptor saccharolyticus* immobilized on activated carbon for thermophilic biohydrogen production. *Environmental Technology & Innovation, 22*, 101477. https://doi.org/10.1016/j.eti.2021.101477

Jones, L. E., & Olsson, G. (2017). Solar photovoltaic and wind energy providing water. *Global Challenges, 1*(5), 1–8. https://doi.org/10.1002/gch2.201600022

Kabir, M. M., Rajendran, K., Taherzadeh, M. J., & Horváth, I. S. (2015). Experimental and economical evaluation of bioconversion of forest residues to biogas using organosolv pretreatment. *Bioresource Technology, 178*, 201–208. https://doi.org/10.1016/j.biortech.2014.07.064

Kainthola, J., Kalamdhad, A. S., & Goud, V. V. (2019). A review on enhanced biogas production from anaerobic digestion of lignocellulosic biomass by different enhancement techniques. *Process Biochemistry, 84*, 81–90. https://doi.org/10.1016/j.procbio.2019.05.023

Karimi, K., & Taherzadeh, M. J. (2015). A critical review on analysis in pretreatment of lignocelluloses: Degree of polymerization, adsorption/desorption, and accessibility. *Bioresource Technology, 203*, 348–356. https://doi.org/10.1016/j.biortech.2015.12.035

Karthikeyan, O. P., Trably, E., Mehariya, S., Bernet, N., Wong, J. W. C., & Carrere, H. (2018). Pretreatment of food waste for methane and hydrogen recovery: A review. *Bioresource Technology, 249*, 1025–1039. https://doi.org/10.1016/j.biortech.2017.09.105

Kaur, K., & Phutela, U. G. (2016). Enhancement of paddy straw digestibility and biogas production by sodium hydroxide-microwave pretreatment. *Renewable Energy, 92*, 178–184. https://doi.org/10.1016/j.renene.2016.01.083

Kim, J. S., Lee, Y. Y., & Kim, T. H. (2015). A review on alkaline pretreatment technology for bioconversion of lignocellulosic biomass. *Bioresource Technology, 199*, 42–48. https://doi.org/10.1016/j.biortech.2015.08.085

Knoema. (2021). *Production statistics - Crops, crops processed.* https://knoema.com/atlas/Malaysia/topics/Agriculture/Crops-Production-Quantity-tonnes/Sugar-cane-production

Korbag, I., Omar, S. M. S., Boghazala, H., & Abusasiyah, M. A. A. (2020). Recent advances of biogas production and future perspective. In A. E. F. Abomohra, M. Elsayed, Z. Qin, H. Ji & Z. Liu (Eds.), *Biogas - Recent Advances and Integrated Approaches* (pp. 1–40). IntechOpen. https://doi.org/10.5772/intechopen.93231

Koupaie, E. H., Dahadha, S., Lakeh, A. B., Azizi, A., & Elbeshbishy, E. (2018). Enzymatic pretreatment of lignocellulosic biomass for enhanced biomethane production - A review. *Journal of Environmental Management, 233*, 774–784. https://doi.org/10.1016/j.jenvman.2018.09.106

Kucharska, K., Rybarczyk, P., Hołowacz, I., Łukajtis, R., Glinka, M., & Kamiński, M. (2018). Pretreatment of lignocellulosic materials as substrates for fermentation processes. *Molecules, 23*(11), 2937. https://doi.org/10.3390/molecules23112937

Kumar, A. K., & Sharma, S. (2017). Recent updates on different methods of pretreatment of lignocellulosic feedstocks: A review. *Bioresource and Bioprocessing, 4*(1), 1–19. https://doi.org/10.1186/s40643-017-0137-9

Kumaran, P., Hephzibah, D., Sivasankari, R., Saifuddin, N., & Shamsuddin, A. H. (2015). A review on industrial scale anaerobic digestion systems deployment in Malaysia: Opportunities and challenges. *Renewable and Sustainable Energy Reviews, 56*, 929–940. https://doi.org/10.1016/j.rser.2015.11.069

Lim, J. W., Ge, T., & Tong, Y. W. (2017). Monitoring of microbial communities in anaerobic digestion sludge for biogas optimisation. *Waste Management, 71*, 334–341. https://doi.org/10.1016/j.wasman.2017.10.007

Lim, Y. F., Chan, Y. J., Abakr, Y. A., Sethu, V., Selvarajoo, A., Singh, A., Lee, J., & Gareth, M. (2021). Review of biowastes to energy in Malaysia: Current technology, scalability and socioeconomic analysis. *Clean Energy Technologies, 4*, 100257. https://doi.org/10.1016/j.clet.2021.100257

Lim, Z. W., & Goh, K. L. (2019). Natural gas industry transformation in Peninsular Malaysia: The journey towards a liberalised market. *Energy Policy, 128*, 197–211. https://doi.org/10.1016/j.enpol.2018.12.049

Ling, Z., Chen, S., Zhang, X., & Xu, F. (2016). Exploring crystalline-structural variations of cellulose

during alkaline pretreatment for enhanced enzymatic hydrolysis. *Bioresource Technology, 224*, 611–617. https://doi.org/10.1016/j.biortech.2016.10.064

Liu, Z., Fels, M., Dragone, G., & Mussatto, S. I. (2021). Effects of inhibitory compounds derived from lignocellulosic biomass on the growth of the wild-type and evolved oleaginous yeast *Rhodosporidium toruloides*. *Industrial Crops and Products, 170*, 113799. https://doi.org/10.1016/j.indcrop.2021.113799

Lizasoain, J., Trulea, A., Gittinger, J., Kral, I., Piringer, G., Schedl, A., Nilsen, P. J., Potthast, A., Gronauer, A., & Bauer, A. (2017). Corn stover for biogas production: Effect of steam explosion pretreatment on the gas yields and on the biodegradation kinetics of the primary structural compounds. *Bioresource Technology, 244*, 949–956. https://doi.org/10.1016/j.biortech.2017.08.042

Lo, J. (2020, December 8). *Malaysian bank to phase out coal finance, in a victory for campaigners.* Climate Change News. https://www.climatechangenews.com/2020/12/08/malaysian-bank-phase-coal-finance-victory-campaigners/

Lopes, A. D. C. P., Ebner, C., Gerke, F., Wehner, M., Robra, S., Hupfauf, S., & Bockreis, A. (2021). Residual municipal solid waste as co-substrate at wastewater treatment plants: An assessment of methane yield, dewatering potential and microbial diversity. *Science of The Total Environment, 804*, 149936. https://doi.org/10.1016/j.scitotenv.2021.149936

Lu, X., Zheng, X., Li, X., & Zhao, J. (2016). Adsorption and mechanism of cellulase enzymes onto lignin isolated from corn stover pretreated with liquid hot water. *Biotechnology for Biofuels, 9*(1), 1–12. https://doi.org/10.1186/s13068-016-0531-0

Ma, S., Li, Y., Li, J., Yu, X., Cui, Z., Yuan, X., Zhu, W., & Wang, H. (2022). Features of single and combined technologies for lignocellulose pretreatment to enhance biomethane production. *Renewable and Sustainable Energy Reviews, 165*, 112489. https://doi.org/10.1016/j.rser.2022.112606

Ma, S., Wang, H., Li, J., Fu, Y., & Zhu, W. (2019). Methane production performances of different compositions in lignocellulosic biomass through anaerobic digestion. *Energy, 189*, 116190. https://doi.org/10.1016/j.energy.2019.116190

Magdalena, J. A., Greses, S., & González-Fernández, C. (2019). Impact of organic loading rate in volatile fatty acids production and population dynamics using microalgae biomass as substrate. *Scientific Reports, 9*(1), 18374. https://doi.org/10.1038/s41598-019-54914-4

Mahidin, M. U. (2019, November 29). *Selected agricultural indicators, Malaysia, 2018*. DOSM. https://www.dosm.gov.my/site/downloadrelease?id=selected-agricultural-indicators-malaysia-2018&lang=English&admin_view=

Matheri, A. N., Ntuli, F., Ngila, J. C., Seodigeng, T., Zvinowanda, C., & Njenga, C. K. (2018). Quantitative characterization of carbonaceous and lignocellulosic biomass for anaerobic digestion. *Renewable and Sustainable Energy Reviews, 92*, 9–16. https://doi.org/10.1016/j.rser.2018.04.070

Malaysian Investment Development Authority (MIDA). (2023). *Preparing for the energy transition*. https://www.mida.gov.my/mida-news/preparing-for-the-energy-transition/

Malaysian Palm Oil Board (MPOB). (2020). *Number and capacities of palm oil sectors 2020*. https://bepi.mpob.gov.my/index.php/en/sectoral-status/sectoral-status-2020/number-a-capacities-of-palm-oil-sectors-2020

Malaysian Palm Oil Board (MPOB). (2023a). *OER performance in Malaysia*. https://prestasisawit.mpob.gov.my/en/oer

Malaysian Palm Oil Board (MPOB). (2023b). *Overview of the Malaysian Oil Palm Industry 2022*. https://bepi.mpob.gov.my/images/overview/overview2022.pdf

Malaysian Palm Oil Council (MPOC). (2021). *Malaysian palm oil industry*. https://mpoc.org.my/malaysian-palm-oil-industry/

McNamara, J. T., Morgan, J. L. W., & Zimmer, J. (2015). A molecular description of cellulose biosynthesis. *Annual Review of Biochemistry, 84*, 895–921. https://doi.org/10.1146/annurev-biochem-060614-033930

Meng, X., Parikh, A., Seemala, B., Kumar, R., Pu, Y., Christopher, P., Wyman, C. E., Cai, C. M., & Ragauskas, A. J. (2018). Chemical transformations of poplar lignin during cosolvent enhanced lignocellulosic fractionation process. *ACS Sustainable Chemistry & Engineering, 6*(7), 8711–8718. https://doi.org/10.1021/acssuschemeng.8b01028

Meraj, S., Liaquat, R., Naqvi, S. R., Sheikh, Z., Zainab, A., Khoja, A. H., Juchelkova, D., & Atabani, A. (2021). Enhanced methane production from anaerobic co-digestion of wheat straw, rice straw, and sugarcane bagasse: A kinetic analysis. *Applied Sciences, 11*(13), 6069. https://doi.org/10.3390/app11136069

Ministry of Economy (MoE). (2023). *National Energy Transition Roadmap (NETR) – Energising the nation, powering our future*. https://ekonomi.gov.my/sites/default/files/2023-08/National%20Energy%20Transition%20Roadmap.pdf

Ministry of Science, Technology and Innovation (MOSTI). (2023). *Hydrogen Economy & Technology Roadmap*. https://www.mosti.gov.my/wp-content/uploads/repository/penerbitan/2023/Hidrogen%20Economy%20&%20Technology%20Roadmap.pdf

Mirmohamadsadeghi, S., Karimi, K., Azarbaijani, R., Yeganeh, L. P., Angelidaki, I., Nizami, A. S., Bhat, R., Dashora, K., Vijay, V. K., Aghbashlo, M., Gupta, G. K., & Tabatabaei, M. (2020). Pretreatment of lignocelluloses for enhanced biogas production: A review on influencing mechanisms and the importance of microbial diversity. *Renewable and Sustainable Energy Reviews, 135*, 110173. https://doi.org/10.1016/j.rser.2020.110173

Mong, G. R., Chong, C. T., Ng, J. H., Chong, W. W. F., Lam, S. S., Ong, H. C., & Ani, F. N. (2020). Microwave pyrolysis for valorisation of horse manure biowaste. *Energy Conversion and Management, 220*, 113704. https://doi.org/10.1016/j.enconman.2020.113704

Mussatto, S. I., Yamakawa, C. K., Van Der Maas, L., & Dragone, G. (2021). New trends in bioprocesses for lignocellulosic biomass and CO2 utilization. *Renewable and Sustainable Energy Reviews, 152*, 111620. https://doi.org/10.1016/j.rser.2021.111620

Mustafa, A. M., Poulsen, T. G., Xia, Y., & Sheng, K. (2016). Combinations of fungal and milling pretreatments for enhancing rice straw biogas production during solid-state anaerobic digestion. *Bioresource Technology, 224*, 174–182. https://doi.org/10.1016/j.biortech.2016.11.028

Oh, T. H., Hasanuzzaman, M., Selvaraj, J., Teo, S. C., & Chua, S. C. (2018). Energy policy and alternative energy in Malaysia: Issues and challenges for sustainable growth – An update. *Renewable and Sustainable Energy Reviews, 81*, 3021–3031. https://doi.org/10.1016/j.rser.2017.06.112

Olatunji, K. O., Ahmed, N. A., & Ogunkunle, O. (2021). Optimization of biogas yield from lignocellulosic materials with different pretreatment methods: A review. *Biotechnology for Biofuels and Bioproducts, 14*(1), 1–34. https://doi.org/10.1186/s13068-021-02012-x

Pan, S. Y., Tsai, C. Y., Liu, C. W., Wang, S. W., Kim, H., & Fan, C. (2021a). Anaerobic co-digestion of agricultural wastes toward circular bioeconomy. *iScience, 24*(7), 102704. https://doi.org/10.1016/j.isci.2021.102704

Pan, S., Liu, Q., Wen, C., Li, Z., Du, L., & Wei, Y. (2021b). Producing biogas from rice straw: Kinetic analysis and microbial community dynamics. *BioEnergy Research, 14*, 1338–1348. https://doi.org/10.1007/s12155-020-10226-4

Patel, A., & Shah, A. R. (2021). Integrated lignocellulosic biorefinery: Gateway for production of second generation ethanol and value added products. *Journal of Bioresources and Bioproducts, 6*(2), 108–128. https://doi.org/10.1016/j.jobab.2021.02.001

Pattiya, A. (2018). Fast pyrolysis. In *Direct Thermochemical Liquefaction for Energy Applications* (pp. 3–28). Elsevier. https://doi.org/10.1016/b978-0-08-101029-7.00001-1

Paudel, S. R., Banjara, S. P., Choi, O. K., Park, K. Y., Kim, Y. M., & Lee, J. W. (2017). Pretreatment of agricultural biomass for anaerobic digestion: Current state and challenges. *Bioresource Technology, 245*, 1194–1205. https://doi.org/10.1016/j.biortech.2017.08.182

Pecha, M. B., & Garcia-Perez, M. (2020). Pyrolysis of lignocellulosic biomass: Oil, char, and gas. In *Bioenergy: Biomass to Biofuels and Waste to Energy* (pp. 581–619). Elsevier. https://doi.org/10.1016/b978-0-12-815497-7.00029-4

Pera, A. Le, Sellaro, M., Migliori, M., Bianco, M., & Zanardi, G. (2021). Dry mesophilic anaerobic digestion of separately collected organic fraction of municipal solid waste: Two-year experience in an industrial-scale plant. *Processes, 9*(2), 1–14. https://doi.org/10.3390/pr9020213

Pérez-Almada, D., Galán-Martín, Á., Der Mar Contreras, M., & Castro, E. (2023). Integrated techno-economic and environmental assessment of biorefineries: Review and future research directions. *Sustainable Energy & Fuels, 7*(17), 4031–4050. https://doi.org/10.1039/d3se00405h

Phuttaro, C., Sawatdeenarunat, C., Surendra, K. C., Boonsawang, P., Chaiprapat, S., & Khanal, S. K. (2019). Anaerobic digestion of hydrothermally-pretreated lignocellulosic biomass: Influence of pretreatment temperatures, inhibitors, and soluble organics on methane yield. *Bioresource Technology, 284*, 128–138. https://doi.org/10.1016/j.biortech.2019.03.114

Preethi, Gunasekaran, M., & Banu, J. R. (2023). Indexing energy and cost of the pretreatment for economically efficient bioenergy generation. *Frontiers in Energy Research, 10*, 1–19. https://doi.org/10.3389/fenrg.2022.1060599

Rahman, K. H. A., Yusof, S. J. H. M., & Ismail, K. S. K. (2022). Renewable energy: The past and the future. In *Green Energy and Technology* (pp. 213–234). Springer. https://doi.org/10.1007/978-981-16-9314-4_10

Rashidi, N. A., Chai, Y. H., & Yusup, S. (2022). Biomass energy in Malaysia: Current scenario, policies, and implementation challenges. *Bioenergy Research, 15*(3), 1371–1386. https://doi.org/10.1007/s12155-022-10392-7

Rezania, S., Oryani, B., Cho, J., Sabbagh, F., Rupani, P. F., Talaiekhozani, A., Rahimi, N., & Ghahroud, M. L. (2020). Technical aspects of biofuel production from different sources in Malaysia - A review. *Processes, 8*(8), 993. https://doi.org/10.3390/pr8080993

Riya, S., Meng, L., Wang, Y., Lee, G., Zhou, S., Toyota, K., & Hosomi, M. (2020). Dry anaerobic digestion for agricultural waste recycling. In A. E-F. Abomohra, M. lsayed, Z. Qin, H. Ji, & Z. Liu (Eds.), *Biogas: Recent Advances and Integrated Approaches* (pp. 1–21). IntechOpen. https://doi.org/10.5772/intechopen.91229

Saelor, S., Kongjan, P., & O-Thong, S. (2017). Biogas production from anaerobic co-digestion of palm oil mill effluent and empty fruit bunches. *Energy Procedia, 138, 717–722*. https://doi.org/10.1016/j.egypro.2017.10.206

Safarian, S., & Unnthorsson, R. (2018). An assessment of the sustainability of lignocellulosic bioethanol production from wastes in Iceland. *Energies, 11(6)*, 1493. https://doi.org/10.3390/en11061493

Sahabat Alam Malaysia. (2020, November 11). *Statistical data on forested and conservation areas in Malaysia*. https://foe-malaysia.org/articles/statistical-data-on-forested-and-conservation-areas-in-malaysia-2/

Saini, J. K., Patel, A. K., Adsul, M., & Singhania, R. R. (2016). Cellulase adsorption on lignin: A roadblock for economic hydrolysis of biomass. *Renewable Energy, 98*, 29–42. https://doi.org/10.1016/j.renene.2016.03.089

Sarangi, P. K., Singh, A. K., Srivastava, R. K., & Gupta, V. K. (2023). Recent progress and future perspectives for zero agriculture waste technologies: Pineapple waste as a case study. *Sustainability, 15*(4), 3575. https://doi.org/10.3390/su15043575

Scarlat, N., Dallemand, J. F., & Fahl, F. (2018). Biogas: Developments and perspectives in Europe. *Renewable Energy, 129*, 457–472. https://doi.org/10.1016/j.renene.2018.03.006

Sustainable Energy Development Authority (SEDA). (2014). *Annual report 2014 – SEDA Malaysia*. http://www.seda.gov.my/pdfdownload/annual-report-2014/

Sustainable Energy Development Authority (SEDA). (2021a). *Malaysia renewable energy roadmap: Pathway towards low carbon energy system*. https://www.seda.gov.my/reportal/wp-content/uploads/2021/12/MyRER_webVer-1.pdf

Sustainable Energy Development Authority (SEDA). (2021b). *Leading the nation towards sustainable energy energy* (pp. 6–13). https://www.seda.gov.my/wp-content/uploads/2021/12/Vol5_Issue13.pdf

Sharma, H. K., Xu, C., & Qin, W. (2017). Biological pretreatment of lignocellulosic biomass for biofuels and bioproducts: An overview. *Waste and Biomass Valorization, 10*(2), 235–251. https://doi.org/10.1007/s12649-017-0059-y

Sharma, S., Tsai, M. L., Sharma, V., Sun, P. P., Nargotra, P., Bajaj, B. K., Chen, C. W., & Dong, C. Di. (2023). Environment friendly pretreatment approaches for the bioconversion of lignocellulosic biomass into biofuels and value-added products. *Environmental, 10*(1), 1–25. https://doi.org/10.3390/environments10010006

Soam, S., Kapoor, M., Kumar, R., Gupta, R. P., Puri, S. K., & Ramakumar, S. S. V. (2018). Life cycle assessment and life cycle costing of conventional and modified dilute acid pretreatment for fuel ethanol production from rice straw in India. *Journal of Cleaner Production, 197*, 732–741. https://doi.org/10.1016/j.jclepro.2018.06.204

Soares, J. F., Confortin, T. C., Todero, I., Mayer, F. D., & Mazutti, M. A. (2019). Dark fermentative

biohydrogen production from lignocellulosic biomass: Technological challenges and future prospects. *Renewable and Sustainable Energy Reviews, 117*, 109484. https://doi.org/10.1016/j.rser.2019.109484

Sorn, V., Chang, K. L., Phitsuwan, P., Ratanakhanokchai, K., & Dong, C. D. (2019). Effect of microwave-assisted ionic liquid/acidic ionic liquid pretreatment on the morphology, structure, and enhanced delignification of rice straw. *Bioresource Technology, 293*, 121929. https://doi.org/10.1016/j.biortech.2019.121929

Su, G., Zulkifli, N. W. M., Ong, H. C., Ibrahim, S., Bu, Q., & Zhu, R. (2022). Pyrolysis of oil palm wastes for bioenergy in Malaysia: A review. *Renewable and Sustainable Energy Reviews, 164*, 112554. https://doi.org/10.1016/j.rser.2022.112554

Sun, Q., Chen, W. J., Pang, B., Sun, Z., Lam, S. S., Sonne, C., & Yuan, T. Q. (2021). Ultrastructural change in lignocellulosic biomass during hydrothermal pretreatment. *Bioresource Technology, 341*, 125807. https://doi.org/10.1016/j.biortech.2021.125807

Tan, S. T., Ho, W. S., Hashim, H., Lee, C. T., Taib, M. R., & Ho, C. S. (2015). Energy, economic and environmental (3E) analysis of waste-to-energy (WTE) strategies for municipal solid waste (MSW) management in Malaysia. *Energy Conversion and Management, 102*, 111–120. https://doi.org/10.1016/j.enconman.2015.02.010

Thomsen, S. T., Spliid, H., & Østergård, H. (2013). Statistical prediction of biomethane potentials based on the composition of lignocellulosic biomass. *Bioresource Technology, 154*, 80–86. https://doi.org/10.1016/j.biortech.2013.12.029

Tiwari, A., Chen, C. W., Haldar, D., Patel, A. K., Dong, C. Di, & Singhania, R. R. (2023). Laccase in biorefinery of lignocellulosic biomass. *Applied Sciences, 13*(8), 4673. https://doi.org/10.3390/app13084673

Triolo, J. M., Pedersen, L., Qu, H., & Sommer, S. G. (2012). Biochemical methane potential and anaerobic biodegradability of non-herbaceous and herbaceous phytomass in biogas production. *Bioresource Technology, 125*, 226–232. https://doi.org/10.1016/j.biortech.2012.08.079

Tu, W. C., & Hallett, J. P. (2019). Recent advances in the pretreatment of lignocellulosic biomass. *Current Opinion in Green and Sustainable Chemistry, 20*, 11–17. https://doi.org/10.1016/j.cogsc.2019.07.004

U.S. Energy Information Administration. (2020). *Biomass and the environment*. https://www.eia.gov/energyexplained/biomass/biomass-and-the-environment.php

Vivekanand, V., Olsen, E. F., Eijsink, V. G. H., & Horn, S. J. (2014). Methane potential and enzymatic saccharification of steam-exploded bagasse. *BioResources, 9*(1), 1311–1324. https://doi.org/10.15376/biores.9.1.1311-1324

Wadchasit, P., Siripattana, C., & Nuithitikul, K. (2020). The effect of pretreatment methods for improved biogas production from oil-palm empty fruit bunches (EFB): Experimental and model. *IOP Conference Series: Earth and Environmental Science, 463*, 012126. https://doi.org/10.1088/1755-1315/463/1/012126

Weide, T., Baquero, C. D., Schomaker, M., Brügging, E., & Wetter, C. (2020). Effects of enzyme addition on biogas and methane yields in the batch anaerobic digestion of agricultural waste (silage, straw, and animal manure). *Biomass and Bioenergy, 132*, 105442. https://doi.org/10.1016/j.biombioe.2019.105442

Wu, Q., Qiang, T. C., Zeng, G., Zhang, H., Huang, Y., & Wang, Y. (2017). Sustainable and renewable energy from biomass wastes in palm oil industry: A case study in Malaysia. *International Journal of Hydrogen Energy, 42*(37), 23871–23877. https://doi.org/10.1016/j.ijhydene.2017.03.147

Xu, N., Liu, S., Xin, F., Zhou, J., Jia, H., Xu, J., Jiang, M., & Dong, W. (2019). Biomethane production from lignocellulose: Biomass recalcitrance and its impacts on anaerobic digestion. *Frontiers in Bioengineering and Biotechnology, 7*, 1–12. https://doi.org/10.3389/fbioe.2019.00191

Xue, S., Song, J., Wang, X., Shang, Z., Sheng, C., Li, C., Zhu, Y., & Liu, J. (2019). A systematic comparison of biogas development and related policies between China and Europe and corresponding insights. *Renewable and Sustainable Energy Reviews, 117*, 109474. https://doi.org/10.1016/j.rser.2019.109474

Yatim, P., Lin, N. S., Lam, H. L., & Choy, E. A. (2017). Overview of the key risks in the pioneering stage of the Malaysian biomass industry. *Clean Technologies and Environmental Policy, 19*(7), 1825–1839. https://doi.org/10.1007/s10098-017-1369-2

Yogalakshmi, K. N., Poornima Devi, T., Sivashanmugam, P., Kavitha, S., Yukesh Kannah, R., Varjani, S., AdishKumar, S., Gopalakrishnan,

K., & Rajesh Banu, J. (2022). Lignocellulosic biomass-based pyrolysis: A comprehensive review. *Chemosphere, 286*, 131824. https://doi.org/10.1016/j.chemosphere.2021.131824

Zafar, S. (2022). *Bioenergy developments in Malaysia.* Bionergy Consult. https://www.bioenergyconsult.com/bioenergy-developments-malaysia/

Zain, M. M., & Mohamed, A. R. (2018). An overview on conversion technologies to produce value added products from CH_4 and CO_2 as major biogas constituents. *Renewable and Sustainable Energy Reviews, 98*, 56–63. https://doi.org/10.1016/j.rser.2018.09.003

Zhang, L., Loh, K. C., & Zhang, J. (2018). Enhanced biogas production from anaerobic digestion of solid organic wastes: Current status and prospects. *Bioresource Technology Reports, 5*, 280–296. https://doi.org/10.1016/j.biteb.2018.07.005

Zhang, S., Wang, Y., & Liu, S. (2020). Process optimization for the anaerobic digestion of poplar (*Populus L.*) leaves. *Bioengineered, 11*(1), 439–448. https://doi.org/10.1080/21655979.2020.1739823

Zhu, J. Y., & Pan, X. (2022). Efficient sugar production from plant biomass: Current status, challenges, and future directions. *Renewable and Sustainable Energy Reviews, 164*, 112583. https://doi.org/10.1016/j.rser.2022.112583

Zoghlami, A., & Paës, G. (2019). Lignocellulosic biomass: Understanding recalcitrance and predicting hydrolysis. *Frontiers in Chemistry, 7*(874), 1–11. https://doi.org/10.3389/fchem.2019.00874

Zulkifli, Z. (2021). Malaysia country report. In P. Han & S. Kimura (Eds.), *Energy Outlook and Energy Saving Potential in East Asia 2020* (pp. 170–190). ERIA. https://www.eria.org/uploads/media/Books/2021-Energy-Outlook-and-Saving-Potential-East-Asia-2020/18_Ch.11-Malaysia.pdf

Zulkifli, A. A., Yusoff, M. Z. M., Manaf, L. A., Zakaria, M. R., Roslan, A. M., Ariffin, H., Shirai, Y., & Hassan, M. A. (2019). Assessment of municipal solid waste generation in Universiti Putra Malaysia and its potential for green energy production. *Sustainability, 11*(14), 3909. https://doi.org/10.3390/su11143909

RESEARCH ARTICLES

Journal of Oil Palm Research Vol. 37 (1) March 2025 p. 44-52
DOI: https://doi.org/10.21894/jopr.2023.0061

SPECIES COMPOSITION OF BIRDS IN OIL PALM AREAS, NORTHERN SARAWAK, BORNEO, MALAYSIA

BETTYCOPA AMIT[1]*; ANGIE SAPIS[1] and NIK SASHA KHATRINA KHAIRUDDIN[1]

ABSTRACT

Birds play an important role in the ecosystem. However, the species composition of birds in oil palm areas and their roles in balancing the ecosystem are still minimally understood. Hence, this study was carried out to investigate them. A study on bird species composition using the point count method in oil palm areas was conducted at three oil palm estates located in Northern Sarawak, Malaysia. A total of 72 bird species belonging to 30 families including one vulnerable and six near-threatened species have been recorded from 123 points. Bird species richness was the highest in Sebungan and Sabaju Estates and the lowest in Taniku Estate. Twenty-six out of 72 species of birds were common to these three different oil palm estates. Seven species consisting of Oriental Magpie Robin, Long-tailed Parakeet, Yellow-vented Bulbul, Greater Coucal, White-breasted Waterhen, Spotted Dove, and Malaysian Pied Fantail were the dominant species recorded in all estates. Ardeidae, Cuculidae, Nectariidae and Cisticolidae were the most diverse bird families in oil palm areas. Knowledge of bird species composition in oil palm areas could provide a better understanding of their importance towards bioindicator species to the ecosystem and the conservation actions to be taken.

Keywords: bioindicator, bird, dominant species, oil palm, species composition.

Received: 14 June 2023; **Accepted:** 24 September 2023; **Published online:** 29 November 2023.

INTRODUCTION

Agriculture development has impacts on biological diversity (Karp *et al.*, 2012), especially for birds that suffer significant global declines due to agricultural progress (Azhar *et al.*, 2011). Managing the agricultural area to reduce negative impacts on bird populations requires a better understanding of the species that inhabit certain agricultural area. Apparently, their implications towards agricultural production, primarily through ecosystem functions which are supposed to benefit humans in terms of pollination, biological pest control, disposal of waste, and cycling of nutrients and birds, have negative impacts on agricultural production (Sekercioglu, 2006; Triplett *et al.*, 2012; Wenny *et al.*, 2011; Whelan *et al.*, 2008). Conservation-production interactions have complex implications in agricultural areas. Therefore, changing management strategies may support the diversity of bird species for the benefit of growers and bird conservation (Luck *et al.*, 2015).

As reported, 26.1% of the land in Malaysia was devoted to agricultural production in 2018 (The World Bank, 2022). In 2021, 5.74 million hectares of land in Malaysia has been developed for oil palm agricultural production [Malaysian Palm Oil Board (MPOB), 2022]. The Malaysian palm oil industry remains committed to producing sustainable palm oil by ensuring a balance between oil palm development, as well as preserving and conserving biodiversity. In order to develop more sustainable oil palm agriculture practices, Malaysia has implemented the Malaysian Sustainable Palm Oil Certification (MSPO) schemes to sustain the production of the Malaysian palm oil supply chain for global market consumption.

Birds are known as bioindicators and act as ecosystem functioning and balancing agents (Kiros *et al.*, 2018; Lim & Mojiol, 2019; Sekercioglu *et al.*, 2016). They are the key groups in earth's

[1] Malaysian Palm Oil Board,
6, Persiaran Institusi, Bandar Baru Bangi,
43000 Kajang, Selangor, Malaysia.

* *Corresponding author e-mail: bettycopa@mpob.gov.my*

biodiversity components (Hasmat *et al.*, 2020) which play important roles as agents of nutrient cycles, pollinators, seed dispersal and control population of their prey (Sekercioglu *et al.*, 2016). There are several factors that influence the composition and distribution of birds in an area such as habitat complexity, foraging site Brickle, nest-site selection or breeding site and shelter (Bradbury *et al.*, 2000; Soderstrom & Part, 2000). Bird assessment is an important tool for biodiversity identification so that subsequent conservation actions can be taken (Amit *et al.*, 2015). Therefore, this study was instituted to assess and understand the bird species composition in oil palm areas located in Bintulu and Miri, Sarawak, Malaysia.

MATERIALS AND METHODS

Study Sites

This study was conducted in three oil palm estates comprising Taniku oil palm estate (TANE) with 5,026 ha in Miri, Sarawak (4°23′44.64″N, 114°06′58.05″E), Tinbarap oil palm estate (TINE) with 13 396 ha in Miri, Sarawak (4°04′11.68″N, 114°15′08.37″E), and Sebungan and Sabaju oil palm estates (SSE) with 9683 ha in Bintulu, Sarawak (3°11′47.99″N, 113°28′11.17″E). The study sites are shown in *Figure 1*, located in Northern Sarawak, Malaysia. These estates have been in operation for approximately 4-21 years and are mostly of peat land area. SSE and TINE have a large-scale peat swamp forest patch (TINE: >200 ha, SSE: >300 ha) in their estates for conservation purposes and some parts of their estates are surrounded by forest. TANE has a small forest patch and is mostly surrounded by other oil palm estates. The summary of the sampling estates is in *Table 1*.

Data Collection

The bird sampling was conducted using the point count method. A total of 123 points (TINE: 56 points, SSE: 44 points, TANE: 23 points) were established and randomly sampled in this study. The sampling was conducted one time for each point. Each point was at least 500 m apart from the other. The sampling was done for 15 min for each point. The detected species and the number of individuals through sighting and sound were recorded. The sound of birds was recorded using an Olympus LS-P4 for further identification. The sampling was conducted in the morning between 06:30 and 10:30.

Data Analysis

Relative abundance was used to determine the percentage of each bird species in each area by dividing the number of species. The relative



Figure 1. Location of three oil palm estates in Northern Sarawak, Malaysia.

TABLE 1. SUMMARY OF THE ESTATES

Estates	Size of the estate (ha)	Number of sampling points	Forest patches within oil palm landscape (ha)	Range of palm age (years old)
TANE	5,026	23	-	10-21
TINE	13,396	56	>200	10-13
SSE	9,683	44	>300	4-13

abundance was calculated from the percentage ratio of individual numbers of a species, divided by the total individual numbers recorded in that area. Species diversity was used to determine the diversity of bird species in each area. Species diversity (*H'*) was calculated using the Shannon-Weiner index (Magurran, 1988). Species richness was calculated using Margalef's Richness Index (R_1) to determine the richness of the birds' species in each area. Species evenness was calculated using Pielou's Evenness Index (E') to determine the evenness of the species distribution of the bird in each area.

RESULTS AND DISCUSSION

Bird Species and Their Conservation Status in Oil Palm Areas

This study recorded 2,621 birds belonged to 72 species and 30 families found from three oil palm estates (*Table 2*), representing 10.7% of the total species of birds (673 species) reported in Borneo Island (Phillipps & Phillipps, 2014). Data analysis as presented in *Table 3* showed that the species distribution was more evenly distributed (Pielou's Evenness Index). Shannon-Weiner Diversity Index indicated bird species have the highest diversity in TANE than SSE and TINE even though both estates showed the richest bird species (Margalef's Richness Index). The high richness of bird species in SSE and TINE is attributed to the presence of forest patches within their oil palm estates and the adjacent forest areas. This finding is similar to the previous studies by Amir *et al.* (2015) and Yaap *et al.* (2010) which mentioned that the retention of forests promotes the biodiversity patches within or around oil palm estates.

Several species listed as threatened under international status, and protected under local conservation status, have been recorded in this study. Under the International Union for Conservation of Nature and Nature Resources (IUCN) Red List of Threatened Species, one Vulnerable (Long-tailed Parakeet) and six near-threatened species (Green Imperial Pigeon, Fluffy-backed tit-babbler, Chestnut-winged Babbler, Black-throated Babbler, Black Hornbill and Green Iora) were recorded in this study (IUCN, 2022). Some noteworthy bird species that are protected under Sarawak Wildlife Protection Ordinance (SWLPO), 1998 were also recorded [The Commissioner of Law Revision Sarawak, (2008)]. These species included three totally protected (Cattle Egret, Green Imperial Pigeon, Black Hornbill) and 16 protected species (Little Egret, Intermediate Egret, Great Egret, Cinnamon Bittern, Yellow Bittern, Striated Heron, Purple Heron, Blue-eared Kingfisher, Stork-billed Kingfisher, Oriental Dwarf Kingfisher, White-breasted Kingfisher, Hill Myna, White-throated Needletail, Long-tailed Parakeet, Grey-and-buff Woodpecker, Black-thighed Falconet) were recorded in this study (*Table 2*). Dusky Munia which primarily feeds on grass seeds, seeds of weeds, and insects and endemic species in Borneo Island was also recorded in this study. Additionally, previous studies also reported the sightings of threatened and endemic species in oil palm estates (Amit *et al.*, 2015; 2021). Identification of bird species especially the endemic species is important in order to estimate the biodiversity conservation status in oil palm estates so that the conservation action plan can be taken to protect these important species from threat.

Bird Species Composition and Ecosystem Values in Oil Palm Areas

Birds are important bioindicators in ecosystems. Type of habitat complexity, food availability, shelter and breeding areas are the important factors that influence the bird's occurrence in an ecosystem for the viability of their population (Soderstrom & Part, 2000). Assessing the bird composition in the oil palm ecosystem is important to identify the biodiversity values and to understand the bird's role in balancing the ecosystems. This study divided the bird species composition according to bird families recorded at each oil palm estate (*Figure 2*). A total of 30 families have been recorded in this study. Overall, a good representation of Ardeidae, Nectariidae, Cuculidae and Columbidae were recorded in oil palm areas.

The most diverse species recorded in this study was the family Ardeidae. TINE recorded seven species, followed by SSE with five species and TANE with three species. The occurrence of the most diverse bird family Ardeidae (bitterns, egrets, heron) in this study with eight species is linked to the presence of aquatic habitats such as water drainage systems in oil

TABLE 2. RELATIVE ABUNDANCE OF BIRD SPECIES AT THREE OIL PALM ESTATES AND THEIR CONSERVATION STATUS UNDER IUCN RED LIST OF THREATENED SPECIES AND SWLPO, 1998

Family	Common species	Scientific name	IUCN	SWLPO	Relative abundance (%)		
					SSE	TINE	TANE
Ardeidae	Little Egret	*Egretta garzetta*	LC	P	0.90	0.15	
	Intermediate Egret	*Ardea intermedia*	LC	P	0.77	0.38	0.56
	Cattle Egret	*Bubulcus ibis*	LC	TP		0.08	
	Great Egret	*Ardea alba*	LC	P		0.08	
	Cinnamon Bittern	*Ixobrychus cinnamomeus*	LC	P	0.51	0.69	1.31
	Yellow Bittern	*Ixobrychus sinensis*	LC	P	0.64	0.31	1.69
	Striated Heron	*Butorides striata*	LC	P	0.26	0.15	
	Purple Heron	*Ardea purpurea*	LC	P			0.19
Nectariidae	Purple-naped Sunbird	*Kurochkinegramma hypogrammica*	LC		0.26		0.56
	Plain Sunbird	*Anthreptes simplex*	LC		1.28	0.54	1.31
	Brown-throated Sunbird	*Anthreptes malacensis*	LC		2.30	2.22	3.75
	Ruby-cheeked Sunbird	*Chalcoparia singalensis*	LC				0.75
	Crimson Sunbird	*Aethopyga siparaja*	LC				0.19
	Little Spiderhunter	*Arachnothera longirostra*	LC		0.51		0.38
	Olive-backed Sunbird	*Cinnyris jugularis*	LC			0.08	
Columbidae	Spotted Dove	*Streptopelia chinensis*	LC		6.91	7.65	6.00
	Zebra Dove	*Geopelia striata*	LC			0.61	
	Grey-capped Emerald Dove	*Chalcophaps indica*	LC		0.13		
	Green Imperial Pigeon	*Ducula aenea*	NT	TP	0.13		
	Pink-necked Green Pigeon	*Treron vernans*	LC		2.43	0.31	6.00
Cuculidae	Plaintive Cuckoo	*Cacomantis merulinus*	LC		0.90	0.84	1.13
	Greater Coucal	*Centropus sinensis*	LC		8.45	6.89	6.57
	Lesser Coucal	*Centropus bengalensis*	LC		1.28	0.23	1.69
	Chestnut-bellied Malkoha	*Phaenicophaeus sumatranus*	LC		0.13	0.54	
	Chestnut-breasted Malkoha	*Phaenicophaeus curvirostris*	LC		0.13		
Timaliidae	Bold-striped Tit-babbler	*Macronus bornensis*	LC		6.40	2.37	2.25
	Fluffy-backed Tit-babbler	*Macronus ptilosus*	NT		0.38		
	Chestnut-winged Babbler	*Stachyris erythroptera*	NT		0.90	0.15	0.38
	Black-throated Babbler	*Stachyris nigricollis*	NT			0.23	
Cisticolidae	Yellow-bellied Prinia	*Prinia flaviventris*	LC		5.38	2.60	4.13
	Ashy Tailorbird	*Orthotomus ruficeps*	LC		0.77	1.68	1.69
	Dark-necked Tailorbird	*Orthotomus atrogularis*	LC		0.13	0.23	
	Rufous-tailed Tailorbird	*Orthotomus sericeus*	LC		1.28	1.68	3.19
Alcedinidae	Blue-eared Kingfisher	*Alcedo meninting*	LC	P	0.13		
	Stork-billed Kingfisher	*Pelargopsis capensis*	LC	P	0.64		0.19
	Oriental Dwarf Kingfisher	*Ceyx erithaca*	LC	P	0.13		
	White-breasted Kingfisher	*Halcyon smyrnensis*	LC	P		0.08	2.63
Pycnonotidae	Yellow-vented Bulbul	*Pycnonotus simplex*	LC		10.63	13.54	7.69
	Olive-winged Bulbul	*Pycnonotus plumosus*	LC		1.92	0.99	2.44
	Asian Red-eyed Bulbul	*Pycnonotus brunneus*	LC			0.08	0.38
Sturnidae	Asian Glossy Starling	*Aplonis panayensis*	LC		1.28	1.99	3.75
	Hill Myna	*Gracula religiosa*	LC	P	1.02	0.15	2.63
	Common Myna	*Acridotheres tristis*	LC				0.38
Accipitridae	Black-shouldered Kite	*Elanus axillaris*	LC		0.51	0.15	
	Crested Serpent Eagle	*Spilornis cheela*	LC		0.77	0.15	0.56
	Changeable Hawk-eagle	*Nisaetus cirrhatus*	LC			0.08	
Dicaeidae	Yellow-rumped Flowerpecker	*Prionochilus xanthopygius*	LC		0.13		
	Orange-bellied Flowerpecker	*Dicaeum trigonostigma*	LC		0.13		
	Yellow-breasted Flowerpecker	*Prionochilus maculatus*	LC			0.08	

TABLE 2. RELATIVE ABUNDANCE OF BIRD SPECIES AT THREE OIL PALM ESTATES AND THEIR CONSERVATION STATUS UNDER IUCN RED LIST OF THREATENED SPECIES AND SWLPO, 1998 (continued)

Family	Common species	Scientific name	IUCN	SWLPO	Relative abundance (%)		
					SSE	TINE	TANE
Hirundinidae	Pacific Swallow	*Hirundo tahitica*	LC		0.13	0.84	3.56
	Barn Swallow	*Hirundo rustica*	LC			2.60	
Estrildidae	Dusky Munia	*Lonchura fuscans*	LC		0.90	0.23	
	Chestnut Munia	*Lonchura atricapilla*	LC			2.68	4.69
Corvidae	Large-billed Crow	*Corvus macrorhynchos*	LC		0.13	0.15	
	Slender-billed Crow	*Corvus enca*	LC				0.19
Aegithinaidae	Green Iora	*Aegithina viridissima*	NT		0.26		
	Common Iora	*Aegithina tiphia*	LC			0.23	
Rallidae	White-breasted Waterhen	*Amaurornis phoenicurus*	LC		6.66	6.35	10.13
Musicapidae	Oriental Magpie-robin	*Copsychus saularis*	LC		11.52	16.83	9.57
Rhipiduridae	Malaysian Pied Fantail	*Rhipidura javanica*	LC		5.51	3.83	2.81
Scolopacidae	Common Sandpiper	*Actitis hypoleucos*	LC		0.13	0.38	
Apodidae	White-throated Needletail	*Hirundapus caudacutus*	LC	P			0.38
Psittaculidae	Long-tailed Parakeet	*Psittacula longicauda*	VUL	P	13.06	16.99	2.63
Laniidae	Long-tailed Shrike	*Lanius schach*	LC		0.13	0.54	
Bucerotidae	Black Hornbill	*Anthracoceros malayanus*	NT	TP	0.13		0.38
Megalaimidae	Blue-eared Barbet	*Psilopogon cyanotis*	LC		0.26		
Passeridae	Eurasian Tree Sparrow	*Passer montanus*	LC		0.51	0.15	
Meropidae	Blue-throated Bee-eater	*Merops viridis*	LC		0.13	0.15	0.75
Picidae	Grey-and-buff Woodpecker	*Hemicircus concretus*	LC	P	0.13		
Artamidae	White-breasted Woodswallow	*Artamus leucorynchus*	LC				0.38
Coraciidae	Oriental Dollarbird	*Eurystomus orientalis*	LC				0.19
Falconidae	Black-thighed Falconet	*Microhierax fringillarius*	LC	P		0.08	

Note: SSE - Sebungan and Sabaju Estate; TINE - Tinbarap Estate; TANE - Taniku Estate; LC - Least Concern; NT - Near Threatened; VUL - Vulnerable; TP - Totally Protected; P - Protected.

TABLE 3. DIVERSITY INDICES FOR THE THREE OIL PALM ESTATES

Data analysis	SSE	TINE	TANE
Shannon-Wiener diversity index, H'	3.02	2.785	3.22
Margalef's richness index, R1	7.51	6.69	6.37
Pielou's evenness index, E	0.40	0.33	0.61

Note: SSE - Sebungan and Sabaju Estate; TINE - Tinbarap Estate; TANE - Taniku Estate.

palm planted on peat land that offer foraging areas for waterbirds. Drainage systems play a significant role in managing water levels in oil palm plantations established in peat land areas for flood-control management systems (Hasnol *et al.*, 2010). According to Azhar *et al.* (2013) the waterbird biodiversity conservation highlights another aspect of these drainage systems. This study stated that properly managed drainage systems can create diverse aquatic habitats that attract various waterbird species. These species are normally observed as solitary or in groups in the drainage system searching for food. Species such as Intermediate Egrets together with Little Egrets have been observed to follow excavators during the maintenance of the drainage system in oil palm estates while searching for food.

Family Nectariidae (sunbirds and spiderhunters) was the second diverse bird family recorded in this study with seven species. Six species were recorded in TANE, SSE four species and TINE three species. The presence of these species might be attributed to the flowering plants, such as native and beneficial flowering plants in oil palm areas. Sunbirds and spiderhunters are nectar feeder specialists which

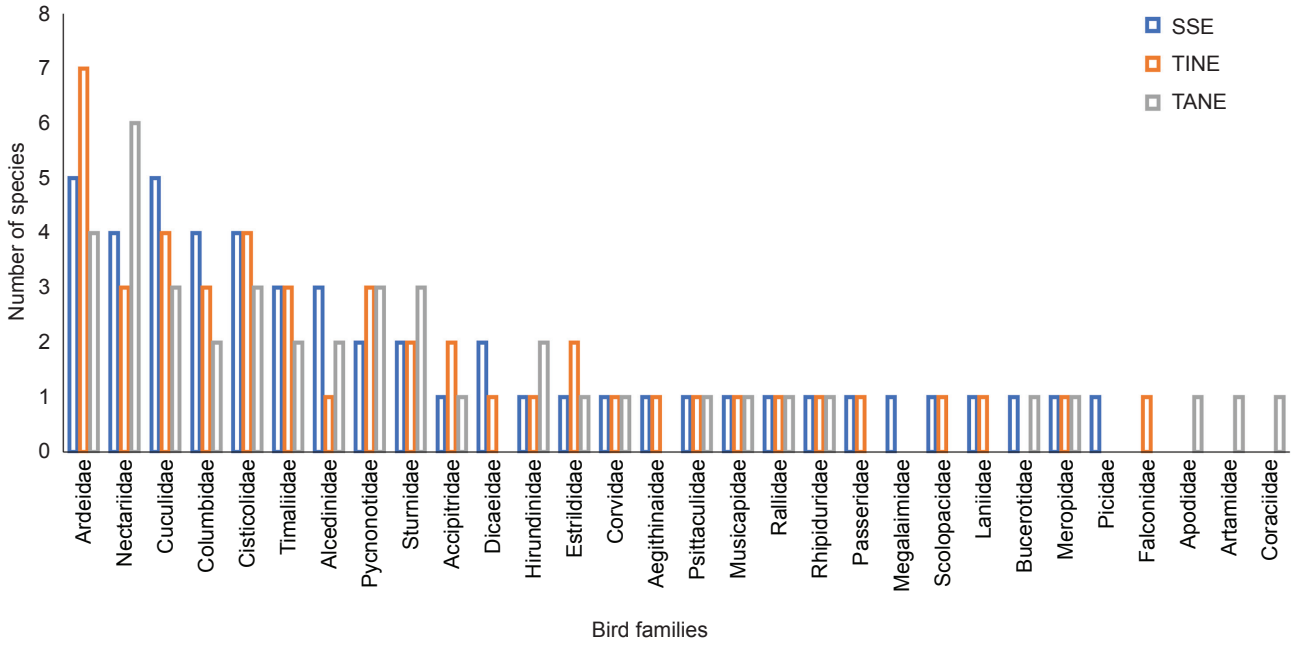


Figure 2. Bird species composition is divided according to bird families recorded at each oil palm estate.

also feed on insects and small berries. These species play an important role as flower pollinator agents in the ecosystems besides bees, insects, bats, and squirrels (Phillipps & Phillips, 2014). Two common sunbirds were recorded in oil palm areas namely, Plain Sunbird and Brown-throated Sunbird. Species such as Olive-backed Sunbird, Brown-throated Sunbird and Little Spiderhunter are normally found in gardens, cultivated or open areas, while the other sunbirds are birds of forest (Phillipps & Phillipps, 2014). Olive-backed Sunbird has been spotted visiting flowers of beneficial plants like *Turnera subulate* in the oil palm estate. These findings showed the importance of flowering plants in supporting and conserving nectar feeders and bird species like sunbirds and spiderhunters in oil palm areas. Other studies also recorded these species in oil palm areas (Amit *et al*., 2021; Hawa *et al*., 2016; Jambari *et al*., 2012; Mohd-Azlan *et al*., 2019).

Family Cuculidae (Cuckoo, Coucals and Malkohas) is the third most diverse family in this study with five species. Five species were found in SSE, TINE with four species and TANE with three species. This family feeds on insects, small vertebrates and fruits (Myers, 2009). Three common cuculid species recorded in oil palm areas were Plaintive Cuckoo, Lesser Coucal and Greater Coucal. Family Columbidae (doves, pigeons) with five species were recorded in this study. SSE recorded four species followed by TINE with three species and TANE with two species. Two species commonly recorded in oil palm areas were Spotted Dove and Pink-necked Pigeon. Myers (2009) mentioned that dove species prefer to feed on grains and seeds, while pigeon feeds on fruits. Pink-necked Pigeon has been observed to feed on *Melastoma* fruits (a native plant) in oil palm areas and this finding is similar to the study by Myers (2009).

Dominant Bird Species and Its Ecosystem Function in Oil Palm Areas

Twenty six out of 72 total species recorded in this study were common in the three oil palm estates. Oriental Magpie-robin, Long-tailed Parakeet, Yellow-vented Bulbul, Greater Coucal, White-breasted Waterhen, Spotted Dove, and Malaysian Pied Fantail were the dominant species recorded in this study. These species are considered dominant species in this study if they exceeded 2% of the total number recorded in each estate and consistently recorded more than 2% at other estates. Oriental Magpie-robin was the most dominant species (relative abundance of more than 5% of the total individuals for each estate), followed by Long-tailed Parakeet, Yellow-vented Bulbul, Greater Coucal, White-breasted Waterhen, Spotted Dove and Malaysian Pied Fantail.

Oriental Magpie Robin is usually seen solitary or sometimes in pairs hopping from one palm frond to another frond, hunting for insects found on the ground in oil palm areas. This species has the common bird sounds that can be heard in oil palm areas, consists of various sound calls. The study conducted by Manshor and Gawin (2020) in a suburban area in Kota Samarahan, Sarawak mentioned that this species has six distinctive

types of call. This species has been reported to feed on all kinds of insects, caterpillars, beetles, grasshoppers, flies, dragonflies and ants in oil palm habitat (Chenon & Susanto, 2006) and hence, have an essential role in controlling the insect pest population in the oil palm area. This species was also reported as a dominant species in oil palm estates by Amit *et al.* (2015) and Azhar *et al.* (2013) through the point count method.

The Long-tailed Parakeet feeds on fruits, seeds, flowers, and lead buds, and is listed as Vulnerable in the IUCN Red List (IUCN, 2022). They have been reported to feed on oil palm fruitlets (Parr & Juniper, 2010). However, in this study, this species was not spotted at the oil palm fruitlets. They are usually observed in a large number of groups around palm fronds and fly from one place to another in the oil palm area with their noisy sound. As the estates have large scale forest patches and are also located adjacent to or surrounded by peat swamp forests, especially SSE and TINE, the abundance of this species might be associated with these features of oil palm areas.

Yellow-vented Bulbul can be found in a wide variety of open areas (Phillipps & Phillipps, 2014). This species was reported as the most abundant bird species using the mist-netting method in the oil palm area by Amit *et al.* (2015). This species is normally observed solitary or sometimes in pairs flying from one palm frond to another palm. It is reported that this bird feeds on a wide range of diets, such as caterpillars, small beetles, wasps, and fruits (Chenon & Susanto, 2006). Amit *et al.* (2015) reported that this species feeds on oil palm pollinators (*Elaeidobius kamerunicus*), insects, small arthropods, and fruits. Hence, due to the open area, they can feed on a wide range of diets available in the oil palm area which may contribute to their abundance in this habitat.

Greater Coucal is a big-sized bird normally observed jumping on the oil palm frond or feeding insects on the ground. Chenon and Susanto (2006) mentioned that this species feeds on small vertebrates and insects such as Hemiptera, Lepidoptera, Orthoptera and Diptera in the oil palm area. Amit *et al.* (2021) also reported that this species was observed to feed on small birds such as Prinia and tailorbirds in the oil palm area. According to Myers (2009), this species feeds on small mammals, nestlings and eggs, lizards, frogs, large insects and invertebrates.

White-breasted Waterhen is a bird that is linked to the presence of water. They are normally observed at the edge of oil palm drainage systems as this system plays a role in flood-control in oil palm planted peat land. This omnivorous bird feeds on small fishes, worms, and aquatic insects but not on the pests of oil palm (Chenon & Susanto, 2006).

The Spotted Dove is a seed eater bird that is frequently observed in groups, feeds on the seed of grasses on the ground at the harvesting paths and the road, and sometimes they are spotted perching on the oil palm fronds.

Malaysian Pied Fantail was also recorded as dominant in the oil palm area in this study. This species is a common fantail that prefers open areas, gardens, mangroves area, and secondary forests (Myers, 2009). They are normally observed to be noisy and constantly fan their tails when flying and sallying and actively feed on insects on the ground and mid-storey. Boles and Christie (2020) mentioned that this species feeds on insects, with items brought to nestlings, including caterpillars, flies, and moths. This species has the potential to prey on insects found in oil palm areas; however, no research has been conducted to determine which insects they prefer to feed on.

Most of the dominant bird species recorded in this study primarily or partially feed on insects. These species include Oriental Magpie-robin, Yellow-vented Bulbul, White-breasted Waterhen, Greater Coucal, and Malaysian Pied Fantail. Hence, this study concludes that oil palm area is capable of providing a good habitat and insects as food resource to support the bird population. It is recommended that all oil palm estates have land patches that have trees and natural vegetation to support the birds' species and biodiversity in their oil palm areas. A study conducted by Soon *et al.* (2022) showed that interaction between insectivorous bird and overall arthropods neither decreased nor increased the number of arthropods, contrary to their expectation that when there is more insectivorous bird predator, there should be less arthropod prey. According to Stevens (2010), higher insectivorous bird abundance could also contribute to the surge in arthropod numbers as food resource.

CONCLUSION

A better understanding of bird composition in oil palm estates provides better information on the status of the bird biodiversity in oil palm areas and their important role in the ecosystem. Through our study, we found that species composition of Ardeidae, Cuculidae, Nectariidae and Cisticolidae were the most diverse bird families in oil palm areas where they play ecological importance in oil palm ecosystems. Thus, high priority should be given to the oil palm areas for conservation and monitoring bird species to support Malaysia as one of the megadiverse bird biodiversity in the world. Further study should be done on the interaction between dominant insectivorous birds and arthropod prey in oil palm areas in order to understand their roles in balancing the ecosystem.

ACKNOWLEDGEMENT

We would like to acknowledge the members of Malaysian Palm Oil Board especially Peat Ecosystem and Biodiversity Unit Mr. Jonathan Anderson, Mr. Royston Stephen and Mr. Tarien Kasi for their technical assistance. We would also like to thank the oil palm estates management of Sarawak Oil Palms Berhad (SOPB) for their assistance throughout the study.

REFERENCES

Amir, A., Noor, H. M., & Hambali, K. (2015). Assessing avian richness and diversity in different regions of oil palm plantation in Selangor, Malaysia. *International Letters of Natural Sciences*, *42*, 28–37. https://doi.org/10.56431/p-l61658

Amit, B., Tuen, A. A., & Kho, L. K. (2021). Bird species richness, abundance and their feeding guild across oil palm development through mist-netting method in Betong, Sarawak. *Journal of Oil Palm Research, 33*(4), 617–628. https://doi.org/10.21894/jopr.2021.0017

Amit, B., Tuen, A. A., Haron, K., Harun, M. H., & Kamarudin, N. (2015). The diet of Yellow-vented Bulbul (*Pycnonotus goiavier*) in oil palm agroecosystems. *Journal of Oil Palm Research, 27*(4), 417–424.

Azhar, B., Lindenmayer, D. B., Wood, J., Fischer, J., Manning, A., McElhinny, C., & Zakaria, M. (2011). The conservation value of oil palm plantation estates, smallholdings and logged peat swamp forest for birds. *Forest Ecology and Management*, *262*(12), 2306–2315. https://doi.org/10.1016/j.foreco.2011.08.026

Azhar, B., Lindenmayer, D. B., Wood, J., Fischer, J., Manning, A., Mcelhinny, C., & Zakaria, M. (2013). The influence of agricultural system, stand structural complexity and landscape context on foraging birds in oil palm landscapes. *Ibis*, *155*(2), 297–312. https://doi.org/10.1111/ibi.12025

Bradbury, R. B., Kyrkos, A., Morris, A. J., Clark, S. C., Perkins, A. J., & Wilson, J. D. (2000). Habitat associations and breeding success of yellowhammers on lowland farmland. *Journal of Applied Ecology*, *37*(5), 789–805. https://doi.org/10.1046/j.1365-2664.2000.00552.x

Brickle, N. W., Harper, D. G., Aebischer, N. J., & Cockayne, S. H. (2000). Effects of agricultural intensification on the breeding success of corn buntings *Miliaria calandra*. *Journal of Applied Ecology*, *37*(5), 742–755. https://doi.org/10.1046/j.1365-2664.2000.00542.x

Boles, W., & Christie, D. (2020). Malaysian Pied-Fantail (*Rhipidura javanica*). *Birds of the World*. https://doi.org/10.2173/bow.piefan1.01

Chenon, R. D., & Susanto, A. (2006). Ecological observations on diurnal birds in Indonesian oil palm plantations. *Journal of Oil Palm Research, Special Issue*, 122–143.

Hasnol, O., Tarmizi, A. M., Haniff, M. H., Darus, F. M., & Mos, H. (2010). Best management practices for oil palm planting on peat: Optimum groundwater table. *MPOB Information Series, No. 472*.

Hawa, A., Azhar, B., Top, M. M., & Zubaid, A. (2016). Depauperate avifauna in tropical peat swamp forests following logging and conversion to oil palm agriculture: Evidence from mist-netting data. *Wetlands*, *36*(5), 899–908. https://doi.org/10.1007/s13157-016-0802-3

International Union for Conservation of Nature and Nature Resources (IUCN). (2022). *IUCN Red List of Threatened Species*. https://www.iucnredlist.org/

Jambari, A., Azhar, B., Ibrahim, N. L., Jamian, S., Hussin, A., Puan, C. L., Noor, H. M., Yusof, E., & Zakaria, M. (2012). Avian biodiversity and conservation in Malaysian oil palm production areas. *Journal of Oil Palm Research, 24*, 1277–1286.

Karp, D. S., Rominger, A. J., Zook, J., Ranganathan, J., Ehrlich, P. R., & Daily, G. C. (2012). Intensive agriculture erodes β-diversity at large scales. *Ecology Letters*, *15*(9), 963–970. https://doi.org/10.1111/j.1461-0248.2012.01815.x

Luck, G. W., Hunt, K., & Carter, A. (2015). The species and functional diversity of birds in almond orchards, apple orchards, vineyards and eucalypt woodlots. *Emu - Austral Ornithology*, *115*(2), 99–109. https://doi.org/10.1071/mu14022

Manshor, Z., & Gawin, D. F. A. (2020). Call types of the Oriental Magpie-robin (*Copsychus saularis*) in suburban areas in Kota Samarahan, Sarawak. *Borneo Journal of Resource Science and Technology*, *10*(1), 37–44. https://doi.org/10.33736/bjrst.2264.2020

Malaysian Palm Oil Board (MPOB). (2022). *Oil palm planted area 2021*. https://bepi.mpob.gov.my/index.php/en/area/area-2021/oil-palm-planted-area-as-at-dec-2021

Magurran, A. E. (1988). *Ecological diversity and its measurement*. Springer Dordrecht. https://doi.org/10.1007/978-94-015-7358-0

Mohd-Azlan, J., Fang, V. A. M., Kaicheen, S. S., Lok, L., & Lawes, M. J. (2019). The diversity of understorey birds in forest fragments and oil palm plantation, Sarawak, Borneo. *Journal of Oil Palm Research, 31*, 437–447. https://doi.org/10.21894/jopr.2019.0033

Myers, S. (2009). *A Field Guide to the Birds of Borneo*. New Holland Publishers.

Parr, M., & Juniper, T. (2010). *Parrots: A Guide to Parrots of the World*. Bloomsbury Publishing.

Phillipps, Q., & Phillipps, K. (2014). *Phillipps's Field Guide to the Birds of Borneo: Sabah, Sarawak, Brunei and Kalimantan* (3rd ed.). Princeton University Press.

Sekercioglu, C. H., Wenny, D., & Whelan, C. J. (2016). *Why Birds Matter: Avian Ecological Functions and Ecosystem Services*. University of Chicago Press.

Söderström, B., & Pärt, T. (2000). Influence of landscape scale on farmland birds breeding in Semi-Natural pastures. *Conservation Biology*, *14*(2), 522–533. https://doi.org/10.1046/j.1523-1739.2000.98564.x

Soon, V., Mohd-Azlan, J., Amit, B., & Tuen, A. A. (2022). The abundance and species richness of insectivorous birds in relation to arthropod assemblages along distance gradient from secondary forest into oil palm plantation in SALCRA, Sarawak. *Malaysian Nature Journal, 74*(3), 347–363.

Stevens, A. (2010). Dynamics of predation. *Nature Education Knowledge, 3*(10), 46.

The Commissioner of Law Revision, Sarawak (2008). Wild Life Protection Ordinance 1998. In *Laws of Sarawak*. Percetakan Nasional Malaysia Berhad. https://www.sarawakforestry.com/pdf/laws/wildlife_protection_ordinance98_chap26.pdf

The World Bank. (2022). *Agricultural land (% of land area).* https://data.worldbank.org/indicator/AG.LND.AGRI.ZS

Triplett, S., Luck, G. W., & Spooner, P. (2012). The importance of managing the costs and benefits of bird activity for agricultural sustainability. *International Journal of Agricultural Sustainability*, *10*(4), 268–288. https://doi.org/10.1080/14735903.2012.700102

Wenny, D. G., DeVault, T. L., Jonson, M. D., Kelly, D., Sekercioglu, C. H., Tomback, D. F., & Whelan, C. J. (2011). The need to quantify ecosystem services provided by birds. *Ornithology*, *128*(1), 1–14. https://doi.org/10.1525/auk.2011.10248

Whelan, C. J., Wenny, D. G., & Marquis, R. J. (2008). Ecosystem services provided by birds. *Annals of the New York Academy of Sciences*, *1134*(1), 25–60. https://doi.org/10.1196/annals.1439.003

Yaap, B., Struebig, M., Paoli, G., & Koh, L. (2010). Mitigating the biodiversity impacts of oil palm development. *CABI Reviews*, 1–11. https://doi.org/10.1079/pavsnnr20105019

Journal of Oil Palm Research Vol. 37 (1) March 2025 p. 53-63
DOI: https://doi.org/10.21894/jopr.2023.0066

APPLICATION OF SEAWEED EXTRACTS IN OIL PALM (*Elaeis guineensis*) SEEDLINGS SUBJECTED TO WATER DEFICIT: PHYSIOLOGICAL, BIOCHEMICAL AND ENZYMATIC RESPONSES

MUHAMMAD DANIAL MOKHTARUDDIN[1]; NUR AIFAA ABD RAZAK[1]; AISAMUDDIN ARDI ZAINAL ABIDIN[1]; NOR IZZATI HUSNA NOORHISHAM[2]; NUR ASNA FAIQAH JOHARI[1] and ZETTY NORHANA BALIA YUSOF[1,2,3]*

ABSTRACT

Water deficit can negatively affect physiological and biochemical responses in plants. The stress-mitigation potential of seaweed extracts (SWEs) Caulerpa lentillifera *(green seaweed) and* Gracilaria edulis *(red seaweed) on oil palm seedlings subjected to water deficit was investigated. Plant height, relative water content, chlorophyll content, soluble protein concentration and the expression of genes coding for thiamine (vitamin B1) biosynthesis enzymes were evaluated. SWE treatments were applied to four-month-old oil palm seedlings under full irrigation (control) and water deficit conditions. Overall, SWE did not affect the height of the seedlings after 60 days of treatment, but the seedlings managed to maintain relative water content of up to 90.00% and chlorophyll and leaf protein content increased up to 50.00% in seedlings treated with red seaweed extract compared to the control. The application of* G. edulis *and* C. lentillifera *SWE induced downregulation of THIC (up to 15.00%) and THI4 (up to 15.46%) expression respectively on day 2 post-treatment as compared to the control. This finding is in line with the postulated role of thiamine in protection against stress in plants and suggests the role of SWE as a biostimulant.*

Keywords: biostimulant, seaweed extracts, thiamine, vitamin B1, water deficit.

Received: 20 March 2023**; Accepted:** 23 October 2023**; Published online:** 27 December 2023.

INTRODUCTION

Elaeis guineensis (Jacq.) is native to Africa and is the commercial species of oil palm planted in Malaysia since 1870 (Basiron, 2007). It started as an ornamental plant and has become a huge industry due to increasing global demands for palm oil in many applications such as food products, cosmetics, and bio-energy (Alam *et al*., 2015). Currently, Malaysia is reported to be the second-largest world producer and exporter of palm oil (Kushairi *et al*., 2018). However, challenges still remain and largely affect the oil palm growth and productivity, and among them is the water deficit (Noor *et al*., 2011). The means to control this situation unfortunately is still very limited. According to Henson and Harun (2005), oil yields depend not only on genetic resources but also on environmental factors such as availability of water, relative humidity, use of fertilisers, soil texture, and cultural practices. Thus, a need to search for alternative stress mitigation techniques to maintain and improve crop production would be very beneficial.

Under water deficit conditions, plants often respond by reducing their growth and metabolic activities (Bonjoch & Tamayo, 2001) as ways to improve plant adaptability towards stress. Apart from that, thiamine has also been reported to have

[1] Department of Biochemistry, Faculty of Biotechnology and Biomolecular Sciences, Universiti Putra Malaysia, 43400 UPM Serdang, Selangor, Malaysia.

[2] Aquatic Animal Health and Therapeutics Laboratory (AquaHealth), Institute of Bioscience, Universiti Putra Malaysia, 43400 UPM Serdang, Selangor, Malaysia.

[3] Bioprocessing and Biomanufacturing Research Complex (BBRC), Universiti Putra Malaysia, 43400 UPM Serdang, Selangor, Malaysia.

* *Corresponding author e-mail: zettynorhana@upm.edu.my*

a role in plant protection against stress, where the level of thiamine content in maize leaves increased when subjected to water deficit (Rapala-Kozik *et al*., 2009). This may be due to thiamine's role in plant defense mechanism through systemic acquired resistance (SAR) by induction of SAR-related genes (Subki *et al*., 2018; 2020). THIC and THI4 gene transcripts in oil palm, key genes in the thiamine biosynthesis pathway, showed an increase in gene expression in conjunction with increasing concentrations of osmotic, salinity, and oxidative stresses (Abidin *et al*., 2016; Idris *et al*., 2018; Rahman *et al*., 2017; Wong *et al*., 2016). Plus, biotic stress and the colonisation of harmless endophytes have also been shown to increase the expression of thiamine biosynthesis genes as well as the accumulation of the vitamin and its intermediates (Kamarudin *et al.,* 2017a; 2017b; Yusof *et al.,* 2015).

Seaweeds have been widely utilised in agriculture and horticulture as a complement to fertilisers because of their various positive effects on crop production, stress tolerance, nutrient uptake, and the quality of products after harvest (Fan *et al*., 2013). The same effects of the physiological responses in crops treated with plant growth-regulatory substances were reported in seaweed extracts (SWEs)-treated plants (Ghaderiardakani *et al*., 2019). SWEs exhibited effects at low concentrations and the effects may involve the synergy between plant-growth promoters (Ghaderiardakani *et al*., 2019). Battacharyya *et al*. (2015) reported that the application of different types of SWEs could improve plants' tolerance towards a wider range of abiotic stresses.

In this study, *Caulerpa lentillifera* and *Gracilaria edulis* were extracted and applied to oil palm seedlings through soil application. *Caulerpa lentillifera* is also known as sea grapes (Guo *et al*., 2015) and belongs to the Chlorophyta phylum. It has high polyunsaturated fatty acids (PUFAs), multiple essential amino acids, dietary fibres, minerals, vitamin C and vitamin A (Chen *et al.,* 2019). *Gracilaria edulis*, a member of the Rhodophyta phylum, produces phycocolloid agar for the biotechnology, medicine, cosmetics, pharmaceutical and food industries (Lee *et al*., 2016). It contains high dietary fibre, ash, essential amino acids, minerals and vitamins (Sakthivel & Devi, 2015). Even though the usefulness of SWEs in attenuating the negative effects of water deficit has been proven in many plants, studies on oil palm have not been addressed to date. It is crucial to find alternatives to stress control in oil palm plantations and the dependency on synthetic and chemical control must be reduced. Hence, the objective of this study is to investigate the physiological and biochemical effects of SWEs on oil palm seedlings subjected to water deficit.

MATERIALS AND METHODS

Collection of Seaweeds

Caulevpa lentillifera and *G. edulis* were collected from Teluk Kemang, Port Dickson, Negeri Sembilan, Malaysia (2°27'14.039"N, 101°51'18.719"E) as shown in *Figure 1*. *Table 1* shows the dominant compounds found in the extract using gas chromatography-mass spectrometry (GC-MS). The seaweeds were handled as described by Aziz *et al.* (2019a) and washed with seawater to remove sand particles, epiphytes and foreign particles followed by water to remove the remaining salt. The seaweeds were freeze-dried to a constant weight before grinding into fine powder and kept at -20˚C until further analysis.

Preparation of Seaweed Crude Extracts

The crude SWEs (*C. lentillifera* and *G. edulis* extract) were prepared by using the Soxhlet extraction method as described previously by Aziz *et al.* (2019c). Ten gram of seaweed powder was packed into a Soxhlet thimble and placed inside a Soxhlet extractor with dichloromethane as solvent. The concentrated crude extract was then kept at 4°C until further use.

Plant Materials and Experimental Design

Four-month-old oil palm seedlings (*Dura* x *Pisifera*) were procured from Felda Global Ventures (FGV) Holdings Berhad, Malaysia. The seedlings were grown and maintained in polyethylene bags under greenhouse conditions at the Transgenic Greenhouse, Institute of Plantation Studies (IKP), UPM, Malaysia. The seedlings were acclimatised under normal nursery practices. *i.e.,* watered with 200 mL twice daily (morning and evening) by using a drip irrigation system. This experiment consists of two watering regimes: Full irrigation (200 mL of water) and water deficit condition (100 mL of water) (Najihah *et al.,* 2019) and four soil application treatments; control (distilled water), positive control (Green Amino-G liquid fertiliser) and liquid SWE (*C. lentillifera* and *G. edulis*). Green Amino-G liquid fertiliser, an organic biostimulant derived from marine products fortified with a range of vitamins and trace minerals was prepared by adding 3-4 mL of fertiliser to 1 L of water. The SWEs with a concentration of 1 mg/mL with a final volume of 20 mL of distilled water were prepared (Salim, 2016). The same amount of 20 mL of each soil application treatment was soil drenched onto the oil palm seedlings every 15 days and sampled at day 60 for physiological analyses (plant height, relative water content, chlorophyll content, and protein content). While

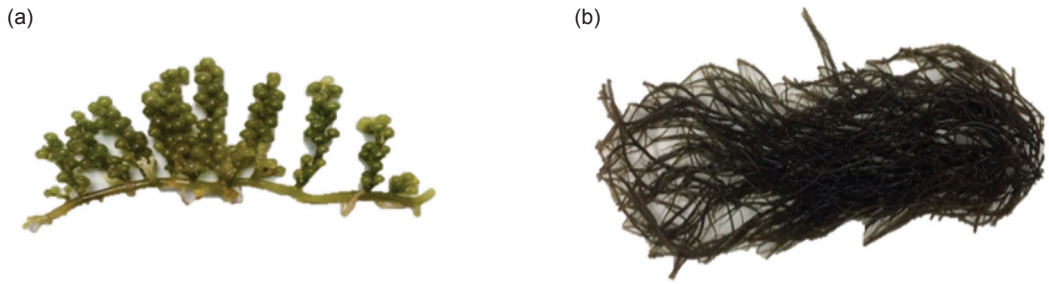


Figure 1. Seaweeds collected in this study are found in abundance in Port Dickson (a) Caulerpa lentillifera, *and (b)* Gracilaria edulis.

TABLE 1. IDENTIFIED COMPOUNDS OF SEAWEED EXTRACTS WITH BIOSTIMULANT POTENTIAL

Compounds
Phytol (Diterpene alcohol)
9,12,15-Octadecatrienoic acid, (Z,Z,Z) (Fatty acid)
n-Hexadecanoic acid (Fatty acid)
Tetradecanoic acid (Fatty acid)

Source: Aziz *et al.* (2019b).

for gene expression analysis, the spear leaves of the seedlings were sampled at day 0, 1 and 2 post-SWE treatment (control, *C. lentillifera* and *G. edulis*). Both experiments were arranged in a completely randomised design (CRD) with three replicates (n=3).

Physiological Analyses

Plant height. Plant height was measured as performed by Sapak *et al.* (2008). The plant height was measured by measuring the seedlings 1 cm above the soil level to the tip of the leaves.

Relative water content (RWC). RWC of the leaves was analysed as done by Sun *et al.* (2011). Six leaf samples of the same size were weighed and recorded as fresh weight (FW). The turgid weight (TW) of the leaf samples was recorded by immersing them in a petri dish with water for 24 hr. The dry weight (DW) of the leaf samples was then recorded after oven-drying at 70ºC for 24 hr. RWC (%) was calculated using Equation (1):

$$[(FW-DW)/(TW-DW)]\times 100 \quad (1)$$

Chlorophyll concentration. The chlorophyll concentration of the leaf samples was determined as performed by Godlewska *et al.* (2016) with a slight modification. Leaf samples at 0.2 g were immersed in 200 mL of methanol for 30 min. The sample was filtered using Whatman filter paper before the absorbance readings were recorded at wavelengths of 645 and 663 nm. The concentration of total chlorophyll (Total Chl) was determined from Equation (2):

$$Total\ Chl = 8.02 \cdot A(663) + 20.2 \cdot A(645) \quad (2)$$

Total soluble proteins. The proteins were extracted using TCA/acetone extraction method as performed by Hassan *et al.* (2014) with a slight modification. The quantification of the protein content was determined using Bradford's (1976) method. The protein concentrations of the samples were calculated using the Equation (1) described previously.

Gene Expression Analysis

Total RNA was extracted as described by Kamarudin *et al.* (2017a) and stored at -80ºC until further use. Reverse transcription was performed using Tetro cDNA Synthesis Kit (Bioline) and stored at -20°C until further use. PCR was performed using MyTaq™ Red Mix (Bioline). Three pairs of primers were used in this study namely actin (housekeeping gene), THIC, and THI4. Actin was used to normalise mRNA levels between different samples. THIC encodes the first enzyme of the pyrimidine branch located in chloroplast, chloroplast stroma and plastid, while, THI4 encodes the enzyme responsible for the biosynthesis of thiamine precursor thiazole. Primers used in this study are shown in *Table 2*.

The PCR cycling conditions include initial denaturation at 95°C for 1 min for 1 cycle, followed by 30 repetitive cycles of denaturation step at 95°C for 15 s, annealing step at 60°C for all primers for 15 s, and extension step at 72°C for 10 s. The final extension step was set at 72°C for 3 min for 1 cycle and then held at 4°C. The PCR product was then subjected to agarose gel electrophoresis and the intensities of the bands obtained were analysed using ImageJ software.

TABLE 2. NUCLEOTIDE SEQUENCES OF THE PRIMERS USED IN THIS STUDY

Gene	Primer sequence (5′-3′)	Amplicon size (bp)
Actin	F : 5′ – CTT GCT CCA AGC AGC ATG A – 3′ R : 5′ – AGA AGC ACT TCC GGT GCA CG – 3′	168
THIC	F : 5′ – AAT GAA GGT CCA GGG CAT – 3′ R : 5′ – GCT GAG GTG ATG TGA TCA – 3′	188
THI4	F : 5′ – ATC GTG GAG CAG TCC GTC T– 3′ R : 5′ – AGC TCG TCG AGG AAG AGG T– 3′	104

Statistical Analysis

Results are expressed as mean ± standard deviation (SD). Statistical analysis was performed using two-way ANOVA and Dunnet post-test. The significant level was set at $P<0.05$ using GraphPad Prism 8.

RESULTS AND DISCUSSION

Physiological Effects of Seaweeds Extract on Oil Palm Seedlings

To observe the effects of the application of SWE on various physiological parameters, data and samples were taken for plant height, relative water content, chlorophyll content, and protein content. In this study, the plant height of seedlings under both conditions showed no significant difference in all treatments as compared to the controls when measured after 60 days (*Figure 2a*). Theoretically, plants respond to any biotic or abiotic stress by decreasing their normal metabolic activities leading to growth reduction (Bonjoch & Tamayo, 2001). SWE has been reported to have a significant effect on the vegetative growth of many crops including soybean (Noli *et. al.*, 2021), coriander (Tursun, 2022), sugarcane (Chen *et al.*, 2021), and tomato (Kumari *et al.*, 2011). However, this could not be seen in this current study as the time point taken may be a bit too short to be able to see any difference in plant height.

On the other hand, oil palm seedlings not treated with SWEs and subjected to a 50% water deficit showed a reduction in RWC as compared to the controls (*Figure 2b*). The result obtained is in accordance with the findings reported by Sun *et al.* (2011) which can vary from one species to the other. However, it could be assumed that under water deficit conditions, the RWC of the seedlings applied with both *C. lentillifera* and *G. edulis* extracts can retain the water content as well as the seedlings applied with the Greenamino-G liquid fertiliser. In this study, the findings agree with what was reported by Santaniello *et al.* (2017), in which SWEs treated plants were able to maintain their RWC of up to 90% throughout the dehydration period. Increased RWC in the stressed plants after the application of seaweed indicated that plants encountered less stress due to high water status. According to Trivedi *et al.* (2017), the compound presents in SWE contributes to greater cytoplasmic water volume and cell expansion for the higher RWC. It is known that the closure of stomata acts as the primary plant defense when subjected to drought stress to save water and maintain turgor (Santaniello *et al.*, 2017; Skirycz & Inzé, 2010). Therefore, an increase in RWC was the likely consequence of stomata closure in preventing excessive water losses.

Under water deficit, the damaged photosynthetic pigments and the thylakoid membrane affect the chlorophyll content. The total chlorophyll content of seedlings under normal and water deficit conditions increased significantly by all treatments as compared to negative control under normal conditions (*Figure 2c*). The results obtained coincide with what has been reported by Latique *et al.* (2013), where bean plants treated with SWEs showed higher chlorophyll content than untreated controls. The same finding by Ghaffar *et al.* (2019) also showed that the water deficit decreased the chlorophyll content in the control treatment. It is well understood that the photosynthetic capability of plant tissues is indicated by the chlorophyll content in the leaves (Hassanzadeh *et al.*, 2009). In addition, the compounds of SWE such as betaines and cytokinin have a role in inhibiting leaf chlorophyll content degradation (Ali *et al.*, 2019).

Protein content in plants is also a good indicator of the status of plant health. The leaf protein content of the seedlings under both conditions increased significantly when applied with *G. edulis* extracts as shown in *Figure 2d*. Previously, Hidangmayum and Sharma (2017) reported that SWEs play an important role in increasing the leaf protein content of onions. The increase in leaf protein may be due to the increased availability and absorption of necessary elements (Ca, Na, K, Mg, N and Zn) present in the SWEs (Erulan *et al.* 2009; Ramya *et al.*, 2011). Low protein concentration in plants is an indicator of damage caused by stress (Bonjoch & Tamayo, 2001). Most plants under stress will activate their stress coping mechanisms which include *de novo* synthesis of stress proteins such as heat shock protein to tolerate abiotic stresses (Akhzari & Pessarakli, 2016). The accumulation of leaf-soluble proteins acts as a nitrogen reserve

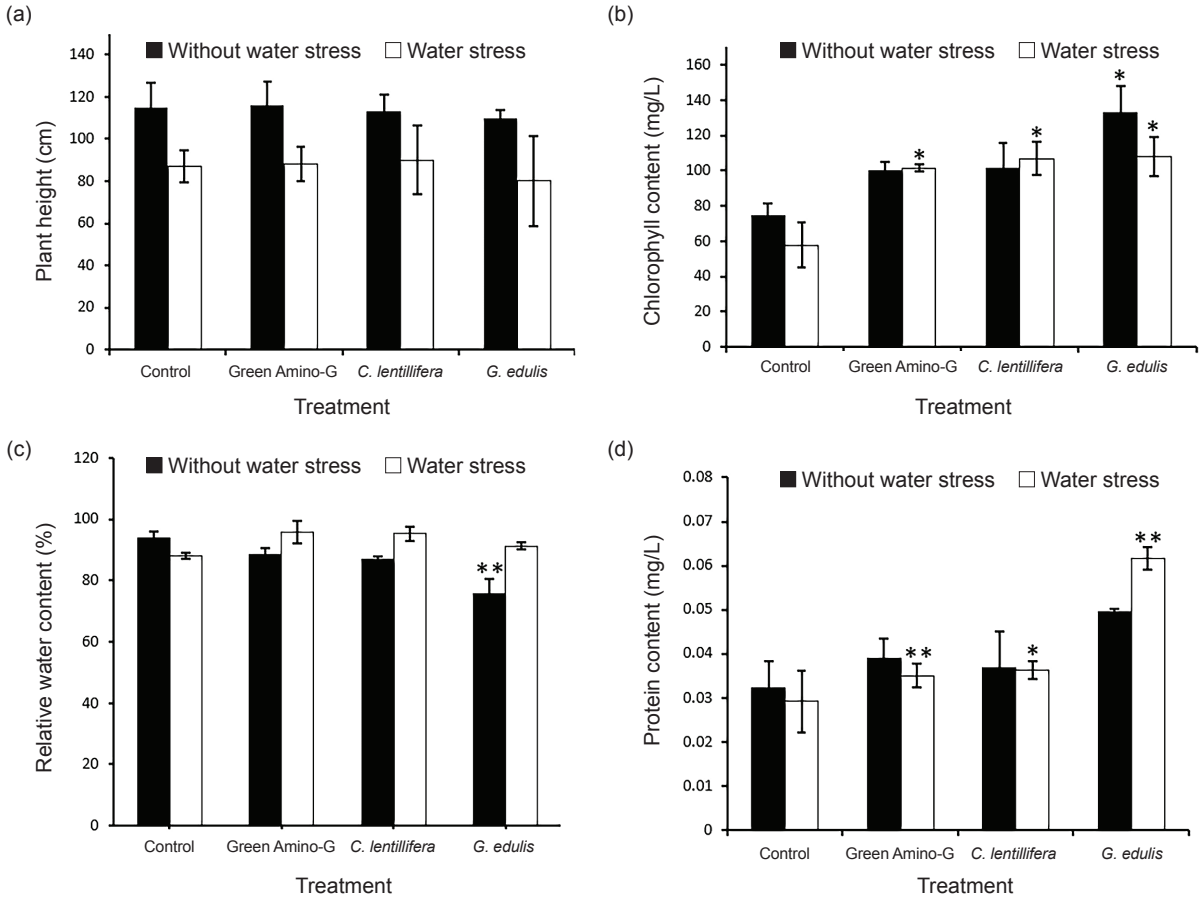


Figure 2. Effects of seaweed extract application towards (a) the plant height, (b) chlorophyll content, (c) relative water content and (d) protein content in oil palm seedlings with and without water deficit and with treatments after 60 days. Data presented are the mean ± standard deviation of three replicates with significant differences of *P<0.05, **P<0.01, *and* ***P<0.001 vs. *control, using one-way ANOVA (Dunnett post-test) on the raw data.*

which will then be used during recovery (Bonjoch & Tamayo, 2001).

Expression of THIC and THI4 Gene Transcripts

Thiamine has been postulated to have a role in protection against stress where studies have shown the upregulation of thiamine biosynthesis genes transcripts in plants treated with various biotic and abiotic stresses (Abidin *et al.*, 2016; Kamarudin *et al.*, 2017b; Wong *et al.*, 2016; Yusof *et al.*, 2015). In this study, the expression of THIC and THI4 gene transcripts were analysed from oil palm spear leaves samples with water deficit following the treatment with 0.1 g/100 mL SWE to determine if SWE may contribute to the mitigation of stress in the plants. The actin, THIC, and THI4 gene fragments were successfully amplified from samples collected on days 0, 1, and 2 post-treatment application. The expression of actin remained constant throughout the experiment (*Figure 3*). However, the expression of both THIC and THI4 gene fragments was postulated to be downregulated in oil palm seedlings under water deficit treated with SWE as the band intensity observed was lower than the control (*Figure 4a* and *4b*).

To further verify the data obtained from the gel electrophoresis, the intensity of the bands amplified was analysed using ImageJ software. The actin band amplified from all samples showed stable intensities throughout the treatment period (*Figure 5a*). Actin is a highly conserved, key cytoskeletal protein involved in numerous structural and functional roles, therefore, regardless of any condition, the actin gene will still be expressed (Ladt *et al.*, 2016). The ImageJ software analysed the gene expression by measuring the peak area under the curve which accounts for the band intensity. Each intensity of the band has different values according to their pixel value read by the ImageJ software. The expression of THIC gene transcript in oil palm seedlings under water deficit without SWE treatment increased from day 0 to day 1 indicating the effects of the stress on the seedlings (*Figure 5b*). However, on day 2, the expression for both genes started to remain constant or decreased slightly indicating the adaptation of the oil palm seedlings towards the water deficiency condition. However, the expression of THIC gene transcript in oil palm seedlings under water deficit treated with SWE showed a decrease in expression as compared to the control. There was a decrease of up to 15.00% in THIC gene expression on day 2 in oil

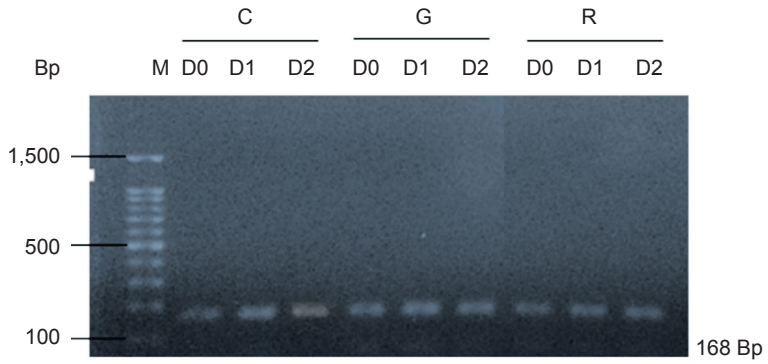


Figure 3. The expression of actin gene transcript from oil palm seedlings with and without SWE treatment from day 0 until day 2 (D0, D1, and D2). M represents 100 bp DNA ladder, C represents oil palm seedlings under water deficit without SWE treatment (control), G represents oil palm seedlings treated with C. lentillifera *(green seaweed) and R represents oil palm seedlings under water deficit treated with* G. edulis *(red seaweed).*

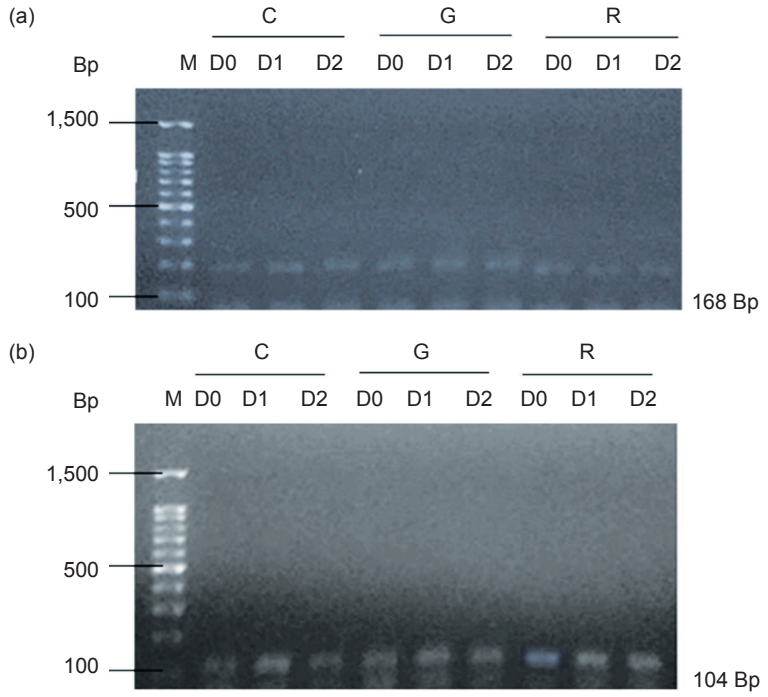


Figure 4. The expression of (a) THIC and (b) THI4 gene transcripts in oil palm seedlings under water deficit with and without SWE treatment from day 0 until day 2 (D0, D1, and D2). M represents 100 bp DNA ladder, C represents oil palm seedlings under water deficit without SWE treatment (control), G represents oil palm seedlings treated with C. lentillifera *(green seaweed) and R represents oil palm seedlings under water deficit treated with* G. edulis *(red seaweed).*

palm seedlings treated with *G. edulis*. The THI4 gene transcript also showed a somewhat similar trend where the expression showed a decrease throughout day 0 to day 2 post-treatment, with up to 15.46% decrement on day 2 in oil palm seedlings treated with *C. lentillifera* (*Figure 5c*).

A study by Abidin *et al.* (2016) and Yee *et al.* (2016) and reported that THIC and THI4 gene transcripts in oil palms increased in conjunction with increasing concentrations of osmotic, salinity and oxidative stresses. These suggest that thiamine biosynthesis is tightly modulated during stress sensing and adaptation. The increase in both genes' expression was also due to the non-cofactor role and cofactor role of thiamine in the metabolic pathways in combating abiotic stress (Goyer, 2010; Jabeen *et al.*, 2020). Thiamine is required as a cofactor in carbohydrate metabolism, NADPH, and ATP synthesis. A huge amount of energy is needed by the oil palm to combat drought stress. Thus, the expression of these two genes must be high enough to synthesise thiamine. Besides that, thiamine also induced the pathway of salicylic acid in the plant. Salicylic acid is known to provide a defense mechanism to the plant. A decrease in gene expression in stress oil palm seedlings treated with SWEs further proved that SWEs could act as a biostimulant

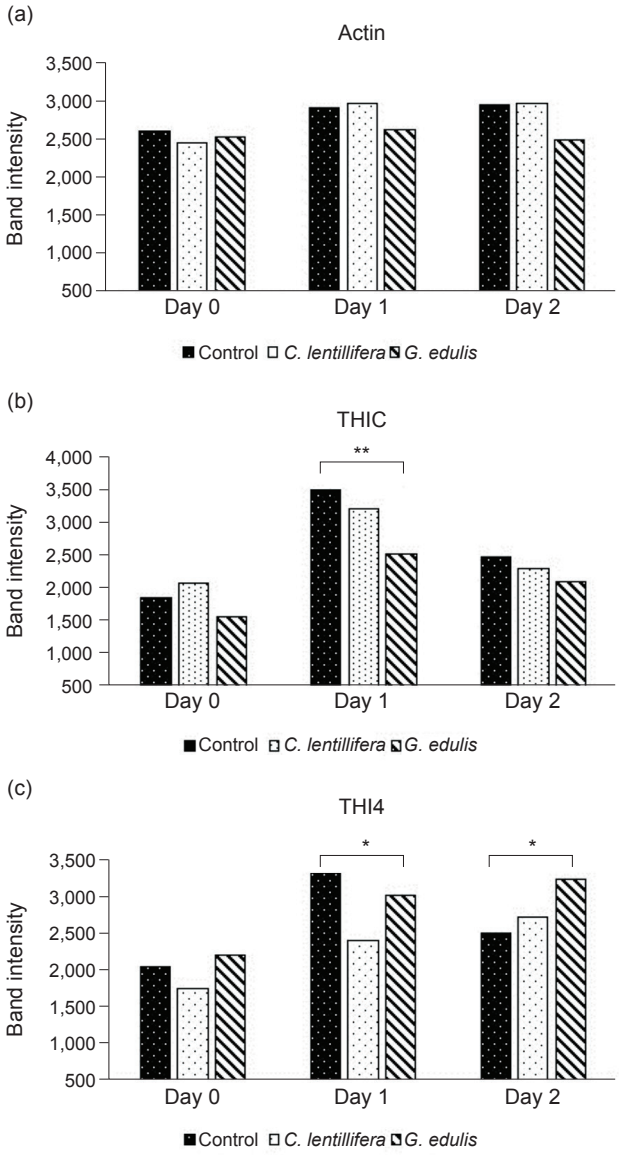


Figure 5. Gene expression analysis of (a) actin, (b) THIC, and (c) THI4 in oil palm seedlings under water deficit with and without SWE treatment from day 0 until day 2 was analysed using ImageJ. Data presented are the mean ± standard deviation of three replicates with significant differences *P<*0.05,* **P<*0.01, and* ***P<*0.001* vs. *control, using one-way ANOVA (Dunnett post-test) on the raw data.*

as it helps the oil palm seedlings combat the drought stress. Thiamine possesses an antioxidant capacity as it has O^{2-}/OH^{-} scavenger properties (Ahn, 2007).

Thiamine is believed to mitigate the effect of water deficit by up-regulating thiamine biosynthesis genes in plants (Tunc-Ozdemir *et al.*, 2009). Under stress conditions, thiamine concentration is known to be high in seeds, roots, and leaves to protect the plant (Ghaffar *et al.*, 2019; Goyer, 2010; Kaya *et al.*, 2015). Particularly, THIC genes are immediately triggered by stress and become the early stress response in *Arabidopsis* plants (Rapala-Kozik *et al.*, 2012). Moreover, thiamine compounds have been proposed to act as antioxidants (Rosado-Souza *et al.*, 2020). The studies reported by Ghaffar *et al.* (2019) and Sayed and Gadallah (2002) also proved that the application of thiamine lessens the negative effects of water deficit on several plants. The upregulation of THIC and THI4 gene transcripts in oil palm seedlings under water deficit without SWE treatment was probably due to the suggested role of thiamine as a signalling molecule in plant response to biotic and abiotic stresses (Goyer, 2010). This finding is consistent with that of Fitzpatrick and Chapman (2020) who reported that the up-regulation of thiamine biosynthesis occurred under stress conditions.

On the other hand, the downregulation of THIC and THI4 gene transcripts in oil palm seedlings treated with SWE could be the stimulatory effects of the SWEs in aiding the plant to combat the water deficiency condition which caused the less requirement of thiamine. Besides, the SWEs application downregulated the expression of THIC and THI4 genes due to the ability of SWEs to reduce the effect of water deficit by stimulating the expression of stress-responsive genes, and suppressing reactive oxygen species (ROS) (Shukla *et al.*, 2019) rather than focusing on thiamine biosynthesis. Furthermore, SWE also showed a significant increase in abscisic acid (ABA) accumulation (Irani *et al.*, 2021) which play a role in inducing various gene expression that encodes important proteins for both biochemical and physiological responses.

It was suggested by Mansori *et al.* (2016) that SWEs treatment influences the ability of the water deficit plants to maintain a balance between the formation and detoxification of oxygen species, leading to amelioration of oxidative stress. A study by Abidin *et al.* (2016) and Wong *et al.* (2016) reported that the expressions of THIC and THI4 gene transcripts in oil palm increased in conjunction with increasing concentrations of osmotic, salinity, and oxidative stresses. These studies suggest that thiamine biosynthesis is tightly modulated during stress sensing and adaptation. The increase in both genes' expression was also due to the non-cofactor role and cofactor role of thiamine in the metabolic pathways (Goyer, 2010). Thiamine is required as a cofactor in carbohydrate metabolism, NADPH, and ATP synthesis. A huge amount of energy is needed by the oil palm to combat drought stress. Thus, the expression of these two genes must be high enough to synthesise thiamine. Besides that, thiamine also induced the pathway of salicylic acid in the plant. Salicylic acid is known to provide a defence mechanism to the plant. A decrease in thiamine biosynthesis gene expression in oil palm seedlings under water deficit treated with SWE further proved that SWE could act as a biostimulant as it helps the oil palm seedlings to combat the stress.

CONCLUSION

In conclusion, *C. lentillifera* and *G. edulis* described in this study have the potential in increasing the chlorophyll content, protein content, and RWC as well as downregulating the expression of the first two enzymes in the thiamine biosynthesis pathway, THIC and THI4 in oil palm seedlings under water deficit. The increment of important biomolecules, as well as water retention capabilities, may be favorable in maintaining stress tolerance in oil palm seedlings. The decrease in the expression of thiamine biosynthesis gene fragments further proved that SWEs could act as biostimulant as it helps the oil palm seedlings combat the stress. This study hoped to open up further possibilities in the exploration of the use of seaweeds as one of the strategies for maintaining the sustainability of the palm oil industry in Malaysia.

ACKNOWLEDGEMENT

This research was funded by Higher Institution Centre of Excellence (HICOE) Research Grant (Innovative Vaccines and Therapeutics Against Fish Diseases) (Project No. 6369100), SATREPS (JICA-JST): COSMOS-MOHE G4-B Research Grant (Microalgae for Sustainable Aquaculture Health: Microalgae Vaccine Delivery System) (Project No. 6300866), and Fundamental Research Grant Scheme (FRGS), Fasa1/2020, KPT Ref. Code: FRGS/1/2020/STG02/UPM/02/4; Project Code: 01-01-20-2227FR; Vote No.: 5540359).

REFERENCES

Abidin, A. A. Z., Yee, S. W., Rahman, N. S. A., Idris, Z. H. C., & Yusof, Z. N. B. (2016). Osmotic, oxidative and salinity stresses upregulate the expressions of thiamine (Vitamin B1) biosynthesis genes (THIC and THI1/THI4) in oil palm (*Elaeis guineensis*). *Journal of Oil Palm Research, 28*(3), 308–319. https://doi.org/10.21894/jopr.2016.2803.07

Ahn, I. P., Kim, S., Lee, Y. H., & Suh, S. C. (2007). Vitamin B1-induced priming is dependent on hydrogen peroxide and the NPR1 gene in *Arabidopsis*. *Plant Physiology, 143*(2), 838–848. https://doi.org/10.1104/pp.106.092627

Akhzari, D., & Pessarakli, M. (2016). Effect of drought stress on total protein, essential oil content, and physiological traits of *Levisticum officinale* Koch. *Journal of Plant Nutrition, 39*(10), 1365–1371. https://doi.org/10.1080/01904167.2015.1109125

Alam, A. F., Er, A. C., & Begum, H. (2015). Malaysian oil palm industry: Prospect and problem. *Journal of Food, Agriculture & Environment, 13*(2), 143–148.

Ali, O., Ramsubhag, A., & Jayaraman, J. (2019). Biostimulatory activities of *Ascophyllum nodosum* extract in tomato and sweet pepper crops in a tropical environment. *PLoS ONE, 14*(5), e0216710. https://doi.org/10.1371/journal.pone.0216710

Aziz, S. D. A., Jafarah, N. F., & Yusof, Z. N. B. (2019a). Phytol-containing seaweed extracts as control for *Ganoderma boninense*. *Journal of Oil Palm Research, 31*(2), 238–247. https://doi.org/10.21894/jopr.2019.0018

Aziz, S. D. A., Jafarah, N. F., Sabri, S., Wahab, M. A. A., & Yusof, Z. N. B. (2019b). Antifungal activities against oil palm pathogen *Ganoderma boninense* from seaweed sources. *Asia-Pacific Journal of Molecular Biology and Biotechnology, 27*, 75–83. https://doi.org/10.35118/apjmbb.2019.027.1.08

Aziz, S. D. A., Jafarah, N. F., Sabri, S., Wahab, M. A. A., & Yusof, Z. N. B. (2019c). Antifungal activity of dichloromethane and hexane extracts of four Malaysian seaweed species against *Ganoderma boninense*. *Malaysian Applied Biology, 48*(3), 189–196. https://jms.mabjournal.com/index.php/mab/article/view/1854

Basiron, Y. (2007). Palm oil production through sustainable plantations. *European Journal of Lipid Science and Technology, 109*(4), 289–295. https://doi.org/10.1002/ejlt.200600223

Battacharyya, D., Babgohari, M. Z., Rathor, P., & Prithiviraj, B. (2015). Seaweed extracts as biostimulants in horticulture. *Scientia Horticulturae, 196*, 39–48. https://doi.org/10.1016/j.scienta.2015.09.012

Bonjoch, N. P., & Tamayo, P. R. (2001). Protein content quantification by Bradford method. In *Handbook of Plant Ecophysiology Technique* (pp. 283–295). Kluwer Academic. https://doi.org/10.1007/0-306-48057-3_19

Bradford, M. M. (1976). A rapid and sensitive method for the quantitation of microgram quantities of protein utilizing the principle of protein-dye binding. *Analytical Biochemistry, 72*(1-2), 248–254. https://doi.org/10.1006/abio.1976.9999

Chen, D., Zhou, W., Yang, J., Ao, J., Huang, Y., Shen, D., Jiang, Y., Huang, Z., & Shen, H. (2021).

Effects of seaweed extracts on the growth, physiological activity, cane yield and sucrose content of sugarcane in China. *Frontiers in Plant Science, 12*, 659130. https://doi.org/10.3389/fpls.2021.659130

Chen, X., Sun, Y., Liu, H., Liu, S., Qin, Y., & Li, P. (2019). Advances in cultivation, wastewater treatment application, bioactive components of *Caulerpa lentillifera* and their biotechnological applications. *PeerJ, 7*, e6118. https://doi.org/10.7717/peerj.6118

Erulan, V., Sourndarapandiyan, P., Thirumaran, G., & Ananthan, G. (2009). Studies on the effect of *Sargassum polycystum* extract on the growth and biochemical composition of *Cajanus cajan* (L.) Mill sp. *American-Eurasian Journal of Agricultural & Environmental Sciences*, *6*(4), 392–399.

Fan, D., Hodges, D. M., Critchley, A. T., & Prithiviraj, B. (2013). A commercial extract of brown macroalga (*Ascophyllum nodosum*) affects yield and the nutritional quality of spinach *in vitro*. *Communications in Soil Science and Plant Analysis, 44*(12), 1873–1884. https://doi.org/10.1080/00103624.2013.790404

Fitzpatrick, T. B., & Chapman, L. M. (2020). The importance of thiamine (vitamin B1) in plant health: From crop yield to biofortification. *Journal of Biological Chemistry, 295*(34), 12002–12013. https://doi.org/10.1074/jbc.rev120.010918

Ghaderiardakani, F., Collas, E., Damiano, D. K., Tagg, K., Graham, N. S., & Coates, J. C. (2019). Effects of green seaweed extract on *Arabidopsis* early development suggest roles for hormone signalling in plant responses to algal fertilizers. *Scientific Reports*, *9*(1), 1983. https://doi.org/10.1038/s41598-018-38093-2

Ghaffar, A., Akram, N. A., Ashraf, M., Ashraf, M. Y., & Sadiq, M. (2019). Thiamin-induced variations in oxidative defense processes in white clover (*Trifolium repens* L.) under water deficit stress. *Turkish Journal of Botany, 43*(1), 58–66. https://doi.org/10.3906/bot-1710-34

Godlewska, K., Michalak, I., Tuhy, A., & Chojnacka, K. (2016). Plant growth biostimulants based on different methods of seaweed extraction with water. *BioMed Research International, 2016*, 5973760. https://doi.org/10.1155/2016/5973760

Goyer, A. (2010). Thiamine in plants: Aspects of its metabolism and functions. *Phytochemistry, 71*(14-15), 1615–1624. https://doi.org/10.1016/j.phytochem.2010.06.022

Guo, H., Yao, J., Sun, Z., & Duan, D. (2015). Effects of salinity and nutrients on the growth and chlorophyll fluorescence of *Caulerpa lentillifera*. *Chinese Journal of Oceanology and Limnology, 33*(2), 410–418. https://doi.org/10.1007/s00343-015-4105-y

Hassan, H., Lau, B. Y. C., & Ramli, U. S. (2014). Extraction methods for analysis of oil palm leaf and root proteins by two-dimensional gel electrophoresis. *Journal of Oil Palm Research, 26*(1), 54–61.

Hassanzadeh, M., Ebadi, A., Panahyan-e-Kivi, M., Eshghi, A. G., Jamaati-e-Somarin, S., Saeidi, M., & Zabihi-e-Mahmoodabad, R. (2009). Evaluation of drought stress on relative water content and chlorophyll content of sesame (*Sesamum Indicum* L.) genotypes at early flowering stage. *Research Journal of Environmental Sciences, 3*(3), 345–350. https://doi.org/10.3923/rjes.2009.345.350

Henson, I. E., & Harun, M. H. (2005). The influence of climatic conditions on gas and energy exchanges above a young oil palm stand in north Kedah, Malaysia. *Journal of Oil Palm Research, 17*(4), 73–91.

Hidangmayum, A., & Sharma, R. (2017). Effect of different concentrations of commercial seaweed liquid extract of *Ascophyllum nodosum* as a plant biostimulant on growth, yield and biochemical constituents of onion (*Allium cepa* L.). *Journal of Pharmacognosy and Phytochemistry, 6*(4), 658–663.

Idris, Z. H. C., Subki, A., Abidin, A. A. Z., & Yusof, Z. N. B. (2018). The effect of oxidative stress towards the expression of thiamine biosynthesis genes (THIC & THI1/THI4) in oil palm (*Elaeis guineensis*). *Tropical Life Sciences Research, 29*(1), 71–85. https://doi.org/10.21315/tlsr2018.29.1.5

Irani, H., ValizadehKaji, B., & Naeini, M. R. (2021). Biostimulant-induced drought tolerance in grapevine is associated with physiological and biochemical changes. *Chemical and Biology Technology in Agriculture, 8*(1), 1–3. https://doi.org/10.1186/s40538-020-00200-9

Jabeen, M., Akram, N. A., Ashraf, M., Alyemeni, M. N., & Ahmad, P. (2020). Thiamin stimulates growth and secondary metabolites in turnip (*Brassica rapa* L.) leaf and root under drought stress. *Physiologia Plantarum, 172*(2), 1399–1411. https://doi.org/10.1111/ppl.13215

Kamarudin, A. N., Idris, A. S., & Yusof, Z. N. B. (2017a). Thiamine biosynthesis gene

expression analysis in *Elaeis guineensis* during interactions with *Hendersonia toruloidea*. *Journal of Oil Palm Research, 29*(2), 218–226. https://doi.org/10.21894/jopr.2017.2902.06

Kamarudin, A. N., Lai, K. S., Lamasudin, D. U., Idris, A. S., & Yusof, Z. N. B. (2017b). Enhancement of thiamine biosynthesis in oil palm seedlings by colonization of endophytic fungus *Hendersonia toruloidea*. *Frontiers in Plant Science, 8*, 1799. https://doi.org/10.3389/fpls.2017.01799

Kaya, C., Ashraf, M., Sonmez, O., Tuna, A. L., Polat, T., & Aydemir, S. (2015). Exogenous application of thiamin promotes growth and antioxidative defense system at initial phases of development in salt-stressed plants of two maize cultivars differing in salinity tolerance. *Acta Physiologiae Plantarum, 37*(1), 1741. https://doi.org/10.1007/s11738-014-1741-3

Kumari, R., Kaur, I., & Bhatnagar, A. K. (2011). Effect of aqueous extract of *Sargassum johnstonii* Setchell & Gardner on growth, yield and quality of *Lycopersicon esculentum* Mill. *Journal of Applied Phycology, 23*, 623–633. https://doi.org/10.1007/s10811-011-9651-x

Kushairi, A., Loh, S. K., Azman, I., Hishamuddin, E., Ong-Abdullah, M., Izuddin, Z. B., Razmah, G., Sundram, S., & Parveez, G. K. A. (2018). Oil palm economic performance in Malaysia and R&D progress in 2017. *Journal of Oil Palm Research, 30*(2), 163–195. https://doi.org/10.21894/jopr.2018.0030

Ladt, K., Ganguly, A., & Roy, S. (2016). Axonal actin in action: Imaging actin dynamics in neurons. *Methods in Cell Biology, 131*, 91–106. https://doi.org/10.1016/bs.mcb.2015.07.003

Latique, S., Chernane, H., Mansori, M., & El-Kaoua, M. (2013). Seaweed liquid fertilizer effect on physiological and biochemical parameters of bean plant (*Phaseolus vulgaris* variety Paulista) under hydroponic system. *European Scientific Journal, 9*(30), 174–191.

Lee, W. K., Lim, P. E., Phang, S. M., Namasivayam, P., & Ho, C. L. (2016). Agar properties of *Gracilaria* species (*Gracilariaceae, Rhodophyta*) collected from different natural habitats in Malaysia. *Regional Studies in Marine Science, 7*, 123–128. https://doi.org/10.1016/j.rsma.2016.06.001

Mansori, M., Chernane, H., Latique, S., Benaliat, A., Hsissou, D., & Kaoua, M. E. (2016). Effect of seaweed extract (*Ulva rigida*) on the water deficit tolerance of *Salvia officinalis* L. *Journal of Applied Phycology, 28*(2), 1363–1370. https://doi.org/10.1007/s10811-015-0671-9

Najihah, T. S., Ibrahim, M. H., Razak, A. A., Nulit, R., & Megat, P. E. W. (2019). Effects of water stress on the growth, physiology and biochemical properties of oil palm seedlings. *AIMS Agriculture and Food, 4*(4), 854–868. https://doi.org/10.3934/agrfood.2019.4.854

Noli, Z. A., Suwirmen, N., Aisyah, N., & Aliyyanti, P. (2021). Effect of liquid seaweed extracts as biostimulant on vegetative growth of soybean. *IOP Conference Series: Earth and Environmental Science, 759*, 012029. https://doi.org/10.1088/1755-1315/759/1/012029

Noor, M. R. M., Harun, M. H., & Jantan, N. M. (2011). Physiological plant stress and responses in oil palm. *Oil Palm Bulletin, 62*, 25–32.

Rahman, N. S. A., Ghazali, N. S., & Yusof, Z. N. B. (2017). Changes in the expressions of thiamine biosynthesis genes (THIC and THI1/THI4) in oil palm (*Elaeis guineensis*) as response to salinity stress. *Crop Research, 18*(4), 634–641. https://doi.org/10.5958/2348-7542.2017.00106.1

Ramya, S. S., Nagaraj, S., & Vijayanand, N. (2011). Influence of seaweed liquid extracts on growth, biochemical and yield characteristics of *Cyamopsis tetragonaloba* (L.) Taub. *Journal of Phytology, 3*(9), 37–41.

Rapala-Kozik, M., Goøda, A., & Kujda, M. (2009). Enzymes that control the thiamine diphosphate pool in plant tissues. Properties of thiamine pyrophosphokinase and thiamine-(di)phosphate phosphatase purified from *Zea mays* seedlings. *Plant Physiology and Biochemistry, 47*, 237–242. https://doi.org/10.1016/j.plaphy.2008.12.015

Rapala-Kozik, M., Wolak, N., Kujda, M., & Banas, A. K. (2012). The upregulation of thiamine (vitamin B1) biosynthesis in *Arabidopsis thaliana* seedlings under salt and osmotic stress conditions is mediated by abscisic acid at the early stages of this stress response. *BMC Plant Biology, 12*, 1–14. https://doi.org/10.1186/1471-2229-12-2

Rosado-Souza, L., Fernie, A. R., & Aarabi, F. (2020). Ascorbate and thiamin: Metabolic modulators in plant acclimation responses. *Plants, 9*(1), 101. https://doi.org/10.3390/plants9010101

Sakthivel, R., & Devi, K. P. (2014). Evaluation of physicochemical properties, proximate and nutritional composition of Gracilaria edulis collected from Palk Bay. *Food Chemistry, 174*, 68–74. https://doi.org/10.1016/j.foodchem.2014.10.142

Salim, B. B. M. (2016). Influence of biochar and seaweed extract applications on growth, yield and mineral composition of wheat (*Triticum aestivum* L.) under sandy soil conditions. *Annals of Agricultural Science, 61*(2), 257–265. https://doi.org/10.1016/j.aoas.2016.06.001

Santaniello, A., Scartazza, A., Gresta, F., Loreti, E., Biasone, A., Tommaso, D. D., Piaggesi, A., & Perata, P. (2017). *Ascophyllum nodosum* seaweed extract alleviates drought stress in *Arabidopsis* by affecting photosynthetic performance and related gene expression. *Frontiers in Plant Science, 8*, 1–15. https://doi.org/10.3389/fpls.2017.01362

Sapak, Z., Meon, S., & Ahmad, Z. A. M. (2008). Effect of endophytic bacteria on growth and suppression of *Ganoderma* infection in oil palm. *International Journal of Agriculture and Biology, 10*(2), 127–132.

Sayed, S., & Gadallah, M. (2002). Effects of shoot and root application of thiamin on salt-stressed sunflower plants. *Plant Growth Regulation, 36*(1), 71-80.

Shukla, P. S., Mantin, E. G., Adil, M., Bajpai, S., Critchley, A. T., & Prithiviraj, B. (2019). *Ascophyllum nodosum*-based biostimulants: Sustainable applications in agriculture for the stimulation of plant growth, stress tolerance, and disease management. *Frontiers in Plant Science, 10*, 655. https://doi.org/10.3389/fpls.2019.00655

Skirycz, A., & Inzé, D. (2010). More from less: Plant growth under limited water. *Current Opinion in Biotechnology, 21*(2), 197–203. https://doi.org/10.1016/j.copbio.2010.03.002

Subki, A., Thaw, S. F. K., & Yusof, Z. N. B. (2018). Regulation of thiamine biosynthesis upon exogenous application of the vitamin in oil palm (*Elaeis guineensis*). *Journal of Oil Palm Research, 30*(2), 236–241. https://doi.org/10.21894/jopr.2018.0028

Subki, A., Ho, C. L., Ismail, N. F. N., Abidin, A. A. Z., & Yusof, Z. N. B. (2020). Identification and characterisation of thiamine pyrophosphate (TPP) riboswitch in *Elaeis guineensis*. *PLoS ONE, 15*(7), e0235431. https://doi.org/10.1371/journal.pone.0235431

Sun, C., Cao, H., Shao, H., Lei, X., & Xiao, Y. (2011). Growth and physiological responses to water and nutrient stress in oil palm. *African Journal of Biotechnology, 10*(51), 10465–10471. https://doi.org/10.5897/AJB11.463

Tunc-Ozdemir, M., Miller, G., Song, L., Kim, J., Sodek, A., Koussevitzky, S., Misra, A. N., Mittler, R., & Shintani, D. (2009). Thiamin confers enhanced tolerance to oxidative stress in *Arabidopsis*. *Plant Physiology, 151*(1), 421–432. https://doi.org/10.1104/pp.109.140046

Tursun, A. O. (2022). Effect of foliar application of seaweed (organic fertilizer) on yield, essential oil and chemical composition of coriander. *PLoS ONE, 17*(6), e0269067. https://doi.org/10.1371/journal.pone.0269067

Trivedi, K., Anand, K. G. V., Kubavat, D., Kumar, R., Vaghela, P., & Ghosh, A. (2017). Crop stage selection is vital to elicit optimal response of maize to seaweed bio-stimulant application. *Journal of Applied Phycology, 29*(4), 2135–2144. https://doi.org/10.1007/s10811-017-1118-2

Wong, S. Y., Aziz, S. D. S., & Yusof, Z. N. B. (2016). Osmotic stress upregulates the transcription of thiamine (vitamin B1) biosynthesis genes (THIC and THI4) in oil palm (*Elaeis guineensis*). *African Journal of Biotechnology, 15*(29), 1566–1574. https://doi.org/10.5897/AJB2016.15222

Yee, Y. Y., Ching, Y. C., Rozali, S., Hashim, N. A., & Singh, R. (2016). Preparation and characterization of poly (lactic acid)-based composite reinforced with oil palm empty fruit bunch fiber and nanosilica. *BioResources, 11*(1), 2269–2286. https://doi.org/10.15376/biores.11.1.2269-2286

Yusof, Z. N. B., Borhan, F. P., Mohamad, F. A., & Rusli, M. H. (2015). The effect of *Ganoderma boninense* infection on the expressions of thiamine (vitamin B1) biosynthesis genes in oil palm (*Elaeis guineensis*). *Journal of Oil Palm Research, 27*(1), 12–18.

Journal of Oil Palm Research Vol. 37 (1) March 2025 p. 64-71
DOI: https://doi.org/10.21894/jopr.2023.0064

In Vitro CULTURAL STUDIES FOR CALLOGENESIS AND EMBRYOGENESIS OF OIL PALM (*Elaeis guineensis* Jacq.) USING SEEDLING AND SPEAR LEAF EXPLANTS

B KALYANA BABU[1]*; R K MATHUR[1]; K SURESH[1]; G RAVICHANDRAN[1]; B SUSANTHI[1] and S TIWARI[1]

ABSTRACT

In oil palm, hybrids are not homogeneous due to their highly heterogeneous nature. However, the generation of homogeneous material is of prime importance, which can be possible only by using somatic embryogenesis using explants like spear leaf and seedling leaf. Evaluation of callogenesis and embryogenesis of oil palm using seedling and spear leaf is reported here. This is the first report on in vitro *production of callus and somatic embryos using leaves as explants in India. Seedling leaf experiment revealed that callus induction ranged from 3%-4% among the four media combinations used in the study. Somatic embryo induction was observed in modified Murashige and Skoog (MS) containing picloram (37.26 µmol). The minimum time required for callus induction was 29 days whereas the maximum time required for initiation of callus was five months and four days. The minimum time required for induction of embryogenic callus was noted to be seven months and five days on two different media, whereas, the maximum time was 11 months and 14 days on modified N6 with dicamba (72.39 µmol) (palm No. 377). The present study opens up the prospect of understanding embryogenesis and manipulating* in vitro *culture conditions to achieve plantlet regeneration in oil palm using leaf explant.*

Keywords: oil palm, seedling leaf, somatic embryo, spear leaf.

Received: 29 May 2023; **Accepted:** 30 October 2023; **Published online:** 26 December 2023.

INTRODUCTION

Oil palm (*Elaeis guineensis* Jacq.) is a monocotyledonous, perennial, cross-pollinating, crop belonging to Arecaceae family, cultivated in Africa, Latin America and Southeast Asia. It is now designated as the world's principal vegetable oil crop credited with high productivity and long life spans (Woittiez *et al.*, 2017). In addition to serving as edible oil, its increasing commercial importance in food, soap and oleo-chemical manufacturing industries; there has been a significant rise in its area under cultivation (19 million hectares) and production of palm oil (81 million tonnes) over the last two decades (Murphy *et al.*, 2021). However, to meet the demand for palm oil by ever-increasing population, the multiplication of oil palm plantlets is required on a commercial scale. Multiplication by conventional vegetative propagation of oil palm is not possible because of the presence of a single growing apex, while the seed propagation technique suffers from limitations like a substantial time required for seed germination (1-3 yr) and a very low germination rate (30%) (Martine *et al.*, 2009). The *in vitro* propagation method has evolved as a promising alternative method for the cultivation of oil palm which could address these limitations and has the potential to increase oil production by 20% (Kushairi *et al.*, 2010). Besides this, superior oil quality, reduced palm height (secondary characters), important agronomic characteristics and healthy quality of seeds found in particular elite oil palm genotype could be uniformly expressed in tissue culture-raised plantlets (Paranjothy *et al.*, 1989).

[1] ICAR-Indian Institute of Oil Palm Research, Pedavegi-534 435, Eluru (Dt), Andhra Pradesh, India.

* *Corresponding author e-mail*: *kalyan_biotek@yahoo.co.in, B.Babu@icar.gov.in*

To date, regeneration of oil palm through somatic embryogenesis has been reported using many explants like immature and mature zygotic embryos (Gomes *et al.,* 2015; 2016; Kanchanapoom & Domyoas, 1999; Monteiro *et al.,* 2017; Teixeira *et al.,* 1995; Thuzar *et al.,* 2011; Wan Nur Syuhada *et al.,* 2016), young plantlets (Scherwinski-Pereira *et al.,* 2010), immature male and female inflorescences (Jayanthi *et al.,* 2015; Rodrigo *et al.,* 2011; Teixeira *et al.,* 1994), immature leaves (Gomes *et al.,* 2017; Hashim *et al.,* 2018), and seedling leaves (Karun & Sajini, 1994). However, an efficient, universal protocol on the somatic embryogenesis and regeneration system of oil palm is lacking and not repetitive due to several factors, such as genotype, age of the parent tree and explant type (Wecks *et al.,* 2019). Every lab has its protocols for the generation of tissue culture plants in oil palm and hence, the present study aimed at standardising the *in vitro* protocols for callusing and somatic embryogenesis by using the spear and seedling leaves. Furthermore, precise details of the protocols are not available because of the commercial interests of business enterprises involved in micropropagation (Hashim *et al.,* 2018). Since somatic embryogenesis of oil palm is difficult to be conducted owing to recalcitrance, woody and perennial nature of the crop, and is also affected by several factors like medium composition, growth regulators and explant source, the present study thus endeavours to evaluate the callogenesis and embryogenesis processes by using two different explant types *i.e.,* seedling and spear leaves, for establishing an efficient *in vitro* regeneration system in oil palm.

MATERIALS AND METHODS

Plant Materials and Culture Initiation

Oil palm seedlings of hybrid *Tenera* (*dura* × *pisifera*) were obtained from the nursery of ICAR-Indian Institute of Oil Palm Research, Pedavegi, Andhra Pradesh, India. The seedlings were first washed with running tap water, and followed by washing with bavistin (1% w/v) for 20 min and finally washed with 20% (v/v) sodium hypochlorite (HiMedia, India) for 20 min. The outermost leaves were removed destructively, keeping a few interior leaves with the middle column, followed by surface sterilisation with 70% (v/v) ethanol (Merck, India) for 30 s and then thoroughly washed with sterile distilled water for three times, followed by blot drying in a laminar air flow cabinet for 5 min. Subsequently, outer leaf whorls were removed and the leaf lamina and leaf base were taken from the central portion, containing the meristematic region, and later were cut into small pieces (0.5-1.0 cm). To initiate cultures, leaves were inoculated on media, *viz*., modified MS (Murashige & Skoog, 1962), modified N6 (Chu *et al.,* 1975), and modified Y3 (Eeuwens & Blake, 1976), supplemented with growth regulators (*Table 1*). The composition of media used in the present experiment is shown *Table 1*. Cultures were sub-cultured every two months on each respective medium, supplemented with growth regulators for six months, and followed by sub-culturing onto a half-strength respective medium with the same concentration of growth regulators for six months. Cultures were incubated at 26°C-27°C temperature and ± 60%-65% relative humidity during the entire course of study. The time required for callus induction, somatic embryo formation and percentage of callus induction and somatic embryo formation were noted.

Ortets were selected on the basis of having high yielding capacity of more than 250 kg yr^{-1}, with good bunch parameters (oil to bunch ratio >25%), vegetative growth and healthy condition of the palm, which is free of pests and diseases. The age of selected ortets was 15 years old. The method followed here as per the earlier reports (Hashim *et al.,* 2018). Briefly, all the thorns were removed and fronds were flattened for the collection of the spear leaves which were present within a cylinder of older leaf petioles at the centre of the palm canopy. Subsequently, older fronds and fruit bunches were removed successively to get the cabbage (younger frond petioles) which was cut without disturbing the shoot apex. The cabbage was then placed in a bag and lowered to the ground and the cut ends of cabbage were immediately covered with aluminium foil and brought to the laboratory. The aluminium foil was later removed from the cut ends and the whole cabbage was checked for breakage, freshness and kept in a disease free condition by disinfecting with 70% (v/v) ethanol (Merck, India). Following that, both ends of the cabbage were trimmed and the cabbage was then placed in a laminar airflow followed by frond marking (Monteiro *et al.* 2017). The outermost petiole was later removed by cutting longitudinally and subsequently internal petioles were removed, until the stacks of spear leaves (immature leaflets) were exposed. The immature leaf stacks were cut at 5-6 cm from the distal ends and discarded to avoid any contamination. To initiate culture, sub-stacks of 5-6 leaflets were taken from the stack of leaflets and transferred to another sterile petri plate for explant cutting. These leaflets were cut into strips of about 2 mm and were inoculated on different types of media as mentioned in *Table 2*. The media preparation method and pH conditions were maintained exactly similar as above for the seedling leaf experiment.

The callus percentage was calculated by taking the number of tubes having callus and divided by the total number of tubes in each replication, and

TABLE 1. COMPOSITION OF MEDIA USED IN OIL PALM TISSUE CULTURE

Nutrient composition of media used in the study (mg L^{-1})			
Chemicals	**Modified MS (1962)**	**Modified N6 (Chu *et al.*, 1975)**	**Modified Y3 (Eeuwens, 1976)**
Macro nutrients			
NH_4Cl	-	-	535
NH_4NO_3	1,650	-	-
$NaH_2PO_4.2H_2O$	-	-	276
KNO_3	1,900	2,830	2,020
$CaCl_2.2H_2O$	440	166	294
$MgSO_4.7H_2O$	370	185	247
KH_2PO_4	-	400	-
KH_2PO_2	170	-	-
$(NH_4)_2SO_4$	-	463	-
KCl	-	-	1,492
Micro nutrients			
H_3BO_3	6.2	1.6	3.10
$MnSO_4.4H_2O$	22.3	4.4	11.2
KI	0.83	0.80	8.30
$ZnSO_4.7H_2O$	8.6	1.5	7.2
$CuSO_4.5H_2O$	0.025	-	0.250
$CoCl_2.6H_2O$	0.025	-	0.240
$Na_2MoO_4.2H_2O$	0.25	-	0.24
NaFeEDTA	37.5	-	-
Na_2EDTA	-	37.2	-
$NaEDTA.2H_2O$	-	-	37.2
$NaMO_4$	-	-	-
$NiCl_2.6H_2O$	-	-	0.024
$FeSO_4.7H_2O$	-	27.8	13.9
Vitamins			
Myo-inositol	100	-	100
Nicotinic acid	0.5	0.5	1.0
Pyridoxine-HCl	0.5	0.5	1.0
Thiamine-HCl	0.1	1.0	2.0
Glycine	200	2	2
Amino acids			
L-Glutamine	100	-	100
L-Arginine	100	-	200
L-Asparagine	100	-	100
Sucrose	30,000	30,000	30,000
Casein hydrolysate	500	500	500
Activated charcoal	3,000	3,000	3,000
Agar	8,000	8,000	8,000

expressed in terms of percentage. Likewise, the embryogenic percentage was calculated by dividing the number of bottles having embryos and divided by the total number of bottles in each replication. The factorial, randomised complete block design experiments were performed with five replications. The critical difference (CD) and least significant difference (LSD) were calculated to determine if any significant difference existed among the treatments.

RESULTS AND DISCUSSION

The induction of nodular calli from seedling leaf veins were observed after 60 days of inoculation, in four media compositions *i.e.,* modified MS + picloram (37.26 µmol), modified MS + picloram (149.06 µmol), modified Y3 + dicamba (10.00 µmol) and modified Y3 + dicamba (19.95 µmol), among the 32 media combinations attempted (data not shown).

It was observed that the callus induction ranged from 3%-4%, among the four media combinations (*Table 3*). The induced primary calli were white and actively proliferating (*Figure 1*).

There was no morphogenic variability among all the induced calli. It was observed that the primary calli after initiation had induced a single somatic embryo in the modified MS containing picloram (37.26 µmol) (when maintained on its respective medium with growth regulators for 240 days, with every two months of sub-culturing and followed by transferring to respective half-strength medium, supplemented with the same concentration of growth regulators for two months) (*Figure 2*). The other media compositions did not induce any somatic embryos. During these periods, there was no incidence of direct embryogenesis which supported the findings of Karun and Sajini (1994). Moreover, in the present study, it was observed that the induced embryo started to deteriorate in the half strength medium, therefore, it was transferred to a full strength medium, supplemented with the same concentration of growth regulator to retain its embryogenecity, which was similar to Hilae and Te Chato (2005), that suggested a full strength MS, rather than half strength MS for oil palm. Moreover, the role of picloram in the induction of the primary calli and somatic embryo as seen in the present study, also supported the earlier findings which mentioned the suitability of picloram to get embryogenic cultures in different palm species *viz.*, areca palm (Karun *et al.*, 2004), peach palm (Steinmacher *et al.*, 2007), and acai palm.

The spear leaves collected from different palms (*Table 2*), and inoculated on different media supplemented with growth regulators, had resulted into the induction of primary and embryogenic calli. It was observed that palm (P-204), when inoculated on media *viz.*, modified MS + Y3 vitamins, with differing α-napthalene acetic acid (NAA) and dicamba concentrations, had resulted in callus initiation in only 19 days. Whereas, the maximum time required for initiation of primary callus was about 154 days from explants derived from palm (P-377) and inoculated onto modified Y3 supplemented with NAA (534.99 µmol). The minimum time required for induction of embryogenic callus from the primary callus was 215 days for palm (P-204), and the maximum time was recorded at 344 days for palm (P-377). The maximum percentage of induction of primary callus was 0.55% for palm (P-377).

TABLE 2. *In Vitro* MORPHOGENIC RESPONSE OF SPEAR LEAF DERIVED CULTURES

Genotype	Media	Primary callus % ± SD	No. of months (M) & days (D) required for initiation of primary callus	No. of months (M) & days (D) required for initiation of embryogenic callus
P-419	Modified Y3 + NAA (179.80 µmol)	0.03 ± 0.01^{a}	2 M & 10 D	11 M & 10 D
	Modified Y3 + NAA (119.87 µmol)	0.07 ± 0.02^{b}	2 M & 10 D	9 M
P-204	Modified MS + Y3 vitamins + NAA (322.23 µmol)	0.03 ± 0.01^{c}	19 D	7 M & 5 D
	Modified MS + Y3 vitamins + Dicamba (72.39 µmol)	0.03 ± 0.01^{c}	19 D	7 M & 5 D
P-377	Modified Y3 + NAA (534.99 µmol)	0.55 ± 0.07^{c}	5 M & 4 D	-
	Modified N6 + Dicamba (72.39 µmol)	0.28 ± 0.03^{c}	4 M & 5 D	11 M & 14 D
P-251	Modified Y3 + Picloram (74.53 µmol)	0.04 ± 0.02^{c}	1 M & 13 D	9 M
	F (cal)	203.001		
	CD 1%	0.057		

Note: Values with similar alphabet are not significantly different.

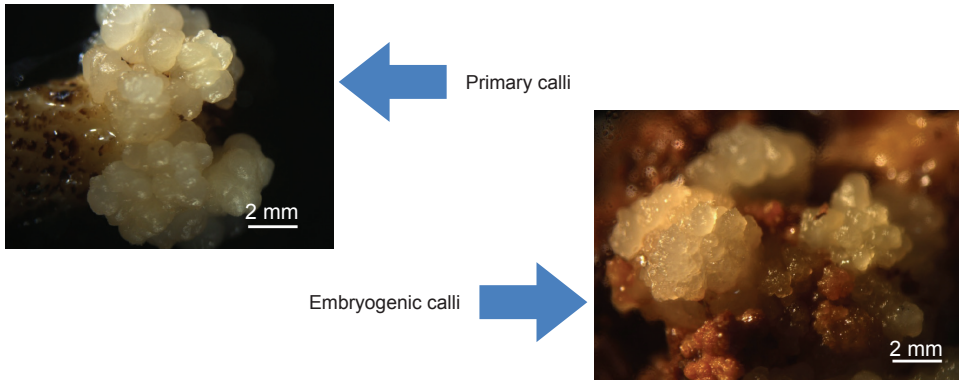


Figure 1. The callus formation in oil palm using seedling leaf tissue.

TABLE 3. *In Vitro* MORPHOGENIC RESPONSE OF SEEDLING LEAF DERIVED CULTURES

Genotype	Media	Primary callus % ± SD
Tenera	Modified MS (1962) + Picloram (37.26 μmol)	4.00 ± 0.51[a]
	Modified MS (1962) + Picloram (149.06 μmol)	3.80 ± 0.35[b]
	Modified Y3 (Eeuwens, 1976) + Dicamba (10.00 μmol)	3.84 ± 0.29[b]
	Modified Y3 (Eeuwens, 1976) + Dicamba (19.95 μmol)	3.77 ± 0.21[b]
	F (cal)	3.799
	CD 5%	0.561

Note: Values with similar alphabet are not significantly different.

However, it was observed that there was no induction of somatic embryo from any embryogenic callus, even after maintaining cultures with high auxin and followed by transferring to half concentration of auxin or no auxin, which was contrary to Rival and Parveez (2005). The present study also showed that long exposure of explants to auxin is not required for the initiation of callus in all the palms which is contrary to Hashim *et al.* (2018), where the minimum and maximum time required for callus initiation ranged between 3-12 months. Since the long-term exposure of explants to auxin is not recommended because of the chances of somaclonal variations, the present findings demonstrated the efficiency of medium compositions for early induction of primary callus. In general, oil palm tissue culture suffers from phenolic oxidation, leading to the browning of explants, and therefore activated charcoal was amended in the media (Teixeira *et al.,* 1994; Patcharapisutsin & Kanchanapoom, 1996). The addition of higher concentration of auxin becomes mandatory to achieve callogenesis, since activated charcoal is non-selective (Yusnita & Hapsaro, 2011) and absorbs part of the plant growth regulator. However, the present findings revealed that the concentration of auxins like 2,4-D and picloram, used in the present study, was comparatively less compared to other studies conducted by Gomes *et al.* (2017), where these were used in the range of 800 and 450 μmol respectively. The similar effect of NAA and dicamba individually in callogenesis has been studied. It was found that a modified Y3 medium supplemented with NAA alone could successfully induce callogenesis. However, some somatic embryos could not be induced, likely due to higher concentrations of NAA used in the present study (179.8 and 119.8 μmol), which might have led to oxidation of cultures and death. Likewise, the role of dicamba in callogenesis and embryogenesis was evaluated in the present study, since dicamba has been used successfully to induce direct and indirect embryogenic callus from tender leaf explants and cultured mature zygotic embryos of oil palm, and has been found suitable for mass propagation of *in vitro* seedlings and mature oil palms. From the present study, it was found that the media *viz.*, modified MS + Y3 vitamins and modified N6 media containing dicamba (72.39 μmol) could induce primary callus and form embryogenic callus, derived from explants of palms (P-204 & P-377) which is in agreement with Te Chato (1998), however, without the formation of somatic embryo. One of the factors which was recently found by Aroonluk *et al.* (2020) indicated that protein phosphorylation mechanism might be playing a major role in the somatic embryogenesis of oil palm. In another set of experiments, a combined effect of auxin and cytokinin for callogenesis was studied. The N6 modified media supplemented with 2,4-D and BAP resulted in the induction of primary callus and embryogenic callus. Although the addition of cytokinin with auxin in oil palm tissue culture is avoided since it causes abnormality, it was still added in the present study to get embryogenic cultures, capable of forming somatic embryos. The identification of genes influencing somatic embryogenesis also helps in screening the germplasm with high potency of embryogenesis (Chan *et al.*, 2020; Zhang *et al.*, 2022). This will facilitate to identify the palms at an early stage for their use in *in vitro* studies. However, it was observed that the addition of cytokinin along with auxin did not bring any change and ultimately no somatic embryo was induced. The possible explanation of failure of embryogenic cultures to produce somatic embryos in all the palms, can be attributed to its genotypic effect and the presence of varying levels of cytokinin which might have interfered in somatic embryogenesis, irrespective of any media composition used. Moreover, auxin concentration used in the present study might have failed to influence cellular activity to interfere with the endogenous hormones which can trigger gene expression towards re-differentiation for somatic embryo induction.

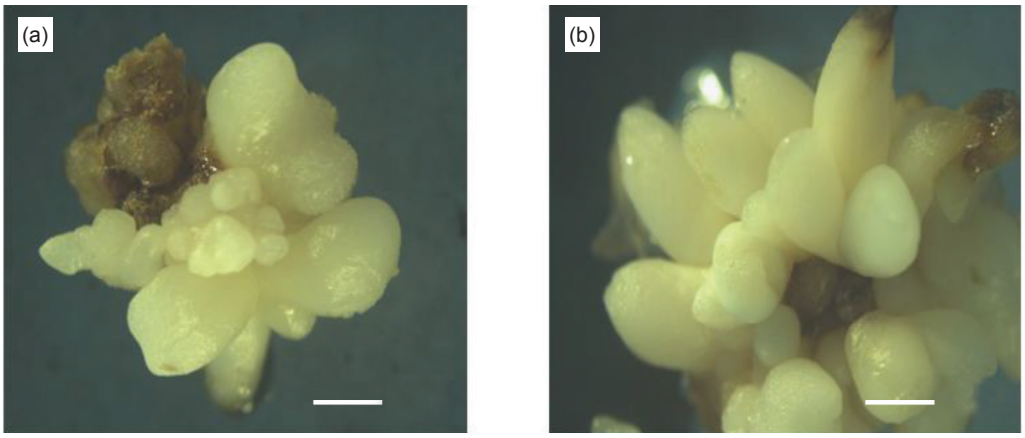


Figure 2. The callus and somatic embryo formation in oil palm by using the spear leaf. (a) Embryo initiation and (b) embryogenic calli with globular and nodular structures (bar = 2 mm).

CONCLUSION

The *in vitro* induction of callogenesis and somatic embryogenesis is a significant step in achieving the *in vitro* organogenesis in oil palm. The present study reported the induction of callus and embryogenic calli from immature leaf and spear leaf explants. The study also reported the minimum time required for initiation of callus, which was 29 days, compared to the maximum time required for initiation of callus, which was about 154 days. Further studies are required to strengthen the *in vitro* regeneration protocols in oil palm, using other explants like immature male inflorescence for generating homogeneous planting material.

ACKNOWLEDGEMENT

The authors would like to acknowledge Director, ICAR-IIOPR, Pedavegi for providing financial support.

REFERENCES

Aroonluk, S., Roytrakul, S., & Jantasuriyarat, C. (2020). Identification and characterization of phosphoproteins in somatic embryogenesis acquisition during oil palm tissue culture. *Plants, 9*(1), 36. https://doi.org/10.3390/plants9010036

Chan, P., Rose, R. J., Murad, A. M. A., Zainal, Z., Ong, P., Ooi, L. C., Low, E. L., Ishak, Z., Yahya, S., Song, Y., & Singh, R. (2020). Early nodulin 93 protein gene: Essential for induction of somatic embryogenesis in oil palm. *Plant Cell Reports, 39*(7), 1395–1413. https://doi.org/10.1007/s00299-020-02571-7

Chu, C. C., Wang, C. C., Sun, C. C., Hsu, C., Yin, K. C., Chu, C. Y., & Bi, F. Y. (1975). Establishment of an efficient medium for another culture of rice through comparative experiments on the nitrogen sources. *Science Sinica, 18*, 659–668.

Eeuwens, C. J. (1976). Mineral requirements for growth and callus initiation of tissue explants excised from mature coconut palms (*Cocos nucifera*) and cultured *in vitro*. *Physiologia Plantarum, 36*(1), 23–28. https://doi.org/10.1111/j.1399-3054.1976.tb05022.x

Gomes, H. T., Bartos, P. M. C., & Scherwinski-Pereira, J. E. (2015). Optimizing rooting and survival of oil palm (*Elaeis guineensis)* plantlets derived from somatic embryos. *In Vitro Cellular & Developmental Biology - Plant, 51*(1), 111–117. https://doi.org/10.1007/s11627-015-9669-x

Gomes, H. T., Bartos, P. M. C., & Scherwinski-Pereira, J. E. (2017). Dynamics of morphological and anatomical changes in leaf tissues of an interspecific hybrid of oil palm during acquisition and development of somatic embryogenesis. *Plant Cell Tissue and Organ Culture (PCTOC), 131*(2), 269–282. https://doi.org/10.1007/s11240-017-1282-8

Gomes, H. T., Bartos, P. M. C., Balzon, T. A., & Scherwinski-Pereira, J. E. (2016). Regeneration of somatic embryos of oil palm (*Elaeis guineensis*) using temporary immersion bioreactors. *Industrial Crops and Products, 89*, 244–249. https://doi.org/10.1016/j.indcrop.2016.05.021

Hashim, A. T., Ishak, Z., Rosli, S. K., Ong-Abdullah, M., Ooi, S. E., & Husri, M. N. (2018). Oil palm (*Elaeis guineensis* Jacq.) somatic embryogenesis. In S. M. Jain & P. Gupta (Eds.), *Stepwise protocols for somatic embryogenesis of important woody plants* (pp. 209–229). Springer.

Hilae, A., & Te Chato, S. (2005). Effect of carbon sources and strength of MS medium on germination of somatic embryos of oil palm (*Elaeis guineensis* Jacq.). *Songklanakarin Journal of Science and Technology, 27*(3), 629–635.

Jayanthi, M., Susanthi, B., Mohan, N. M., & Mandal, P. K. (2015). *In vitro* somatic embryogenesis and plantlet regeneration from immature male inflorescence of adult *dura* and *tenera* palms of *Elaeis guineensis* (Jacq.). *SpringerPlus, 4*, 256. https://doi.org/10.1186/s40064-015-1025-4

Kanchanapoom, K., & Domyoas, P. (1999). The origin and development of embryoids in oil palm (*Elaeis guineensis* Jacq.) embryo culture. *Science Asia, 25*, 195–202.

Karun, A., & Sajini, K. K. (1996). Plantlet regeneration from leaf explants of oil palm seedlings. *Current Science*, *71*(11), 922–926. https://www.cabdirect.org/cabdirect/abstract/19971610101

Karun, A., Siril, E. A., Radha, E., & Parthasarathy, V. A. (2004). Somatic embryogenesis and plantlet regeneration from leaf and inflorescence explants of arecanut (*Areca catechu* L.). *Current Science, 89*, 1623–1628.

Kushairi, A., Tamizi, A. H., Zamzuri, I., Ong-Abdullah, M., Samsul Kamal, R., Ooi, S. E. & Rajanaidu, N., (2010, May 29). *Production performance and advances in oil palm tissue culture* [Paper presentation]. International Society of Oil Palm Breeders (ISOPB) Seminar on Advances in Oil Palm Tissue Culture, Yogyakarta, Indonesia.

Martine, M. B., Laurent, K. K., Pierre, B. J., Eugene, K. K., Hilaire, K. T., & Justin, K. Y. (2009). Effect of storage and heat treatments on the germination of oil palm (*Elaeis guineensis* Jacq.) seed. *African Journal of Agricultural Research, 4*(10), 931–937. https://doi.org/10.5897/ajar.9000233

Monteiro, T. R., Freitas, E. O., Nogueira, G. F., & Scherwinski-Pereira, J. E. (2017). Assessing the influence of subcultures and liquid medium during somatic embryogenesis and plant regeneration in oil palm (*Elaeis guineensis* Jacq.). *The Journal of Horticultural Science and Biotechnology, 93*(2), 196–203. https://doi.org/10.1080/14620316.2017.1360156

Murashige, T., & Skoog, F. (1962). A revised medium for rapid growth and bio assays with tobacco tissue cultures. *Physiologia Plantarum*, *15*(3), 473–497. https://doi.org/10.1111/j.1399-3054.1962.tb08052.x

Murphy, D. J., Goggin, K., & Paterson, R. R. M. (2021). Oil palm in the 2020s and beyond: Challenges and solutions. *CABI Agriculture & Bioscience, 2*, 39. https://doi.org/10.1186/s43170-021-00058-3

Parajothy, K., Rohani, O., Tan. C. C., Tan C. S. & Tarmizi, A. H. (1989). Current status and strategies of oil palm tissue culture research. In *PORIM International Palm Oil Development Conference,* 109-121.

Patcharapisutsin, W., & Kanchanapoom, K. (1996). Somatic embryogenesis and plantlet regeneration from oil palm (*Elaeis guineensis* Jacq.) callus. *Journal of the Science Society of Thailand, 22*, 13–20. https://www.thaiscience.info/Journals/Article/JSST/10422220.pdf

Rao, P. S., & Ganapathi, T. R. (1993). Micropropagation of palms. In M. R. Ahuja (Ed.), *Micropropagation of Woody Plants* (pp. 405–421). Springer.

Ree, J. F., & Guerra, M. P. (2015). Palm (*Arecaceae*) somatic embryogenesis. In Vitro *Cell & Developmental Biology – Plant, 51*, 589–602. https://doi.org/10.1007/s11627-015-9722-9

Rival, A., & Parveez, G. K. A. (2005). *Elaeis guineensis* oil palm. In R. E. Litz, F. Pliego-Alfaro, & J. I. Hormaza (Eds.), *Biotechnology of Fruit and Nut Crops* (pp. 113-143). CABI Publishing.

Rodrigo, D. S. G., Da Silva Tatiane, L., Z, N., Erluce, G. L., & Jonny, E. S. P. (2011). Initial requirements for embryogenic calluses initiation in thin cell layers explants from immature female oil palm inflorescences. *African Journal of Biotechnology, 10*(52), 10774–10780. https://doi.org/10.5897/ajb11.152

Scherwinski-Pereira, J. E., Da Guedes, R. S., Fermino, P. C. P., Silva, T. L., & Costa, F. H. S. (2010). Somatic embryogenesis and plant regeneration in oil palm using the thin cell layer technique. In Vitro *Cellular & Developmental Biology - Plant*, *46*(4), 378–385. https://doi.org/10.1007/s11627-010-9279-6

Steinmacher, D. A., Cangahuala-Inocente, G. C., Clement, C. R., & Guerra, M. P. (2007). Somatic embryogenesis from peach palm zygotic embryos. In Vitro *Cellular & Developmental Biology - Plant*, *43*(2), 124–132. https://doi.org/10.1007/s11627-007-9032-y

Te Chato, S. (1998). Fertile plant from young leaves-derived somatic embryos of oil palm. *Songklanakarin Journal of Science and Technology, 20*, 7–13.

Teixeira, J. B., Söndahl, M. R., Nakamura, T., & Kirby, E. G. (1995). Establishment of oil palm cell suspensions and plant regeneration. *Plant Cell Tissue and Organ Culture (PCTOC)*, *40*(2), 105–111. https://doi.org/10.1007/bf00037662

Teixeira, J. B., Söndahl, M. R., & Kirby, E. G. (1994). Somatic embryogenesis from immature inflorescence of oil palm. *Plant Cell Reports, 13*, 247–250. https://doi.org/10.1007/bf00233313

Thuzar, M., Vanavichit, A., Tragoonrung, S., & Jantasuriyarat, C. (2011). Efficient and rapid plant regeneration of oil palm zygotic embryos cv. *Tenera* through somatic embryogenesis. *Acta Physiologiae Plantarum, 33*(1), 123–128. https://doi.org/10.1007/s11738-010-0526-6

Wan Nur Syuhada, W. S., Rasid, O. A., & Parveez, G. K. A. (2016). Evaluation on the effects of culture medium on regeneration of oil palm plantlets from immature embryos (IE). *Journal of Oil Palm Research, 28*(2), 234–239.

Woittiez, L. S., Van Wijk, M. T., Slingerland, M., Van Noordwijk, M., & Giller, K. E. (2017). Yield gaps in oil palm: A quantitative review of contributing factors. *European Journal of Agronomy*, *83*, 57–77. https://doi.org/10.1016/j.eja.2016.11.002

Yusnita, N., & Hapsoro, D. (2011). *In vitro* callus induction and embryogenesis of oil palm (*Elaeis guineensis* Jacq.) from leaf explants. *HAYATI Journal of Biosciences*, *18*(2), 61–65. https://doi.org/10.4308/hjb.18.2.61

Zhang, A., Li, Y., Yarra, R., Li, R., Cao, H., & Jin, L. (2021). Genome-wide identification of WUSCHEL-related homeobox gene family and their expression analysis during somatic embryogenesis in oil palm (*Elaeis guineensis*). *Tropical Plant Biology*, *15*(1), 55–64. https://doi.org/10.1007/s12042-021-09299-y

Journal of Oil Palm Research Vol. 37 (1) March 2025 p. 72-84
DOI: https://doi.org/10.21894/jopr.2023.0062

ANALYSIS OF PUTATIVE *EgBBM* PROMOTER BINDING PROTEINS DURING OIL PALM SOMATIC EMBRYOGENESIS

KAMOLWAN KHIANCHAIKHAN[1]; SUVICHARK AROONLUK[2]; SUPACHAI VUTTIPONGCHAIKIJ[1,3] and CHATCHAWAN JANTASURIYARAT[1,3]*

ABSTRACT

BABY BOOM (BBM) *gene has been identified as a crucial factor in regulating somatic embryogenesis in plants. During this process, high levels of* BBM *expression are observed. Nonetheless, the mechanisms regulating the expression of* BBM *during somatic embryogenesis in oil palm remain unclear. In this study, we cloned and examined the* cis*-regulatory elements of the* EgBBM *promoter. Our analysis revealed the presence of* cis*-regulatory elements, such as ABRE, as-1, G-box, Sp1, STRE, ARE, CAT-Box and MYB, which are similar to those found in the promoters of* AtBBM *and* OsBBM1. *In addition, we conducted a DNA-protein pull-down assay followed by mass spectrometry to identify the potential binding proteins of the* EgBBM *promoter. Several proteins were related to histone modification through direct and indirect interaction for controlling the* EgBBM *expression. Therefore, this study highlighted a complex regulatory network formation of histone modification and putative* EgBBM *binding proteins through both DNA-protein and protein-protein interactions. Our findings provide valuable insights into the factors that influence the role of* EgBBM *in oil palm tissue culture during somatic embryogenesis.*

Keywords: *BABY BOOM (BBM)*, DNA-protein pull-down assay, somatic embryogenesis.

Received: 21 April 2023; **Accepted:** 30 October 2023; **Published online:** 29 November 2023.

INTRODUCTION

Elaeis guineensis Jacq., commonly known as the African oil palm, is a widely cultivated plant species used for oil production. The oil palm has three types of fruit: *Dura* (thick-shell), *Pisifera* (shell-less), and *Tenera* (thin-shell), which is a hybrid between *Dura* and *Pisifera* and is preferred for commercial palm oil production. Because *Tenera* oil palm produces segregated yields through seed production, it is more effective to grow elite oil palm plants true to their type through tissue culture, which also increases oil yield compared to commercial *Dura* x *Pisifera* seedlings (Wahid *et al*., 2015). However, the indirect somatic embryogenesis process used in oil palm tissue culture takes a long time (Konan *et al*., 2009), and regulating gene expression associated with this process can improve its efficiency.

Previous reports have established that *BABY BOOM (BBM)*, a member of the AP2/ERF family of transcription factors, is a crucial regulator of plant embryogenesis (Boutilier *et al*., 2002). The *BBM* gene, which encodes two AP2 DNA-binding domains, is expressed at high levels during somatic embryogenesis in certain plant species (Irikova *et al*., 2012; Kulinska-Lukaszek *et al*., 2012; Nic-Can *et al*., 2013). Moreover, *BBM* ectopic expression in specific plant species can induce somatic embryo

[1] Department of Genetics, Faculty of Science, Kasetsart University, 10900 Bangkok, Thailand.

[2] Program in Agriculture, Faculty of Agriculture and Life Sciences, Chandrakasem Rajabhat University, 10900 Bangkok, Thailand.

[3] Center for Advanced Studies in Tropical Natural Resources, National Research University-Kasetsart (CASTNAR, NRU-KU), Kasetsart University, 10900 Bangkok, Thailand.

* *Corresponding author e-mail: fscicwj@ku.ac.th*

formation (Deng *et al*., 2009; Ouakfaoui *et al*., 2010; Passarinho *et al*., 2008). In oil palm, *EgBBM* gene was investigated in the expression through RT-PCR and in-situ hybridisation. *EgBBM* gene was highly expressed in somatic embryos and proliferating tissues such as the early development of leaf primordia, root initials and provascular tissues (Morcillo *et al*., 2007; Wachananawat *et al*., 2017). The expression of the *BBM* gene can be regulated by various factors, including epigenetic mechanisms such as DNA methylation and histone modifications, which can influence chromatin accessibility and gene expression and are commonly observed during somatic embryo development (Duarte-Aké & De-la-Peña, 2016; Kumar & Van Staden 2017; Osorio-Montalvo *et al*., 2018). Previous studies have reported that the expression of *BBM* gene can be regulated by epigenetic modifications, such as DNA methylation and histone modification. For instance, H3K27me3, a mark associated with transcriptional repression, is detected at different levels on the *BBM* gene during somatic embryogenesis in certain plant species like coffee and *Arabidopsis* (Borg *et al*., 2020; Nic-Can *et al*., 2013). Furthermore, the binding of various proteins to the *cis*-regulatory elements in the *BBM* promoter is crucial for regulating its expression. However, the proteins that control the expression of *BBM* during oil palm somatic embryogenesis remain unknown. Therefore, this study focused on the analysis of *cis*-regulatory elements in *EgBBM* promoter and the identification of the putative *EgBBM* binding protein with DNA-protein pull-down assay followed by mass spectrometry.

The DNA-protein pull-down assay is a technique that can be utilised to identify DNA-binding proteins (Chaparian & Van Kessel, 2020). This method is effective in identifying promoter-binding proteins for gene regulation (Schlag *et al*., 2020). In this study, we analysed the promoter sequence of the oil palm *BBM* (*EgBBM*) gene and utilised the *EgBBM* promoter pull-down assay to identify potential proteins that may regulate *EgBBM* expression. Ultimately, understanding the regulation of *EgBBM* expression may help to shorten the somatic embryogenesis process in oil palm tissue culture.

MATERIALS AND METHODS

DNA Extraction and *EgBBM* Promoter Cloning

To obtain the *EgBBM* promoter sequence, DNA was extracted from oil palm leaf using the C-TAB method (Semagn, 2014), and a specific region 2458 base pairs upstream of the transcriptional start site was amplified using the *pEgBBM*_F (5′-ACCCTCCGTACTTAAATCAGTG-3′) and *pEgBBM*_R (5′-TTTGAGGAGAAGAGAAGG GAAG-3′) primers (NCBI accession number NM_001303564.1). The PCR reaction consisted of 35 cycles of 98°C for 10 s, 56°C for 45 s, and 72°C for 1 min, followed by a final extension at 72°C for 5 min. The resulting *EgBBM* promoter sequence was cloned into the pGEM®-T Easy vector (Promega, Wisconsin, USA), and the positive clones were selected for DNA sequencing using a barcode-tagged sequencing service provided by U2Bio Thailand.

Analysis of *EgBBM* Promoter Sequence

The PlantCARE database (https://bioinformatics.psb.ugent.be/webtools/plantcare/html/) was used to search for *cis*-regulatory elements in the *EgBBM* promoter sequence (*EgBBM* promoter sequence was submitted in an appendix). Tbtools software (https://github.com/CJ-Chen/TBtools) was then used to visualise these *cis*-regulatory elements.

Preparation of Biotinylated dsDNA Fragment of *EgBBM* Promoter

A specific region 2,458 base pairs of the *EgBBM* promoter fragments were amplified from the pGEM®-T Easy vector containing *EgBBM* promoter using biotinylated primers; *pEgBBM*_biotin_F (5′-biotin-ACCCTCCGTACTTAAATCAGTG-3′) and *pEgBBM*_biotin_R (5′-biotin-TTTGAGGAGAA GAGAAGGGAAG-3′). The PCR reaction conditions were as follows: 35 cycles of 98°C for 10 s, 56°C for 45 s, and 72°C for 1 min, followed by a final extension at 72°C for 5 min. The resulting biotinylated dsDNA fragment of the *EgBBM* promoter was purified using the MEGAquick-spin™ Plus Total Fragment DNA Purification Kit (iNtRON Biotechnology, Seongnam, Republic of Korea), and its quantity was determined using Nanodrop 2000 (Thermo Fisher, Massachusetts, USA).

Protein Extraction

Fifteen-week-old *Tenera* zygotic embryo explants from the Golden *Tenera* (KB) variety were cultured on callus induction medium. After three months, embryogenic callus was transferred to somatic embryo maturation medium until somatic embryo appeared (Thuzar *et al*., 2011). Total proteins were extracted from oil palm somatic embryo tissues at three to five months, including globular, torpedo, and cotyledon stages, which is the *EgBBM*-expressed stage (*Figure 1*). The tissue sample was ground in liquid nitrogen and dissolved in an ice-cold extraction buffer containing 10% glycerol, 25 mM Tris (pH 7.5), 1 mM EDTA, 150 mM NaCl, 2% w/v PVPP, 10 mM dithiothreitol, 1X protease inhibitor cocktail (Sigma), and 0.1% Tween 20 (Sigma). The mixture was then centrifuged at

4,200 xg for 30 min at 4°C, and the resulting supernatant was collected and filtered through a 0.45 µm syringe filter (De La Concepcion *et al*., 2018). The concentration of soluble protein was determined using the Bradford's method (Bio-Rad protein assay, Bio-Rad Laboratory, CA) and stored at -80°C. To perform SDS-PAGE, 10 µg of protein sample was separated on a 15% denaturing discontinuous polyacrylamide gel at 150V for 50 min and then stained with Bio-Safe Coomassie G-250 stain (Bio-Rad Laboratories, Inc., USA).

Promoter Pull-down Assay

A DNA-protein binding pulldown assay was conducted to identify proteins that bind to the *EgBBM* promoter according to Wu (2006). The assay involved mixing 4 µg of biotinylated dsDNA fragment of *EgBBM* promoter, 400 µg of total extracted proteins, and 40 uL of streptavidin agarose beads with 70% slurry in 500 µL of PBSI buffer. The mixture was incubated on a rocking platform at gentle speed for 3 hr at 4ºC and then centrifuged at 550 xg for 1 min at 4ºC. The pellet was collected and washed with 500 µL of PBSI buffer for three times, resuspended in 50 µL of 2X Laemmli sample buffer, and incubated at 95ºC for 5 min. The supernatant was collected and separated using 15% SDS-PAGE gel at 150V for 50 min and stained with Bio-Safe Coomassie G-250 stain. The concentration of promoter-binding proteins was measured by the Bradford's method (Bio-Rad protein assay, Bio-Rad Laboratory, CA), and 300 µg of these proteins were identified by Mass spectrometry (MS).

In-solution Digestion, Nano-LC-MS/MS Analysis and Data Analysis

The proteomic analysis was carried out at the Proteomics Services Center, Center for Research and Innovation, Faculty of Medical Technology, Mahidol University, Nakhon Pathom, Thailand. The promoter-binding proteins were cleaned up using Clean-up kit (GE Healthcare, USA) before dissolving the protein pellets in 8 M urea. The reduced proteins were then alkylated and digested with Trypsin, Gold (Promega, USA) for 16 hr at 37°C. The samples were dried in a CentriVap DNA Concentrator (Labconco Co., Kansas City, Missouri, USA), resuspended in 0.1% formic acid (FA), and cleaned up by C18 Zip tip. The cleaned peptide was then dried in the CentriVap and stored at -80°C until further processing. Finally, the sample was resuspended in 0.1% formic acid and the peptide concentration measured by Nano drop 1000 (Thermo Fisher Scientific, Bremen, Germany).

Peptides were analysed on an LC-MS/MS system including a Nano-liquid chromatograph (Dionex Ultimate 3000, RSLCnano System, Thermo Scientific) in combination with a CaptiveSpray source/Quadrupole ion trap mass spectrometer (Model Q-ToF Compact, Bruker, Germany). A linear gradient elution of Solvent B was used over 90 min at a flow rate of 300 nL/min and a column temperature of 60°C. The MS acquisition rate was set at 6 Hz, and AutoMSn CID fragmentation experiments were performed.

The peptide sequence was searched on the UNIPROT-*Elaeis guineensis* database using the MASCOT (Version 2.3) searching engine. Search parameters in MASCOT MS/MS Ions search were followed by carbamidomethyl at cysteine residues as fixed modification, oxidation on methionine were set as variable modifications, peptide tolerance ±1.6 Da, MS/MS fragment tolerance ±0.8 Da.

RESULTS AND DISCUSSION

***EgBBM* Promoter Sequence Analysis**

The promoter region is responsible for regulating the expression of a gene by integrating signals from various transcription factors (TFs)

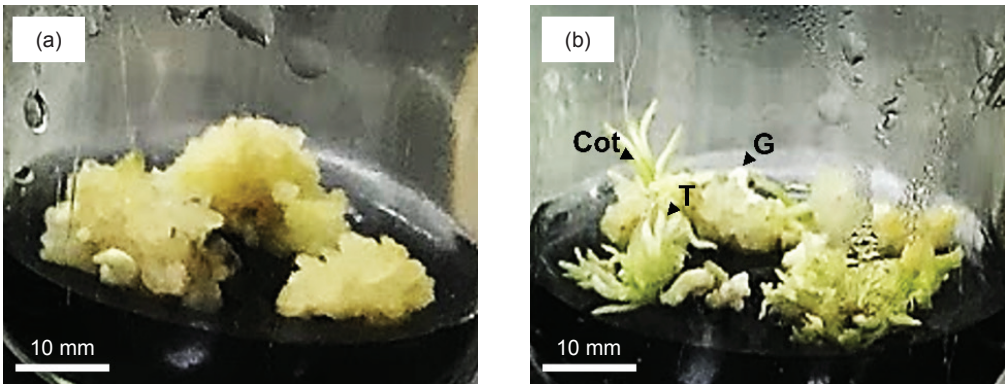


Figure 1. The oil palm tissues; (a) embryogenic callus at 3 months on callus induction medium and (b) somatic embryo tissues at 3-5 months including globular (G), torpedo (T) and cotyledon (Cot) stages on somatic embryo maturation medium used in this study, scale bar.

to establish a specific pattern of gene expression. In this study, the *EgBBM* promoter was analysed for *cis*-regulatory elements using the PlantCARE database. The promoter region of *EgBBM* gene contains several *cis*-regulatory elements involved in hormone response, light response, condition specificity, plant tissue specificity, transcription factor binding, unnamed factors, and common elements (*Table 1*). The presence of these *cis*-regulatory elements suggests that they may be involved in the regulation of *EgBBM* expression by recruiting factor binding in the promoter region. It is noteworthy that some *cis*-regulatory elements are shared with the promoters of *AtBBM* and *OsBBM1*, which have been shown to be active in promoting gene expression.

The promoter region of *EgBBM*, which comprises *cis*-regulatory elements involved in hormone response, was analysed in this study. ABRE elements, known to play a role in ABA responsiveness, were found predominantly in the promoter regions of *EgBBM*, *AtBBM*, and *OsBBM1* (*Figure 2a*). These elements are recognised and bound to by the ABRE-BINDING PROTEIN/FACTOR (AREB/ABF) bZIP transcription factors, which help regulate ABA-responsive gene expression. In *Arabidopsis*, ABI5, a member of the AREB/ABF transcription factor family, has been found to be involved in seed maturation and germination by regulating the expression of *Late Embryogenesis Abundant* (*LEA*) genes. ABI5 directly binds to the ABRE element in the *AtEM6* promoter region in response to ABA, thereby activating late embryogenesis pathways following seed germination. ABI5 has also been shown to interact with the embryogenesis-related genes *LEC1* and *FUS3*, which regulate germination sensitivity to ABA and suppress vivipary. The TGA protein belongs to the basic region leucine zipper (bZIP) family and contains a bZIP DNA binding domain that interacts with activation sequence-1 (as-1) element for MeJA and SA responsiveness in regulating defense responses. TGA1 and TGA4 are required for shoot apical meristem (SAM) maintenance, flowering, and inflorescence architecture through their interaction with BLADE-ON-PETIOLE1 (BOP1) and BOP2.

The promoter regions of *EgBBM*, *AtBBM*, and *OsBBM1* contain shared *cis*-regulatory elements involved in light response, such as the G-box element and Sp1 element (*Figure 2b*). The G-box element is bound by bHLH and bZIP families, which regulate cell elongation, seed germination, and gene expression, while the Sp1-binding element is recognised by zinc finger proteins Sp1, although it has not been extensively studied in plants. These promoter regions also contain condition specific elements such as STRE and ARE elements (*Figure 2c*), which induce various stresses through zinc finger transcription factors and activate hypoxia-responsive genes, respectively (Gasch *et al*., 2015; Kuang *et al*., 2017; Walley *et al*., 2007). The CAT-box element, essential for meristem expression, is also present (*Figure 2d*). Moreover, MYB transcription factor binding element is common in the promoter regions of all three plant species (*Figure 2e*). MYB transcription factors have a wide range of biological functions, including cell division and differentiation, hormone responses, environmental factor responses, plant development, and metabolism (Li *et al*., 2019). For example, MYB118 promotes the formation of somatic embryos and upregulates the expression of *LEC1* gene, which is associated with embryonic development (Wang *et al*., 2008).

Identification of Putative Proteins Regulating *EgBBM* Expression

The study aimed to identify proteins that interact with the *EgBBM* promoter during the oil palm somatic embryo stages. DNA-protein pull-down assay was conducted, and the result showed that proteins with molecular weights of approximately 25 kDa were detected in both treatment and negative control, while a protein with a molecular weight of 15 kDa was detected only in the treatment group. This protein was considered a potential candidate for binding to the *pEgBBM* fragment. To further investigate the differences in protein profiles between the two groups, total eluted-DNA binding proteins in the treatment and negative control were identified using mass spectrometry (MS) (*Figure 3*).

The DNA-protein pull-down assay identified 495 proteins specifically observed in the *pEgBBM*-binding protein treatment, and several putative proteins were reported to be involved in embryogenesis as shown in *Table 2*. These candidate proteins were presented as putative binding partners to the *EgBBM* promoter or as proteins that indirectly regulate *EgBBM* gene expression through protein interactions.

Histone deacetylases and histone acetyltransferases are involved in the regulation of gene expression through multi-subunit protein complexes, which achieve specific cellular functions (Kurdistani & Grunstein, 2003). Histone deacetylation is commonly associated with the suppression of gene expression. In grapevine, the effect of NaB, an inhibitor of histone deacetylases, on *BBM* gene expression during somatic embryogenesis was investigated, and the result showed a significant upregulation of *BBM* gene expression in the presence of 0.5 mM NaB (Martínez *et al*., 2021).

TABLE 1. FUNCTIONAL CATEGORY OF *CIS*-REGULATORY ELEMENTS OF *EgBBM* PROMOTER USING PLANTCARE

Name	Conserved sequence	Number	Function	*AtBBM*	*OsBBM1*
Hormone response element					
ABRE	ACGTG	5	ABA responsiveness	✓	✓
ERE	ATTTTAAA	3	Ethylene responsiveness		✓
as-1	TGACG	2	MeJA and SA responsiveness	✓	✓
JERE	AGACCGCC	1	MeJA responsiveness		
TCA	TCATCTTCAT	1	SA responsiveness	✓	
AuxRR-core	GGTCCAT	1	Auxin responsiveness		
Light response element					
G-Box	CACGTT	5	Light responsiveness	✓	✓
GA-motif	ATAGATAA	1	Light responsiveness		✓
GATA-motif	AAGGATAAGG	1	Light responsiveness	✓	
ATCT-motif	AATCTAATCC	1	Light responsiveness		
TCT-motif	TCTTAC	1	Light responsiveness	✓	
TCCC-motif	TCTCCCT	1	Light responsiveness		✓
Sp1	GGGCGG	1	Light responsiveness	✓	✓
Condition specific element					
STRE	AGGGG	6	Stress responsiveness	✓	✓
ARE	AAACCA	2	Anaerobic induction	✓	✓
DRE	TACCGACAT	1	Dehydration responsiveness		
DRE core	GCCGAC	1	Dehydration responsiveness		✓
WRE3	CCACCT	1	Wounding responsiveness		✓
GC-motif	CCCCCG	1	Anoxic specific inducibility	✓	
O2-site	GATGACATGG	1	Zein metabolism regulation	✓	
Plant tissue specific element					
A-Box	CCGTCC	4	Meristem specific activation		✓
CAT-Box	GCCACT	1	Meristem expression	✓	✓
Transcription factor binding element					
MYB	TAACTG/CAACCA	5	MYB binding	✓	✓
MYC	CAT(T/G)TG	4	MYC binding	✓	✓
W-Box	TTGACC	4	WRKY binding	✓	✓
HD-ZIP III	GTAAT(G/C)ATTAC	2	HD-ZIP III binding		
OCT	CGCGGATC	2	Octamer binding		

Note: Number indicated the number of *cis*-regulatory element contained in 2,458 bp of *EgBBM* promoter. *AtBBM* indicated the cis-regulatory element in the promoter region of *BBM* gene in *Arabidopsis*. *OsBBM1* indicated the cis-regulatory element in the promoter region of *BBM1* gene in rice. ✓ indicated sharing of the *cis*-regulatory element in the promoter region of *AtBBM1* gene and/or *OsBBM1*.

Furthermore, SCL15, a transcription factor in the GRAS family, has been reported to interact with histone deacetylases as the protein complex to repress the expression of embryonic genes during the embryo-to-seedling transition (Guo *et al*., 2015; Jaiswal *et al*., 2022). SCL14, on the other hand, acts as a transcriptional coactivator with TGA transcription factors to promote the SCL14 target gene expression (Fode *et al*., 2008). TGA2.2 has been reported to promote the defense-responsive genes, while TGA2.1 has a crucial role in plant development (Thurow *et al*., 2005). Both SCL and TGA proteins are considered to play an important role in regulating *EgBBM* expression during somatic embryogenesis.

In addition, previous studies have shown that TGA2.2 and TGA2.1 can interact with Nonexpressor of Pathogenesis-Related 1 (NPR1) to activate the expression of *PR* genes (Niggeweg *et al*., 2000; Thurow *et al*., 2005). NPR1 has been proposed

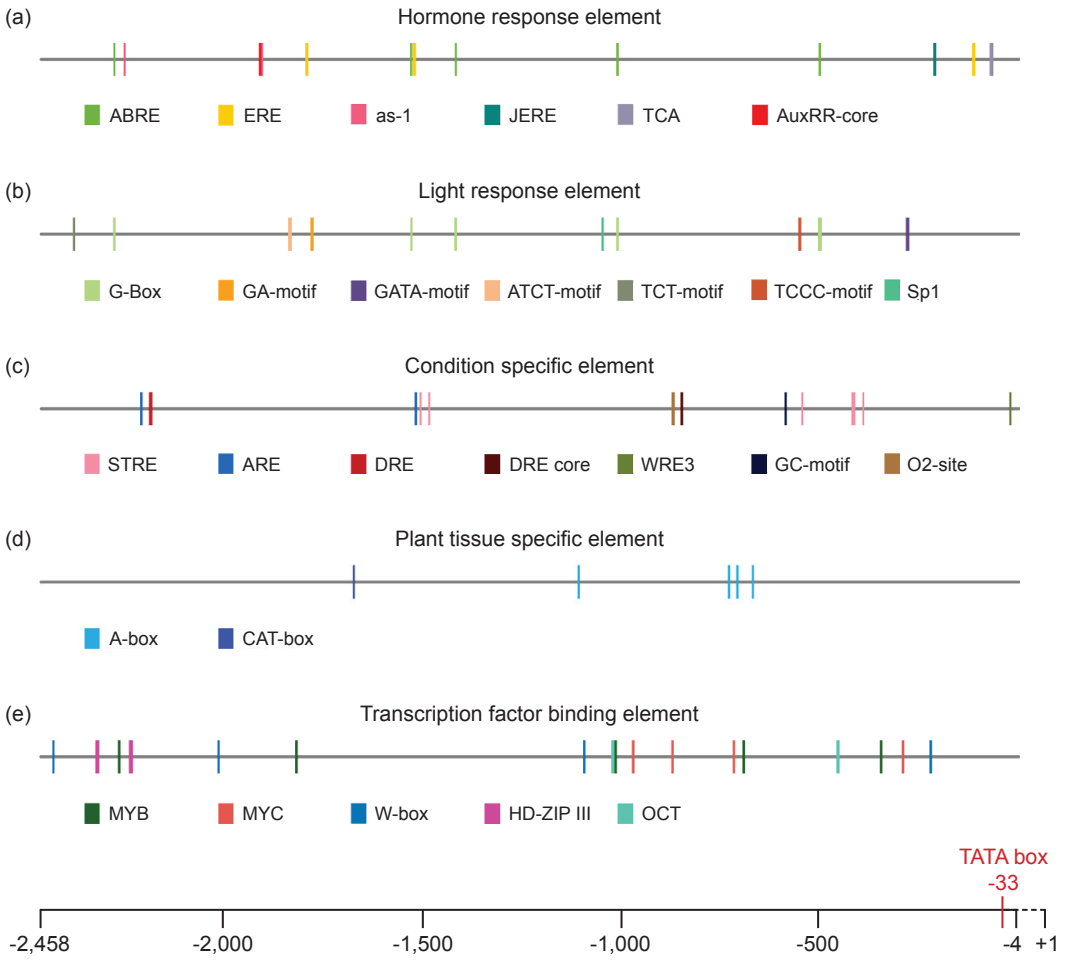


Figure 2. Distribution of cis*-regulatory elements within 2,458 base pairs upstream of the transcriptional start site of the* EgBBM *promoter sequence. Different elements indicated by different box colors. (a) Hormone response elements included ABRE element (ACGTG), ERE element (ATTTTAAA), as-1 element (TGACG), JERE element (AGACCGCC), TCA element (TCATCTTCAT) and AuxRR-core element (GGTCCAT). (b) Light response elements included G-Box element (CACGTT), GA-motif element (ATAGATAA), GATA-motif element (AAGGATAAGG), ATCT-motif element (AATCTAATCC), TCT-motif element (TCTTAC), TCCC-motif element (TCTCCCT) and Sp1 elements (GGGCGG). (c) Condition specific element included STRE element (AGGGG), ARE element (AAACCA), DRE element (TACCGACAT), DRE core element (GCCGAC), WRE3 element (CCACCT), GC-motif element (CCCCCG), and O2-site element (GATGACATGG). (d) Plant tissue specific element included A-Box element (CCGTCC) and CAT-Box element (GCCACT). (e) Transcription factor binding element included MYB (TAACTG/CAACCA), MYC (CAT(T/G)TG), HD-ZIP III (GTAAT(G/C)ATTAC), WRKY (W-Box; TTGACC) and Octamer (OCT; CGCGGATC) binding elements.*

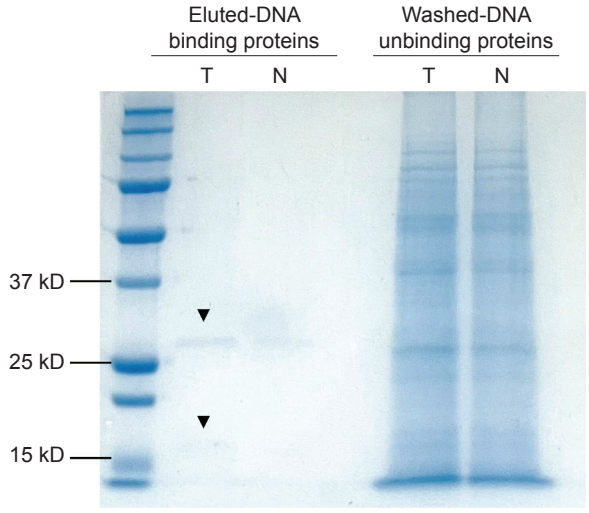


Figure 3. Separation of pEgBBM*-binding proteins and* pEgBBM*-unbinding protein by DNA-protein binding pull-down assay using 15% SDS-PAGE at 150V for 50 min. T (as treatment) indicated the mixture of extracted-somatic embryo protein,* pEgBBM *fragment, and streptavidin agarose bead. N (as negative control) indicated the mixture of extracted-somatic embryo protein and streptavidin agarose bead without* pEgBBM *fragment. Arrow indicated protein detection.*

to deactivate Suppressor of NPR1-1, Inducible 1 (SNI1), as the phenotype of the *npr1* mutant can be restored by the *sni1* mutation (Durrant *et al*., 2007; Li *et al*., 1999). SNI1-mediated transcriptional repression involves a highly conserved mechanism that affects chromatin modification (Mosher *et al*., 2006). Interestingly, SNI1 shares structural similarity with Armadillo repeat proteins, homologous to ARABIDILLO (Coates *et al*., 2006; Mosher *et al*., 2006; Moody *et al*., 2016), which were identified as putative *EgBBM* promoter-binding proteins in this study. ARABIDILLO 1 and 2 have been reported to promote lateral root development and seed germination in *Arabidopsis*, similar to the role of the *BBM* gene (Coates *et al*., 2006; Galinha *et al*., 2007; Moody *et al*., 2016; Ouakfaoui *et al*., 2010). Furthermore, CRF5, another putative *EgBBM* promoter-binding protein identified in this study, has been shown to play an important role in growth and development in *Arabidopsis* by upregulating the expression of Suppressor of NPR1-1, Constitutive1 (SNC1) (Zou *et al*., 2017).

RCF3 is a small subunit of the RFC complex that has been shown to regulate cell proliferation and pathogen resistance in *Arabidopsis* (Xia *et al*., 2009). The *rcf3-1* mutation can enhance the expression of *pathogenesis-related* (*PR*) genes, and the phenotype of *rcf3-1* is similar to that of *sni1*. Although the interaction between RFC3 and SNI1 could not be detected through the yeast-two hybrid assay, RFC3 may negatively regulate *PR* genes by indirectly interacting with SNI1 and affecting chromatin modification (Mosher *et al*., 2006; Xia *et al*., 2009).

In this study, WRKY71, a putative *EgBBM* promoter-binding protein, is functionally related to leaf senescence and overlapped with WRKY53 in *Chimonanthus praecox* (Huang *et al*., 2019). CpWRKY71 is highly expressed in flowers and senescing leaves, and its overexpression in *Arabidopsis* promotes precocious leaf senescence (Huang *et al*., 2019). Furthermore, WRKY71/EXB1 plays an important role in axillary meristem (AM) initiation in the control of shoot branching by regulating the auxin pathway in *Arabidopsis* (Guo *et al*., 2015).

Retinoblastoma-related protein (RBR) is a vital protein for cell division, differentiation, and stem cell maintenance in *Arabidopsis* root and it is regulated by the GRAS family member SCR (Borghi *et al*., 2010; Wildwater *et al*., 2005). RBR also cooperates with PRC2 during cell differentiation and development and PRC1 acts downstream of PRC2 to maintain gene repression (Kuwabara & Gruissem, 2014; Margueron & Reinberg, 2011). PRC1 represses the embryonic trait by suppressing the *BBM* gene expression during vegetative growth in *Arabidopsis*, but PRC2 subunit mutation does not affect *BBM* expression (Chen *et al*., 2010; Ikeuchi *et al*., 2015; Mozgová *et al*., 2017).

AHL10, a nuclear-localised protein with an AT-hook motif, binds to AT-rich DNA and recruits other transcription factors to regulate transcriptional regulation. It interacts with ADM to reestablish histone modifications after fertilisation in the endosperm (Jiang *et al*., 2017). Additionally, it is directly dephosphorylated by HAI1 to control plant growth under drought stress and regulate gene expression (Wong *et al*., 2019). RAV1 and RAV2-like proteins contain both AP2 and B3 DNA binding domains and are putative *EgBBM* promoter-binding proteins. RAV1 is a negative regulator in ABA signaling and interacts with SnRK2 to modulate gene expression (Feng *et al*., 2014). The ABRE *cis*-regulatory element, bound by ABI5 protein, is present in the *EgBBM* promoter, suggesting that the RAV1-ABI5 regulatory network may play a crucial role in *EgBBM* expression during somatic embryogenesis.

PIF1 is a bHLH transcription factor that binds to the G-box *cis*-regulatory element during light-dependent seed germination inhibition in *Arabidopsis* (Oh *et al*., 2009). PIF1 activates ABA and jasmonic signaling, which inhibit seed germination, while it represses GA and brassinosteroid signaling, which promote seed germination (Oh *et al*., 2009).

TRN1 plays a crucial role in cell-specific differentiation of radial dimension during early leaf and root development in *Arabidopsis* (Cnops *et al*., 2006). The establishment of radial symmetry in roots occurs during embryogenesis and is maintained throughout postembryonic growth. This process requires the participation of the SCR protein, which is essential for embryonic stem cell niche specification (Salvi *et al*., 2018).

Histone modifications play a critical role in regulating *EgBBM* gene expression during somatic embryogenesis. FRI, a scaffold protein, recruits various chromatin modifications to modify chromatin structure, including H3K4 methyltransferase complex COMPASS-like, Histone acetyltransferase of the MYST family1 (HAM1), SWR1 chromatin remodeling complex (SWR1-C), and ubiquitin-conjugating enzyme 1 (UBC1), forming a FRI-containing super complex that promotes the transcriptional activation of the flowering gene, *FLOWERING LOCUS C* (*FLC*) gene during embryogenesis in *Arabidopsis* (Choi *et al.,* 2009; 2011; Li *et al*., 2018). Furthermore, MRG1 is a protein localised to euchromatin that interacts with H3K36me3 and histone H4-specific acetyltransferases (HAM1 and HAM2) to recruit histone acetylation at the promoter region of the *FLC* gene, leading to the activation of *FLC* gene expression (An *et al*., 2020; Xu *et al*., 2014).

Several bZIP transcription factors have been identified as potential *EgBBM* promoter-binding proteins involved in seed and embryo development. bZIP53 is a transcriptional regulator of the seed

TABLE 2. PUTATIVE *EgBBM* PROMOTER-BINDING PROTEINS

Accession No.	Protein name	Protein mass (kDa)	Protein sequence coverage	MOWSE score	Peptide sequence	Putative binding *cis*-regulatory element
LOC105032345	Scarecrow-like protein 15 (SCL15)	59	9.8	69	APPPGLR	-
LOC105032336	Histone deacetylase 15	70	22.3	30	GDPLGCCDVTPAGYAQMTHMLTGLSQGK	-
LOC105053122	Replication factor C subunit 3 (RCF3)	40	7.9	29	LSNGDMR	-
LOC105053961	ARABIDILLO 1 protein	100	4.0	28	IVLRNLEHHQLEASI	-
LOC105053872	AT-hook motif nuclear-localised protein 10 (AHL10)	37	44.0	27	DDRDSPR	AT-rich element binding
LOC105047044	AP2/ERF and B3 domain-containing transcription repressor RAV2-like	41	17.0	25	RNMPAAAAAGGLGLSQALGGAQR	ABRE *cis*-regulatory element (Indirect binding)
LOC105033317	TORNADO 1 protein (TRN1)	16	13.1	24	DGVVAILR	-
LOC105035615	Transcription factor TGA2.2	40	8.9	22	MASLDMAASAVGAELDMGKLAFPR	-
LOC105039935	bZIP transcription factor 53	17	15.2	22	MSSVPAPQTSGSEEDAQLIVDER	G-box *cis*-regulatory element
LOC105053422	Histone acetyltransferase	63	18.6	22	GATGPSGQQNAAAAASLMPGIVVK	-
LOC105057643	Chromatin remodeling 5 protein (CRF5)	198	6.1	22	IVQQHEVSYKQTR	-
LOC105038489	Transcription factor MYB54-like	37	13.4	21	SHFHDLSLRSSYHPYR	MYB *cis*-regulatory element
LOC105051995	bZIP transcription factor 12-like	32	39.7	21	NIYGDGTAAAASPATPFGGDAGEKAAPPPLAR	G-box *cis*-regulatory element
LOC105047023	bZIP transcription factor 11	17	17.0	20	ASSNGTSSGSSALFPGSGEAVMDRK	G-box *cis*-regulatory element
LOC105051512	FRIGIDA-like protein (FRI)	63	10.3	18	VSQIKAGNMSPGGQNETNER	-
LOC105051764	Histone deacetylase 14	40	28.7	18	GSGEGTTLNLPLPGGSVMMLMR	-
LOC105042616	Transcription factor bHLH93-like	38	31.8	17	QEMGMDEQSLLQELFAPWR	G-box *cis*-regulatory element
LOC105046537	AP2/ERF and B3 domain-containing transcription factor RAV1	40	11.2	17	RSMPAGGYGGGLGLR	ABRE *cis*-regulatory element (Indirect binding)
LOC105054681	Homeobox-leucine zipper protein ROC5-like	86	34.5	16	GQDEMSQLGVIGGVGDGSGDK	-
LOC105055793	Phytochrome interacting factor1 (PIF1)	40	27.0	16	MGSSAVAEAVRQLFMEEDDIASWIHYQIGEDGGGDMYR	G-box *cis*-regulatory element
LOC105035176	Retinoblastoma-related protein (RBR)	115	12.7	15	VLETMCR	-
LOC105047232	WRKY transcription factor 71	38	4.5	14	GFNTSCSSPEMFGPR	W-box *cis*-regulatory element
LOC105059243	Phytochrome interacting factor-like 15 (PIL15)	53	42.3	14	PMVPSFRSPNMGMAMADQTR	G-box *cis*-regulatory element
LOC105061003	MRG1 protein	37	11.7	14	DAKSAEK	-

maturation (*MAT*) gene in *Arabidopsis* and is expressed in embryos and endosperm of maize grains (Alonso *et al*., 2009; Lv *et al*., 2021). bZIP11 is co-expressed with bZIP53 and highly expressed in the chalazal pole and globular seed in *Brassica napus*, where it binds to G-box *cis*-regulatory elements to modulate auxin-induced transcription by interacting with histone acetylation machinery (Ehlert *et al*., 2006; Khan *et al*., 2022; Weiste & Dröge-Laser, 2014; Ziegler *et al*., 2019). Additionally, bZIP12, which is related to ABA signaling, was specifically and highly expressed in the early embryo stage during zygotic embryo development in oil palm, and was found to be co-expressed with the *BBM* gene (Zhang *et al*., 2022).

CONCLUSION

In this study, we cloned the *EgBBM* promoter to investigate the *cis*-regulatory elements in this region and identify putative *EgBBM* promoter-binding proteins using a DNA-protein pull-down assay. Our findings revealed that developmental processes, hormone response, and transcription factor binding were represented in *EgBBM* promoter. Moreover, several proteins were involved in histone modification, leading to the establishment of a complex regulatory network involving interactions between DNA-proteins and protein-proteins. Through our research, we have gained valuable insights into the factors that impact the function of *EgBBM* in oil palm tissue culture, specifically during the process of somatic embryogenesis.

ACKNOWLEDGEMENT

This research and innovation activity is funded by the National Research Council of Thailand (NRCT) as of the fiscal year 2021, and the Royal Golden Jubilee (RGJ) Ph.D Program (Grant No. PHD/0001/2560), through the National Research Council of Thailand (NRCT), Thailand Research Fund (TRF), and Kasetsart University Research and Development Institute (KURDI).

REFERENCES

Alonso, R., Oñate-Sánchez, L., Weltmeier, F., Ehlert, A., Diaz, I., Dietrich, K., Vicente-Carbajosa, J. S., & Dröge-Laser, W. (2009). A pivotal role of the Basic Leucine Zipper transcription factor bZIP53 in the regulation of *Arabidopsis* seed maturation gene expression based on heterodimerization and protein complex formation. *Plant Cell, 21*(6), 1747–1761. https://doi.org/10.1105/tpc.108.062968

An, Z., Yin, L., Liu, Y., Peng, M., Shen, W. H., & Dong, A. (2020). The histone methylation readers MRG1/MRG2 and the histone chaperones NRP1/NRP2 associate in fine-tuning *Arabidopsis* flowering time. *Plant Journal, 103*(3), 1010–1024. https://doi.org/10.1111/tpj.14780

Borg, M., Jacob, Y., Susaki, D., LeBlanc, C., Buendía, D., Axelsson, E., Kawashima, T., Voigt, P., Boavida, L., Becker, J., Higashiyama, T., Martienssen, R., & Berger, F. (2020). Targeted reprogramming of H3K27me3 resets epigenetic memory in plant paternal chromatin. *Nature Cell Biology, 22*, 621–629. https://doi.org/10.1038/s41556-020-0515-y

Borghi, L., Gutzat, R., Fütterer, J., Laizet, Y., Hennig, L., & Gruissem, W. (2010). *Arabidopsis* RETINOBLASTOMA-RELATED is required for stem cell maintenance, cell differentiation, and lateral organ production. *Plant Cell, 22*(6), 1792–1811. https://doi.org/10.1105/tpc.110.074591

Boutilier, K., Offringa, R., Sharma, V. K., Kieft, H., Ouellet, T., Zhang, L., Hattori, J., Liu, C. M., Van Lammeren, A. A., Miki, B. L., Custers, J. B., & Van Lookeren Campagne, M. M. (2002). Ectopic expression of *BABY BOOM* triggers a conversion from vegetative to embryonic growth. *Plant Cell, 14*(8), 1737–1749. https://doi.org/10.1105/tpc.001941

Chaparian, R. R., & Van Kessel, J. C. (2020). Promoter pull-down assay: A biochemical screen for DNA-binding proteins. In K. Turksen (Ed.), *Stem Cell Renewal and Cell-Cell Communication* (pp. 165–172). Springer.

Chen, D., Molitor, A., Liu, C., & Shen, W. H. (2010). The *Arabidopsis* PRC1-like ring-finger proteins are necessary for repression of embryonic traits during vegetative growth. *Cell Research, 20*(12), 1332–1344. https://doi.org/10.1038/cr.2010.1

Choi, J., Hyun, Y., Kang, M. J., In Yun, H., Yun, J. Y., Lister, C., Dean, C., Amasino, R. M., Noh, B., Noh, Y. S., & Choi, Y. (2009). Resetting and regulation of FLOWERING LOCUS C expression during *Arabidopsis* reproductive development. *Plant Journal, 57*(5), 918–931. https://doi.org/10.1111/j.1365-313x.2008.03776.x

Choi, K., Kim, J., Hwang, H. J., Kim, S., Park, C., Kim, S. Y., & Lee, I. (2011). The FRIGIDA complex activates transcription of FLC, a strong flowering repressor in *Arabidopsis*, by recruiting chromatin modification factors. *Plant Cell, 23*(1), 289–303. https://doi.org/10.1105/tpc.110.075911

Cnops, G., Neyt, P., Raes, J., Petrarulo, M., Nelissen, H., Malenica, N., Luschnig, C., Tietz, O., Ditengou, F., Palme, K., Azmi, A., Prinsen, E., & Van Lijsebettens, M. (2006). The *TORNADO1* and *TORNADO2* genes function in several patterning processes during early leaf development in *Arabidopsis thaliana*. *Plant Cell, 18*(4), 852–866. https://doi.org/10.1105/tpc.105.040568

Coates, J. C., Laplaze, L., & Haseloff, J. (2006). Armadillo-related proteins promote lateral root development in *Arabidopsis*. *Proceedings of the National Academy of Sciences, 103*(5), 1621–1626. https://doi.org/10.1073/pnas.0507575103

De La Concepción, J. C., Franceschetti, M., Maqbool, A., Saitoh, H., Terauchi, R., Kamoun, S., & Banfield, M. J. (2018). Polymorphic residues in rice NLRs expand binding and response to effectors of the blast pathogen. *Nature Plants, 4*, 576–585. https://doi.org/10.1038/s41477-018-0194-x

Deng, W., Luo, K., Li, Z., & Yang, Y. (2009). A novel method for induction of plant regeneration via somatic embryogenesis. *Plant Science, 177*(1), 43–48. https://doi.org/10.1016/j.plantsci.2009.03.009

Duarte-Aké, F., & De-La-Peña, C. (2016). Epigenetic advances in somatic embryogenesis in sequenced genome crops. In V. Loyola-Vargas & N. Ochoa-Alejo (Eds.), *Somatic Embryogenesis: Fundamental Aspects and Applications* (pp. 81–102). Springer.

Durrant, W. E., Wang, S., & Dong, X. (2007). *Arabidopsis* SNI1 and RAD51D regulate both gene transcription and DNA recombination during the defense response. *Proceedings of the National Academy of Sciences, 104*(10), 4223–4227. https://doi.org/10.1073/pnas.0609357104

Ehlert, A., Weltmeier, F., Wang, X., Mayer, C. S., Smeekens, S., Vicente-Carbajosa, J., & Dröge-Laser, W. (2006). Two-hybrid protein-protein interaction analysis in *Arabidopsis* protoplasts: Establishment of a heterodimerization map of group C and group S bZIP transcription factors. *Plant Journal, 46*(5), 890–900. https://doi.org/10.1111/j.1365-313x.2006.02731.x

Feng, C. Z., Chen, Y., Wang, C., Kong, Y. H., Wu, W. H., & Chen, Y. F. (2014). *Arabidopsis* RAV1 transcription factor, phosphorylated by SnRK2 kinases, regulates the expression of *ABI3*, *ABI4*, and *ABI5* during seed germination and early seedling development. *Plant Journal, 80*(4), 654–668. https://doi.org/10.1111/tpj.12670

Fode, B., Siemsen, T., Thurow, C., Weigel, R., & Gatz, C. (2008). The *Arabidopsis* GRAS protein SCL14 interacts with class II TGA transcription factors and is essential for the activation of stress-inducible promoters. *Plant Cell, 20*, 3122–3135. https://doi.org/10.1105/tpc.108.058974

Galinha, C., Hofhuis, H., Luijten, M., Willemsen, V., Blilou, I., Heidstra, R., & Scheres, B. (2007). PLETHORA proteins as dose-dependent master regulators of *Arabidopsis* root development. *Nature, 449*(7165), 1053–1057. https://doi.org/10.1038/nature06206

Gasch, P., Fundinger, M., Müller, J. T., Lee, T., Bailey-Serres, J., & Mustroph, A. (2015). Redundant ERF-VII transcription factors bind to an evolutionarily conserved *cis*-motif to regulate hypoxia-responsive gene expression in *Arabidopsis*. *Plant Cell, 28*(1), 160–180. https://doi.org/10.1105/tpc.15.00866

Guo, D., Zhang, J., Wang, X., Han, X., Wei, B., Wang, J., Li, B., Yu, H., Huang, Q., Gu, H., Qu, L. J., & Qin, G. (2015). The WRKY Transcription Factor WRKY71/EXB1 controls shoot branching by transcriptionally regulating RAX genes in *Arabidopsis*. *Plant Cell, 27*(11), 3112–3127. https://doi.org/10.1105/tpc.15.00829

Huang, R., Liu, D., Huang, M., Ma, J., Li, Z., Li, M., & Sui, S. (2019). *CpWRKY71*, a WRKY transcription factor gene of wintersweet (*Chimonanthus praecox*), promotes flowering and leaf senescence in *Arabidopsis*. *International Journal of Molecular Sciences, 20*, 5325. https://doi.org/10.3390/ijms20215325

Ikeuchi, M., Iwase, A., Rymen, B., Harashima, H., Shibata, M., Ohnuma, M., Breuer, C., Morao, A. K., de Lucas, M., De Veylder, L., Goodrich, J., Brady, S. M., Roudier, F., & Sugimoto, K. (2015). PRC2 represses dedifferentiation of mature somatic cells in *Arabidopsis*. *Nature Plants, 1*(7), Article 15089. https://doi.org/10.1038/nplants.2015.89

Irikova, T., Grozeva, S., & Denev, I. (2012). Identification of *BABY BOOM* and *LEAFY COTYLEDON* genes in sweet pepper (*Capsicum annuum* L.) genome by their partial gene sequences. *Plant Growth Regulation, 67*, 191–198. https://doi.org/10.1007/s10725-012-9676-4

Jaiswal, V., Kakkar, M., Kumari, P., Zinta, G., Gahlaut, V., & Kumar, S. (2022). Multifaceted roles of GRAS transcription factors in growth and stress responses in plants. *iScience, 25*(9), Article 105026. https://doi.org/10.1016/j.isci.2022.105026

Jiang, H., Moreno-Romero, J., Santos-González, J., De Jaeger, G., Gevaert, K., Van De Slijke, E., & Köhler, C. (2017). Ectopic application of the repressive histone modification H3K9me2 establishes post-zygotic reproductive isolation in *Arabidopsis thaliana*. *Genes & Development, 31*, 1272–1287. https://doi.org/10.1101/gad.299347.117

Khan, D., Ziegler, D. J., Kalichuk, J. L., Hoi, V., Huynh, N., Hajihassani, A., Parkin, I. A. P., Robinson, S. J., & Belmonte, M. F. (2022). Gene expression profiling reveals transcription factor networks and subgenome bias during *Brassica napus* seed development. *Plant Journal, 109*(3), 477–489. https://doi.org/10.1111/tpj.15587

Konan, K. E., Durand-Gasselin, T., Kouadio, Y. J., Flori, A., Rival, A., Duval, Y., & Pannetier, C. (2009). *In vitro* conservation of oil palm somatic embryos for 20 years on a hormone-free culture medium: Characteristics of the embryogenic cultures, derived plantlets, and adult palms. *Plant Cell Reports, 29*, 1–13. https://doi.org/10.1007/s00299-009-0787-y

Kuang, Z., Pinglay, S., Ji, H., & Boeke, J. D. (2017). Msn2/4 regulate expression of glycolytic enzymes and control transition from quiescence to growth. *eLife, 6*, Article e29938. https://doi.org/10.7554/elife.29938

Kulinska-Lukaszek, K., Tobojka, M., Adamiok, A., & Kurczynska, E. U. (2012). Expression of the *BBM* gene during somatic embryogenesis of *Arabidopsis thaliana*. *Biologia Plantarum, 56*, 389–394. https://doi.org/10.1007/s10535-012-0105-3

Kumar, V., & Van Staden, J. (2017). New insights into plant somatic embryogenesis: An epigenetic view. *Acta Physiologiae Plantarum, 39*, Article 194. https://doi.org/10.1007/s11738-017-2487-5

Kurdistani, S. K., & Grunstein, M. (2003). Histone acetylation and deacetylation in yeast. *Nature Reviews Molecular Cell Biology, 4*(4), 276–284. https://doi.org/10.1038/nrm1075

Kuwabara, A., & Gruissem, W. (2014). *Arabidopsis* retinoblastoma-related and polycomb group proteins: Cooperation during plant cell differentiation and development. *Journal of Experimental Botany, 65*(10), 2667–2676. https://doi.org/10.1093/jxb/eru069

Li, J., Han, G., Sun, C., & Sui, N. (2019). Research advances of MYB transcription factors in plant stress resistance and breeding. *Plant Signaling & Behavior, 14*(8), Article 1613131. https://doi.org/10.1080/15592324.2019.1613131

Li, X., Zhang, Y., Clarke, J. D., Li, Y., & Dong, X. (1999). Identification and cloning of a negative regulator of systemic acquired resistance, SNI1, through a screen for suppressors of NPR1-1. *Cell, 98*(3), 329–339. https://doi.org/10.1016/s0092-8674(00)81962-5

Li, Z., Jiang, D., & He, Y. (2018). FRIGIDA establishes a local chromosomal environment for *FLOWERING LOCUS C* mRNA production. *Nature Plants, 4*(10), 836–846. https://doi.org/10.1038/s41477-018-0250-6

Lv, H., Li, X., Li, H., Hu, Y., Liu, H., Wen, S., Li, Y., Liu, Y., Huang, H., Yu, G., Huang, Y., & Zhang, J. (2021). Gibberellin induced transcription factor bZIP53 regulates CesA1 expression in maize kernels. *PLoS ONE, 16*(3), e0244591. https://doi.org/10.1371/journal.pone.0244591

Margueron, R., & Reinberg, D. (2011). The polycomb complex PRC2 and its mark in life. *Nature, 469*(7330), 343–349. https://doi.org/10.1038/nature09784

Martínez, Ó., Arjones, V., González, M. V., & Rey, M. (2021). Histone deacetylase inhibitors increase the embryogenic potential and alter the expression of embryogenesis-related and dac-encoding genes in grapevine (*Vitis vinifera* L., cv. Mencía). *Plants, 10*(6), 1164. https://doi.org/10.3390/plants10061164

Moody, L. A., Saidi, Y., Gibbs, D. J., Choudhary, A., Holloway, D., Vesty, E. F., Bansal, K. K., Bradshaw, S. J., & Coates, J. C. (2016). An ancient and conserved function for Armadillo-related proteins in the control of spore and seed germination by abscisic acid. *New Phytologist, 211*(3), 940–951. https://doi.org/10.1111/nph.13938

Morcillo, F., Gallard, A., Pillot, M., Jouannic, S., Aberlenc-Bertossi, F., Collin, M., Verdeil, J. L., & Tregear, J. W. (2007). *EgAP2-1*, an *AINTEGUMENTA-like* (AIL) gene expressed in meristematic and proliferating tissues of embryos in oil palm. *Planta, 226*, 1353–1362. https://doi.org/10.1007/s00425-007-0574-3

Mosher, R. A., Durrant, W. E., Wang, D., Song, J., & Dong, X. (2006). A comprehensive structure-function analysis of *Arabidopsis* SNI1 defines essential regions and transcriptional repressor activity. *Plant Cell, 18*(7), 1750–1765. https://doi.org/10.1105/tpc.105.039677

Mozgová, I., Muñoz-Viana, R., & Hennig, L. (2017). PRC2 represses hormone-induced somatic

embryogenesis in vegetative tissue of *Arabidopsis thaliana*. *PLoS Genetics, 13*(1), 1006562. https://doi.org/10.1371/journal.pgen.1006562

Nic-Can, G. I., Lopez-Torres, A., Barredo-Pool, F., Wrobel, K., Loyola-Vargas, V. M., Rojas-Herrera, R., & De-la-Pena, C. (2013). New insights into somatic embryogenesis: *LEAFY COTYLEDON1*, *BABY BOOM1*, and *WUSCHE-RELATED HOMEOBOX4* are epigenetically regulated in *Coffea canephora*. *PLoS ONE, 8*(8), e72160. https://doi.org/10.1371/journal.pone.0072160

Niggeweg, R., Thurow, C., Weigel, R., Pfitzner, U., & Gatz, C. (2000). Tobacco TGA factors differ with respect to interaction with NPR1, activation potential, and DNA-binding properties. *Plant Molecular Biology, 42*(5), 775–788. https://doi.org/10.1023/a:1006319113205

Oh, E., Kang, H., Yamaguchi, S., Park, J., Lee, D., Kamiya, Y., & Choi, G. (2009). Genome-wide analysis of genes targeted by PHYTOCHROME INTERACTING FACTOR 3-LIKE5 during seed germination in *Arabidopsis*. *Plant Cell, 21*(2), 403–419. https://doi.org/10.1105/tpc.108.064691

Osorio-Montalvo, P., Sáenz-Carbonell, L., & De-la-Peña, C. (2018). 5-Azacytidine: A promoter of epigenetic changes in the quest to improve plant somatic embryogenesis. *International Journal of Molecular Sciences, 19*(10), 3182. https://doi.org/10.3390/ijms19103182

Ouakfaoui, S. E., Schnell, J., Abdeen, A., Colville, A., Labbe, H., Han, S., Baum, B., Laberge, S., & Miki, B. (2010). Control of somatic embryogenesis and embryo development by AP2 transcription factors. *Plant Molecular Biology, 74*, 313–326. https://doi.org/10.1007/s11103-010-9674-8

Passarinho, P., Ketelaar, T., Xing, M., Van Arkel, J., Maliepaard, C., Hendriks, M. W., Joosen, R., Lammers, M., Herdies, L., Boer, B. D., Van Der Geest, L., & Boutilier, K. (2008). *BABY BOOM* target genes provide diverse entry points into cell proliferation and cell growth pathways. *Plant Molecular Biology, 68*, 225–237. https://doi.org/10.1007/s11103-008-9364-y

Salvi, E., Di Mambro, R., Pacifici, E., Dello Ioio, R., Costantino, P., Moubayidin, L., & Sabatini, S. (2018). SCARECROW and SHORTROOT control the auxin/cytokinin balance necessary for embryonic stem cell niche specification. *Plant Signaling & Behavior, 13*(8), 1507402. https://doi.org/10.1080/15592324.2018.1507402

Schlag, K., Steinhilber, D., Karas, M., & Sorg, B. L. (2020). Analysis of proximal *ALOX5* promoter binding proteins by quantitative proteomics. *FEBS Journal, 287*(20), 4481–4499. https://doi.org/10.1111/febs.15259

Semagn, K. (2014). Leaf tissue sampling and DNA extraction protocols. In P. Besse (Ed.), *Molecular Plant Taxonomy: Methods in Molecular Biology* (pp. 53-67). Humana Press. https://doi.org/10.1007/978-1-62703-767-9_3

Thurow, C., Schiermeyer, A., Krawczyk, S., Butterbrodt, T., Nickolov, K., & Gatz, C. (2005). Tobacco bZIP transcription factor TGA2.2 and related factor TGA2.1 have distinct roles in plant defense responses and plant development. *Plant Journal, 44*(1), 100–113. https://doi.org/10.1111/j.1365-313x.2005.02513.x

Thuzar, M., Vanavichit, A., Tragoonrung, S., & Jantasuriyarat, C. (2011). Efficient and rapid plant regeneration of oil palm zygotic embryos cv. *Tenera* through somatic embryogenesis. *Acta Physiologiae Plantarum, 33*, 123–128. https://doi.org/10.1007/s11738-010-0526-6

Wachananawat, B., Vuttipongchaikij, S., & Jantasuriyarat, C. (2017). Cloning and gene expression of *BABY BOOM* (*BBM*) in oil palm embryogenesis. *Thai Journal of Science and Technology, 6,* 44-52.

Wahid, M. B., Abdullah, S. N. A., & Henson, I. E. (2015). Oil palm - Achievements and potential. *Plant Production Science, 8*(3), 288–297. https://doi.org/10.1626/pps.8.288

Walley, J. W., Coughlan, S., Hudson, M. E., Covington, M. F., Kaspi, R., Banu, G., Harmer, S. L., & Dehesh, K. (2007). Mechanical stress induces biotic and abiotic stress responses via a novel *cis*-element. *PLoS Genetics, 3*(10), e172. https://doi.org/10.1371/journal.pgen.0030172

Wang, X., Niu, Q. W., Teng, C., Li, C., Mu, J., Chua, N. H., & Zuo, J. (2008). Overexpression of PGA37/*MYB118* and *MYB115* promotes vegetative-to-embryonic transition in *Arabidopsis*. *Cell Research, 19*(2), 224–235. https://doi.org/10.1038/cr.2008.276

Weiste, C., & Dröge-Laser, W. (2014). The *Arabidopsis* transcription factor bZIP11 activates auxin-mediated transcription by recruiting the histone acetylation machinery. *Nature Communications, 5*(1), 3883. https://doi.org/10.1038/ncomms4883

Wildwater, M., Campilho, A., Perez-Perez, J. M., Heidstra, R., Blilou, I., Korthout, H., Chatterjee, J., Mariconti, L., Gruissem, W., & Scheres, B. (2005). The RETINOBLASTOMA-RELATED gene regulates stem cell maintenance in *Arabidopsis* roots. *Cell, 123*(7), 1337–1349. https://doi.org/10.1016/j.cell.2005.09.024

Wong, M. M., Bhaskara, G. B., Wen, T. N., Lin, W. D., Nguyen, T. T., Chong, G. L., & Verslues, P. E. (2019). Phosphoproteomics of *Arabidopsis* highly ABA-Induced1 identifies AT-Hook-Like10 phosphorylation required for stress growth regulation. *Proceedings of the National Academy of Sciences, 116*(6), 2354–2363. https://doi.org/10.1073/pnas.1819971116

Wu, K. K. (2006). Analysis of protein-DNA binding by streptavidin-agarose pulldown. In *Methods in Molecular Biology, 338*, 281–290. Humana Press. https://doi.org/10.1385/1-59745-097-9:281

Xia, S., Zhu, Z., Hao, L., Chen, J. G., Xiao, L., Zhang, Y., & Li, X. (2009). Negative regulation of systemic acquired resistance by Replication Factor C Subunit3 in *Arabidopsis*. *Plant Physiology, 150*(4), 2009–2017. https://doi.org/10.1104/pp.109.138321

Xu, Y., Gan, E. S., Zhou, J., Wee, W. Y., Zhang, X., & Ito, T. (2014). *Arabidopsis* MRG domain proteins bridge two histone modifications to elevate expression of flowering genes. *Nucleic Acids Research, 42*(17), 10960–10974. https://doi.org/10.1093/nar/gku781

Zhang, A., Jin, L., Yarra, R., Cao, H., Chen, P., & Martin, J. J. (2022). Transcriptome analysis reveals key developmental and metabolic regulatory aspects of oil palm (*Elaeis guineensis* Jacq.) during zygotic embryo development. *BMC Plant Biology, 22*(1), Article 112. https://doi.org/10.1186/s12870-022-03459-2

Ziegler, D. J., Khan, D., Kalichuk, J. L., Becker, M. G., & Belmonte, M. F. (2019). Transcriptome landscape of the early *Brassica napus* seed. *Journal of Integrative Plant Biology, 61*(5), 639–650. https://doi.org/10.1111/jipb.12812

Zou, B., Sun, Q., Zhang, W., Ding, Y., Yang, D. L., Shi, Z., & Hua, J. (2017). The *Arabidopsis* chromatin-remodeling factor CHR5 regulates plant immune responses and nucleosome occupancy. *Plant Cell Physiology, 58*(12), 2202–2216. https://doi.org/10.1093/pcp/pcx155

Journal of Oil Palm Research Vol. 37 (1) March 2025 p. 85-95
DOI: https://doi.org/10.21894/jopr.2023.0065

ANTIFUNGAL VOLATILE ORGANIC COMPOUNDS (VOCs) FROM A STRAIN OF *Fusarium foetens* AGAINST *Ganoderma boninense*

ANISA LUTFIA[1]* and BEDAH RUPAEDAH[1]

ABSTRACT

Basal Stem Rot (BSR) caused by Ganoderma boninense *poses a threat to the sustainability of oil palm (*Elaeis guineensis *Jacq.), a valuable export commodity in Southeast Asia. This study focuses on evaluating the potential of an indigenous strain of* Fusarium*, as a biocontrol agent for BSR. The research involves chemical characterisation and laboratory testing. Molecular identification confirmed the isolate as* Fusarium foetens*, an unconventional biocontrol agent that showed promising results in experimental settings. In the disc vapour assay, discs containing volatile organic compounds (VOCs) effectively inhibited the growth of* G. boninense *by up to 60%. Analysis of scanning electron microscopy (SEM) imagery suggested that the inhibition might be attributed to cell wall damage and internal disruption caused by the VOCs. Four major VOCs were identified and ranked based on their relative peak area (%), including 2,3-Pyrazinedicarboximide (15.54%), 2-(2-Butoxyethoxy) ethyl thiocyanate (11.43%), 3,5-Dimethoxyphenol (11.40%) and Indolylmethylthiohydroximate (5.56%), with other minor compounds accounting for less than 5.00%. Docking simulations using PyRx software were performed to analyse the binding affinity between selected VOCs and the virulent protein, xyloglucan-specific endo-beta-1,4-glucanase (XEG). Interestingly, two compounds, 2,3-Pyrazinedicarboximide and indolylmethylthiohydroximate, had exhibited binding affinities similar to that of hexaconazole, a standard antifungal agent used in BSR management.*

Keywords: antifungi, basal stem rot, *Fusarium*, molecular docking, xyloglucanase.

Received: 26 June 2023; **Accepted:** 30 October 2023; **Published online:** 27 December 2023.

INTRODUCTION

Plant pathogens, also known as phytopathogens, pose a major risk to both agriculture and global food security by inducing various plant diseases that result in significant economic losses. The oil palm (*Elaeis guineensis* Jacq.), a valuable export commodity in Southeast Asia, particularly in Indonesia and Malaysia, faces threats to its production and sustainability, due to basal stem rot (BSR), predominantly caused by *Ganoderma boninense* Pat., a basidiomycete fungi. Despite ongoing research efforts, the exact infection mechanism of *G. boninense* in oil palm plantations and its sporadic spread still remains elusive (Bharudin *et al*., 2022).

The management of BSR presents significant difficulties and challenges due to the infective dikaryotic mycelium that arises from the mating between mycelia and newly germinated basidiospores (Pilotti *et al*., 2003; 2018). To date, an effective and integrated disease management method to prevent the spread of *G. boninense* and sustainably reduce the incidence of the disease has not been discovered (Siddiqui *et al*., 2021). Various methods have been employed to control the spread of infection, including soil mounding, manual removal of infected tissues and *G. boninense* fruiting bodies, as well as the use of fungicides such as hexaconazole (Hushiarian *et al*., 2013; Idris *et al*., 2010). Hexaconazole has been considered relatively

[1] Research Center for Applied Microbiology, National Research and Innovation Agency, Jl. Raya Jakarta-Bogor Km. 46, Cibinong, Bogor, West Java 16911, Indonesia.

* *Corresponding author e-mail: anis031@brin.go.id*

effective in reducing the incidence of *G. boninense* infection and infestation in healthy, mature oil palm trees (Khoo & Chong, 2023; Nur-Rashyeda *et al.*, 2022). However, its efficacy decreases when faced with melanised mycelium, basidiospores, and pseudosclerotia of *G. boninense* (Susanto *et al.*, 2005). The continuous use of hexaconazole also carries specific risks, particularly concerning the accumulation of residues on oil palm leaves, detectable for at least 70 days after application (Muhamad *et al.*, 2012).

Various groups of microorganisms, including actinomycetes, bacteria and fungi, have been investigated as potential biological control agents for *G. boninense*. However, their efficacy is still being assessed, both as individual isolates and consortia, in laboratory and field-scale experiments (Bharudin *et al.*, 2022; Shariffah-Muzaimah *et al.*, 2015; 2020). This study aims to assess the effectiveness of a soil fungus belonging to the unique group of *Fusarium*, through both *in vitro* and *in silico* experiments. In addition, the volatile organic compounds (VOCs) produced by this fungus and its effects will be investigated against the *G. boninense* colony. VOCs are a blend of volatile metabolites produced by both microbial and plant sources, which is referred to as "volatilome". They are distinguished by functional effects in the soil, greater ability to disperse, and stronger antifungal properties (Tilocca *et al.*, 2020). Through this research, novel opportunities are sought for harnessing non-pathogenic strains of soil microbes, as potential candidates in the development of antifungal agents.

MATERIALS AND METHODS

Biological Materials and Molecular Identification

The soil fungus, *Fusarium* sp. isolate F2, was obtained from healthy and non-infected oil palm plantation soils in Bogor, Indonesia. Soil samples were serially diluted to 10^8 dilutions. Fungal isolation was carried out using Potato Dextrose Agar (PDA), followed by incubation at 25°C for two to three days (Ali *et al.*, 2016). The pathogenic fungus, *G. boninense* strain SSU008, utilised in this study, was collected from the Oil Palm Research Center (PPKS) Marihat, Simalugun Regency, North Sumatra, Indonesia. The isolates were maintained on PDA medium. To determine their molecular identity, the fungal specimen (isolate F2) was commercially sent to Macrogen, Inc. (Singapore). The genomic DNA was amplified using a pair of ITS1 (5′-TCCGTAGGTGAACCTGCGG-3′) and ITS4 (5′-TCCTCCGCTTATTGATATGC-3′) primer, assembled and analysed for similarity against an online database using BLASTn for the ITS-rDNA region (Xie *et al.*, 2008). The fungal species were identified by constructing a phylogenetic tree or dendrogram, which displayed the species phylogeny and clustering analysis among accessions using MEGA11 (Tamura *et al.*, 2021). The confirmed species was then submitted as an online accession to GenBank and assigned the accession code *Fusarium foetens* F2 (OR186217).

VOCs Production of *Fusarium foetens* F2 in Submerged Fermentation

For the production of VOCs, potato dextrose broth (PDB) was employed as the fermentation medium (Vieira *et al.*, 2008). The fungus, *F. foetens* F2, was cultivated in a 250 mL flask containing 50 mL of PDB at a temperature of 28°C for 14 days. To obtain the cell-free supernatant (CFS), the fermentation broth was filtered using Whatman filter paper No. 1 in a Büchner funnel. Subsequently, the CFS was separated by centrifugation at 10,000 ×g for 15 min. The resulting CFS was subjected to extraction using laboratory-grade ethyl acetate (EtOAc) in a 1:1 ratio. The mixture was vigorously shaken for 3 days. The ethyl acetate layer was then separated and decanted, followed by evaporation *in vacuo* to concentrate the crude VOC-containing extract and to remove EtOAc solvent using a Buchi Rotavapor® R-300.

Antifungal Vapour Assay of VOCs and Microscopy Analysis of *G. boninense*

To evaluate the antifungal activity of the VOCs produced by the fungus, *F. foetens* F2 against *G. boninense*, a modified disc diffusion or vapour assay was conducted (Bismarck *et al.*, 2020). An agar plug (ø6 mm) of the 5-day-old colony of *G. boninense* was inoculated and placed at the centre of a potato dextrose agar (PDA) medium. In the lid of the agar plate, a disc containing an extract of EtOAc or saturated VOCs was positioned. The plates were then incubated for five days at 28°C, with the lids facing upwards. A control plate consisting solely of the *G. boninense* colony in the centre was also prepared. The assay was performed in triplicate. The percentage of radial growth inhibition (%) was calculated using Equation (1):

$$(\%) = [(D1 - D2) / D1] \times 100\%, \quad (1)$$

D1 represents the radial growth (mm) of the control plate, and D2 represents the radial growth of the treated plates. For analysis of the treated colony or mycelium, the surface morphology was examined using a scanning electron microscope (JSM-6510LA JEOL SEM). The slide was fixed and coated with platinum (35 s: 30 mA) using 10 kV.

GC-MS Profiling of VOCs

Qualitative analysis of the crude VOCs-containing extracts was performed using an Agilent column (Type 19091S-433: 93.92873 DB-5MS UI, 5% Phenyl Methyl Silox) with dimensions of 30 m × 250 µm × 0.25 µm. The temperature range for injection was set from 0°C to 325°C, with a final hold time of 1 min. The analysis was conducted on an Agilent-type 7890 gas chromatograph (GC) coupled with a 5977A mass selective detector (MSD).

***In Silico* Molecular Docking**

Prediction of binding sites of selected VOCs produced by *F. foetens* F2 and their affinities, to xyloglucan-specific endo-beta-1,4-glucanase (XEG) (PDB ID: 3VL8) was performed through a molecular docking analysis (Yoshizawa *et al.*, 2012). The water molecules were removed from the protein using the BIOVIA Discovery Studio 2021 Client 21.1.0 software. The PyRx ver. 0.8 software (Dallakyan & Olson, 2015) was used for the docking simulation. The three-dimensional (3D) conformers of the VOCs were obtained from PubChem site (Bethesda, MD, USA). The results of molecular docking were visualised and analysed for binding affinity/energy (ΔG, kcal/mol) and similarity of binding site residues.

RESULTS AND DISCUSSION

Fusarium sp. F2, a soil fungus thriving in a local oil palm plantation, was successfully isolated. Its presence in asymptomatic regions free from *G. boninense* infection and BSR led to the hypothesis that it may possess antagonistic traits.

In previous studies, researchers have also isolated microbial strains and isolates that demonstrated antagonistic effects against the same pathogenic fungus. These strains were obtained either from the rhizosphere or as endophytes residing in healthy areas (Pramudito *et al.*, 2020; Yurnaliza *et al.*, 2014). Based on the bioinformatics analysis and phylogenetic inference within the ITS-rDNA region, the isolate was then identified as *F. foetens* F2 (*Figure 1*). Some studies have well documented this species as a pathogenic fungus affecting *Begonia elatior* and its hybrids and also potato plants, resulting in plant wilting and abnormal growth (Liu *et al.*, 2023; Tschöpe *et al.*, 2007). However, the presence of *F. foetens* in the oil palm plantation poses an intriguing question that demands further investigation. It is crucial to determine whether this fungus has the potential to cross-infect oil palm or just as a non-virulent rhizopheric fungal strain. The only negative aspect associated with *Fusarium* in oil palm was reported in relation to *F. sacchari*, which is a moderately virulent strain but less prevalent in distribution, including Indonesia. This species is recognised as one of the causal agents responsible for crown spear rot (CSR) or crown disease in young oil palms (Suwandi *et al.*, 2012). On the contrary, it is also widely recognised that specific non-pathogenic strains of *Fusarium* can provide crop protection against *F. oxysporum* pathogens (Iida *et al.*, 2022). Thus, it is plausible to consider that a similar phenomenon may occur with *G. boninense*. Among the extensively studied cases, Fo47 (*F. oxysporum*) stood out, as it established colonisation on the root surface and the surrounding soils in the vicinity of root epidermal cells. This colonisation enables Fo47 to effectively compete with pathogens for essential nutrients (Bolwerk *et al.*, 2005).

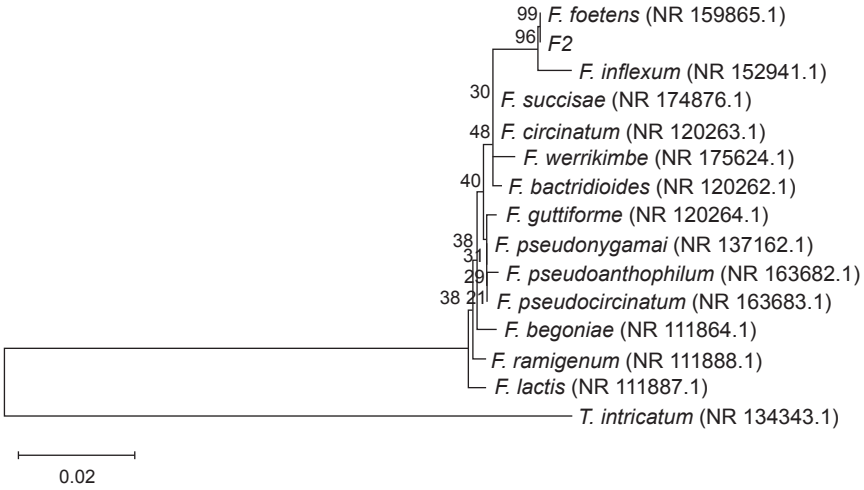


Figure 1. Phylogenetic tree of isolate F2 based on the alignment of ITS-rDNA from Fusarium *spp. and* T. intricatum *as an outgroup. Sequence alignment and tree construction were performed by MEGA11 using the neighbour-joining method and tested with 1000× bootstrapping.*

Through the disc vapour assay, the growth of the *G. boninense* colony was inhibited (*Figure 2*). The contactless exposure of *F. foetens* F2 to the pathogen demonstrated that inhibition occurred as a result of prolonged exposure to VOCs. The final observation on day 5 showed the highest growth inhibition of 63.64%, with the colony diameter reduced to 32 mm, which was much smaller compared to the control plate of *G. boninense* without VOCs (88 mm). However, it should be noted that studies examining *Fusarium* strains against *G. boninense* are still limited, as is the use of volatilisation assays to explore the potential of volatiles. Several studies have reported inhibition using VOCs from other microbial sources, particularly actinobacteria such as *Nocardiopsis alba* and *Streptomyces* spp., which exhibited varying levels of effectiveness (Budi *et al.,* 2022; Islamiati *et al.,* 2022; Widada *et al.,* 2021). The percentage of inhibition achieved through VOCs produced by a collection of peatland actinobacteria ranged between 4.47% and 20.23% against *G. boninense*, which was lower compared to this study (Budi *et al.,* 2022). According to Islamiati *et al.* (2022), an inhibition of 55% was achieved using the double-dish sets (DDS) method by exposing the colony of *Streptomyces* sp. GMR22 to the *G. boninense* colony. In a study conducted by Widada *et al.* (2022), the two-petri-dish method was employed, where *G. boninense* and *N. alba* strains were inoculated side by side. The highest inhibition rate, reaching 62.60%, was observed on the fifth day, which was similar to recent findings. Despite employing different inoculation methods, it can be inferred that the VOCs generated by antagonistic biocontrol agents possess considerable potential against *G. boninense*.

The ultrastructure of *G. boninense* was examined using SEM imagery after exposure to VOCs from *F. foetens* F2, and comparisons were made with the control (*Figure 3*). The treated mycelial network appeared thinner, wrinkled, but more compact compared to the control. This was evident from the hyphal arrangement, which showed reduced empty spaces. At 8,000× magnification, the control mycelium exhibited a normal and intact mycelia, while the mycelia exposed to VOCs appeared shriveled and incomplete. This was observed through disrupted branching or potential degeneration within the mycelium. Fungal cell walls typically contain 50%-60% of the dry weight of the cell wall, with β-(1-3)-glucan being the predominant component (Latgé, 2007). This β-(1-3)-glucan constitutes up to around 40% of the total fungal cell volume and serves as a common target for antifungal compounds (Gow *et al.,* 2017). The antifungal activity of *F. foetens* VOCs is likely linked to the destabilisation of cell wall structures and cytoskeleton in *G. boninense*, particularly involving chitin, glucan, and tubulin proteins (Islamiati *et al.,* 2022; Takeshita *et al.,* 2014). The incomplete extension of hyphae in specific branches may be attributed to internal damage or interactions with the VOCs, the exact mechanisms of which are currently unknown. The combination of external and intracellular damage may lead to an imbalance in homeostasis, ultimately impeding the overall growth of the *G. boninense* colony.

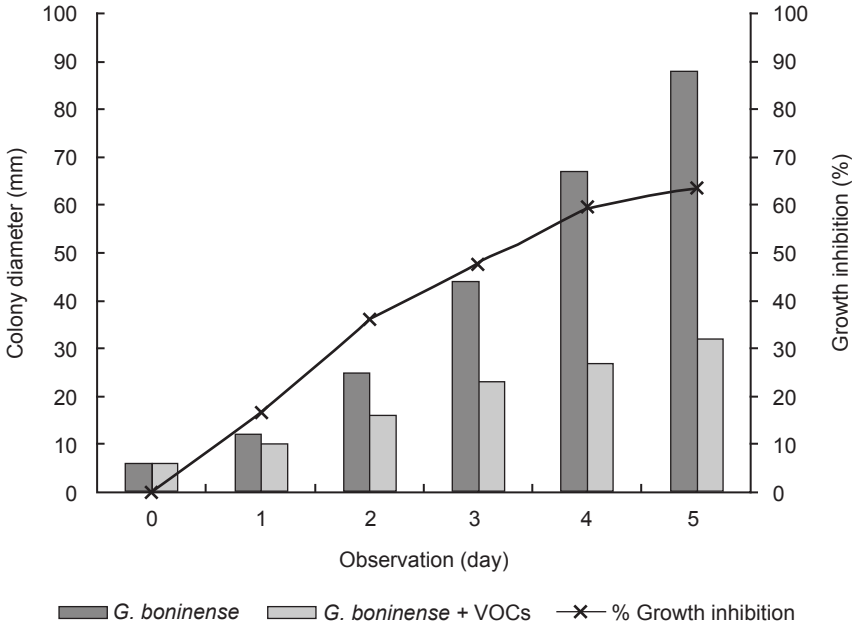


Figure 2. Inhibition of G. boninense *by volatile organic compounds (VOCs) of* F. foetens *F2.*

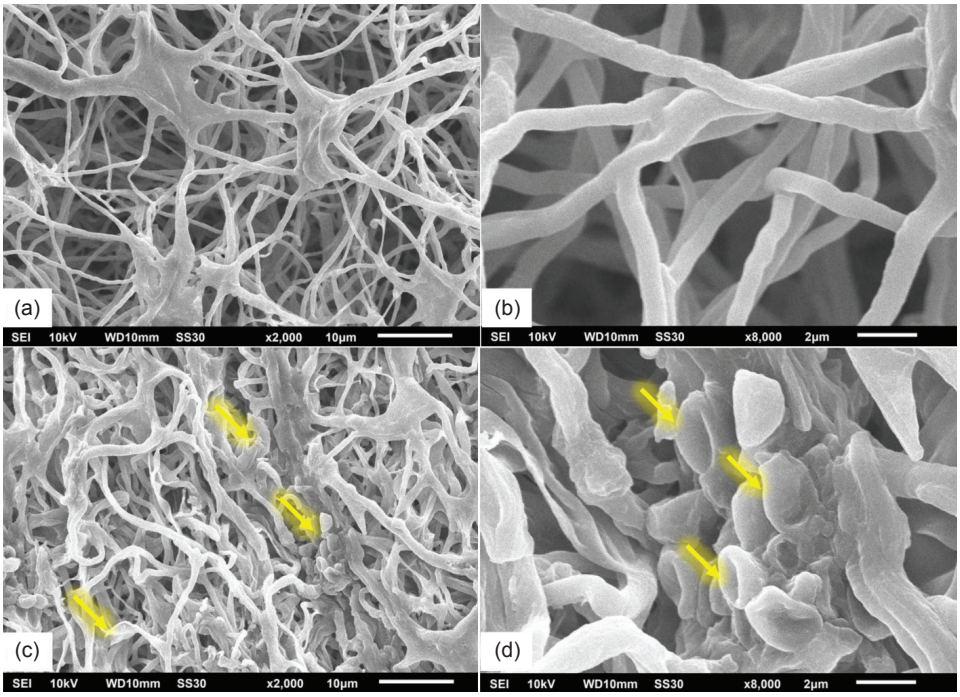


Figure 3. (a) The ultrastructure of G. boninense *in control plate at 2,000× and (b) 8,000× magnification. (c) The ultrastructure of* G. boninense *after 5-d exposure to VOCs of* F. foetens *F2 at 2,000× and (d) 8,000× magnification. The yellow arrows indicate visual evidence of hyphal abnormalities following VOCs exposure, including shrinkage, contraction, and branch deformation.*

A total of 45 VOCs were identified and confirmed by comparing their similarity percentages with the database (*Figure 4*). Among these, four major components were identified based on their relative peak areas (%): 2,3-Pyrazinedicarboximide (15.54%), 2-(2-Butoxyethoxy) ethyl thiocyanate (11.43%), 3,5-Dimethoxyphenol (11.40%), Indolylmethylthiohydroximate (5.56%) and other minor compounds (<5.00%).

These compounds will be further analysed using an *in silico* approach as anti *G. boninense.* The compound, 2,3-Pyrazinedicarboximide or 5h-Pyrrolo[3,4-b]pyrazine-5,7(6h)-dione ($C_6H_3N_3O_2$) belongs to a class of heterocylic compounds or cyclic imides, which are valuable bioactive compounds with a wide range of biological activities (Hassanzadeh & Jafari, 2018). The hydrophobic nature of cyclic imides and their N-derivatives allows for enhanced membrane permeability, facilitating their interaction with intracellular targets. This properties is advantageous for their potential as drug candidates, as it increase their ability to reach their target sites within cells (Patil & Rajput, 2014). Specifically, 2,3-Pyrazinedicarboximide has not been reported or directly tested for its activity against *G. boninense* or its antifungal activity against other species. However, several studies have documented inhibitory activity of other derivatives and related cyclic imides against *Candida albicans, C. krusei, C. tropicalis, Geotrichum candidum, Trichophyton mentagrophytes*, and *T. rubrum* (Gayoso *et al*., 2006; Sortino *et al*., 2008). 2-(2-Butoxyethoxy) ethyl thiocyanate or lethane ($C_9H_{17}NO_2S$) is an organosulfur compound or isothiocyanate that is commonly used as insecticides (Tsao *et al.,* 2002). Isothiocyanates, in their various forms, have been recognised for their antifungal properties against a wide array of plant pathogens, particularly *Alternaria brassicicola, F. oxysporum, Rhizoctonia solani*, and *Sclerotinia sclerotiorum*. Additionally, human-pathogenic strains such as those belonging to the *Candida* genus are also susceptible to these compounds. The mechanisms of action include growth inhibition, suppression of sclerotia or spore germination, and prevention of biofilm formation (Plaszko *et al.,* 2021). Therefore, based on the findings of this study, the compound produced by *F. foetens* could be regarded as the first report in VOCs. The phenol derivative, 3,5-Dimethoxyphenol ($C_8H_{10}O_3$) is characterised by the presence of two methoxy ($-OCH_3$) groups attached to the benzene ring at positions 3 and 5 that could be present as antifungal compound in VOCs. Phenols and phenolics are essential compound classes, recognised for their natural antifungal properties against *G. boninense*. Their mechanism of action involves the suppression of enzymes responsible for the degradation of wood and cell walls (Surendran *et al.*, 2017). In a more recent study by Fernanda *et al.* (2021), the inhibitory effects of benzoic acid, a phenol compound, was investigated at concentrations of 5 mM and above. The findings revealed that these concentrations

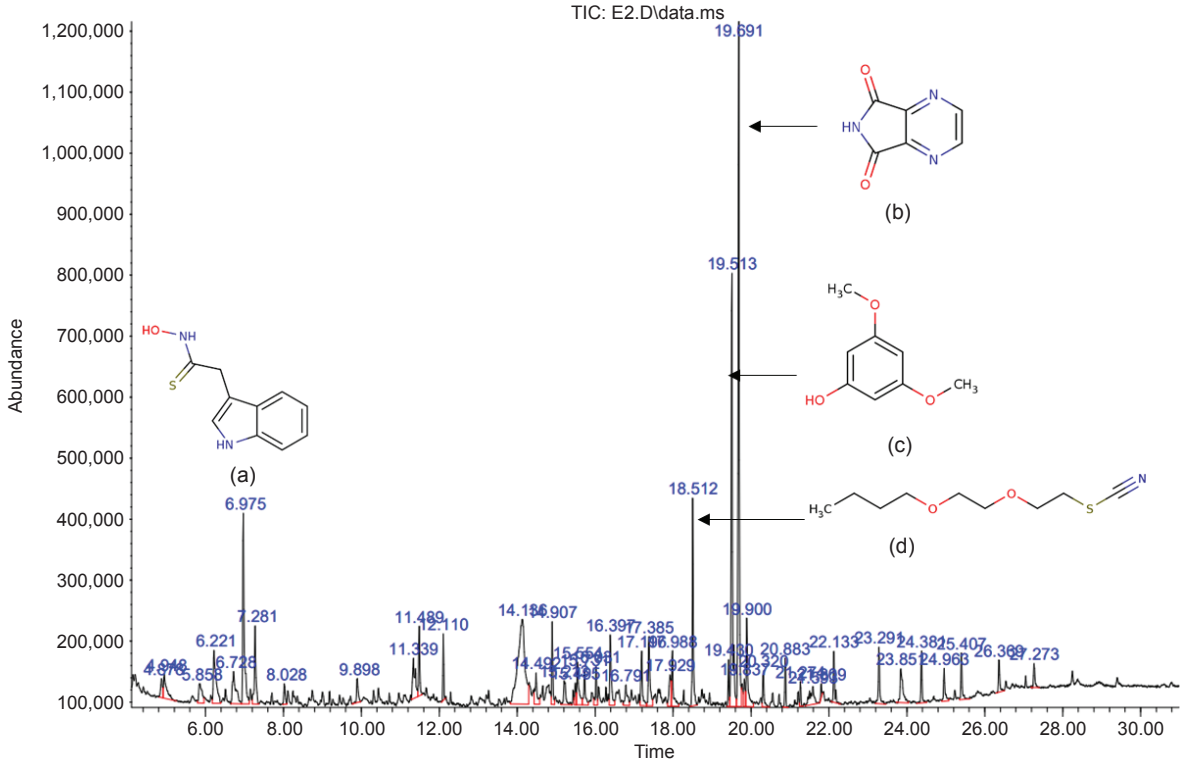


Figure 4. GC-MS spectra of volatiles emitted from F. foetens *F2. Chemical structure of four selected VOCs: (a) Indolylmethylthiohydroximate, (b) 2,3-Pyrazinedicarboximide, (c) 3,5-Dimethoxyphenol, and (d) 2-(2-Butoxyethoxy) ethyl thiocyanate. The numbers above the spectrum indicate the retention time (in min) of each identified compound.*

effectively hindered or delayed the establishment of the pathogen in oil palm wood, through cell mortality. Indolylmethylthiohydroximate or indolylmethylthiohydroximic acid ($C_{10}H_{10}N_2OS$) is a distinct form of glucosinolates that possesses an indole moiety (referred to as indole GSs), and it is currently known to exist as a component in the plant defence and abiotic stress response of *Arabidopsis thaliana* (Brader *et al.*, 2001; Zhao *et al.*, 2017). Some glucosinolates play a crucial role in defence against bacterial pathogens when activated upon pathogen attack (Rask *et al.*, 2000). However, there are currently no reports on the presence of indolylmethylthiohydroximate or its constituents as VOCs in fungi. It is then possible that the chemical cocktails found in the VOCs of *F. foetens* F2 may have the potential to be developed as antifungal agents in the future.

Xyloglucanases (XEG) are classified as cell wall-degrading enzymes (CWDEs) that specifically hydrolyse xyloglucan, a major component of hemicellulose in the plant cell wall, consisting of β-1,4-glucan linkages. This enzyme, categorised as a glycoside hydrolase, plays a significant role in phytopathogenic fungi, including possibly *G. boninense*. The enzyme can function as pathogen-associated molecular patterns (PAMPs), triggering PAMP-triggered immunity (PTI) (Zhang *et al.*, 2021). Interestingly, their PAMP activity may be separate from their enzymatic activity, as evidenced by *Verticillium dahlia* (Gui *et al.*, 2017). Through comprehensive genomic screening of various bacteria, fungi, oomycetes, and plant species, it has been observed that homologous protein sequences of XEG are exclusively present and widely distributed among microbial taxa, while absent in plants (Raflei *et al.*, 2021). Consequently, XEG becomes a potential target for antifungal treatment. As no native ligand was identified from the crystallography data, hexaconazole was then assigned as a standard antifungal agent in oil palm, as a reference, and compared it with four selected VOCs derived from *F. foetens*.

The interaction between hexaconazole and XEG protein resulted in a total of 16 bonds, including Van der Waals, π-alkyl, π-anion, and π-π stacked interactions. Van der Waals interactions were observed at three specific amino acid positions (Val-64, Ile-133, Phe-207) as depicted in *Figure 5*. No hydrogen bonds were formed during the simulation. Docking analysis of the ligand and XEG protein demonstrated a high-affinity value, indicated by an increased negative docking score (Du *et al.*, 2016). Hexaconazole exhibited a slightly lower affinity (-5.4 kcal/mol) to the XEG protein compared to the other two VOCs, namely 2,3-Pyrazinedicarboximide (-5.5 kcal/mol) and indolylmethylthiohydroximate (-5.5 kcal/mol) (*Table 1*). Both VOCs showed comparable activity and affinity to the standard antifungal agent

hexaconazole in the simulation. The interaction of ligands with proteins through hydrogen bonds or Van der Waals interactions contributes to the stability of ligand-protein complexes (De Freitas & Schapira, 2017), which may lead to stronger antimicrobial activity. According to *Table 1*, all simulated VOCs from *F. foetens* exhibited a greater number of hydrogen bond interactions during protein-ligand interactions in comparison to hexaconazole. This indicates a propensity to function as more effective inhibitors of XEG activity due to their enhanced capacity for maintaining stability through hydrogen bonding interactions. The hydrogen bond interactions of 2,3-pyrazinedicarboxamide were observed with the amino acids Ser-36, Ser-56, and Ser-54, while indolylmethylthiohydroximate formed hydrogen bonds with Asp-26, Asp-105, and Glu-119 (*Figure 6*). Therefore, it is confirmed that 2,3-pyrazinedicarboxamide and indolylmethylthiohydroximate may possess antifungal activities.

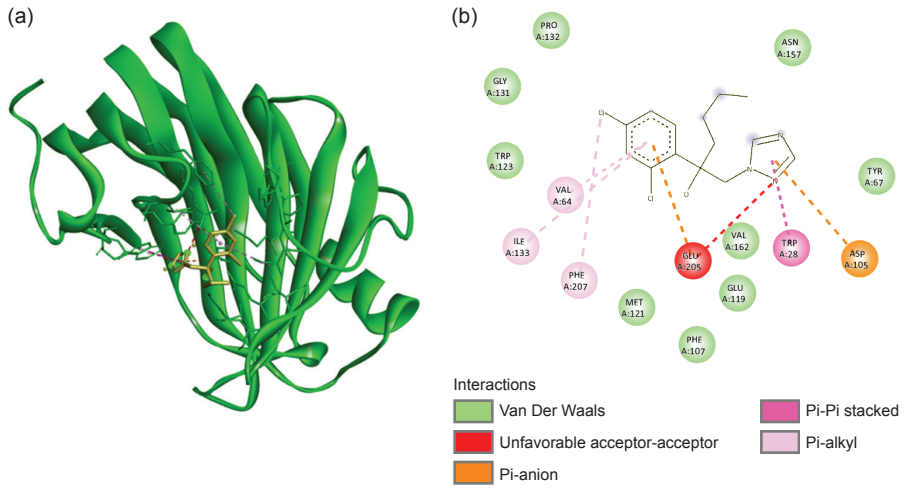


Figure 5. (a) Binding sites of the standard antifungi, hexaconazole (yellow) to xyloglucanaseprotein (green) and (b) Two dimensional (2D) visualisation of hexaconazole and xyloglucanaseprotein interaction.

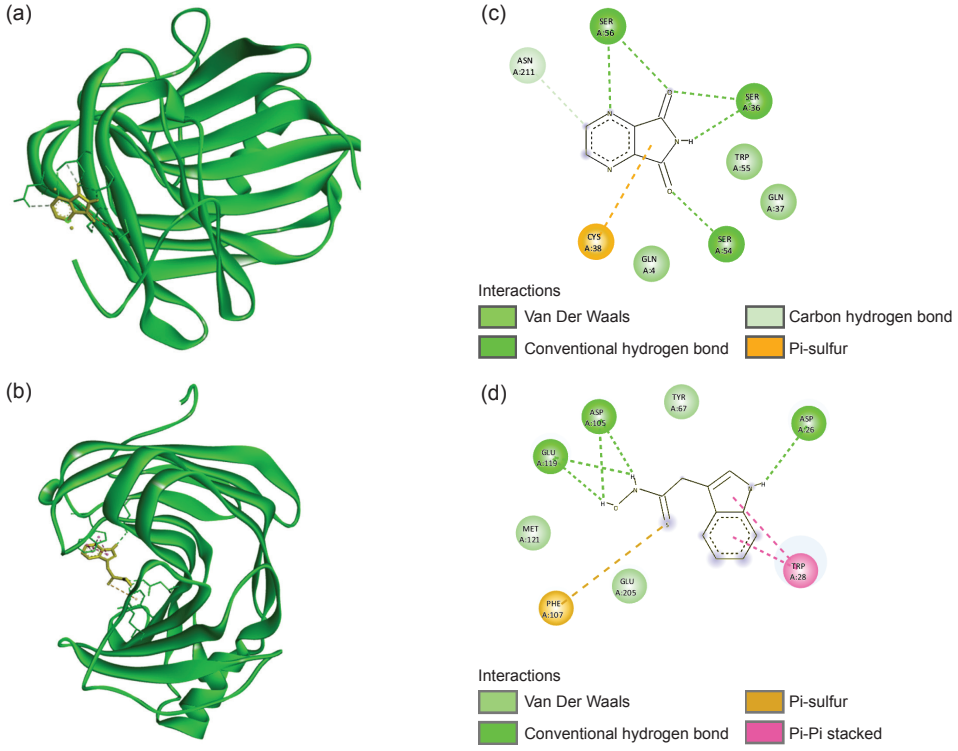


Figure 6. Docking visualisation of two volatiles by F. foetens *F2: (a) 2,3-pyrazinedicarboximide (yellow) and (b) indolylmethylthiohydroximate (yellow) to xyloglucanaseprotein (green). The 2D interaction of (c) 2,3-pyrazinedicarboximide and (d) indolylmethylthiohydroximate.*

TABLE 1. BINDING ENERGY BETWEEN XEG PROTEIN AND HEXACONAZOLE AND SELECTED VOCs AS TEST OF LIGANDS

Compound	Molecular weight (g/mol)	No. of H bonds	Binding energy (kcal/mol)
Hexaconazole (Standard)	314.20	-	-5.4
2,3-Pyrazinedicarboximide	149.11	3	-5.5
Indolylmethylthiohydroximate	206.27	3	-5.5
3,5-Dimethoxyphenol	154.16	3	-4.7
2-(2-Butoxyethoxy)ethyl thiocyanate	203.30	2	-3.1

CONCLUSION

Fusarium foetens F2, a soil fungus found in healthy oil palm plantations, emit VOCs that exhibit potent antifungal activity against *G. boninense*. These VOCs effectively inhibit the growth of *G. boninense* and cause both external and internal damage to its cells. Among the VOCs emitted by the fungus, four major compounds have been identified as the most prevalent. Notably, 2,3-pyrazinedicarboximide and indolylmethylthiohydroximate have displayed a strong binding affinity to XEG protein, a virulent factor of *G. boninense*, as revealed by molecular docking simulations. The results indicate a potential candidate for the future development of biocontrol and antifungal agents for managing BSR in oil palm.

ACKNOWLEDGEMENT

Financial support for the research was provided by LPDP - the Ministry of Finance of the Republic of Indonesia (RIIM - Technical Program No. PRN-018512262) for 2022-2024 years. The research was also supported by the facilities, scientific and technical support from the Laboratory of Biotechnology, National Research and Innovation Agency through *E-Layanan Sains*-BRIN.

REFERENCES

Ali, S. R. A., Safari, S., Thakib, M. S., Bakeri, S. A., & Ghani, N. A. A. (2016). Soil fungal community associated with peat in Sarawak identified using 18S rDNA marker. *Journal of Oil Palm Research, 28*(2), 161–171. https://doi.org/10.21894/jopr.2016.2802.03

Bharudin, I., Wahab, A. F. F. A., Samad, M. A. A., Yie, N. X., Zairun, M. A., Bakar, F. D. A., & Murad, A. M. M. (2022). Review update on the life cycle, plant-microbe interaction, genomics, detection and control strategies of the oil palm pathogen *Ganoderma boninense*. *Biology, 11*(2), 251. https://doi.org/10.3390/biology11020251

Bismarck, D., Dusold, A., Heusinger, A., & Muller, E. (2020). Antifungal in vitro activity of essential oils against clinical isolates of *Malassezia pachydermatis* from canine ears: A report from a practice laboratory. *Complementary Medicine Research, 27*, 143–154. https://doi.org/10.1159/000504316

Brader, G., Tas, E., & Palva, E. T. (2001). Jasmonate-dependent induction of indole glucosinolates in *Arabidopsis* by culture filtrates of the nonspecific pathogen *Erwinia carotovora*. *Plant Physiology, 126*(2), 849–860. https://doi.org/10.1104/pp.126.2.849

Budi, M. B. S., Giyanto, & Tondok, E. T. (2022). Isolation of actinomycetes from peatland to suppress the growth of *Ganoderma boninense*, the causal agent of basal stem rot disease in oil palm. *Biodiversitas: Journal of Biological Diversity, 23*, 5914–5922. https://doi.org/10.13057/biodiv/d231145

Bolwerk, A., Lagopodi, A. L., Lugtenberg, B. J. J., & Bloemberg, G. V. (2005). Visualization of interactions between a pathogenic and a beneficial *Fusarium* strain during biocontrol of tomato foot and root rot. *Molecular Plant-Microbe Interactions, 18*, 710–721. https://doi.org/10.1094/MPMI-18-0710

Dallakyan, S., & Olson, A. J. (2015). Small-molecule library screening by docking with PyRx. *Methods in Molecular Biology, 1263*, 243–250. https://doi.org/10.1007/978-1-4939-2269-7_19

De Freitas, R. F., & Schapira, M. (2017). A systematic analysis of atomic protein-ligand interactions in the PDB. *MedChemComm, 8*, 1970–1981. https://doi.org/10.1039/c7md00381a

Du, X., Li, Y., Xia, Y. L., Ai, S. M., Liang, J., Sang, P., Ji, X. L., & Liu, S. Q. (2016). Insights into protein-ligand interactions: Mechanisms, models, and methods. *International Journal of Molecular Sciences, 17*, 144. https://doi.org/10.3390/ijms17020144

Fernanda, R., Siddiqui, Y., Ganapathy, D., Ahmad, K., & Surendran, A. (2021). Suppression of *Ganoderma boninense* using benzoic acid: Impact on cellular ultrastructure and anatomical changes in oil palm wood. *Forests, 12*, 1231. https://doi.org/10.3390/f12091231

Gayoso, C. W., Lima, E. O., Souza, E. L., Filho, V. C., Trajano, V. N., Pereira, F. O., & Lima, I. O. (2006). Antimicrobial effectiveness of maleimides on fungal strains isolated from onychomycosis. *Brazilian Archives of Biology and Technology, 49*, 661–664. https://doi.org/10.1590/S1516-89132006000500016

Gow, N. A. R., Latgé, J. P., & Munro, C. A. (2017). The fungal cell wall: Structure, biosynthesis, and function. *Microbiology Spectrum, 5*, 1–25. https://doi.org/10.1128/microbiolspec.FUNK-0035-2016

Gui, Y. J., Chen, J. Y., Zhang, D. D., Li, N. Y., Li, T. G., Zhang, W. Q., Wang, X. Y., Short, D. P. G., Li, L., Guo, W., Kong, Z. Q., Bao, Y. M., Subbarao, K. V., & Dai, X. F. (2017). *Verticillium dahliae* manipulates plant immunity by glycoside hydrolase 12 proteins in conjunction with carbohydrate-binding module 1. *Environmental Microbiology, 19*, 1914–1932. https://doi.org/10.1111/1462-2920.13695

Hassanzadeh, F., & Jafari, E. (2018). Cyclic imide derivatives: As promising scaffold for the synthesis of antimicrobial agents. *Journal of Research in Medical Sciences, 23*, 53. https://doi.org/10.4103/jrms.JRMS_539_17

Hushiarian, R., Yusof, N. A., & Dutse, S. W. (2013). Detection and control of *Ganoderma boninense*: Strategies and perspectives. *SpringerPlus, 2*, 1–12. https://doi.org/10.1186/2193-1801-2-555

Idris, A. S., Arifurrahman, R., & Kushairi, A. (2010). *Hexaconazole as a preventive treatment for managing* Ganoderma *in oil palm*. MPOB Information Series, 75. MPOB

Iida, Y., Ogata, A., Kanda, H., Nishi, O., Sushida, H., Higashi, Y., & Tsuge, T. (2022). Biocontrol activity of nonpathogenic strains of *Fusarium oxysporum*: Colonization on the root surface to overcome nutritional competition. *Frontiers in Microbiology, 13*, 826677. https://doi.org/10.3389/fmicb.2022.826677

Islamiati, E. D., Widada, J., Wahyuningsih, T. D., & Widianto, D. (2022). Volatile organic compounds of *Streptomyces* sp. GMR22 inhibit growth of two plant pathogenic fungi. *Agricultural and Natural Resources, 56*, 899–908. https://doi.org/10.34044/j.anres.2022.56.5.04

Khoo, Y. W., & Chong, K. P. (2023). *Ganoderma boninense*: General characteristics of pathogenicity and methods of control. *Frontiers in Plant Science, 14*, 1156869. https://doi.org/10.3389/fpls.2023.1156869

Latgé, J. P. (2007). The cell wall: A carbohydrate armour for the fungal cell. *Molecular Microbiology, 66*, 279–290. https://doi.org/10.1111/j.1365-2958.2007.05872.x

Liu, L., Jin, X., Lu, X., Guo, L., Lu, P., Yu, H., & Lv, B. (2023). Mechanisms of surfactin from *Bacillus subtilis* SF1 against *Fusarium foetens*: A novel pathogen inducing potato wilt. *Journal of Fungi, 9*, 367. https://doi.org/10.3390/jof9030367

Muhamad, H., Zainol, M., Sahid, I., & Seman, I. A. (2012). Determination of hexaconazole in field samples of an oil palm plantation. *Drug Testing and Analysis, 4*, 112–117. https://doi.org/10.1002/dta.1351

Nur-Rashyeda, R., Idris, A. B., Sundram, S., Zainol-Hilmi, N. H., & Ming, S. C. (2022). A field evaluation on fungicides application to control upper stem rot (USR) disease in oil palm caused by *Ganoderma* spp. *Journal of Oil Palm Research, 35*, 320–329. https://doi.org/10.21894/jopr.2022.0037

Patil, M. M., & Rajput, S. S. (2014). Succinimides: Synthesis, reaction, and biological activity. *International Journal of Pharmaceutics and Pharmaceutical Sciences, 6*, 8–14. https://innovareacademics.in/journals/index.php/ijpps/article/view/2715/9249

Pilotti, C. A., Gorea, E. A., & Bonneau, L. (2018). Basidiospores as sources of inoculum in the spread of *Ganoderma boninense* in oil palm plantations in Papua New Guinea. *Plant Pathology, 67*, 1841–1849. https://doi.org/10.1111/ppa.12915

Pilotti, C. A., Sanderson, F. R., & Aitken, E. A. B. (2003). Genetic structure of a population of *Ganoderma boninense* on oil palm. *Plant Pathology, 52*, 455–463. https://doi.org/10.1046/j.1365-3059.2003.00870.x

Plaszkó, T., Szűcs, Z., Vasas, G., & Gonda, S. (2021). Effects of glucosinolate-derived isothiocyanates on fungi: A comprehensive review on direct effects, mechanisms, structure-activity relationship data and possible agricultural applications. *Journal of Fungi, 7*(7), 539. https://doi.org/10.3390/jof7070539

Pramudito, T. E., Agustina, D., Budinarta, W., Nguyen, T. K. N., Prihatna, C., & Suwanto, A. (2020). Identification and characterization of antifungal compounds from a *Burkholderia* strain against plant pathogenic fungi. *Malaysian Journal of Microbiology, 16*(3), 245–252. https://doi.org/10.21161/mjm.190524

Raflei, V., Vélëz, H., & Tzelepis, G. (2021). The role of glycoside hydrolases in phytopathogenic fungi and oomycetes virulence. *International Journal of Molecular Sciences, 22*(17), 9359. https://doi.org/10.3390/ijms22179359

Rask, L., Andreasson, E., Ekbom, B., Eriksson, S., Pontoppidan, B., & Meijer, J. (2000). Myrosinase: Gene family evolution and herbivore defense in Brassicaceae. *Plant Molecular Biology, 42*(1), 93–114. https://doi.org/10.1023/A:1006380021658

Shariffah-Muzaimah, S. A., Idris, A. S., Madihah, A. Z., Dzolkhifli, O., Kamaruzzaman, S., & Cheong, P. C. H. (2018). Isolation of actinomycetes from the rhizosphere of oil palm (*Elaeis guineensis* Jacq.) for antagonism against *Ganoderma boninense*. *Journal of Oil Palm Research, 27*, 19–29.

Shariffah-Muzaimah, S. A., Idris, A. S., Nur-Rashyeda, R., Naidu, Y., Zainol-Hilmi, N. H., & Norman, K. (2020). Impact of pre-inoculating soil with *Streptomyces* sp. GanoSA1 on oil palm growth and *Ganoderma* disease development. *Biocatalysis and Agricultural Biotechnology, 29,* 101814. https://doi.org/10.1016/j.bcab.2020.101814

Siddiqui, Y., Surendran, A., Paterson, R. R. M., Ali, A., & Ahmad, K. (2021). Current strategies and perspectives in detection and control of basal stem rot of oil palm. *Saudi Journal of Biological Sciences, 28*, 2840–2849. https://doi.org/10.1016/j.sjbs.2021.02.016

Sortino, M., Filho, V. C., Correa, R., & Zacchino, S. (2008). N-Phenyl and N-phenylalkyl-maleimides acting against *Candida* spp.: Time-to-kill, stability, interaction with maleamic acids. *Bioorganic & Medicinal Chemistry, 16*, 560–568. https://doi.org/10.1016/j.bmc.2007.08.030

Surendran, A., Siddiqui, Y., Saud, H. M., Ali, N. S., & Manickam, S. (2017). The antagonistic effect of phenolic compounds on ligninolytic and cellulolytic enzymes of *Ganoderma boninense*, causing basal stem rot in oil palm. *International Journal of Agriculture and Biology, 19*, 1437–1446. https://doi.org/10.17957/IJAB/15.0439

Susanto, A., Sudharto, P. S., & Purba, R. Y. (2005). Enhancing biological control of basal stem rot disease (*Ganoderma boninense*) in oil palm plantations. *Mycopathologia, 159*(2), 153–157. https://doi.org/10.1007/s11046-004-4438-0

Suwandi, A., Akino, S., & Kondo, N. (2012). Common spear rot of oil palm in Indonesia. *Plant Disease, 96*, 537–543. https://doi.org/10.1094/PDIS-08-10-0569

Takeshita, N., Manck, R., Grün, N., de Vega, S. H., & Fischer, R. (2014). Interdependence of the actin and the microtubule cytoskeleton during fungal growth. *Current Opinion in Microbiology, 20*, 34–41. https://doi.org/10.1016/j.mib.2014.04.005

Tamura, K., Stecher, G., & Kumar, S. (2021). MEGA11: Molecular evolutionary genetics analysis version 11. *Molecular Biology and Evolution, 38*, 3022–3027. https://doi.org/10.1093/molbev/msab120

Tilocca, B., Cao, A., & Migheli, Q. (2020). Scent of a killer: Microbial volatilome and its role in the biological control of plant pathogens. *Frontiers in Microbiology, 11*, 41. https://doi.org/10.3389/fmicb.2020.00041

Tsao, R., Peterson, C. J., & Coats, J. R. (2002). Glucosinolate breakdown products as insect fumigants and their effect on carbon dioxide emission of insects. *BMC Ecology, 2*, 5. https://doi.org/10.1186/1472-6785-2-5

Tschöpe, B., Hey, M., Wohanka, W., & Hennig, F. (2007). Characterisation and identification of *Fusarium foetens*, causative agent of wilting and stem rot of *Begonia elatior* hybrids (*Begonia* × *hiemalis*) by its volatile compounds. *European Journal of Horticultural Science, 72*(4), 151–157.

Vieira, G. R. T., Liebl, M., Tavares, L. B. B., Paulert, R., & Junior, A. S. (2008). Submerged culture conditions for the production of mycelial biomass and antimicrobial metabolites by *Polyporus tricholoma* Mont. *Brazilian Journal of Microbiology, 39*(3), 561–568. https://doi.org/10.1590/S1517-838220080003000029

Widada, J., Damayanti, E., Alhakim, M. R., Yuwono, T., & Mustofa, M. (2021). Two strains of airborne *Nocardiopsis alba* producing different volatile organic compounds (VOCs) as biofungicide for *Ganoderma boninense*. *Microbiology Letters, 368*, 1–10. https://doi.org/10.1093/femsle/fnab138

Xie, J., Fu, Y., Jiang, D., Li, G., Huang, J., Li, B., Hsiang, T., & Peng, Y. (2008). Intergeneric transfer of ribosomal genes between two fungi. *BMC Evolutionary Biology, 8*, 87. https://doi.org/10.1186/1471-2148-8-87

Yoshizawa, T., Shimizu, T., Hirano, H., Sato, M., & Hashimoto, H. (2012). Structural basis for inhibition of xyloglucan-specific endo-beta-1,4-glucanase (XEG) by XEG-protein inhibitor. *Journal of Biological Chemistry, 287*(22), 18710–18716. https://doi.org/10.1074/jbc.M112.350520

Yurnaliza, Aryantha, I. N. P., Esyanti, R. R., & Susanto, A. (2014). Antagonistic activity assessment of fungal endophytes from oil palm tissues against *Ganoderma boninense* Pat. *Plant Pathology Journal, 13*(4), 257–267. https://doi.org/10.3923/ppj.2014.257.267

Zhang, L., Yan, J., Fu, Z., Shi, W., Ninkuu, V., Li, G., Yang, X., & Zeng, H. (2021). FoEG1, a secreted glycoside hydrolase family 12 protein from *Fusarium oxysporum*, triggers cell death and modulates plant immunity. *Molecular Plant Pathology, 22*(4), 522–538. https://doi.org/10.1111/mpp.13041

Zhao, L., Wang, C., Zhu, F., & Li, Y. (2017). Mild osmotic stress promotes 4-methoxy indolyl-3-methyl glucosinolate biosynthesis mediated by the MKK9-MPK3/MPK6 cascade in *Arabidopsis*. *Plant Cell Reports, 36*(4), 543–555. https://doi.org/10.1007/s00299-017-2101-8

Journal of Oil Palm Research Vol. 37 (1) March 2025 p. 96-109
DOI: https://doi.org/10.21894/jopr.2024.0005

INSECT COMMUNITY ASSOCIATED WITH *Ganoderma* BASIDIOCARPS IN OIL PALM PLANTATIONS OF SABAH

MUHAMMAD NURUL YAQIN SYARIF[1]; SHAMALA SUNDRAM[1]*; SITI NURULHIDAYAH AHMAD[1]; MOHAMED MAZMIRA MOHD MASRI[1] and IDRIS ABU SEMAN[1]

ABSTRACT

Ganoderma *basal stem rot (BSR) is currently one of the most important diseases in oil palm. The disease transmission is predominantly through root-to-root contact in soil. However, the role of* Ganoderma *basidiospores remains ambiguous in the transmission process despite millions being produced during active phase of fungus. Five plantations in Sabah, Malaysia with varying incidences of* Ganoderma *BSR (6.0%-9.8%) were selected for the study. A total of 543 basidiocarps were collected and assessed. At least 55 arthropods were associated with* Ganoderma *basidiocarps. Among these arthropods, 8 species were found carrying the basidiospores internally or externally. Handsome fungus beetles,* Eumorphus *spp. were found to be strongly associated as vector of* Ganoderma *disease, but this requires further investigation. This study could potentially provide an insight on the sporadic spread of BSR which was not conceivable via root-to-root contact.*

Keywords: basal stem rot, insect vector, upper stem rot.

Received: 24 June 2023; **Accepted:** 14 November 2023; **Published online:** 10 January 2024.

INTRODUCTION

Malaysia is among the two major palm oil suppliers across the world, which signifies the importance of oil palm to Malaysia's economy. The oil palm industry plays a crucial role in the agricultural and economic development of the country (Parveez *et al.*, 2020). Malaysia has entered the 4th generation planting and has celebrated its centennial anniversary after its humble introduction in 1917. After decades of cultivation, the country's golden crop is seriously threatened by *Ganoderma* basal stem rot (BSR) infection, prevalent in all oil palm areas regardless of the soil type. The disease has no immediate curative control and has been managed to remain below the economic threshold through a combination of integrated approaches: Cultural, biological, and chemical (Nur-Rashyeda *et al.*, 2022).

Three *Ganoderma* species have been reported to cause *Ganoderma* BSR and upper stem rot (USR) in oil palm, namely: (1) *G. boninense*, (2) *G. zonatum*, and (3) *G. miniatocinctum* (Idris *et al.*, 1999; Rees *et al.*, 2007). The primary transmission of the disease is through root-to-root contact with the fungal inoculum present in the field, while the basidiospores have implications for the distribution and genetic diversity of *Ganoderma* sp. (Rees *et al.*, 2007). *Ganoderma* is a white rot fungus that produces basidiocarps, which, upon maturity, release millions of basidiospores in the field. The disease epidemiology validates the role of root-to-root contact in the disease's spread in the field, but the role of spores remains ambiguous. Despite the ambiguity of their role, basidiospores are believed to be the primary source of inoculum (Pilotti *et al.*, 2018). Basidiospores are able to germinate and grow on different parts of oil palm including the cut surfaces of fronds, peduncles, and stems (Rees *et al*. 2012). However, the high level of *G. boninense* heterogeneity in oil palm plantations based on previous genetic studies has generated arguments for root-to-root contact as the main method of BSR disease spread (Miller *et al.*, 1999; Pilotti, 2005; Pilotti *et al.*, 2004). Additionally, the occurrence of USR in oil palm plantations has driven the hypothesis that insects are possible vectors of *Ganoderma* disease spread through the dispersal

[1] Malaysian Palm Oil Board,
6, Persiaran Institusi,
Bandar Baru Bangi,
43000 Kajang, Selangor, Malaysia.

* *Corresponding author e-mail: shamala@mpob.gov.my*

of its airborne basidiospores. Oil palms infected with USR differ in their decaying location, whereby it is situated on the upper section of the trunk and the basidiocarps emerge approximately 1-2 m above ground level (Rees *et al.*, 2012). In addition, the sporadic BSR incidences in the field further validate the need to determine the contribution of insects as *Ganoderma* vectors, despite the claim that previous crops were a source of disease inoculum initiating a new infection (Turner, 1965).

Oil palm plantation is a monocrop habitat that host a diverse community of insects that vary in their roles in the ecosystem, ranging from beneficial ones such as parasitoids and pollinators to damaging insects such as the bagworm and rhinoceros beetle that feed on plants. The presence of insects in the oil palm plantation is signified as part of the food web, with different feeding systems and ingestions depending on their mouthparts and physiological adaptations (Yadav, 2003). Regardless of their roles, insects have their own unique, specific niche in the oil palm ecosystem including the association of insects and microorganisms that form a range of symbiotic and pathogenic relationships (Wielkopolan *et al.*, 2021). Thus, insects could be considered as both pest and reservoir, as well as vector of plant pathogen. To date, more than 700 plant diseases are known to be vector-borne threats to food health and security worldwide (Fletcher & Wayadande, 2002; Hammond & Bedendo, 2005; Hogenhout *et al.*, 2008; Weintraub & Beanland, 2006). Vector density, feeding activity on the host, vector longevity during pre- and post-infection, incubation period, and vector competency are some of the factors affecting vectorial capacity that determine the effectiveness of vector-borne pathogens (Chuche *et al.*, 2017).

Ganoderma basidiocarp could provide food and breeding sites for several insect species which subsequently contribute to the biodiversity richness and composition of insects. This has been implied in other studies where Polyporacea fungi were used as breeding and hosting sites for fungivorous insects (Fäldt *et al.*, 1999; Jonsell & Nordlander, 1995; Yamashita *et al.*, 2015). However, there has been no publication or report on the diversity of the insects cohabiting with the basidiocarps in the oil palm plantations specifically.

Therefore, the aim of this study was to conduct a generic census on the diversity of the insect community surrounding the *Ganoderma* infected palms and the community of insects cohabiting within *Ganoderma* basidiocarps (fruiting bodies). This was followed by insect species identification using key taxonomic characteristics, basidiospore carrying assessment, and finally, establishing the association potential of the insects as vectors in spreading the disease in oil palm.

MATERIALS AND METHODS

Study Sites

Five oil palm plantations located in Sabah, Malaysia were selected for the insect sampling, focusing on the *Ganoderma* infected palms. The *Ganoderma* disease incidence was determined by ground census and labelling of infected palms. The percentage of disease incidence was calculated by the number of infected palms (basidiocarps presence) over total palms of 5 ha planting area. The percentage of disease incidence was between 6.0% and 9.8% across five sampling sites: Kota Marudu, Beaufort, Tawau, Kunak and Lahad Datu (*Figure 1*).

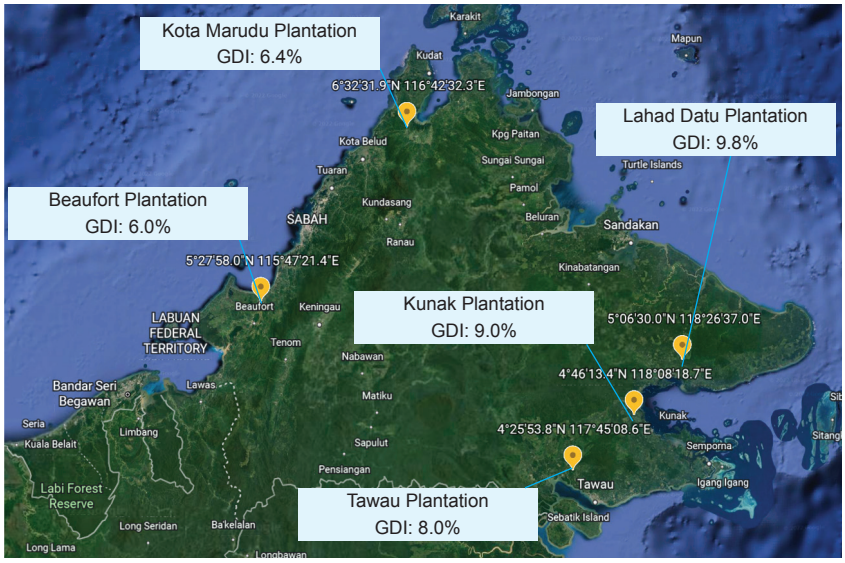


Figure 1. The selected five study sites with varying Ganoderma *disease incidences (GDI) of basal stem rot (BSR) and upper stem rot (USR) in Sabah.*

Insect Species Richness Surrounding *Ganoderma* Basidiocarp

The *Ganoderma* infected palms with the presence of basidiocarps were labelled prior to the sampling activity. Only BSR infected palms were selected in the study as shown in *Figure 2*. Three *Ganoderma* basidiocarps, irrespective of its stage of maturity, were collected from the infected palms, placed into a sterile plastic container, and brought to the laboratory. A total of 543 basidiocarps of *Ganoderma* were collected for the insect enumeration. All insects either in contact with or surrounding the palms were handpicked, and the basidiocarps were placed in a small container and labeled accordingly. The basidiocarps were broken into pieces using hand pressure, and all the insects inside the brackets were carefully removed using soft forceps to ensure the retrieved insects were not physically injured. These insects were classified taxonomically before being subjected to enumeration. The insect classification was based on published taxonomic key such as Zettler *et al.* (2016) for identification to orders, Hölldobler and Wilson (1990) for ants, Strohecker (1949; 1968) for *Eumorphus* spp.

Presence and Viability of *Ganoderma* Basidiospore

Externally. The sampled insects from the basidiocarp were brought to the laboratory for further examination for the presence of *Ganoderma* basidiospores. The insects were dipped into 5 mL sterile distilled water and the suspensions was observed under microscope. The detection of basidiospores was carried out according to the morphological characteristics stated by Rees *et al.* (2012) *i.e.*, basidiospore dimensions were 9.8 × 4.5 µm (mean), reddish brown, narrow ellipsoid with a visible hilar appendage, and often containing a large vacuole. Each sampled insect was dipped into 1 mL of sterile distilled water with 0.02% Tween 80®.

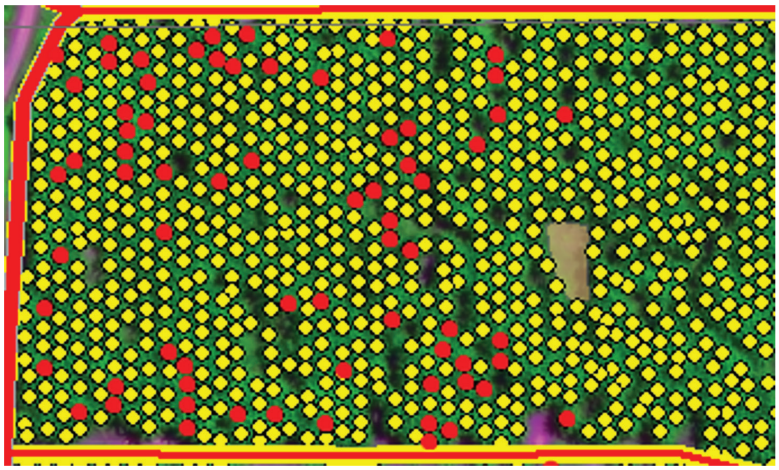
Internally. Insects were removed from the suspension, blotted carefully using sterile tissue, and left to dry for 10 min. The insects were dissected using a sterile dissecting scalpel to expose the inner section of the bodies, followed by dipping into 1 mL of sterile distilled water.

All the resulting suspension were then placed on a glass slide and observed under a Leica DM750 compound microscope to examine the presence of *Ganoderma* basidiospores. This method was adapted from Dhileepan (1992) for examining the pollen carrying capacity of *Elaeidobius kamerunicus*. Any positive presence of basidiospores was quantified using a hemocytometer. The suspension was then immediately spread onto potato dextrose agar (PDA) and *Ganoderma* selective medium (GSM) prepared as previously described in Ariffin and Idris (1992) to observe the identity and viability of the basidiospores.

RESULTS AND DISCUSSION

Species Richness of the Arthropods Associated to *Ganoderma* Basidiocarps

After sampling and data collection from five different plantations in Sabah, 53 species of arthropods were found. Most of the infected palms in the sampled estates had been dominated by Tenebrionids followed by Formicids, as shown in *Table 1*. Some of the insects' pictures are shown in *Figure 3*. Non-insect arthropods were mainly decomposers, and predatory spiders feeding on the abundance of insects located at the base of palm. It was also noted that the presence of *Ganoderma* basidiocarps may have increased the species



Note: Red circle - infected palm.

Figure 2. The map of the oil palm plantation in Lahad Datu selected for insect sampling.

richness of the palm base due to the colonisation by fungivorous insects for breeding and feeding sites. The largest insect order associated with *Ganoderma* basidiocarps was Coleoptera. According to research undertaken in temperate and boreal climates, many Coleoptera and Diptera employ enormous fungal fruiting bodies as both food and habitat (Hammond & Lawrence, 1989; Hanski, 1989; Yamashita & Hijii, 2003). Research on host use patterns of fungivorous insects shows monophagy and oligophagy are commonly seen in Coleoptera that feed on bracket fungi (Nordlander, 2004; Orledge & Reynolds, 2005; Paviour-Smith, 1960), whereas many Diptera that feed on agaric fungi are observed as polyphagy (Jaenike, 1978; Yamashita & Hijii, 2007). Meanwhile, the high biodiversity value (HBV) is a riparian area initiated by MPOB to conserve the flora and fauna along the gazetted river inside the plantations (*Figure 4*). Therefore, there is a possibility that the high number of species recorded in Lahad Datu was influenced by the species migration from this area. There are some common insects found associated with *Ganoderma* in this study which also found in the riparian area. *Dolichoderus* sp., *Anoplolepis* sp., *Camponotus* sp., *Oecophylla smaragdina*, *Polyrhachis furcata* were previously found in the riparian zones of Sungai Sepetang, Sungai Rembau and Sungai Chukai in Peninsular Malaysia (Abdullah *et al*., 2019) but these are ants commonly present in the ecosystems. Pitfall trapping in primary and secondary forest of Danum Valley Field Centre and Sungai Bole found abundance of *Onthophagus* spp. which is also commonly known as dung beetles (Holloway *et al*., 1992). Another insect collection study from bracket fungi of Borneon tropical forest also found insect species from the following genera: *Physodera*, *Tachys*, *Cis*, *Eumorphus*, *Sepedophilus*, *Staphylinidae*, *Amarygmus*, *Pentaphylus* and *Platydema* (Yamashita *et al*., 2015). All of these beetles could also be found associated with the *Ganoderma* basidiocarps in this study.

It was also noted that Tenebrionids were commonly found in most of the plantations (>70%). Generally, Tenebrionid pests feed on plant materials including decaying matter, wood, leaf litter, pollen and fungal and algal matters (Darya *et al.*, 2016). This is explained by the decaying process caused by *Ganoderma* sp. within the palm base, which may have served as a feeding substrate for this pest. Tenebrionid species commonly reside in primary forests and are easily affected by continuous forest development (Grimm & Schawaller, 2021). Thus, the abundance and presence of Darkling beetles in the oil palm planting area is predictable, while the presence of *Ganoderma* and the decaying process subsequently attracted those other associated insects.

When comparing the presence from other insect orders associated with *Ganoderma* basidiocarp, there is a higher possibility of Coleopterans as disease vectors due to the fact that some of them complete their life cycle during the course of feeding, breeding, and living inside the basidiocarps. Komonen (2003) suggested that fruiting bodies of wood-decaying macrofungi can be considered hotspots of insect diversity after concluding that the insect communities occurring within are rich in species, many of which show preference for a specific fungal host. Previous studies reported that fungal odour have a role in inviting insects living on fungi (Bengtsson *et al*., 1991; Fäldt *et al*., 1999; Jonsell & Nordlander, 1995; Pacioni *et al*., 1991) or on decayed substrates of the infection (Honda *et al*., 1988; Pfeil & Mumma, 1993; Phelan & Lin, 1991; Pierce *et al*., 1991). Jonsell and Norlander (2004) even concluded that more than half (53%) of the insect species breeding in bracket fungi appeared to be monophagous.

Interestingly, insects such as *Cis* sp., *Eledona* sp. and *Pentaphyllus* sp. were found to bore tunnels inside the *Ganoderma* basidiocarps while feeding on the fungi. Fäldt *et al.* stated in (1999) that many insects that develop under the bark of logs are frequently found on the hymenium of fruiting bodies, where they feed on spores. The patchy distribution of *Ganoderma* basidiocarps may not serve as a predictable breeding or feeding site for insects. The Ciidae family, also called the minute tree fungus beetle, is well known for infesting Polyporacea fungi such as *Fomes fomentarius* and *Ganoderma lucidum*. This could account for the greater diversity of insects in *Ganoderma* infected areas, which draws fungivorous insects.

Among the Coleopterans, *Eumorphus minor* (*Figure 5a*), was found in colony on the surface of *Ganoderma* basidiocarps. This species was identified based on the taxonomic key by Strohecker (1949; 1968). The features of this species matched the taxonomic key of having an elytral margin narrow along the shoulder, an epipleuron, a dark suture, an elytral surface dull and purplish brown, and bicolored femora. Unlike the other Coleopterans mentioned, *Eumorphus* spp. or handsome fungus beetles do not reside entirely inside the basidiocarp. They were observed to intermittently move in and out of the basidiocarps of *Ganoderma* despite colonising and feeding on the basidiocarps. Endomychids behave like any other mycophagous beetles, wandering regularly onto and even nibble on any substrate, including plant tissue (Shockley *et al.*, 2009). There are also reports on *Eumorphus quadriguttatus* (Illiger) infesting betel pepper plants, *Piper betel* (L.) (Piperaceae) (Mondal *et al.*, 2003). These beetles gradually leave the fruiting bodies upon afternoon to reach darker places around the palm base, usually between the silts of the oil palm roots. This observation shows that handsome fungus beetle prefers dark and moist places for shelter and only emerges for feeding.

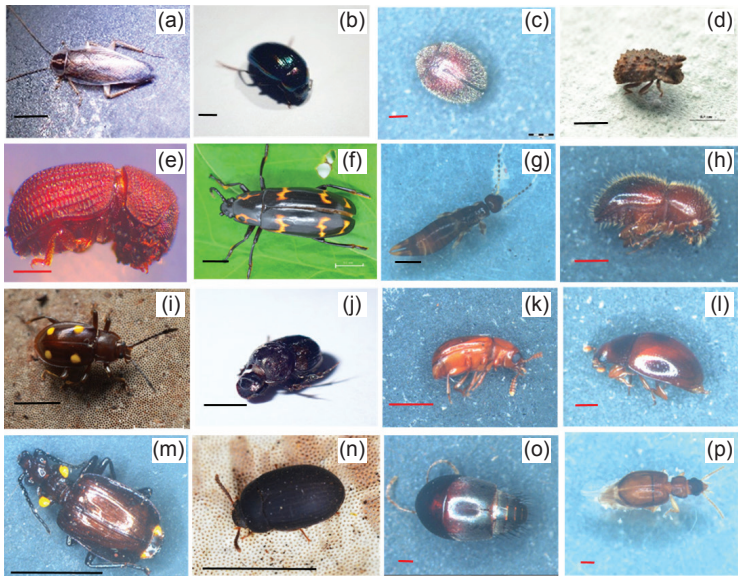
TABLE 1. DIVERSITY OF ARTHROPODS COLLECTED FROM FIVE SAMPLING ESTATES IN SABAH AND TOXONOMIC CLASSIFICATIONS

No.	Scientific name	Common name	MPOB Phase 2 Lahad Datu	Mawao Estate Beaufort	Langkon Estate Kota Marudu	Madai Estate Kunak	Merotai Besar Estate Tawau	Class	Order / Sub-order	Family / Superfamily
1	*Amarygmus* sp.	Darkling beetle	+	+	+	+	+	Insecta	Coleoptera	Tenebrionidae
2	*Amphicrossus* sp.	Sap beetle	+	-	-	-	-	Insecta	Coleoptera	Nitidulidae
3	*Anoplolepis gracilipes*	Red ant	+	+	+	+	+	Insecta	Hymenoptera	Formicidae
4	*Blattella asahinai*	Asian cockroach	+	+	+	+	+	Insecta	Blattodea	unidentified
5	*Bolitotherus cornutus*	Forked fungus beetle	+	+	+	+	+	Insecta	Coleoptera	Tenebrionidae
6	*Camponotus* sp.	Black carpenter ant	+	+	+	+	+	Insecta	Hymenoptera	Formicidae
7	*Camponotus* sp.	Carpenter ant 2	+	+	+	+	+	Insecta	Hymenoptera	Formicidae
8	*Cis* sp.	Minute tree fungus beetle	+	+	+	+	+	Insecta	Coleoptera	Ciidae
9	*Coptotermes kalshoveni*	Termite	-	+	-	-	-	Insecta	Isoptera	Rhinotermitidae
10	*Dolichodores* sp.	Black ant	+	+	+	+	+	Insecta	Hymenoptera	Formicidae
11	*Eledona* sp.	Unidentified	+	+	+	+	+	Insecta	Coleoptera	Tenebrionidae
12	*Encaustes* sp.	Pleasing fungus beetle	+	-	-	-	-	Insecta	Coleoptera	Erotylidae
13	*Euborellia annulipes*	Earwig	+	+	+	+	+	Insecta	Dermaptera	Forficulidae
14	*Eumorphus dilatatus tarittus*	Handsome fungus beetle	+	+	-	-	+	Insecta	Coleoptera	Endomychidae
15	*Eumorphus austerus*	Four spotted handsome fungus beetle	+	+	+	+	+	Insecta	Coleoptera	Endomychidae
16	*Eumorphus minor*	Handsome fungus beetle	+	+	-	-	-	Insecta	Coleoptera	Endomychidae
17	*Eumorphus quadrinotatus*	Handsome fungus beetle	+	+	-	-	-	Insecta	Coleoptera	Endomychidae
18	*Eumorphus dihaani*	Handsome fungus beetle	+	-	-	-	-	Insecta	Coleoptera	Endomychidae
19	*Eumorphus micans*	Handsome fungus beetle	+	-	-	-	-	Insecta	Coleoptera	Endomychidae
20	*Lioptera* sp.	Pleasing fungus beetle	+	-	-	-	-	Insecta	Coleoptera	Erotylidae
21	*Mycomya rondani*	Fungus gnat	-	+	+	-	-	Insecta	Diptera	Mycetophyllidae
22	*Oecophylla smaragdina*	Weaver ant	+	+	+	+	+	Insecta	Hymenoptera	Formicidae
23	*Onthophagus* sp.	Dung beetle	+	-	-	-	-	Insecta	Coleoptera	Scarabaeidae
24	*Oryctes rhinoceros*	Rhinoceros beetle	-	-	+	-	-	Insecta	Coleoptera	Scarabaeidae
25	*Pentaphyllus* sp.	Unidentified	+	+	+	+	+	Insecta	Coleoptera	Tenebrionidae
26	*Phalacrus* sp.	Unidentified	+	-	-	-	-	Insecta	Coleoptera	Phalacridae
27	*Physodera chalceres*	Ground beetle	+	-	-	-	-	Insecta	Coleoptera	Carabidae

TABLE 1. DIVERSITY OF ARTHROPODS COLLECTED FROM FIVE SAMPLING ESTATES IN SABAH AND TOXONOMIC CLASSIFICATIONS (continued)

No.	Scientific name	Common name	MPOB Phase 2 Lahad Datu	Mawao Estate Beaufort	Langkon Estate Kota Marudu	Madai Estate Kunak	Merotai Besar Estate Tawau	Class	Order / Sub-order	Family / Superfamily
28	*Platydema ruficorne*	Darkling beetle	+	-	-	-	-	Insecta	Coleoptera	Tenebrionidae
29	*Polyrachis* sp.	Ants	+	+	+	+	+	Insecta	Hymenoptera	Formicidae
30	*Porcellionides pruinosus*	Woodlice	+	+	+	+	+	Malacostraca	Isopoda	Porcellionidae
31	*Sepedophilus* sp.	Crab like -rove beetle	+	+	+	-	-	Insecta	Coleoptera	Staphylinidae
32	*Sepedophilus* sp.	Rove beetle	+	+	+	+	+	Insecta	Coleoptera	Staphylinidae
33	*Solenopsis* sp.	Fire ant	+	+	+	+	+	Insecta	Hymenoptera	Formicidae
34	*Tachy* sp.	Ground beetle	+	-	-	-	-	Insecta	Coleoptera	Carabidae
35	*Trigoniulus corallinus*	Red garden millipade	+	+	+	+	+	Diplopoda	Spirobolida	unidentified
36	Unidentified 1	Unidentified	+	-	-	-	-	Insecta	Coleoptera	Curculionidae
37	Unidentified 2	Cricket	+	+	+	+	+	Insecta	Orthoptera	unidentified
38	Unidentified 3	Flat bug 1	+	+	+	+	+	Insecta	Heteroptera	Aradidae
39	Unidentified 4	Darkling beetle 1	+	-	-	-	-	Insecta	Coleoptera	Tenebrionidae
40	Unidentified 5	Flat bug 2	+	+	+	+	+	Insecta	Heteroptera	Aradidae
41	Unidentified 6	Leiochrinini beetle	+	-	-	-	-	Insecta	Coleoptera	Tenebrionidae
42	Unidentified 7	Damsel bug	+	+	+	+	+	Insecta	Hemiptera	Nabidae
43	Unidentified 8	Palm weevil	+	+	-	-	-	Insecta	Coleoptera	Curculionidae
44	Unidentified 9	Brown darkling beetle	+	-	-	-	-	Insecta	Coleoptera	Tenebrionidae
45	Unidentified 10	Scorpion	+	+	+	+	+	Arachnida	unidentified	unidentified
46	Unidentified 11	Spider 1	+	+	+	-	-	Arachnida	unidentified	unidentified
47	Unidentified 12	Spider 2	+	+	+	-	-	Arachnida	unidentified	unidentified
48	Unidentified 13	Sap beetle 1	+	-	-	-	-	Insecta	Coleoptera	Nitidulidae
49	Unidentified 14	Sap beetle 2	+	-	-	-	-	Insecta	Coleoptera	Nitidulidae
50	Unidentified 15	Flat bug 3 (black)	+	+	-	-	-	Insecta	Heteroptera	Aradidae
51	Unidentified 16	Sap beetle 4	+	-	-	-	-	Insecta	Coleoptera	Nitidulidae
52	Unidentified 17	Ground beetle	+	-	-	-	-	Insecta	Coleoptera	Carabidae
53	Unidentified 18	Ant 1	+	+	+	+	+	Insecta	Hymenoptera	Formicidae
54	Unidentified 19	Ant 2	+	+	+	+	+	Insecta	Hymenoptera	Formicidae
55	*Xylosandrus carrassiuculus*	Asian ambrosia beetle	-	-	+	-	-	Insecta	Coleoptera	Curculionidae

Note: "+" - present; "- " - absent; ---- grey highlights in the table indicates the presence of insect species in all five sampling sites in Sabah.



Note: (a) *Blattella asahinai*; (b) *Amarygmini* sp.; (c) *Amphicrossus* sp.; (d) *Bolitotherus cornutus*; (e) *Eledona* sp.; (f) *Encaustes* sp.; (g) *Euborellia annulipes*; (h) *Xylosandrus crassiusculus*; (i) *Eumorphrus micans*; (j) *Onthopagus* sp.; (k) *Penthaphyllus* sp.; (l) *Phalacrus* sp. (*Phlacridae*); (m) *Physodera chalceres*; (n) *Platydema ruficorne*; (o) *Sepedophilus* sp.; (p) *Tachys* sp.
Scale Bars: ——— : 0.5 cm ——— : 0.5 mm

Figure 3. Close up of the insect community captured from the five study sites in Sabah.

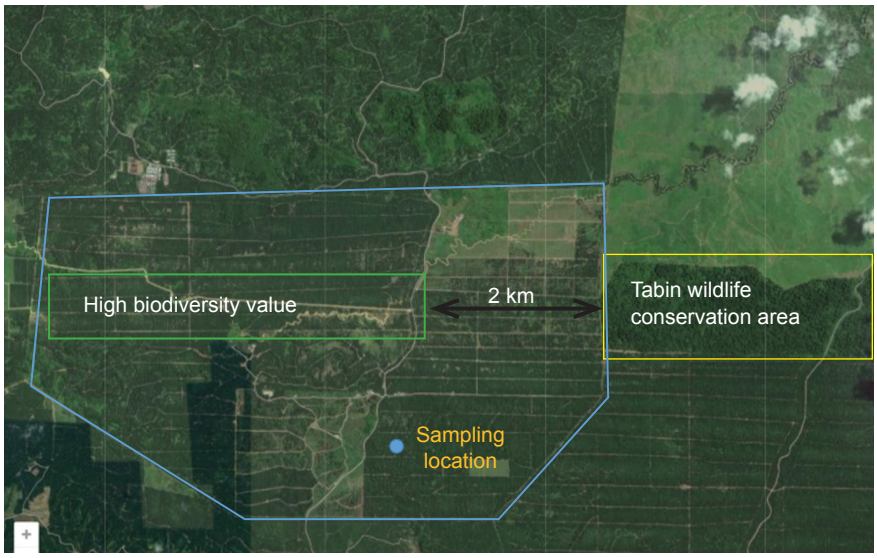


Figure 4. Sampling area in Lahad Datu (study site) bordered by Tabin wildlife conservation area and high biodiversity area.

Previously, *Episcapha quadrimaculata* was reported by Idris (2013) to be associated as a vector of *Ganoderma* BSR dispersal in Peninsular Malaysia due to its common presence in the basidiocarps. This species belongs to Erotylidae family or commonly known as pleasing fungus beetles, a different family than handsome fungus beetle which is Endomychidae. Erotylidae were generally synonym to the bracket fungus pest. *Megalodacne* spp. also an Erotylids was reported to infest bracket fungi found on dead trees and stumps (Skelley, 1999). Contrary to the findings of Idris (2013), *E. quadrimaculata* was not detected in Sabah; instead, two other Erotylids: *Lioptera* sp. and *Eucastes* sp. were found in solitude.

There were six *Eumorphus* spp. discovered on the basidiocarp of *Ganoderma* in MPOB Phase 2 and Mawao Estate, but these species were found in solitude. The six species were *E. minor*, *E. austerus*, *E. dihaani*, *E. micans*, *E. dilatatus tirittus* (*Figure 5c*), and *E. quadrinotatus* (*Figure 5b*) based on Strohecker's descriptions. Only *E. dihaani* and *E. micans* were not found in Mawao estate. The wide spread *Eumorphus* spp. in South East Asia region has led to the assumption that this genus is endemic to this region (Yusup & Eris, 2020).



Note: Notice the distinct four yellow spots on the dorsal view.

Figure 5. Handsome fungus beetles (a) Eumorphus minor *(b)* Eumorphus quadrinotatus *and (c)* Eumorphus dilatatus turittus.

Interestingly, *E. austerus* samples were occasionally observed to secrete yellow fluids from their femoral apex, which subsequently spread a pungent odour; a similar observation was reported by Brown (1985). And all the *Eumorphus* spp. were confirmed to carry the basidiospores of *Ganoderma,* internally and externally, making them an obvious candidate as vectors for BSR disease transmission. The PDA viability test further validated the cultured basidiospores as viable (*Table 2*). This is the first finding indicating *Eumorphus* spp. as one of the common insects from the *Ganoderma* basidiocarps on oil palm in Malaysian. In a study conducted by Yamashita *et al.* (2015), fungivorous insects' diversity was assessed by collecting brackets of forest-growing fungal species. The study reported that *Eumorphus* spp. had the dominance of presence compared to other families of Coleopteran species within the *Ganoderma* spp. basidiocarps.

Presence and Viability of *Ganoderma* Basidiospores

The list of insects with viable spore germination through the PDA plating is shown in *Table 2* below. *Eumorphus* spp. were carrying *Ganoderma* basidiospores (*Figure 6*) in both internal and external parts of their bodies.



Figure 6. The presence of Ganoderma *basidiospores found inside* Eumorphus aestrus *body observed on a hemocytometer.*

TABLE 2. *Ganoderma* BASIDIOSPORE PRESENCE AND VIABILITY

No.	Scientific name	Common name	Basidiospore		Viability
			External	Internal	
1	*Amarygmus* sp.	Darkling beetle	+	-	/
2	*Amphicrossus* sp.	Sap beetle	-	-	
3	*Anoplolepis gracilipes*	Red ant	-	-	
4	*Blattella asahinai*	Asian cockroach	-	-	
5	*Bolitotherus cornutus*	Forked fungus beetle	+	+	/
6	*Camponotus* sp.	Black carpenter ant	-	-	
7	*Camponotus* sp.	Carpenter ant 2	-	-	
8	*Cis* sp.	Minute tree fungus beetle	+	-	/
9	*Coptotermes kalshoveni*	Termite	-	-	
10	*Dolichodores* sp.	Black ant	-	-	
11	*Eledona* sp.	Unidentified	+	-	X
12	*Encaustes* sp.	Pleasing fungus beetle	-	-	
13	*Euborellia annulipes*	Earwigs	-	-	
14	*Eumorphus dilatatus tarittus*	Handsome fungus beetle	+	+	/
15	*Eumorphus austerus*	Four spotted handsome fungus beetle	+	+	/
16	*Eumorphus minor*	Handsome fungus beetle	+	+	/
17	*Eumorphus quadrinotatus*	Handsome fungus beetle	+	+	/
18	*Eumorphus dihaani*	Handsome fungus beetle	+	+	/
19	*Eumorphus micans*	Handsome fungus beetle	+	+	/
20	*Lioptera* sp.	Pleasing fungus beetle	-	-	
21	*Mycomya rondani*	Fungus gnat	-	-	
22	*Oecophylla smaragdina*	Weaver ant	-	-	
23	*Onthophagus* sp.	Dung beetle	-	-	
24	*Oryctes rhinoceros*	Rhinoceros beetle	-	-	
25	*Pentaphyllus* sp.	Unidentified	+	-	X
26	*Phalacrus* sp.	Unidentified	-	-	
27	*Physodera chalceres*	Ground beetle	-	-	
28	*Platydema ruficorne*	Darkling beetle	+	-	/
29	*Polyrachis* sp.	Ant	-	-	
30	*Porcellionides pruinosus*	Woodlice	+	+	/
31	*Sepedophilus* sp.	Crab-like rove beetle	-	-	
32	*Sepedophilus* sp.	Rove beetle	-	-	
33	*Solenopsis* sp.	Fire ant	-	-	
34	*Tachy* sp.	Ground beetle	-	-	
35	*Trigoniulus corallinus*	Red garden millipade	-	-	
36	Unidentified 1	Unidentified	-	-	
37	Unidentified 2	Cricket	-	-	
38	Unidentified 3	Flat bug 1	+	-	/
39	Unidentified 4	Darkling beetle 1	+	-	X
40	Unidentified 5	Flat bug 2	+	-	/
41	Unidentified 6	Leiochrinini beetle	-	-	

TABLE 2. *Ganoderma* BASIDIOSPORE PRESENCE AND VIABILITY (continued)

No.	Scientific name	Common name	Basidiospore		Viability
			External	Internal	
42	Unidentified 7	Damsel bug	-	-	
43	Unidentified 8	Palm weevil	-	-	
44	Unidentified 9	Brown darkling beetle	-	-	
45	Unidentified 10	Scorpion	-	-	
46	Unidentified 11	Spider 1	-	-	
47	Unidentified 12	Spider 2	-	-	
48	Unidentified 13	Sap beetle 1	-	-	
49	Unidentified 14	Sap beetle 2	-	-	
50	Unidentified 15	Flat bug 3 (black)	+	-	/
51	Unidentified 16	Sap beetle 4	-	-	
52	Unidentified 17	Ground beetle	-	-	
53	Unidentified 18	Ant 1	-	-	
54	Unidentified 19	Ant 2	-	-	
55	*Xylosandrus carrassiuculus*	Asian ambrosia beetle	-	-	

Note: "+" - present; "-" - absent; "/" - viable; X - non-viable.

From *Table 2*, there were 17 arthropods which were able to carry basidiospores externally and eight of them also carried the basidiospores internally. The viability of the basidiospores was determined and 14 of them carried viable basidiospores. Darkling beetles such as *Cis* sp., *Eledona* sp. and *Pentaphyllus* sp. that were feeding on *Ganoderma* fruiting bodies were only found carrying the spore outside (externally) their bodies. *Eumorphus* spp. were often found underneath the fruiting bodies feeding on the basidiospores, which allowed the *Ganoderma* basidiospores to remain intact internally and externally on their bodies. Meanwhile, the darkling beetles, usually present on the top surface of the fruiting bodies, bore into the *Ganoderma* basidiocarps, mining and building tunnels. In polypores fungi, the basidiospores are released from the underneath structure of the basidiocarp, where the pores are located. The darkling beetles were more often found travelling on the top surface of the basidiocarps, which may have contributed to the fact that they had limited contact with the basidiospores of *Ganoderma*. It has been reported that *Bolitotherus cornutus*, the forked fungus beetle, favours the tissues and spores of bracket fungi, including *Ganoderma applanatum*, *G. tsugae* and *Fomes fomentarius* (Liles, 1956; Pace, 1967). We found *Bolitotherus cornutus* to be associated with the basidiocarps of *Ganoderma*, and they were found in all five sampling locations (*Table 1*).

All basidiospores from internal and external collections of the insects were spread on the GSM agar surface, but unfortunately none of the spores were found viable. According to Ariffin *et al.* (2000), GSM was developed to isolate and confirm *Ganoderma* infected tissues but was not tested for spores. Since the insects were directly collected on *Ganoderma* fruiting bodies, the possibility that the basidiospores were not *Ganoderma* was very low. However, the high content of different chemicals will not be conducive to the germination of these basidiospores. The GSM is a mixture of antibiotics, fungicides and tannic acids that provides the selective growth conditions for infected *Ganoderma* tissues while eliminating and suppressing the growth of other microbes associated with oil palm to achieve a pure culture of *Ganoderma* (Ariffin *et al.*, 2000). The formulation was suitable to directly conduct an *in-situ* plating of infected tissues of *Ganoderma* in the field (Sundram *et al.*, 2015). Meanwhile, fungal spores are robust structures of the fungi kingdom and are well known to withstand harsh environmental conditions for survival (Sephton-Clark *et al.*, 2018). These robust structures will only break their dormancy and begin their germination once exposed to favourable conditions, which may explain their inability to germinate on GSM. Germination in fungal spores is the mechanism that converts the spore from a dormant biological organism to one that is vegetatively compatible and capable of sexual or asexual reproduction. Therefore, a final attempt to recover the viability of the basidiospores was conducted on PDA, and the monokaryons were indeed viable. However, we encountered high levels of cross-contamination (bacteria) because the spores were not subjected to any form of surface sterilisation.

CONCLUSION

The importance of insect transmission of plant diseases has generally been overlooked and greatly underestimated. Insects are capable of facilitating the entry of a pathogen into its plant host through wounds made above ground or below ground of the plant structures. Based on findings in the current study, we could conclude that insect community visiting *Ganoderma* basidiocarps were mainly from Coleoptera and Hymenoptera orders. We also observed that insects were able to carry and move the spores. Although GSM was unable to germinate the basidiospores, it was the PDA spread that confirmed the viability of the spores. This study is the first report that enlists the possible insects as potential vectors for *Ganoderma* BSR disease in oil palm plantations in Sabah. Among the 16 species of insects detected to have a positive presence of basidiospores, the handsome fungus beetle, *Eumorphus* spp. indeed has the biggest possibility of transmitting the basidiospores. Further investigation should include assays to obtain pure cultures of the basidiospores, followed by identification via molecular tools. Additionally, research should also include insects sampling in the other states of Malaysia for comparison, especially Sarawak, the state with the worst infection by USR. All the possible vectors should be screened against healthy palms to validate initiation of infection due to the role of vectors.

ACKNOWLEDGEMENT

We would like to thank Sindy Maurice Goulip, Mohd Masri Madsali and Safrin Laupa of the Entomology and Integrated Pest Management Unit, MPOB Lahad Datu for their assistance in this project. A special thanks to MPOB Sessang team, Saharul Abillah Mohamad and Mohamad Rosman Sulaiman for their advice. A sincere appreciation is also extended to Jumain Sinring, Irwan Salleh and Sutrisno from the Plant Pathology and Biosecurity Unit.

REFERENCES

Abdullah, N. A., Radzi, S. N. F., Asri, L. N., Idris, N. S., Husin, S., Sulaiman, A., Khamis, S., Sulaiman, N., & Hazmi, I. R. (2019). Insect community in riparian zones of Sungai Sepetang, Sungai Rembau and Sungai Chukai of Peninsular Malaysia. *Biodiversity Data Journal, 7*, e34752. https://doi.org/10.3897/bdj.7.e35679

Ariffin, D., Idris, A. S., & Singh, G. (2000). Status of *Ganoderma* in oil palm. In J. Flood, P. D. Bridge, & M. Holderness (Eds.), Ganoderma *diseases of perennial crops* (pp. 49-68). CABI Publishing.

Ariffin, D., & Idris, A. S. (1992). *The* Ganoderma *selective medium (GSM)*. PORIM Information Series No. 8. MPOB.

Bengtsson, G., Hedlund, K., & Rundgren, S. (1991). Selective odor perception in the soil collembola *Onychiurus armatus*. *Journal of Chemical Ecology*, *17*(11), 2113–2125. https://doi.org/10.1007/bf00987995

Brown, J. W. L. (1985). The quadrimaculate color pattern in beetles and a possible mimicry complex. In G. E. Ball (Ed.), *Taxonomy, phylogeny, and zoogeography of beetles and ants* (pp. 432-436). Dr. W. Junk Publishers.

Chuche, J., Auricau-Bouvery, N., Danet, J., & Thiéry, D. (2016). Use the insiders: Could insect facultative symbionts control vector-borne plant diseases? *Journal of Pest Science*, *90*(1), 51–68. https://doi.org/10.1007/s10340-016-0782-3

Darya, H., Azura, A. N., Lau, W. H., Izfa, R. H., Maa, A., & Ahmed, A. M. (2016). Distribution of darkling beetles (Tenebrionidae) in Malaysia. *Journal of Entomology and Zoology, 4*(5), 1113–1117.

Dhileepan, K. (1992). Pollen carrying capacity, pollen load and pollen transferring ability of the oil palm pollinating weevil *Elaeidobius kamerunicus* Faust in India. *Oleagineux, 47*(2), 55–61.

Fäldt, J., Jonsell, M., Nordlander, G., & Borg-Karlson, A. K. (1999). Volatiles of bracket fungi *Fomitopsis pinicola* and *Fomes fomentarius* and their functions as insect attractants. *Journal of Chemical Ecology, 25*(3), 567–590. https://doi.org/10.1023/a:1020958005023

Fletcher, J., & Wayadande, A. (2002). Fastidious vascular-colonizing bacteria. *The Plant Health Instructor,* 2. https://www.apsnet.org/edcenter/Pages/Fastidious.aspx

Grimm, R., & Schawaller, W. (2021). Checklist for the darkling beetles of Borneo (Coleoptera: Tenebrionidae s.str.). *Integrative Systematics: Stuttgart Contributions to Natural History, 2*(1), 61–82. https://doi.org/10.18476/insy.v02.a5

Hammond, P. M., & Lawrence, J. F. (1989). Mycophagy in insects: A summary. In N. Wilding, N. M. Collins, P. F. Hammond, & J. F. Webber (Eds.), *Insect-fungus interactions* (pp. 275-324). Academic Press.

Hammond, R. W., & Bedendo, I. P. (2005). Molecular confirmation of *maize rayado fino virus* as the Brazilian corn streak virus. *Scientia Agricola, 62*(6), 601–603. https://doi.org/10.1590/s0103-90162005000600015

Hanski, I. (1989). Fungivory: Fungi, insects and ecology. In N. Wilding, N. M. Collins, P. F. Hammond, & J. F. Webber (Eds.), *Insect-fungus interactions* (pp. 25-68). Academic Press.

Hogenhout, S. A., Ammar, E. D., Whitfield, A. E., & Redinbaugh, M. G. (2008). Insect vector interactions with persistently transmitted viruses. *Annual Review of Phytopathology, 46*(1), 327–359. https://doi.org/10.1146/annurev.phyto.022508.092135

Hölldobler, B., & Wilson, E. O. (1990). *The ants*. Belknap Press.

Holloway, J. D., Kirk-Spriggs, A. H., & Khen, C. V. (1992). The response of some rainforest insect groups to logging and conversion to plantation. *Philosophical Transactions of the Royal Society B: Biological Sciences, 335*(1275), 425–436. https://doi.org/10.1098/rstb.1992.0034

Honda, H., Ishiwatari, T., & Matsumoto, Y. (1988). Fungal volatiles as oviposition attractants for the yellow peach moth, *Conogethes punctiferalis* (Guenee) (Lepidoptera: Pyralidae). *Journal of Insect Physiology, 34*(3), 205–211. https://doi.org/10.1016/0022-1910(88)90051-0

Idris, A. S. (1999). *Basal stem rot (BSR) of oil palm (*Elaeis guineensis *Jacq.) in Malaysia: Factors associated with variation in disease severity* [Doctoral dissertation]. University of London.

Idris, A. S. (2013). Current status of R&D on *Ganoderma* disease in Malaysia. *PALMAS, 34*, 71–80.

Jaenike, J. (1978). Resource predictability and niche breadth in the *Drosophila quinaria* species group. *Evolution, 32*(3), 676–678. https://doi.org/10.2307/2407734

Jonsell, M., & Nordlander, G. (1995). Field attraction of Coleoptera to odours of the wood-decaying polypores *Fomitopsis pinicola* and *Fomes fomentarius*. *Annales Zoologici Fennici, 32*(4), 391–402. https://ci.nii.ac.jp/naid/10011409227

Jonsell, M., & Nordlander, G. (2004). Host selection patterns in insects breeding in bracket fungi. *Ecological Entomology, 29*(6), 697–705. https://doi.org/10.1111/j.0307-6946.2004.00654.x

Komonen, A. (2003). Hotspots of insect diversity in boreal forests. *Conservation Biology, 17*(4), 976–981. https://doi.org/10.1046/j.1523-1739.2003.02076.x

Liles, M. P. (1956). A study of the life history of the forked fungus beetle, *Bolitotherus cornutus* (Panzer) (Coleoptera: Tenebrionidae). *Ohio Journal of Science, 56*(6), 329–337.

Miller, R. N. G., Holderness, M., Bridge, P. D., Chung, G. F., & Zakaria, M. H. (1999). Genetic diversity of *Ganoderma* in oil palm plantings. *Plant Pathology, 48*, 595–603. https://doi.org/10.1046/j.1365-3059.1999.00390.x

Mondal, S., Ray, R., & Ghorai, M. (2003). Observation on the destruction of piper betel plant by *Eumorphus quadriguttatus* (Coleoptera: Endomychidae). *Bionotes, 5*, 51.

Nur-Rashyeda, R., Idris, A. S., Sundram, S., Zainol-Hilmi, N. H., & Ming, S. C. (2022). A Field evaluation on fungicides application to control Upper Stem Rot (USR) disease in oil palm caused by *Ganoderma* spp. *Journal of Oil Palm Research, 35*(2), 320–329. https://doi.org/10.21894/jopr.2022.0037

Orledge, G., & Reynolds, R. (2005). Fungivore host-use groups from cluster analysis: Patterns of utilisation of fungal fruiting bodies by ciid beetles. *Ecological Entomology, 30*, 620–641. https://doi.org/10.1111/j.0307-6946.2005.00727.x

Pace, A. E. (1967). *Life history and behavior of a fungus beetle, Bolitotherus cornutus (Tenebrionidae)* [Occasional paper]. The Museum of Zoology University of Michigan. https://deepblue.lib.umich.edu/handle/2027.42/57089

Pacioni, G., Bologna, M. A., & Laurenzi, M. (1991). Insect attraction by Tuber: A chemical explanation. *Mycological Research, 95*(12), 1359–1363. https://doi.org/10.1016/s0953-7562(09)80385-7

Parveez, G. K. A., Hishamuddin, E., Loh, S. K., Ong-Abdullah, M., Salleh, K. M., Bidin, M. N. I. Z., Sundram, S., Hasan, Z. A. A., & Idris, Z. (2020). Oil palm economic performance in Malaysia and R&D progress in 2019. *Journal of Oil Palm Research, 32*(2), 159–190. https://doi.org/10.21894/jopr.2020.0032

Paviour-Smith, K. (1960). The fruiting-bodies of macrofungi as habitats for beetles of the family Ciidae (Coleoptera). *Oikos, 11*, 43–71. https://doi.org/10.2307/3564883

Pfeil, R. M., & Mumma, R. O. (1993). Bioassay for evaluating attraction of the phorid fly, *Megaselia halterata* to compost colonized by the commercial mushroom, *Agaricus bisporus*, and to 1-octen-3-ol and 3-octanone. *Entomologia Experimentalis et Applicata, 69*(2), 137–144. https://doi.org/10.1111/j.1570-7458.1993.tb01736.x

Phelan, L. P., & Lin, H. (1991). Chemical characterization of fruit and fungal volatiles attractive to dried-fruit beetle *Carpophilus hemipterus* (L.) (Coleoptera: Nitidulidae). *Journal of Chemical Ecology, 17*(6), 1253–1272. https://doi.org/10.1007/bf01402948

Pierce, A. M., Pierce Jr., H. D., Oehlschlager, A. C., & Borden, J. H. (1991). 1-octen-3-ol, attractive semiochemical for foreign grain beetle, *Ahasverus advena* (Waltl) (Coleoptera: Cucujidae). *Journal of Chemical Ecology, 17*(3), 567–580. https://doi.org/10.1007/bf00982127

Pilotti, C. A. (2005). Stem rots of oil palm caused by *Ganoderma boninense*: Pathogen biology and epidemiology. *Mycopathologia, 159*, 129–137. https://doi.org/10.1007/s11046-004-4435-3

Pilotti, C. A., Gorea, E. A., & Bonneau, L. (2018). Basidiospores as sources of inoculum in the spread of *Ganoderma boninense* in oil palm plantations in Papua New Guinea. *Plant Pathology, 67*, 1841–1849. https://doi.org/10.1111/ppa.12915

Pilotti, C. A., Sanderson, F. R., Aitken, E. A. B., & Armstrong, W. (2004). Morphological variation and host range of two *Ganoderma* species from Papua New Guinea. *Mycopathologia, 158*, 251–265. https://doi.org/10.1023/b:myco.0000041833.41085.6f

Rees, R. W., Flood, J., Hasan, Y., & Cooper, R. M. (2007). Effects of inoculum potential, shading, and soil temperature on root infection of oil palm seedlings by the basal stem rot pathogen *Ganoderma boninense*. *Plant Pathology, 56*(5), 862–870. https://doi.org/10.1111/j.1365-3059.2007.01621.x

Rees, R. W., Flood, J., Hasan, Y., Wills, M. A., & Cooper, R. M. (2012). *Ganoderma boninense* basidiospores in oil palm plantations: Evaluation of their possible role in stem rots of *Elaeis guineensis*. *Plant Pathology, 61*(3), 567–578. https://doi.org/10.1111/j.1365-3059.2011.02533.x

Sephton-Clark, P. C., Muñoz, J. F., Ballou, E. R., Cuomo, C. A., & Voelz, K. (2018). Pathways of pathogenicity: Transcriptional stages of germination in the fatal fungal pathogen *Rhizopus delemar*. *mSphere, 3*(5), e00418. https://doi.org/10.1128/msphere.00403-18

Shockley, F. W., Tomaszewska, K. W., & McHugh, J. V. (2009). Review of the natural history of the handsome fungus beetles (Coleoptera: Cucujoidea: Endomychidae). *Insecta Mundi, 0072*, 1–24. https://doi.org/10.5281/zenodo.4531527

Skelley, P. E. (1999). Pleasing fungus beetles, *Pseudischyrus*, *Tritoma*, *Megalodacne*, *Ischyrus* spp. (Insecta: Coleoptera: Erotylidae). *EDIS*, *2003*(14). https://doi.org/10.32473/edis-in248-1999

Strohecker, H. F. (1949). The genus *Spathomeles* Gerstaecker, with the description of a new species from Borneo (Coleoptera: Endomychidae). *Proceedings of the Hawaiian Entomological Society, 13*(03), *437–444*. http://hdl.handle.net/10125/16195

Strohecker, H. F. (1968). A synopsis of the genus *Eumorphus* (Coleoptera: Endomychidae). *Pacific Insects, 10*(1), 79–112.

Sundram, S., Meon, S., Seman, I. A., & Othman, R. (2015). Application of arbuscular mycorrhizal fungi with *Pseudomonas aeruginosa* UPMP3 reduces the development of *Ganoderma* basal stem rot disease in oil palm seedlings. *Mycorrhiza, 25*(5), 387–397. https://doi.org/10.1007/s00572-014-0620-5

Turner, P. D. (1965). The incidence of *Ganoderma* disease of oil palms in Malaya and its relation to previous crop. *Annals of Applied Biology, 55*(3), 417–423. https://doi.org/10.1111/j.1744-7348.1965.tb07954.x

Wielkopolan, B., Jakubowska, M., & Obrępalska-Stęplowska, A. (2021). Beetles as plant pathogen vectors. *Frontiers in Plant Science, 12*, 748093. https://doi.org/10.3389/fpls.2021.748093

Weintraub, P. G., & Beanland, L. (2006). Insect vectors of phytoplasmas. *Annual Review of Entomology, 51*, 91–111. https://doi.org/10.1146/annurev.ento.51.110104.151039

Yadav, M. (2003). *Physiology of Insects*. Discovery Publishing House.

Yamashita, S., & Hijii, N. (2003). Effects of mushroom size on the structure of a mycophagous arthropod community: Comparison between infracommunities with different types of

resource utilization. *Ecological Research, 18*, 131–143. https://doi.org/10.1046/j.1440-1703.2003.00541.x

Yamashita, S., & Hijii, N. (2007). The role of fungal taxa and developmental stage of mushrooms in determining the composition of the mycophagous insect community in a Japanese forest. *European Journal of Entomology, 104*, 225–233. https://doi.org/10.14411/eje.2007.035

Yamashita, S., Ando, K., Hoshina, H., Ito, N., Katayama, Y., Kawanabe, M., & Itioka, T. (2015). Food web structure of the fungivorous insect community on bracket fungi in a Bornean tropical rain forest. *Ecological Entomology, 40*(4), 390–400. https://doi.org/10.1111/een.12200

Yusup, C. A., & Eris, D. D. (2020). Hubungan serangga dengan *Ganoderma*: Media penyebaran pasif. *Bioteknologi & Bioindustri, 7*(1), 4–6.

Zettler, J. A., Mateer, S. C., Link-Pérez, M., Bailey, J. B., Demars, G., & Ness, T. (2016). To key or not to key: A new key to simplify and improve the accuracy of insect identification. *American Biology Teacher, 78*(8), 626–633. https://doi.org/10.1525/abt.2016.78.8.626

Journal of Oil Palm Research Vol. 37 (1) March 2025 p. 110-121
DOI: https://doi.org/10.21894/jopr.2023.0063

ANALYSIS OF THE ENERGY CONSUMPTION OF MOTORISED CIRCULAR SAW WHEN CUTTING OIL PALM FROND

SUN QUN[1]* and ZAIDI MOHD RIPIN[1]

ABSTRACT

Existing pruning technique uses the sickle or chisel, manually or mechanically powered using small internal combustion engine. The current challenge of going for zero carbon emission for the oil palm industry requires the replacement of all internal combustion engines with battery powered electrical tools. It is important to reduce the force and power consumption of the cutting process which can affect the number of cuts made per battery charge. One efficient cutting process is the use of a circular saw which is widely adopted in the lumber processing but not in the oil palm harvesting. Cutting the oil palm fronds with a circular saw has never been studied before. In the paper, the mechanism of energy consumption in the circular saw-cutting process of oil palm fronds is studied, and the model of power (w) and work (J) is established. Comparing the test results with the theoretical values calculated by the model, indicating that no significant difference in cutting work model for the oil palm fronds ($38<F<145$, $0.72<R^2<0.91$, $P<0.05$) based on the different cutting conditions. The validated cutting energy equation is used in the optimisation of the cutting process of a 100 mm base wide of an oil palm frond resulting in the minimum cutting energy of 330 J for rotational speed of 1,000 rpm and feed rate of 10 mm/s.

Keywords: cutting force, energy consumption model, friction, frond, oil palm.

Received: 15 April 2023**; Accepted:** 3 October 2023**; Published online:** 5 December 2023.

INTRODUCTION

Oil palm is an important economic crop covering large swathes of arable land in Southeast Asia, Africa, South America and now extending to southern China. It contributed significantly to the world edible oil market (Meijide *et al.,* 2017). The integration of circular saw cutting in oil palm harvesting brings forth a range of benefits. Firstly, it improves efficiency by enabling faster and more precise cutting, leading to increased productivity and reduced labour requirements. Secondly, the precise and controlled cutting action of the circular saw minimises damage to the fronds, ensuring higher-quality harvested produce. Moreover, by optimising cutting parameters and implementing energy-efficient practices based on power consumption models, the overall cost of harvesting can be significantly reduced. This reduction in costs translates into improved profitability for farmers and greater competitiveness in the global market.

Maintenance of the tree requires periodical pruning of the fronds typically done as part of the harvesting of the oil palm fruit bunch (Jasim *et al.,* 2017). Research in the mechanics of cutting of oil palm fronds covered the effect of cutting angle and frond maturity on the specific reaction force and the energy requirement using spring assisted sickle (Jelani *et al.,* 1998) and normal sickle (Jelani *et al.,* 1999). Another cutting study was conducted on the chopping of empty fruit bunches, where it was shown that increasing the peripheral cutting speed increased the cutting power (Suryanto *et al.,*

[1] School of Mechanical Engineering,
Universiti Sains Malaysia (USM),
14300 Nibong Tebal, Penang, Malaysia.

* *Corresponding author e-mail: Sq842943050@outlook.com*

2009). All these were experimentally based and no cutting power model was developed. In order to improve the cutting performance of the current harvester tools, a cutting model is needed. The process of cutting with a spring-assisted sickle may involve some degree of energy wastage. A portion of the force applied to the spring may be absorbed or converted into other forms of energy instead of being entirely transmitted to the stalk for cutting. This can lead to decreased efficiency and necessitate a greater amount of energy to accomplish the same task. Spring-assisted sickles possess a more complex structure, including the spring mechanism, compared to circular saw cutting method. This potentially increases the costs and workload associated with maintenance. If the spring becomes damaged or malfunctions, repair or replacement is required, adding additional time and resource costs.

There is limited research on using circular saws for cutting oil palm fronds. However, there have been numerous research achievements in using circular saws for cutting other plants, which have significantly improved efficiency. The knowledge gained from research on circular saws in cutting other plants can be applied to the context of oil palm leaf stalks. Although there may be variations in the physical properties and cutting requirements of different plant species, the principles and insights gained from previous studies can serve as valuable references for developing efficient cutting methods for oil palm fronds. Meng (2018) described a method of an explicit kinetic simulation and experimental study of circular saw cutting system of mulberry cutting machine and carried out the orthogonal simulation for the optimisation of the combinations of operating parameters of the circular saw in cutting dynamic parameters. Li *et al.* (2022) studied the circular saw cutting force of apple branches and showed that cutting speed and the branch diameter had a significant effect on the cutting force, while the sawtooth number had a small effect on the cutting force. Abbood *et al.* (2018) studied three different cutting angles and their effect on cutting time. A randomised complete block design with three replications was used in the experiment. The results showed that 45° cutting angle was superior in obtaining the shortest time of frond cutting is 4.30 s. Jasim *et al.* (2017) evaluated the effects of motorised vibration cutters on some operational characteristics used for date palm fronds which indicated that the solution found in the oil palm harvesting can be readily applied to date palms. Abbood (2020) showed that frond strength influences the frond chopping force in particular the cutting angle. Eliçin *et al.* (2019) studied the cutting of grapes vines and determined that the cutting force and energy values increased with increasing knife-cutting angle from 0°-40°. The maximum cutting force, cutting strength, cutting energy and specific cutting energy was observed at 0° cutting angle as 319.3 N, 11.30 MPa, 2.393 N and 0.08464 J mm^{-2} respectively. On the modelling front, the theoretical sawing power of a circular saw was calculated by (Gao, 2016). Chu (2017) showed that the cutting work and the effect of rotational speed, feed rate and the inclination angle. Dong (2017) researched the single-factor tests to study the feed rate of the header, rotation speed, the inclination angle of the disc cutter and the diameter of the straw. Xie (2019) discussed the research on the optimisation of cutting parameters of sugarcane. It is clear that the theoretical modelling of the cutting process is an important part of the minimisation of the cutting force and power.

Circular saw cutting has emerged as a powerful tool for enhancing efficiency and quality in oil palm harvesting. By understanding the dynamics of circular saw cutting on oil palm fronds and establishing reliable power consumption models, we can unlock the full potential of this technique. The adoption of circular saw cutting in oil palm harvesting offers numerous advantages, including increased efficiency, improved quality, cost reduction, and reduced labour requirements. By embracing this innovative approach, the oil palm industry can achieve sustainable and profitable growth while meeting the rising global demand for this valuable crop. The paper shows the development of the model for the cutting power and work parameters of circular saw used in the cutting of the oil palm fronds. These cutting parameters are compared with the measured values obtained from cutting test bench to verify the accuracy of the model. To the best knowledge of the authors, the cutting model of a cutting power of a circular saw on the oil palm fronds has never been reported before. The industrial relevance of this work is the model can be used to theoretically determine the cutting power of a new cutting device based on the rupture modulus of the palm fronds other parameters and can be used to develop a new cutting tool to further improve the frond cutter for the oil palm harvesting and pruning.

MATERIALS AND METHODS

Establishment of Kinematics Model for Sawing Oil Palm Fronds

The oil palm frond is in general wide at the base and tapering to the end of the frond. In this work the cutting of the frond would start at the centre where the frond was the thickest and move through the apex of the triangle to the top of the frond which is the widest. The setup is as shown in *Figure 1a* where the circular saw is located at the bottom of the frond.

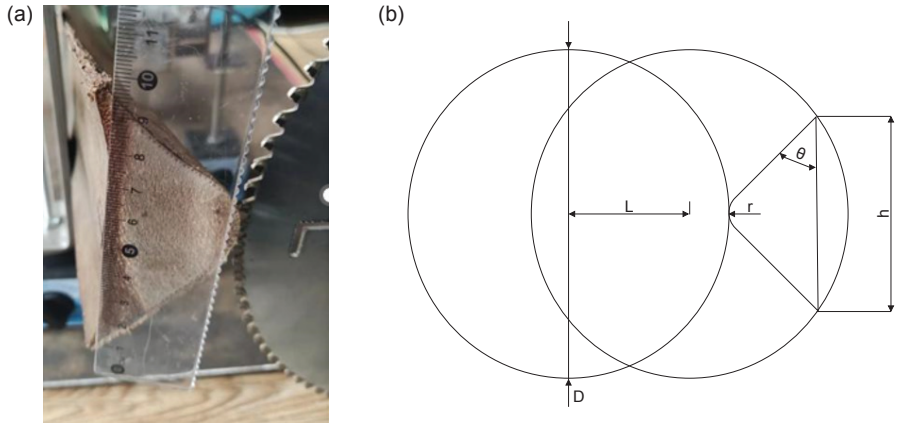


Figure 1. (a) Section of oil palm and (b) schematic diagram of sawing oil palm fronds.

The section can be regarded as an isosceles triangle with an obtuse angle and an arc top angle. It can be simplified as *Figure 1b*. The maximum width of the cutting cross section of h fronds, θ was the included angle of the fronds, and r was the fillet radius of the bottom edge of the fronds.

As shown in *Figure 1b*, assuming that the parameters to be solved are the total travel of the circular saw from the initial cutting position to the final cutting position (L), required time (t_1) and cutting area ($S_{Fronds\text{-}area}$) the Equations (1) to (4) are derived based on the geometry of the frond based on *Figure 1b*.

$$L = \frac{1}{2} \cdot h \cdot \tan\theta - \left(\frac{r}{\sin 45°} - r_e\right) + \left(\frac{D}{2} - \sqrt{\left(\frac{D}{2}\right)^2 - \left(\frac{h}{2}\right)^2}\right) \quad (1)$$

$$t_1 = \frac{L}{\mu} \quad (2)$$

$$= \frac{1}{u} \cdot \left[\frac{1}{2} \cdot h \cdot \tan\theta - (\sqrt{2}\text{-}1) \cdot r + \frac{D - \sqrt{D^2 - h^2}}{2}\right] \quad (3)$$

The area of the fronds cutting part:

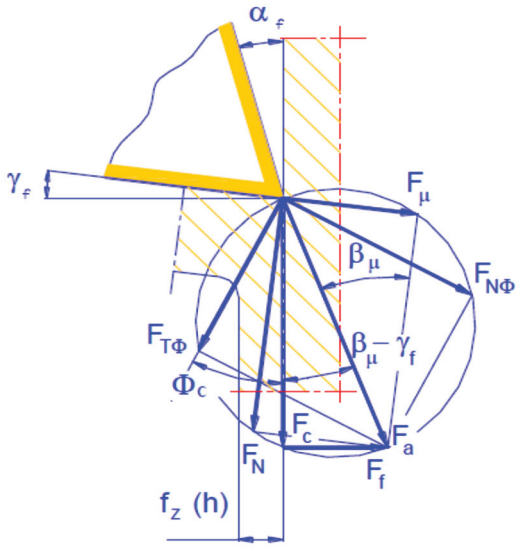
$$S_{Fronds\text{-}area} = \frac{1}{2} \cdot h \cdot \tan\theta \cdot \left(\frac{h}{2}\right) - \left(r^2 - \frac{\pi \cdot r^2}{4}\right) \quad (4)$$

where D is the circular saw diameter, h is the maximum width of the cross section of the fronds, θ is the side angle of the fronds, r is the fillet radius of the bottom edge of the fronds, u is the feed rate of the tool.

Power Calculation Model for Sawing Oil Palm Fronds

Cutting feed power of sawing oil palm fronds. According to Hlásková *et al.* (2015), the mechanical process of material separation from the saw work piece (*i.e.*, chip formation) could be described as an orthogonal process (two-dimensional deformation). The forces acting on the tooth could be represented in the classical approach by Ernst and Merchant's force circle is shown in *Figure 2*.

F_a is the active force, F_c is the cutting force, F_f is the thrust force (passive), F_μ is the friction force on the rake face, F_N is the normal force to the rake face, $F_{T\phi}$ is the force required to shear the wood along the shear plane, $F_{N\phi}$ is the normal force on the shear plane, α_f is the clearance angle, ϕ_c is the shear angle, γ_f is the rake angle, and β_μ is the friction angle (Hlásková *et al.*, 2015).



Source: Hlásková *et al.*, 2015.

Figure 2. Simplified cutting process model with Ernst and Merchant's force circle.

The cutting power for one saw blade during the cutting stroke of a sash gang saw, in which both chip momentum (Hlásková *et al.*, 2015) and a ploughing effect caused by tooth cutting edge dullness (Wang *et al.*, 2013) were disregarded, follows Equation (5).

The shear angle ϕ_c, for the necessary aim of this study, can be calculated for larger values of feed per tooth f_c with the Merchant's equation (because for large uncut chip values ϕ_c was constant) (Atkins, 2003) [Equation (6)].

$$\beta_\mu = \tan^{-1}(\mu) \tag{5}$$

$$\phi_c = (\pi/4) - (1/2)(\beta_\mu - \gamma_f) \tag{6}$$

μ is the friction coefficient of the cutting section of the oil palm fronds measured by the test. γ_f is the rake angle of the circular saw.

Sawing productivity f of the circular saw when sawing the work piece [Equation (7)].

$$f = \frac{S_{Fronds\text{-}area}}{t_1} = \frac{1/4 \cdot (h^2 \cdot \tan\theta + \pi \cdot r^2) - r^2}{\frac{1}{u} \cdot [\frac{1}{2} \cdot h \cdot \tan\theta - (\sqrt{2}\text{-}1) \cdot r + \frac{D - \sqrt{D^2 - h^2}}{2}]} \tag{7}$$

During sawing, the sawing deformation work per unit volume of the fronds to be cut is A [Equation (8)].

$$A = \frac{k(1+\cot\phi_c)(\sin\theta_1 - \sin\theta_2)}{(\theta_1 - \theta_2)\cos\bar{\alpha}} \approx k(1+\cot\phi_c) \tag{8}$$

k was the rupture modulus of the fronds, and test for Sampling Method according to (Intara *et al.*, 2013). ϕ_c is the shear angle when the circular saw is cutting.

The cutting feed power during the sawing process P_1 can be deduced through Equation (9).

$$P_1 \approx \frac{ABf}{10^6} = \frac{f(\vartheta + 0.0006D)A}{10^6} = \frac{f(\vartheta + 0.0006D) \cdot k(1+\cot\phi_c)}{10^6} \tag{9}$$

$$= \frac{[(h^2 \cdot \tan\theta + \pi \cdot r^2) - 4r^2] \cdot (\vartheta + 0.0006D) \cdot k(1+\cot\phi_c)}{\frac{4}{u} \cdot [\frac{1}{2} \cdot h \cdot \tan\theta - (\sqrt{2}\text{-}1) \cdot r + \frac{D - \sqrt{D^2 - h^2}}{2}]} \tag{10}$$

From the Equation 9 and 10, ϑ is the thickness of the tool (*mm*), ϕ_c is the shear angle when the circular saw is cutting (°), and D is the diameter of the tool (*m*).

Power required for bending work piece. When sawing the work-piece, saw tooth just touches the work-piece, the work-piece will produce bending deformation under the external force. The bending deformation energy will also consume part of the power. In the sawing process, the power consumed by the bending deformation of the work piece is P_2, therefore,

$$P_2 = \frac{U_{bend}}{5t_{bend}} \tag{11}$$

The P_2 is the bending deformation energy of the work piece. It is found that the value of P_2 is very small, almost zero and can be ignored.

Clamping saw power for sawing oil palm frond. In the process of sawing the workpiece, a slit was formed at the sawing position of the circular saw. The inner wall of the front limited the deformation of the circular saw during sawing. When the workpiece was sawed at a constant speed, the circular saw was subjected to the friction of the side wall of the slit, which inevitably consumed a certain amount of cutting work. The power P_3 consumed to overcome the friction is called the power of the saw clamp [Equation (12)].

$$P_3 = \frac{\mu V (\frac{f_d}{c})}{102} \tag{12}$$

where, V is the linear speed, μ is the friction coefficient of the cutting section of the oil palm fronds measured by the test, and c is the dynamic load factor of circular saw. f_d is the dynamic load amplitude of the circular saw (if V<2 mm/s, then f_d = 0.0006; if 2 mm/s<V<5 mm/s, then f_d = 0.0009; if 5 mm/s<V<10 mm/s, then f_d = 0.0015; and if V>10 mm/s, then f_d = 0.0028.). The final comprehensive cutting power of the oil palm fronds is as follows:

$$P_{total} = P_1 + P_2 + P_3 \tag{13}$$

The final cutting work result J can be obtained by multiplying the total power P_{total} required for circular saw cutting and the time t_1 required for cutting as Equation 13.

$$J = P_{total} \cdot t_1 \tag{14}$$

The method used in this study was an idealised cutting condition, which did not represent the frond in its natural state, but was most closely supported as a cantilever beam. The application of the weight of the frond at the free end reduced the friction power, as the bending moment of the frond weight helped to open up the cut part of the frond and reduced the normal force and the ensuing friction force on the radial cutter saw. However, the simplified support used in this study was easy to replicate by other researchers in order to obtain comparable cutting data. The same approach had been adopted in the study for static cutting force by Jelani *et al.* (1998).

Experimental Study

The experimental work was carried out in two different stages, the first stage was to characterise the frond properties in terms of the modulus of rupture and the friction coefficient between the frond and the circular saw. These were the required parameters for the cutting model and the second stage was the measurement of the cutting force and power of the circular saw when cutting the fronds.

Experimental measurement of the frond rupture modulus* (k) *and friction coefficient. In order to determine the rupture modulus of the frond, the specimen was prepared from the fronds of an eight year old oil palm tree obtained from a plantation in Yunnan, China. These specimens were then tested in the tensile test equipment (Zwick, CTM tensile test equipment). Samples were prepared and tested according to the storage period from fresh to 10, 20, and 30 days. Three sets of appropriately sized samples (*Figure 3*) were selected. The weight of each fresh sample was recorded, and the average weight (W) was calculated. After placing the samples for 10 days, the average weight (W_1) was recorded. After a natural resting period of 20 days, the average weight (W_2) was recorded. Similarly, after a natural resting period of 30 days, the average weight (W_3) was recorded. The percentage of moisture content W_c in the oil palm fronds were calculated using Equation (15).

$$W_c = \frac{W - W_{1or2or3}}{W} \times 100\% \quad (15)$$

The moisture content of the specimens was determined to be 58%, 43%, 31% and 12% respectively. The samples were prepared such that they were free from burr and stored in the cupboard for airing under natural ventilation, and the dimensions of specimens were shown in the *Figure 3* below.



Figure 3. The samples of fronds.

The tensile test was carried out on the specimen as shown in *Figure 4*. The load was applied on the specimen at 2 min/mm speed until fracture where the computer automatically records the required breaking force of the specimen.



Figure 4. The measurement test of rupture modulus.

***Measurement of the friction coefficient* (μ).** The sample for the friction coefficient test was made in specimen with the width of 100 mm. The inclined angle technique used, which consisted of a high-speed camera analysis system, a high-speed camera, LED fill light, protractor, and friction coefficient measuring slope meter, and the sliding surface was made of 65 Mn tool steel to best represent the circular saw.

The sliding distance and time of the test piece on the friction coefficient tester were calculated by high-speed camera and then the sliding acceleration of the test piece was calculated. The dynamic friction coefficient of the test piece on the 65 Mn tool steel surface can be calculated according to the force balance equation of the test piece on the slope. By utilising a high-speed camera to capture the displacement of both specimen and the 65 Mn tool steel at various time points, we proceed to calculate the dynamic friction coefficient. The specific procedural framework for elucidating this process can be delineated as follows.

As shown in *Figure 5*, the shooting frequency was set to 120 pictures/s under the high-speed shooting state, so the sliding time of the test piece in each frame was 8.33 ms. The sliding time of the test piece can be obtained by calculating the difference between the number of frames between the start position and the end position and the sliding distance of the test piece can be measured. The dynamic friction coefficient (μ) of the test piece

on the surface of 65 Mn tool steel can be calculated by Equation (16).

$$\mu_k = \frac{2 \cdot S}{g \cdot \cos\theta' \cdot t_2^2} \tag{16}$$

where, θ' is the inclination angle of the inclinometer, S is the distance travelled between two successive photos and t_2 is the time lapse between the frames of the photos.

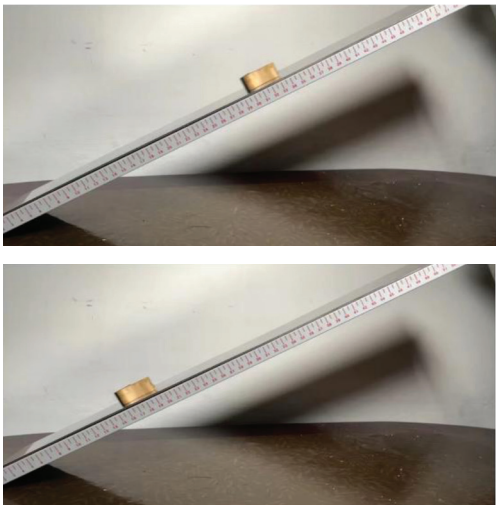
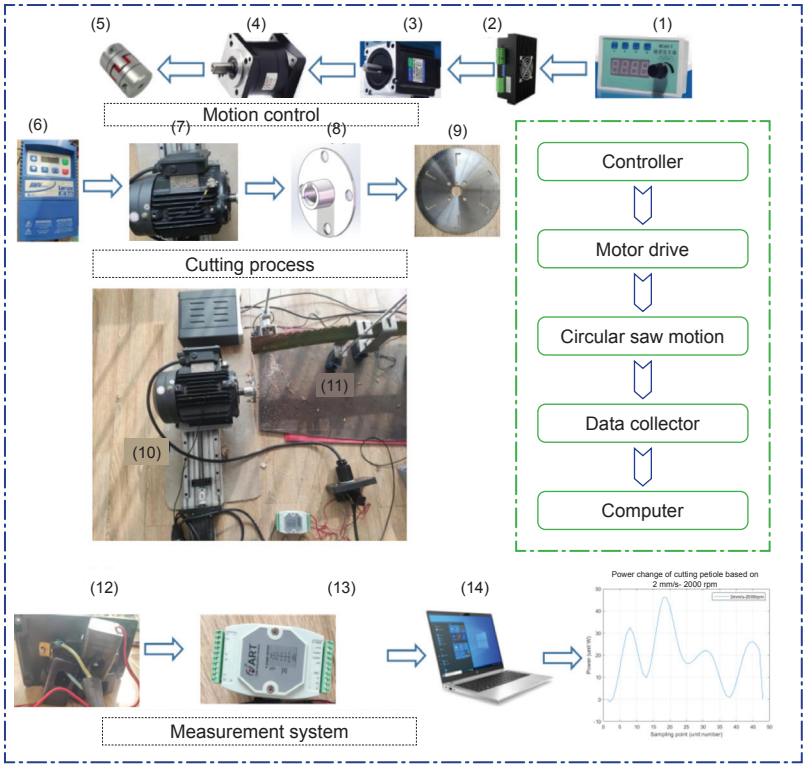


Figure 5. Determination process of friction coefficient from two successive photos.

Measurement of power of circular saw when cutting frond. The power of the circular saw motor was measured by the multi-function power meter. The multi-function power meter transmitted the data to the Personal Computer (PC) through the serial port data converter. The PC stored the data in real time through the serial port debugging software, and then converted it into a curve chart through Matlab software to obtain the power time domain diagram in the cutting process. *Figure 6* showed the ART data acquisition system for multi-function power meter to measure the power of the three-phase motor (ABB - 2.2kw - 4P - asynchronous motor). Three current sensors were clamped to each wire as shown in *Figure 6* respectively in order to measure the current through the U, V, W lines of the three-phase supply.

The ART was powered by voltage and these were then connected to the motor three-phase voltage, and voltage data of the motor was directly collected by ART. The 485 to 232 serial port data converters connected the multi-functional power instrument with the PC host. The multi-functional power instrument was the serial port of 485, and the PC host was the serial port of 232 (Xie, 2019) and this was combined with Modbus communication protocol for data conversion and acquisition of the PC. The data transmitted from multi-function power meter to PC was hexadecimal data, which was converted to decimal data through Modbus protocol of serial port debugging software.



Note: (1) - Controller; (2) - Step driver; (3) - Stepper motor; (4) - Decelerator; (5) - Coupling; (6) - Frequency transformer; (7) - AC motor; (8) - Cutter coupling; (9) - Circular saw; (10) - Feed assembly; (11) - Fixed structure; (12) - Sensor; (13) - Acquisition instrument; (14) - Computer.

Figure 6. The overall setup of the cutting power measurement.

Cutting test of oil palm fronds was conducted based on the oil palm comprehensive cutting test bench. The test conditions were the (1) feed rate at 2, 4, 8 and 12 mm/s, (2) rotation speed of the circular saw at 1,000-2,600 rpm. The data sets obtained were used to verify the value of power consumption obtained from the model.

The Process Diagram for Model Establishment and Validation

In summary, the establishment and validation of the cutting model for oil palm fronds are demonstrated through three specific steps, as illustrated in *Figure 7*.

RESULTS AND DISCUSSION

Fronds Characterisation

Rupture modulus. *Figure 8* below shows the rupture modulus as a function of moisture content. The normal drying of the specimens produces moisture content of 12%-58% and the results of the fracture modulus show that the strength of the frond increases almost linearly as the moisture content is reduced. The maximum rupture modulus is 43 MPa at 12% moisture and the lowest rupture modulus 28 MPa as in *Figure 8*. It is well known that woody specimens have similar regular pattern and increases the fracture toughness as the moisture content reduces. The fracture modulus of oil palm or king palm fronds ranged from 19-44 MPa at different water content (Chen, 2012; Wang, 2016; Wu, 2013).

The results of regression analysis *Figure 8* shows that $P<0.05$ the moisture content has a significant impact on the rupture modulus k. In other words, the significant linear relationship between rupture modulus k and moisture content has been verified. The tissue structure of oil palm fronds with different moisture content has a great impact on the variation of the required rupture force, and there is a linear correlation between the variation of oil palm fronds rupture modulus k and the moisture content of fronds. The moisture content continues to decrease with the extension of storage time, which causes to more serious fibrillation of fronds. Lower moisture content will lead to the ability to resist fracture (rupture modulus k) is enhanced. Lin (2012) developed rupture modulus model for wood species using moisture content (MC) as parameters. It seemed reasonable to expect that the main force would decrease with increased MC.

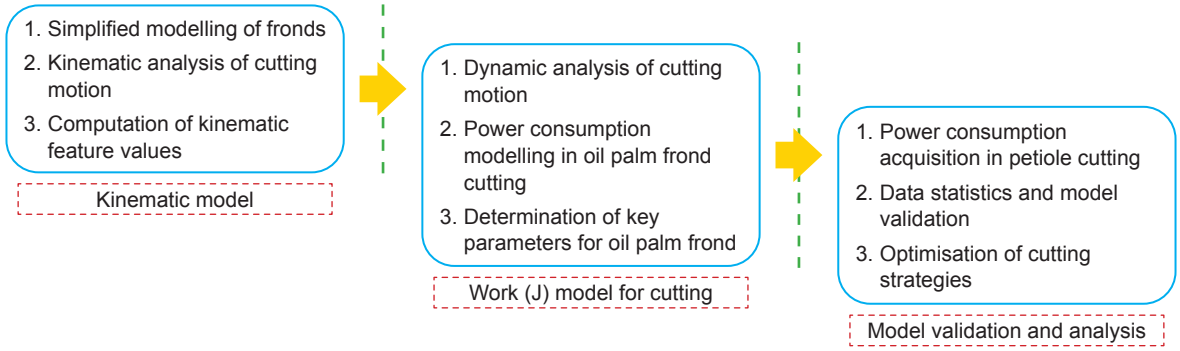


Figure 7. The process diagram for model establishment and validation.

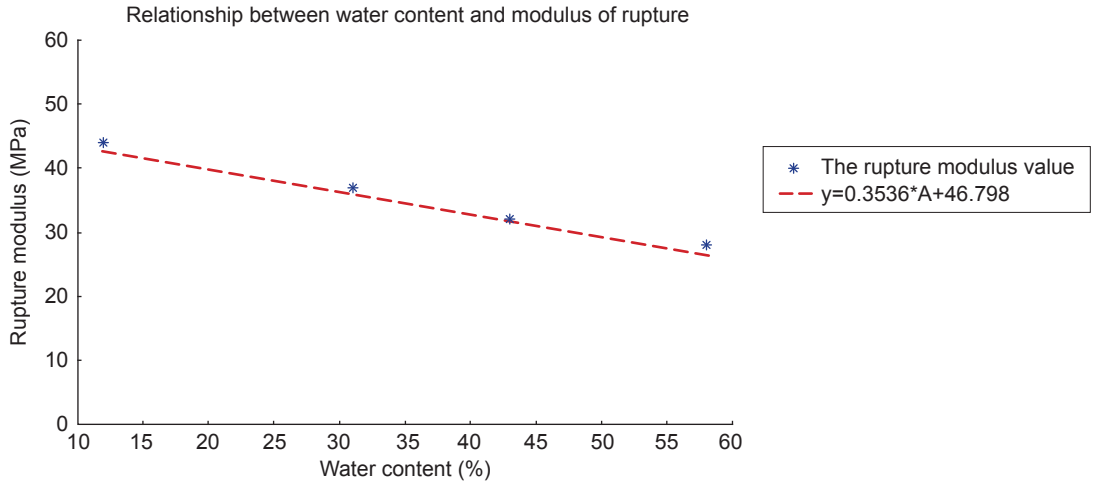


Figure 8. Effect of moisture content on the modulus of rupture of oil palm frond.

Friction coefficient of frond and circular saw. The critical angle of sliding of the test piece on the inclined plane was tested and was determined to be at 30°. The test was conducted for angles above the critical angle in order to find the variation of friction coefficient with the speed and the angle of inclination of up to 50° was tested for. The results are shown in *Figure 9* below. In this figure the general trend is that the friction, which coefficient is reducing with the sliding speed and this compares well with the trend of static friction which is higher than the kinetic friction as generally observed. The friction coefficient is highest at 0.55 at 0.75 m/s sliding speed and lowest at 0.41 at the sliding speed of 1.1 m/s is shown in the *Figure 9*. The trend of the data observed here correlates well with the data obtained elsewhere on wood specimen (Guan *et al.*, 1983; McMillin *et al.*, 1970; Murase *et al.*, 1978) for the case where the wood moisture content was large, the friction coefficient decreased with the increase of sliding speed. With the increase of sliding speed, the bond stability becomes weaker, and the friction coefficient also decreases. The moisture content of fresh oil palm frond tested here was more than 50%, belonging to high moisture content (Li & Zhang, 2018). The results obtained here is to be used as a guideline in the modelling of the cutting process.

Cutting Work of Circular Saw when Cutting Fronds

Figure 10 shows the different cutting power for several rotational speed of the circular saw, the Y-axis coordinate represents the cutting work (J) between the rotation speed and the cutting work under the working condition of the circular saw cutting feed rate of 2, 4, 8 and 12 mm/s. The cutting work was directly related to the rotation speed and feed rate. The cutting work had a linear function to rotation speed. Guedes *et al.* (2020), Li *et al.* (2022) and Nasir *et al.* (2018) studied the power consumption of cutting different types of wood (pine, tobacco fronds, ash *etc.*) using a circular saw. They also concluded that the power consumption increases linearly with the increase in the rotational speed of the circular saw. From the perspective of kinematic transmission laws, the power consumption model equation and experimental results are consistent with existing research results. Xie (2019) studied the power consumption of sugarcane cutting within the range of tool speed conditions of 250-500 rpm. It was found that the power consumption required for complete cutting of sugarcane falls within the range of 400-800 J.

The experimental data and research (*Figure 10*) results show that large gap between the individual data and the prediction results does not affect the final significance determine, which may be caused by the vibration of the circular saw and the uneven distribution of the texture of the cut body (Porankiewicz *et al.*, 2011). The data for the cutting work has a certain degree of dispersion, which is a normal phenomenon in the test. In general, it can be seen that there is a significant relationship between the test data and cutting work model for the oil palm fronds under the condition of rotation speed from 1,000-2,600 rpm and the feed rate of 2, 4, 8 and 12 mm/s. The distribution correlation coefficient ranges 0.72-0.91, ranges 38.12-144.35 and $P<0.05$. The red dotted line is the theoretical line from the model developed (Equation 13) and the correlation is good with R-square values, F statistic values and P values for the cases investigated. The significance of the model is statistically robust. It can be said the cutting model developed is validated.

The model developed here is based on a limited sample size. Increasing the sample size will effectively diminish the errors resulting from coupling effects. There is also a need to investigate the tooth profile which can strongly affect the

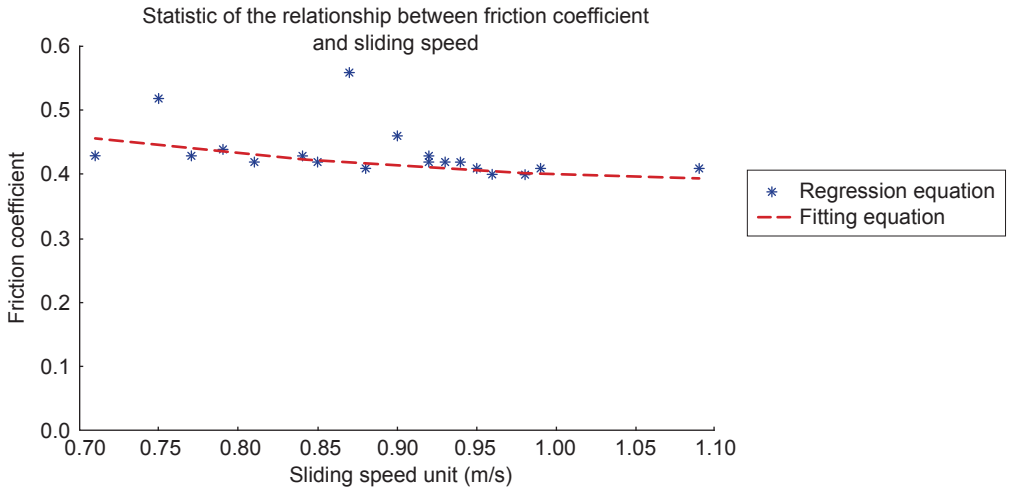


Figure 9. Variation of friction coefficient of oil palm frond with sliding speed.

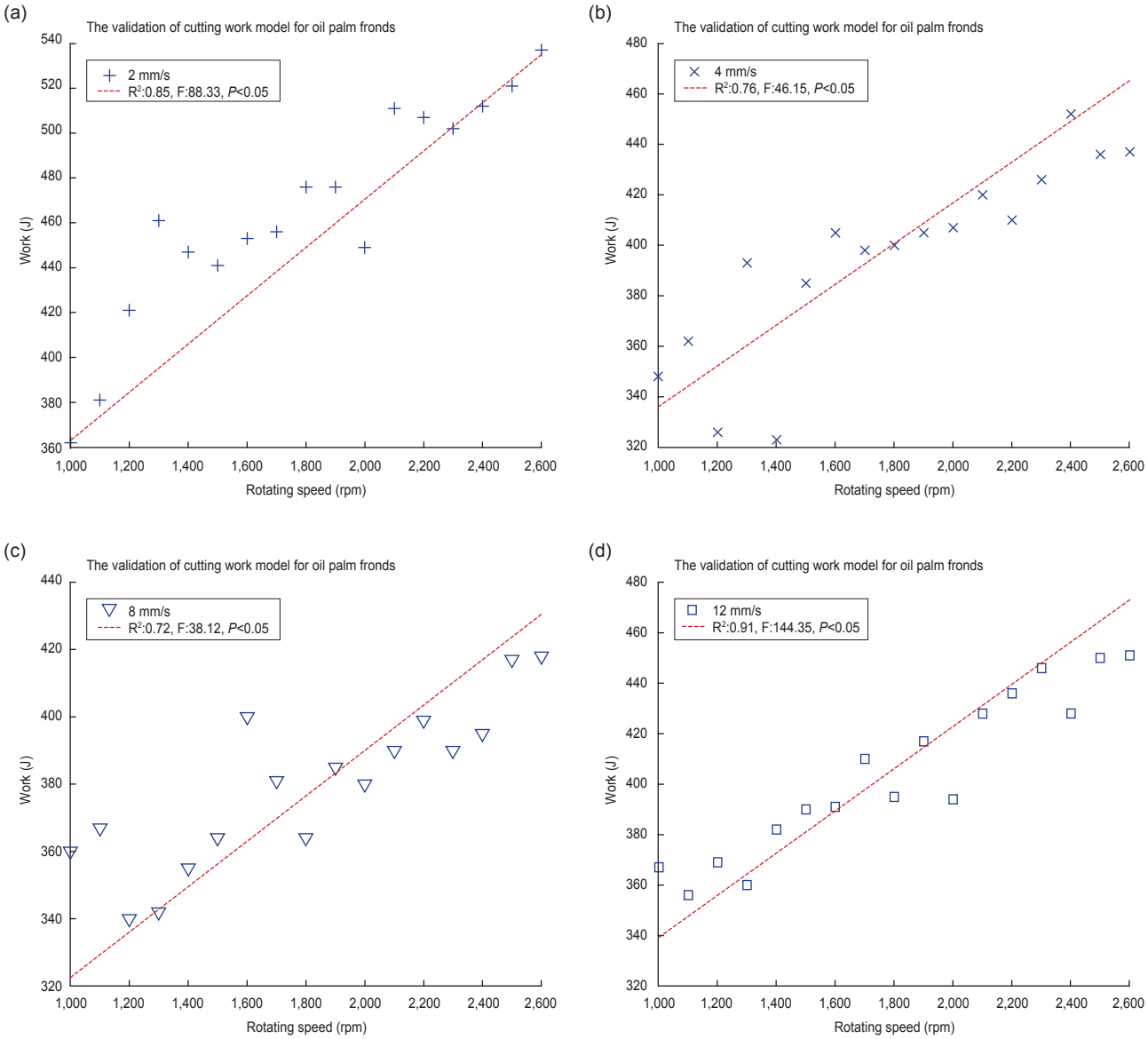


Figure 10. Theoretical cutting work (red line) and experimental reading (+,×,▽, □) for various feed rate (a) 2 mm/s, (b) 4 mm/s, (c) 8 mm/s and (d) 12 mm/s respectively.

cutting force and the effect of the angle of the saw relative to the frond fibre orientation as the current study only consider cutting perpendicular to the fibre of the frond. It would also be appropriate to study the theoretical cutting model for the existing sickle type harvester and the chisel type harvester. This can enable the resulting models to be compared with the radial saw cutter investigated here.

Optimisation of the Cutting Parameters

The model of the circular saw cutting process can now be used to determine the effect of the operating parameters on the work done for the cutting process. In this study, the range of the cutting parameters considered are 1-12 mm/s of feed rate and 1,000-3,000 rpm rotation speed of the circular saw. The results of those are shown in the *Figure 11* below. The energy consumed reduces linearly with the reduction of circular saw rotation speed and the variation of the energy consumed with the feed rate cannot be simply described as linear. When the feed rate of the circular saw increases from 1-3 mm/s, the cutting work decreases sharply. When the feed rate of the circular saw reaches 5 mm/s, the cutting work reaches the first peak bottom. When the feed rate of the circular saw increases from 6-12 mm/s, the cutting work of the cutting reaches the second peak bottom, which is the lowest point of energy consumption. When the feed rate of circular saw is 10 mm/s, the cutting work is the minimum. Within the range investigated, the minimum energy consumed is at circular saw rotation speed of 1,000 rpm and 10 mm/s feed rate.

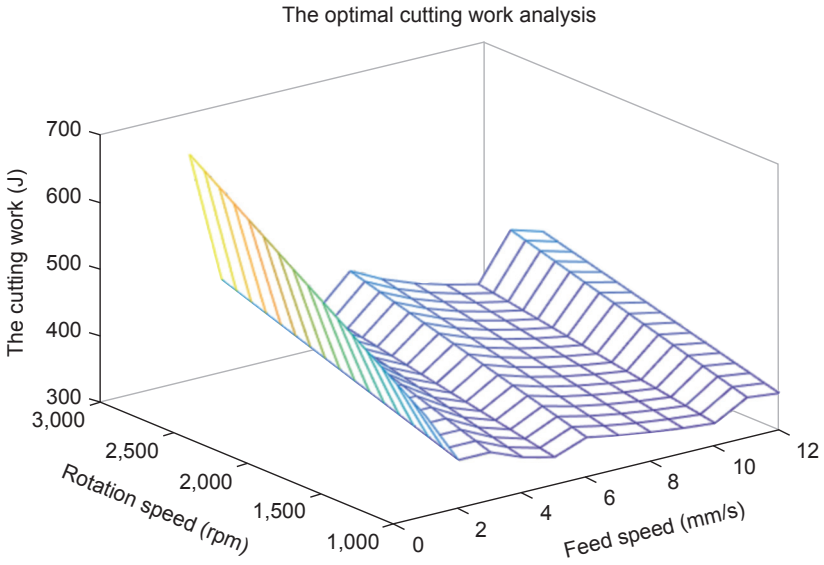


Figure 11. Analysis of optimal cutting work based on different working conditions.

Challenges and Future Work

The model developed here is based on a limited sample size. In particular, the age of the fronds and also the different size. There is also a need to investigate the tooth profile which can strongly affect the cutting force and the effect of the angle of the saw relative to the frond fibre orientation as the current study only consider cutting perpendicular to the fibre of the frond. It would also be appropriate to study the theoretical cutting model for the existing sickle type harvester and the chisel type harvester. This can enable the resulting models to be compared with the radial saw cutter investigated here.

CONCLUSION

Experimentally determined characteristics of the fronds used in this study are the rupture modulus (28-43 MPa) and friction coefficient for different sliding speed (0.41-0.55 at 0.75-1.10 m/s) measured at moisture content of (12%-58%). A frond cutting model was developed based on the Ernst and Merchant's force circle and the energy consumption based on the cutting power and clamping power expenditure. The energy consumption of the circular saw from the model is verified with the measured cutting energy of (330-540 J) at 1,000-2,600 rpm and feed rate of 2-12 mm/s ($0.72<R^2<0.91$, $P<0.05$). The validated cutting energy equation is used in the optimisation of the cutting process of a 100 mm base wide of an oil palm frond resulting in the minimum cutting energy of 330 J for rotational speed of 1,000 rpm and feed rate of 10 mm/s.

ACKNOWLEDGEMENT

The authors are grateful to the insightful comments suggested by the editor and the anonymous reviewers.

REFERENCES

Abbood, S. M. (2020). Effect of moisture ratio and cutting angles on force required to cut date palm fronds. *Biochemical and Cellular Archives, 20*(1), 1995–1997. https://doi.org/10.35124/bca.2020.20.1.1995

Abbood, S. M., Abbood, M. R., & Jasim, A. A. (2018). Manufacturing and testing of date palm vibration motorized fronds cutter. *Iraqi Journal of Agricultural Sciences, 49*(3), 763–773.

Atkins, A. (2003). Modelling metal cutting using modern ductile fracture mechanics: Quantitative explanations for some longstanding problems. *International Journal of Mechanical Sciences, 45*(2), 373–396. https://doi.org/10.1016/s0020-7403(03)00040-7

Chen, L. (2012). *Research on multi-scale model and mechanical properties of branching system of the family Palmae* (Master's thesis). South China University of Technology, Guangzhou.

Chu, H. (2017). *Design and experimental research of cutting key device for collecting potato stalk* (Doctoral dissertation). China Agricultural University.

Dong, R. (2017). *Simulation and experimental study on cutting process of silage corn harvesting header* (Master's thesis). Jilin University.

Eliçin, A. K., Sessiz, A., & Pekitkan, F. G. (2019). Effect of various knife type, cutting angle and speed on cutting force and energy of grape cane. *European Journal of Science and Technology*, 519–525. https://doi.org/10.31590/ejosat.532914

Gao, Z. (2016). *The bionic design of circular saw blade for metal cutting* (Master's thesis). Jilin University.

Guan, N., Thunell, B., & Lyth, K. (1983). On the friction between steel and some common swedish wood species. *European Journal of Wood and Wood Products*, *41*(2), 55–60. https://doi.org/10.1007/bf02612232

Guedes, T. O., Moreira da Silva, J. R., Hein, P. R. G., & Ferreira, S. C. (2020). Cutting energy required during the mechanical processing of wood species at different drying stages. *Maderas. Ciencia y Tecnología, 22*(4), 477–482. https://doi.org/10.4067/S0718-221X2020005000406

Hlásková, L., Orlowski, K. A., Kopecký, Z., & Jedinák, M. (2015). Sawing processes as a way of determining fracture toughness and shear yield stresses of wood. *BioResources, 10*(3), 5381–5394. https://doi.org/10.15376/biores.10.3.5381-5394

Intara, Y. I., Mayulu, H., & Radite, P. (2013). Physical and mechanical properties of oil palm frond and stem bunch for developing pruner and harvester machinery design. *International Journal of Science and Engineering, 4*(2), 69–74. https://doi.org/10.12777/ijse.4.2.2013.69-74

Jasim, A. A., Abbood, M. R., & Abbood, S. M. (2017). Effect of knives type on some operational characteristics for a locally assembled motorized vibration cutter used for date palm fronds pruning. *International Journal of Environment, Agriculture and Biotechnology, 2*(4), 1597–1600. https://doi.org/10.22161/ijeab/2.4.19

Jelani, A. R., Ahmad, D., Hitam, A., Yahya, A., & Jamak, J. (1998). Force and energy requirements for cutting oil palm frond. *Journal of Oil Palm Research, 10*(2), 10–24.

Jelani, A. R., Ahmad, D., Hitam, A., Yahya, A., & Jamak, J. (1999). Reaction force and energy requirement for cutting oil palm fronds by spring powered sickle cutter. *Journal of Oil Palm Research, 11*(2), 114–122.

Li, C., Zhang, H., Wang, Q., & Chen, Z. (2022). Influencing factors of cutting force for apple tree branch pruning. *Agriculture, 12*(2), 312. https://doi.org/10.3390/agriculture12020312

Li, P., Wang, S., Xiong, B., Tang, X., Tong, Y., Gao, S., Wen, S., Huang, M., Duan, Z., & Chen, Q. (2022). Laser cutting tobacco slice experiment: Effects of cutting power and cutting speed. *Open Physics, 20*(1), 977–983. https://doi.org/10.1515/phys-2022-0034

Li, W., & Zhang, Z. (2018). Research progress of friction behaviour in wood cutting. *China Wood Industry, 32*(6), 23–27. https://doi.org/10.19455/j.mcgy.20180606

Lin, X. (2012). *Calculation research on force and energy parameters of the metal sawing process of circular sawing machine* (Master's thesis). Central South University, Hunan.

McMillin, C. W., Lemoine, T. J., & Manwiller, F. G. (2007). Friction coefficient of Oven-Dry spruce pine on steel, as related to temperature and wood properties. *Wood and Fiber Science, 2*(1), 6–11. https://wfs.swst.org/index.php/wfs/article/download/681/681

Meijide, A., Röll, A., Fan, Y., Herbt, M., Niu, F., Tiedemann, F., June, T., Rauf, A., Hölscher, D., & Knohl, A. (2017). Controls of water and energy fluxes in oil palm plantations: Environmental variables and oil palm age. *Agricultural and Forest Meteorology, 239*, 71–85. https://doi.org/10.1016/j.agrformet.2017.02.034

Meng, Y., Wei, J., Wei, J., Chen, H., & Cui, Y. (2018). An ANSYS/LS-DYNA simulation and experimental study of circular saw blade cutting system of mulberry cutting machine. *Computers and Electronics in Agriculture, 157*, 38–48. https://doi.org/10.1016/j.compag.2018.12.034

Murase, Y. (1978). Effect of surface roughness of steel and wood variables on repeated friction between wood and steel. *Japan Wood Research, 24*(5), 865–872.

Nasir, V., Mohammadpanah, A., & Cool, J. (2018). The effect of rotation speed on the power consumption and cutting accuracy of guided circular saw: Experimental measurement and analysis of saw critical and flutter speeds. *Wood Material Science and Engineering, 15*(3), 140–146. https://doi.org/10.1080/17480272.2018.1508167

Porankiewicz, B., Axelsson, B., Grönlund, A., & Marklund, B. (2011). Main and normal cutting forces by machining wood of Pinus sylvestris. *BioResources*, *6*(4), 3687–3713. https://doi.org/10.15376/biores.6.4.3687-3713

Suryanto, N. H., Ahmad, N. D., Yahya, N. A., Akande, N. F. B., & Syahrita, N. K. (2009). Technical note: Cutting tests of oil palm empty fruit bunches. *Transactions of the ASABE*, *52*(3), 723–726. https://doi.org/10.13031/2013.27388

Wang, H., Chang, L., Ye, L., & Williams, J. G. (2013). Micro-cutting tests: A new way to measure the fracture toughness and yield stress of polymeric nanocomposites. *Proceedings of the 13th International Conference on Fracture*, 1–12. https://www.gruppofrattura.it/ocs/index.php/ICF/icf13/paper/viewFile/11399/10778

Wang, N. (2016). *Multi-scale modeling of royal palm tissue and the bionic applications based on its tissue structure* (Doctoral dissertation). South China University of Technology, Guangzhou.

Wu, H. (2013). *Research on structure and mechanical property of the family Palmae and bionic design of wind turbine* (Master's thesis). South China University of Technology, Guangzhou.

Xie, L. (2019). *Design and parameter optimization of stalk chopping, leaf stripping and top breaking devices for sugarcane harvester* (Doctoral dissertation). Zhejiang University.

Journal of Oil Palm Research Vol. 37 (1) March 2025 p. 122-130
DOI: https://doi.org/10.21894/jopr.2023.0060

CORROSION SIMULATION OF AUTOMOTIVE MATERIALS UNDER EXPOSURE IN BIODIESEL

S Y CETIN[1,2]*; M A MALEQUE[3]; H H MASJUKI[2]; A HAMDANI[2] and M M RAHMAN[4]

ABSTRACT

Biodiesel being an eco-friendly and renewable alternative fuel has gained attention due to its clean nature. However, the corrosion behaviour of automotive component materials in the presence of biodiesel is well known. Therefore, a computational fluid dynamics simulation on corrosion phenomena of automotive component materials has been done under exposure of biodiesel over varying time intervals. Two different types of steel materials (carbon steel and stainless steel) were chosen for the simulation of corrosion under biodiesel exposure. However, the corrosion was predominantly observed in both carbon steel and stainless steel materials. A notable finding emerged as stainless steel demonstrated significantly superior corrosion resistance compared to carbon steel when subjected to biodiesel-induced corrosion. Furthermore, the corrosion resistance of both stainless steel and carbon steel was found to be within the acceptable range for utilising biodiesel in automotive engines. This finding underscores the viability of biodiesel as a sustainable and viable alternative fuel for the automotive industry.

Keywords: automotive materials, biodiesel, CFD simulation, corrosion.

Received: 13 April 2023; **Accepted:** 4 October 2023; **Published online:** 29 November 2023.

INTRODUCTION

Corrosion is an undesirable phenomenon that affects the durability of materials and is caused by an electrochemical interaction between metals with their environment. This process arises from prolonged exposure to hostile environmental conditions, impacting the reliability and safety of various alloys (Mitrović *et al*., 2018). In everyday life, corrosion represents a common form of surface degradation that affects metallic structures negatively and employs a considerable economic impact. Industrial and personal assets such as automotive engine components, underground piping systems, bridges, storage tanks, furniture with metal accessories and household items such as kettles and white goods can all succumb to corrosion. From automotive engine components to underground piping systems, bridges, storage tanks, and household utilities, such as kettles and white goods are subjected to corrosion. In the sphere of design, the importance of considering corrosion when incorporating metallic materials is considerable. Consequently, considering corrosion during material design becomes imperative. While its effects may not be immediately evident, the damage it inflicts gradually surfaces over time (The Electrochemical Society, 2016). Corrosion occurs in the presence of corrosive media, typically acidic or basic solutions, where metals react according to their composition and electrochemical properties. This phenomenon manifests in various types, as depicted in *Figure 1* (Oxyplast UK Limited, 2018).

Biodiesel presents a promising cleaner energy source, derived from renewable resources, holding significant potential as a future alternative fuel.

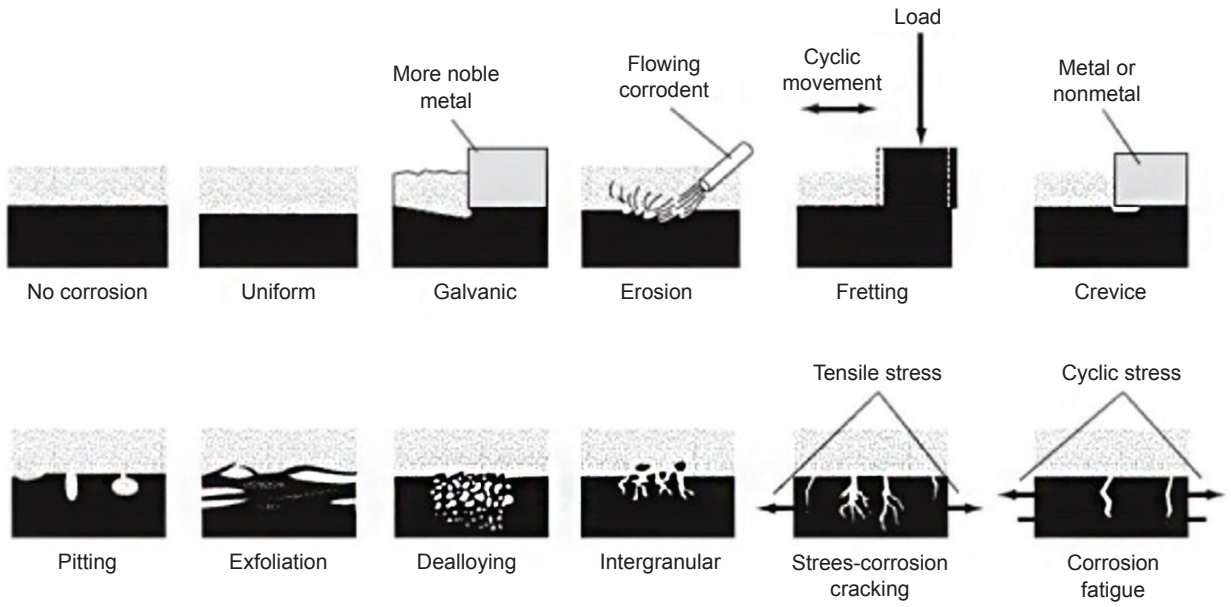
[1] Institute of Structural Durability and Railway Technology, Graz University of Technology, 8010 Graz, Austria.

[2] Department of Mechanical Engineering, International Islamic University Malaysia, 53100 Kuala Lumpur, Malaysia.

[3] Department of Manufacturing and Materials Engineering, International Islamic University Malaysia, 53100 Kuala Lumpur, Malaysia.

[4] College of Engineering, Universiti Malaysia Pahang Al-Sultan Abdullah, 26300 Pahang, Malaysia.

* *Corresponding author e-mail: s.y.cetin@tugraz.at*



Source: Oxyplast UK Limited (2018).

Figure 1. Various types of corrosion.

Countries with agricultural economies can reduce their dependence on oil by using biodiesel. It's superior lubricating properties can reduce wear on engine components and extend the engine life (Maleque *et al.*, 2015). Moreover, biodiesel is an environmentally friendly fuel which makes it promising for the future, such as reduced toxic exhaust emissions and minimised visible smoke during ignition, highlight its appeal (Maleque *et al.*, 2015). Nonetheless, biodiesel does possess some disadvantages, including aggressive corrosive tendencies that limit its industrial utilisation (Jakeria *et al.*, 2015). The presence of dissolved water, emulsified water, oxygen and free fatty acids in biodiesel adversely affects automobile engine components, leading to corrosion (Maleque & Abdulmumin 2014). Researchers have identified the hygroscopic nature and oxidation of biodiesel as potential threats to the integrity of metallic components in automotive engines (Sazzad *et al.*, 2016). Consequently, it is evident that biodiesel has a detrimental impact on automotive engine components, particularly regarding the interaction with metallic materials which is subjected to corrosion.

Technological developments in automobile industry are advancing with each passing day, hence, manufacturers continually pursue materials with superior resistance, strength, usability, and affordability. After paying attention on the interaction and corrosive effects between metals and biodiesel, research has been undertaken on this subject in the recent times. Baena and Calderón (2020), studied corrosive dynamics of carbon steel and stainless steel under biodiesel exposure for 3, 6 and 12 months periods. As a result of the study, the corrosion rates observed 0.001000, 0.000500 and 0.000240 mm/yr, respectively. Complementing these findings, referring to Ahmmad *et al.* (2018), stainless steel showed approximately 0.000500 mm/yr corrosion rate in presence of biodiesel for 2 months. Sterpu *et al.* (2012) found that the corrosion rate of carbon steel was 0.000855 mm/yr after 49 days of immersion period by sunflower oil biodiesel. These divergent results across different investigations can be attributed to a variety of variables such as temperature variations, movement of metal components, the specific type of biodiesel used, the velocity of the biodiesel fluid and other unique experimental conditions. This underlines the multifaceted and complex nature of the corrosive process involved in this context. The tribological behaviour of the metal components with several factors such as temperature, sliding time, biodiesel conditions and non-aqueous phase are investigated by Maleque *et al.* (2000). The complex nature of this corrosive process necessitates the use of different models to predict corrosion rates under varying parameters, ultimately reducing the need for numerous experiments (Anderko & Young, 1999).

Very minimum information on the computational fluid dynamics (CFD) simulation study that realistically addresses possible damage on metal surfaces, allowing the identification of potential failures in presence of biodiesel are

available in literature. Such simulations can prove biodiesel's corrosive behaviour on metals and help to identify suitable material for automotive engine components. It is believed that simulation studies yield results close to real-life conditions, however, experimental studies under similar conditions are necessary for comparison and verification. Therefore, the main aim of this work is to simulate corrosion phenomena of automotive component materials under exposure of biodiesel over varying time intervals.

MATERIALS AND METHODS

Materials

In this study, stainless steel and carbon steel were used as representative materials. Renowned for their robust strength, both stainless steel and carbon steel are commonly used in the automotive industry. Stainless steel is an iron-based alloy that contains 10.5% or more of chromium and a maximum of 1.2% carbon thus resulting a self-regenerative surface layer that provides remarkable corrosion resistance. The nomenclature `stainless steel` derives from the fact that these steels do not stain, corrode and rust unlike many other types of steel. Owing to its alloy characteristics and type, this material is frequently referred to as corrosion-resistant steel.

Therefore, stainless steel has a high resistance to corrosion and oxidation in many natural and artificial environment. Conversely, carbon steels are iron-carbon alloys, which contain manganese, silicon, sulphur and phosphorus. All the properties of carbon steels are directly related to their respective structures, depending on the amount of carbon content. Thereby, hardness, yield and tensile strength increase with the increase in the amount of carbon content. Following the thread of investigation previously established by (Maleque *et al.*, 2022), the present study maintains the focus on the same chemical composition for both stainless steel and carbon steel. This strategy allows for a consistent examination and correlation of results, ensuring that the results remain robust and meaningful within the overarching context of the original research.

3D Modelling

In the modelling phase of this simulation, two identical sketches were meticulously designed and the biodiesel liquid environment was created in ANSYS Fluent and ANSYS Mechanical. Subsequent to the completion of the sketching process, the contact relation has been created between materials and the liquid. Following these initial steps, all bodies within the simulation were meshed. *Figure 2* presents the meshed geometry of the corrosion simulation specimens and palm biodiesel environment.

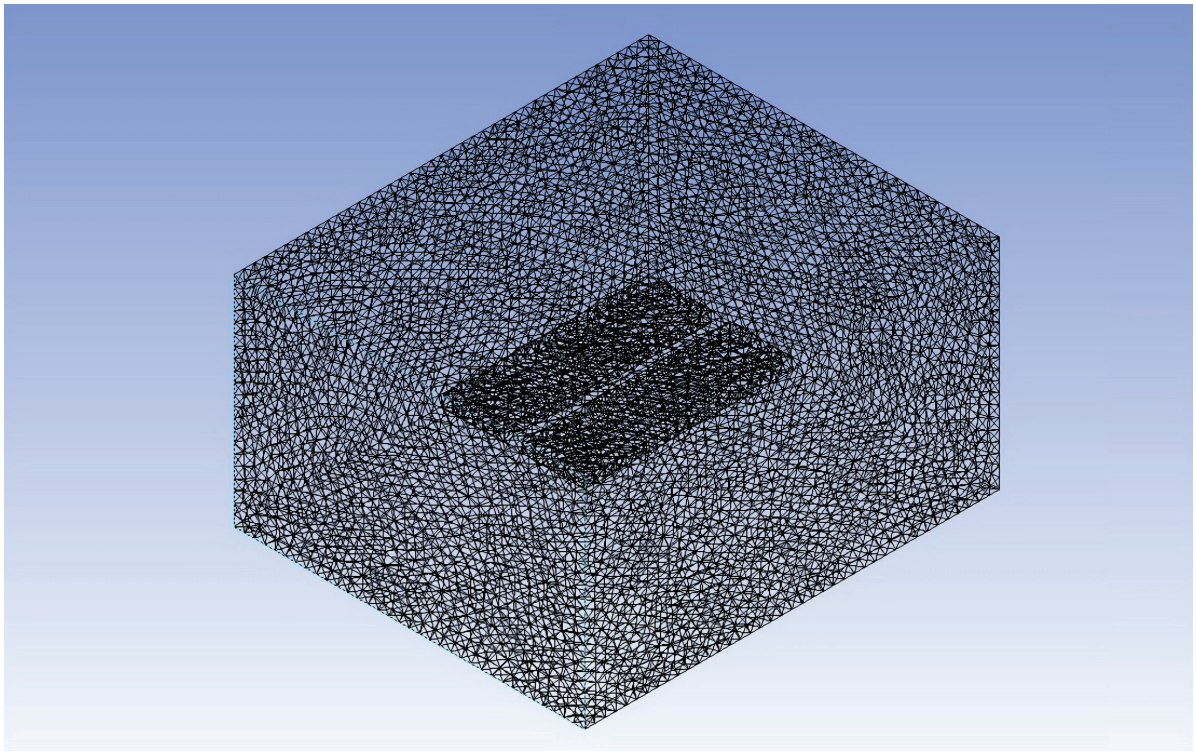


Figure 2. Meshed geometry of corrosion analysis.

Simulation Procedure

Numerous simulation methods are available, such as numerical simulation, computational simulation and computer aided simulation *etc.* A crucial aspect of simulation is the definition of the simulation procedure before the process is initiated. Real-life conditions, including simulation time, temperature, pressure and the characteristics of the liquid to be used, should be replicated as accurately as possible in the simulation. The corrosive impact of biodiesel on automotive engine components is widely recognised. Therefore, predicting the severity, type and exposure time of biodiesel corrosion is of great importance. Proactive measures can be taken based on early detection of corrosion. Consequently, material surfaces can either be reinforced or alternative materials can be considered for the engine components. In addition, a realistic simulation can help to minimise the factors that potentiate the corrosion, thereby ensuring enhanced durability and life of the components.

At the beginning of the simulation study, boundary box was created. As can be seen in *Figure 3*, biodiesel entered through the inlet section of the boundary box and, left the system by the outlet section after contact with specimens of stainless steel and carbon steel.

The reference temperature was regulated at 25°C as the room temperature. The pressure-velocity method was preferred as "coupled" to keep high accuracy of the results. Furthermore, standard wall functions were used together with the realisable k-epsilon model. The simulation performed for 100 iterations. The entry of biodiesel liquid was provided from the inlet section of the boundary box at a constant speed of 1 m/s.

Finally, the calculation method of the test determined and adjusted. The type of transport model was selected and the reaction set as "volumetric". Turbulence-chemistry interaction was determined as "Eddy-Dissipation". Palm biodiesel was given 1 m/s velocity for ease of calculation. "Inlet diffusion" and "Diffusion Energy Source" was activated as options of the model. In consequence, the "mass fraction of O_2" was taken as a reference for the corrosion rate.

Corrosion Rate Measurement

Recognising the extensive toolbox available for the investigation of corrosion phenomena, it is worthwhile to acknowledge the contribution of established electrochemical techniques, although their application is outside the boundary of this particular study, which used computational fluid dynamics simulation as its primary investigative tool. Among these acknowledged electrochemical methodologies, polarisation curves represent a fundamental analytical resource providing a graphical correlation between the electrode potential and the corresponding current. Through this relationship, a comprehensive assessment of corrosion rates can be made, thereby delineating the degree of corrosion resistance inherent in the materials under investigations. Similarly, Electrochemical Impedance Spectroscopy (EIS) which uses modest voltage or current perturbations to provoke a system response, is another laudable technique. The resultant impedance characteristics grant us to assess the performance of materials under different environmental conditions, providing valuable insight into the dynamics of the corrosion process. Furthermore, potentiometric polarisation, a technique characterised by gradual change in electrode potential to establish a comprehensive current versus potential profile, provides a significant depth of understanding

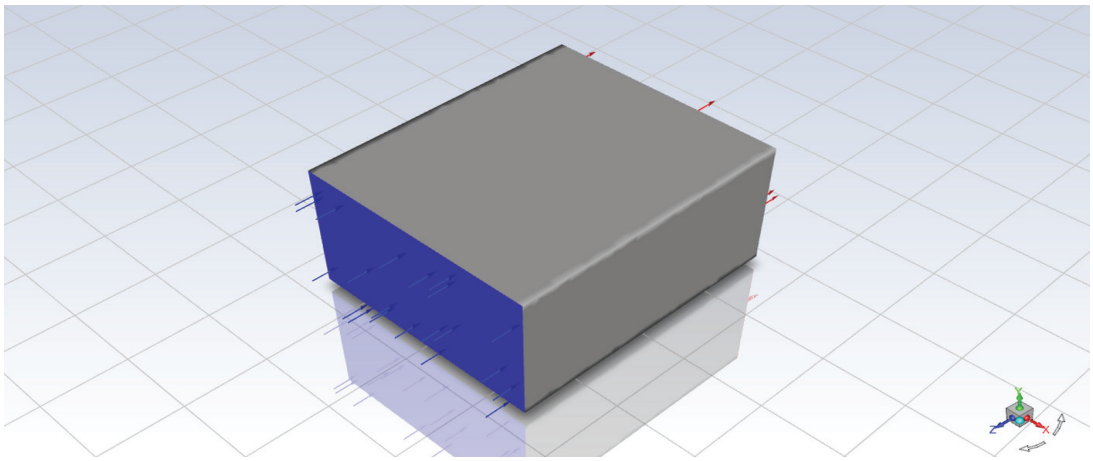


Figure 3. Boundary box.

of the kinetics of corrosion reactions. The value of this technique lies in its ability to clarify the mechanisms and rates of electrochemical process.

This study pursued an alternative but equally rigorous route, using computational simulations to elucidate the behaviour of materials under biodiesel exposure. The unit of measures is defined as the metal mass that moves away from unit surface in unit time. In general, the unit used to express corrosion rate is g/dm^2 per year.

$$\frac{g}{dm^2 \times yr} \quad (1)$$

As another unit, metal thickness reduction over a certain period of time can also be used.

$$\frac{mm}{yr} \quad (2)$$

The corrosion rate can be found by the help of the formula that is shown in Equation (3):

$$Corrosion\ rate\left(\frac{mm}{yr}\right) = \frac{K \times W}{DAT} \quad (3)$$

where, K is a constant, W is the weight loss in milligrams, D is the metal density in g/cm^3, A is the area of the test specimen in m^2 and T is the exposure time in hours. Besides, the mass fraction is one of the preferred parameters in corrosion studies to analyse the interaction between metal and chemical substances. Equation (4) shows the general equation for mass fraction.

$$W_i = \frac{m_i}{m_t} \quad (4)$$

where mass fraction of specimen is W_i, component mass m_i and m_t is the total mass of the mixture.

RESULTS AND DISCUSSION

Corrosion rates for materials predicted are based on the data obtained from the simulation software. Since the ANSYS software is not suitable for real-time long interaction tests, weight loss was considered for the corrosion rate calculations. In general, "mm/yr" is used as the corrosion rate which means the metal thickness in mm that was removed from the surface of the material by corrosion in one year. Equation (3) presents the formula of corrosion rate. Moreover, the mass fraction formula is presented in Equation (4). Herein, the simulation was performed for the mass fraction of O_2 of both materials. Based on the simulation results, maximum mass fraction of carbon steel monitored was 1.04×10^{-1}. Besides, stainless steel showed 1.68×10^{-1} mass fraction of O_2. *Table 1* presents the mass fraction of O_2 in different regions of both carbon steel and stainless steel specimens.

According to the simulation results, after three months of exposure to biodiesel, the corrosion rate of carbon steel was recorded as 0.000213 mm/yr. Meanwhile, stainless steel exhibited a corrosion rate of 0.000193 mm/yr over the same exposure time. Besides, carbon steel displayed 0.000106 mm/yr and stainless steel displayed 0.000096 mm/yr for 6 months of contact with palm biodiesel. After 1 yr of exposure, it was observed that corrosion rate of carbon steel decreased to 0.000053 mm/yr. Furthermore, stainless steel displayed 0.0000482 mm/yr of corrosion rate. *Figure 4* presents corrosion rates of stainless steel and carbon steel under exposure of palm biodiesel at different time periods. Moreover, *Figure 5* shows corroded surfaces of the materials after exposure of palm biodiesel. From a metallurgical point of view, the corrosion behaviour of both carbon steel and stainless steel when exposed to biodiesel can be interpreted in terms of their respective material compositions and the way they interact with the

TABLE 1. MASS FRACTION OF O_2 OF THE MATERIALS

Reference position of carbon steel (m)	Mass fraction of O_2 for carbon steel	Mass fraction of O_2 for stainless steel	Reference position of stainless steel (m)
0.012	1.16×10^{-2}	9.41×10^{-2}	0.027
-0.008	2.16×10^{-2}	9.38×10^{-2}	0.032
0.000	5.08×10^{-2}	1.01×10^{-1}	0.043
0.002	7.25×10^{-2}	1.68×10^{-1}	0.049
0.009	9.07×10^{-2}	1.29×10^{-1}	0.052
0.018	1.04×10^{-1}	4.90×10^{-2}	0.057

Note: Reference coordinate is (-0.012 m, 0.058 m), carbon steel placed (-0.012 m, 0.018 m) and stainless steel placed (0.027 m, 0.057 m).

corrosive environment. Carbon steel, which has mainly higher mass fraction of oxygen, indicates more extensive oxidation, resulting in a slightly higher corrosion rate. This phenomenon mainly due to the absence of a protective oxide layer that could resist corrosive agents. On the other hand, stainless steel, an alloy with a significant chromium content, exhibits a lower corrosion rate. The chromium in the alloy reacts with oxygen in the environments to form a thin, adherent, invisible surface layer of chromium-rich oxide. This layer is self-repairing and provides a barrier to prevent oxygen diffusion to the underlying steel surface. Thus, slowing the corrosion process. The slightly lower mass fraction of oxygen found in stainless steel compared to carbon steel in the simulation study is evidence of this inherent corrosion resistance property. The results of this study also demonstrate that the corrosion rate for both types of steel decreases over time when exposed to biodiesel, suggesting a possible adaptation or saturation effect of the corrosive biodiesel environment. These findings provide valuable insights for material selection in industries where equipment is exposed to similar corrosive conditions.

Although there is no common corrosion rate as standards for palm biodiesel, carbon steel and stainless steel, it is important to note that these rates are inherently variable. Furthermore, they depend on the number of factors such as material composition, environmental conditions and the specific operating parameters under which they are utilised. Particularly in the industrial applications, the specific requirements of the materials may vary due to the dynamic nature of their role, requiring an adaptable approach to corrosion management. The adaptability of materials and the diversity of their applications underline the importance of a sophisticated understanding and management of material corrosion in different industrial contents. The way metallic materials degrade or corrode in biodiesel blends is influenced by several factors. These include the chemical composition of the fuel, how long the material is immersed in the fuel and the environmental conditions. According to the Dharma *et al.* (2023) the rate at which mild steel corrodes decreases as the amount of biodiesel in the fuel increases. The reason behind this finding is that biodiesel contains less sulphur and aromatic compounds than regular diesel fuel. These compounds are known to contribute to metal corrosion. Biodiesel also contains more oxygen and fatty acid methyl esters which can form a protective layer on the metal, slowing down corrosion. However, the impact of biodiesel on the rate which metal corrodes is not simple. It can be influenced by other factors such as the type of metal, impurities in the fuel and environmental conditions. Therefore, more research is needed to fully understand how metallic materials corrode in biodiesel blends and to find the effective ways to handle these corrosion problems in engines running on biodiesel.

The results of the current investigation are broadly consistent with previous research, although the existence of the minor variations due to different experimental conditions is acknowledged (*Table* 2). The study by Fazal *et al.* (2011) reported a corrosion

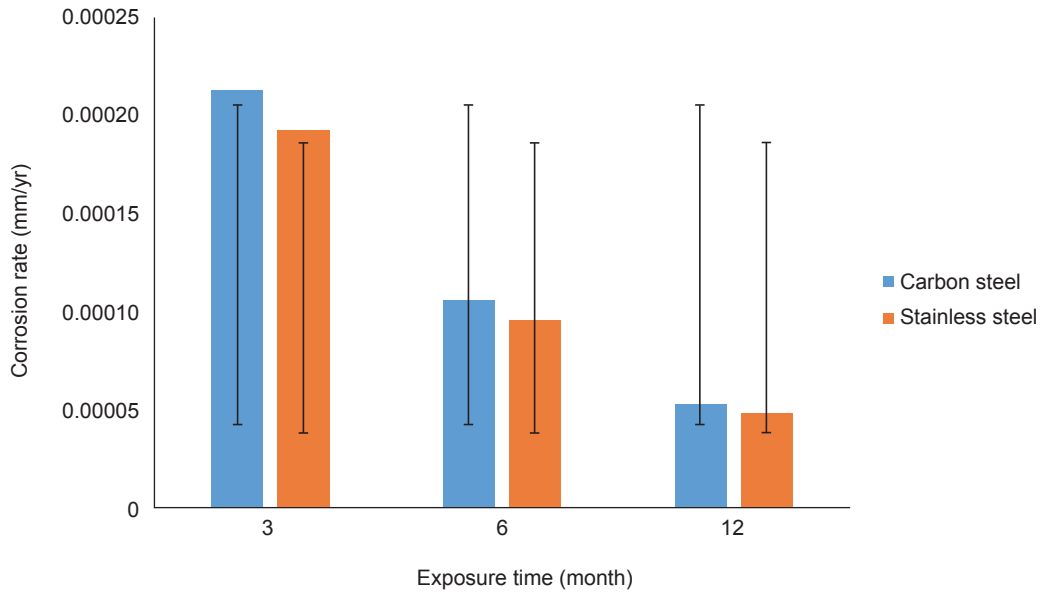


Figure 4. Corrosion rates of the materials.

rate for mild carbon steel in biodiesel approximately 0.001320 mm/yr after 1,200 hr of immersion test. Although, the results show slightly higher values than those obtained in this study, considering the difference between the immersion times in both studies, the results provide evidence that these two studies can support each other. Similarly, Fazal *et al.* (2010) investigated the corrosion rate of stainless steel in palm biodiesel and diesel at 80°C for 1,200 hr. The authors reported the corrosion rate of stainless steel immersed in diesel and biodiesel as 0.000586 and 0.000879 mm/yr respectively. Therefore, these results explicitly demonstrate the effect of temperature on the results. Likewise, Alves *et al.* (2019) investigated the influence of stainless steel corrosion on the oxidative stability of biodiesel during storage. The study explored the relationship between biodiesel degradation and corrosion of stainless steel used for storage. The authors measured lower corrosion rates for stainless steel in biodiesel conditions ranging from approximately 0.00000381 to 0.00001905 mm/yr than those found in this study. Thangavelu *et al.* (2015) analysed the effect of biodiesel blends on corrosion rate, fuel properties and fuel composition changes. The carbon steel specimens were exposed to static immersion test for 800 hr at 25°C-30°C and 400 hr at 60°C respectively. The corrosion rate of carbon steel in biodiesel was found to be 0.1817 and 0.2612 mpy which are approximately equals to 0.004615 mm/yr and 0.006634 mm/yr at room temperature and 60°C, respectively. As highlighted earlier, the differences may be due to the immersion time, the use of different fuel blends and test conditions, emphasising the role of certain fuel properties influencing the corrosion rates. In addition, some chronic differences can be observed between simulation-based studies and experimental analyses performed in laboratory environments. These differences may be due to the limitations of the simulation software, the use of incorrect parameter inputs, incomplete or incorrect implementation of the simulation process, and inadequate conditions for the experiments. Therefore, it is very important to determine the most appropriate conditions to use as input in simulation studies. In the current simulation study, the most suitable conditions evaluated and attempts were made to emphasise the importance of simulation studies in predicting the corrosive properties of materials in advance. However, it should be noted that an experimental study that fully meets the same conditions is required for a complete and accurate comparison.

TABLE 2. CORROSION RATES OF PREVIOUS EXPERIMENTAL STUDIES ON STAINLESS STEEL AND CARBON STEEL WITH DIFFERENT KIND OF BIODIESEL

Biodiesel type	Temperature (°C)	Duration (hr)	Corrosion rate		References
			Stainless steel	Carbon steel	
Palm oil	80	600	0.015 mpy	-	Fazal *et al.* (2010)
	60	-	-	0.1497 mm/yr	Prasojo *et al.* (2019)
Palm biodiesel	25	2,190	0.000213 mm/yr	0.0001930 mm/yr	Present work
		4,382	0.000107 mm/yr	0.0000965 mm/yr	
		8,765	0.000530 mm/yr	0.0000482 mm/yr	
Fatty acid methyl esters (FAME)	At room temperature	720	0.00055 mpy	-	Alves *et al.* (2019)
			0.00045 mpy		
		1,440	0.00020 mpy		
Fatty acid ethyl esters (FAEE)		2,160	0.00015 mpy		
			0.00015 mpy		
			0.00015 mpy		
Sunflower oil	25-30	1,176	-	0.000855 mm/yr	Sterpu *et al.* (2012)
Rapeseed oil				0.000760 mm/yr	
Corn oil				0.001164 mm/yr	

Note: mpy - mils per year.

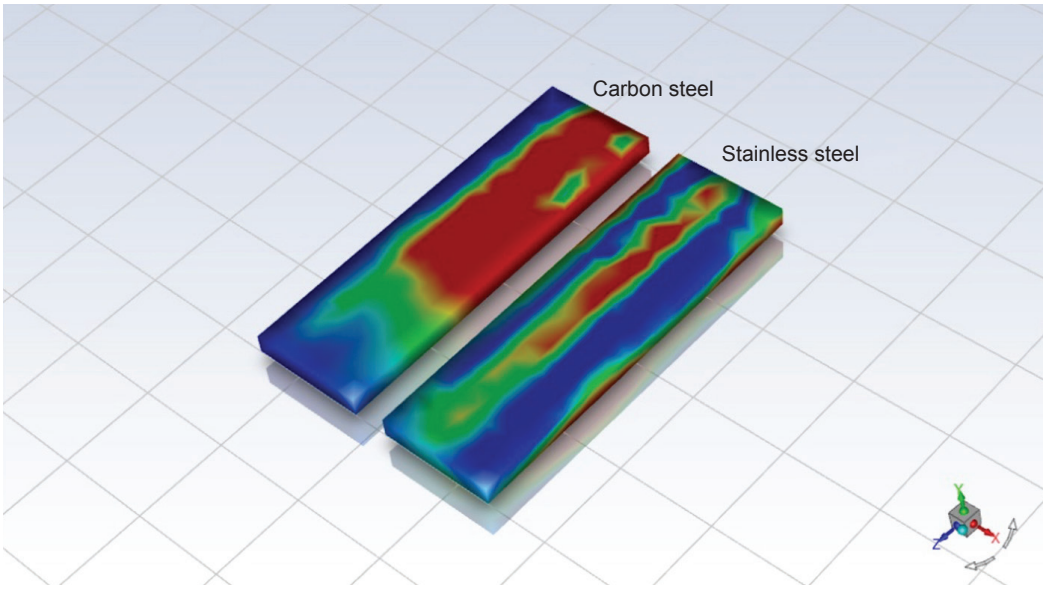


Figure 5. Corroded surfaces of carbon steel and stainless steel after biodiesel exposure.

CONCLUSION

Corrosion, with its potential to cause product loss and contamination, it is highly demanded to consider its effect and pre-determine the behaviour with materials. In this pursuit, the utilisation of simulation tools, incorporating basic material properties, emerges as a highly effective and scientifically sound approach to predict corrosion behaviour when exposed to biodiesel. The simulation employed palm biodiesel as the operating liquid at 25°C. This study shows that it was feasible to simulate corrosion behaviour of automotive component materials under biodiesel for the prediction of such phenomenon in real life. It is possible to achieve the process parameters for the corrosion rate providing accurate predictions for stainless steel and carbon steel specimens under biodiesel exposure with the ANSYS simulation software. The findings showcased a corrosion rate of 0.000213 mm/yr for carbon steel specimens after three months of biodiesel exposure, while stainless steel specimens exhibited a slightly lower corrosion rate of 0.000193 mm/yr over the same duration. After one year of exposure, corrosion rates were recorded at 0.000053 mm/yr for carbon steel and 0.0000482 mm/yr for stainless steel, respectively. As a conclusion, this study illustrates the efficiency of simulation studies to predict the behaviour of materials, saving valuable time and resources in the process. Nonetheless, to validate these results under real-time operations, it remains crucial to conduct future experimental studies, ensuring the exact conditions are met.

ACKNOWLEDGEMENT

The authors would like to acknowledge to the Malaysian Tribology Society (MYTRIBOS) for funding this research through project No. MIG-0005-2021 and also to the International Islamic University of Malaysia (IIUM) for technical supports that made this study possible.

REFERENCES

Ahmmad, M. S., Hassan, M. B. H., & Kalam, M. A. (2018). Comparative corrosion characteristics of automotive materials in *Jatropha* biodiesel. *International Journal of Green Energy*, *15*(6), 393–399. https://doi.org/10.1080/15435075.2018.1464925

Alves, S., Dutra-Pereira, F., & Bicudo, T. (2019). Influence of stainless steel corrosion on biodiesel oxidative stability during storage. *Fuel*, *249*, 73–79. https://doi.org/10.1016/j.fuel.2019.03.097

Anderko, A., & Young, R. D. (1999, April 25). *Simulation of CO_2/H_2S corrosion using thermodynamic and electrochemical models* [Paper presentation]. Corrosion 99, Texas, USA.

Baena, L. M., & Calderón, J. A. (2020). Effects of palm biodiesel and blends of biodiesel with organic acids on metals. *Heliyon, 6*(5), e03735. https://doi.org/10.1016/j.heliyon.2020.e03735

Dharma, S., Silitonga, A. S., Shamsuddin, A. H., Sebayang, A. H., Milano, J., & Sebayang, R. (2023).

Properties and corrosion behaviors of mild steel in biodiesel-diesel blends. *Energy Sources, Part A: Recovery, Utilization, and Environmental Effects, 45*(2), 3887–3899. https://doi.org/10.1080/15567036.2019.1668883

Fazal, M. A., Haseeb, A. S. M. A., & Masjuki, H. H. (2010). Comparative corrosive characteristics of petroleum diesel and palm biodiesel for automotive materials. *Fuel Processing Technology, 91*(10), 1308–1315. https://doi.org/10.1016/j.fuproc.2010.04.016

Fazal, M. A., Haseeb, A. S. M. A., & Masjuki, H. H. (2011). Effect of temperature on the corrosion behavior of mild steel upon exposure to palm biodiesel. *Energy, 36*(5), 3328–3334. https://doi.org/10.1016/j.energy.2011.03.028

Jakeria, M. R., Fazal, M. A., & Haseeb, A. S. M. A. (2015). Effect of corrosion inhibitors on corrosiveness of palm biodiesel. *Corrosion Engineering, Science and Technology, 50*(1), 56–62. https://doi.org/10.1179/1743278214Y.0000000208

Maleque, A., & Abdulmumin, A. A. (2014). Tribocorrosion behaviour of biodiesel: A review. *Tribology Online, 9*(1), 10–20. https://doi.org/10.2474/trol.9.10

Maleque, A., Cetin, S. Y., Masjuki, H. H., & Hamdani, A. (2022). Wear simulation of automotive engine component materials under biodiesel. *Journal of Mechanical Engineering and Science, 16*(4), 9167–9174. https://doi.org/10.15282/jmes.16.4.2022.02.0726

Maleque, M. A., Masjuki, H. H., & Haseeb, A. S. M. A. (2000). Effect of mechanical factors on tribological properties of palm oil methyl ester blended lubricant. *Wear, 239*(1), 117–125. https://doi.org/10.1016/S0043-1648(00)00319-7

Maleque, M. A., Ghazal, B., Ali, M. Y., Hayyan, M., & Saleh, A. A. (2015). Corrosion of surface-modified AISI 4340 steel in *Jatropha* biodiesel. *Advanced Materials Research, 1115*, 243–246. https://doi.org/10.4028/www.scientific.net/AMR.1115.243

Mitrović, R. M., Momčilović, D. B., & Atanasovska, I. D. (2018). Determination of critical size of corrosion pit on mechanical elements in hydro power plants. *Applied Engineering Letters Journal of Engineering and Applied Sciences*, *3*(1), 1–5. https://doi.org/10.18485/aeletters.2018.3.1.1

Oxyplast UK Limited. (2018). Different types of corrosion. *https://oxyplastuk.com/technical/different-types-of-corrosion/*

Prasojo, B., Kurniyanto, H. B., Azis, R. T., So'im, S., & Haqin, A. R. (2019). Effect of flow rate and temperature on erosion corrosion rate of crude palm oil against elbow A53 grade B carbon steel material. *IOP Conference Series: Materials Science and Engineering, 462*, 012038. https://doi.org/10.1088/1757-899X/462/1/012038

Sazzad, B. S., Fazal, M. A., Haseeb, A. S. M. A., & Masjuki, H. H. (2016). Retardation of oxidation and material degradation in biodiesel: A review. *RSC Advances, 6*(65), 60244–60263. https://doi.org/10.1039/C6RA10016C

Sterpu, A. E., Dumitru, A. I., & Popa, M. F. (2012). Corrosion behavior of steel in biodiesel of different origin. *Analele Universitatii "Ovidius" Constanta - Seria Chimie, 23*(2), 143 – 148. https://doi.org/10.2478/v10310-012-0024-3

Thangavelu, S. K., Chelladorai, P., & Ani, F. N. (2015). Corrosion behaviour of carbon steel in biodiesel-diesel-ethanol (BDE) fuel blend. *MATEC Web of Conferences, 27*, 01011. https://doi.org/10.1051/matecconf/20152701011

The Electrochemical Society. (2016). Corrosion and corrosion prevention. *What is corrosion?* https://www.electrochem.org/corrosion-science

Journal of Oil Palm Research Vol. 37 (1) March 2025 p. 131-147
DOI: https://doi.org/10.21894/jopr.2024.0002

EXPERIMENTAL INVESTIGATIONS ON TRIBOLOGICAL ASSESSMENT AND NO_x EMISSIONS OF PALM BIODIESEL BLENDED WITH OLEIC ACID AND ETHANOL

KARTHIC RAJA M[1]; KAMALESH A SORATE[1]* and PURNANAND V BHALE[1]

ABSTRACT

Tribological behaviour of biodiesel should be investigated to get confidence for long-term engine usage. Also, the higher nitrous oxide (NO_x) level from the biodiesel-fueled engine is observed. Tribological assessment and engine performance of lower blends of palm biodiesel (B10, B20) are available in the literature. Due to limited reserves of fossil fuels, the demand for biodiesel is increasing day by day. To fulfil this demand, the higher blends of biodiesel (such as B80, B90) should be investigated. Hence, this study aimed to investigate the tribological and NO_x assessment of the higher blends of palm biodiesel. Palm biodiesel was produced by transesterification and blended with oleic acid (OA) and ethanol (E). Biodiesel blends such as 100% biodiesel (B100), 80% biodiesel + 20% oleic acid (B80OA20), 90% (80% biodiesel + 20% oleic acid) + 10% ethanol (B80OA20E10), 90% biodiesel+10% oleic acid (B90OA10) and 95% (90% biodiesel + 10% oleic acid) + 5% ethanol (B90OA10E5) were prepared. Pin on disc machine was used for tribological study and diesel engine was used for NO_x analysis. Nearly 40% reduction in wear and 48% reduction in friction were observed for B80OA20 compared to B90OA10, while B90OA10E5 exhibited the lowest frictional force among all the test fuels. During tribological assessment, two blends B80OA20 and B80OA20E10 showed satisfactory performance and were further studied for NO_x analysis. Also, these two blends lower NO_x emissions by 12% and 2%, respectively, compared to B100.

Keywords: biodiesel blends, friction, oleic acid, transesterification, wear.

Received: 23 June 2023; **Accepted:** 31 October 2023; **Published online:** 9 January 2024.

INTRODUCTION

Fatty acid methyl ester, commonly known as biodiesel, is derived from edible, nonedible feedstocks and waste cooking oils, recently microalgae (Atmanli, 2020). Biodiesel can be produced by conventional transesterification, hydrodynamic cavitation reactor, electrolysis, ultrasonication and microwave methods (Tabatabaei *et al.*, 2019). The thermophysical properties of biodiesel were found to be comparable with petrodiesel (Verma *et al.*, 2021). Biodiesel showed an increase in fuel consumption and a decrease in brake thermal efficiency. In addition, biodiesel showed less exhaust emissions except nitrous oxide (NO_x) compared to diesel (Tamilselvan *et al.*, 2017).

Unlike other feedstocks used for biodiesel production, oil palm is a perennial crop, thereby being a reliable raw material source. Palm oil in crude and refined form accounts for over one-third of vegetable oil production. Palm oil cultivation stood at nearly 73 million tonnes for 2018-2019, estimated to rise to 240 million tonnes by 2050 (Tillis, 2019). The palm oil yield per hectare of a plantation is over ten times higher than other feedstocks (Mekhilef *et al.*, 2011). Palm oil can be transesterified into biodiesel using a 12:1 methanol to oil molar ratio, NaOH as catalyst

[1] Renewable and Sustainable Energy Laboratory, Department of Mechanical Engineering, Sardar Vallabhbhai National Institute of Technology, Surat, Gujarat, India.

* *Corresponding author's e-mail: kasorate@med.svnit.ac.in*

(0.6 w/v), and a reaction temperature of 60°C for 60 min (Benjumea *et al.*, 2007). In other study, palm biodiesel was prepared using a transesterification process (reaction temperature 60°C for 60 min; 10:1 methanol to oil molar ratio, KOH as catalyst (1.4 w%; stirring 250 rpm). Engine performance of B20 blend showed that brake specific fuel consumption (BSFC) increases while brake thermal efficiency (BTE) and emission decreases except NO_x as compared to diesel (Rosha *et al.*, 2019). *Table 1* shows the European Standards of NO_x emission.

The lubrication properties of fuel/biofuel can increase the engine's life. Biodiesel generally possess better lubricity than diesel (Mishra & Goswami, 2017). Tribological properties depend upon the load and temperature. Diesel engine components such as fuel pumps and injectors are lubricated by fuel itself. The wear and friction properties of the biodiesel samples should be equivalent to or better than that of the conventional diesel used in automobiles. It was found that the addition of nanoparticles and alcohol improves the lubricity of B30 (diesel-palm-sesame) biodiesel (Mujtaba *et al.*, 2020). For Aamla biodiesel, the tribological properties were affected at higher loads and higher temperatures compared to low loads and lower temperatures (Singh *et al.*, 2018). The lubricating characteristics of biodiesel in terms of friction and wear decrease as the temperature of the fuel rises (Haseeb *et al.*, 2009). Compared to diesel, the wear and friction coefficients of B20 (palm and cottonseed biodiesel) were lower.

The long hydrocarbon chains of biodiesel decreased the friction and improved lubrication (Jamshaid *et al.*, 2021). Biodiesel was found corrosive to engine components when stored for long durations (Sorate & Bhale, 2013; 2018), but its better lubricity resulted in less friction and wear (Fazal *et al.*, 2014). The wear and friction coefficient reduces as the biodiesel concentration increases from B10 to B100. It's because of the compositional nature of biodiesel (Fazal *et al.*, 2013). Tertiary blends of biodiesel improved the lubrication property of palm (B10) biodiesel when blended with plastic pyrolysis biodiesel and waste cooking oil biodiesel (Awang *et al.*, 2022). Through tribological testing, biolubricants were found the most promising lubricant. *Jatropha* biolubricant was tested for tribological characteristics. The use of a 20% *Jatropha* biolubricant blend was found to be efficient in minimising friction and wear on the pins used in the tests (Anand *et al.*, 2021).

Engine performance of palm oil biodiesel blends was found to be satisfactory except NO_x emissions (Lim & Teong, 2009). Palm oil biodiesel contains about 49.2% oleic acid, palmitic acid (43.3%) and stearic acid (5.4%). Oleic acid is a good carrier of hydrogen and oxygen (Ali *et al.*, 2015). Hydrogen concentration (up to 5%) demonstrates a minor reduction in NO_x. However, as H_2 concentration rises, NO_x levels rise as well. A controlled increase in oleic acid content resulted in a reduction in NO_x emissions for Karanja (*Pongamia*) biodiesel (Dinesha *et al.*, 2017; Mohan *et al.*, 2021). The use of B10, B20 biodiesel from rice bran and Pongamia, along with hydrogen enrichment (7 L/min), can improve brake thermal efficiency by up to 6%. However, when compared to diesel, the NO_x from blended biodiesel with hydrogen increases by up to 13% (Kanth & Debbarma, 2021). Diesel, on the other hand, produced more NO_x than algae, or Jatropha oil (Krishania *et al.*, 2020). Water emulsified biodiesel can reduce harmful emissions. Emulsified palm biodiesel (B10, B15 and B20) were prepared using ultrasonication. A decrease in NO_x was observed for emulsified fuel. However, the calorific value decreases, and viscosity increases with an increase in the blending ratio (Azahari *et al.*, 2016).

The properties of biodiesel can be improved by adding additives. Further improvements to the combustion phenomenon can be made, resulting in lower emissions (Gaur *et al.*, 2022). The addition of 2% ethanol lowers the smoke emissions. It was found that adding ethanol to canola biodiesel reduces emissions (Öztürk & Can, 2022). Compared to diesel, biodiesel emits more NO_x due to oxygen in biodiesel. NO_x emissions were revealed as a result of a higher combustion temperature. There have also been initiatives taken across the globe on the production of second-generation ethanol. The plant-based feedstock would help to improve the farmer's income. Although ethanol is not an ideal alternative fuel for diesel engines, it can be added to reduce fuel viscosity, and density as well as improve the cold flow performance (Yilmaz *et al.*, 2017).

The binary blends of waste oil biodiesel with higher alcohols (propanol, n-butanol and 1-pentanol) on semi-low temperature combustion in diesel engines showed lower NO_x emissions (Atmanli & Yilmaz, 2019). On the other hand, the ternary blends of diesel, crude vegetable oil and n-butanol showed an increase in oxides of nitrogen (Atmanli *et al.*, 2015). Combustion of diesel, rapeseed oil, and n-butanol in turbocharged engines showed an increase in NO_x formation (Ileri *et al.*, 2015; Örs

TABLE 1. NO_x EMISSION STANDARDS OF EUROPEAN HEAVY DUTY DIESEL ENGINE

Tier	Euro I	Euro II	Euro III	Euro IV	Euro V	Euro VI
Year	1992	1996	2000	2005	2008	2013
NO_x level (g/kWh)	8.0	7.0	5.0	3.5	2.0	0.4

et al., 2020). Moreover, a quaternary blend of diesel, waste oil biodiesel, soybean oil and higher alcohols showed an 11.9% reduction in oxides of nitrogen (Yilmaz *et al.*, 2017). The optimised diesel, butanol, and cottonseed oil blend also showed decreased NO_x for variable speed engines (Atmanli *et al.*, 2016). Along with experimental methods, predicting methods such as the response surface method and least-squares support vector machine models can be used for engine performance and emission parameters (Ileri *et al.*, 2016).

The web of science data analysis was done on 10th October, 2023 for the availability of research papers in the area of biodiesel, palm biodiesel, NO_x reduction and tribology. A total 44,849 research articles were found. Out of this, 4,273 articles were found related to palm biodiesel. Out of 4,273, only 140 were found on NO_x reduction and 46 were found on tribology. The data is presented as shown in *Figure 1*.

Sufficient work related to tribological behaviour and emissions of lower blends such as B10, and B20 of biodiesel with conventional diesel has been reported in the literature. The novelty of this research paper is that higher blends (B80 and B90) of palm biodiesel on tribology and emission are investigated which is very exiguous in the open literature. Also, studies related to the reduction of NO_x emission by means of blending with oxygenated compounds are very limited. Therefore, the main aim of this study is to investigate experimentally the tribological assessment and NO_x emissions of higher blends of palm biodiesel blended with oleic acid and ethanol. The materials and methodology related to biodiesel feedstock selection, production, characterisation, tribological characteristics, engine testing, and results are discussed in subsequent sections. The flowchart of the work performed is shown in *Figure 2*.

MATERIALS AND METHODS

Refined palm oil was obtained from the nearby convenience store, while diesel was purchased from a local fuel station. A local supplier provided methanol, KOH (potassium hydroxide), OA (oleic acid), and ethanol.

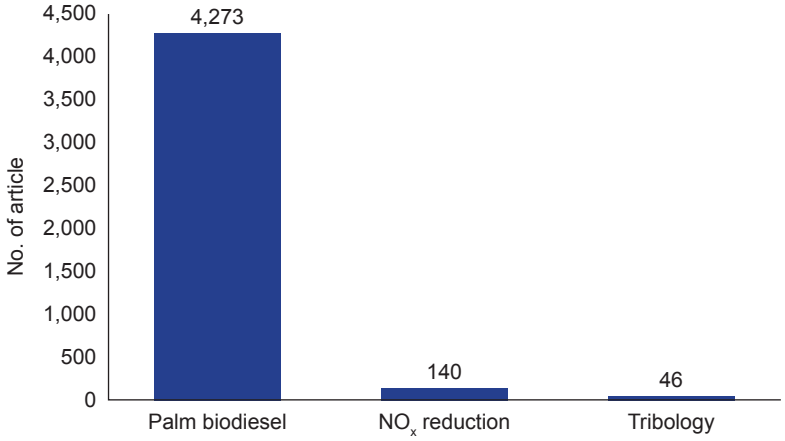


Figure 1. Number of research articles available in the area of palm biodiesel.

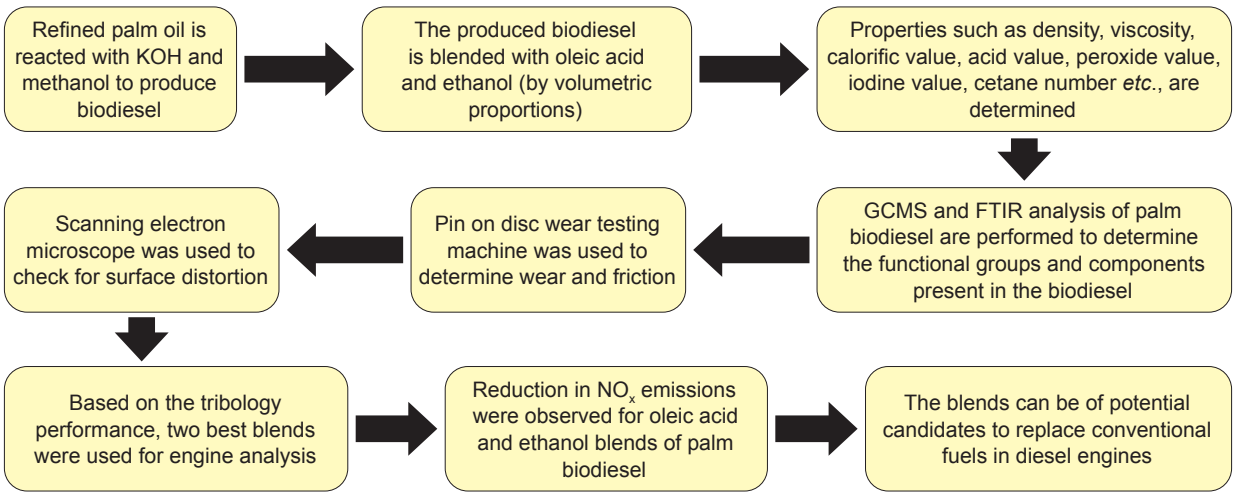


Figure 2. Flowchart of the work.

Transesterification

The palm oil was mixed and heated to 60°C using a magnetic stirrer. A borosilicate condenser with water as a coolant was used to cool the methanol solution. Methanol - oil molar ratio of 1:7 and 1.2% w/v of KOH were used as the catalyst. The stirring speed was maintained at 700 rpm. The reaction was carried out for an hour while maintaining the temperature at 60°C. The resulting solution was placed in a decantation flask and left undisturbed for an hour. The crude glycerol and the biodiesel separated due to the density difference. Glycerol was removed and the remaining solution was water-washed to remove dissolved KOH and other impurities. The fatty acid methyl ester was heated in the oven to vaporise moisture in the solution. The entire process of transesterification is depicted in *Figure 3*.

The blending of the test fuels was carried out based on volumetric proportions, and five test fuels, namely B100 (100% palm biodiesel), B90OA10 (90% palm biodiesel + 10% oleic acid), B90OA10E5 [95% (90% palm biodiesel + 10% oleic acid) + 5% ethanol], B80OA20 (80% palm biodiesel + 20% oleic acid) and B80OA20E10 [90% (80% palm biodiesel + 20% oleic acid) + 10% ethanol], were prepared.

Characterisation

The quality of the produced biodiesel depends on many factors, such as the properties of feedstock, the catalyst used, reaction parameters, *etc.*, Certain physio-chemical parameters must be evaluated to check the quality of produced biodiesel. Some of the critical attributes of liquid fuel include density, kinematic viscosity, calorific value, pour point, cloud point, acid value (AV), peroxide value (PV), iodine number, saponification number and cetane number (CN). All biodiesel and its blends were characterised to ensure compliance with ASTM (American Society for Testing and Materials) and EN (European Standards) standards.

The energy content of the biodiesel blends was determined using a LECO 350 bomb calorimeter. The density was measured as per ASTM D1298 standard. The viscosity of the test fuels was assessed using a Redwood viscometer. The flashpoint was measured with Cleveland open-cup apparatus. A cloudy white appearance was observed at the temperature known as cloud point. The pour point is the temperature where biodiesel loses its flowability and is determined by adding 3°C to the observed temperature. The detailed procedure for determining the AV, PV and CN is mentioned in Annexures A, B and C respectively. Fourier Transform InfraRed (FTIR) spectroscopy is the most widely used tool to predict the functional groups present in biodiesel. FTIR spectroscopy was carried out using a Shimadzu IRAffinity-1S spectrometer. The procedure of FTIR is mentioned in Annexure D. The instruments used for evaluating the characteristics of the test fuels of the study are shown in *Figure 4*.

The contents of the fatty acids in palm biodiesel were determined using gas chromatography and mass spectrometry (SHIMATZU QP 2010). By comparing their retention durations to those of a typical methyl ester of fatty acids, the composition of methyl ester was determined.

Configuration of Pin on Disc (POD) Wear Tester

Ducom POD wear tester was used to perform a tribological assessment of the sample. Pins made of stainless steel were used in the process. This test measured the amount of wear and frictional force. The apparatus consists of a pin that provides a normal load. A uniform volume flow of 10 mL/min of test fuel was maintained over the disc to ensure proper contact with the pin. The rpm, load, time, and offset distance from the centre are given as input to the wear and friction monitor. Diesel was used to compare with the results of biodiesel and its blends. Scanning Electron Microscope (SEM) was used to study the surface of pin tips post POD testing. The experimental setup and the specifications of the tribometer are described in *Figure 5* and *Table 3* respectively.

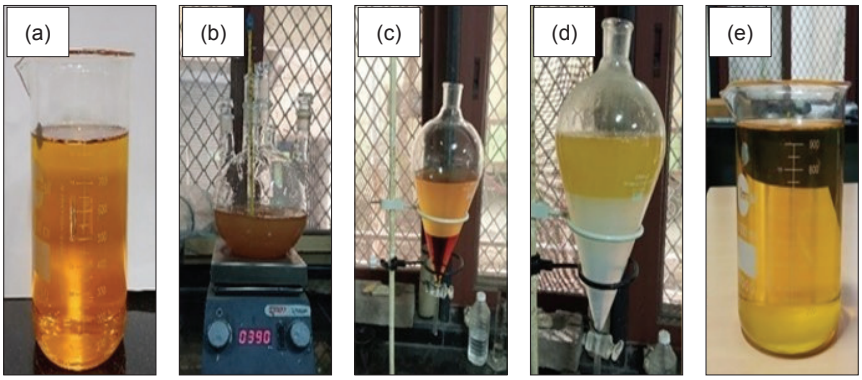


Figure 3. Transesterification process (a) refined palm oil, (b) reactor vessel, (c) glycerol separation, (d) water washing and (e) palm biodiesel.



Figure 4. Instruments used for the characterisation study.

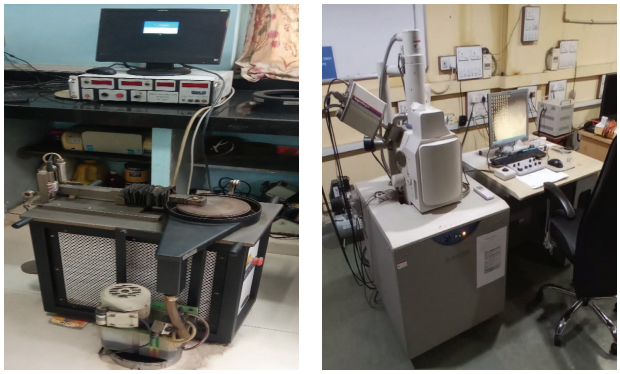


Figure 5. Experimental setup of the POD wear tester and SEM used in the study.

TABLE 3. SPECIFICATIONS OF POD WEAR TESTER AND PARAMETERS SET FOR THE STUDY

Make	Ducom
Disc speed	200-2,000 rpm
Normal load range	5-200 N
Wear range	± 2 mm
Least count	1 ± 1% μ
Frictional force range	0 to 200 N
Accuracy	0.1 ± 2.0% N
Load	5 kg
Rotating speed	200 rpm
Sliding distance	1,500 m
Time	720 s
Temperature	30°C

Configuration of Engine Test Rig

Based on the characterisation and tribological study, conventional diesel and three biodiesel test fuels B100, B80OA20 and B80OA20E10, were chosen for engine testing. A computerised test rig consisting of four-strokes, a 5.2 kW diesel engine, and Testo gas analyser was used to evaluate engine performance, emissions, and combustion of test fuels. The specifications and details of instrumentation used in the engine setup and the experimental setup of the test rig are depicted in *Table 4* and *Figure 6* respectively.



Figure 6. Experimental setup of the engine test rig.

TABLE 4. SPECIFICATIONS OF THE CI ENGINE

Make	Kirloskar TV1
General details	Four-strokes, CI, vertical, constant speed, water-cooled, single cylinder
Bore × stroke (mm)	87.5 × 110
Compression ratio	17.5
Capacity (cc)	661
Rated output (kW)	5.2 at 1,500 rpm
Piezo sensor make	PCB Piezotronics, Model HSM111A22
Inlet valve opening / Inlet valve closing	4.5° before TDC / 35.5° after BDC
Exhaust valve opening / Exhaust valve closing	35.5° before BDC / 4.5° after TDC
Injection advance	23° before TDC

Note: CI - compression ignition; BDC - bottom dead centre; TDC - top dead centre.

The load to the engine was applied with a dynamometer. The constituents of exhaust gases were measured using an emission analyser. Data on fuel flow, torque, water flow rate, and other parameters were obtained using a data-gathering system.

Uncertainty Analysis

The validity of the obtained results depends upon the instruments' accuracy and techniques used in the process. The characterisation, engine testing, and tribological studies involve the use of many instruments and equipment, which leads to the need to perform uncertainty analysis. Each experiment was carried out thrice, and the average was presented. The uncertainties of the individual experiments carried out in this research work are shown in *Table 5*. The uncertainty of the results was calculated using the root mean square approach and was found to be ± 2.1%.

$$\text{Overall uncertainty} = \sqrt{\begin{matrix}CV^2 + Density^2 + KV^2 + AV^2 + \\ PV^2 + Wear^2 + Friction^2 + BTE^2 + \\ BSFC^2 + CO^2 + NO_x^{\ 2} + CO_2^{\ 2}\end{matrix}}$$

$$= \sqrt{\begin{matrix}0.5^2 + 0.4^2 + 0.6^2 + 0.5^2 + 0.6^2 + \\ 0.2^2 + 0.7^2 + 0.7^2 + 0.4^2 + 0.6^2 + \\ 0.3^2 + 1.2^2\end{matrix}}$$

$$= \pm 2.1\%$$

where, KV is kinematic viscosity, AV is acid value, PV is peroxide value, BTE is brake thermal efficiency, BSFC is brake specific fuel consumption, CO is carbon monoxide and CO_2 is carbon dioxide.

RESULTS AND DISCUSSION

The results obtained from the experimentation of biodiesel and its blends are discussed in the following section. The characterisation, tribology, and engine testing of the blended test fuels will also be discussed in this section.

Characterisation of Biodiesel Blends

The characterisation of biodiesel and blends was carried out, and is listed in *Table 6*. Blending OA with B100 reduced the CV and PV but increased the density and acid value. The blending of OA increased the acid value beyond the permissible limit. The viscosity of the OA was also higher than pure biodiesel. 10% blending restricts the kinematic viscosity within the allowable limit. Further blending takes it beyond the permissible limit of 6 mm^2/s as per ASTM standards. The cold flow properties of OA measured is lower than B100. Thus, blending reduced the cloud and pour point, and ethanol addition further augmented them. The addition of ethanol reduced the calorific value of the blended test fuels.

The FTIR analysis of the palm biodiesel produced by transesterification is illustrated in *Figure 7*. The bending vibration at a wavenumber of 1,743.650 and 1,168.862 cm^{-1} represents the C=O and C-O bonds of the esters, respectively. The stretching band at 2,854.648 cm^{-1} denotes the formation of alkanes. These peaks reflect the ester component in the biodiesel sample (Abdullah *et al*., 2017). A significant difference was seen in the fingerprint region corresponding to 900-1,500 cm^{-1}. The rocking vibration of C-H can be noted at 721.37 cm^{-1}. A more substantial peak was observed for the biodiesel sample than palm oil, indicating the conversion of triglycerides to fatty acid methyl esters during transesterification (Kamaronzaman *et al*., 2020). The comparison plot indicates fatty acid methyl ester formation obtained post-transesterification.

From GC-MS analysis, the percentages of palmitic acid (C16:0), oleic acid (C18:1), linoleic acid (C18:2) and stearic acid (C18:0) in palm biodiesel are respectively 41.25, 38.91, 11.65 and 5.73.

TABLE 5. UNCERTAINTY ANALYSIS OF EXPERIMENTATION

Instrument used	Accuracy	Uncertainty (%)
Calorific value (CV)	± 0.5%	± 0.5
Density	± 0.01 g/cc	± 0.4
Kinematic viscosity (KV)	± 1.0%	± 0.6
Acid value (AV)	± 0.1 mL	± 0.5
Peroxide value (PV)	± 0.2 mL	± 0.6
Wear	± 1.0% µm	± 0.2
Friction	± 2.0% N	± 0.7
BTE	± 0.5%	± 0.7
BSFC	± 0.5 kg/kWh	± 0.4
CO_2	± 0.2% vol	± 0.6
NO_x	± 10 ppm	± 0.3
CO	± 10 ppm	± 1.2

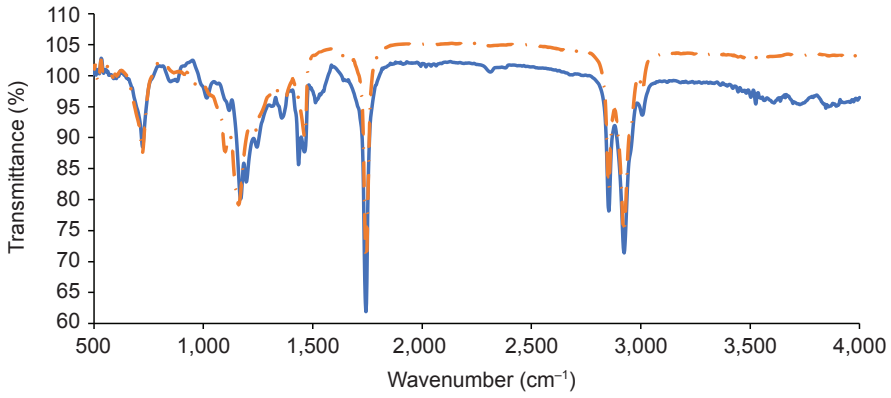


Figure 7. FTIR spectroscopy of palm oil and B100.

TABLE 6. MEASURED PHYSIO-CHEMICAL CHARACTERISTICS OF BIODIESEL AND ITS BLENDS

Property	Standards	Limit	B100	B90OA10	B90OA10E5	B80OA20	B80OA20E10	OA	Diesel
Calorific value (kJ/kg)	ASTM D6751	-	40,493.17	40,014.52	39,013.07	39,827.91	38,845.12	39,516.20	42,000
Cloud point (°C)	ASTM D2500	-3 to -12	17	11	8	5	3	1	-6
Pour point (°C)	ASTM D97	-15 to -16	14	8	5	2	0	-2	-30
Kinematic viscosity @ 40°C (cSt)	ASTM D445	1.9 to 6.0	4.59	5.65	5.1646	8.16	5.7732	18.74	4.6
Density (kg/m^3)	ASTM D1298	820-860	866.67	873	869	881	876	906.67	830
Flashpoint (°C)	ASTM D93	130	176	182	85	185	92	192	58
Acid value (mg KOH/g)	ASTM D664	0.5 maximum	0.369	17.403	16.3158	34.465	30.44025	198.5	-
Free fatty acid (%)		-	0.185	8.74	8.1988	17.32	15.296	99.75	-
Peroxide value (meq/kg)	AOAC 965.33		16.614	13.745	14.730	10.896	13.698	2.904	-
Iodine value (gI_2/100 g)	EN-14111	-	57.975	61.17	58.111	64.364	57.927	89.921	-
Saponification value	-	-	207.452	206.53	196.206	205.65	185.05	198.25	-
Cetane number	-	47 minimum	59.565	58.968	54.463	58.3717	51.067	53.5985	48

Pin on Disc (POD) Wear Testing

The following section discusses the friction characteristics, wear analysis, and surface morphology of the pins used in POD testing.

Friction analysis. Lubrication is required to reduce the friction in different engine components, thereby reducing wear and improving the engine's life span. The frictional force obtained for each sample with respect to sliding distance is as shown in *Figure 8a*. The fluctuation is due to the variation in surface roughness and contact area of the pin tip with the disc. The blends and additives of palm biodiesel show a lesser frictional force than that of conventional diesel. A significant reduction in friction force was observed upon ethanol addition. The B80OA20E10 reduced the frictional force by 43% on average with reference to B80OA20, thereby showing the least frictional force compared to all the test fuels. The presence of ester groups (RCOOR) provides sufficient adhesion to form a tribofilm with the pin surface, exhibiting better anti-friction capability (Chan *et al.*, 2018). The higher viscosity of sample oil reduces the metal-to-metal contact during the experimentation (Kurre & Yadav, 2022). This explains the reduction in friction force on addition upon blending of OA to B100. The addition of ethanol further reduced the frictional force of the blend. The high polarity of ethanol aids in reducing the contact between pin and the disc (Sorate & Bhale, 2014).

Wear analysis. *Figure 8b* demonstrates the wear in the pins with respect to distance. The amount of wear generated in each pin tip of different test fuels was calculated by finding the difference in wear at the start and end of the experimentation. The wear was the highest in the B100 sample, with 53.03 µm after the entire run. Nearly 25% reduction in wear has been recorded for B90OA10 compared to B100. The wear observed in the pins by B80OA20 was lower than diesel. The addition of

OA has significantly reduced the wear of the pin. Nearly 40% reduction in wear and 48% reduction in friction was observed for B80OA20 compared to B90OA10. The B90OA10E5 reduced wear by 11% compared to B90OA10. On the contrary, 10% ethanol additive to B80OA20 increases the wear by 70% to 40.47 µm. The blending of OA by 20% has reduced the wear by nearly 55% compared to B100 sample. The reduction in wear of B80OA20 and B90OA10 might be due to the higher composition of unsaturated compounds than B100, which aids in forming a stronger layer of film between the metals (Zaid *et al.*, 2020). The shorter carbon chains in the esters and higher polarity of compounds enhance the lubricity of the test sample (Sorate & Bhale, 2014). Hence, ethanol having higher polarity, act as an emulsifier forming strong emulsions with B80OA20.

Surface morphology analysis. The surface morphology of the pin post-wear testing for the test fuels is shown in *Figure 9*. The obtained micrographs can be correlated with the friction force and wear, as shown in *Figure 8a* and *8b*. Indentations are present for B100 in the direction parallel to the wear, indicating abrasion. The B100 has a lower viscosity than OA blends, leading to higher surface contact with the disc. The images for the diesel show severe delamination of the pin surface (Maleque *et al.*, 2000). Surface distortion in the form of pits can be observed in B90OA10 and B80OA20 samples. Bubbles in the order of 300 µm^2 can be observed for the B80OA20E10 sample. This may be due to the agglomeration of ethanol molecules on the pin surface. The level of micro-pitting was observed to be higher for B90OA10 compared with the B80OA20 sample.

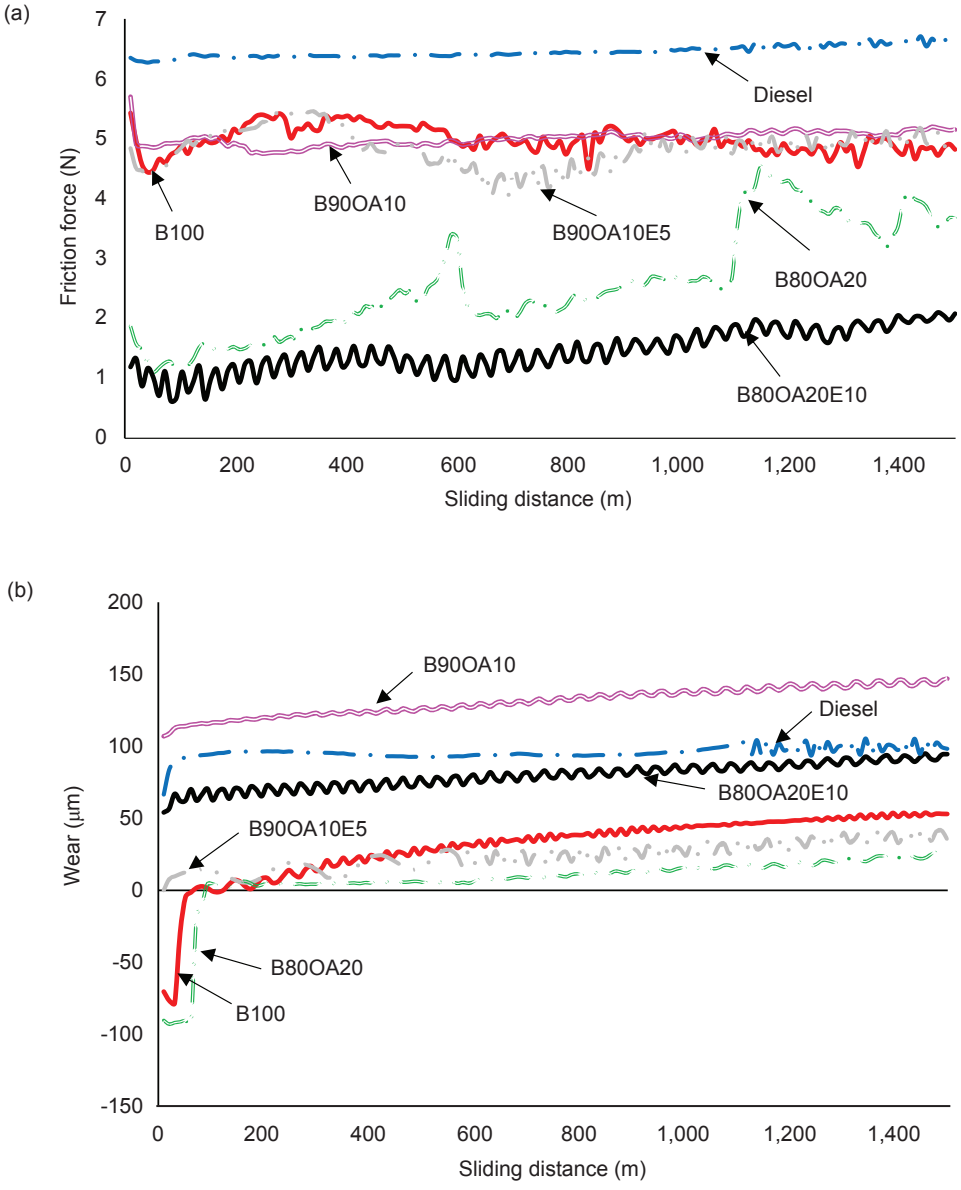


Figure 8. (a) Friction force variation and (b) wear of pins for different test fuels with respect to sliding distance.

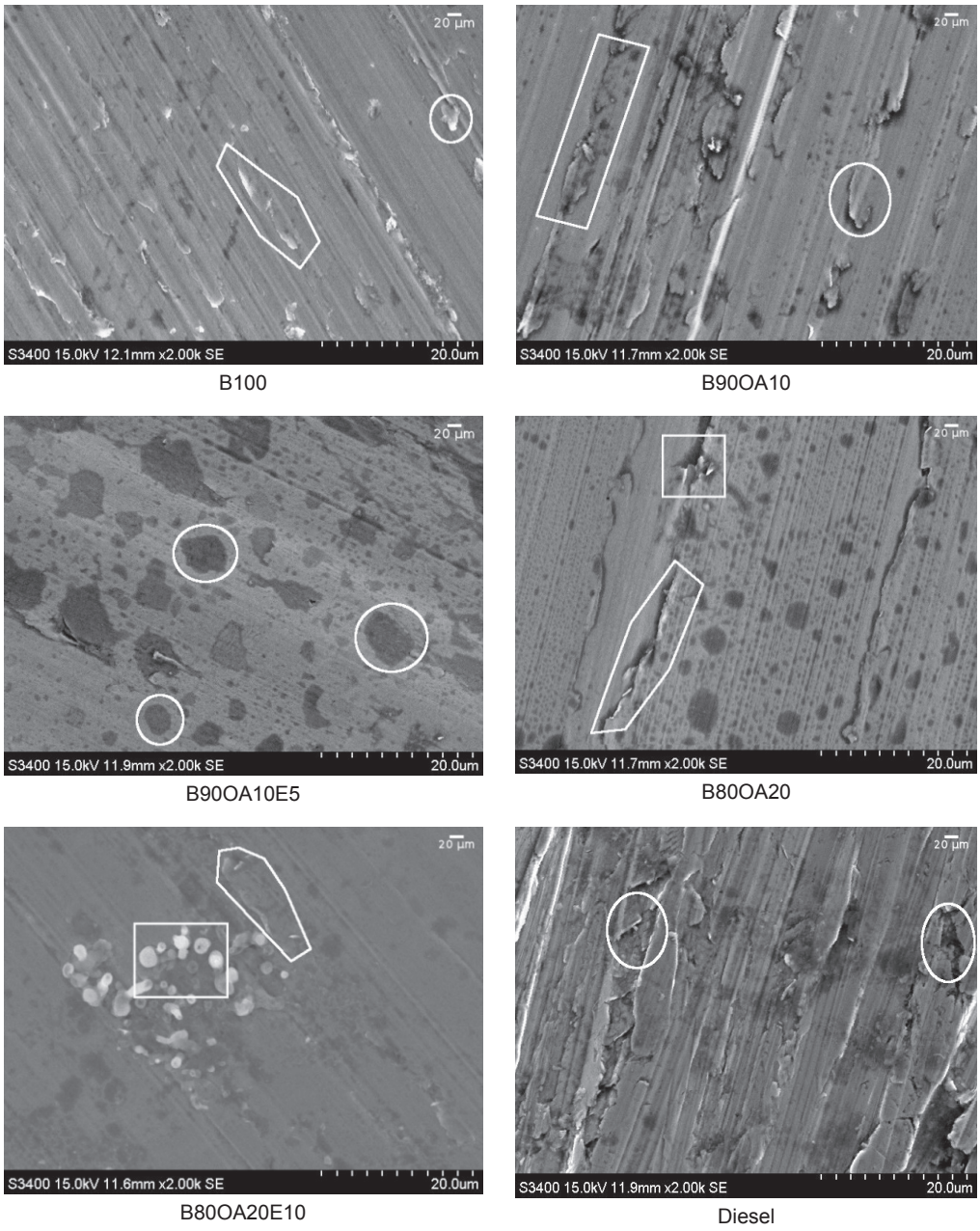


Figure 9. SEM micrographs of pin tip after POD wear test.

Engine Performance, Combustion and Emission Analysis

This section discusses the engine performance, combustion, and emission of B100, B80OA20, B80OA20E10 and diesel.

Brake thermal efficiency (BTE). BTE is the ratio of brake power available at the output of the shaft to the heat supplied by the fuel. *Figure 10a* presents the BTE of all the test fuels varying with brake mean effective pressure (BMEP). Conventional diesel exhibits the highest BTE of 35.22%, followed by B80OA20, B100 and B80OA20E10 of 33.49%, 32.29% and 32.02%, respectively, at BMEP of 5.5 bar. Performance is improved using fuel with a higher heating value and lower flash point. Complete fuel combustion is ensured by high cylinder pressure and temperature, leading to greater efficiency. The result obtained for the conventional diesel was consistent with the literature (Rajamohan *et al.*, 2022). The higher density and kinematic viscosity of biodiesel blends account for the decrease in BTE compared to diesel (Sakthivel *et al.*, 2017). On the contrary, adding OA to B100 has shown a positive effect on BTE, increasing it by 3% compared with B100. This can be explained by the fact that OA contains oxygenated molecules, which improve fuel burning (Mohan *et al.*, 2021). The lower calorific value of B80OA20E10 has led to lower BTE among

all the samples. Due to ethanol's lower boiling point, the fuel mixture burns ineffectively during combustion (Rahiman *et al.*, 2021).

Brake specific fuel consumption (BSFC) (kWh). The fuel consumption for a unit kilowatt hour of power generation for different test fuels is shown in *Figure 10b*. The brake power is directly proportional to BMEP; hence, fuel consumption decreases with a rise in BMEP. Conventional diesel shows the lowest BSFC of 0.23 kg/kWh at 5.5 bar BMEP while B100 and B80OA20E10 exhibit BSFC of 0.28 kg/kWh. The BSFC increases by 0.01 to 0.28 kg/kWh on addition of 10% ethanol to B80OA20. Increased calorific value and reduced viscosity of the diesel help in the finer mixing of the fuel, reducing fuel consumption (Rajamohan *et al.*, 2022). A very minuscular effect in fuel consumption is observed between B100 and B80OA20, with the latter showing a slightly higher consumption than the former. The increase in BTE of B80OA20 compared to B100 has led to a reduction in BSFC.

Peak pressure. Peak cylinder pressure for various fuels with respect to crank angle (in °) is shown in *Figure 11a*. The 0° indicates the TDC of the engine cylinder. A slight ignition delay can be observed for all the test fuels due to the atomisation and premixing stage of combustion. However, the B100 sample attained peak pressure at 47.51 bar at 8° compared to B80OA20 at 9°. The B80OA20 exhibits nearly a 15% rise in the peak pressure to 55.43 bar compared to the 47.95 bar attained by the B100 sample. Higher viscosity and density of B80OA20 cause poor fuel atomisation. Thus, fuel gets accumulated, and a greater quantity of fuel gets injected inside the combustion chamber, leading to a rise in the peak pressure. *Table 6* illustrates that B80OA20 possesses a viscosity nearly double that of B100. Ethanol addition to B80OA20 has lowered the blend's viscosity and CN. However, it has raised the peak pressure to 60.87 bar, comparable to 61.99 bar attained by conventional diesel. This may be due to the vaporisation of ethanol before the ignition phase (Rahiman *et al.*, 2021). The lower CN and higher latent heat of vaporisation of B80OA20E10 would have augmented the peak pressure (Kim *et al.*, 2020). The peak pressure relies on the oxidation level attained during the premixing phase of combustion.

Cumulative heat release rate (CHRR). CHRR was plotted with respect to the crank angle (in °), as shown in *Figure 11b*. The rate at which the flame consumes the unburned mass of fuel charge is

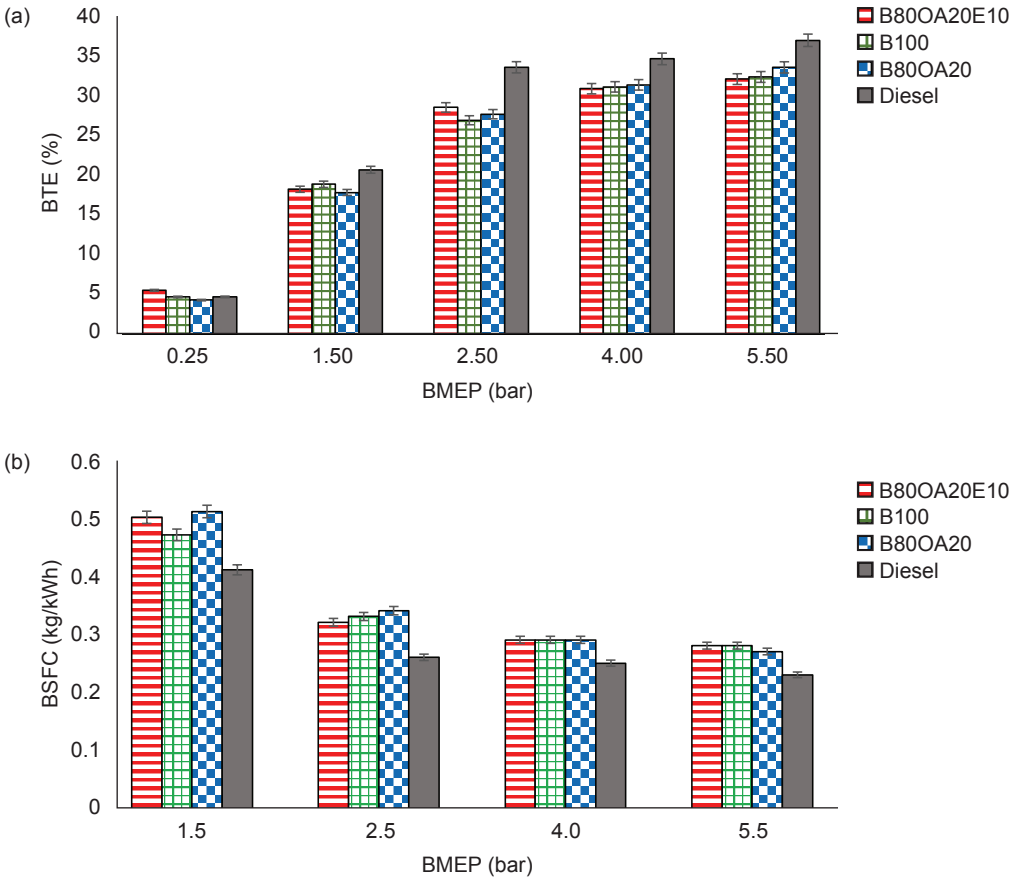


Figure 10. Variation in (a) BTE and (b) BSFC with respect to BMEP.

known as CHRR. The diesel exhibits the highest CHRR of 1.08 kJ at 63°, while the B100 shows the least CHRR of 0.61 kJ at 47°. Lower CN has increased the ignition delay of diesel compared to biodiesel and its blends. The shorter ignition delay period caused by the higher CN of B100 allows fuel to ignite more quickly and easily. The higher CN of B100 has lowered the ignition delay period compared to B80OA20 and B80OA20E10. Adding OA increased the CHRR by 36% to 0.83 kJ at 53° and B80OA20E10 recorded a CHRR of 0.95 kJ at 57°. The increase in CHRR was due to the increase in adiabatic flame temperature (Kim *et al.*, 2020). The higher oxygenated and hydrogen components in the B80OA20 than in B100 aid in complete combustion, resulting in higher CHRR (Mohan *et al.*, 2021). The higher viscosity and density lead to fuel accumulation in the cylinder, increasing the fuel available for combustion (Santhoshkumar *et al.*, 2019).

Exhaust gas temperature. The exhaust gas temperature of different test fuels is shown in *Figure 12a*. Diesel showed the highest temperature of 321°C, followed by B100 and B80OA20E10 at 320°C and 314°C at 5.5 bar. All the test fuels show an increase in temperature with BMEP. B80OA20 has a greater viscosity, resulting in poor atomisation. The lower calorific value of biodiesel and higher CN leads to lower exhaust gas temperature (Enweremadu & Rutto, 2010). Higher temperature augments the formation of NO_x emissions (Rajamohan *et al.*, 2022).

NO_x emissions. As shown in *Figure 12b*, an increasing trend in NO_x emissions with the BMEP can be observed for all test fuels. Higher in-cylinder temperature and pressure favor NO_x emissions. NO_x majorly consists of NO and NO_2. NO formation is profound at lean air-fuel ratio. At lean fuel conditions, combustion NO is formed.

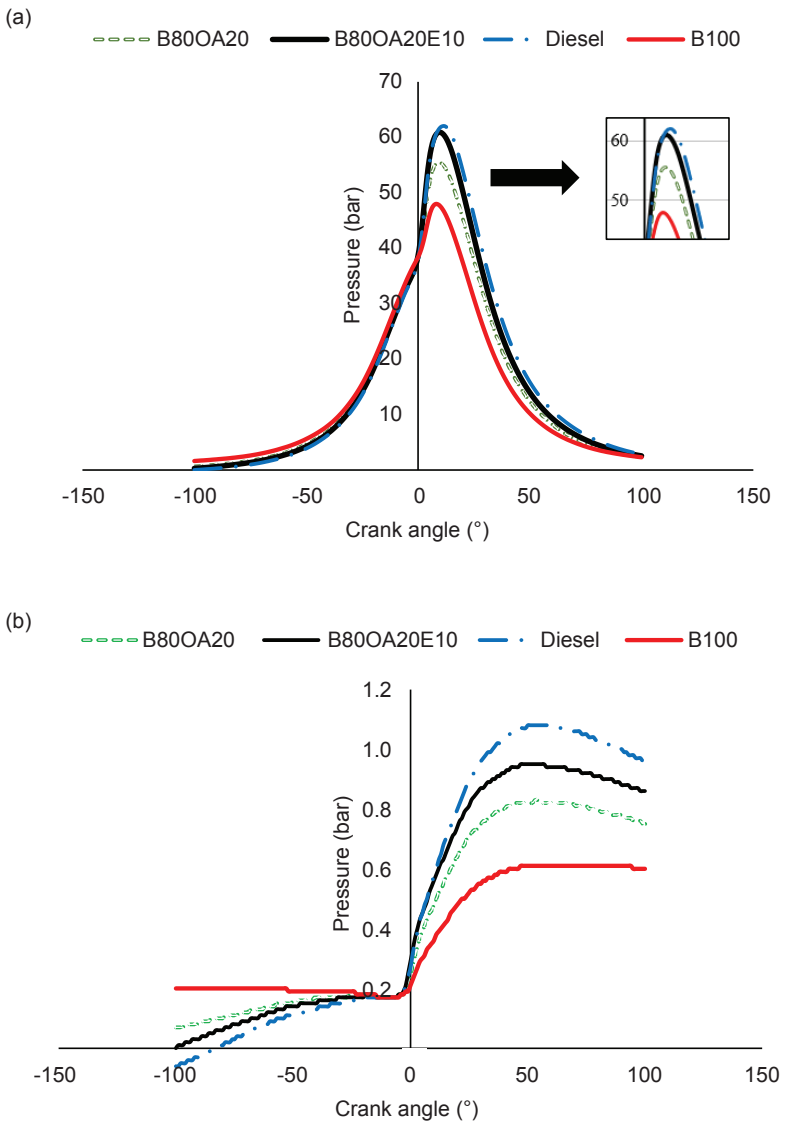
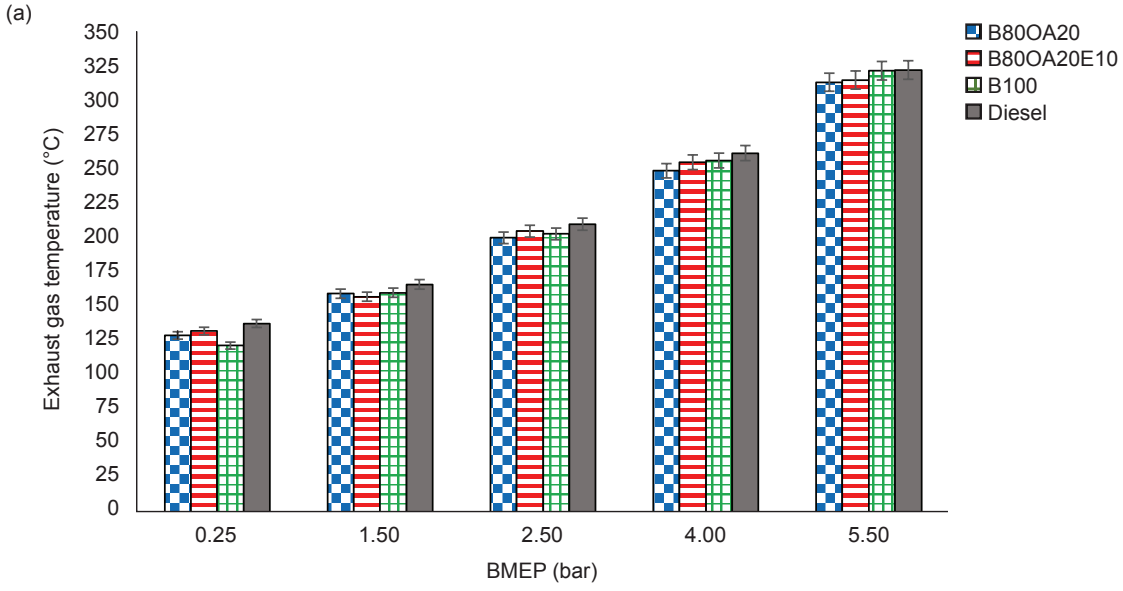


Figure 11. (a) Peak pressure and (b) cumulative heat release rate (CHRR) with respect to crank angle.

Zeldovich mechanism governs the NO_x formation (Shote *et al.*, 2018). At lean fuel conditions, more air is available for combustion. As a result, the nitrogen and oxygen present in the air starts reacting with the fuel at a higher temperature, increasing NO_x emissions. Adding OA has shown a positive impact in reducing NO_x emissions. B100 has shown the highest NO_x emission of 769 ppm among all the samples at 5.5 bar BMEP. The oxygen in the fatty acids of biodiesel aids atmospheric nitrogen's reaction, thereby augmenting NO_x formation. However, with the addition of 20% OA by volume, the emissions have decreased by 17.3% to 636 ppm. OA has a higher viscosity, lower boiling point and higher evaporation rate; hence it supports NO_x emission reduction when blended with biodiesel. The higher density of palm biodiesel gives a higher residence time for the fuel to stay in the high-temperature region, which increased the NO_x emission. Another reason might be due to the higher bulk modulus of compressibility of biodiesel, advancing the injection timing. The presence of hydrogen concentrations also helps in reducing NO_x emissions, and OA ($C_{18}H_{34}O_2$), being a carrier of hydrogen, aids in the reduction of NO_x. Oxygenated compounds reduce the flame temperature and thus improve combustion efficiency. NO_x emissions increased by 11.3% for B80OA20E10. Adding ethanol reduced the blend's density and viscosity, resulting in lower NO_x emission than B100. Similar trends were also observed by some researchers (Lee *et al.*, 2020).

CO emissions. *Figure 12c* displays the change in CO emissions with BMEP for all test fuels. A decreasing trend is noticed for all the test fuels. Adding ethanol by 10% to B80OA20 increased the emissions by nearly 25% to 571 ppm at 5.5 bar pressure. While performing the combustion in a stoichiometric air-fuel ratio, the hydrocarbons present in the fuel would get oxidised to CO_2 and H_2O (Lee *et al.*, 2020). In fuel-rich conditions, these hydrocarbons do not oxidise to CO_2 and instead form CO, indicating an incomplete oxidation condition. A lower carbon to hydrogen ratio in B100 might have reduced CO emissions (Niyas & Shaija, 2022). The addition of ethanol leads to viscosity reduction and enhances the atomisation of fuel in the injector. However, the results indicate a higher CO emission for B80OA20E10. Ethanol's higher latent heat and evaporative cooling effect would have resulted in partial combustion. Additionally, higher ignition delay would have increased the CO emissions (Shahir *et al.*, 2015).

CO_2 emissions. *Figure 12d* indicates CO_2 emissions, and all the test fuels show an increasing trend with BMEP. The B80OA20E10 shows the highest emission of 7.560% volume, followed by 7.400% volume from the B100 sample and 7.353% volume by diesel at 5.5 bar BMEP. The B80OA20 sample showed the lowest emission of 7.230% volume. The CO_2 emissions get augmented with the rise in BMEP for all the test fuels. The complete oxidation of the fuel leads to the formation of CO_2 (Rajamohan *et al.*, 2022). The higher CO_2 emissions indicate the degree of complete combustion. The formation of CO_2 is highly favourable for renewable sources of fuel as it aids in maintaining a closed carbon cycle, thereby reducing global warming (Sakthivel *et al.*, 2019). An explicit trade-off is observed in the sample's CO and CO_2 emissions trends for B100, B80OA20 and diesel. However, B80OA20E10 showed the highest CO and CO_2 emissions. A higher quantity of oxides of carbon is produced when oxygen is available in fuel.



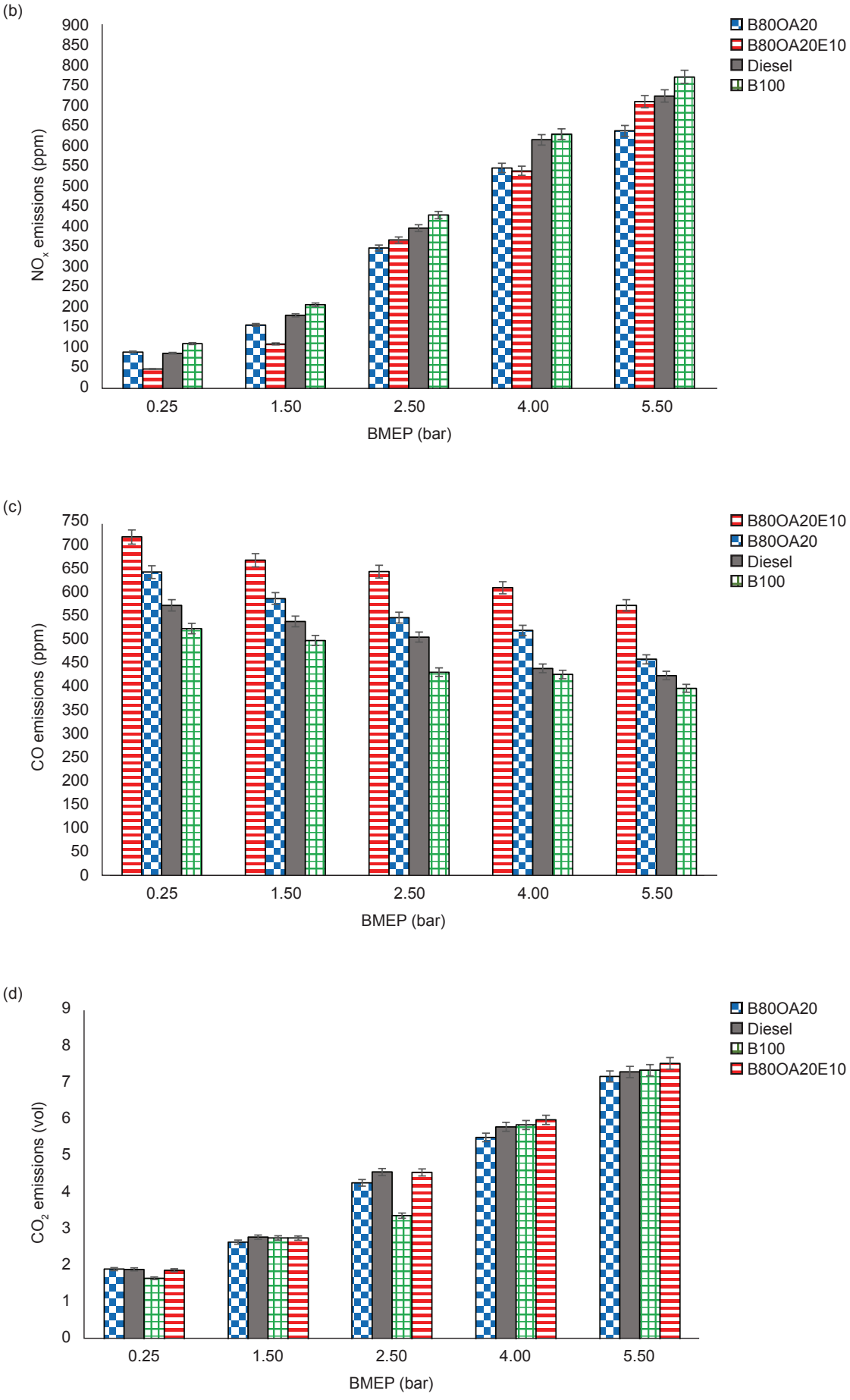


Figure 12. (a) Exhaust gas temperature, (b) NO_x emissions, (c) CO emissions and (d) CO_2 emissions with respect to BMEP.

CONCLUSION

The prepared biodiesel and blends were characterised by following the required standards. The properties of prepared biodiesel and blends were found to be comparable with diesel. A tribological assessment was carried out using POD machine. A decrease in frictional force for biodiesel and its blends was observed. Wear and SEM analysis showed comparable results of biodiesel and its blends with diesel. The following conclusions are 1) Analysis of friction force, wear and SEM images showed that B80OA20 and B80OA20E10 blends showed better results than B90OA10 and B90OA10E5. Wear reduced by 48% in B80OA20 when compared with B90OA10, while B80OA20E10 showed the least frictional force. 2) The blends namely, B80OA20 and B80OA20E10 were studied for engine and emission analysis and compared with diesel and B100. However, the tested blend showed less BTE in comparison with diesel but the addition of OA with palm biodiesel (B80OA20) showed a 3% increase in BTE when compared to B100. On the other hand, adding ethanol in B80OA20 showed minuscular decrease in BTE compared to B100. An increase in cylinder pressure is observed in B80OA20 and B80OA20E10 compared to B100. 3) The critical contribution of this study is that B80OA20 and B80OA20E10 showed a decrease in NO_x level and improved tribological behaviour when compared to B100 and diesel. Also, these two blends lower NO_x emissions by 12% and 2%, respectively, compared to B100 and 4) Hence, the higher blends of palm biodiesel with oleic acid were practical from tribological and NO_x emission points of view.

The authors recommend future studies on the engine material compatibility, oxidation stability, and long-term endurance of palm biodiesel blended with oleic acid (B80OA20) and ethanol (B80OA20E10) that will help to gain more confidence amongst engine manufacturers and the automotive industry.

ACKNOWLEDGEMENT

The corresponding author gratefully acknowledges the financial support provided by S. V. National Institute of Technology, Surat, India by seed funding file number: Dean (R&C)/Seed Money/2021-2022/11171 and project number: 2021-22/DoME/27.

REFERENCES

Abdullah, N., Sianipar, R. N. R., Ariyani, D., & Nata, I. F. (2017). Conversion of palm oil sludge to biodiesel using alum and KOH as catalysts. *Sustainable Environment Research, 27*(6), 291–295. https://doi.org/10.1016/j.serj.2017.07.002

Ali, O. M., Mamat, R., Abdullah, N. R., & Abdullah, A. A. (2015). Analysis of blended fuel properties and engine performance with palm biodiesel-diesel blended fuel. *Renewable Energy, 86*, 59–67. https://doi.org/10.1016/j.renene.2015.07.103

Anand, G., Yick, J., & Kabir, S. N. (2021). Rheological and tribological properties of *Jatropha curcas* biolubricants at various blend concentrations. *Biofuels, 13*(5), 623–630. https://doi.org/10.1080/17597269.2020.1833410

Atmanli, A. (2020). Experimental comparison of biodiesel production performance of two different microalgae. *Fuel, 278*, 118311. https://doi.org/10.1016/j.fuel.2020.118311

Atmanli, A., & Yilmaz, N. (2019). An experimental assessment on semi-low temperature combustion using waste oil biodiesel/C3-C5 alcohol blends in a diesel engine. *Fuel, 260*, 116357. https://doi.org/10.1016/j.fuel.2019.116357

Atmanli, A., Ileri, E., & Yilmaz, N. (2016). Optimization of diesel-butanol-vegetable oil blend ratios based on engine operating parameters. *Energy, 96*, 569–580. https://doi.org/10.1016/j.energy.2015.12.091

Atmanli, A., Ileri, E., Yuksel, B., & Yilmaz, N. (2015). Extensive analyses of diesel-vegetable oil-n-butanol ternary blends in a diesel engine. *Applied Energy, 145*, 155–162. https://doi.org/10.1016/j.apenergy.2015.01.071

Awang, M. S. N., Zulkifli, N. W. M., Abbas, M. M., Zulkifli, S. A., Kalam, M. A., Yusoff, M. N. A. M., Daud, W. M. A. W., & Ahmad, M. H. (2022). Effect of diesel-palm biodiesel fuel with plastic pyrolysis oil and waste cooking biodiesel on tribological characteristics of lubricating oil. *Alexandria Engineering Journal, 61*(9), 7221–7231. https://doi.org/10.1016/j.aej.2021.12.062

Azahari, S. R., Salahuddin, B. B., Noh, N. A. M., Nizah, R., & Rashid, S. A. (2016). Physico-chemical and emission characterization of emulsified biodiesel/diesel blends. *Biofuels, 7*(4), 337–343. https://doi.org/10.1080/17597269.2015.1135374

Benjumea, P., Agudelo, J., & Agudelo, A. (2007). Basic properties of palm oil biodiesel-diesel blends. *Fuel, 87*(10), 2069–2075. https://doi.org/10.1016/j.fuel.2007.11.004

Chan, C. H., Tang, S. W., Mohd, N. K., Lim, W. H., Yeong, S. K., & Idris, Z. (2018). Tribological behaviour of biolubricant base stocks and additives. *Renewable and Sustainable Energy Reviews, 93*, 145–157. https://doi.org/10.1016/j.rser.2018.05.024

Dinesha, P., Jagannath, K., & Mohanan, P. (2017). Effect of varying 9-octadecenoic acid (oleic fatty acid) content in biofuel on the performance and emission of a compression ignition engine at varying compression ratio. *Biofuels, 9*(4), 441–448. https://doi.org/10.1080/17597269.2016.1275491

Enweremadu, C. C., & Rutto, H. L. (2010). Combustion, emission and engine performance characteristics of used cooking oil biodiesel: A review. *Renewable and Sustainable Energy Reviews, 14*(9), 2863–2873. https://doi.org/10.1016/j.rser.2010.07.036

Fazal, M. A., Haseeb, A. S. M. A., & Masjuki, H. H. (2013). Investigation of friction and wear characteristics of palm biodiesel. *Energy Conversion and Management, 67*, 251–256. https://doi.org/10.1016/j.enconman.2012.12.002

Fazal, M. A., Haseeb, A. S. M. A., & Masjuki, H. H. (2014). A critical review on the tribological compatibility of automotive materials in palm biodiesel. *Energy Conversion and Management, 79*, 180–186. https://doi.org/10.1016/j.enconman.2013.12.002

Gaur, A., Dwivedi, G., Baredar, P., & Jain, S. (2022). Influence of blending additives in biodiesel on physiochemical properties, engine performance, and emission characteristics. *Fuel, 321*, 124072. https://doi.org/10.1016/j.fuel.2022.124072

Haseeb, A. S. M. A., Sia, S. Y., Fazal, M. A., & Masjuki, H. H. (2009). Effect of temperature on tribological properties of palm biodiesel. *Energy, 35*(3), 1460–1464. https://doi.org/10.1016/j.energy.2009.12.001

Ileri, E., Atmanli, A., & Yilmaz, N. (2015). Comparative analyses of n-butanol-rapeseed oil-diesel blend with biodiesel, diesel, and biodiesel-diesel fuels in a turbocharged direct injection diesel engine. *Journal of Energy Institute, 89*(4), 586–593. https://doi.org/10.1016/j.joei.2015.06.004

Ileri, E., Atmanli, A., Yilmaz, N., Karaoglan, A., Okkan, U., & Kocak, M. S. (2016). Predicting the engine performance and exhaust emissions of a diesel engine fuelled with hazelnut oil methyl ester: The performance comparison of RSM and LSSVM. *Journal of Energy Resources Technology, 138*(5), 052206. https://doi.org/10.1115/1.4032941

Jamshaid, M., Masjuki, H. H., Kalam, M. A., Zulkifli, N. W. M., Arslan, A., & Qureshi, A. A. (2021). Experimental investigation of performance, emissions and tribological characteristics of B20 blend from cottonseed and palm oil biodiesels. *Energy, 239*, 121894. https://doi.org/10.1016/j.energy.2021.121894

Kamaronzaman, M. F. F., Kahar, H., Hassan, N., Hanafi, M. F., & Sapawe, N. (2020). Analysis of biodiesel product derived from waste cooking oil using Fourier transform infrared spectroscopy. *Materials Today Proceedings, 31*, 329–332. https://doi.org/10.1016/j.matpr.2020.06.088

Kanth, S., & Debbarma, S. (2021). Comparative performance analysis of diesel engine fuelled with hydrogen enriched edible and non-edible biodiesel. *International Journal of Hydrogen Energy, 46*(17), 10478–10493. https://doi.org/10.1016/j.ijhydene.2020.10.173

Kim, H. Y., Ge, J. C., & Choi, N. J. (2020). Effects of ethanol-diesel on the combustion and emissions from a diesel engine at a low idle speed. *Applied Sciences, 10*(12), 4153. https://doi.org/10.3390/app10124153

Krishania, N., Rajak, U., Verma, T. N., Birru, A. K., & Pugazhendhi, A. (2020). Effect of microalgae, tyre pyrolysis oil and Jatropha biodiesel enriched with diesel fuel on performance and emission characteristics of CI engine. *Fuel, 278*, 118252. https://doi.org/10.1016/j.fuel.2020.118252

Kurre, S. K., & Yadav, J. (2022). A review on bio-based feedstock, synthesis, and chemical modification to enhance tribological properties of biolubricants. *Industrial Crops and Products, 193*, 116122. https://doi.org/10.1016/j.indcrop.2022.116122

Lee, C. C., Tran, M., Tan, B. T., Scribano, G., & Chong, C. T. (2020). A comprehensive review on the effects of additives on fundamental combustion characteristics and pollutant formation of biodiesel and ethanol. *Fuel, 288*, 119749. https://doi.org/10.1016/j.fuel.2020.119749

Lim, S., & Teong, L. K. (2009). Recent trends, opportunities, and challenges of biodiesel in Malaysia: An overview. *Renewable and Sustainable Energy Reviews, 14*(3), 938–954. https://doi.org/10.1016/j.rser.2009.10.027

Maleque, M. A., Masjuki, H. H., & Haseeb, A. S. M. A. (2000). Effect of mechanical factors on tribological properties of palm oil methyl ester blended lubricant. *Wear, 239*(1), 117–125. https://doi.org/10.1016/s0043-1648(00)00319-7

Mekhilef, S., Siga, S., & Saidur, R. (2011). A review on palm oil biodiesel as a source of renewable fuel. *Renewable and Sustainable Energy Reviews, 15*(4), 1937–1949. https://doi.org/10.1016/j.rser.2010.12.012

Mishra, V. K., & Goswami, R. (2017). A review of production, properties and advantages of biodiesel. *Biofuels, 9*(2), 273–289. https://doi.org/10.1080/17597269.2017.1336350

Mohan, S., Dinesha, P., & Bekal, S. (2021). NO_x reduction of biodiesel engine using pongamia ester with oleic acid and optimization of operating conditions using particle swarm optimization. *International Journal of Hydrogen Energy, 46*(52), 26665–26676. https://doi.org/10.1016/j.ijhydene.2021.05.124

Niyas, M. M., & Shaija, A. (2022). Performance evaluation of diesel engine using biodiesels from waste coconut, sunflower, and palm cooking oils, and their hybrids. *Sustainable Energy Technologies and Assessments*, *53*, 102681. https://doi.org/10.1016/j.seta.2022.102681

Mujtaba, M. A., Cho, H. M., Masjuki, H. H., Kalam, M. A., Farooq, M., Soudagar, M. E. M., Gul, M., Ahmed, W., Afzal, A., Bashir, S., Raju, V. D., Yaqoob, H., & Syahir, A. Z. (2020). Effect of alcoholic and nano-particles additives on tribological properties of diesel-palm-sesame-biodiesel blends. *Energy Reports, 7*, 1162–1171. https://doi.org/10.1016/j.egyr.2020.12.009

Öztürk, E., & Can, Ö. (2022). Effects of EGR, injection retardation and ethanol addition on combustion, performance and emissions of a DI diesel engine fueled with canola biodiesel/diesel fuel blend. *Energy, 244*, 123129. https://doi.org/10.1016/j.energy.2022.123129

Rahiman, M. K., Santhoshkumar, S., Subramaniam, D., Avinash, A., & Pugazhendhi, A. (2021). Effects of oxygenated fuel pertaining to fuel analysis on diesel engine combustion and emission characteristics. *Energy, 239*, 122373. https://doi.org/10.1016/j.energy.2021.122373

Rajamohan, S., Gopal, A. H., Muralidharan, K. R., Huang, Z., Paramasivam, B., Ayyasamy, T., Nguyen, X. P., Le, A. T., & Hoang, A. T. (2022). Evaluation of oxidation stability and engine behaviors operated by Prosopis juliflora biodiesel/diesel fuel blends with presence of synthetic antioxidant. *Sustainable Energy Technologies and Assessments, 52*, 102086. https://doi.org/10.1016/j.seta.2022.102086

Rosha, P., Mohapatra, S. K., Mahla, S. K., Cho, H., Chauhan, B. S., & Dhir, A. (2019). Effect of compression ratio on combustion, performance, and emission characteristics of compression ignition engine fueled with palm (B20) biodiesel blend. *Energy, 178*, 676–684. https://doi.org/10.1016/j.energy.2019.04.185

Sakthivel, R., Ramesh, K., Purnachandran, R., & Shameer, P. M. (2017). A review on the properties, performance and emission aspects of the third generation biodiesels. *Renewable and Sustainable Energy Reviews, 82*, 2970–2992. https://doi.org/10.1016/j.rser.2017.10.037

Sakthivel, R., Ramesh, K., Marshal, S. J. J., & Sadasivuni, K. K. (2019). Prediction of performance and emission characteristics of diesel engine fuelled with waste biomass pyrolysis oil using response surface methodology. *Renewable Energy, 136*, 91–103. https://doi.org/10.1016/j.renene.2018.12.109

Santhoshkumar, A., Thangarasu, V., & Anand, R. (2019). Performance, combustion, and emission characteristics of DI diesel engine using Mahua biodiesel. In *Advanced Biofuels* (pp. 291-327). Woodhead Publishing. https://doi.org/10.1016/b978-0-08-102791-2.00012-x

Shahir, S. A., Masjuki, H. H., Kalam, M. A., Imran, A., & Ashraful, A. M. (2015). Performance and emission assessment of diesel-biodiesel-ethanol/bioethanol blend as a fuel in diesel engines: A review. *Renewable and Sustainable Energy Reviews, 48*, 62–78. https://doi.org/10.1016/j.rser.2015.03.049

Shote, A. S., Betiku, E., & Asere, A. A. (2018). Characteristics of CO and NO_x emissions from combustion of transmethylated palm kernel oil-based biodiesel blends in a compression ignition engine. *Journal of King Saud University - Engineering Sciences, 31*(2), 178–183. https://doi.org/10.1016/j.jksues.2018.02.005

Singh, Y., Singh, P., Sharma, A., Choudhary, P., Singla, A., & Singh, N. K. (2018). Optimization of wear and friction characteristics of *Phyllanthus emblica* seed oil based lubricant using response

surface methodology. *Egyptian Journal of Petroleum, 27*(4), 1145–1155. https://doi.org/10.1016/j.ejpe.2018.04.001

Sorate, K. A., & Bhale, P. V. (2013). Impact of biodiesel on fuel system materials durability. *Journal of Scientific and Industrial Research, 72*(01), 48–57.

Sorate, K. A., & Bhale, P. V. (2014). Biodiesel properties and automotive system compatibility issues. *Renewable and Sustainable Energy Reviews, 41*, 777–798. https://doi.org/10.1016/j.rser.2014.08.079

Sorate, K. A., & Bhale, P. V. (2018). Corrosion behavior of automotive materials with biodiesel: A different approach. *SAE International Journal of Fuels and Lubricants, 11*(2), 147–162. https://doi.org/10.4271/04-11-02-0007

Tabatabaei, M., Aghbashlo, M., Dehhaghi, M., Panahi, H. K. S., Mollahosseini, A., Hosseini, M., & Soufiyan, M. M. (2019). Reactor technologies for biodiesel production and processing: A review. *Progress in Energy and Combustion Science, 74*, 239–303. https://doi.org/10.1016/j.pecs.2019.06.001

Tamilselvan, P., Nallusamy, N., & Rajkumar, S. (2017). A comprehensive review on performance, combustion and emission characteristics of biodiesel fuelled diesel engines. *Renewable and Sustainable Energy Reviews, 79*, 1134–1159. https://doi.org/10.1016/j.rser.2017.05.176

Tillis, P. (2019, February 19). *How the world got hooked on palm oil*. The Guardian. https://www.theguardian.com/news/2019/feb/19/palm-oil-ingredient-biscuits-shampoo-environmental

Verma, T. N., Shrivastava, P., Rajak, U., Dwivedi, G., Jain, S., Zare, A., Shukla, A. K., & Verma, P. (2021). A comprehensive review of the influence of physicochemical properties of biodiesel on combustion characteristics, engine performance and emissions. *Journal of Traffic and Transportation Engineering (English Edition), 8*(4), 510–533. https://doi.org/10.1016/j.jtte.2021.04.006

Yilmaz, N., Atmanli, A., & Vigil, F. M. (2017). Quaternary blends of diesel, biodiesel, higher alcohols and vegetable oil in a compression ignition engine. *Fuel, 212*, 462–469. https://doi.org/10.1016/j.fuel.2017.10.050

Zaid, M., Kumar, A., & Singh, Y. (2020). Lubricity improvement of the raw jojoba oil with TiO_2 nanoparticles as an additive at different loads applied. *Materials Today Proceedings, 46*, 3165–3168. https://doi.org/10.1016/j.matpr.2020.07.437

Journal of Oil Palm Research Vol. 37 (1) March 2025 p. 148-159
DOI: https://doi.org/10.21894/jopr.2024.0001

SEDIMENT FORMATION IN A PALM OIL BIODIESEL BLEND IN A SHIP FUEL TANK

JAJANG AMIR HIDAYAT[1]; BAMBANG SUGIARTO[1]*; YULIANTO SULISTYO NUGROHO[1]; AHMAD SYIHAN AUZANI[1]; HARI SETIAPRAJA[2] and SITI YUBAIDAH[2]

ABSTRACT

In this study, sediment formation in a ship fuel tank fuelled with a blend of 30% palm biodiesel (B30) was evaluated. The main objective was to understand sediment formation during fuel storage over different storage periods, which has not been previously reported. In this study, B30 was evaluated for cleanliness, water content, contaminants and other properties before it was stored in a ship fuel tank for 30 days. Regular sampling was conducted every two days during this storage period to monitor and analyse sediment formation. After a storage period of 30 days, B30 exhibited density comparable to its initial condition, with a difference of less than 0.1%. However, its viscosity showed an increase of 1.2%. In contrast, no significant difference was observed in fuel cleanliness based on ISO 4406 and in the measured water content. The amount of sediment formed was consistent up to the 19th day, but from the 20th to the 30th day, it rapidly increased logarithmically, with a 312% mass increase by the 30th day. Additionally, morphological and FTIR analyses showed that the sediment consisted of agglomerated asphaltene and saturated fatty acids. This study reveals that quality control and specific treatments are required in B30 to suppress the formation of sediments.

Keywords: cleanliness, palm oil biodiesel, sediment formation, storage stability.

Received: 12 April 2023; **Accepted:** 31 October 2023; **Published online:** 2 January 2024.

INTRODUCTION

Biodiesel is a new form of renewable energy (He & Van Gerpen, 2012) that consists of fatty acid methyl esters (FAME) or ethyl esters, which are sourced from animal or vegetable fats through a transesterification process (Mehmood *et al*., 2016; Sebayang *et al*., 2023). These fuels are environmentally friendly and promising alternatives that can meet the world's energy needs as a substitute for fossil fuels (Sun & Li, 2019). The fuel is classified as low-emission, nontoxic and easily decomposable (Garcia *et al*., 2020; Okoye *et al*., 2019; Sun & Li, 2019).

In Indonesia, various studies have been conducted to improve biodiesel FAME properties and reduce dependence on fossil fuels. Indonesia has been using a mixture of 30% biodiesel and 70% diesel fuel (B30), and the biodiesel proportion will soon increase to 40%. The Indonesian government has mandated biodiesel use in the industrial sector, land and sea transportation [Minister of Energy and Mineral Resources (MEMR), 2014]. Biodiesel implementation in Indonesia is strongly supported by the successful durability testing of biodiesel-blended fuel, particularly for land applications, including truck, train, bus and passenger car transport, which have no issues.

However, the use of biodiesel for marine vessels still presents numerous challenges, especially under environmental conditions with high water content and condensation on the walls of storage tanks. These factors require careful consideration, as they significantly affect biodiesel quality (Fregolente *et al*., 2012). In addition, the large capacity of ship tanks differs from that of land

[1] Faculty of Mechanical Engineering,
Universitas Indonesia,
Depok 16424, Indonesia.

[2] Research Centre for Conversion and Conservation Energy,
National Innovation Research Agency (BRIN) Serpong,
South Tangerang Banten 15314, Indonesia.

* *Corresponding author e-mail: bangsugi@eng.ui.ac.id*

vehicles. On board the vessel, the fuel tank cannot be completely depleted, leading to the mixing of old fuel with new fuel during refuelling. Moreover, ships move dynamically to various regions, which pose a challenge for maintaining fuel quality when refuelling in different places.

Differences in raw material suppliers will affect changes in properties such as density, viscosity, cleanliness and water content (Fersner & Galante-Fox, 2014; Rao & Reddy, 2023). Viscosity, cleanliness, and density are also important properties of biodiesel (Ramos *et al*., 2008). Viscosity also dramatically affects ignition in the engine and will determine the fuel's combustion quality. High viscosity will cause large spray size and can cause poor combustion (Ceriani *et al*., 2007; Tesfa *et al*., 2010). Biodiesel blends can reduce viscosity by approximately 12.9% (Lin, 2013). Viscosity can also cause a decrease in the quality of injection and decreased pressure (Srichai *et al*., 2018). Density is critical because it affects the quality of the mixture in the combustion chamber, the energy produced, and the injection system (Li *et al*., 2019; Noor *et al*., 2018; Tesfa *et al*., 2010). Density will affect the atomisation of the fuel (Silitonga *et al*., 2016). High density will cause incomplete combustion (Erdmann *et al*., 2019).

The water content in biodiesel can originate from condensation at the tank's surface and the accumulation of fuel vapours (Hill & Hill, 2008). The presence of water allows the formation of microorganisms in biodiesel (Hettige & Sheridan, 1989; Zhang *et al*., 2011). Biodiesel also has hygroscopic properties, *i.e.*, it quickly absorbs water from the environment. Water absorption can lead to the formation of fatty acids, resulting in corrosion issues (Fregolente *et al*., 2012). Furthermore, the high water content will cause sedimentation at the bottom of the tank and can drive the growth of microorganisms (Passman, 2013). The presence of microorganisms can impact the deterioration of biodiesel fuel quality. These conditions are attributed to the composition of biodiesel, which contains an ester that is readily used by microorganisms, unlike hydrocarbons (Hettige & Sheridan, 1989). The presence of these microorganisms can result in the emergence of contaminants, resulting in sludge development (Chao *et al*., 2010).

Various types of contaminants have been found in biodiesel, such as glycerine, water, sulfur, sterile glucosides, microbial sediments and other sediments that need further research and exceptional attention to maintain the quality of biodiesel (Fersner & Galante-Fox, 2014; He & Van Gerpen, 2012). These contaminants have caused significant detrimental effects (Fersner & Galante-Fox, 2014), so various methods have been taken to avoid this situation. If this problem occurs continuously, it will cause fuel filters to become clogged, shorten their service life and even cause the engine to not operate optimally because it cannot supply sufficient fuel flow (Jaroonjitsathian *et al*., 2016; Thangamani *et al*., 2021). Wang *et al*. (2009) reported that steryl glucoside (SG) was the main contributor to the formation of deposits in soybean biodiesel. In addition, SG is a natural derivative of vegetable or animal oil. It can contribute to problems with the flow ability of biodiesel and biodiesel mixtures and lead to clogged filters (Lee *et al*., 2007). Moreover, deposits will cause the injector to clog (Kumar, 2017). Therefore, these deposits can form on the injectors, valves and piston crowns due to the mixing of biodiesel with diesel (Sugiarto *et al*., 2020a; 2020b). The deposit composition leads to dead ends and corrosion (Hidayat & Sugiarto, 2020; Sugiarto *et al*., 2021).

Various studies have examined the formation of sediments from multiple sources in established storage tanks. Tang *et al*. (2008) used a 20% soy, cottonseed and biodiesel base with 80% ultra-low sulfur diesel (ULSD) to observe precipitate formation. They conducted precipitate testing using glass bottles for storage. Bücker *et al*. (2010) utilised 0%, 5%, 10% and 20% biodiesel soy oil to determine the growth of microbial contaminants by simulating storage. Tang *et al*. (2008) conducted research to determine the growth of fungi in various mixtures of biodiesel from soybeans as a function of time in the laboratory. Mushrush *et al*. (2011) investigated the stability of sediment formed from 5% soybean biodiesel in a borosilicate brown glass bottle. Na-Ranong and Kitchaiya (2014) used pure biodiesel to determine the effect of contaminants such as monoglycerides, diglycerides and triglycerides on biodiesel storage. Gozan *et al*. (2022) conducted precipitation tests to predict contaminant formation using a 20% FAME and 80% diesel fuel (B20) medium based on monoglyceride content in tanks on land. Silva *et al*. (2021) predicted the effect of the addition of 20% and 10% soybean biodiesel to marine diesel on sludge formation over 28 days of storage with a simulated storage method.

Many of these research studies focused on the formation of contaminants under simulated conditions instead of actual conditions, such as those in existing ship tanks. Moreover, only a few studies have fully accounted for the factors that affect storage, including environmental conditions, variations in the quality of biodiesel fuel sources, and requirements for transportation equipment during conveyance from producers to consumers. Therefore, this study investigated sediment formation based on actual conditions on a ship, especially in tropical areas, such as Indonesia, which has not been reported previously. When a ship operates, it will depart from one site and travel to various other sites and refuel in particular areas and the different fuels will mix in the ship's tanks. Refuelling in specific areas cannot be avoided because the vessel cannot

return to the initial refuelling point. Due to different refinery technologies, the different fuels might have varying properties.

Therefore, this study aimed to measure the growth of contaminants in the dynamic fuel tanks of vessels and to study the effect of storage time on changes in the properties of palm biodiesel. The amount of sediment formed from a palm methyl ester blend fuel with a volume ratio of 30% biodiesel and 70% diesel fuel (B30) in the fuel tank of a ship was measured at various storage times, which other researchers have not reported. Therefore, the result can be used to predict how quickly sediment can accumulate to form sludge in fuel tanks. Furthermore, fuel cleanliness, viscosity, density and water content were tested to study the properties of palm biodiesel in a dynamic storage tank in specific periods.

MATERIALS AND METHODS

Fuels

In this study, the fuel used was a B30 biodiesel mixture supplied by two filling points and sourced from a ship's tank. The ship's tank was cleaned first above the docking in the shipyard before it was loaded into the ship. Then, the ship's tank was filled with biodiesel fuel using a barge and a tanker truck. In this study, the B30 palm biodiesel blended fuels came from two places in Indonesia, Sample 1 (X) and Sample 2 (Y). The visual appearance of both samples is shown in *Figure 1*. Sample 1 is brighter with fewer small black particles than Sample 2. Visual inspection showed that both samples were free from water content.



Figure 1. Visual appearance of (a) Sample 1(X) and (b) Sample 2 (Y).

The fuel storage tank was first loaded with Sample 1 at a volume of 18,000 L, and two days later, it was refilled with 1,600 L of Sample 2. Then, fresh samples of Samples 1 and 2 were taken directly from a tanker truck to evaluate fuel characteristics. The storage tank capacity was 20,000 L, and it had dimensions of 4.50 × 3.40 × 1.25 m for the tank's length, width, and height. The vessel tank was made of steel.

Sediment Test

Sediment formation was measured in B30 fuel based on the total contaminants in B30 palm biodiesel in the ship's tank. Fuel samples were taken from the source tank during filling and from the vessel directly after filling from the tank's bottom, middle, and top. Samples were taken at filling time and every two days thereafter for one month.

The aim of the B30 fuel contaminants test was to determine the amount of sediment collected at a particular total contaminant value, the formation of contaminants in the ship's tanks, and the feedstock's effect on contaminant formation. This test was performed to measure sediment formation caused by the accumulation of contaminants. The first test samples for Sample 1 and Sample 2 were treated by placing 100 mL of each B30 sample in a closed 100 mL separating funnel. Each sample was vacuum filtered through 0.8 micron filter paper.

For the second test, samples were taken from the bottom, middle, and top of the tank with volumes reaching 1 L every two days for 30 days. 100 mL of each sample of B30 was placed in a closed 100 mL separatory funnel. Each sample was vacuum-filtered through 0.8 micron filter paper. A Whatman™ cellulose acetate membrane filter was used to filter B30 fuel, and it had a 47 mm diameter and 0.8 micron particle retention. The sediment retained on the filter paper was washed with a petro-ether, dried under vacuum, and then weighed.

Characteristics of Biodiesel Blends

The fuel properties tested, including viscosity at 40°C and density at 15°C measured using Anton PAAR SVM 3001 cold properties and using ASTM D445 and ASTM D1298 standards, respectively, reflect the cleanliness of the biodiesel fuel mixture. The device has good repeatability and reproducibility, approximately 0.10% and 0.35%, respectively. Cleanliness was measured using the Argo Hytos OP Count Particle Counter using standard ASTM D7596, and water content was measured using Karl Fischer Coulometric Titration using standard D1744. The first test samples consisted of Sample 1 and Sample 2, and the second test consisted of samples from the ship's tanks,

which were taken at random from the bottom of the tank based on storage time. Specifically, sample 1+2 (1st day) was from 1 day of storage, 1+2 (15th day) was from 15 days of storage, and 1+2 (30th day) was from 30 days of storage.

The measurement uncertainty value was obtained from the uncertainty that arises from statistical data involving the calculation of several parameters, including the arithmetic mean, standard deviation, and degrees of freedom based on test reports and measuring instrument data sheets. All experimental steps are depicted in the flowchart shown in *Figure 2*.

RESULTS AND DISCUSSION

Viscosity and Density

Viscosity testing was conducted in this study to determine changes that occurred during fuel storage in the ship's fuel tank. Based on the results in *Table 1*, it can be seen that the results obtained for the viscosity of Sample 1 originating from source X showed a high value of approximately 3.45 mm^2/s, while that from source Y, namely, Sample 2, had a lower viscosity value of 3.23 mm^2/s. According to the MEMR, the values should be in the range of 2.00-4.50 mm^2/s, and according to ASTM D6751, it should be between 1.90-6.00 mm^2/s. Therefore, the sample met both standards. However, that value of Sample X was close to the maximum allowable limit. After mixing Sample 1 and 2 (X + Y), the viscosity changed to 3.30 mm/s^2 and continued to increase up to 30 days of storage and may have continued to increase with increasing storage time. If it continued to increase, it would affect the atomisation of biodiesel used as engine fuel (Ayoob & Fadhil, 2019), and if the viscosity is very high, it can cause large jet size and lead to poor combustion (Ceriani *et al*., 2007; Tesfa *et al*., 2010). Based on the maximum standard permitted by the MEMR, the value should be 2.0-4.5 mm^2/s (MEMR, 2019), and according to ASTM D6751, it should be between 1.90 and 6.00 mm^2. Therefore, the sample met both standards.

The results in *Table 1* for the density test show that the density value was relatively stable, as in previous studies where the density tended to be stable after approximately a month of storage (Hidayat *et al*., 2021). In *Table 1*, Sample 1 is the biodiesel from site X showing a high value of 836 kg/m^3 compared to Sample 2 from site Y, at 832 kg/m^3. After samples X and Y (1+2) were mixed, the density changed to 835 kg/m^3 and continued to increase up to 30 days of storage. Based on the maximum standard permitted by the MEMR, the density value should be 810-860 kg/m^3, and based on these results, it was below the permitted quality standard of the MEMR (MEMR, 2019). However, based on ASTM D 6751, biodiesel density must be 860-880 kg/m^3, and according to EN 14214, it should be in the 860-900 kg/m^3 range. Therefore, the density of biodiesel from X and Y sources did

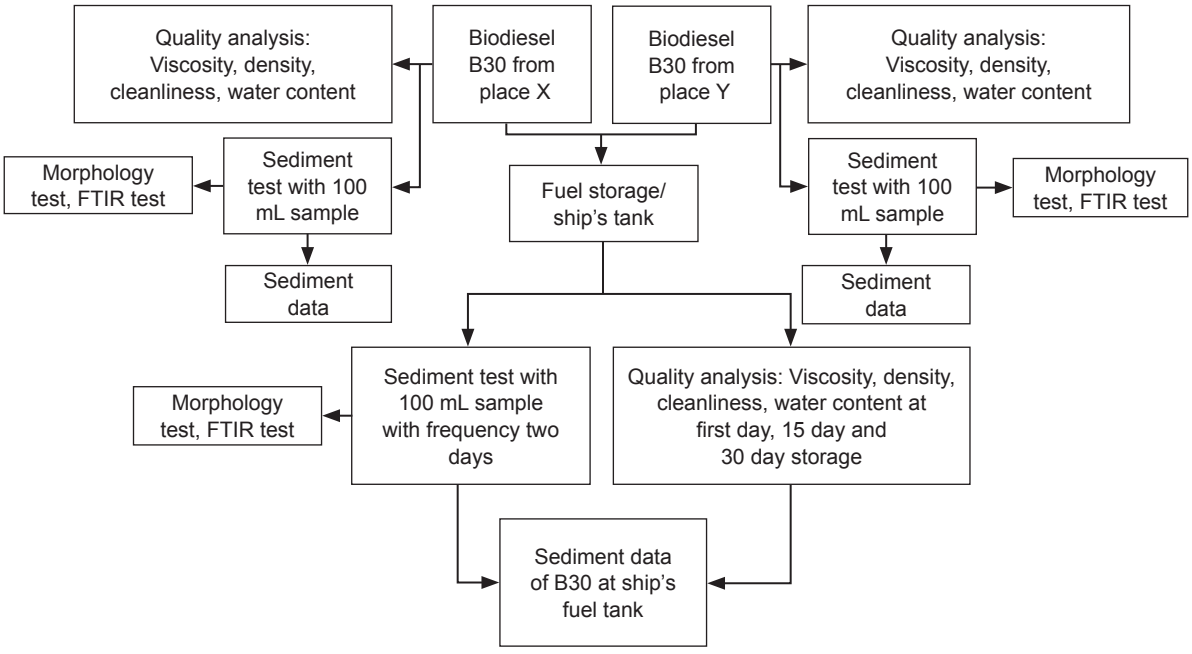


Figure 2. Flowchart of the sediment test to measure sludge formation in the ship's fuel tanks.

not meet these two standards, so it would affect the atomisation of biodiesel used as engine fuel (Silitonga *et al*., 2016).

TABLE 1. VISCOSITY AND DENSITY RESULTS

No.	Sample	Viscosity (mm^2/s)	Density (kg/m^3)
1	1	3.45	836
2	2	3.23	832
3	1+2 (1st day)	3.30	835
4	1+2 (15th day)	3.32	835
5	1+2 (30th day)	3.34	835

Cleanliness and Water Content

The method used for cleanliness testing was the ASTM D7596 standard. Additionally, the most common standard code for the amounts of contaminants screened is ISO 4406. The purpose of this code is to simplify the reporting of particle count data by converting the number of particles into broad classes or regulations, in which a value increase of one generally indicates a doubling of the level of contamination, as shown in *Table 2*. The standard sizes used are 4, 6 and 14 µm. The results of the tests carried out are listed in *Table 3* and *4*.

Table 3 shows the distribution of contaminants from the test results based on filter sizes of 4, 6 and 14 µm. *Table 4* shows the results for converting the number of contaminants to the ISO 4406 code. The table shows the level of cleanliness of the test samples based on storage time. The highest cleanliness results obtained for Sample 1, namely, at 4 microns (366,472), 6 microns (110,971), and 14 microns (5,871), with a cleanliness code of 26/24/20 compared to the others. In Sample 2, the cleanliness test results were at 4 microns (82,339), 6 microns (26,912), and 14 microns (286), with a cleanliness code of 24/22/15. This result shows that a difference in refuelling location leads to differences in cleanliness levels. Based on the test results, the two samples did not meet the standards set by the Worldwide Fuels Charter, namely, 18/16/13 for 4, 6 and 14 µm, respectively [International Organization for Standardization (ISO), 2017].

TABLE 2. ALLOCATION OF SCALE NUMBER ISO 4406

Number of particle (mm)		Scale number
More than	Up to and including	
2,500,000		>28
1,300,000	2,500,000	28
640,000	1,300,000	27
320,000	640,000	26
160,000	320,000	25
80,000	160,000	24
40,000	80,000	23
20,000	40,000	22
10,000	20,000	21
5,000	10,000	20
2,500	5,000	19
1,300	2,500	18
640	1,300	17
320	640	16
160	320	15
80	160	14
40	80	13
21	40	12
10	20	11

Source: (ISO, 2017).

After mixing, there was a change in the level of cleanliness. For the 1+2 sample (1st day), the distribution of contaminants at sizes of 4 microns (26,404), 6 microns (8,100), and 14 microns (551) had the cleanliness code 22/20/16; for the 1+2 sample (15th day), contaminant distribution at sizes of 4 microns (21,624), 6 microns (6,107), and 14 microns (373) had a cleanliness code 22/20/16; and in sample 1+2 (30th day), the distribution of contaminants at sizes of 4 microns (27,511), 6 microns (8,149), and 14 microns (587) had the cleanliness code 22/20/16. The test results showed a decrease in the distribution of contaminants or an increase in the cleanliness code level compared to the blending of Sample 1 and Sample 2. However, these results did not meet the standards set by the Worldwide Fuels Charter. The maximum cleanliness limits of diesel fuel specified by the Worldwide Fuels Charter are 18/16/13 for 4, 6 and 14 µm, respectively (ISO, 2017). If this condition is not resolved, it will lead to injector blockage and affect engine performance.

TABLE 3. CLEANLINESS TEST RESULTS

Sample	>4 µm	>6 µm	>14 µm
1	366,472	110,971	5,871
2	82,339	26,912	286
1+2 (1st day)	26,404	8,100	551
1+2 (15th day)	21,624	6,107	373
1+2 (30th day)	27,511	8,149	587

The test results show that the blending of different biodiesels affects the level of cleanliness of the biodiesel blend. In addition, the dynamic movement of ships affects the distribution of contaminants and the level of cleanliness of the blended biodiesel fuel with varying test results.

TABLE 4. CLEANLINESS TEST RESULTS BASED ON ISO 4406 CODE

Sample	>4 µm	>6 µm	>14 µm
1	26	24	20
2	24	22	15
1+2 (1st day)	22	20	16
1+2 (15th day)	22	20	16
1+2 (30th day)	22	20	16

Source: (ISO, 2017).

Water is the primary source of contaminants in fuel. Testing for water content was carried out based on ASTM D1744, with the results listed in *Table 5* which shows that Sample 2 had higher water content, at 395 ppm, compared to Sample 1, at 372 ppm. These results indicate that the different refuelling locations also differ with respect to the water content of the fuel. The two samples did not meet the maximum average set by the government, namely, 300 ppm (MEMR, 2019).

After fuel mixing, the water content decreased by 313 ppm and was relatively stable over 30 days of storage in the ship's tank. However, the sample did not meet the maximum average set by the government, 300 ppm (MEMR, 2019). If this continued, the fuel properties would impact the occurrence of corrosion and the growth of microorganisms, which would cause the formation of sludge at the bottom of the tank, which would lead to filter blockage, clogged injectors and a clogged fuel system.

TABLE 5. WATER CONTENT RESULTS

Sample	Water content (ppm)
1	372
2	395
1+2 (1st day)	313
1+2 (15th day)	312
1+2 (30th day)	313

Sediment Formation Test Results

The sediment content values for the biodiesel B30 from locations X and Y were 0.031 ± 0.006 g/L and 0.017 ± 0.011 g/L, respectively. These results show that the sediment content in fuel from city X was higher than that in city Y. These results indicate differences in the quality of biodiesel fuel from these samples.

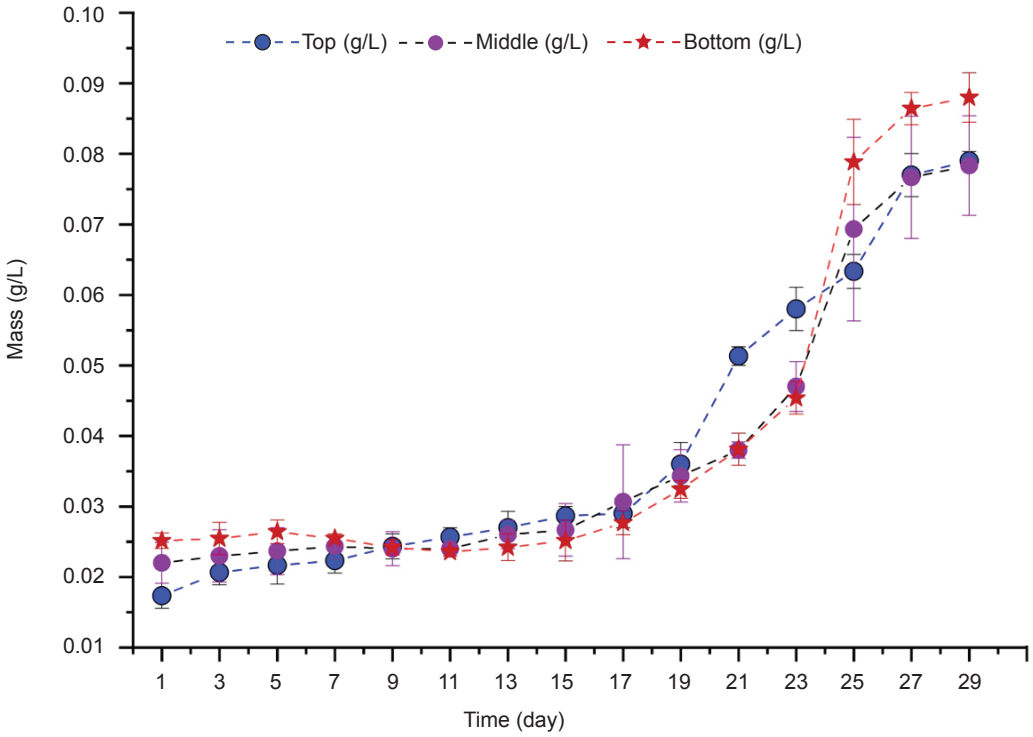


Figure 3. Sediment formation test results.

The test results for the average sediment formation after the mixing of fuels from the two sources in the ship's tanks are shown in *Figure 3* which indicates the mass of contaminants in each layer (top, middle and bottom) of the tank during storage. Under the initial conditions, the mass at the bottom of the tank was higher than that at the middle and top of the tank.

At the beginning of storage, a lower sediment mass was obtained at the top of the tank, namely, 0.016 g/L, this value was the lowest among the sections. Then, with storage time, there was an increase in sediment mass over 30 days of storage. At the top of the tank, the highest addition of sediment mass compared to the others occurred on Day 21, which was an increase of 0.016 g/L from the previous day. The total sediment from the top was less than that from the middle and bottom. In the middle tank, the highest increase occurred on Day 25 compared to the previous day of 0.028 g/L, with a sediment mass of 0.075. On the 25th day, there was a high degree of error compared to the other days, namely, 0.013. However, the error observed was still small. On Day 17 and Day 30, there was also a high degree of error in the middle of the tank, with errors of 0.0081 and 0.0087, respectively. At the bottom of the tank at the beginning of storage, the sediment mass was higher than that in the other sections, namely, 0.026 g/L. Based on the data, on the 25th day, there was a large difference in sediment mass at the bottom of the tank, with an average sediment concentration of 0.081 g/L and an error of 0.0024. Based on these results, most contaminants were located at the bottom of the tank, amounting to 0.621 g/L. The value at the top was 0.582 g/L and that in the middle of the tank was 0.588 g/L. These results are similar to results reported by Gozan *et al*. (2022) who noted that most contaminants are present at the bottom.

During fuel storage, there was an increase in the mass of contaminants, although there were some fluctuations. This occurred because ships at sea operate under unstable conditions and sea waves rock the ship so contaminants are re-suspended from the bottom of the tank, unlike during fuel storage on land or other stationary places. During the first 17 days, the ship was at port, then it began its sea voyage, and then the ship was at port again from the 25th day to the 30th day of storage. Based on this, the aggregation of contaminants occurs when the biodiesel is in a stationary state, and the presence of sea waves can help suppress the aggregation of contaminants. However, these results show an increase of approximately 312% in the mass of contaminants during the 30-day storage period.

Morphology

This study evaluated sediment morphology to study sediment formation in the fuel storage tank of a ship. Morphological analysis was conducted with an optical microscope (HIROX KH-8700). Sample 1 has a different morphology than Sample 2, as shown in *Figure 4*. Sample 2 was found to exhibit small black particles that covered the sediment filter. These could be considered impurities that originated from diesel fuel, not biodiesel, as impurities in biodiesel mainly appear under low-temperature conditions (Paryanto *et al*., 2022). Asphaltene can be derived from marine fuel oil with a low H/C ratio, high aromatic content, and strong polarity (Zhou *et al*., 2023). Asphaltene can agglomerate with saturated monoglycerides of biodiesel due to the negative interaction energy between each component, increasing sediment formation from its agglomeration.

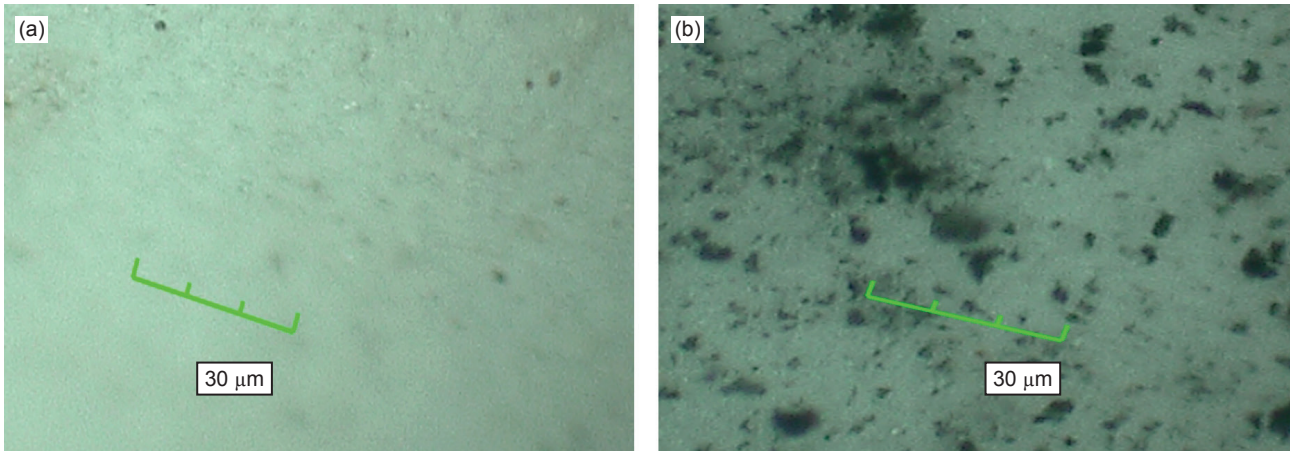


Figure 4. Morphology of sediment formed in (a) Sample 1 and (b) Sample 2.

Figure 5 shows the granular form and sediment distribution across the filter media on the 10th, 25th, and 30th day after fuel sampling. The sediment on the 10th day exhibited small granular particles that covered the filter media, and more prominent granules were observed at several positions. Biodiesel sediment formation occurs mainly due to biodiesel's high saturated monoglyceride content, especially when the fuel is exposed to low-temperature environments below its cloud point. Furthermore, agglomerates continuously formed, developing into more prominent granules that covered the filter media, as shown in *Figure 5b*.

On the 30th day of fuel storage, more significant sediments could be observed covering the filter media. Here, agglomeration between asphaltene and biodiesel is indicated in black and this is considered the reason for the higher sediment content on the 30th day compared with the other days, as shown in *Figure 3*.

Fourier Transform Infrared Spectroscopy (FTIR) Results

A spectrum of wavenumber (cm^{-1}) with percentage transmission (% T) was obtained with FTIR, with *Figure 6* showing the sample area based on the storage time of Sample 1, Sample 2, Sample 1+2 (1st day), Sample 1+2 (25th day) and Sample 1+2 (30th day).

This test was carried out to determine the functional groups present in the B30 biodiesel mixture with storage time. *Figure 6* shows the results of representative FTIR B30 spectra with storage time. *Figure 6* shows a type of mid-IR spectrum (400-4,000 cm^{-1}) that is divided into four regions: The first region is a single bond between 4,000-2,500 cm^{-1}, the second is a triple bond between 2,500-2,000 cm^{-1}, the third is a double bond between 2,000-1,500 cm^{-1}, and the fourth is the fingerprint bond region between 1,500-600 cm^{-1}. *Figure 6* shows six absorption peaks at 2,923, 2,849, 1,747, 1,463, 1,169 and 728 cm^{-1}. The visible peaks observed at 2,923 and 2,849 cm^{-1} indicate saturated aliphatic hydrocarbons of methylene C-H, as shown in *Figure 6* (Coates, 2000), and are related to the stretching absorption of glyceride bonds of oleic, linoleic and palmitic acids (Ayoob & Fadhil, 2019). These peaks also corresponded to aromatic hydrocarbons, indicating asphaltene (Zhou *et al*., 2003).

Figure 6 also clearly shows the presence of carbonyl functional groups, which are represented by the 1,747 cm^{-1} and 1,169 cm^{-1} peaks associated with the stretching of CO_2 double bonds (C-O) and CO_2 single bonds (C-O) (Dharma *et al*., 2016). An aliphatic methylene group with a C-H bond at wavenumber 1,463 cm^{-1} can be attributed to CH_3 from lipids and COO- from amino acids (Ong & Nomanbhay, 2022). The wavenumber 722 cm^{-1} is a *cis* double bond of a disubstituted olefin (Lim *et al*., 2018). The peak at 722 cm^{-1} is associated with the bending of the C-C double bond. There was a decrease in spectral absorption at the peak 1,170 cm^{-1}. This condition indicates increased CO_2 stretching (Sebayang *et al*., 2023) at storage times of more than three weeks. Each line in *Figure 6* shows the same pattern with the wavenumbers and transmittance marked for C-H (2,700-3,000 cm^{-1}), C=O (1,500-1,800 cm^{-1}) and C-O (600-1,400 cm^{-1}). The ester molecule (palm biodiesel) is visible in the C-O and C=O spectra. There is no reaction due to free radicals because there is no -O-H chain in the figure (*Figure 6*), which implies a reduced oxygen level. This is supported by the presence of substantial (73%) -C-H (2,923 cm^{-1}) and weak -O-H bonds (98%).

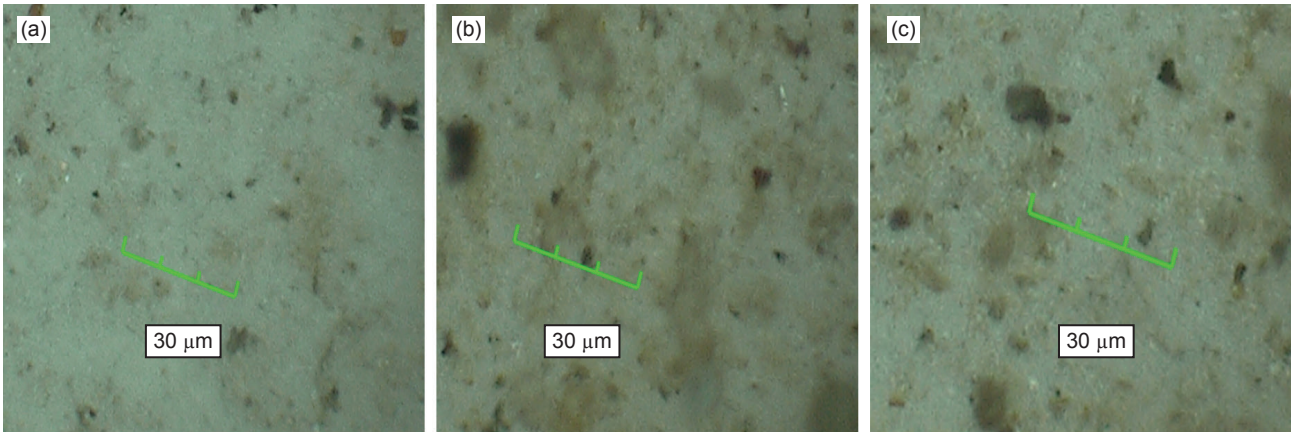


Figure 5. Morphology of sediment formed on the (a) 10th day, (b) 25th day, and (c) 30th day of mixed fuel storage.

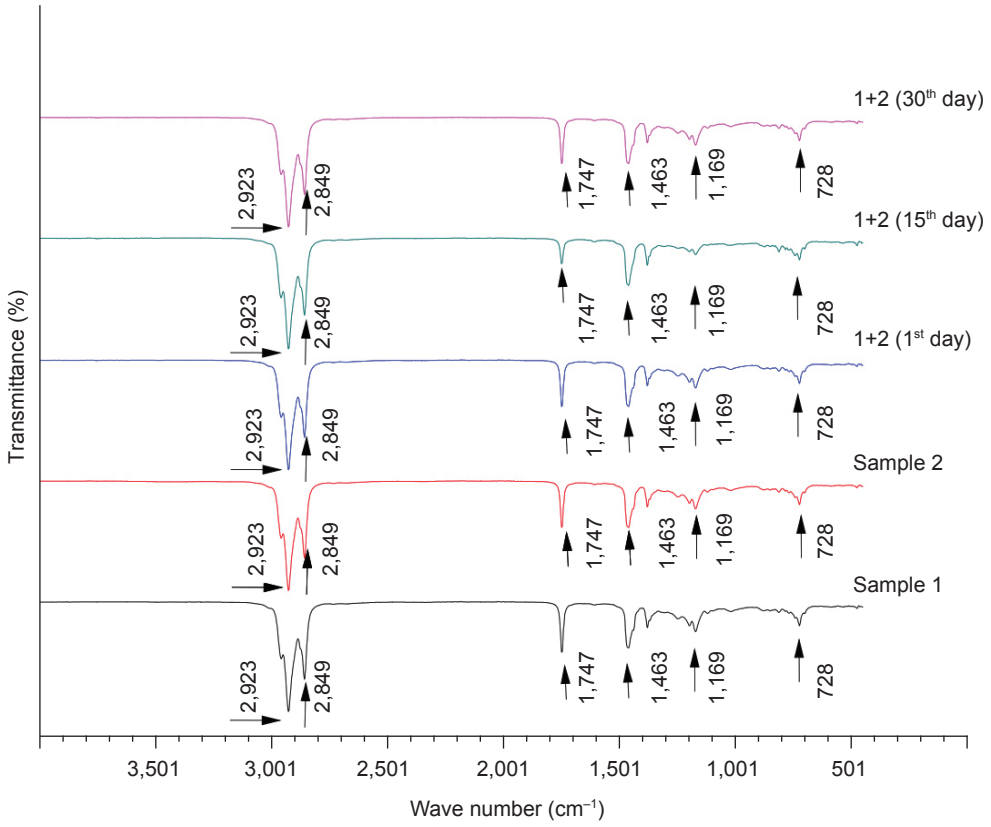


Figure 6. FTIR results.

CONCLUSION

In this study, tests on the characteristics of biodiesel B30 were carried out, including its cleanliness, viscosity, density, and water content. The results of this study show that differences in biodiesel sources affect these characteristics. In addition, the length of storage time plays a role in changing these characteristics. The results of the sediment test for biodiesel-diesel mixtures stored in ship tanks under actual conditions demonstrated the formation of contaminants with storage time. Based on the sediment test results, contaminants significantly increased after storage times longer than 20 days. This study showed an unstable distribution of contaminants between the bottom, middle and top of the ship's tank. These results indicate that fuel properties are unstable when the fuel is stored in a ship's tank in contrast to its storage in stationary fuel tanks, such as on land, where most contaminants remain at the bottom of the tank. The length of storage time is very influential on the formation of contaminants and it can be seen that there is an increase in contaminants after three weeks of storage. This condition dramatically affects the strategy for handling biodiesel blend storage in ship tanks. In addition, the quality of the biodiesel fuel mixture from the filling source is of particular concern during tank filling, as the blended fuel deteriorates as the storage period increases.

The interaction of asphaltene with water and other sediments, the prediction of sediment accumulation in a ship's fuel tank, the determination of the tank cleaning period, and detailed influences of various factors, such as multiple biodiesel properties, should be further studied to obtain better knowledge of the formation of contaminants. Sediment composition must be studied in greater detail in future studies to find countermeasures to sediment formation.

ACKNOWLEDGEMENT

This study was funded by the Ministry of Education, Culture, Research and Technology (KEMDIKBUDRISTEK) through the Doctoral Dissertation Research Assignment Program for Fiscal Year 2022 under grant agreement number NKB-1001/UN2.RST/HKP.05.00/2022.

REFERENCES

Ayoob, A. K., & Fadhil, A. B. (2019). Biodiesel production through transesterification of a mixture of non-edible oils over lithium supported on activated carbon derived from scrap tires. *Energy Conversion and Management, 201*, 112149. https://doi.org/10.1016/j.enconman.2019.112149

Bücker, F., Santestevan, N. A., Roesch, L. F., Jacques, R. J. S., Peralba, M. D. C. R., Camargo, F. A. D. O., & Bento, F. M. (2010). Impact of biodiesel on biodeterioration of stored Brazilian diesel oil. *International Biodeterioration & Biodegradation, 65*(1), 172–178. https://doi.org/10.1016/j.ibiod.2010.09.008

Ceriani, R., Gonçalves, C. B., Rabelo, J., Caruso, M., Cunha, A. C. C., Cavaleri, F. W., Batista, E. A. C., & Meirelles, A. J. A. (2007). Group contribution model for predicting viscosity of fatty compounds. *Journal of Chemical & Engineering Data, 52*(3), 965–972. https://doi.org/10.1021/je600552b

Chao, Y., Liu, N., Zhang, T., & Chen, S. (2010). Isolation and characterization of bacteria from engine sludge generated from biodiesel-diesel blends. *Fuel, 89*(11), 3358–3364. https://doi.org/10.1016/j.fuel.2010.05.041

Coates, J. (2000). Interpretation of infrared spectra, a practical approach. In *Encyclopedia of Analytical Chemistry: Applications, Theory and Instrumentation*. Wiley and Sons. https://doi.org/10.1002/9780470027318.a5606

Dharma, S., Masjuki, H. H., Ong, H. C., Sebayang, A. H., Silitonga, A. S., Kusumo, F., & Mahlia, T. M. I. (2016). Optimization of biodiesel production process for mixed *Jatropha curcas - Ceiba pentandra* biodiesel using response surface methodology. *Energy Conversion and Management, 115*, 178–190. https://doi.org/10.1016/j.enconman.2016.02.034

Erdmann, M., Böhning, M., & Niebergall, U. (2019). Physical and chemical effects of biodiesel storage on high-density polyethylene: Evidence of co-oxidation. *Polymer Degradation and Stability, 161*, 139–149. https://doi.org/10.1016/j.polymdegradstab.2019.01.018

Fersner, A. S., & Galante-Fox, J. M. (2014). Biodiesel feedstock and contaminant contributions to diesel fuel filter blocking. *SAE International Journal of Fuels and Lubricants, 7*, 783–791. https://doi.org/10.4271/2014-01-2723

Fregolente, P. B. L., Fregolente, L. V., & Wolf, M. R. M. (2012). Water content in biodiesel, diesel, and biodiesel-diesel blends. *Journal of Chemical & Engineering Data, 57*, 1817–1821. https://doi.org/10.1021/je300279c

Garcia, R., Figueiredo, F., Brandão, M., Hegg, M., Castanheira, É., Malça, J., Nilsson, A., & Freire, F. (2020). A meta-analysis of the life cycle greenhouse gas balances of microalgae biodiesel. *International Journal of Life Cycle Assessment, 25*, 1737–1748. https://doi.org/10.1007/s11367-020-01780-2

Gozan, M., Paryanto, I., Darmawan, M. A., Sahlan, M., Hermansyah, H., Rismana, E., Arbianto, A. D., Prakoso, T., Aroua, M. K., & Cognet, P. (2022). Prediction of B20 storage tank precipitate removal based on biodiesel monoglyceride content. *Chemical Engineering, 6*, 7. https://doi.org/10.3390/chemengineering6010007

He, B. B., & Van Gerpen, J. H. (2012). Analyzing biodiesel for contaminants and moisture retention. *Biofuels, 3*(3), 351–360. https://doi.org/10.4155/bfs.12.19

Hettige, G. E., & Sheridan, J. E. (1989). Interactions of fungi contaminating diesel fuel. *International Biodeterioration, 25*(4), 299–309. https://doi.org/10.1016/0265-3036(89)90004-3

Hidayat, J., & Sugiarto, B. (2020). Characteristic, structure, and morphology of carbon deposit from biodiesel blend. *Evergreen, 7*, 609–614. https://doi.org/10.5109/4150514

Hidayat, J., Sugiarto, B., Akbar, R. N., Fajar, N. A., Cekas, G. N., & Yubaidah, S. (2021). Analysis of the effect of biodiesel storage on changes in characteristics and deposits. *AIP Conference Proceedings, 070003*. https://doi.org/10.1063/5.0063918

Hill, E. C., & Hill, G. C. (2008). Microbial contamination and associated corrosion in fuels, during storage, distribution and use. *Advanced Materials Research, 38*, 257–268. https://doi.org/10.4028/www.scientific.net/AMR.38.257

International Organization for Standardization (ISO). (2017). *ISO 4406 Hydraulic fluid power-fluids-method for coding the level of contamination by solid particles.*

Jaroonjitsathian, S., Noomwongs, N., & Boonchukosol, K. (2016). Comprehensive experimental study on the effect of biodiesel/diesel blended fuel on common-rail DI diesel

engine technology. *International Journal of Automotive Technology, 17*, 289–298. https://doi.org/10.1007/s12239-016-0029-6

Kumar, N. (2017). Oxidative stability of biodiesel: Causes, effects and prevention. *Fuel*, *190*, 328–350. https://doi.org/10.1016/j.fuel.2016.11.001

Lee, I., Pfalzgraf, L. M., George, B. P., Erica, P., & Troy, H. (2007, April 6). The role of sterol glucosides on filter plugging. *Biodiesel Magazine.* https://biodieselmagazine.com/articles/the-role-of-sterol-glucosides-on-filter-plugging-1566

Li, T., Zhang, X., Zhang, C., Li, R., Liu, J., Zhang, H., Han, P., Zheng, Z., & Fan, C. (2019). A density functional theory study on the acid-catalyzed transesterification mechanism for biodiesel production from waste cooking oils. *Journal of the American Oil Chemists' Society, 96*, 137–145. https://doi.org/10.1002/aocs.12178

Lim, S. Y., Mutalib, M. S. A., Khaza'ai, H., & Chang, S. K. (2018). Detection of fresh palm oil adulteration with recycled cooking oil using fatty acid composition and FTIR spectral analysis. *International Journal of Food Properties, 21*, 2428–2451. https://doi.org/10.1080/10942912.2018.1522332

Lin, C. Y. (2013). Effects of biodiesel blend on marine fuel characteristics for marine vessels. *Energies, 6*, 4945–4955. https://doi.org/10.3390/en6094945

Mehmood, M. A., Ibrahim, M., Rashid, U., Nawaz, M., Ali, S., Hussain, A., & Gull, M. (2016). Biomass production for bioenergy using marginal lands. *Sustainable Production and Consumption, 9*, 3–21. https://doi.org/10.1016/j.spc.2016.08.003

Ministry of Energy and Mineral Resources (MEMR). (2014). *Second amendment to the regulation of the Minister of Energy and Mineral Resources number 32 of 2008 concerning the supply, utilization, and trade system of biofuels as other fuels.* https://www.bpdp.or.id/wp-content/uploads/2018/12/Permen-ESDM-Nomor-20-Tahun-2014-Tentang-Perubahan-Kedua-Atas-Permen-ESDM-Nomor-32-Tahun-2008.pdf

Ministry of Energy and Mineral Resources (MEMR). (2019, November 18). *Specification of biodiesel-diesel blend (B30) in Indonesia*. https://www.esdm.go.id/en/media-center/news-archives/b30-trial-these-are-b30-specs

Noor, C. M., Noor, M., & Mamat, R. (2018). Biodiesel as alternative fuel for marine diesel engine applications: A review. *Renewable and Sustainable Energy Reviews*, *94*, 127–142. https://doi.org/10.1016/j.rser.2018.05.031

Mushrush, G. W., Willauer, H. D., Wynne, J. H., Lloyd, C. T., & Bauserman, J. W. (2011). Storage tank stability of soybean-derived biodiesel. *Energy Sources, Part A: Recovery, Utilization, and Environmental Effects, 33*, 2303–2308. https://doi.org/10.1080/15567030903530590

Na-Ranong, D., & Kitchaiya, P. (2014). Precipitation above cloud point in palm oil based biodiesel during production and storage. *Fuel, 122*, 287–293. https://doi.org/10.1016/j.fuel.2014.01.003

Rao, D. N., & Reddy, A. S. (2023). Effects on the performance and emission characteristics of CRDI diesel engine fueled with ethanol, acid oil methyl ester biodiesel, and diesel blends. *Materials Today: Proceedings*. https://doi.org/10.1016/j.matpr.2023.06.065

Okoye, P. U., Longoria, A., Sebastian, P. J., Wang, S., Li, S., & Hameed, B. H. (2019). A review on recent trends in reactor systems and azeotrope separation strategies for catalytic conversion of biodiesel-derived glycerol. *Science of the Total Environment, 719*, 134595. https://doi.org/10.1016/j.scitotenv.2019.134595

Ong, M. Y., & Nomanbhay, S. (2022). Optimization study on microwave-assisted hydrothermal liquefaction of Malaysian macroalgae *Chaetomorpha sp.* for phenolic-rich bio-oil production. *Energies, 15*(11), 3974. https://doi.org/10.3390/en15113974

Paryanto, I., Budianta, I. A., Alifia, K. C. H., Hidayatullah, I. M., Darmawan, M. A., Prakoso, T., Indarto, A., & Gozan, M. (2022). Modelling of fuel filter clogging of B20 fuel based on the precipitate measurement and filter blocking test. *ChemEngineering, 6*(1), 84. https://doi.org/10.3390/chemengineering60600

Passman, F. J. (2013). Microbial contamination and its control in fuels and fuel systems since 1980 – A review. *International Biodeterioration & Biodegradation, 81*, 88–104. https://doi.org/10.1016/j.ibiod.2012.08.002

Ramos, M. J., Fernández, C. M., Casas, A., Rodríguez, L., & Pérez, Á. (2008). Influence of fatty acid composition of raw materials on biodiesel properties. *Bioresource Technology, 100*(1), 261–268. https://doi.org/10.1016/j.biortech.2008.06.039

Sebayang, A. H., Ideris, F., Silitonga, A. S., Shamsuddin, A. H., Zamri, M. F. M. A., Pulungan, M. A., Siahaan, S., Alfansury, M., Kusumo, F., & Milano, J. (2023). Optimization of ultrasound-assisted oil extraction from *Carica candamarcensis*: A potential Oleaginous tropical seed oil for biodiesel production. *Renewable Energy, 211*, 434–444. https://doi.org/10.1016/j.renene.2023.04.099

Silitonga, A. S., Masjuki, H. H., Ong, H. C., Kusumo, F., Mahlia, T. M. I., & Bahar, A. H. (2016). Pilot-scale production and the physicochemical properties of palm and *Calophyllum inophyllum* biodiesels and their blends. *Journal of Cleaner Production, 126*, 654–666. https://doi.org/10.1016/j.jclepro.2016.03.057

Silva, T. L., Cazarolli, J. C., Pizzolato, T. M., Guedes Frazzon, A. P., Mann, M. B., Frazzon, J., John, D. K., Ferrão, M. F., Rampelotto, P. H., D'Alessandro, E. B., Antoniosi Filho, N. R., & Bento, F. M. (2021). Microbial sludge formation in Brazilian marine diesel oil (B0) and soybean methylic biodiesel blends (B10 and B20) during simulated storage. *Fuel, 308*, 121905. https://doi.org/10.1016/j.fuel.2021.121905

Srichai, P., Ewphun, P. P., Charoenphonphanich, C., Karin, P., Tongroon, M., & Chollacoop, N. (2018). Injection characteristics of palm methyl ester blended with diesel using Zuech's chamber. *International Journal of Automotive Technology, 19*(3), 535–545. https://doi.org/10.1007/s12239-018-0051-y

Sugiarto, B., Hidayat, J. A., Akbar, R. N., Fajar, N. A., & Cekas, G. N. (2021). Analysis of the effect of biodiesel storage conditions on deposit growth with the FTIR (Fourier Transform InfraRed) test. *AIP Conference Proceedings, 2376*, 070004. https://doi.org/10.1063/5.0063925

Sugiarto, B., Hidayat, J. A., Suryantoro, M., Setiapraja, H., Yubaidah, S., & Dani, R. C. (2020a). Effect of biodiesel oxidation on deposit growth rate in the combustion chamber. *AIP Conference Proceedings, 030037*. https://doi.org/10.1063/5.0013746

Sugiarto, B., Mulyono, A. B., Hidayat, J. A., Suryantoro, M. T., Setiapraja, H., Yubaidah, S., Irfin, A., & Geo, R. (2020b). Characteristic of deposit growth in Indonesian national standard biodiesel, export grade biodiesel, and hydrotreated biodiesel using hot chamber test rig method. *AIP Conference Proceedings, 030036*. https://doi.org/10.1063/5.0013745

Sun, S., & Li, K. (2019). Biodiesel production from phoenix tree seed oil catalyzed by liquid Lipozyme TL100L. *Renewable Energy, 151*, 152–160. https://doi.org/10.1016/j.renene.2019.11.006

Tang, H., Salley, S. O., & Ng, K. Y. S. (2008). Fuel properties and precipitate formation at low temperature in soy-, cottonseed-, and poultry fat-based biodiesel blends. *Fuel, 87*(14), 3006–3017. https://doi.org/10.1016/j.fuel.2008.04.030

Tesfa, B., Mishra, R., Gu, F., & Powles, N. (2010). Prediction models for density and viscosity of biodiesel and their effects on fuel supply system in CI engines. *Renewable Energy, 35*(12), 2752–2760. https://doi.org/10.1016/j.renene.2010.04.026

Thangamani, S., Sundaresan, S. N., Kannappan, S. S., Barawkar, V. T., & Jeyaseelan, T. (2021). Impact of biodiesel and diesel blends on the fuel filter: A combined experimental and simulation study. *Energy, 227*, 120526. https://doi.org/10.1016/j.energy.2021.120526

Wang, H., Tang, H., Salley, S., & Ng, K. Y. S. (2009). Analysis of sterol glycosides in biodiesel and biodiesel precipitates. *Journal of the American Oil Chemists' Society, 87*(2), 215–221. https://doi.org/10.1007/s11746-009-1489-x

Zhang, T., Chao, Y., Liu, N., Thompson, J., Garcia, M., He, B. B., Van Gerpen, J., & Chen, S. (2011). Case study of biodiesel-diesel blends as a fuel in marine environment. *Advances in Chemical Engineering & Science, 1*(1), 65–71. https://doi.org/10.4236/aces.2011.12011

Zhou, D., Wei, H., Tan, Z., Xue, S., Qiu, Y., & Wu, S. (2023). Biodiesel as dispersant to improve the stability of asphaltene in marine very-low-sulfur fuel oil. *Journal of Marine Science and Engineering, 11*(2), 315. https://doi.org/10.3390/jmse11020315

Zhou, P., Fet, A., Michelsen, O., & Fet, K. (2003). A feasibility study of the use of biodiesel in recreational boats in the United Kingdom. *Proceedings of the Institution of Mechanical Engineers, Part M: Journal of Engineering for the Maritime Environment, 217*(4), 149–158. https://doi.org/10.1243/147509003322255859

Journal of Oil Palm Research Vol. 37 (1) March 2025 p. 160-171
DOI: https://doi.org/10.21894/jopr.2024.0006

PHYSICOCHEMICAL AND RHEOLOGICAL PROPERTIES OF RED PALM OLEIN OLEOGELS MADE WITH BEESWAX AS THE OLEOGELATOR

ANNISA NOOR RACHMAWATI[1]; NUR WULANDARI[1,2]* and EKO HARI PURNOMO[1,2]

ABSTRACT

Red palm olein (RPO) is a source of carotenoids that can act as provitamin A and pigment. RPO is liquid at room temperature and heating degrades carotenoids easily. Modifying RPO into a solid by oleogelation is essential to expand its application in food products. This study aimed to identify the physicochemical and rheological properties of RPO oleogels, using beeswax as the oleogelator, including crystal morphology and formation, solid fat content, total carotenoid content and colour analysis. This study consisted of three stages: Characterisation of the raw materials, preparation of RPO oleogels (0%-10% beeswax), and characterisation of the RPO oleogels. RPO starts to form as a solid at 3% beeswax with a melting point of 40.61 ± 1.73°C (solid at room temperature) and 557.73 ± 10.28 ppm of total carotenoid. Furthermore, increasing the beeswax concentration increased the compacity of the needle-shaped crystal structure, which has an impact on the rheological properties of the oleogels, including the higher linear viscoelastic region, yield stress, melting point and stability against frequency and temperature. RPO oleogel viscoelasticity showed a positive relationship with solid fat content. However, increasing beeswax concentration significantly decreases the total carotenoids of RPO oleogels, while increasing the lightness and yellowish colour of the oleogels.

Keywords: beeswax, oleogel, red palm olein.

Received: 7 July 2023; **Accepted:** 27 November 2023; **Published online:** 23 January 2024.

INTRODUCTION

Red palm olein (RPO) contains higher carotenoids, especially 85% of β-carotene, than other palm oil products (Eze *et al*., 2021; Nainggolan & Sinaga, 2021). RPO is produced from crude palm oil containing 500-700 ppm of carotenoids through degumming, deacidification and fractionation. Technically, its processing is conducted without bleaching or deodorisation, enabling the retention of carotenoids in crude palm oil (Dewi *et al*., 2023; Purnama *et al*., 2020). Carotenoids in RPO increase retinol levels in the blood serum, which justifies their use in cases of vitamin A deficiency (Harlen *et al*., 2018; Loganathan *et al*., 2017). Treatment of vitamin A deficiency is important because it causes metabolic disorders, metaplasia (changes in cell function), infectious diseases, immunoglobulin dysregulation, anaemia, promyelocytic leukaemia, xerophthalmia (failure to produce tears), cancer development and death (Carazo *et al*., 2021; Surman *et al*., 2020).

RPO consists of 42.23% palmitic acid (C:16-1), 41.58% oleic acid (C:18-1), and 10.71% linoleic acid (C:18-2), and for this reason, it is liquid at room temperature (Marliyati *et al*., 2021; Nainggolan & Sinaga, 2021). The carotenoids in RPO begin to degrade significantly at 60°C, leading to its limited application in food products (Sarah, 2018). Therefore, it is necessary to modify RPO to make

[1] Department of Food Science and Technology, Faculty of Agricultural Engineering & Technology, IPB University, Bogor 16680, Indonesia.

[2] Southeast Asian Food and Agricultural Science and Technology (SEAFAST) Centre, IPB University, Bogor 16680, Indonesia.

* *Corresponding author e-mail: wulandari_n@apps.ipb.ac.id*

it solid at room temperature while maintaining its carotenoid content. A modified RPO, which is in solid form, can be formulated for several food products that require raw fat materials, such as margarine, spread, and shortening (Hasibuan *et al.*, 2019; Wang *et al.*, 2021).

Oleogelation is an alternative to the conventional method that facilitates the mixing of oil and oleogelator through heating, followed by crystallisation through cooling to produce an oleogel. This process can minimise changes in the fatty acid composition and the formation of *trans* fatty acids by selecting an effective oleogelator (Samateh *et al.*, 2018). Natural waxes can form fat crystal networks at concentrations of less than 10% (Morales *et al.*, 2023; Sena *et al.*, 2022). Among natural wax, beeswax is often used in oleogelation, considering that Indonesia is among the world's top 20 largest beeswax-exporting countries. In addition, the beeswax market has experienced a significant growth in the last five years and is predicted to continue to grow until 2029 (SEAIR, 2023).

Oleogels are viscoelastic mixtures of liquid and solid lipids that possess specific properties that change owing to certain forces or disturbances (Han *et al.*, 2021; Naeli *et al.*, 2021; Pang *et al.*, 2020; Xu *et al.*, 2022). This has provoked research interests in the rheological analysis of viscoelastic materials. However, the profiles and rheological characteristics of RPO oleogels remain unknown. Therefore, this study aimed to identify the rheological properties of RPO oleogels using a beeswax oleogelator. The rheological properties were confirmed by morphological analysis and solid fat content (SFC). Morphological analyses were performed to observe the crystal morphology and formation of the oleogel. SFC is one of the parameters commonly used by the food industry in developing fat-based foods. In addition, considering the high carotenoid contents in RPO, this study determined the carotenoid content and colour of RPO oleogels at different beeswax concentrations.

MATERIALS AND METHODS

Samples

RPO was obtained from Carotino Sdn. Bhd. (Johor, Malaysia), and the beeswax was obtained from Babybees (Jakarta, Indonesia). The RPO is liquid at room temperature. It contained 60.93% unsaturated fatty acids mainly oleic and linoleic acids and 0.04% free fatty acids. The beeswax is solid at room temperature. It had 5.55 mg KOH/g of acid value, 97.55 mg KOH/g of ester value, 61°C slip melting point, and 110.04 mg KOH/g of saponification value.

Reagents

Wijs reagent, potassium iodate (≥99.5%), potassium iodide (≥99.5%), sodium thiosulfate (99.5%-101.0%), glacial acetic acid (≥99.8%), ethanol (≥99.5%), sodium hydroxide (≥97.0%), cyclohexane (≥99.5%), phenolphthalein (≥99.9%), amylum indicator (≥99.9%) and ethanol (95.1%-96.9%) were purchased from Merck (Darmstadt, Germany). Isooctane (≥99.0%) was purchased from SmartLab Indonesia (Jakarta, Indonesia), while distilled water was procured from a laboratory in the Department of Food Science and Technology at IPB University (Bogor, Indonesia). Demineralised water was procured by PT Laboratorindo Jaya Perkasa (Sidoarjo, Indonesia).

RPO Characterisation

RPO characterisation followed the standard method of the Indonesian National Standard 9098:2022 for Red Cooking Oil [Badan Standardisasi Nasional (BSN), 2022], concerning colour by Model F Lovibond Tintometer (England), odour and taste with organoleptic test, moisture content and volatile matter by UN55 Memmert Oven (Germany), iodine number, peroxide value, free fatty acid content, and total carotenoids by Uvmini-1240 Shimadzu UV-Vis spectrophotometer (Germany), and pelican oil. Pelican oil contains minerals that cannot be saponified in an alkaline alcohol-water solution.

Oleogelation

RPO and beeswax with a total mass of 10 g were heated at 65°C for 20 min in a LabTech LSB-015S shaking water bath (Indonesia). Subsequently, the mixture was cooled to 5°C for 24 hr (Kamali *et al*, 2019). The beeswax concentrations were 0%, 1%, 2%, 3%, 4%, 5%, 6%, 7%, 8%, 9% and 10% in duplicates.

Critical Gelling Concentration

Determination of critical gelling concentration was carried out visually by inverting the oleogel test tube at 25°C. The formation of a solid phase in the oleogel was indicated by a non-flowing oleogel (Flöter *et al.*, 2021).

Morphology Analysis

Melted oleogels were dropped onto a preheated slide and immediately covered with a cover slip. It was stored at 5°C for 24 hr. The crystal morphology of the RPO oleogels was observed using a CX31-P Olympus polarised microscope (Japan), at 1000× magnifications (Pang *et al.*, 2020).

Rheology

The rheological properties were analysed using Anton Paar MCR 92 rheometers (Austria). Rheological analysis consisted of amplitude, frequency and temperature sweep. An amplitude sweep was carried out at a strain of 0.01%-100.00%, with angular frequency of 10 rad/s at 25°C. A frequency sweep was performed in the linear viscoelastic region (LVR) with a frequency of 0.1-100.0 rad/s and a temperature of 25°C. The temperature sweep was carried out 25°C-90°C with 5°C/min and an angular frequency of 10 rad/s at linear viscoelastic region (LVR) (Barroso *et al*., 2022). This analysis was performed using PP50/S (beeswax and oleogel 1%-10% beeswax) and CP50-1 (RPO and oleogel 0% beeswax) geometries.

Melting Point

The melting point was determined from the result of the temperature sweep in rheology analysis. This melting point is an estimated melting point that was determined by the crossover point of G′ and G″, affected by temperature (Atik *et al.*, 2022).

Solid Fat Content

Solid fat content (SFC) was analysed by MQ20 Minispec nuclear magnetic resonance (NMR) analyser (Germany). The sample was heated at 100°C for 15 min in a water bath. The water bath was then turned off and the sample was left in the water bath for 30 min. They were re-heated in a water bath at 60°C for 5 min and transferred to a water bath at 0°C for 60 min. Samples were analysed at temperatures of 0°C, 10°C, 20°C, 30°C, 40°C, 50°C, 60°C, 70°C and 80°C or until the sample showed SFC of 0% [American Oil Chemists' Society (AOCS), 2022).

Total Carotenoid

The total carotenoid content was analysed using a UVmini-1240 Shimadzu UV-Vis spectrophotometer (Germany). Samples (0.1-0.5 g) were diluted with isooctane in a 25 mL volumetric flask, then analysed in a UV-Vis spectrophotometer at a wavelength of 446 nm [International Organization for Standardization (ISO), 2011).

Colour Characterisation

The colour was analysed using a Minolta CR-400 chromameter. The chromameter was calibrated on standard white and black plates. Colour analysis was performed by placing a homogeneous sample in a cylindrical tube with a diameter of 2 cm and a height of 1 cm (Papadaki *et al.*, 2020).

Statistical Analysis

The experimental design of this study was a completely randomised design (CRD) with two treatment replicates and all tests were repeated in duplicate. Data were analysed by analysis of variance (ANOVA) using the IBM SPSS Statistics 25 software with an alpha of 5%.

RESULTS AND DISCUSSION

Characteristics of Red Palm Olein

Table 1 shows that the RPO samples fully complied with the quality requirements of Indonesian National Standard (SNI 9098:2022) for Red Cooking Oil. The samples were of high quality and were made from high-quality raw materials; thus, they could be used as food ingredients.

TABLE 1. RPO CHARACTERISTICS BASED ON INDONESIA NATIONAL STANDARD (SNI 9098:2022)

Parameter	Quality requirements on SNI 9098:2022	Analysis results
Colour (Lovibond unit)		
Red	≥10	15.07 ± 0.06
Yellow	≥10	10.03 ± 0.06
Odour	Normal	Normal
Taste	Normal	Normal
Moisture content and volatile matter (%)	≤0.15	0.06 ± 0.02
Iodine number (g iod/100 g)	≥56.00	60.93 ± 0.52
Peroxide value (meq O_2/kg)	≤10.00	7.85 ± 0.32
Free fatty acid content (%)	≤0.50	0.04 ± 0.00
Total carotenoids (mg/kg)	≥400.00	657.24 ± 15.67
Pelican oil	Negative	Negative

Critical Gelling Concentration

As shown in *Figure 1*, the RPO oleogels with 0%, 1% and 2% beeswax flowed to the bottom of the tube due to gravity, indicating that the oleogels were liquid and could flow without additional force. However, the control sample (without beeswax) moved completely to the bottom of the tube and no oleogel remained at the top. Intriguingly, the RPO oleogel with 1% beeswax left residual oleogel on the inner tube wall. Visually, the remaining sample left in the tube appeared orange at the top of the test tube of the sample containing 2% beeswax, indicating it contained more residue than that containing 1% beeswax. A slower flow time indicated higher viscosity and higher resistance because it has more friction (Jia *et al.*, 2022).

In contrast, RPO oleogel with 3%-10% beeswax did not flow to the tube bottom after inversion. This indicated that the sample was solid at room temperature. Higher beeswax concentrations resulted in more solid oleogels (Han *et al.*, 2021; Pang *et al.*, 2020; Zbikowska *et al.*, 2022). About 3% beeswax is the minimum amount required to make the RPO oleogel solid at room temperature. Therefore, the critical gelling concentration of the RPO oleogel with beeswax as oleogelator is 3%.

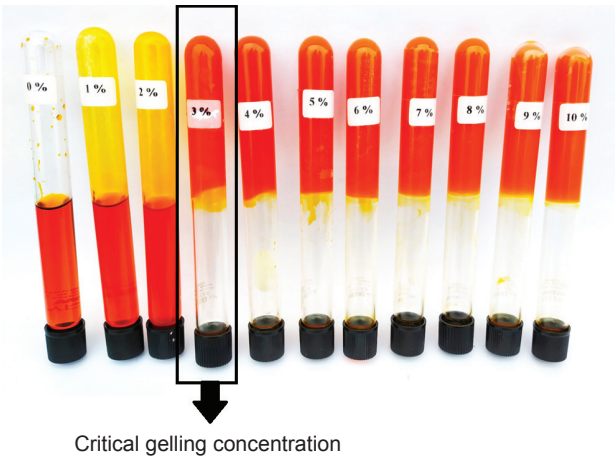


Figure 1. Critical gelling concentration of RPO oleogel.

Morphology Analysis

Figure 2 shows that the RPO oleogels had needle-shaped crystals. Its crystal morphology is characteristic of an oleogel that uses beeswax as the oleogelator (Chen *et al.*, 2021; Gómez-Estaca *et al.*, 2019; Pang *et al.*, 2020). RPO oleogel with 3%-10% beeswax has a compact crystal structure. Higher beeswax concentration resulted in denser crystal structures. Our results are consistent with that of Pang *et al.* (2020) in that the crystals are denser with higher concentration of beeswax in oleogels, either with camellia oil, sunflower oil, flaxseed oil or soybean oil. RPO oleogel with 10% beeswax is known to contain fluorescent molecules in the beeswax.

In contrast, RPO and RPO oleogel with 0% beeswax (control) had no crystal structure, therefore they were liquid at room temperature. Notably, the control oleogel (with 0% beeswax) was an RPO which underwent an oleogelation process without adding the beeswax. The RPO oleogels with 1% and 2% beeswax had needle-like crystals but did not have a compact structure. This result is consistent with the observations of the critical gelation concentrations, which indicated that the transition concentration was 3%. When viewed through a polarised microscope, compact crystal structures were formed at the transition concentrations. The crystal structure of beeswax had trapped the RPO into a solid form.

Rheology

Amplitude sweep results. The linear viscoelastic region (LVR) and yield stress were determined using an amplitude sweep. The maximum shear strain value at the LVR (LVR limit) was determined based on the shear strain value at the storage modulus (G'), loss modulus (G''), or complex modulus (G*) with a 5% difference from the shear strain value using a horizontal line plot (ISO, 2015). The LVR is the range in which at a given disturbance (shear strain or shear stress) on the sample, it does not damage the structure of the samples (Mezger, 2021). In this study, it was evident that beeswax had significantly affected the LVR (*Figure 3*). Higher levels of beeswax resulted in a wider range of LVR. A wider LVR indicates that the sample is more resistant to disturbances in the form of shear strain. Beeswax increases the strength and stability of the three-dimensional bonds to stabilise the RPO structure against shear strain treatment (Chai *et al.*, 2022; Espert *et al.*, 2022). However, the LVR for the RPO oleogels with 0% and 1% beeswax could not be identified because they were Newtonian fluids. The viscosity of a Newtonian fluid is not affected by the force applied to the flow and a very small shear strain can cause sample deformation (Alexander, 2017; Gagliardi, 2020; Hariyadi *et al.*, 2019).

The yield stress is the minimum force required to flow a material, such as a liquid generally possessed by non-Newtonian fluids (Hariyadi *et al.*, 2019). This analysis revealed that increased beeswax oleogelator levels increased the yield stress (*Figure 4*). The yield stress is associated with the length of the saturated fatty acid chains in the beeswax and the crystal structure of the oleogel. Beeswax mainly contains C24-C36 fatty acids, most of which are saturated fatty acids (approximately 85%). However, the dominant saturated fatty acids chain length was C14-C31, with a long-

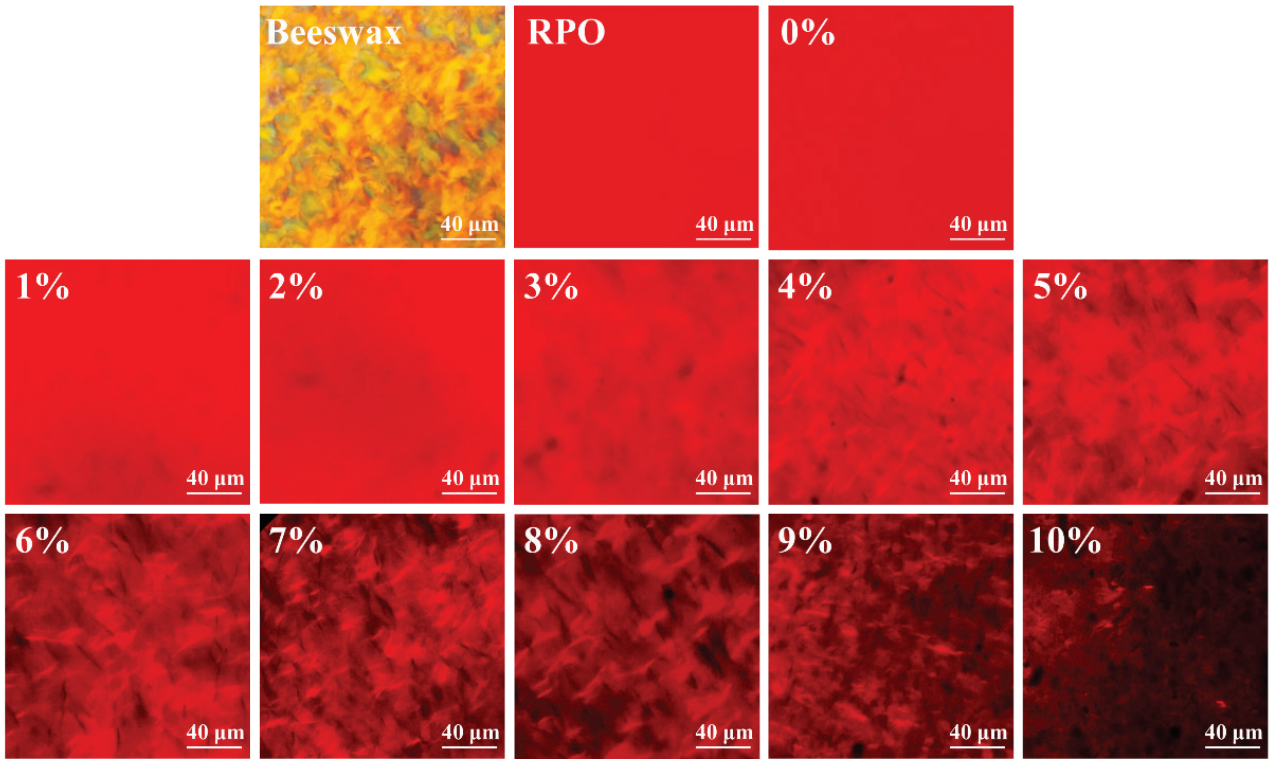


Figure 2. Needle-shaped crystal of beeswax, RPO and RPO oleogels.

chain of even-numbered palmitate wax esters and fatty acids (Chasan *et al.*, 2021; Doan *et al.*, 2016a; Szulc *et al.*, 2020). As explained in the morphology analysis section, the higher beeswax concentration caused a denser crystal structure. A denser crystal structure resulted in a higher elastic modulus value; therefore, a stronger force was required to destroy the oleogel structure. Therefore, the yield stress increased as the beeswax concentration increased.

Frequency sweep results. Changes in the frequency given to the sample markedly alter G′ and G″. Values are specific to each sample and frequency. In addition, the G′ and G″ have the same value at the crossover point. The crossover point is indicated by the angular frequency required to achieve a loss factor of 1 (Sivakanthan *et al.*, 2023). The loss factor is the ratio of loss modulus to storage modulus. In the case of RPO oleogels with 0%-3% beeswax, the higher concentration of beeswax resulted in a higher crossover point (*Figure 5*). A higher crossover point indicates that a higher frequency is required to change the RPO oleogel phase, from the solid to the liquid phase. In addition, the higher the concentration of beeswax, the more stable the RPO oleogel structure (Doan *et al.*, 2016b; Kwon & Chang, 2022; Sivakanthan *et al.*, 2023).

Moreover, G′ is higher than G″ at frequency below the crossover point, suggesting that the sample is solid. Conversely, above the crossover point, G′ was lower than G″, indicating that the sample was liquid. Previous studies have discovered different types of oleogels, including walnut oleogels with monoglycerides, sunflower seed oleogels with carnauba wax, hazelnut oleogels with carnauba wax and olive oleogels with carnauba wax, with similar results (Pehlivanoglu *et al.*, 2021; Sun *et al.*, 2021).

In addition, the higher concentration of beeswax had increased G′ and G″. However, the crossover points of the RPO oleogel with 4%-10% beeswax could not be identified. Oleogels with 4%-10% beeswax had a crossover point of more than 100 rad/s, exceeding the detection limit of the rheometer used. Thus, they were not analysed further in this study. However, these results demonstrated that the angular frequency range of 0.10-100.00 rad/s was unable to change the 4%-10% oleogel phase from solid to liquid.

Temperature Sweep Results. The addition of the beeswax oleogelator to the formulation of the RPO oleogel was aimed at increasing the melting point of RPO. Beeswax, which has elevated long-chain fatty acids, immobilises RPO fatty acid molecules in a three-dimensional matrix, formed from the beeswax needle crystals. Beeswax can transform RPO from liquid to solid at room temperature. In this study, the melting point of RPO had increased significantly with the addition of beeswax (*Table 2*).

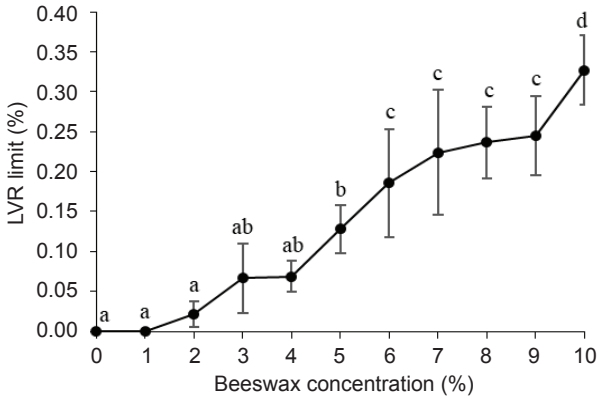


Figure 3. Linear viscoelastic region (LVR) limit of red palm olein oleogels. Distinct letters show significant differences between the LVR limit of the samples (two-way ANOVA; Duncan test: p*-value ≤0.05).*

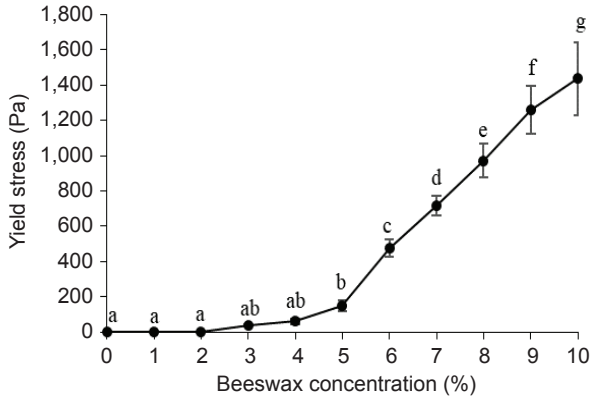


Figure 4. Yield stress of red palm olein oleogels. Distinct letters show significant differences between the yield stress of the samples (two-way ANOVA; Duncan test: p*-value ≤0.05).*

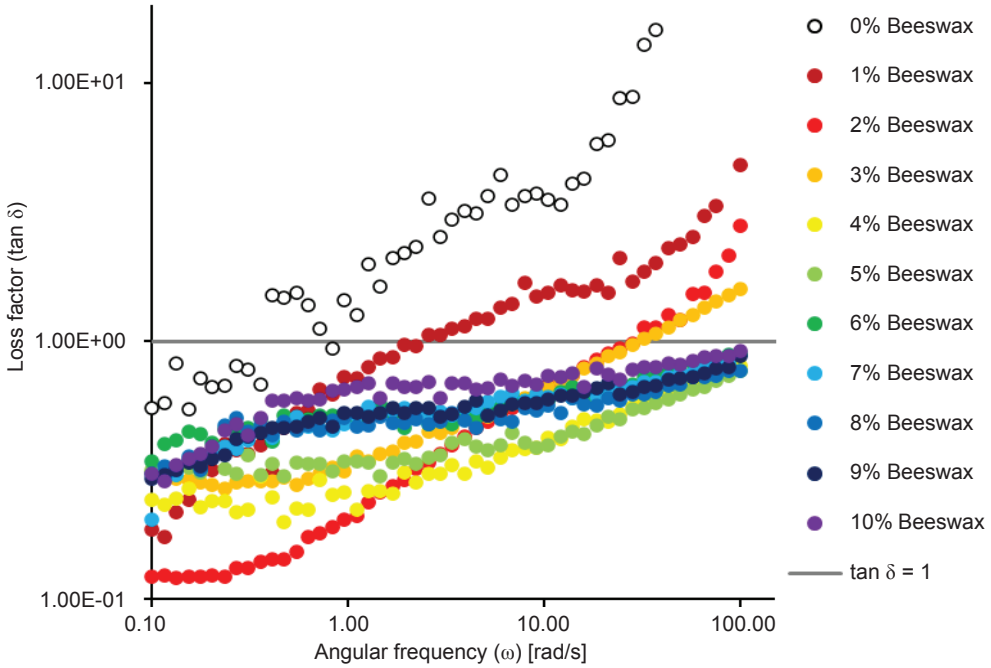


Figure 5. Frequency sweep results of red palm olein oleogels.

TABLE 2. MELTING POINT OF RED PALM OLEIN OLEOGELS

Beeswax concentration (%)	Melting point (°C)
0	<25.00
1	<25.00
2	26.94 ± 1.87 [a]
3	40.61 ± 1.73 [bc]
4	39.83 ± 1.49 [b]
5	41.87 ± 2.04 [bc]
6	42.90 ± 0.34 [c]
7	45.65 ± 1.87 [d]
8	46.26 ± 1.51 [d]
9	46.82 ± 1.45 [d]
10	47.29 ± 1.56 [d]

Note: Values are the mean ± standard deviation (n=4). Distinct superscript letters indicate significant differences between the melting points of the samples (two-way ANOVA; Duncan's test: $p \leq 0.05$).

The RPO oleogels with 0% and 1% beeswax had melting points of less than the room temperatures (<25°C). It indicated that the oleogels were liquid at room temperature. The RPO oleogel with 2% beeswax had a melting point around room temperatures (26.94°C ± 1.87°C). RPO oleogels with 0% beeswax (control) and 1%-2% beeswax did not form a three-dimensional matrix that firmly trapped the oil molecules. On the other hand, RPO oleogels with 3%-10% beeswax had melting points higher than 25°C, so they were solid at room temperature. This indicated that a minimum of 3% beeswax in the RPO oleogel was in solid form at room temperature.

This melting point of the RPO oleogel was comparable to the results of visual analysis of critical gelation concentrations. RPO oleogel with a melting point above room temperatures (about 25°C) is in solid form at room temperatures, which can be visually identified from the RPO oleogel that was motionless after tube inversion. Oleogel with 3% beeswax had the lowest concentration of beeswax, whose melting point was above 25°C, with a critical gelling concentration of RPO oleogel at 3%. The melting point indicates the temperature limits at which the gel structure can be maintained during heating. These are important for making decisions and controlling the texture, emulsion stability, homogeneity, and other qualities of food during processing.

Solid Fat Content

RPO showed solid fat content (SFC) of 58.89% ± 0.46% at 0°C, but it turned to 0% at 20°C. This suggests that at a temperature of 20°C, the RPO was entirely in the liquid phase. In contrast, beeswax had a higher SFC than the RPO samples and all RPO oleogel samples at all temperature levels. The SFC of beeswax was 92.21% ± 0.04% at 0°C and reached 0% at 60°C. The SFC value is directly proportional to the melting point of the sample. A higher melting point corresponds to a higher temperature for 0% of SFC.

The melting point profile changed markedly owing to the addition of beeswax to the RPO oleogels. A higher beeswax concentration shifted the SFC chart pattern to the right (*Figure 6*). However, the RPO oleogel had a similar pattern of SFC reduction with temperature as the RPO SFC. The increase in the SFC of oleogels resulted from the 3-dimensional structure of the oleogelator, which can trap oils, enhancing the content of saturated fatty acids in the oleogel (Pehlivanoglu *et al*., 2021). Another study revealed that the SFC of a crude palm oil oleogel with 5% beeswax was higher than that of a cooking oil oleogel with 5% beeswax at all temperatures. It is clearly understandable that CPO has a higher saturated fatty acid content than palm cooking oil, even though it comes from a similar source, that is palm oil (Suriaini *et al*., 2022). In our experiment, the SFC results were consistent with the results of the melting point analysis during the temperature sweep. When the SFC reached 0%, the temperature was aligned with the melting point of the RPO oleogel. This indicated that the melting point had represented at solid-to-liquid phase transition. A SFC of 0% indicates that the sample is completely liquid.

The temperature range required to achieve a SFC of 0% was close to the melting point analysis results, based on the temperature sweep. RPO oleogel with 2% beeswax had SFC 0% at 30°C, while the melting point of this oleogel was 26.94 ± 1.87°C. The SFC 0% was achieved by RPO oleogel with 3%-5% beeswax at 40°C, while RPO oleogel with 6%-10% beeswax reached SFC 0% at 50°C. Therefore, the rheological properties obtained by temperature sweep analysis can replace SFC in determining the transition temperature between the solid and liquid phases at a more specific temperature.

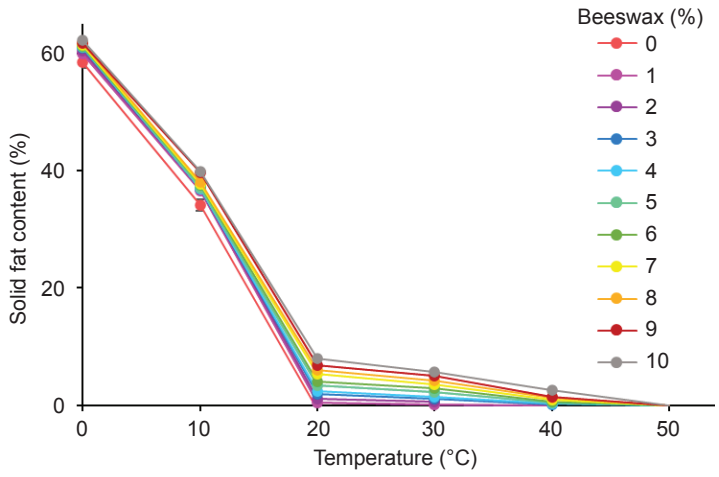


Figure 6. Solid fat content of red palm olein oleogels.

Total Carotenoid

The total carotenoid in RPO and beeswax reached 670.77 ± 1.81 ppm and 94.18 ± 1.69 ppm, respectively. The combination of RPO and beeswax in RPO oleogels at a particular ratio contained various levels of total carotenoids. The results showed that beeswax reduced the total carotenoids contents of the RPO oleogels. In this study, the carotenoid content in the RPO oleogel with 1% beeswax was higher than that in the RPO with 0% beeswax (control). However, the addition of beeswax exceeding 1% significantly increased the total carotenoid content of the RPO oleogels (*Figure 7*). The increase in the total carotenoid content caused by oleogelation protects specific carotenoid compounds (Pușcaș *et al.*, 2022). Although increasing the beeswax concentration decreased the total carotenoid levels, adding up to 10% beeswax resulted in high total carotenoid levels of 483.27 ± 2.53 ppm. Thus, RPO oleogels can be used as food ingredients and sources of provitamin A.

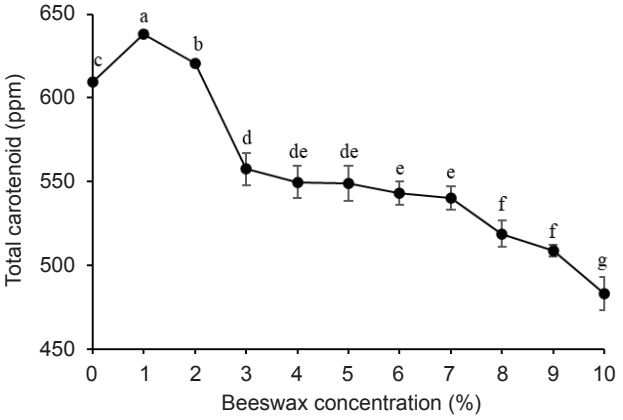


Figure 7. Total carotenoid of red palm olein oleogels. Distinct letters show significant differences between the LVR limit of the samples (two-way ANOVA; Duncan test: p≤*0.05).*

Colour Attributes

Colour analysis showed that all the oleogel samples were orange. The beeswax colour was pale yellow and the RPO colour was orange-red. The lightness of the control samples was higher than that of the RPO samples. Noticeably, the orange colour of the RPO oleogels darkened up to a beeswax concentration of 2%. The lightness of the oleogel containing 3% beeswax was higher than that of the oleogel containing 2% beeswax. At beeswax concentration of 3% onward, the colour pattern (L, a*, b*) was similar, but they differed compared with 0%-2% beeswax samples (*Figure 8*), highlighting the impact of the transition phase (liquid at <3% beeswax; solid at ≥3% beeswax) on the physical appearance of samples. A higher beeswax concentration resulted in a higher lightness level of the RPO oleogels. This is due to the reduced proportion of RPO. The RPO oleogel, a solid at room temperature, had a paler colour than the liquid RPO oleogel. Therefore, the lightest oleogel sample was the RPO oleogel with 10% beeswax. RPO has the most significant colour effects on oleogel, primarily towing to the carotenoids, which produce a yellow to red colour, due to the presence of conjugated double bonds in the polyene chain (Cvetkovic & Nikolic, 2017; Maoka, 2019).

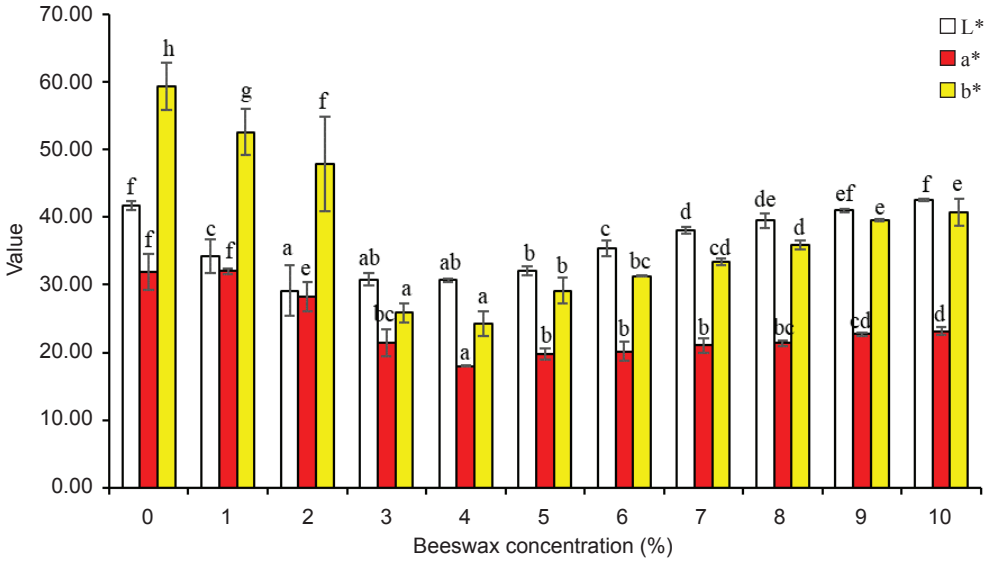


Figure 8. Colour of red palm olein oleogels.

CONCLUSION

An RPO oleogel was successfully prepared from RPO by adding beeswax as an oleogelator. We found that a minimum concentration of 3% beeswax is needed to produce a solid oleogel at room temperatures, which is critical in gelling concentration. The oleogelation process induced remarkable changes in the rheological characteristics, SFC, total carotenoids and colour. The results showed that a higher concentration of beeswax produced a more compact needle crystal structure, a wider LVR, a higher yield stress, a higher crossover point, a higher melting point and a higher temperature of SFC 0%. RPO oleogel with 3% beeswax showed a significant parameter transition, resulting in compact crystal structures that immobilised the RPO, with an LVR limit of 0.02% ± 0.04%, yield stress of 38.3675 ± 8.1864 Pa, and a melting point of 40.61°C ± 1.73°C. However, a higher concentration of beeswax yielded a lower total carotenoid content in the RPO oleogels. The decrease in the total carotenoids content correlated with the resulting colour. The lower total carotenoid content also corresponded to a lighter colour of the RPO oleogels, which tended to be yellowish. These RPO oleogels can be used as alternative raw materials as sources of provitamin A for fat-based food products, such as margarine, spreadable products and shortening.

ACKNOWLEDGEMENT

We would like to express our deepest gratitude to Department of Food Science and Technology, IPB University for facilitating this research.

REFERENCES

Alexander, D. E. (2017). *Nature's machines: An introduction to organismal biomechanics*. Academic Press.

American Oil Chemists' Society (AOCS). (2022). *AOCS official method Cd 16b–93: Solid fat content (SFC) by low-resolution nuclear magnetic resonance, direct method*.

Atik, D. S., Demirci, M., Toker, O. S., & Palabiyik, I. (2022). Development of a novel rheological method for determining melting properties of gelatin-based gummies. *International Journal of Biological Macromolecules, 209*(1), 385–395. https://doi.org/10.1016/j.ijbiomac.2022.04.002

Barroso, L., Karatay, G., & Hubinger, M. (2022). Effect of potato starch hydrogel: Glycerol monostearate oleogel ratio on the physico-rheological properties of bigels. *Gels, 8*(11), 694–711. https://doi.org/10.3390/gels8110694

Badan Standardisasi Nasional (BSN). (2022). *SNI 9098:2022 Minyak makan merah*.

Carazo, A., Macáková, K., Matoušová, K., Krčmová, L. K., Protti, M., & Mladěnka, P. (2021). Vitamin A update: Forms, sources, kinetics, detection, function, deficiency, therapeutic use and toxicity. *Nutrients, 13*(5), 1703. https://doi.org/10.3390/nu13051703

Chai, X., Zhang, Y., Shi, Y., & Liu, Y. (2022). Crystallization and structural properties of oleogel-based margarine. *Molecules, 27*(8952), 1–12. https://doi.org/10.3390/molecules27248952

Chasan, R., Rosenberg, D., Kimscha, F., Beeri, R., Golan, D., Ayelet, D., Galili, E., & Spiteri, C. (2021). Bee products in prehistoric Southern Levant: Evidence from the lipid organic record. *Royal Society Open Science, 8*, 1–21. https://doi.org/10.1098/rsos.210950

Chen, Y., Gavaliatsis, T., Kuster, S., Stadeli, C., Fischer, P., & Windhab, E. J. (2021). Crust treatments to reduce bread staling. *Current Research in Nutrition & Food Science, 4*, 182–190. https://doi.org/10.1016/j.crfs.2021.03.004

Cvetkovic, D. J., & Nikolic, G. S. (2017). *Carotenoids*. IntechOpen. https://doi.org/10.5772/65523

Dewi, E. K., Mardawati, E., & Nurhasanah, S. (2023). Color changes evaluation on crude palm oil processing into red palm oil and palm cooking oil as a visual indicator of β-carotene content in oils. *Biomass Biorefinery & Bioeconomy, 1*(1), 25–29.

Dinkgreve, M., Paredes, J., Denn, M. M., & Bonn, D. (2016). On different ways of measuring the yield stress. *Journal of Non-Newtonian Fluid Mechanics, 238*, 233–241. https://doi.org/10.1016/j.jnnfm.2016.11.001

Doan, C. D., Tavernier, I., Sintang, M. D. B., Danthine, S., de Walle, D. V., Rimaux, T., & Dewittinck, K. (2016a). Crystallization and gelation behavior of low- and high-melting waxes in rice bran oil: A case-study on berry wax and sunflower wax. *Food Biophysics, 12*(1), 97–108. https://doi.org/10.1007/s11483-016-9467-y

Doan, C. D., To, C. M., De Vrieze, M., Lynen, F., Danthine, S., Brown, A., Dewettinck, K., & Patel,

A. R. (2016b). Chemical profiling of the major components in natural waxes to elucidate their role in liquid oil structuring. *Food Chemistry, 214*, 717–725. https://doi.org/10.1016/j.foodchem.2016.07.123

Espert, M., Hernández, M. J., Sanz, T., & Salvador, A. (2022). Rheological properties of emulsion templated oleogels based on xanthan gum and different structuring agents. *Current Research in Nutrition & Food Science, 5*, 564–570. https://doi.org/10.1016/j.crfs.2022.03.001

Eze, S. O., Orji, J. N., Okechukwu, V. U., Omokpariola, D. O., Umeh, T. C., & Oze, N. R. (2021). Effect of processing method on carotenoid profiles of oils from three varieties of Nigerian palm oil (*Elaeis guineensis*). *Biophysical Chemistry, 12*, 23–31. https://doi.org/10.4236/jbpc.2021.123003

Flöter, E., Wettlaufer, T., Conty, V., & Scharfe, M. (2021). Oleogels – Their applicability and methods of characterization. *Molecules, 26*(6), 1–19. https://doi.org/10.3390/molecules26061673

Gagliardi, M. (2020). Rheology of polymer coatings. In S. M. Rangappa, J. Parameswaranpillai, & S. Siengchin (Eds.), *Polymer coatings: Technologies and applications* (pp. 117-136). CRC Press.

Gómez-Estaca, J., Pintado, T., Jimenez-Colmenero, F., & Cofrades, S. (2019). Assessment of a healthy oil combination structured in ethyl cellulose and beeswax oleogels as animal fat replacers in low-fat, PUFA-enriched pork burgers. *Food Bioprocessing Technology, 12*, 1068–1081. https://doi.org/10.1007/s11947-019-02281-3

Han, W., Chai, X., Liu, Y., Xu, Y., & Tan, C. P. (2021). Crystal network structure and stability of beeswax-based oleogels with different polyunsaturated fatty acid oils. *Food Chemistry, 381*, 131745. https://doi.org/10.1016/j.foodchem.2021.131745

Hariyadi, P., Purnomo, E. H., & Kusnandar, F. (2019). Aliran dan transportasi fluida. In P. Hariyadi (Ed.), *Landasan teknik pangan* (pp. 91-158). IPB Press.

Harlen, W. C., Muchtadi, T. R., & Palupi, N. S. (2018). β-Carotene bioavailability of palm oil emulsion drink in rats (*Rattus norvegicus*) blood plasma and liver. *International Food Research Journal, 25*(4), 1349–1356.

Hasibuan, H., Akram, A., Putri, P., & Rangkuti, B. T. (2019). Pembuatan margarin dan baking shortening dari minyak sawit merah dan aplikasinya dalam produk bakery. *Agritech, 38*(4), 353–363. https://doi.org/10.22146/agritech.32162

International Organization for Standardization (ISO). (2011). *ISO 17932:2011: Palm oil - Determination of the deterioration of bleachability index (DOBI) and carotene content*.

International Organization for Standardization (ISO). (2015). *ISO 6721-10:2015: Plastics - Determination of dynamic mechanical properties - Complex shear viscosity using a parallel-plate oscillatory rheometer*.

Jia, X., Chiu, Q., Zhu, Z., Ding, Q., & Gao, P. (2022). Influence of fluid flood viscosity on internal flow characteristics of conveying pump. *Frontiers in Nutrition, 9*. https://doi.org/10.3389/fnut.2022.910589

Kamali, E., Sahari, M. A., Barzegar, M., & Ahmadi, G. H. (2019). Novel oleogel formulation based on amaranth oil: Physicochemical characterization. *Food Science & Nutrition, 7*(6), 1986–1996. https://doi.org/10.1002/fsn3.1018

Kwon, U. H., & Chang, Y. H. (2022). Rheological and physicochemical properties of oleogel with esterified rice flour and its suitability as a fat replacer. *Foods, 12*(2), 10–19. https://doi.org/10.3390/foods11020242

Loganathan, R., Subramaniam, K. M., Radhakrishnan, A. K., Choo, Y. M., & Teng, K. T. (2017). Health-promoting effects of red palm oil: Evidence from animal and human studies. *Nutritional Reviews, 75*(2), 98–113. https://doi.org/10.1093/nutrit/nuw054

Maoka, T. (2019). Carotenoids as natural functional pigments. *Journal of Natural Medicines, 74*(1), 1–16. https://doi.org/10.1007/s11418-019-01364-x

Marliyati, S., & Rimbawan, H. (2021). Karakteristik fisikokimia dan fungsional minyak sawit merah. *Jurnal Gizi Komunitas Indonesia, 10*(1), 83–94.

Mezger, T. (2021). *Applied rheology* (8th ed.). Anton Paar GmbH.

Morales, E., Iturra, N., Contardo, I., Quilaqueo, M., Franco, D., & Rubilar, M. (2023). Fat replacers based on oleogelation of beeswax/shellac wax

and healthy vegetable oils. *Food Science and Technology, 185*, 1–10. https://doi.org/10.1016/j.lwt.2023.115144

Naeli, M. H., Milani, J. M., Farmani, J., & Zargaraan, A. (2021). Developing and optimizing low-saturated oleogel shortening based on ethyl cellulose and hydroxypropyl methyl cellulose biopolymers. *Food Chemistry, 369*, 130963. https://doi.org/10.1016/j.foodchem.2021.130963

Nainggolan, M., & Sinaga, A. G. S. (2021). Characteristics of fatty acid composition and minor constituents of red palm olein and palm kernel oil combination. *Journal of Advanced Pharmaceutical Technology & Research, 12*(1), 22–26. https://doi.org/10.4103/japtr.JAPTR_91_20

Pang, M., Shi, Z., Lei, Z., Ge, Y., Jiang, S., & Cao, L. (2020). Structure and thermal properties of beeswax-based oleogels with different types of vegetable oil. *Grasas y Aceites, 71*(4), 1–11. https://doi.org/10.3989/gya.0806192

Papadaki, A., Kopsahelis, N., Freire, D., Mandala, I., & Koutinas, A. (2020). Olive oil oleogel formulation using wax esters derived from soybean fatty acid distillate. *Biomolecules, 10*(106), 1–9. https://doi.org/10.3390/bio10010106

Pehlivanoglu, H., Akcicek, A., Can, M. A., Karasu, S., Demirci, M., & Yilmaz, M. T. (2021). Effect of oil type and concentration on solid fat contents and rheological properties of watery oleogels. *Rivista Italiana delle Sostanze Grasse*, *98*(3), 177–186.

Purnama, K. O., Setyaningsih, D., Hambali, E., & Taniwiryono, D. (2020). Processing, characteristics, and potential application of red palm oil – A review. *International Journal of Oil Palm, 3*(2), 40–55. https://doi.org/10.35876/ijop.v3i2.47

Pușcaș, A., Mureșan, A., Socaci, S., Dulf, F., Muste, S., Fetea, F., Semeniuc, C. A., Bunea, A., Mureșan, V., & Pintea, A. (2022). Cold-pressed pumpkin seed oil fatty acids, carotenoids, volatile compounds profiles, and infrared fingerprints as affected by storage time and wax-based oleogellation. *Journal of the Science of Food and Agriculture, 103*(2), 680–691. https://doi.org/10.1002/jsfa.12180

Rege, S. A., Momin, S. A., Wadekar, S. D., & Bhowmick, D. N. (2013). Formulation of a functional fat spread stabilized by natural antioxidants and emulsifiers. *Malaysian Journal of Nutrition, 19*(1), 121–130.

Samateh, M., Sagiri, S., & John, G. (2018). Molecular oleogels: Green approach in structuring vegetable oils. In A. Marangoni & N. Garti (Eds.), *Edible oleogels (2nd ed.,)* (pp. 415-438). AOCS Press. https://doi.org/10.1016/b978-0-12-814270-7.00018-6

Sarah, M. (2018). Carotenoids preservation during sterilization of palm fruit using microwave irradiation. *Journal of Engineering and Applied Sciences, 13*(3), 1009–1014.

SEAIR. (2023). *Beeswax exporters.* https://www.seair.co.in/beeswax-exporters

Sena, B., Dhal, S., Sahu, D., Sarkar, P., Mohanty, B., Jarzebski, M., Wieruszewski, M., Behera, H., & Pal, K. (2022). Variations in microstructural and physicochemical properties of soy wax/soybean oil-derived oleogels using soy lecithin. *Polymers, 14*(19), 3928. https://doi.org/10.3390/polym14193928

Sivakanthan, S., Fawzia, S., Mundree, S., Madhujith, T., & Karim, A. (2023). Optimization and characterization of new oleogels developed based on sesame oil and rice bran oil. *Food Hydrocolloids, 142*, 108839. https://doi.org/10.1016/j.foodhyd.2023.108839

Sun, H., Xu, J., Lu, X., Xu, Y., Regenstein, J. M., Zhang, Y., & Wang, F. (2021). Development and characterization of monoglyceride oleogels prepared with crude and refined walnut oil. *Food Science and Technology, 154*, 1–10. https://doi.org/10.1016/j.lwt.2021.112769

Suriaini, N., Arpi, N., Syamsudin, Y., & Supardan, M. D. (2022). Characteristics of palm oil-based oleogel and its potency as a shortening replacer. *South African Journal of Chemical Engineering, 43*, 197–203. https://doi.org/10.1016/j.sajce.2022.11.003

Surman, S. L., Penkert, R. R., Sealy, R. E., Jones, B. G., Marion, T. N., Vogel, P., & Hurwitz, J. L. (2020). Consequences of vitamin A deficiency: Immunoglobulin dysregulation, squamous cell metaplasia, infectious disease, and death. *International Journal of Molecular Sciences, 21*(15), 1–17. https://doi.org/10.3390/ijms21155570

Szulc, J., Machnowski, W., Kowalska, S., Jachowicz, A., Ruman, T., Steglińska, A., & Gutarowska, B. (2020). Beeswax-modified textiles: Method of preparation and assessment of antimicrobial properties. *Polymer, 12*(2), 344–359. https://doi.org/10.3390/polym12020344

Wang, X., Wang, S., Nan, Y., & Liu, G. (2021). Production of margarines rich in unsaturated fatty acids using oxidative-stable vitamin C-loaded oleogel. *Journal of Oleo Science, 70*(8), 1059–1068. https://doi.org/10.5650/jos.ess20264

Xu, H., Li, T., Zhang, H. X., Shi, C. H., Cao, J. Q., & Zhang, X. R. (2022). The application of oleogels in food products: Classification, preparation, and characterization. *Acta Alimentaria, 51*(4), 462–478. https://doi.org/10.1556/066.2022.00099

Zbikowska, A., Onacik-Gür, S., Kowalska, M., Sowiński, M., Szymańska, I., Żbikowska, K., Marciniak-Łukasiak, K., & Werpachowski, W. (2022). Analysis of stability, rheological and structural properties of oleogels obtained from peanut oil structured with yellow beeswax. *Gels, 8*(7), 448. https://doi.org/10.3390/gels8070448

Journal of Oil Palm Research Vol. 37 (1) March 2025 p. 172-180
DOI: https://doi.org/10.21894/jopr.2024.0009

INVERSE VULCANISED POLYSULPHIDE ADSORBENT FROM WASTE COOKING PALM OIL FOR Cu^{2+} REMOVAL

MOHD FAIZAL ALI[1]; NANCY NUBUR LIBAT[1]; HANNAH NISA ADAWIYAH[1]; ABDULLAH NAYEEM[1,2] and JUN HASLINDA SHARIFFUDDIN[1,3]*

ABSTRACT

Heavy metals are considered to be toxic to humans. Commonly produced by petrochemical plants and pesticide productions, various techniques have been utilised to treat wastewater contaminated with heavy metal such as copper (Cu^{2+}). This article focuses on using adsorption by utilising polysulphide adsorbent to treat wastewater via inverse vulcanisation. The huge amount of waste cooking palm oil (WCO) that is generated daily in Malaysia has motivated the study to produce a low-cost adsorbent with high removal efficiency. The polysulphide adsorbent was prepared with sulphur powder and waste cooking oil with a ratio of 9:1. The effect of contact time, initial Cu^{2+} concentration, and adsorbent dosage were studied using a batch adsorption process. The highest removal efficiency was 77.81% obtained while using 5 g of adsorbent dosage to treat 5 mg/L of Cu^{2+} aqueous solution. The Freundlich and Langmuir isotherm was used for modelling Cu^{2+} adsorption in an aqueous medium which was modelled best by the Langmuir isotherm. Overall, these results confirmed polysulphide as a low-cost and potential adsorbent to remove Cu^{2+} from wastewater.

Keywords: heavy metal removal, inverse vulcanisation, polysulphide adsorbent, waste cooking palm oil, waste to wealth.

Received: 27 July 2023**; Accepted:** 27 November 2023**; Published online:** 29 January 2024.

INTRODUCTION

The adverse effects of heavy metal wastewater on human health and the aquatic system have concerned the scientific community. Heavy metal wastewater is toxic and carcinogenic in nature and sometimes is released without prior wastewater treatment. Globally, almost 78% of heavy metal wastewater remains untreated, which bioaccumulates along the food chain because of its non-degradable nature (Jones *et al.*, 2021; Kumar *et al.*, 2019; Worthington *et al.*, 2017). Copper (Cu^{2+}), an important micronutrient element, has a crucial role in bone formation with the help of enzymes and proteins, but extreme intake of this heavy metal wastewater can lead to brutal health damage including renal and hepatic damage, widespread capillary damage, mucosal irritation and corrosion, severe gastrointestinal and central nervous system irritation, and necrotic changes in the kidney and liver (Arbabi & Golshani, 2016). Highly concentrated Cu^{2+} wastewater damages the osmoregulatory mechanism of the freshwater resources which also endangers the living organisms of the freshwater ecosystem. Different industries such as paint and pigments, metal plating and cleaning, petroleum refineries, smelting, mining, wood pulp, paper board and fertiliser production are responsible for Cu^{2+} wastewater (Braga & Ricardo, 2021). Ion exchange, coagulation and precipitation, membrane filtration, distillation, reverse osmosis and adsorption have been explored so far to remove Cu^{2+} from aqueous solution (Ramos *et al.*, 2016; Rashed *et al.*, 2023). To deal with Cu^{2+} wastewater, the adsorption process has been proven as an effective method (Ciobanu *et al.*, 2023). However, the high price and

[1] Faculty of Chemical and Process Engineering Technology, Universiti Malaysia Pahang Al-Sultan Abdullah, Lebuhraya Persiaran Tun Khalil Yaakob, 26300 Gambang, Kuantan, Pahang, Malaysia.

[2] Department of Soil Sciences and Agri-food Engineering, Université Laval, Quebec, QC, G1V 0A6 Canada.

[3] Centre for Sustainability of Mineral and Resource Recovery Technology (Pusat SMaRRT), Universiti Malaysia Pahang Al-Sultan Abdullah, Lebuh Persiaran Tun Khalil Yaakob, 26300 Kuantan, Pahang, Malaysia.

* *Corresponding e-mail: junhaslinda@umpsa.edu.my*

the nature of metal selectivity of the commercial adsorbents have caused some difficulties in the application of commercial adsorbents for Cu^{2+} wastewater adsorption (Emenike *et al.*, 2022).

Recently, inverse vulcanised polysulphides have been used as adsorbents to remove heavy metals in wastewater (Nayeem *et al.*, 2023). Inverse vulcanisation utilises the surplus amount of elemental sulphur obtained from sour gas and refinery treatment plants all over the world exceeding almost 70 million tonnes per year (Nayeem *et al.*, 2022a). Inverse vulcanisation enabled the use of a wide range of crosslinking monomers, which include cooking oils, agro-wastes, inorganic refinery by-products, *etc.* (Chalker *et al.*, 2019). The vinylic double bonds in the monomers break down during inverse vulcanisation and react with sulphur to form sustainable polysulphides (Chalker *et al.*, 2019). A recent investigation done by Nayeem *et al.* (2022b) showed the use of waste cooking palm oil (WCO) in inverse vulcanisation, which created a new way to deal with the threat of environmental hazards caused by WCO (Nayeem *et al.*, 2022b). The use of different crosslinkers, simple synthesis process, and high selectivity towards heavy metals have made the inverse vulcanised polysulphide adsorbents suitable for heavy metal wastewater treatment (Chalker *et al.*, 2021; Nayeem *et al.*, 2022a).

Polysulphide was prepared in the current study from sulphur and WCO to remove Cu^{2+} ions. The ratio of sulphur to WCO was 9:1. The characterisation of polysulphides was done using FTIR, TGA, and SEM-EDX to understand the functional bonds, thermal and morphological characteristics. The Cu^{2+} removal was studied by varying the parameters including dosages, initial Cu^{2+} concentration, and contact time. Later, isothermal studies were done by Langmuir and Freundlich isothermal models.

MATERIALS AND METHODS

Materials

Sulphur powder (Sigma Aldrich, USA, S_8 reagent grade sublimed powder, ±99.5%), sodium chloride (NaCl), (Sigma Aldrich, USA, ACS reagent, ≥99.5%), copper nitrate [$Cu(NO_3)_2$], (Merck, Germany, >230 mesh ASTM) were used as received for polysulphide preparation and Cu^{2+} solution preparation. WCO was sourced from the café of Universiti Malaysia Pahang Al-Sultan Abdullah (UMPSA), Gambang campus and used prior to the removal of existing impurities due to the frying process by 0.224 µm syringe filter. Deionised water (Millipore Elix 5, USA) was produced at the chemical lab (FTKKP), UMPSA.

Polysulphide Synthesis Via Inverse Vulcanisation

The synthesis process was followed by the method done by Abraham *et al.* (2018) and Nayeem *et al.* (2022b) with some minor modifications (Abraham *et al.*, 2018; Nayeem *et al.*, 2022b). About 9 g of sulphur powder and 3 g of NaCl were weighed according to 3:1 and ground using mortar and pestle to make a fine and homogenous mixture. The mixture was heated in a 50 mL beaker at 195°C and 450 rpm on a hot plate. After 8-10 min the mixture became orange in colour to ensure the complete ring opening of the S-S bond (Chung *et al.*, 2013). Then, WCO of 10 wt.% of sulphur was slowly poured into the mixture using a syringe and heated up for the next 60 min to reach the gel point for successful polymerisation (Gomez *et al.*, 2016). As WCO is not a completely unsaturated vegetable oil, over 9:1 ratio may result in a large amount of unreacted sulphur. This phenomenon was physically observed in a study of the liquid sulphur-oil solution which was not polymerised at all (Worthington *et al.*, 2017). The mixture was then cooled at room temperature for 90 min and ground into a fine powder using a pestle and mortar. The powder was rinsed with deionised water and was stirred at 600 rpm for 30 min to remove the NaCl that was added earlier which acted as porogen. Then the polymer was placed in a vacuum drier for 12 hr at 50°C.

Polysulphide Characterisation

The functional groups of the polysulphides were studied using FTIR with ATR (Thermo Fisher Nicolet iS5, USA) over the range of 400-4,000 cm^{-1}. The thermal stability of the polysulphide was observed through TGA (Hitachi STA7200, Japan) at a constant heating rate of 10°C min^{-1} from 30°C up to 700°C. Gaseous N_2 was used to create an inert environment. The surface morphology and elemental analyses were studied using scanning electron microscopy (SEM) equipped with an energy dispersive X-ray (EDX) system (Hitachi TM3030 Plus, Japan). During analysis, a platinum (Pt) sputter coat was applied to keep the sample surface uncharged. The main attributes of the adsorbents including the specific surface area, pore size, pore volume and pore distribution were studied through N_2 adsorption-desorption isotherm by a Micromeritics ASAP 2020 system based on the BET method.

Batch Adsorption of Cu^{2+}

A 100 mg L^{-1} of Cu^{2+} stock solution was prepared in a 50 mL beaker using deionised water (Darweesh *et al.*, 2022). Later, different Cu^{2+} solutions (1, 3 and 5 mg L^{-1}) were prepared through serial dilution to study the effect of initial Cu^{2+} concentration on the

adsorption process. Cu^{2+} removal was studied using batch adsorption technique at room temperature. About 100 mL of each concentration was stirred at 450 rpm for 2 hr in a 200 mL beaker. To record the Cu^{2+} concentration of the solution, 2 mL of sample was collected at a regular interval (every 20 min), centrifuged (Thermo Scientific MicroCL 21, USA) and run through atomic absorption spectroscopy (AAS). The effects of the adsorption parameters on Cu^{2+} removal were studied like adsorbent dosages, initial Cu^{2+} concentration and time. Numeric values of these parameters used in this study were varied according to the previous studies (Cheraghipour & Pakshir, 2021; Gonçalves *et al.*, 2021; Stanković *et al.*, 2019). Three different dosages (1, 3 and 5 g 100 mL^{-1}) were used to study the effect of dosages on Cu^{2+} adsorption.

The equilibrium concentration of the adsorbed Cu^{2+} was calculated with the help of Equation (1).

$$q_e = \frac{(C_o - C_e) \times V}{M} \quad (1)$$

Here, q_e denotes adsorption capacity (mg g^{-1}). V stands for the total volume of solution (L) and, M for the mass of adsorbent amount (g). The initial and equilibrium concentration (mg L^{-1}) of Cu^{2+} in solution are denoted respectively by C_0 and C_e. The percentage of Cu^{2+} removal is denoted by R which is calculated using the following Equation (2).

$$R(\%) = \frac{C_o - C_e}{C_o} * 100\% \quad (2)$$

Adsorption isotherm was analysed using both Langmuir [Equation (3)] and Freundlich [Equation (4)] isothermal model (Ciobanu *et al.*, 2023; Nayeem *et al.*, 2023).

$$\frac{1}{q_e} = \frac{1}{q_m} + \frac{1}{q_m K_L}\frac{1}{C_e} \quad (3)$$

Here, the maximum possible amount of Cu^{2+} that can be adsorbed per unit mass of adsorbent (mg g^{-1}) and constant for adsorption equilibrium is expressed by q_m and K_L, respectively.

$$logq_e = logK_L + \frac{1}{n} logc_e \quad (4)$$

Adsorption intensity for Freundlich isothermal model is denoted by 1/n.

RESULTS AND DISCUSSION

Characterisation of Polysulphide Adsorbent

Generally, FTIR indicates the functional bonds through the characteristic spectral peaks. *Figure 1* shows the FTIR spectra for the synthesised polysulphide compound. The figure depicts the basic characteristic peaks in the spectrum of polysulphide. From the previous study, the characteristic peak at 3,005 cm^{-1} resembled the vinylic bond of C=C, which was not observed in *Figure 1* and transformed to C-C to form the C-S

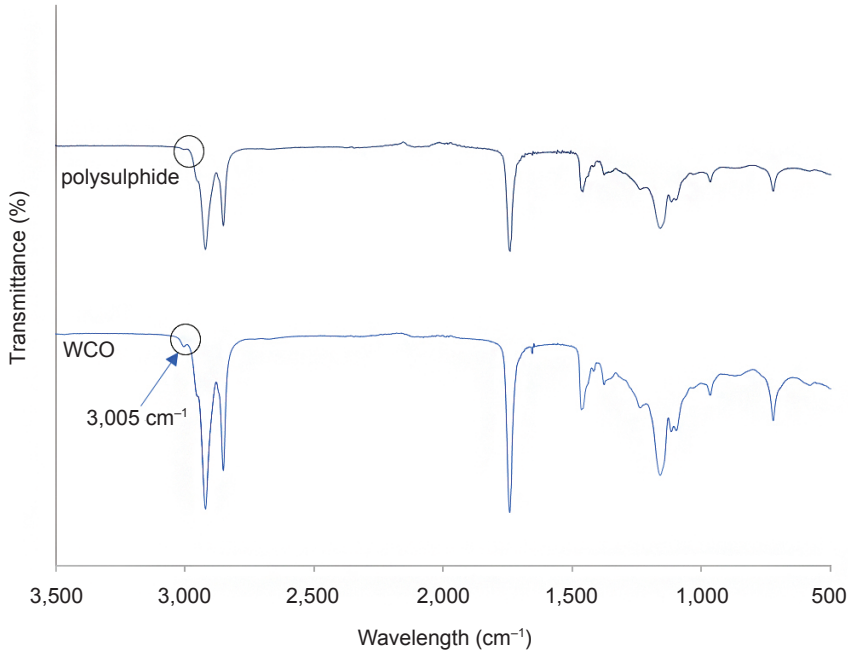


Figure 1. FTIR spectra of polysulphides via inverse vulcanisation.

polymeric chain during inverse vulcanisation (Nayeem *et al.*, 2022b). It demonstrates the successful polymerisation of WCO and sulphur. The observations obtained from FTIR follows the similar trends with the previous studies (Gomez *et al.*, 2016; Stanković *et al.*, 2019).

TGA curve showed the decomposition of polysulphide adsorbent in *Figure 2* where at first, the weight decreases slowly. Then, it becomes faster after 200°C. Maximum decomposition was a recorded at 289.6°C with 36.6% mass loss. Generally, WCO shows a single-step degradation. However, polysulphides produced from different vegetable oils through inverse vulcanisation tend to exhibit a two-step degradation (Nayeem *et al.*, 2022b; Tikoalu *et al.*, 2020).

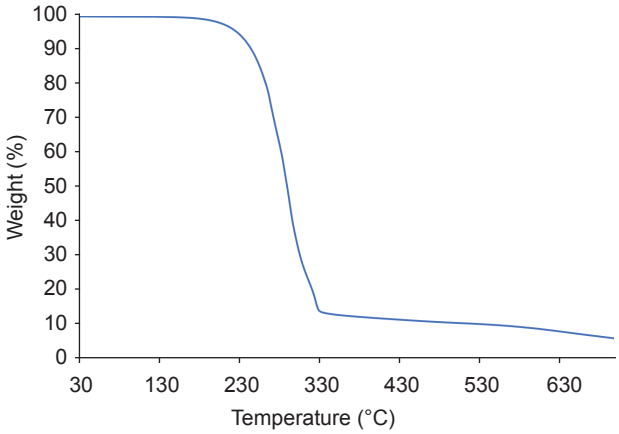


Figure 2. TGA of inverse vulcanised polysulphide adsorbent.

The SEM image of synthesised polysulphide adsorbent with 90 wt.% sulphur has been shown in *Figure 3*. The prepared polysulphide adsorbent has an irregular surface that is shaped like small bricks of different sizes and shapes. The polysulphides present a seemingly rough surface that indicates a high surface area for the adsorption. EDX image presented in *Figure 3*e shows that the percent amount of carbon, oxygen and sulphur composition in the adsorbent is 51.10%, 2.26% and 46.64% respectively.

Effect of Different Parameters

Effect of dosages. The effect of adsorbent dosages on Cu^{2+} removal from wastewater was investigated using three different loadings of polysulphide adsorbents, which were 1, 3 and 5 g respectively. The experiment was conducted at 35°C and a contact time of 120 min with a constant Cu^{2+} initial concentration of 5 mg L^{-1}. The Cu^{2+} removal rate in *Figure 4* indicated an increase in the percentage removal from 41.25%-77.81% as the dosage was increased to 5 g from 1 g. At higher adsorbent dosages, there were higher unoccupied adsorption sites for removal of Cu^{2+}. As mentioned by Azman *et al.* (2020), the amount of adsorbed ions is increased as more surface area, active sites and functional groups can be obtained with higher dosages (Azman *et al.*, 2020). As depicted in *Figure 4*, Cu^{2+} adsorption capacity decreased with higher adsorbent dosage. A similar trend was noticed in a previous study where adsorption

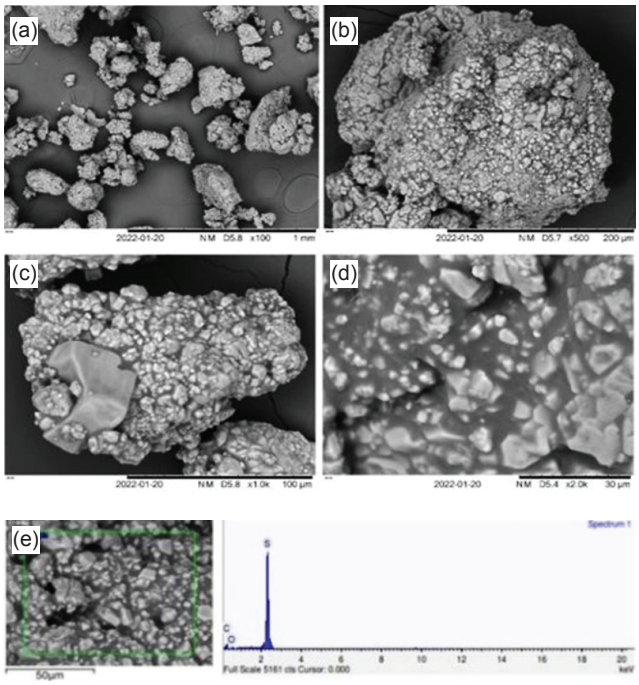


Figure 3. SEM images of prepared polysulphide adsorbent from waste cooking oil and sulphur (a) 100X (b) 500X (c) 1000X (d) 2000X and (e) EDX image.

sites remained unsaturated during the removal because the higher amount of dosages produced more active adsorption sites and introduced steric hindrance for the polysulphide to adsorb the Cu^{2+} ions (Ezeh *et al.*, 2017).

Effect of initial Cu^{2+} concentration. The effect of initial Cu^{2+} concentration on the percentage removal is presented in *Figure 5*. The removal percentage dropped from 68.88%-42.87% while the initial Cu^{2+} concentration increased. On the contrary, the Cu^{2+} adsorption capacity increased from 0.03-0.11 mg g^{-1} when the initial concentration was raised from 1-5 mg L^{-1}. The maximum removal was 68.88% at 1 mg L^{-1} of Cu^{2+} solution. Because of steric hindrance, the active sites of the polysulphide adsorbent would be surrounded with more Cu^{2+} in the solution when the initial Cu^{2+} concentration was comparatively higher. Therefore, the equilibrium adsorption capacity of polysulphide adsorbent rises with the increasing Cu^{2+} which enhances the adsorption process (Azman *et al.*, 2020). On the other hand, the removal rate tended to decrease at lower initial Cu^{2+} concentration, as the Cu^{2+} ions were removed by the sufficient available active sites of the polysulphide adsorbent (Radnia *et al.*, 2012).

Effect of contact time. The removal efficiency of Cu^{2+} was studied as a function of contact time at the initial concentration of 5 mg L^{-1} at 35°C and adsorbent dosage of 2 g, which is presented in *Figure 6*. For predicting the equilibrium adsorption, it is crucial to consider the effect of contact time on the adsorption of metal ions on any adsorbent (Emenike *et al.*, 2022). As depicted in the figure, the adsorption of Cu^{2+} into the polysulphide adsorbent increased with the increasing contact time. A similar trend was reported in a previous study (Gorzin & Abadi, 2017). At 0-80 min, the adsorption of Cu^{2+} removal was very fast. The contact time

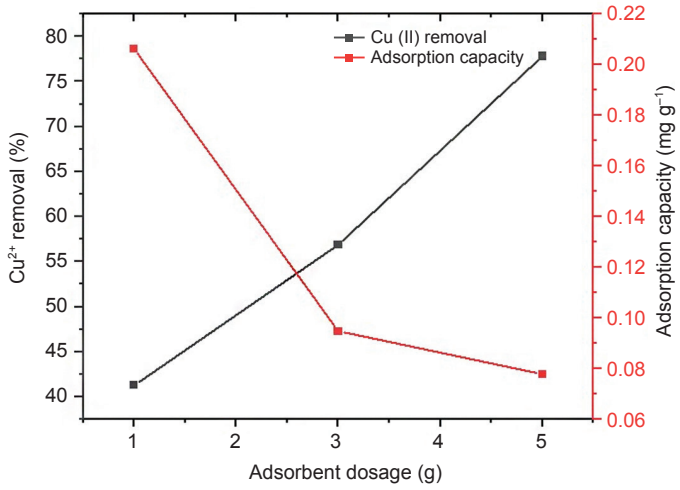


Figure 4. Effect of adsorbent dosage on the percentage removal and Cu^{2+} adsorption capacity (C0= 5 mg L^{-1}, T= 35°C).

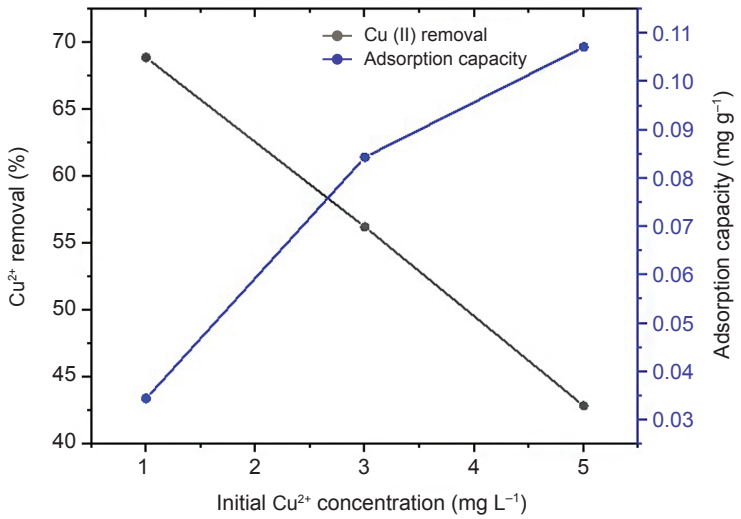


Figure 5. Effect of initial Cu^{2+} concentration on adsorption capacity and percentage removal (C0= 1 mg L^{-1}, T= 35°C and adsorbent dosage = 2 g).

needed for Cu^{2+} solution to achieve equilibrium was 80 min and saturated between 80-120 min with 77.81% of Cu^{2+} uptake. Initially, the removal rate and Cu^{2+} uptake capacity were rapid. Later, a gradual decline was observed at an equilibrium time beyond which no discernible rise in the removal rate and adsorption capacity was found. The initial rapid adsorption was caused by the abundance and availability of the active sites on polysulphide adsorbents. The active sites were rapidly occupied by Cu^{2+} ions and then became saturated upon reaching equilibrium (Ezeh *et al.*, 2017; Gorzin & Abadi, 2017).

Adsorption isotherm. Adsorption isotherm is important to understand the removal process. In this study, Cu^{2+} removal was analysed by both Langmuir and Freundlich isotherm. But the process fitted better by Langmuir isotherm. The R^2 value of Langmuir value was higher than the Freundlich model. The Cu^{2+}-polysulphide interaction is the main reason behind this (Ko *et al.*, 2021). *Figure 7* represents the isothermal curves for both Langmuir and Freundlich isothermal models with a brief exhibition of their parameters in *Table 1*. The R^2 value is closer to 1 for Langmuir model, which means it is more favourable and efficient.

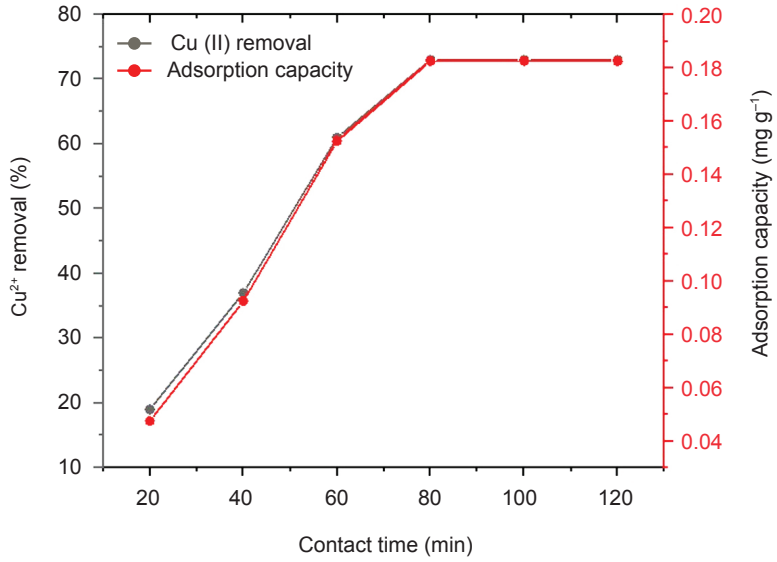


Figure 6. Effect of contact time on adsorption capacity and percentage removal (C0= 5 mg L^{-1}, T= 35°C and adsorbent dosage = 2 g).

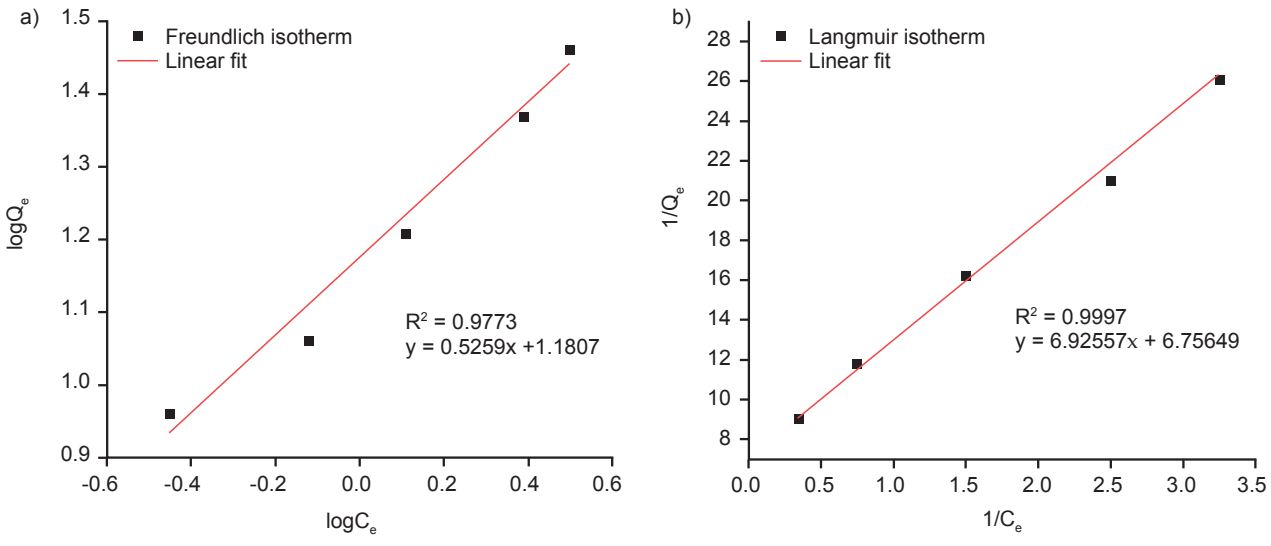


Figure 7. Adsorption isotherm graph of Cu^{2+} removal (a) Freundlich, and (b) Langmuir model.

TABLE 1. PARAMETERS OF ISOTHERMAL STUDY OF Cu^{2+} REMOVAL

Langmuir				Freundlich		
Q_{max}	K_L	R_L	R^2	K_f	1/n	R^2
0.1480	0.9755	2.9755	0.99977	15.1600	1.90146	0.9773

The highest removal recorded in this study is 77.81%. It was achieved using a relatively higher polysulphide adsorbent dosage (5 g in 5 mg L^{-1} Cu^{2+} solution) which is higher than other heavy metals using the same adsorbent (Nayeem *et al*., 2023). There are several factors behind this removal percentage for Cu^{2+} in this study. The surface area, pore volume and pore diameter were 19.59 m^3 g^{-1}, 0.018 cm^3 g^{-1} and 36.83 Å, respectively. Although the surface of the polysulphide was modified using NaCl, the attributes of the surface of the adsorbent were not high. The investigations showed that NaCl provides lesser surface area compared to other modifications processes such as electrospinning, carbonisation and supercritical carbon foaming (Nayeem *et al*., 2023). Moreover, the assumed hydrophobic nature and absence of hydrogen bonds of the vegetable oil based polysulphide adsorbent played a role for relatively low removal percentage (Hasell *et al*., 2016; Lin *et al*., 2019; Mann *et al*., 2021).

CONCLUSION

In this study, polysulphides were prepared from sulphur and waste cooking oil in the ratio of 9:1 by inverse vulcanisation. The study was carried out to investigate the ability of polysulphide adsorbent in the removal of Cu^{2+} ions. It was found that the adsorption is highly influenced by the following parameters such as initial Cu^{2+} concentrations, adsorbent dosage, and contact time. The percentage removal of Cu^{2+} was increased, with the increase of adsorbent dosage. On the other hand, the Cu^{2+} removal efficiency was decreased when the initial Cu^{2+} concentration was increased. The highest percentage removal of copper was recorded at 77.81% with 5 g of adsorbent in 5 mg L^{-1} in aqueous solution. It was found that the equilibrium time for Cu^{2+} adsorption onto polysulphide adsorbent was 80 min. The data obtained best fitted the Langmuir isotherm model with R^2= 0.9997. The results retrieved from this study have proven the ability of polysulphide adsorbent as a low-cost adsorbent. With proper research and development that can be carried out in the future, it shall be useful to be used in an up-scale treatment of contamination of other heavy metals, not only copper.

ACKNOWLEDGEMENT

The study was supported through RDU 1901185 (Ref. FRGS/1/2019/TK02/UMP/02/22).

REFERENCES

Azman, N. A. A., Mohd-Azoddein, A., & Ali, M. F. (2020). Polymer sorbent for mercury removal from aqueous solution. *IOP Conference Series: Materials Science and Engineering, 736*(5), 052020. https://doi.org/10.1088/1757–899X/736/5/052020

Abraham, A. M., Kumar, S. V., & Alhassan, S. M. (2017). Porous sulphur copolymer for gas-phase mercury removal and thermal insulation. *Chemical Engineering Journal*, *332*, 1–7. https://doi.org/10.1016/j.cej.2017.09.069

Arbabi, M., & Golshani, N. (2016). Removal of copper ions Cu (II) from industrial wastewater: A review of removal methods. *International Journal of Epidemiological Research, 3*(3), 283–293.

Braga, E. S., & Ricardo, R. D. (2021). Background concentration of copper and cadmium in water from a high industrialized and urban coastal system (Baixada Santista, Brazil) - Contribution to a monitoring program. *Journal of Geosciences and Environmental Protection, 9*(1), 132–150. https://doi.org/10.4236/gep.2021.91011

Chalker, J. M., Worthington, M. J. H., Lundquist, N. A., & Esdaile, L. J. (2019). Synthesis and applications of polymers made by inverse vulcanization. *Topics in Current Chemistry*, *377*(3). https://doi.org/10.1007/s41061-019-0242-7

Chalker, J. M., Mann, M., Worthington, M. J. H., & Esdaile, L. J. (2021). Polymers made by inverse vulcanization for use as mercury sorbents. *Organic Materials*, *03*(02), 362–373. https://doi.org/10.1055/a-1502-2611

Cheraghipour, E., & Pakshir, M. (2020). Environmentally friendly magnetic chitosan nano-biocomposite for Cu(II) ions adsorption and magnetic nano-fluid hyperthermia: CCD-RSM design. *Journal of Environmental Chemical Engineering*, *9*(2), 104883. https://doi.org/10.1016/j.jece.2020.104883

Chung, W. J., Griebel, J. J., Kim, E. T., Yoon, H., Simmonds, A. G., Ji, H. J., Dirlam, P. T., Glass, R. S., Wie, J. J., Nguyen, N. A., Guralnick, B. W., Park, J., Somogyi, Á., Theato, P., Mackay, M. E., Sung, Y., Char, K., & Pyun, J. (2013). The use of

elemental sulfur as an alternative feedstock for polymeric materials. *Nature Chemistry*, *5*(6), 518–524. https://doi.org/10.1038/nchem.1624

Ciobanu, A. A., Bulgariu, D., Ionescu, I. A., Puiu, D. M., Vasile, G. G., & Bulgariu, L. (2023). Evaluation of thermodynamic parameters for Cu(II) ions biosorption on algae biomass and derived biochars. *Symmetry, 15*(8), 1500. https://doi.org/10.3390/sym15081500

Darweesh, M. A., Elgendy, M. Y., Ayad, M. I., Ahmed, A. M., Elsayed, N., & Hammad, W. (2022). Adsorption isotherm, kinetic, and optimization studies for copper (II) removal from aqueous solutions by banana leaves and derived activated carbon. *South African Journal of Chemical Engineering*, *40*, 10–20. https://doi.org/10.1016/j.sajce.2022.01.002

Emenike, E. C., Adeniyi, A. G., Omuku, P. E., Okwu, K. C., & Iwuozor, K. O. (2022). Recent advances in nano-adsorbents for the sequestration of copper from water. *Journal of Water Process Engineering*, *47*, 102715. https://doi.org/10.1016/j.jwpe.2022.102715

Ezeh, K. A., Ogbu, I. C., Akpomie, K. G., Ojukwu, N. C., & Ibe, J. C. (2017). Utilizing the sorption capacity of local Nigerian sawdust for attenuation of heavy metals from solution: Isotherm, kinetic, and thermodynamic investigations. *The Pacific Journal of Science and Technology, 18*(1), 251–264.

Gomez, I., Mecerreyes, D., Blazquez, J. A., Leonet, O., Youcef, H. B., Li, C., Gómez-Cámer, J. L., Bondarchuk, O., & Rodriguez-Martinez, L. (2016). Inverse vulcanization of sulfur with divinylbenzene: Stable and easy processable cathode material for lithium-sulfur batteries. *Journal of Power Sources*, *329*, 72–78. https://doi.org/10.1016/j.jpowsour.2016.08.046

Gonçalves, F. J., Gurgel, L. V. A., Soares, L. C., Teodoro, F. S., Ferreira, G. M. D., Coelho, Y. L., Da Silva, L. H. M., Prim, D., & Gil, L. F. (2021). Application of pyridine-modified chitosan derivative for simultaneous adsorption of Cu(II) and oxyanions of Cr(VI) from aqueous solution. *Journal of Environmental Management*, *282*, 111939. https://doi.org/10.1016/j.jenvman.2021.111939

Gorzin, F., & Abadi, M. B. R. (2017). Adsorption of Cr(VI) from aqueous solution by adsorbent prepared from paper mill sludge: Kinetics and thermodynamics studies. *Adsorption Science & Technology*, *36*(1-2), 149–169. https://doi.org/10.1177/0263617416686976

Hasell, T., Parker, D. J., Jones, H. A., McAllister, T., & Howdle, S. M. (2016). Porous inverse vulcanised polymers for mercury capture. *Chemical Communications, 52*(31), 5383–5386. https://doi.org/10.1039/C6CC00938G

Jones, E. R., Van Vliet, M. T. H., Qadir, M., & Bierkens, M. F. P. (2021). Country-level and gridded estimates of wastewater production, collection, treatment and reuse. *Earth System Science Data*, *13*(2), 237–254. https://doi.org/10.5194/essd-13-237-2021

Ko, L., Huang, Y., & Lin, Y. A. (2021). Bipyridine-containing polysulfide materials for broad-spectrum removal of heavy metals from water. *ACS Applied Polymer Materials*, *3*(7), 3363–3372. https://doi.org/10.1021/acsapm.1c00259

Kumar, V., Parihar, R. D., Sharma, A., Bakshi, P., Sidhu, G. P. S., Bali, A. S., Karaouzas, I., Bhardwaj, R., Thukral, A. K., Gyasi-Agyei, Y., & Rodrigo-Comino, J. (2019). Global evaluation of heavy metal content in surface water bodies: A meta-analysis using heavy metal pollution indices and multivariate statistical analyses. *Chemosphere*, *236*, 124364. https://doi.org/10.1016/j.chemosphere.2019.124364

Lin, H., Lai, Y., & Liu, Y. (2019). Cross-linkable and Self-foaming polysulfide materials for repairable and mercury capture applications. *ACS Sustainable Chemistry & Engineering*, *7*(4), 4515–4522. https://doi.org/10.1021/acssuschemeng.8b06815

Mann, M., Luo, X., Tikoalu, A. D., Gibson, C. T., Yin, Y., Al-Attabi, R., Andersson, G. G., Raston, C. L., Henderson, L. C., Pring, A., Hasell, T., & Chalker, J. M. (2021). Carbonisation of a polymer made from sulfur and canola oil. *Chemical Communications, 57*(51), 6296–6299. https://doi.org/10.1039/D1CC01555A

Nayeem, A., Ali, M. F., & Shariffuddin, J. H. (2022a). Synthesis and applications of inverse vulcanized polysulfides from bio-crosslinkers. *Materials Today Proceedings, 57*, 1095–1100. https://doi.org/10.1016/j.matpr.2021.09.397

Nayeem, A., Ali, M. F., & Shariffuddin, J. H. (2022b). Polysulfide synthesis using waste cooking palm oil via inverse vulcanization. *Chemical Engineering Technology, 45*(5), 971–978. https://doi.org/10.1002/ceat.202100465

Nayeem, A., Ali, M. F., & Shariffuddin, J. H. (2023). The recent development of inverse vulcanized polysulfide as an alternative adsorbent for heavy metal removal in wastewater. *Environmental*

Research, 216, 114306. https://doi.org/10.1016/j.envres.2022.114306

Radnia, H., Ghoreyshi, A. A., Younesi, H., & Najafpour, G. D. (2012). Adsorption of Fe(II) ions from aqueous phase by chitosan adsorbent: Equilibrium, kinetic, and thermodynamic studies. *Desalination and Water Treatment*, *50*(1-3), 348–359. https://doi.org/10.1080/19443994.2012.720112

Ramos, S. N. D. C., Xavier, A. L. P., Teodoro, F. S., Gil, L. F., & Gurgel, L. V. A. (2015). Removal of cobalt(II), copper(II), and nickel(II) ions from aqueous solutions using phthalate-functionalized sugarcane bagasse: Mono- and multicomponent adsorption in batch mode. *Industrial Crops and Products*, *79*, 116–130. https://doi.org/10.1016/j.indcrop.2015.10.035

Rashed, M. N., Arifien, A. E., & El-Dowy, F. A. (2023). Preparation and characterization of nanomuscovite by intercalation method for adsorption of heavy metals from polluted water. *Environmental Geochemistry and Health*, *45*(7), 5127–5144. https://doi.org/10.1007/s10653-023-01545-4

Stankovic, S., Sostaric, T., Bugarcic, M., Janicijevic, A., Pantovic-Spajic, K., & Lopicic, Z. (2019). Adsorption of Cu(II) ions from synthetic solution by sunflower seed husks. *Acta Periodica Technologica*, *50*, 268–277. https://doi.org/10.2298/apt1950268s

Tikoalu, A. D., Lundquist, N. A., & Chalker, J. M. (2020). Mercury sorbents made by inverse vulcanization of sustainable triglycerides: The plant oil structure influences the rate of mercury removal from water. *Advanced Sustainable Systems*, *4*(3), 1–9. https://doi.org/10.1002/adsu.201900111

Worthington, M. J. H., Kucera, R. L., Albuquerque, I. S., Gibson, C. T., Sibley, A., Slattery, A. D., Campbell, J. A., Alboaiji, S. F. K., Muller, K. A., Young, J., Adamson, N., Gascooke, J. R., Jampaiah, D., Sabri, Y. M., Bhargava, S. K., Ippolito, S. J., Lewis, D. A., Quinton, J. S., Ellis, A. V., . . . Chalker, J. M. (2017). Laying waste to mercury: Inexpensive sorbents made from sulfur and recycled cooking oils. *Chemistry - a European Journal*, *23*(64), 16219–16230. https://doi.org/10.1002/chem.201702871

SHORT COMMUNICATION

Journal of Oil Palm Research Vol. 37 (1) March 2025 p. 181-186
DOI: https://doi.org/10.21894/jopr.2024.0040

DEVELOPMENT OF qPCR PRIMER FOR *Ganoderma boninense* DETECTION IN SOIL

HUN JIAT, TUNG[1]*; YIT KHENG, GOH[1] and WEI CHEE, WONG[1]

ABSTRACT

Quantitation of pathogenic Ganoderma *species presence in oil palm plantation soil is crucial for basal stem rot (BSR) disease management where implemented disease control practices could be validated. Quantitative polymerase chain reaction (qPCR) has been widely applied in quantification of various pathogens in soil and plant tissues due to its high sensitivity. In this study, primers designed based on internal transcribed spacer (ITS) sequences were utilised for detection of pathogenic* Ganoderma *species. Its specificity and detection efficiency were tested using* Ganoderma *inoculated and non-inoculated soil samples. As for qPCR applications, primer IGbF-R was proven to be specific to* Ganoderma boninense*, and capable of amplifying its synonyms (*G. orbiforme *and* G. miniatocinctum*) in* Ganoderma *inoculated soil.*

Keywords: basal stem rot, DNA quantification, *Elaeis guineensis*, soil.

Received: 3 January 2024**; Accepted:** 9 July 2024**; Published online:** 28 August 2024.

INTRODUCTION

The commercially cultivated oil palm (*Elaeis guineensis*) is vulnerable to the attacks by various important fungal diseases, particularly vascular wilt (*Fusarium oxysporum*), bud rot (*Phytophthora palmivora*) and BSR (*Ganoderma boninense*) in different continents of the world (Corley & Tinker, 2016). Root-to-inoculum sources had been proposed as one of the routes of disease transmission by *G. boninense,* in particularly replanting of oil palm at areas previously infected by BSR (Rees *et al*., 2009). Appearance of the multiple unopened spears, skirting or downward snapping of the green fronds and yellowing of the fronds are some of the common visual foliar symptoms observed in the oil palms with BSR (Rees *et al*., 2009). Disease rotting of the stem bole and manifestation of fungal masses or fruiting bodies are some of the common visual symptoms associated with BSR (Rees *et al*., 2007). Unfortunately, once either one of the above symptoms' manifests, BSR disease is well-established and at a late stage.

Detection of *G. boninense* in the oil palm tissues have been studied through non-molecular and molecular approaches (Chong *et al*., 2017; Naher *et al*., 2013). Some of the non-molecular methods explored are a) *Ganoderma*-selective medium (GSM) for pure culture isolation (Ariffin & Idris, 1992); and b) detection of *G. boninense* through ergosterol analysis (Chong *et al*., 2017). Other detection approaches, namely e-nose system, spectroscopy, remote sensing, and ultrasonic, have also been explored and reviewed (Naher *et al*., 2013; Siddiqui *et al*., 2021). For molecular diagnostic methods, techniques such as PCR and loop-mediated isothermal amplification (LAMP) were reported. For instance, PER44-123 and LR1 primers (amplicon size: ~580 bp) were capable of amplifying *G. boninense, G. miniatocinctum* and *G. zonatum* (pathogenic *Ganoderma* species in oil palm plantations), but not in other tested *Ganoderma* species (Idris *et al*., 2003). In a separate study, Gan1 and Gan2 primers (amplicon size: 167 bp) had been developed to detect *Ganoderma* DNA. Unfortunately, this primer-set will also amplify other saprophytes (*Aspergillus, Rhizopus* and *Penicillium* species) of oil palms with a range of DNA fragment sizes (Utomo & Niepold, 2000). The LAMP method, albeit published, the primer sequences were not reported.

[1] Advanced Agriecological Research Sdn. Bhd., 11, Jalan Teknologi 3/6, Taman Sains, 47810 Petaling Jaya, Selangor, Malaysia.

* *Corresponding author e-mail: tunghj@aarsb.com.my*

Quantification of the pathogens with qPCR in plants has been reported (Luchi *et al.*, 2020). This method has also been adopted for quantifying *Ganoderma* DNA in ramets or clonal materials under semi-controlled and sterile conditions (Chow *et al*., 2017; Goh *et al*., 2016). However, successful application of qPCR for *Ganoderma* DNA quantification in environmental soil samples is limited. Thus, in this study, we reported the development of specific qPCR primers for *Ganoderma* DNA quantification in oil palm plantation soil samples.

MATERIALS AND METHODS

Fungal, Bacterial and Actinomycetous Isolates and Growth Conditions

A total of seven fungal, one bacterial and five actinomycetous cultures were isolated from Typic Endoaquept (3°55′33.4″N, 100°48′51.7″E) and Typic Quartzipsamments (3°55′44.6″N, 100°48′36.2″E) series soils of an oil palm estate in Perak, Malaysia (*Table 1*). They were maintained and inoculated on malt extract agar (MEA, Difco) (for fungi), trypticase soy agar (TSA, Difco) (for bacteria) and actinomycetes isolation agar (AIA, Difco) (for actinomycetes) prior to DNA extraction. Ten *Ganoderma* spp. isolates and one *Heterobasidion annosum* isolate (*Table 1*) were purchased from CBS-KNAW Fungal Biodiversity Centre, National Agriculture and Food Research Organization (NARO) and Centre for Agriculture and Bioscience International (CABI). All the fungal cultures were incubated at 24°C, while bacterial and actinomycetous cultures were incubated at 28°C, both in the dark. Genomic DNAs of all the pure cultures of fungi, bacteria and actinomycetes were extracted with the FastDNA Spin Kit (MP Biomedicals, USA).

Soil Samples from the Oil Palm Field

Two different soils, namely Typic Kandiudults (coordinates: 3°16′13.36″N; 101°27′18.62″E) and Typic Quartzipsamments (coordinates: 3°55′44.6″N, 100°48′36.2″E) were collected from inter-palm areas at the soil depth of approximately 0-15 cm and portion of the soils were autoclaved twice at 121°C for 30 min (Rusli *et al*., 2016). Both autoclaved and non-autoclaved soils were inoculated with *G. boninense* colonised rubber wood block (RWB) for nursery infection studies and all the treatments were in triplicates following the procedures outlined previously (Goh *et al*., 2022). The soil samples in polybags were collected and subjected to DNA extraction after five months of post-nursery-infection. Briefly, soil samples were collected approximately 1 cm from the *Ganoderma*-inoculated or non-inoculated RWB and 1 cm from the soil surface using sterilised spatula. Soil samples were then processed by breaking them into small pieces and removing the intact shells, root fragments and wood debris using sterilised forceps prior to sieving through the 2 mm sieve and homogenisation (Goh *et al*., 2020; Strohm, 2015). The processed soils were then stored at -80°C prior to DNA extraction. Prior to DNA extraction, the soil samples were then treated with propidium monoazide (PMA) (Biotium, CA, USA) following previously described protocols (Joo *et al*., 2019). For each replicate, soil total DNA was extracted from approximately 0.4 g soil sample using DNeasy PowerSoil Kit (Qiagen, Inc., CA, USA) and three extractions were conducted for the respective samples. The extracted DNAs were then pooled into one composite prior to qPCR analyses.

Primer Design

Alignment of internal transcribed spacer (ITS) region for 12 *G. boninense* isolates sampled from across Peninsular Malaysia was performed using Geneious 11.1.5 (https://www.geneious.com). From the alignment, constant region (defined as no SNPs) between the 12 isolates were identified and submitted to PrimerQuest (https://www.idtdna.com/SciTools) for primer design. The parameters for qPCR primers design were: a) Optimal primer Tm at 62°C (± 3°C), b) GC at 50% (± 15%) and c) primer size at 22 bp (± 3 bp). The range of amplicon size was set from 75-150 bp. The primer set which satisfied the qPCR parameters were selected for further testing.

Quantitative Real-time Polymerase Chain Reaction (qPCR)

In addition to the selected primer set in this study, another *Ganoderma*-specific primer set *i.e.*, Gan1 (5′-TTGACTGGGTTGTAGCTG-3′) and Gan2 (5′-GCGTTACATCGCAATACA-3′) (Utomo & Niepold, 2000) were included for comparison in qPCR assays using genomic DNAs from the microbial isolates (*Table 1*) and soil DNAs. The qPCR reactions were performed in QuantStudio™ 6 Flex system (Applied Biosystems, USA). Reaction mixture comprised 10 µL KAPA Sybr Fast qPCR kit (KAPA BioSystems, USA), 0.5 µL of 10 µM each forward and reverse primers, 7 µL sterile water, and 2 µL of 10 ng/µL DNA template. Assays were performed in three technical replicates. The qPCR thermal cycling was performed with pre-incubation at 95°C for 3 min, followed by 40 cycles of 95°C for 3 s and 60°C for 20 s with fluorescence data acquisition at the end of each cycle. The dissociation curve was carried out at 95°C for 15 s,

60°C for 1 min and 95°C for 15 s. Additionally, melt curve analysis was carried out at 60°C for 1 min and 95°C for 15 s. Standard curve was constructed using the cycle threshold (Ct) values of a series of ten-fold diluted *G. boninense* PER71 DNA (between 335 ng/µL and 0.003 ng/µL). Detection and quantification of *G. boninense* DNA using both pure microbial cultures and soil samples were performed by comparing the Ct values for the respective samples against the standard curve. The melt curve was generated to examine the specificity of amplification.

RESULTS AND DISCUSSION

The forward primer IGbF (5′- GCAGCGAAAT GCGATAAGTAATG -3′) and reverse primer IGbR (5′-CCGCAAAGAGATTGTAGGTTGA-3′) (produces 140 bp amplicon) found to be the only primer set that fulfilled the criteria for qPCR primer design. When the amplicons of primer IGbF-R and Gan1-2 from three isolates of *G. boninense* DNA were visualised on 2.50% (w/v) agarose gel, both primer sets yielded one single band with the expected amplicon size. Correspondingly, the melt curve plot displayed a single peak in both IGbF-R and Gan1-2. The amplification efficiency determined by standard curve for IGbF-R was 95.74% followed by Gan1-2 with 68.32% (*Figure 1*). Amplification of other fungi and bacteria was not observed for both sets of primers. Primers IGbF-R showed amplification only for *G. boninense* and its synonyms (*G. orbiforme* and *G. miniatocinctum*). In a separate study, the pathogenicity of *G. orbiforme* IMI375255 and *G. miniatocinctum* IMI337035 in oil palm seedlings was established with nursery infection (unpublished data). The disease index and disease severity index were comparable with *G. boninense* control. The melting point of IGbF-R for *G. boninense*, *G. miniatocinctum* and *G. orbiforme* are similar at 80.62°C, given that the sequences of region amplified are identical.

For PCR amplification of *G. boninense* pure cultures, 28 isolates obtained from a single oil palm estate showed positive amplification using IGbF-R primer set. Subsequent testing using DNAs extracted from soil samples (oil palm nursery polybag), with and without *Ganoderma* inoculum were quantified using both primers IGbF-R and Gan1-2 for comparison of the qPCR

TABLE 1. FUNGAL, BACTERIAL AND ACTINOMYCETOUS ISOLATES INCLUDED FOR DETERMINATION OF PRIMER SPECIFICITY TEST

Microbial isolates	Isolate/Culture	GenBank accession	Culture collection*	Amplification	
				IgbF-R	Gan1-2
Ganoderma applanatum	IMI344119	N/A	CABI	X	√
G. tropicum	CBS128582	N/A	CBS-KNAW	X	√
G. weberianum	CBS219.36	MH855780.1	CBS-KNAW	X	√
G. miniatocinctum#	IMI337035	MN490055.1	CABI	√	√
G. colossus	CBS216.36	N/A	CBS-KNAW	X	√
G. orbiforme#	IMI375255	N/A	CABI	√	√
G. boninense	MAFF305601	N/A	NARO	√	√
Ganoderma sp.	MAFF243200	N/A	NARO	X	√
G. gibbosum	MAFF244236	N/A	NARO	X	√
G. applanatum	MAFF305600	N/A	NARO	X	√
G. boninense	PER71	MN490049.1	MPOB	√	√
Heterobasidion annosum	CBS869.87	N/A	CBS-KNAW	X	X
Trichoderma harzianum	D10	OK584118	AAR	X	X
T. simmonsii	D15	OK584471	AAR	X	X
T. yunnanense	D27	OK584679	AAR	X	X
T. simmonsii	B3	OM978939	AAR	X	X
T. yunnanense	D6	OK584477	AAR	X	X
Aspergillus ochraceopetaliformis	D11	OK584475	AAR	X	X
A. protuberus	D8	OK576909	AAR	X	X
Terrabacter koreensis	B15	N/A	AAR	X	X
T. koreensis	208	OM919535	AAR	X	X
Streptomyces abikoensis	M24	OK576703	AAR	X	X
S. abikoensis	M30	OK576707	AAR	X	X
Pseudomonas aeruginosa	D25	OK576699	AAR	X	X
Nocardia bhagyanarayanae	209	OK602688	AAR	X	X

Note: Positive amplification is denoted by "√" and negative amplification denoted by "x". *Ganoderma* sp. denoted with "#" are synonymous with *G. boninense*. CABI - Centre for Agriculture and Bioscience International; CBS-KNAW - Fungal Biodiversity Centre, NARO - National Agriculture and Food Research Organization; MPOB - Malaysian Palm Oil Board; and AAR - Advanced Agriecological Research Sdn. Bhd.; N/A - not available.

detection efficiency and sensitivity. Both primers showed positive detection of *Ganoderma* DNA in all inoculated soil samples with mean Ct value ranging from 17.04 to 23.70 (*Table 2*). Inoculated soils that were sterilised prior to nursery infection experiment showed slightly lower mean Ct value (*i.e.*, early amplification of target) compared to non-sterilised inoculated samples (ranges from 1.0%-8.5% difference) in both Typic Kandiudults and Typic Quartzipsamments soils. This observation indicated a higher *Ganoderma* population in the sterilised soil compared to non-sterilised soil. This observation agrees with Rees *et al*. (2009) study where *G. boninense* is shown to be a poor competitor in non-sterile soil. In this study, all primer sets were able to amplify *Ganoderma* DNA in two different soil types tested. Typic Kandiudults have sandy clay texture with approximate pH 4.5. Meanwhile, Typic Quartzipsamments have coarse sandy texture with shell deposits, higher pH and total calcium in comparison to Typic Kandiudults (Goh *et al*., 2022). In general, the IGbF-R primer set was more sensitive in detection when compared to Gan1-2 as the mean Ct value is lower in all samples tested. There was no amplification in non-inoculated soil samples regardless of sterilisation status (mean Ct value >27.00). Detection of pathogenic *Ganoderma* in soil by qPCR primers developed in this study could potentially be used for rapid pathogen screening in oil palm plantations. The primers designed using ITS region which are known to have several copies in genome increased the sensitivity of the primers for detection. Although the primers were shown to be able to detect *G. boninense* in inoculated soil, the inoculum size used in this nursery study was substantial (rubber wood block inoculum is approximately 8.42% of soil volume in polybags). Hence, it may not necessarily reflect true detection sensitivity for soil in oil palm plantations. Nevertheless, the detection of pathogenic *Ganoderma* sp. is still plausible when optimised soil DNA extraction protocol is incorporated into the workflow. Additionally, the primers developed are not suited for absolute, but limited to relative quantification. This is due to the multiple copies of ITS present in *Ganoderma* genome and the primers could amplify several pathogenic *Ganoderma* species.

CONCLUSION

A reliable and economical repeating test to determine the presence of *Ganoderma* species is prerequisite for effective BSR disease management. However, a precise *G. boninense* detection method is scarced due to low sequence variability for designing of primer and a wide collection of microbial cultures is required for its specificity

TABLE 2. MEAN Ct VALUE OF *Ganoderma* DNA IN POLYBAG'S SOIL

***Ganoderma* inoculation**	**Sterilisation**	**Mean Ct value**	
		IGbF-R	**Gan1-2**
With	Non-sterilised	19.72	21.47
		20.09	21.83
		18.08	21.60
		17.84	19.28
		17.04	18.09
		21.41	22.89
	Average	**19.03**	**20.86**
	Sterilised	22.41	23.13
		20.38	21.88
		23.23	23.70
		19.43	21.12
		21.93	22.22
		17.50	19.37
	Average	**20.81**	**21.90**
Without	Non-sterilised	30.54	30.19
		29.52	27.90
		33.50	32.12
		32.58	32.03
		29.03	27.08
		29.21	28.02
	Average	**30.73**	**29.56**
	Sterilised	33.03	32.12
		28.52	27.62
		33.27	32.39
		35.18	34.09
		31.50	29.61
		34.68	31.79
	Average	**32.70**	**31.27**

Note: Total of six replicates from each parameter (inoculation status and sterilisation) were quantified via qPCR.

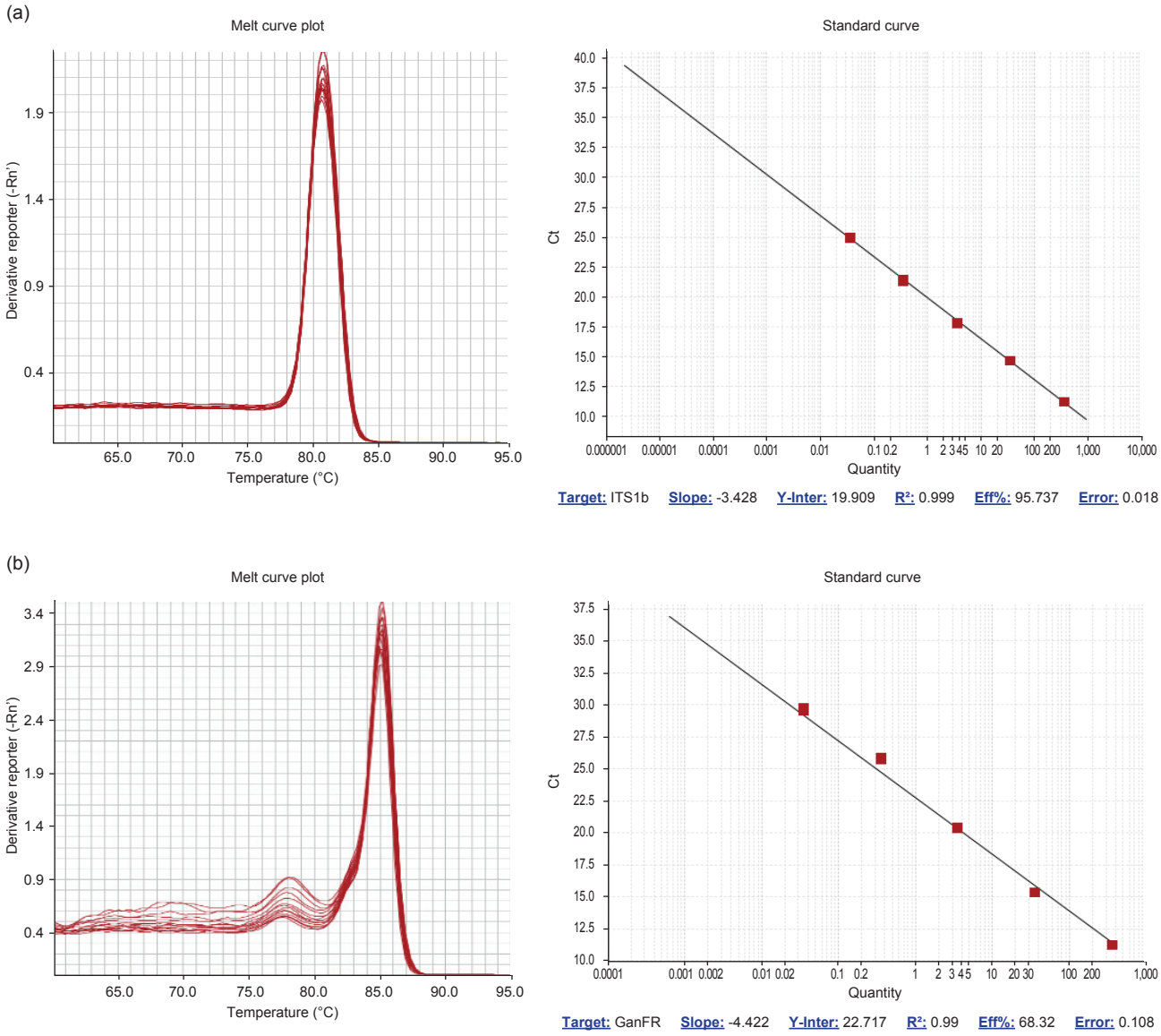


Figure 1. Melt curve plot and standard curve of (a) IGbF-R and (b) Gan1-2 constructed using G. boninense *pure culture DNA.*

evaluation. In this study, primer IGbF-R was developed based on the ITS sequences of *G. boninense* isolates sampled from different regions of Peninsular Malaysia. The primer specificity in detecting *G. boninense* and its synonym *G. orbiforme* and *G. miniatocinctum* was proven by verifying using 11 *Ganoderma* spp., and a collection of fungal and bacteria isolated from oil palm plantation soil. The effectiveness of IGbF-R was confirmed through successful amplification of the DNAs of *G. boninense* in two different soil types *i.e.*, Typic Kandiudults and Typic Quartzipsamments under nursery conditions which inoculum of *G. boninense* was present. Current application of IGbF-R is limited for nursery experimental trial. A robust IGbF-R-based qPCR system could be developed in near future to aid in detecting *G. boninense*, and quantitative monitoring of this fungal pathogen in oil palm plantations over generation of plantings.

ACKNOWLEDGEMENT

H.J.T. isolated and PCRed *G. boninense* isolates in this study, performed data analysis and prepared manuscript. Y.K.G. performed all qPCR related works and procured other *Ganoderma* spp and soil sample. W.C.W. designed the primer, edited and reviewed the manuscript. The authors would like to thank AAR Principals, Boustead Plantations Berhad and Kuala Lumpur Kepong Berhad for funding this research, and for their permission to publish the data in this article.

REFERENCES

Ariffin, D., & Idris, A. S. (1992). *The* Ganoderma *selective medium (GSM)*. PORIM Information Series No. 8. MPOB.

Chong, K. P., Dayou, J., & Alexander, A. (2017). Current detection methods of *G. boninense* infection in oil palm. In K. P. Chong, J. Dayou, & A. Alexander (Eds.), *Detection and control of* Ganoderma boninense *in oil palm crop* (pp. 13-20). Springer International Publishing.

Chow, Y. Y., Rahman, S., & Ting, A. S. Y. (2017). Understanding colonization and proliferation potential of endophytes and pathogens in planta via plating, polymerase chain reaction, and ergosterol assay. *Journal of Advanced Research, 8*, 13–21. https://doi.org/10.1016/j.jare.2016.10.008

Corley, R. H. V., & Tinker, P. B. (2016). Diseases of the oil palm. In R. H. V. Corley & P. B. Tinker (Eds.), *The oil palm* (pp. 399-436). Blackwell Publishing.

Goh, K. M., Dickinson, M., Alderson, P., Yap, L. V., & Supramaniam, C. V. (2016). Development of an *in planta* infection system for the early detection of *Ganoderma* spp. in oil palm. *Journal of Plant Pathology, 98*, 255–264. https://doi.org/10.4454/jpp.v98I2.019

Goh, Y. K., Zoqratt, M. Z. H. M., Goh, Y. K., Ayub, Q., & Ting, A. S. Y. (2020). Determining soil microbial communities and their influence on *Ganoderma* disease incidences in oil palm (*Elaeis guineensis*) via high-throughput sequencing. *Biology, 9*(12), 424. https://doi.org/10.3390/biology9120424

Goh, Y. K., Zoqratt, M. Z. H. M., Goh, Y. K., Ayub, Q., & Ting, A. S. Y. (2022). Discovering naturally-occurring microbiota in disease-suppressive soil: Potential role of biological elements in suppressing *Ganoderma boninense*. *Biological Control, 165*, 104787. https://doi.org/10.1016/j.biocontrol.2021.104787

Idris, A. S., Yamaoka, M., Hayakawa, S., Basri, M. W., Noorhasimah, I., & Ariffin, D. (2003). *PCR technique for detection of Ganoderma*. MPOB Information Series No. 188. MPOB.

Joo, S., Park, P., & Park, S. (2019). Applicability of propidium monoazide (PMA) for discrimination between living and dead phytoplankton cells. *PLoS ONE, 14*, e0218924. https://doi.org/10.1371/journal.pone.0218924

Luchi, N., Santini, A., Salvianti, F., & Pinzani, P. (2019). Early detection of fungal plant pathogens by real-time quantitative PCR: The case of *Diplodia sapinea* on pine. *Methods in Molecular Biology*, 95–104. https://doi.org/10.1007/978-1-4939-9833-3_8

Naher, L., Yusuf, U. K., Ismail, A., Tan, S. G., & Mondal, M. M. A. (2013). Ecological status of Ganoderma and basal stem rot disease of oil palms (*Elaeis guineensis* Jacq.). *Australian Journal of Crop Science*, *7*(11), 1723–1727. http://www.cropj.com/naher_7_11_2013_1723_1727.pdf

Rees, R. W., Flood, J., Hasan, Y., & Cooper, R. M. (2007). Effects of inoculum potential, shading and soil temperature on root infection of oil palm seedlings by the basal stem rot pathogen *Ganoderma boninense*. *Plant Pathology*, *56*(5), 862–870. https://doi.org/10.1111/j.1365-3059.2007.01621.x

Rees, R. W., Flood, J., Hasan, Y., Potter, U., & Cooper, R. M. (2009). Basal stem rot of oil palm (*Elaeis guineensis*); mode of root infection and lower stem invasion by *Ganoderma boninense*. *Plant Pathology*, *58*(5), 982–989. https://doi.org/10.1111/j.1365-3059.2009.02100.x

Rusli, M. H., Idris, A. S., & Cooper, R. M. (2016). Evaluation of Malaysian soils for potential suppressiveness of Fusarium wilt of oil palm caused by *Fusarium oxysporum* f. sp. *elaeidis*. *Journal of Microbial and Biochemical Technology, 8*, 459–464. https://doi.org/10.4172/1948-5948.1000325

Siddiqui, Y., Surendran, A., Paterson, R. R. M., Ali, A., & Ahmad, K. (2021). Current strategies and perspectives in detection and control of basal stem rot of oil palm. *Saudi Journal of Biological Sciences*, *28*(5), 2840–2849. https://doi.org/10.1016/j.sjbs.2021.02.016

Strohm, J. H. T. (2015). *The influence of agricultural tillage practices on soil biodiversity* (Master's thesis). The University of Guelph.

Utomo, C., & Niepold, F. (2000). Development of diagnostic methods for detecting Ganoderma-infected oil palms. *Journal of Phytopathology*, *148*(9–10), 507–514. https://doi.org/10.1046/j.1439-0434.2000.00478.x

JOURNAL OF OIL PALM RESEARCH

GUIDE FOR AUTHORS

(for more details, kindly visit http://jopr.mpob.gov.my)

Type of Articles

1. **Regular Article**
   Full-length original empirical investigations, consisting of introduction, materials and methods, results and discussion, conclusions. Original work must provide references and an explanation on research findings that contain new and significant findings. Conclusion should be brief and focus on the research output, should not be in point form. These papers should not exceed 6,000 words of text (including tables, figures and references) and generally not more than a total of 10 figures and tables. After peer-review, the article word count limit can be extended to a maximum of 8,000 words to better address the reviewers' and editors' comments. Any additional figures or tables can be included in the supplementary data. Please note that papers submitted to JOPR will be sent back to authors because of poor figure resolution or exceeding the number of figures permitted.

2. **Short Communication**
   Significant new information to readers of the Journal in a short but complete form. Preferably not exceeding 3,000 words (including tables, figures and references), and is intended for rapid publication. They are not intended for publishing preliminary results or to be a reduced version of regular article.

3. **Review Article**
   Critical evaluation of materials about current research that have already been published by organising, integrating, and evaluating previously published materials. Re-analyses as meta-analysis and systemic reviews are encouraged. Review articles provide systemic overview, evaluation and interpretation of research in a given field. They should not exceed 12,000 words (excluding references only) and should contain no more than a total of 20 figures and tables. Any additional figures or tables can be included in the supplementary data. Please note that papers submitted to JOPR will be sent back to authors because of poor figure resolution or exceeding the number of figures permitted. The same information should not be repeated in a figure and a table.

Language

Please write your text in good English (US or UK). We do not accept mixture of US and UK English in one manuscript. All spelling must be checked carefully.

JOPR's Template

JOPR's template, which is a standard format that facilitates the manuscript writing and copyediting process. This template is created to provide a detail and clear house style of JOPR. The template is drafted according to JOPR's house style, but in standard word version format. When writing a paper, authors need to format their papers to fit into the journal's house style. To make this easier, Word templates are available for many of other established journals, ready for them to download and apply to their research paper format. It is crucial for author to write a research paper while considering formatting. Each journal has its own guidelines for formatting; hence, the template defines how an article will look when it is published online or in print.

JOPR's Aims & Scope

This is established to provide a detail and clear aims and scope for author reference. Authors should declare in the cover letter how the research fits the aims and scope of JOPR.

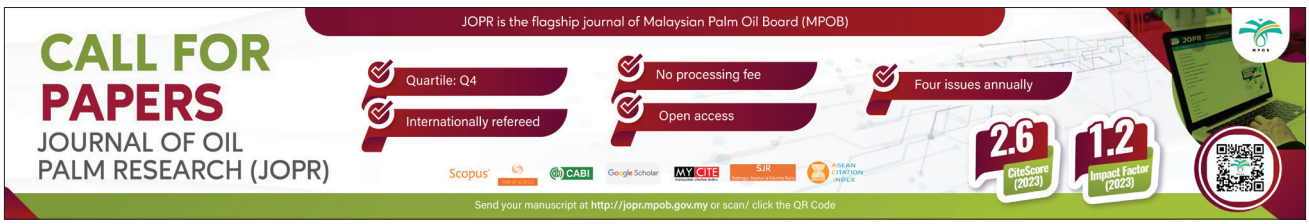
JOPR's House Style

A detail listing of JOPR's house style for authors and a checklist to facilitate the copyediting process and standardise the copyediting process. The JOPR's house style remains the same and is drafted into a detail version for author's reference.

Manuscript Submission

- Manuscripts should be submitted via: https://www2.cloud.editorialmanager.com/jopres/
- JOPR does not permit dual submission, publication and/or any archive platform (preprint) in violation of journal ethical practices.

For more details and to download the JOPR's House Style and Template, kindly visit http://jopr.mpob.gov.my



Contents of the Coming Issue
Journal of Oil Palm Research
Vol. 37 (2) June 2025*

- Oil Palm Economic Performance in Malaysia and R&D Progress in 2024
  Ahmad Parveez Ghulam Kadir; Razmah Ghazali; Abrizah Othman; Madihah Ahmad Zairun; Teh Soek Sin; Voon Phooi Tee; Parthiban Kannan; Nur Ain Mohd Hassan; Zainab Idris and Ramle Moslim

- Spent Bleaching Earth as Value-added Material to Material Construction Applications: A Review
  Fardin Hasibuan; Mohd Kamel Wan Ibrahim and Nugroho Pratomo Ariyanto

- Applications of Organic Fungicides, Endophytic Bacteria, Biofungicides, and Biostimulants in Curative Control of *Ganoderma*
  Deden Dewantara Eris; Agustin Sri Mulyatni; Irma Kresnawaty; Tri Panji; Priyono; Larasati Mardhika; Kuwat Triyana and Happy Widiastuti

- Material Circularity Indicator for Thai Oil Palm Industry
  Nongnuch Poolsawad; Muthita Kachapoch; Jantima Samneangngam and Thanwadee Chinda

- Batch System Clarification of Two Varieties of Palm Oil: Kinetics and Thermodynamics
  Edna Tah; Godlove Nfor Njeshu; Divine Nde Bup; Cerile Woumbo; Alix Ntongme Mboukap and Hilaire Womeni

- Species Identification of the Fatty Acid Composition of the Margarines and Spreads
  Maksat Serikov; Meruyet Nurgaliyeva; Assya Serikbayeva; Zhulduz Suleimenova and Karima Myrzabek

- The First Record of the White-throated Kingfisher, *Halcyon smyrnensis*, Breeding in Borneo, Indonesia
  Muhamad Silmi; Mahfud Huda; Ali Amran; Suryadi; Mislan; Fila Istina Machid; Aldino Fauzil Fanani; Agustina Kristin Handayani and Carl Traeholt

Note: * Subject to change.